Technical Report
TR-20-14
September 2020

Corrosion of copper after 20 years exposure in the bentonite field tests LOT S2 and A3

Adam Johannes Johansson
Daniel Svensson
Andrew Gordon
Helen Pahverk
Oskar Karlsson
Johannes Brask
Martin Lundholm
David Malmström
Fredrik Gustavsson

SVENSK KÄRNBRÄNSLEHANTERING AB

SWEDISH NUCLEAR FUEL
AND WASTE MANAGEMENT CO

Box 3091, SE-169 03 Solna
Phone +46 8 459 84 00
skb.se

SVENSK KÄRNBRÄNSLEHANTERING

ISSN 1404-0344
SKB TR-20-14
ID 1900516
September 2020

Corrosion of copper after 20 years exposure in the bentonite field tests LOT S2 and A3

Adam Johannes Johansson, Daniel Svensson
Svensk Kärnbränslehantering AB

Andrew Gordon, Helen Pahverk
Rise Kimab

Oskar Karlsson, Johannes Brask, Martin Lundholm,
David Malmström, Fredrik Gustavsson
Swerim

Keywords: Field tests, Bentonite, Copper, Corrosion, LOT.

Summary

Long term test of buffer materials (LOT) is a series of field tests aimed to study the behaviour of bentonite clay during extended periods of heated exposure to a repository-like environment in the Äspö Hard Rock Laboratory (HRL). Originally, seven test parcels were installed in 1996–1999, and since then, several parcels have been retrieved and the bentonite clay has been examined thoroughly in several reports. Components of copper were present in the test parcels, and although not intended or prepared for detailed corrosion analysis, these components have been examined as far as possible, regarding the nature and extent of their corrosion. In this report, copper components from the test parcels S2 and A3 are examined after 20 years exposure to the heated environment, conditioned by bentonite clay in the Äspö HRL. The results are discussed in the context of copper corrosion in earlier examined test parcels of the LOT series, similar field tests, and the conceptual corrosion model applied in SKB's safety assessments for the KBS-3 technology.

Sammanfattning

Long-term test of buffertmaterials (LOT) är en serie fältförsök som syftar till att studera hur bentonitlera påverkas under längre perioder av uppvärmning och exponering i en förvarsliknande miljö i Äspölaboratoriet. Sju försökspaket installerades mellan åren 1996 och 1999. Flera av dessa har sedan återtagits och bentonitleran har analyserats grundligt i ett flertal rapporter. I försökspaketen fanns även komponenter av koppar och även om dessa inte varit avsedda eller preparerade för detaljerad korrosionsanalys, har kopparmaterialet undersökts så långt som möjligt med avseende på korrosionens art och omfattning. I den här rapporten analyseras kopparkomponenter från försökspaketen LOT S2 och A3 som återtogs 2019. Kopparmaterialet hade då exponerats under 20 års tid i den uppvärmda och förvarsliknande miljön. Resultaten av analyserna diskuteras mot bakgrund av kopparkorrosion i tidigare undersökta försökspaket i LOT-serien, andra fältförsök med koppar, samt den konceptuella korrosionsmodell som tillämpas i SKB:s säkerhetanalys för Kärnbränsleförvaret.

Contents

1 Introduction

1.1 Background

The field test Long Term Test of Buffer Material (LOT) was initiated more than twenty years ago, with the aim to study the behaviour of bentonite clay (buffer material) under repository-like conditions, e.g. regarding heating and interaction with a corroding metal surface. In the late 1990's seven test parcels were installed at ca 450 m depth in the Äspö Hard Rock Laboratory (HRL). Each parcel consisted of 38 bentonite rings (100 mm high) stacked around a 4 700 mm long copper pipe (diameter 108 mm), which contained a heater (Figures 1-1 and 1-2). Initially, there was a small gap between the copper pipe and the bentonite rings, which prevented interaction between the materials. After saturation and swelling of the clay due to intrusion of groundwater, direct contact was established, which allowed interaction between the clay and the copper surface. The LOT series originally contained seven test parcels, differing mainly by their maximum temperature (Table 1-1).

Since the extent of corrosion of the large copper heater surface is difficult to quantify with accuracy, but could in principle be of importance for the analysis of clay-metal interactions, each test parcel in the LOT-series also contained four copper coupons with accurately determined initial weights, which allows gravimetric analysis and evaluation of the average corrosion depth.

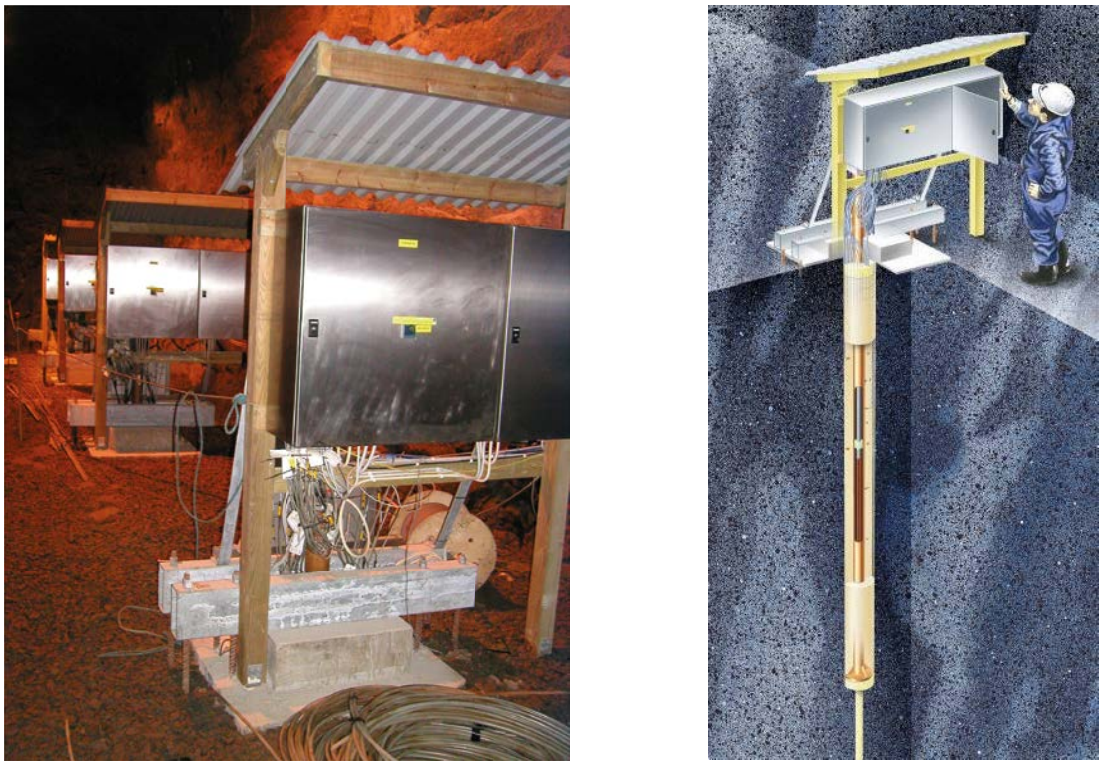

Figure 1-1. *Left: Photo of the test site in the Äspö HRL. Right: Schematic drawing of a LOT test parcel after installation. Reproduced from Sandén and Nilsson (2020).*

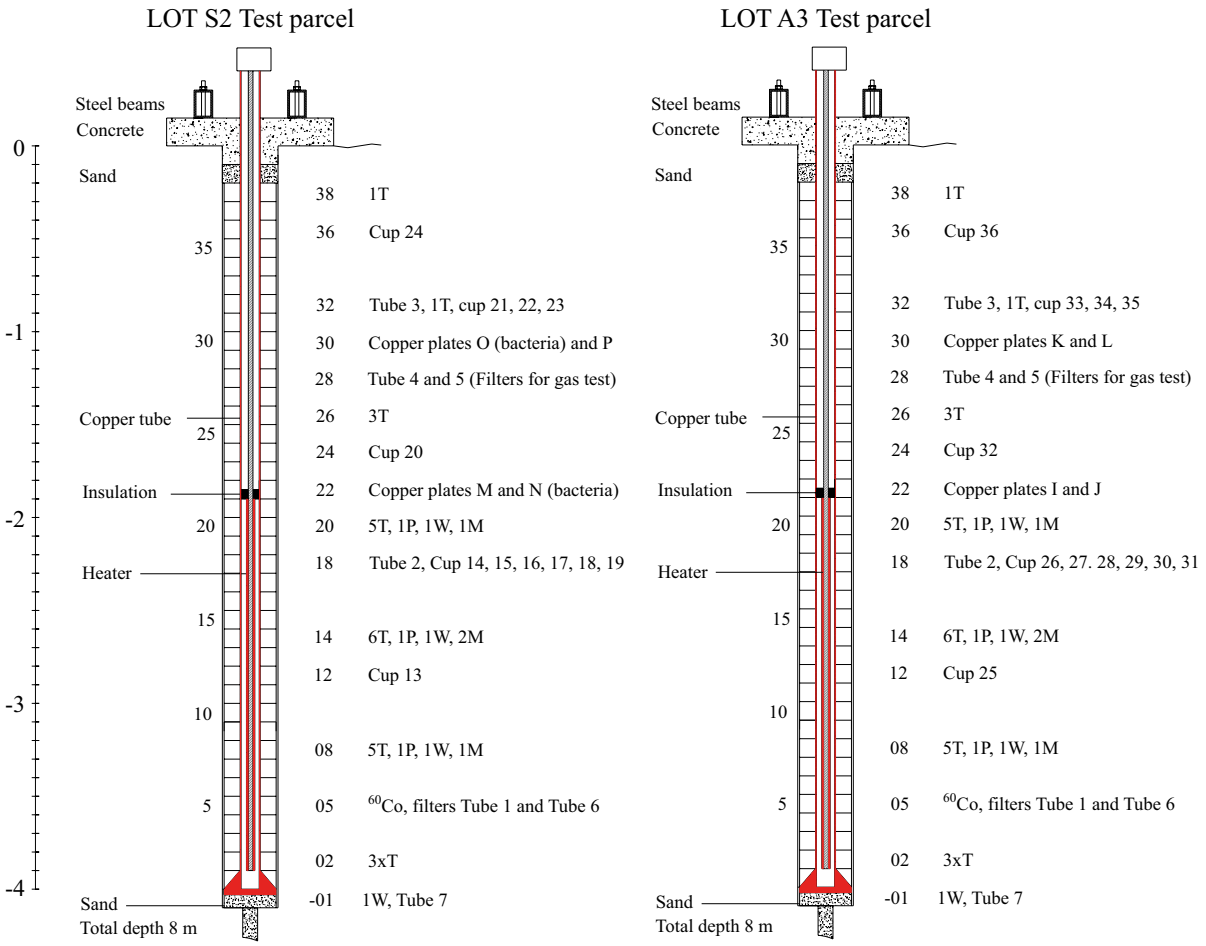

Figure 1-2. *Schematic illustrations of the principal design of the test parcels LOT S2 and LOT A3. Instruments and specimens in the different blocks are described to the right of each illustration. The orange line shows the position of the central copper pipe. Copper coupons ("plates") were mounted in bentonite blocks 22 and 30 in each test parcel. Reproduced from Sandén and Nilsson (2020).*

Table 1-1. Test matrix for the LOT series. A = adverse conditions, S = standard conditions, T = temperature. The test parcels S2 and A3 are examined herein.

Test parcel	Max T (°C)	Installed	Terminated	Time (years)
A1	130	Nov 1996	Mars 1998	1.3
A0	150	Dec 1999	Nov 2001	1.9
A2	120–150	Oct 1999	Jan 2006	6.1
A3	120–150	Oct 1999	Sep 2019	20
S1	90	Oct 1996	Feb 1998	1.4
S2	90	Sep 1999	Oct 2019	20
S3	90	Sep 1999	ongoing	-

In this report, copper components and bentonite clay in contact with copper components from the recently retrieved S2 and A3 test parcels are examined regarding the extent and form of corrosion. Comparison will be made with previously retrieved field experiments and with the conceptual corrosion model applied by SKB in the safety assessment of a KBS-3 repository at the Forsmark site. Details of the retrieval procedure, together with results from long-term measurements and physical data of the bentonite clay are presented in a report by Sandén and Nilsson (2020). More detailed chemical examination of the bentonite clay will be presented in separate reports.

1.2 Corrosive agents – oxygen and sulfide

In the experimental environment, i.e. copper embedded in bentonite clay in contact with saline groundwater, there are two oxidants capable of corroding copper, these are O_2 and sulfide (HS^-/H_2S). On a short timescale, residual O_2 may be present e.g. in the pore volume of the bentonite clay and in initially existing gaps in the experimental setup. Copper can react with O_2 to directly form the solid Cu^+ corrosion product Cu_2O:

$$4Cu(s) + 4OH^- \rightarrow 2Cu_2O(s) + 2H_2O + 4e^- \text{ (anodic reaction)} \quad \text{(Equation 1)}$$

$$O_2 + 2H_2O + 4e^- \rightarrow 4OH^- \text{ (cathodic reaction)} \quad \text{(Equation 2)}$$

$$4Cu(s) + O_2 \rightarrow 2Cu_2O(s) \text{ (total reaction)} \quad \text{(Equation 3)}$$

However, depending on the solution conditions, intermediate Cu^{2+} species may also form, either by direct oxidation of copper metal

$$2Cu + O_2 + 4H^+ \rightarrow 2Cu^{2+} + 2H_2O \quad \text{(Equation 4)}$$

or by the homogeneous oxidation of aqueous Cu^+ species

$$4Cu^+ + O_2 + 2H_2O \rightarrow 4Cu^{2+} + 4OH^- \quad \text{(Equation 5)}$$

The fate of aqueous Cu^{2+} species depend on solution conditions, the Cu^{2+} species may precipitate as solid compound (e.g. $Cu_2(OH)_3Cl$), adsorb on the bentonite clay (via cation exchange), or react further with metallic copper via the comproportionation reaction:

$$Cu^{2+} + Cu(s) \rightarrow 2Cu^+ \quad \text{(Equation 6)}$$

The Cu^+ species can in turn precipitate as Cu_2O or stabilize as a chloride complexes, e.g. $CuCl_2^-$ (King et al. 2010).

By experience from repository-like field tests and laboratory experiments, the main solid corrosion product adherent to the copper surface is typically Cu_2O (Huttunen-Saarivirta et al. 2017, Johansson 2019, Karnland et al. 2009, King et al. 2010, 2013), however, depending on the composition of the groundwater, Cu^{2+} phases such as $Cu_2(OH)_3Cl$ or $Cu_2(OH)_2CO_3$ have been observed (Karnland et al. 2009, Rosborg 2013, Wersin and Kober 2017). Copper adsorbed on the bentonite clay has also been observed (Karnland et al. 2009).

Corrosion driven by direct reactions with O_2 may, of course, only proceed as long as there is O_2 in the system. However, as indicated by Equation 6, corrosion can also proceed if there is Cu^{2+} present in the near field. Nevertheless, from a mass balance point of view, the maximum amount of corrosion caused by entrapped oxygen will be the same, even if the route goes via intermediate Cu^{2+} species.

In the LOT experiments there were several sources of O_2 present initially; air contained by the bentonite porosity, air contained by the porosity of sand above and below the test parcel, an air filled macroscopic gap between the copper tube and bentonite rings, and an initially air filled gap between the bentonite rings and the rock surface of the bore hole. In addition there were seven Ti-tubes mounted at different hights in each test parcels (denoted “Tube X” in Figure 1-2), which were open to the Äspö tunnel for four months before starting the supply of water for which they were intended (Sandén and Nilsson 2020).

The rate of O_2 consumption by copper corrosion and by other processes depends on the experimental conditions, e.g. density and swelling pressure of the clay, degree of water saturation, temperature, clay volume to copper surface ratio, mineral composition of the clay, the presence of aerobic microorganisms etc. Experiments with unsaturated bentonite clay indicated that O_2 depletion of the gas phase took 2 to 10 months, depending on e.g. the surface pre-treatment of the copper heater used in the experiments (Birgersson and Goudarzi 2018, Åkesson et al. 2020). Grandia et al. (2006) concluded based on a theoretical model that anoxic conditions will be reached after about one month after saturation of the bentonite, while electrode potentials (E_{corr} and E_h) in the MiniCan experiments have shown that it took up to a few months to reach low and stable potentials (Smart et al. 2015). More rapid O_2 consumption has also been reported in laboratory tests (Lazo et al. 2003, Muurinen and Carlson 2010), while per-

cent levels O_2 could still be measured after a few years in the large scale Febex experiment (Giroud 2014). It is evident that the time it takes to reach complete depletion of O_2 in a repository, or a field test, depends on several parameters. Exactly how long it took to reach depletion of O_2 in the LOT test parcels is not known, but given the results summarised above, it was probably less than a year.

On a longer timescale, sulfide from the groundwater or produced locally by sulfate reducing bacteria (SRB), can diffuse through the bentonite clay and contribute to corrosion of the copper surface by the formation of mainly chalcocite, Cu_2S (Chen et al. 2010, Smith et al. 2004, 2007a):

$2Cu(s) + OH^- + HS^- \rightarrow Cu_2S(s) + H_2O + 2e^-$ (anodic reaction) (Equation 7)

$2H^+ + 2e^- \rightarrow H_2$ (cathodic reaction) (Equation 8)

$2Cu(s) + HS^- + H^+ \rightarrow Cu_2S(s) + H_2$ (total reaction) (Equation 9)

However, to understand the development of sulfide films on copper in field tests like LOT it is important to note that Cu_2S is also formed as a substitution product when Cu_2O reacts with sulfide (Smith et al. 2007b, Hollmark et al. 2012, Kristiansen et al. 2015, Stenlid et al. 2017):

$Cu_2O(s) + HS^- \rightarrow Cu_2S(s) + OH^-$ (Equation 10)

Since the concentration of sulfide in the Äspö groundwater is low (typically ~ 10^{-6} M) and since diffusion through compacted bentonite clay is slow, the supply of sulfide to the copper surface limits the process effectively. In earlier test parcels from the LOT series and similar field tests, only minor amounts of copper sulfide were found at or near the copper surfaces analysed and its contribution to corrosion was small compared with the O_2 driven corrosion (Karnland et al. 2009, Johansson 2019).

1.3 Development of the physicochemical environment

After the test parcels LOT S2 and A3 had been installed in their boreholes it took ca 4 months before the experiments were started, i.e. before the heaters were switched on. During this period the components of the test parcels had rock temperature of ca 15 °C. When the heating was started the temperatures measured at various positions in the bentonite increased and reached its steady state values within a year from start (Sandén and Nilsson 2020). The maximum temperatures given in Table 1-1 are for the surface of the central copper pipes in each test parcel, reaching up to 90 °C in the S series, and 120 °C at least in the A series. Contour plots of the temperature distributions in LOT S2 and A3 have been made using direct measurements and an interpolation program (Figure 1-3). The temperature readings used for the graphs were made the 5th August 2019 i.e. the day before the heaters were stopped (Sandén and Nilsson 2020). As illustrated by the plots, the temperature of the pipe surface varied along its length, depending on the distance from the heater inside the copper pipe. At distances further from the heater the temperature fell to ca 50 – 60 °C at the position of the coupon in block 22 in the A3 test parcel, while the same position in the S2 test parcel was slightly lower (Figure 1-3). In both test parcels the average temperature around the coupons in block 30 was 20 – 30 °C.

During the operation of the experiments in the Äspö HRL, the evolution of the clay systems were monitored. The swelling pressure developed over periods of 1 – 4 years at most positions monitored in the test parcels, although at some positions it took even longer. The final swelling pressure in LOT S2 ranged between 2.1 and 3.75 MPa, while the range for A3 was 1.5 to 3.75 MPa. The degree of saturation was nearly 100 % in most parts of both test parcels, however, the clay in the hottest region of parcel A3 was a bit lower, varying from 94 to 97 %. The density of the clay at retrieval was significantly lower near the top and bottom of each parcel, mostly below 1 450 kg/m^3, while the density in the middle of the parcels varied within 1 500 – 1 550 kg/m^3. Further details of these measurements can be found in Sandén and Nilsson (2020).

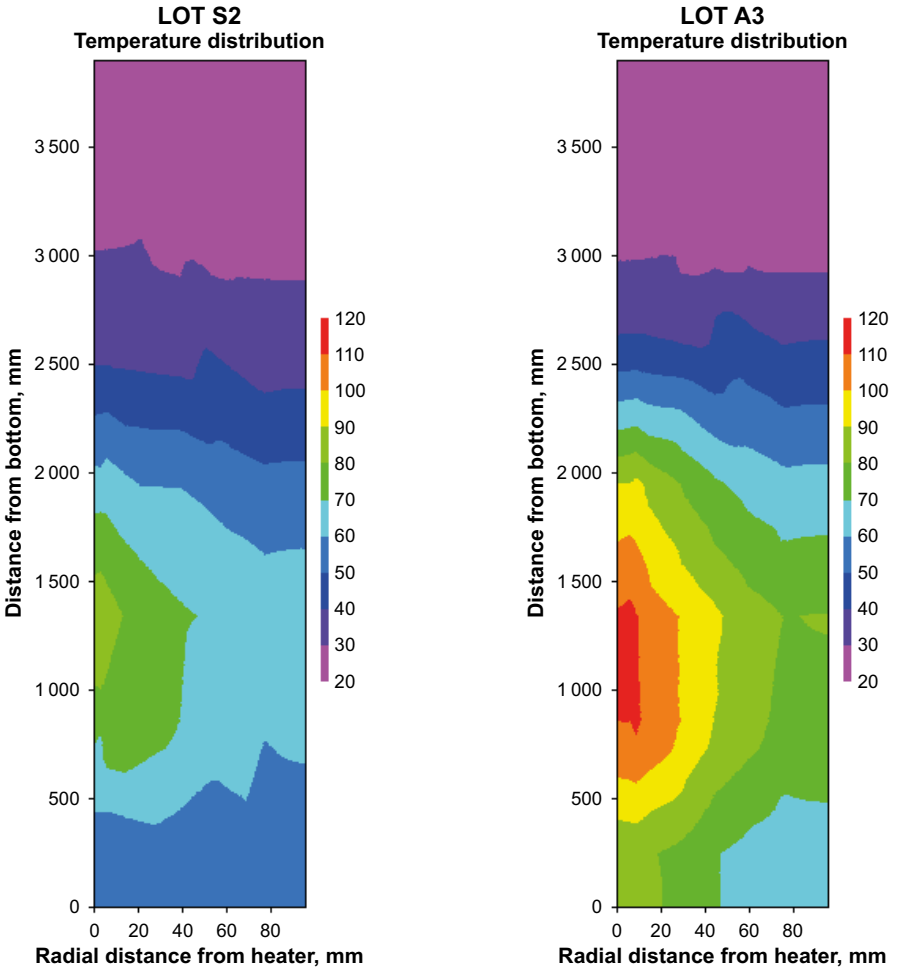

Figure 1-3. *Contour plots showing the temperature distribution in LOT S2 (left) and LOT A3 (right). Reproduced from Sandén and Nilsson (2020).*

As the specific location of the LOT experiments in the Äspö HRL was found to be relatively dry, a water supply hole (HG0038B01) was drilled into the northern wall where a water-bearing fracture was found a few meters into the rock. Its water pressure was found to be around 1.2 MPa and the flow was sufficient to support all test holes in the LOT series. The water supply hole was packed off and a system of titanium tubes was used to inject water into the test holes (Sandén and Nilsson 2020). The chemical composition of the formation water from the supply borehole has been analysed several times during the operation of the experiments (Table 1-2). During the period 2000-04-14 to 2018-11-06 the formation water of the borehole became slightly more alkaline and saline, while sulfide has been very low during the hole period.

Table 1-2. Main composition of the formation water in water supply bore hole (HG0038B01).

HG0038B01	Na^+	K^+	Ca^{2+}	Mg^{2+}	HCO_3^-	Cl^-	SO_4^-	Br^-	F^-	Si	HS^-	pH	E.C.
Units	mM	mM	mM	mM	mM	mM	mM	mM	mM	mM	mM		mS/m
2000-04-14	98.7	0.24	43.4	2.21	0.85	185	4.84	0.50	na	0.18	na	7.4	1750
2001-09-26	104	0.25	49.6	2.15	0.71	195	4.94	0.62	0.13	0.20	0.0006	7.4	1930
2006-10-02	98.7	0.26	56.6	1.90	0.21	219	5.57	0.62	0.08	0.21	0.0003	7.6	2170
2012-05-08	104	0.22	56.6	1.83	0.22	205	5.10	0.55	0.09	0.21	< 0.0006	7.7	2080
2018-11-06	132.7	0.30	75.6	1.45	0.13	266	5.78	0.83	0.09	0.17	< 0.0006	7.8	2553

1.4 Retrieval and samples

The test parcels LOT S2 and A3 were retrieved during fall 2019. The retrieval procedure is described further in Sandén and Nilsson (2020). At the time of the retrieval, the copper coupons in the test parcels had been exposed for 20 years in the experimental installations at ca 450 m depth the Äspö HRL. After being removed from the bentonite, the copper samples were vacuum-packed in sealed aluminium foil bags within less than an hour in order to prevent extensive exposure to air during transport and prior to analysis. The copper coupons and parts of the copper pipes have been subjected to various analysis techniques in order to determine the nature and extent of copper corrosion. Since the start of the LOT experiments two copper coupons were stored under dry indoor conditions in order to serve as reference specimens. A spare copper pipe, made of the same material as the pipes in the LOT experiments and kept in a non-heated storage, served as a reference specimen for the pipes. These reference specimens are also examined in this report. Sampling of the bentonite blocks was done during retrieval of the test parcels and the samples were kept at the Äspö HRL, where the analyses presented herein were conducted. The samples are further described in Section 2.1.

1.5 Limitations of LOT as a corrosion experiment

As already mentioned, LOT (Long-term test of buffer materials) was planned as a series of bentonite experiments, and was thus not intended or designed for detailed studies of copper corrosion. After the initiation of the experiment it has been decided to analyse copper corrosion in LOT as far as possible, and it is thus important to be aware of the limitations of LOT as a copper corrosion experiment. Concerning the copper components it is important to note the following:

- Due to the size of the copper pipe it was not possible to quantify corrosion depth in terms of mass-loss using standardised gravimetric methods. Instead, an indirect measure of the copper concentration in the bentonite near the copper surface has been used to estimate the corrosion depth. This method seems to perform well but is not standardized for measuring corrosion.
- The surface of the copper pipe was not characterised regarding surface topography or deposits before the start of the experiment, meaning that it is not strictly possible to conclude how the surface topography has changed during the experiment and how it has been affected by corrosion.
- The copper pipe was not made of SKB's reference material for the KBS-3 canister, i.e. oxygen-free phosphorous doped copper (Cu-OFP), but was made of a standard de-oxygenated copper (SS 5015-04). Corrosion of this material in repository-like environments has not been studied outside the LOT series.
- The lower part of the copper pipe was welded to a bottom plate, also made of copper. The upper part of the copper pipe (ca 0.7 m) was in direct contact with the atmosphere in the Äspö tunnel (Figure 1-1). Since the upper end of the pipe was open, the interior of the pipe was filled with air during the whole exposure. The corrosion of the upper part and inner pipe surface has thus not occurred under repository-like conditions. In order to assure that the weld at the bottom plate was not leaking air into the clay system, the tightness of the weld before installation was tested using helium gas (Sandén and Nilsson 2020).
- The copper coupons were intended for gravimetric analysis and their weights were determined to sufficient accuracy. However, although one side of the coupons was polished, their surface topography was not pre-characterised, meaning that the examination of corrosion morphology is inherently uncertain.

Other limitations of LOT as a corrosion experiment concern the development of redox conditions in the near environment:

- Due to the existence of macroscopic gaps and porous materials in the test parcels, there are uncertainties in the exact amount of O_2 available initially. Further uncertainty regarding the availability of O_2 comes from that the Ti-tubes used to speed up the water saturation process were open to the Äspö tunnel during 4 months after installing the test parcels.
- Neither the redox potential (E_h), nor the corrosion potential (E_{corr}) of the copper components were monitored, meaning that it is not known on what time-scale the near field environment became oxygen free.

2 Materials and methods

2.1 Samples and analysis overview

The samples were retrieved by staff from SKB and Clay Technology during September and October 2019. Bentonite samples were kept at the Äspö HRL where the bentonite analyses were later conducted. In order to prevent any adverse effects of exposure to air during transport and prior to analysis the copper samples were vacuum packed in Al-foil bags. The samples were then transported to RISE KIMABs facilities in Kista, Stockholm. There, the Al-foil bags were opened and the samples were photographed before being placed in a containment tent which was purged with nitrogen gas in order to maintain a low oxygen environment. The flow of nitrogen was checked every day and logged. This method ensured that the samples had been exposed to air for less than one hour in total during the retrieval procedure at Äspö HRL and during unpackaging at RISE KIMAB before the analyses were carried out. The samples received and the analysis methods employed are summarised in Table 2-1. Photographs of the as received samples and the reference samples are available in Appendix A.

The coupons were made of SKB's reference material for the KBS-3 canister, i.e. oxygen free phosphorous doped copper (Cu-OFP), containing less than 5 wt-ppm oxygen and 30 – 70 wt-ppm phosphorous. The coupons had dimensions 60 × 15 × 1.5 mm, and had one milled and one polished side. As indicated in Figure 1-2, two of the coupons in LOT S2 were immersed in a bacterial growth medium before being installed in the test parcel. It is unfortunate that detailed information about this procedure has been lost during the two decades since the experiment was installed, however, communication with persons involved in the installation of LOT suggests that the growth medium contained sulfate reducing bacteria (SRB). Reference coupons were also analysed. These were made of the same material but had been stored in a dry indoor environment during the exposure of the test parcels in the Äspö HRL. The reference coupons had dimensions 50 × 23 × 1.5 mm.

The copper pipe was made of a standard deoxidised copper quality (SS 5015-04), containing 99.85 % Cu and 150 – 400 wt-ppm P. The samples examined herein were taken from bentonite blocks 21 to 23 from each of the two test parcels, with ca 50 mm margin into blocks 20 and 24. The samples were thus ca 400 mm long. A spare pipe (also SS 5015-04) that had been kept in a non-heated storage since the installation of the LOT experiments has been analysed as a reference material regarding its content of O and H.

Corrosion products on the coupons were analysed using X-ray diffraction (XRD) and scanning electron microscopy (SEM) with energy dispersive scattering (EDS). One coupon from each test parcel was also cross-sectioned and examined using SEM-EDS and high-resolution transmission electron microscopy (HR-TEM). Gravimetric analysis was made to evaluate the average corrosion depth on three coupons from ach test parcel. Finally, light optical microscopy (LOM) was used to examine the surface topography of the coupons before and after the removal of the corrosion products done in the gravimetric analysis.

Corrosion products on the pipe samples were analysed using SEM-EDS. The elemental composition of the material near the surface of the pipe samples were analysed using glow discharge optical emission spectroscopy (GDOES) and the hydrogen content of the material was measured using Leco gas fusion analysis.

The bentonite clay was of the type MX-80 (Wyoming, USA). It consists of approximately 80 wt% montmorillonite, which is a smectite mineral belonging to the layer silicate group. The smectite layers expand upon hydration and shrinks upon drying. Smectites are cation exchangers, as the positive ions that neutralises the negative silicate layers are replaceable, e.g. from Na^+ to Ca^{2+}. Additionally the bentonite contains several accessory minerals such as quartz, calcite, feldspar, gypsum, pyrite, and a low amount of organic carbon.. X-ray fluorescence spectroscopy (XRF) was used to measure the concentration of copper and other major elements in the bentonite clay near the copper surfaces. This was done in order to estimate the extent of corrosion on various parts of the copper pipes. Variations in the elemental composition of the bentonite samples were examined using SEM-EDS, and the mineralogical composition was analysed using powder XRD. In all cases the bentonite was dried prior to any milling or analysis, either at room temperature or for approximately 30 minutes at 60 °C in order to make milling of the clay possible. All handling of the bentonite samples was done in air. All samples were more or less in equilibration with the ambient relative humidity of approximately 40 – 60 %. In a few cases, the water content was determined, this was done at 105 °C in a ventilated oven for 24 hours.

Table 2-1. Summary of copper samples and analysis methods employed.

				Analysis methods							
Test parcel	**Description**	**ID**	**Material**	**XRD**	**SEM/EDS surface**	**SEM/EDS cross-sect.**	**TEM cross-sect.**	**Mass Loss**	**LOM**	**Leco H**	**GDOES**
A3	Coupon	I	Cu-OFP	X	X	-	-	X	X	-	-
A3	Coupon	J	Cu-OFP	X	X	-	-	X	X	-	-
A3	Coupon	K	Cu-OFP	X	X	X	X	-	X	-	-
A3	Coupon	L	Cu-OFP	X	X	-	-	X	X	-	-
A3	Pipe section	-	SS 5015-04	-	X	X	-	-	-	X	X
S2	Coupon	M	Cu-OFP	X	X	-	-	X	X	-	-
S2	Coupon	N	Cu-OFP	X	X	X	X	-	X	-	-
S2	Coupon	O	Cu-OFP	X	X	-	-	X	X	-	-
S2	Coupon	P	Cu-OFP	X	X	-	-	X	X	-	-
S2	Pipe section	-	SS 5015-04	-	X	X	-	-	-	X	X
Ref.	Spare pipe	-	SS 5015-04	-	-	-	-	-	-	X[a]	-
Ref.	Unexposed coupon	K	Cu-OFP	X	X	-	-	X	X	-	-
Ref.	Unexposed coupon	L	Cu-OFP	X	X	-	-	X	X	-	-

[a] For the spare copper pipe, the content of both H and O was analysed with Leco.

2.2 Surface examination of corrosion products

In order to characterise crystalline corrosion products on the coupons surfaces, X-ray diffraction (XRD) was applied. The instrument was a Bruker D8 Discover, with Kα beam (1.54 Å), which can obtain measurements approximately 5 µm deep into the surface. Data were collected between 10° and 100° (2θ). The peak identification is according to best match by the Bruker analysis software DIFFRAC.EVA.

Scanning electron microscope (SEM) images of the surfaces of both coupons and pipe samples, were obtained with a Zeiss Supra scanning electron microscope with a Field Emission Gun (FEG) as electron source. The electron beam energy was 15 keV and the working distance was about 10 mm. A detector for backscattered electrons was used. The microscope was equipped with a detector for energy dispersive spectroscopy (EDS) which was used for elemental analysis of small areas of the samples, carried out to a depth of about 1 µm into the surface. No carbon coating was applied to the samples analysed. Due to the morphology and filtering effects of corrosion products the analysis results should be interpreted as semi-quantitative at best, and as such an accuracy of the measurement values cannot be strictly defined (Appendix B).

2.3 Examination of surface cross-sections

The copper coupons A3/K and S2/N were selected and cross-sectioned in order to examine the corrosion morphology and the composition of the corrosion products at depth. Using 1 out of 4 coupons per test parcel for this purpose was a trade-off between the value of information gained from examination of cross-sections, and the statistical quality of the gravimetric analysis. The particular coupons were chosen as to examine one coupon from each test parcel (S2 and A3), and one coupon from each block position (blocks 22 and 30). SEM-EDS was used to analyse the elemental composition of the corrosion products, while transmission electron microscopy (TEM) was applied in an attempt to further identify the nature of sulfur-rich particles and deposits.

In total, 4 samples (lamellae) for TEM analysis were prepared using focused ion beam machining (FIB), 2 lamellae from each coupon. The lamellae were cut at the bottom of selected pits that had been observed using SEM-EDS and where the highest levels of sulfur had been found. The lamellae were prepared using FIB with a FEI Strata DB235 instrument, using the in situ lift-out technique. A metal-organic precursor consisting of Pt and C was deposited using the electron beam to protect the area of interest from the high energy ions during milling and preparation of the lamellae. The lamellae were then transferred to special grids which are of the correct dimensions for analysis in the TEM, then polished to electron transparency with successively lower beam currents, to achieve a sharper ion beam and less surface damage on the final lamellae. During the final step of preparation, the lamellae were cleaned using low energy ions (5 keV) to remove the most of the affected layer on both sides of the lamellae. This method results in approximately 5 nm of amorphous layers on each side of the lamellae instead of the originally ca 20 – 30 nm.

The lamellae were examined in a JEOL 2001F TEM equipped with an EDS detector from Oxford Instruments and a Gatan Trideum energy filter for Electron Energy-Loss Spectroscopy (EELS). When performing EDS and EELS, the TEM was run in STEM mode (scanning TEM) so that the beam is scanned over the sample and elemental information collected from each pixel separately. Further details of the TEM analysis are given in Appendix C.

For the pipe samples, representative type areas were selected based on their visual appearance. These areas were then cut and examined in cross-section with SEM-EDS. In total 12 samples were examined for each pipe, including 2 samples from the inner surface of each pipe.

2.4 Gravimetric analysis

To evaluate the mass loss for the corrosion coupons the principle method of repeated pickling according to standard SS-EN ISO 8407:2014 was used. Initial weights of the coupons were obtained by Clay Technology before the start of the LOT experiments. The corroded specimens were chemically cleaned, removing the corrosion products by pickling. Repeated pickling is typically needed to remove all corrosion products. The specimen is weighed after each cleaning treatment and the procedure is repeated until the mass loss between two treatments is very small, and comparable to the mass loss of a reference specimen. Both the metal and the corrosion products determine what chemical cleaning solution is suitable to use.

From the examination of previously retrieved test parcels from the LOT series, it was expected that the corrosion products on the coupons would consist mainly of cuprite (Cu_2O) and so a pickling solution of sulfamic acid (5 wt%) was selected and was applied for 5 minutes with a cleaning interval of 1 minute. The appearance of the coupons after pickling indicated that corrosion products still remained at the surface.

XRD analysis on the pickled coupon S2/P revealed weak signals indicating the presence of cuprite (Cu_2O) and chalcocite (Cu_2S). Therefore, in order to complete the mass loss, a second pickling step was tried using hydrochloric acid (50 wt%) for 20 minutes with cleaning intervals of 5 minutes (also in accordance with SS-EN ISO 8407:2014). This procedure was first tested on coupon S2/P with shorter cleaning intervals, before being implemented on the remaining coupons to confirm the efficiency of the method and to ensure that it had no adverse effects on the base material (copper metal). This was confirmed by measuring the surface defect depths before and after pickling.

After the second pickling step in hydrochloric acid, and despite that the mass loss data suggested that all corrosion products had been removed, it was noted that some staining of the surface still remained. Since the coupon S2/P had a slightly lower mass loss than the other coupons, it was decided to try a third pickling step using sulfuric acid (9.5 wt%). This method had been applied to coupons in previously retrieved LOT test parcels and is also in accordance with SS-EN ISO 8407:2014. Finally, in an attempt to get the coupon S2/P completely free of surface deposits, cathodic electrolytic cleaning was applied using a KCl solution (according to SS-EN ISO 7407:2014 E.3.1.). The final pickling and reduction steps gave only a minor increase in the mass loss. Full details of the pickling procedure can be found in Appendix D.

2.5 Examination of surface topography

The surface topography of the coupons was examined using light optical microscopy (LOM). All types of defects on the milled side of the coupon were counted and measured using a Nikon Epiphot microscope equipped with a digital camera Kappa DX40. The depths of the defects were measured using the calibrated focus of the microscope, with an accuracy of ± 1 µm. This was done before and after pickling. After pickling the area analysed was limited to 0.5 cm^2.

2.6 Material elemental composition

Glow discharge optical emission spectroscopy (GDOES) uses a plasma gas to melt the top 5 µm of the sample and then analyses the resulting gas for elemental content. The instrument used was a LECO GDS 850A. For the profile measurements performed, the detection limit is estimated as 0.1 % and the accuracy would be one or a few %. Calibration was carried out using certified reference materials of aluminium (1257), brass (2161-5), copper (Cu0x), ceramic (Ker1), stainless steel (SDN-71 and SUS hot-rolled steel for oxygen content), aluminium-silicon (ST4), and cast iron (c1145A).

The sample surface needs to be flat in order to create a vacuum seal between the sample and the instrument. To flatten the samples a vice was used (with clean paper between the sample and instrument). Each sample was analysed in triplicates. The measured spots can be seen in Figure 2-1.

Figure 2-1. *Sections of pipe A3 (left) and S2 (right) for GDOES analysis. The small circles visible on the surfaces are the spots of analysis.*

A common method for determination of the hydrogen content in steel and other metals is melt extraction. In this method the sample (around 1 g) is melted in a graphite crucible by passing a high current through the latter. Elements such as H, C, N and O are extracted as gases to be mixed with the argon carrier gas. After removing the other components of the gas mixture by chemical traps, H is measured by its influence on the thermal conductivity of the remaining H_2/Ar mixture. After calibration, this measure can give the H content of the sample.

The apparatus used for this analysis was a Leco Rhen 602. Leco's reference samples are used for calibration of the instrument. The precision of the method, as measured by repeated measurements on references, is around 0.2 ppm when H is present at the 1 ppm level. There may be a small additional absolute error depending on the method (e.g. sample preparation) and references used in the calibration. The scale defined by Leco's methods and samples is however well established.

Reference pipe material, kept in a non-heated indoor storage during the LOT experiments, was also analysed. The pipe was analysed for H and O bulk concentration using a Leco Rhen 602 and a Leco TC 436 device respectively, Leco's reference samples were used for calibration of the instruments.

Samples of ca 1 g were extracted (ca 5 × 5 × 5 mm) for the Leco analysis. The samples were taken from the outer surface of the pipe, which was either analysed *as-received*, ground or ground and filed. The ground samples were subjected to abrasive paper to remove the surface oxides, whilst the ground and filed samples were also subjected to filing using a clean file that has been first used on another part of the pipe in order to remove any surface contaminants from the surface of the file.

2.7 Analysis of copper in bentonite

In order to estimate the corrosion depth on different parts of the copper pipes, X-ray fluorescence spectroscopy (XRF) was used to measure the copper content in bentonite samples that had been in contact with the copper surfaces. The equipment used was a Panalytical Epsilon spectrometer using a Rh X-ray tube. The measurement setup was the standard provided from the manufacturer (Omnian). The Omnian application was modified in the way that the measurement time was doubled at the lower energy programs resulting in a total measuring time of approximately 15 minutes per sample. The samples were, if needed, dried at 60 °C, milled using a ball mill and compacted without any other additions into small blocks. Each compacted sample block was measured on both sides resulting in two data points for each sample. The XRF does not measure elements with atomic number lower than 11 (Na). The elements are typically reported as oxides and the sum is normalized to 100 %.

In order to characterize crystalline phases of corrosion products or precipitates in the bentonite, powder XRD was applied. The equipment used was a Panalytical XPert diffractometer using a Cu X-ray tube, and a PIXcel detector. A programmable divergence slit was used, and data were typically collected in the interval of 4 – 80 degrees two theta. The samples were milled in an agate mortar prior to the measurement, and if needed dried at 60 °C. If the sample amount was low, a zero background silicon substrate was used as a sample holder, otherwise, backloaded standard sample holders were used.

The morphology and elemental composition of bentonite samples in contact with copper components was examined with SEM-EDS. The instrument was a Hitachi TM4000 Plus SEM with a Bruker SCU EDS detector. The sample was air dried, and mounted on conductive tape prior to examination in the microscope. The sample was not embedded or coated. Standard settings from the manufacturer optimized for EDS were used. The EDS evaluation was done using the standards included in the software provided by the manufacturer. The EDS detector is calibrated on a routine basis at the laboratory.

3 Results

3.1 Visual appearance of the copper components at retrieval

When the test parcels were retrieved, the bentonite clay embedding the copper pipes was still in place and the test parcels were surrounded by rock as a result of how the drilling to remove the test parcels was performed. Details of the retrieval and disassembly of the LOT S2 and A3 test parcels can be found in Sandén and Nilsson (2020).

The first copper surfaces that became visible during the retrieval were the bottom plates welded to the central copper pipes (Figure 3-1). As indicated in Figure 1-2, the bore holes below the experimental test parcels were filled with sand, i.e. there was no bentonite clay in contact with the bottom plates. The upper left photo in Figure 3-1 shows the bottom plate of A3 when the test parcel was still surrounded by rock. Some of the sand which filled up the hole below the test parcel is still present and some bentonite is visible on the side of the bottom plate. It may be noted in Figures 3-1 and 3-2 that blue-green deposits had formed under the bottom plates in both test parcels, as well as on the side of the bottom plate in A3. Although not apparent in the photographs, the mid part of the S2 bottom plate also had a slightly blue-green appearance. A sample of the blue-green deposit was later analysed with SEM-EDS and XRD (Appendix I). The EDS analysis indicated high levels of chlorine and the XRD showed good agreement with the diffraction pattern of $Cu_2(OH)_3Cl$, an expected corrosion product of copper in the presence of O_2 and chloride (Karnland et al. 2009).

The copper pipes became visible after the test parcels had been segmented by breaking off the rock masses, removing the Ti-tubes and cables to the thermo-elements, and finally cutting the clay and pipe assembly using a saw. The appearance of the copper pipes in the two test parcels were similar (Figure 3-3). Both pipes had areas with dark brown to nearly black appearances, as well as areas with a lighter copper-like appearance. The pipe from A3 appeared to have slightly larger dark areas than the pipe from S2, although areas of both types were found on both pipes. The dark staining of the copper pipes in LOT S2 and A3 was similar to the appearance of the pipe in LOT A2, see Figures A2-2, A8-4 and A8-6 in Karnland et al. (2009). There were also areas where a thin layer of bentonite clay was still adherent to the surface, and areas with a white deposit forming a reticulated pattern (see for example the mid left photo in Figure 3-3). The latter was very similar with observations made in both LOT S1 and A0, see e.g. Figure 4-13 in Karnland et al. (2000), and has been identified as precipitates of $CaSO_4$ (see further Section 3.6).

LOT A3 bottom plate

LOT S2 bottom plate

Figure 3-1. *Appearance of the bottom plates immediately after retrieval. Note the blue-green deposits. Upper left: Bottom plate of A3 when it was still surrounded by rock. Lower left: Bottom plate of A3 when the pipe was still embedded in the bentonite. Right: Bottom plate of S2.*

A3 pipe lower part (block 1-3)

S2 pipe lower part (block 1-3)

Figure 3-2. *Appearance of the lower part of the copper pipes immediately after retrieval.*

A3 pipe sections

S2 pipe sections

Figure 3-3. *Appearance of the copper pipes in LOT A3 and S2 immediately after uncovering the pipes.*

As discussed in the introduction, the copper pipes were open to the Äspö tunnel during the whole experiment. The exposure of the inner pipe surface to air and humidity was clearly visible on some parts and especially the lower parts of the pipe showed signs of corrosion (Figure 3-4). Further examination of cross-sectioned samples of the copper pipes inner surfaces in SEM revealed a thin corrosion film (< 1 µm thick), and pits of about a few µm deep (Appendix F).

Pipe interior bottom A3

Pipe interior bottom S2

Pipe interior A3

Figure 3-4. *Appearance of the interior of the copper pipes in LOT A3 and S2 immediately after retrieval.*

The appearance of the copper coupons was similar to that of the pipes. Some areas were brown while others were very dark, almost black. Some of the coupons had small areas appearing metallic and a thin grey layer (likely bentonite) covered parts of some coupons (Appendix A). There was no clear difference in the appearance between the coupons from the two test parcels, and neither between the coupons in block 22 and block 30. However, there was a difference in appearance when comparing the coupons from LOT S2 and A3 with coupons from previously retrieved test parcels S1 and A0. While the coupons from LOT S2 and A3 were generally darker than coupons from S1 and A0, the latter had developed blue-green corrosion products (see e.g. Figure B-1 in Karnland et al. 2011), which were absent on the coupons in both S2 and A3. On the other hand, the coupons from LOT A2 appeared both dark and with some blue-green corrosion products (see e.g. Figure A3-1 in Karnland et al. 2009).

3.2 Appearance of samples in as-received condition

3.2.1 Copper coupons

When the copper samples arrived at RISE KIMAB, the coupons from test parcel A3 were still buried within bentonite lumps and were carefully extracted by using hand tools not to damage or scratch the coupon surfaces and compromise the gravimetric analysis. The coupons from test parcel S2 were partially withdrawn from the bentonite clay and could be directly placed in sample bags. All coupons were washed with deionised water prior to subsequent analyses in order to remove as much clay as possible. In Figures 3-5 and 3-6 below the surfaces of the coupons as well as the adjacent bentonite surfaces can be seen. Photographs of all as-received samples can be found in Appendix A.

Figure 3-5. *Corrosion coupon A3/L with surrounding bentonite clay.*

Figure 3-6. *Corrosion coupon S2/M with surrounding bentonite clay.*

3.2.2 Copper pipe samples

Two pipe samples from blocks 21–23 of test parcels A3 and S2 were also delivered to RISE KIMAB in sealed aluminium bags and were photographed in as-received condition prior to analyses. The pipes were partially covered with a thin layer of bentonite clay, and it could be seen that the surfaces varied in appearance with some areas apparently having a thicker or more dense oxide layer than others (Figures 3-7, 3-8 and Appendix A).

Figure 3-7. *Pipe sample A3 in as-received condition.*

Figure 3-8. *Pipe sample S2 in as-received condition.*

3.3 Examination of copper coupons

3.3.1 Corrosion products and morphology

The first analysis carried out on the coupons was XRD directly onto the surfaces in their as received state. Analyses of the surfaces showed that the corrosion products were comprised of mainly Cu_2O (cuprite), possibly with small amounts of Cu_2S (chalcocite), see Figure 3-9. The identification of the sulfide phase was made difficult due to interference in the diffraction pattern caused by the copper metal, which are seen as peaks at regular intervals from the copper peak at position 43 on the x-axis. Components of bentonite clay were also identified.

The SEM-EDS data can be reviewed in two steps. First, analysis at 100× magnification was done for an area of a few mm^2 of each coupon, which can give an idea of the average elemental composition of the corrosion products and other surface deposits (see Table 3-1, based on Figures C-3, C-6, C-9, C-12, C-15, C-18, C-21, and C-24 in Appendix C). It was observed that Cu and O were the most abundant elements on the surfaces. Part of the O comes from the corrosion product Cu_2O, while another part comes from SiO_2 in the bentonite clay. The amount of S was generally low in comparison with O, but it may be noted that the amount of S was slightly higher on the coupons in block 30 as compared to those in block 22. For the coupons in block 22, the amount of S was only ca 1 – 2 at% which is similar to the amount of Ca, meaning that S could partly be present as precipitated $CaSO_4$ from the bentonite. For the coupons from block 30, the amount of S was higher, ca 6 – 9 at%, which seems too high to be explained by $CaSO_4$ precipitation only, i.e. indicating in agreement with the XRD analysis that a Cu_xS phase had formed as a corrosion product. For comparison, the level of S in EDS spectra for the reference coupons was in most cases below detection and in all cases less than 1 at% (Appendix C).

Secondly, by looking at EDS data from spots of the surfaces and at higher magnifications, there were a few observations of enhanced amounts of S at positions where the amounts of Ca (from $CaSO_4$) and Fe (from FeS_2) were very low, which further indicates the formation of a Cu_xS corrosion product (e.g. Figure 3-10, and Figures C-11 and C-14 in Appendix C). Figure 3-10 shows the SEM-EDS analyses for coupons A3/I and S2/P, where darker areas appear to be bentonite clay (enhanced Si and Al), and lighter areas have a tendency for higher concentrations of S.

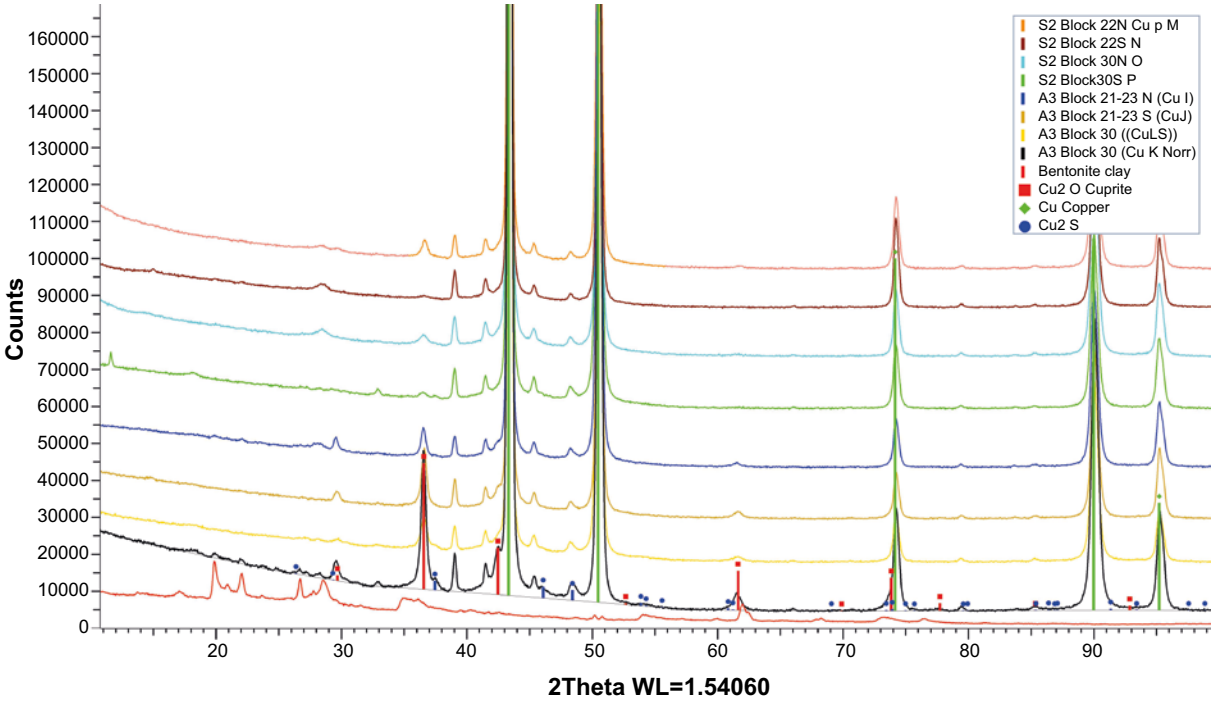

Figure 3-9. *XRD pattern obtained for the surfaces of the corrosion coupons.*

Table 3-1. EDS data of copper coupons at 100× magnification (at%).

Coupon	Block	O	Si	S	Cu	Ca	Fe
A3/I	22	50.8	12.1	2.0	22.6	3.1	0.4
A3/J	22	68.7	3.2	0.7	23.7	1.6	0.2
A3/K	30	28.7	5.7	7.8	53.9	0.3	0.2
A3/L	30	34.9	8.7	8.7	42.4	0.4	0.3
S2/M	22	40.2	10.5	2.2	37.3	0.5	0.3
S2/N	22	37.3	10.3	1.5	44.3	1.4	0.3
S2/O	30	38.7	9.3	5.9	38.5	0.5	0.3
S2/P	30	40.9	11.5	7.3	33.3	0.4	0.4

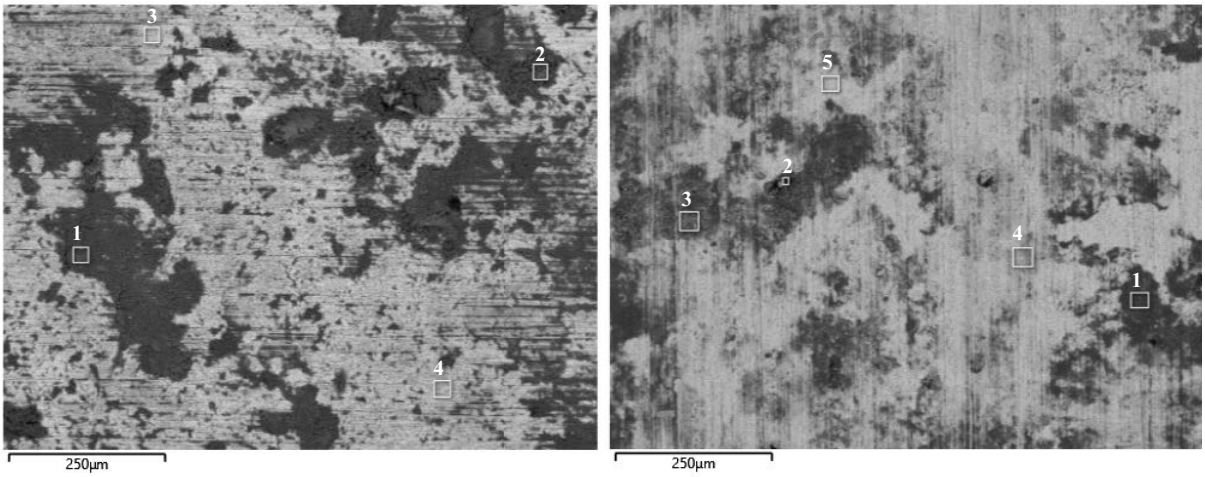

Element (At%)	1	2	3	4
O	61.90	61.58	28.00	31.34
Na	3.06	2.89	1.55	1.74
Mg	1.30	0.89	0.30	0.54
Al	8.73	5.30	1.44	1.62
Si	21.46	25.12	2.69	3.74
S	0.26	0.37	2.70	3.94
Cl		0.04	0.16	0.18
K	0.11	0.18		
Ca	0.42	0.16	0.20	0.38
Ti	0.03	0.08		
Fe	0.88	0.58		0.15
Cu	1.85	2.80	62.97	56.37
Total	100.00	100.00	100.00	100.00

Element (At%)	1	2	3	4	5
O	61.78	51.58	53.07	35.29	11.44
Mg	1.36	1.33	1.25	0.80	
Al	7.57	7.89	6.15	3.60	0.59
Si	21.24	26.61	15.28	8.36	1.10
S	1.79	3.22	5.59	10.55	10.50
Cl	0.05		0.09	0.14	
K	0.05	0.15			
Ca	0.68	0.71	0.52	0.48	0.22
Fe	0.77	0.56	0.52	0.26	
Cu	4.69	7.94	17.54	40.51	76.15
Total	100.00	100.00	100.00	100.00	100.00

Figure 3-10. *SEM micrographs with associated EDS analysis results. Copper coupons A3/I (left) and S2/P (right). Magnification ×300.*

Prior to evaluating the mass loss of the corrosion coupons, it was decided to save one coupon from each test series in order to examine the corrosion product and morphology in cross-section. The coupons A3/K and S2/N were chosen for this purpose and were cut before being cast in epoxy resin and polished. The polished cross-sections were then examined under the SEM and their elemental compositions were analysed with EDS. Figures 3-11 to 3-14 below show the appearance of the corroded interfaces in cross-sections and the corresponding EDS analysis for selected SEM micrographs of each coupon. The cross-sections revealed roughly corroded interfaces with pits densely distributed over the surface. The pits and surface defects observed in the micrographs were found to be less than 10 µm deep. The SEM-EDS analysis revealed a thin layer of corrosion product, ca 360 nm on coupon S2/N (Appendix B, Figure B-40). The surface film was generally composed of Cu and O, with lower levels of S. In some of the cross-sections there was a tendency for decreasing S levels toward the copper surface, although exceptions are found and in many cases the levels of S were too low to analyse any trends in its distribution. The full set of SEM images taken is presented in Appendix B and further details of the EDS analyses are given in Appendix C.

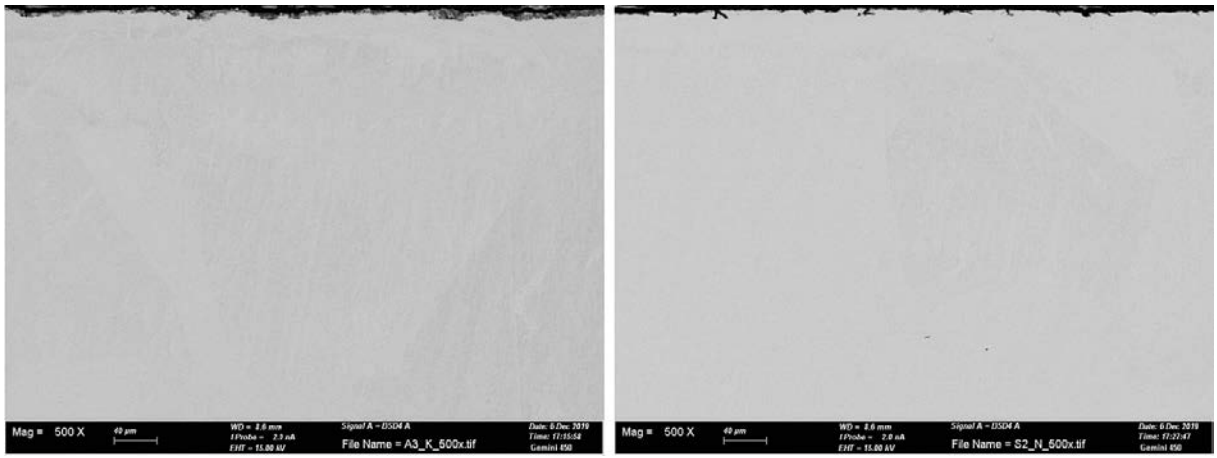

Figure 3-11. *SEM image of cross-section of coupons A3/K (left) and S2/N (right), magnification ×500.*

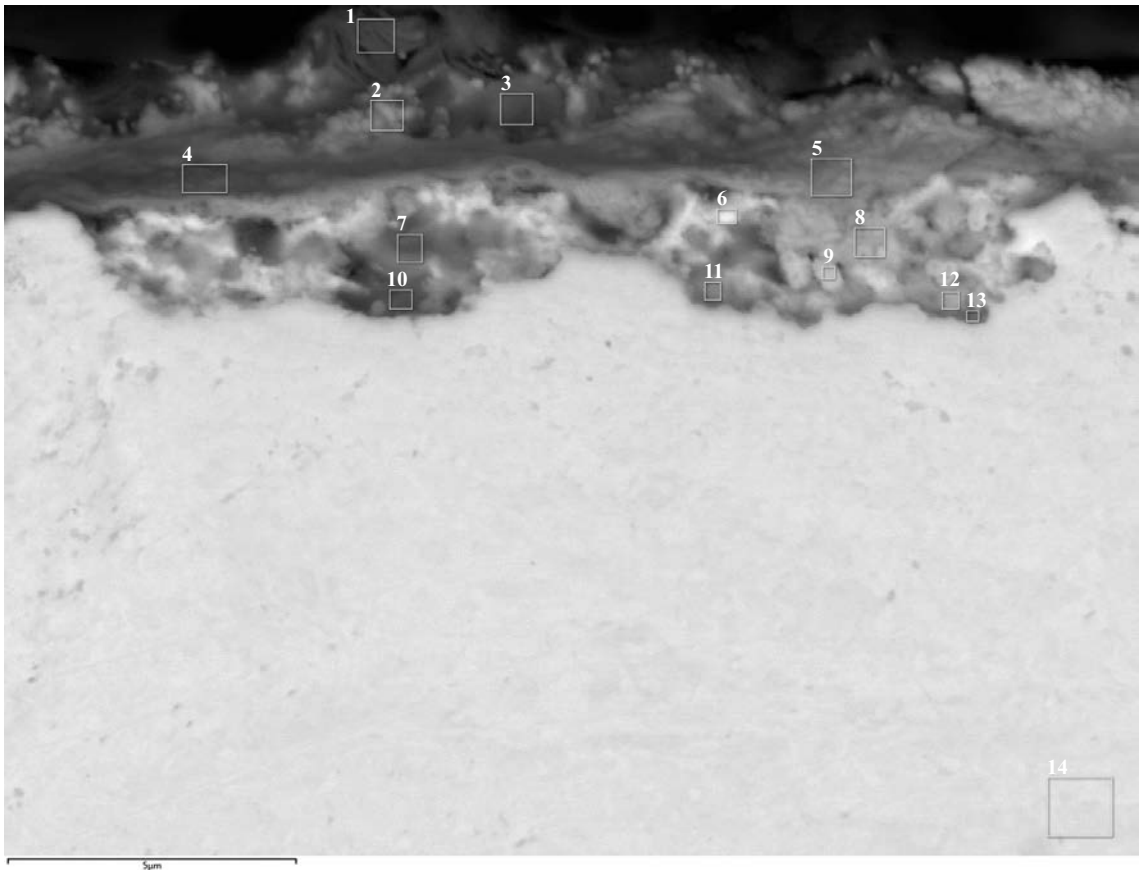

Element (At%)	O	Na	Mg	Al	Si	S	Cl	Ca	Fe	Cu	Total
1	41.32	6.02	3.61	9.22	26.20	3.21		0.78	5.47	4.17	100.00
2	47.90	4.57	1.40	4.66	12.40	6.02	0.21	0.32	1.64	20.88	100.00
3	58.46	2.57	0.63	2.34	21.73	3.11	0.08	0.14	0.57	10.36	100.00
4	22.27		0.69	1.72	4.80	15.91	0.20	0.15	1.16	53.10	100.00
5	21.16		0.55	1.58	3.69	13.69	0.20		1.43	57.68	100.00
6	15.49		0.74	0.93	2.01	3.92	0.14		1.41	75.35	100.00
7	29.73		0.39	0.28	12.24	1.50		0.22	0.91	54.73	100.00
8	17.68		0.50	0.70	2.81	9.31	0.37		1.17	67.47	100.00
9	20.77			0.71	2.47	3.28	0.94		0.91	70.92	100.00
10	19.49			0.41	5.80	0.45		0.27	1.01	72.57	100.00
11	20.41		0.46	0.73	7.76	0.59			0.95	69.10	100.00
12	14.40			0.89	2.80	6.07	0.20		1.03	74.62	100.00
13	18.01			0.55	6.76	2.55			0.90	71.22	100.00
14	0.91			0.64					0.60	97.85	100.00

Figure 3-12. *SEM image of corrosion coupon A3/K in cross section, magnification ×14 000, with associated EDS analysis results.*

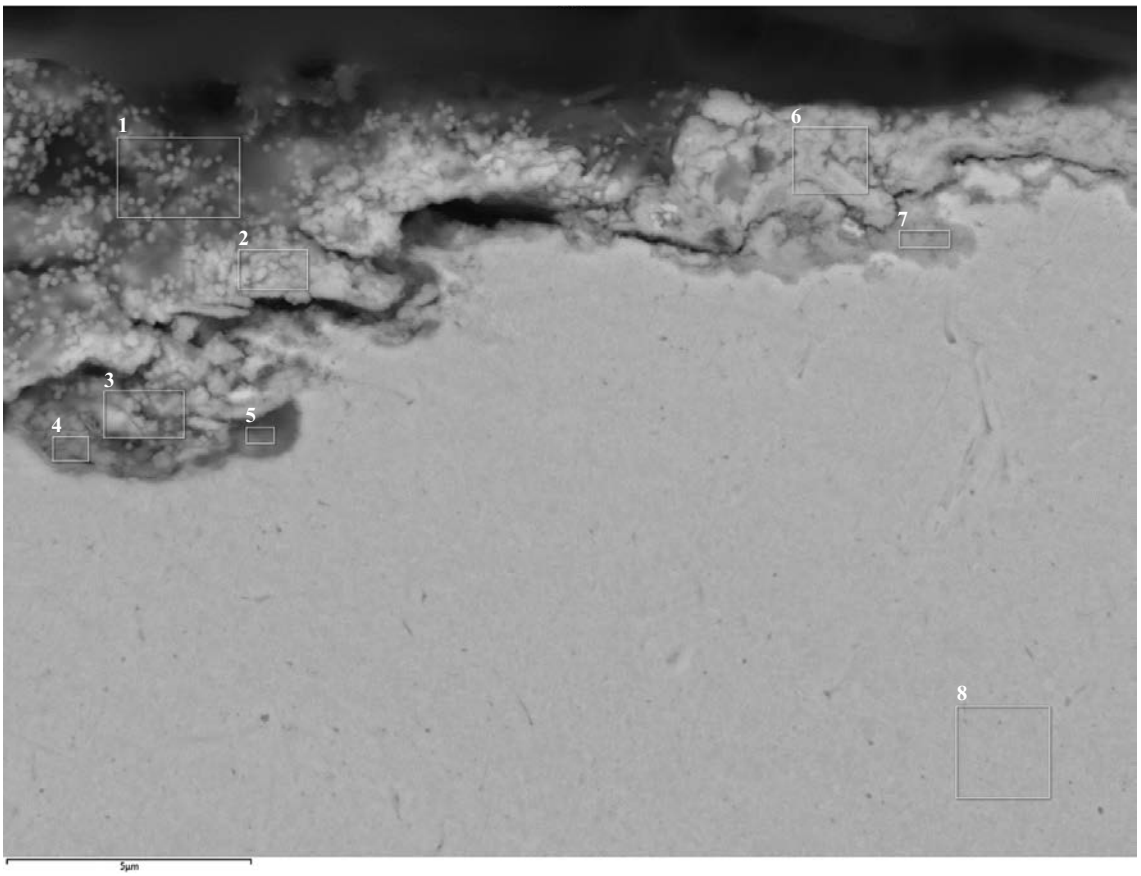

Element (At%)	1	2	3	4	5	6	7	8
O	37.48	22.01	25.20	18.03	12.26	13.93	4.65	0.45
Mg	1.88	0.38	0.62	0.34				
Al	7.88	1.68	1.90	0.71				
Si	20.12	3.98	4.58	1.75	0.52	1.99		
S	11.49	13.43	10.10	4.52	1.98	16.17	0.89	
Cl	0.10	0.26	0.30			0.22		
Ca	0.46							
Cu	20.59	58.27	57.29	74.66	85.25	67.69	94.46	99.55
Total	100.00	100.00	100.00	100.00	100.00	100.00	100.00	100.00

Figure 3-13. *EDS analysis of a cross-sectioned sample of coupon A3/K.*

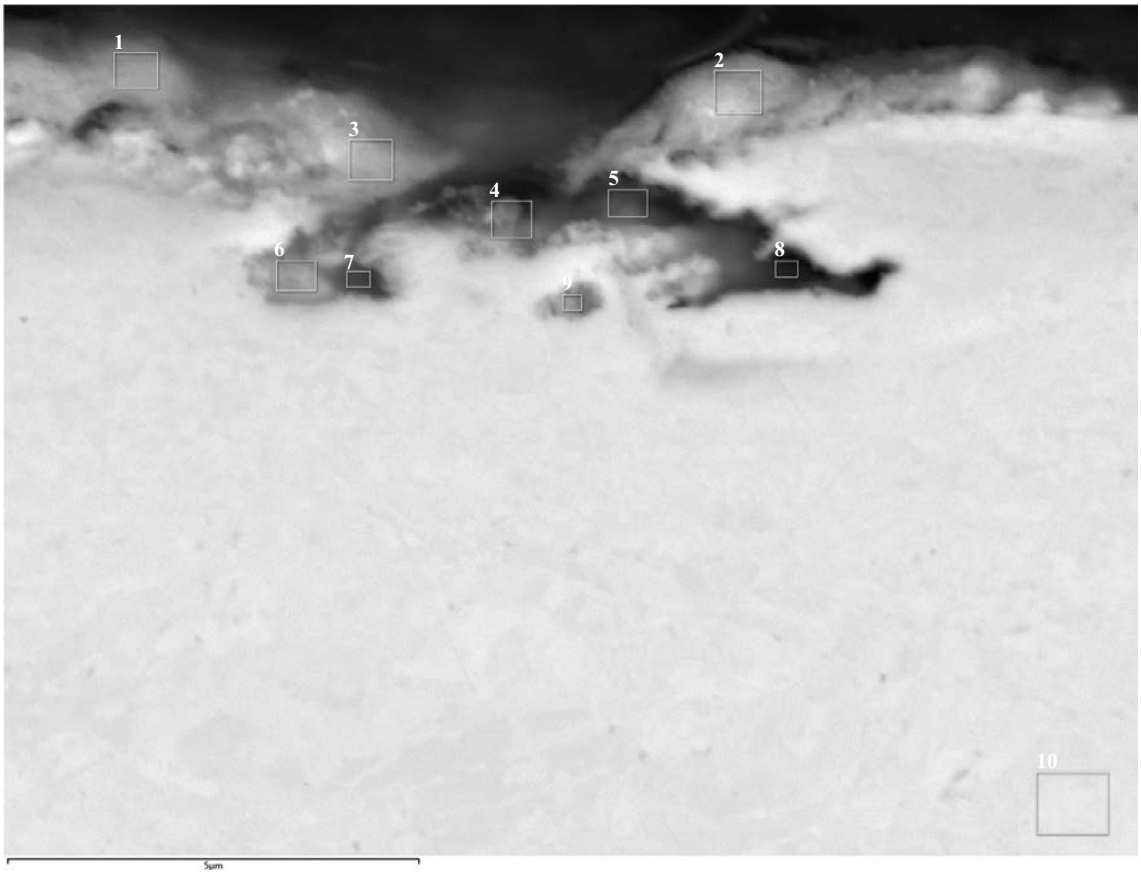

Element (At%)	O	Na	Mg	Al	Si	S	Cl	Ca	Fe	Cu	Total
1	37.64	4.98	1.37	2.45	7.75	5.17	0.07	0.38	2.04	38.14	100.00
2	32.12	3.80	1.98	2.04	5.90	5.17		0.40	2.24	46.35	100.00
3	31.60	3.61	0.94	2.72	7.08	5.75		0.35	2.68	45.27	100.00
4	21.05	2.59	1.10	1.66	2.63	2.78		0.31	1.51	66.39	100.00
5	19.35	2.98	0.80	1.36	2.47	2.88		0.18	1.46	68.51	100.00
6	7.58		0.41	0.73	0.55	0.68			1.34	88.71	100.00
7	11.64		0.36	0.79	0.66	0.68			1.39	84.48	100.00
8	8.31			0.26	0.63	1.43			2.46	86.92	100.00
9	2.04			0.43		0.42			1.81	95.30	100.00
10	1.09			0.66	0.18				0.83	97.24	100.00

Figure 3-14. *SEM image of corrosion coupon S2/N in cross section, magnification ×20 000, with associated EDS analysis results.*

In order to further examine corrosion products or deposits found to have a higher content of S, TEM was applied on FIB cut lamellae from the A3/K and S2/N coupons. The investigation revealed the presence of small particles near the copper surface inside the pits. On coupon A3/K, these particles were found to be agglomerates (50 – 80 nm) consisting of smaller (5 – 10 nm) nanoparticles (Figure 3-15 and further details in Appendix C). On a lamella from coupon S2/N, the particles seemed to be slightly larger, with no particles smaller than 20 nm detected. These particles were found in the clay near the copper surface. Closer to the copper surface, a more compact and ca 250 nm thick layer was found. From the EDS analysis, the sulfur rich particles and layers appear to have Cu:S ratios close to that of Cu_2S (Figure 3-16). Further analysis of the layers and nanoparticles, using the selected area electron diffraction (SAED) technique indicated the existence of Cu_2S on both coupons, as well as Cu_2O on the S2/N coupon (Appendix C).

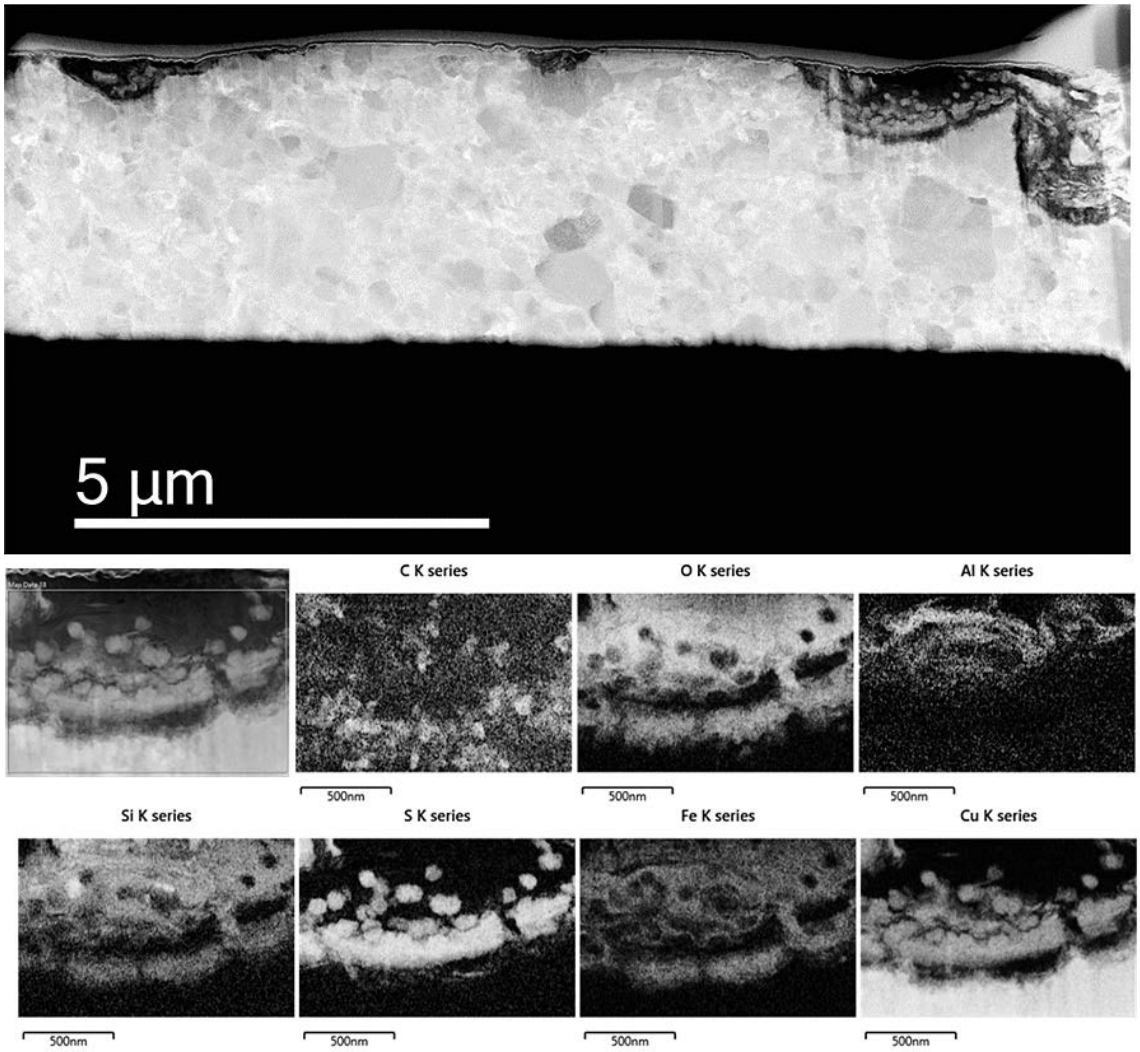

Figure 3-15. *EDS maps of a FIB cut lamella from coupon A3/K.*

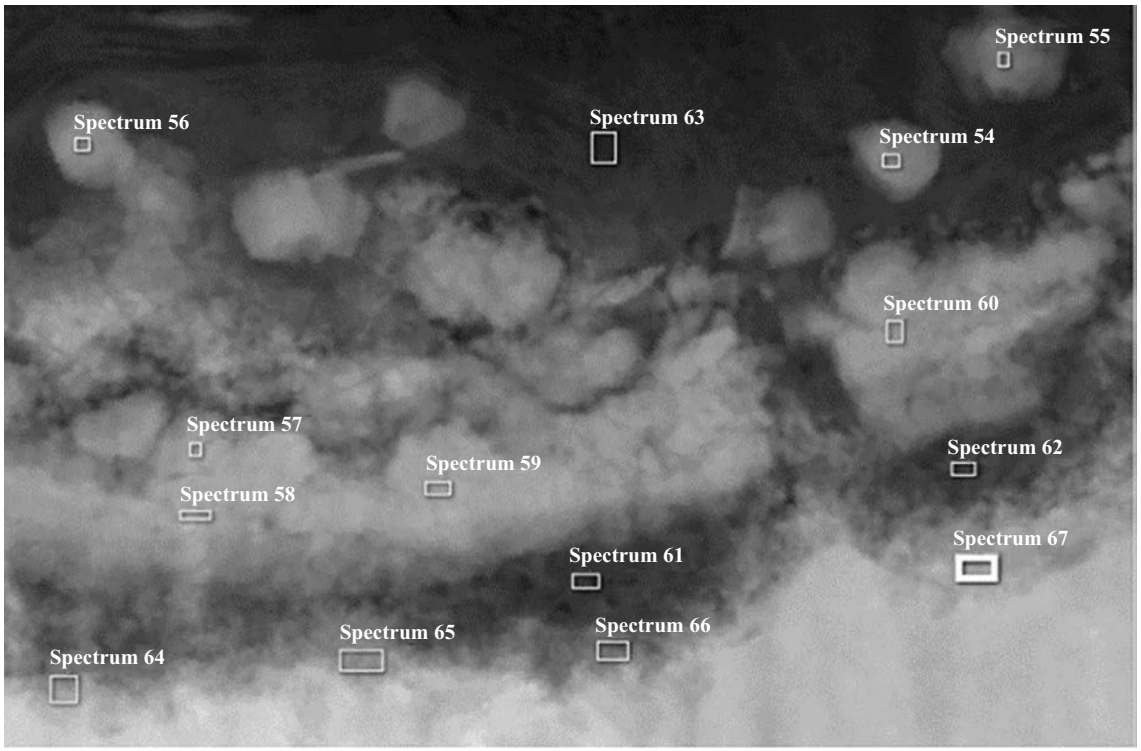

Element (At%)	54	55	56	57	58	59	60	61	62	63	64	65	66	67
O	9.51	22.86	21.39	13.5	5.16	5.53	0	67.12	69.69	71.86	21.63	30.24	40.63	28.7
Na	0	0	0	0	0	0	0	3.3	2.93	1.75	0	0	0	0
Mg	0	0	0	0	0	0	0	0	0	0	0	0	0	0
Al	0	0	0	0	0	0	0	0	0	3.08	0	0	0	0
Si	1.79	2.93	1.97	2.68	0	0	0	8.11	6.79	13.96	1.01	1.68	3.27	1.36
S	32.43	24.41	25.06	26.75	30.62	29.61	34.43	0	1.3	0	1.38	0.83	2.24	0
Cl	0	0	0	0	0	0	0	0	0	0	0	0	0	0
Ca	0	0	0	0	0	0	0	0	0	0	0.63	0	0	0
Fe	0	1.93	3.31	1.54	0	0	0	19.11	15.99	8.37	2.81	2.72	7.92	2.46
Cu	56.27	47.87	48.27	55.52	64.22	64.85	65.57	2.35	3.3	0.98	72.54	64.53	45.95	67.48
Total	100	100	100	100	100	100	100	100	100	100	100	100	100	100

Figure 3-16. *Detailed EDS analysis of a FIB cut lamella from coupon A3/K.*

3.3.2 Gravimetric analysis

The average corrosion depth of the coupons varied from 0.7 µm to 1.3 µm (Table 3-2 and Appendix D). After the initial pickling procedure, the mass-loss of five of the coupons corresponded to corrosion depths between ca 1 µm and 1.3 µm, while for coupon S2/P the corrosion depth was only 0.5 µm. Since coupon S2/P still appeared stained after the pickling, further attempts were made to remove the staining and possibly increasing the mass-loss. This was done by first pickling in H_2SO_4 for a total of 14 minutes, then electrolytic cleaning according to SS-EN ISO 8407:2017 (method E.3.1) for a total of 12 minutes (at one minute intervals) for each side of the coupon. The additional cleaning steps resulted in an additional mass-loss of coupon S2/P corresponding to ca 0.2 µm corrosion (Table 3-2).

Table 3-2. Mass loss and corrosion depths of the copper coupons.

Coupon	Mass loss		Corrosion		
	g	g/m²	g/m²,yr*	µm/yr*	µm
Pickling ref.	0.0006	0.2094	-	-	-
Ref L	0.0016	0.6458	0.0323	0.0036	0.072
Ref K	0.0035	1.3945	0.0697	0.0078	0.156
A3/I	0.0172	8.4885	0.4244	0.0477	0.954
A3/J	0.0234	11.5041	0.5752	0.0646	1.292
A3/L	0.0181	8.9252	0.4463	0.0501	1.002
S2/M	0.0217	10.7183	0.5359	0.0602	1.204
S2/O	0.0238	11.7589	0.5879	0.0661	1.322
S2/P	0.0088	4.3310	0.2165	0.0243	0.486
S2/P**	0.0105	5.2037	0.2602	0.0292	0.584
S2/P***	0.0120	5.9307	0.2965	0.0333	0.666

* Integrated corrosion rates are calculated for the whole exposure period of 20 years.
** Coupon S2/P was further pickled in H_2SO_4 for 14 minutes.
*** Coupon S2/P was further electrolytically cleaned for 12 minutes in KCl according to E3.1 in SS-EN ISO 8407:2014.

3.3.3 Surface topography

The surface topography of the coupons was examined by optical microscopy before and after removal of corrosion products by pickling. All pits and surface defects deeper than 6 µm were measured and the five deepest pits on each coupon were tabulated (Tables 3-3 and 3-4). Selected areas of 0.5 cm^2 were analysed before and after pickling in order to estimate the pit density or distribution of pits. It should be noted that the procedure of measuring the pit depths unavoidably includes using the corroded surface as the reference point. Comparing the data in Tables 3-3 and 3-4, there seems to be a tendency for more and deeper pits after removal of the corrosion products by the pickling method described in Section 2.4 above. One possibility that could explain this tendency would be that the pickling method could have affected the topography of the copper surface. However, it is also possible that pits measured before pickling may have been obscured by surface deposits, i.e. corrosion products and bentonite clay. It is further worth noting that no surface characterisation was carried out prior to exposure in the LOT experiment, meaning that it is not clear how the topography is related to corrosion during exposure. It may be noted that the reference samples had several surface defects around 20 µm in depth already before removal of the corrosion products, despite the fact that their mass-losses corresponded to only ca 0.1 µm corrosion (Table 3-2). Full details of the topographic analysis can be found in Appendix E along with photographs of the pits before and after pickling.

Table 3-3. Topographic analysis of coupons before removal of corrosion products. The pit density was evaluated for an area of 0.5 cm².

	5 deepest pits (µm)					Pit density	
Coupon	1	2	3	4	5	No.pits	Pits/cm²
Ref K	25	19				2	4
Ref L	22	18	11			1	2
A3/I	8					1	2
A3/J	13	12	11	10	9	7	14
A3/K	7	6				1	2
A3/L	17	9	8	8	7	6	12
S2/M	12	8	6			2	4
S2/N	9	5	5	4		1	2
S2/O	16	14	13	13	12	7	14
S2/P	14	13	13	10	9	6	12

Table 3-4. Topographic analysis of coupons after removal of corrosion products. The pit density was evaluated for an area of 0.5 cm².

	5 deepest pits (µm)					Pit density	
Coupon	1	2	3	4	5	No.pits	Pits/cm²
Ref K	28	28	25	24	23	20	40
Ref L	25	23	23	22	22	18	36
A3/I	16	12	11	10	10	5	10
A3/J	39	22	13	10	10	11	22
A3/L	9	8	8	7	7	5	10
S2/M	57	26	15	13	12	14	28
S2/O	20	16	14	14	12	12	24
S2/P	39	14	12	8	8	5	10

In addition to unintentional surface defects and corrosion pits, the microscopic examination of the coupons found a mark from a Vickers hardness indention made on coupon K from LOT A3 (Figure E-19). The opening of the indentation mark at the surface is rhombic and ca 50 × 70 µm. The shape of the indentation mark remains but one corner seems to be affected by the corrosion process.

3.4 Examination of copper pipe samples

3.4.1 Corrosion products and morphology

Analysis of the pipe surfaces with SEM-EDS over an area of a few mm^2, showed similar elemental composition as for the coupons, i.e. high levels of Cu, O and Si, and generally lower levels of S (Table 3-5 and Appendix G). The white deposit on the sample from A3 had a higher content of S but also enhanced levels of Ca and O, indicating the precipitation of $CaSO_4$ (from the bentonite).

Table 3-5. Selected EDS data of copper pipe samples at 100× magnification (at%).

Sample area	O	Si	S	Ca	Fe	Cu
A3 pipe “white”	46.2	10.5	12.3	21.1	1.1	3.5
A3 pipe “dark”	29.1	16.9	4.2	1.2	1.1	38.2
S2 pipe “Cu”	16.4	7.9	1.3	2.1	0.7	61.6
S2 pipe “dark”	23.4	16.0	3.7	1.2	1.4	41.8

Cross-sectioned samples of the copper pipe surfaces appeared generally rough with frequently occurring pits or defects densely distributed over the observed interfaces, see Figures 3-17 to 3-20. The pits were generally wide and shallow, and the deepest pit found was ca 25 µm (Appendix F). The surface deposits on the pipe samples contained high levels of O, likely from both the corrosion product Cu_2O and from bentonite clay, as indicated by a generally high content of Si. The content of S was generally low (from < 1 at% up to a few at%), but a few observations of enhanced S levels were made. On the pipe sample from S2, an enhanced level of S (12 at%) was found on the surface, however, the same spot also had an enhanced level of Ca (11 at%), indicating that the deposit was $CaSO_4$ from the bentonite clay (Figure G-52). EDS data from spots nearby showed lower levels of both S and Ca, which however also seemed to match with $CaSO_4$. Another observation of enhanced S was made inside a shallow pit found on the sample from S2 (Figure 3-20). Here, the level of S was 16 to 26 at% and the levels of O and Si were both lower than what was generally found. Since there was no correlation of S with either Ca ($CaSO_4$) or Fe (FeS_2), this observation suggests the formation of a Cu-S phase. Many of the cross-sections were very low in S (< 3 at%) and only occasionally high levels (> 10 at%) were detected. Due to the low levels of S, the presence of bentonite, and significant levels of Ca (precipitation of $CaSO_4$) it was difficult to analyse the distribution of Cu-S phases in the corrosion products. Full details of the EDS analyses are included in Appendix G, and images of the cross-sections are reported in Appendix F.

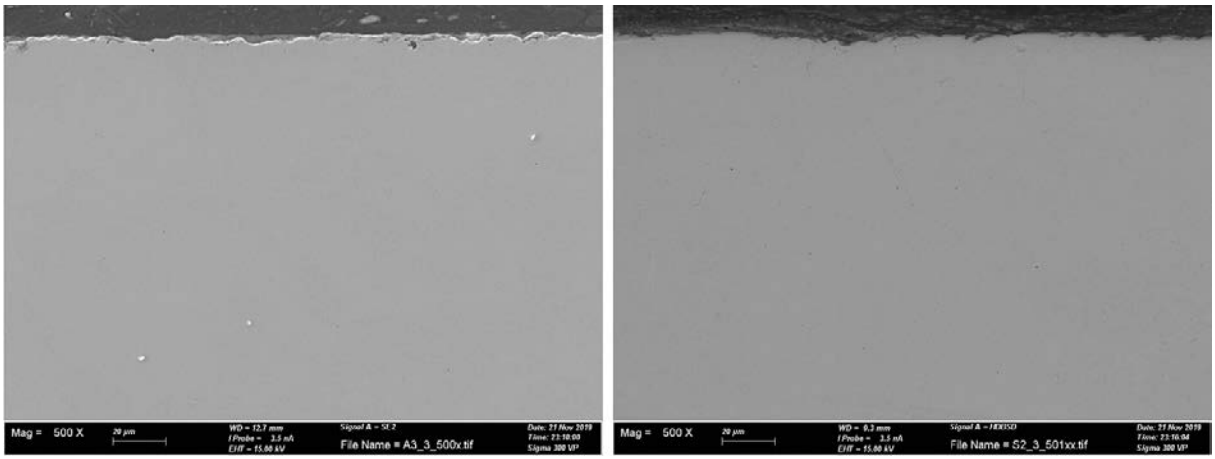

Figure 3-17. *SEM images of cross-sections of samples from pipes A3 (left) and S2 (right). Magnification ×500.*

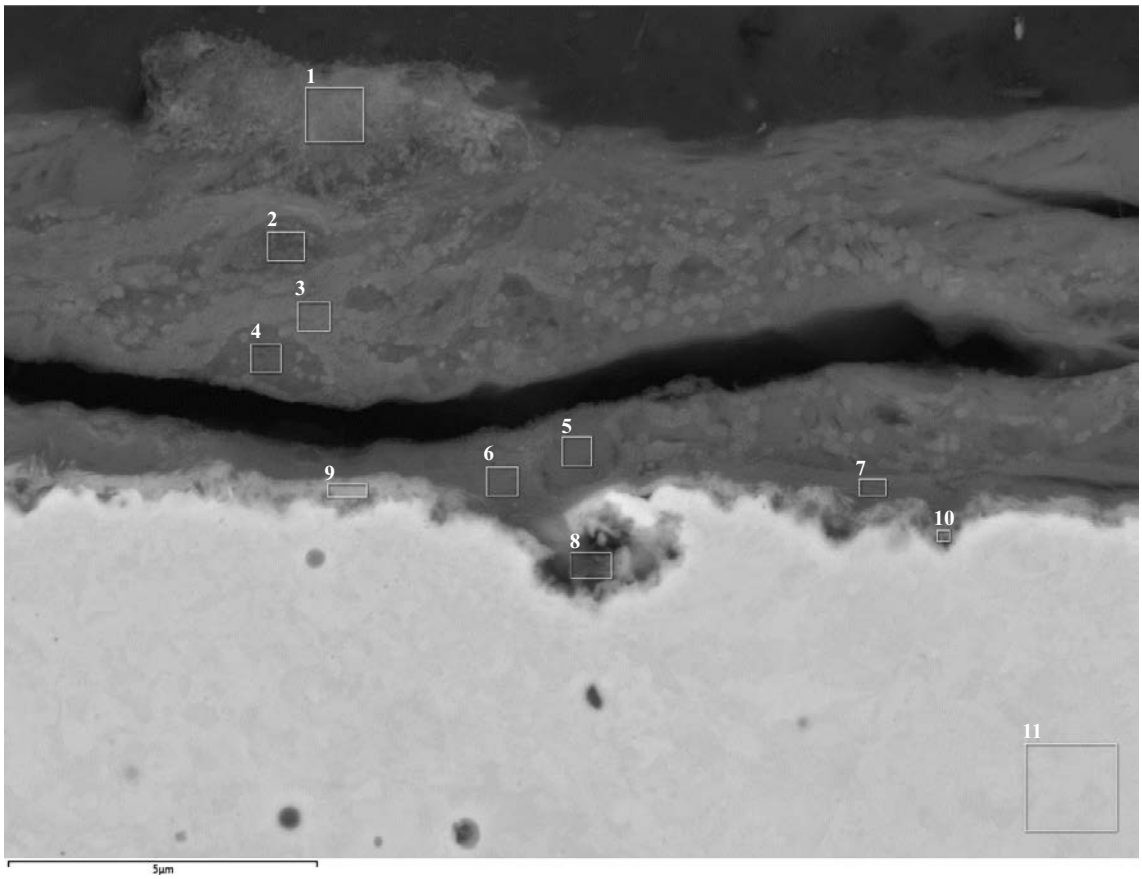

Element (At%)	O	Mg	Al	Si	S	Cl	Ca	Fe	Cu	Total
1	53.97	0.89	4.25	22.22	0.25	0.19	3.60	0.43	14.20	100.00
2	58.03	1.16	6.37	23.89	0.51	0.04	2.15	0.57	7.24	100.00
3	61.29	1.28	6.81	18.10	0.31	0.06	4.48	0.67	6.91	100.00
4	64.70	1.09	4.99	13.30	0.35	0.06	10.78	0.43	4.22	100.00
5	64.46	0.79	4.32	24.45	0.19	0.06	0.78	0.28	4.61	100.00
6	59.06	1.36	8.02	20.39	0.32	0.16	0.77	0.75	9.09	100.00
7	57.22	1.64	9.09	20.79	0.16	0.12	0.50	0.77	9.21	100.00
8	42.11	1.11	6.19	13.45	1.60	0.74	0.32	0.62	33.87	100.00
9	47.79	1.25	6.07	12.44	2.41	0.46	1.07	0.34	28.18	100.00
10	36.33	1.28	5.89	12.32	0.93	0.42	0.86	0.37	41.50	100.00
11	1.35		0.75						97.90	100.00

Figure 3-18. *SEM image of pipe sample A3 in cross section, magnification × 15 000, with associated EDS analysis results.*

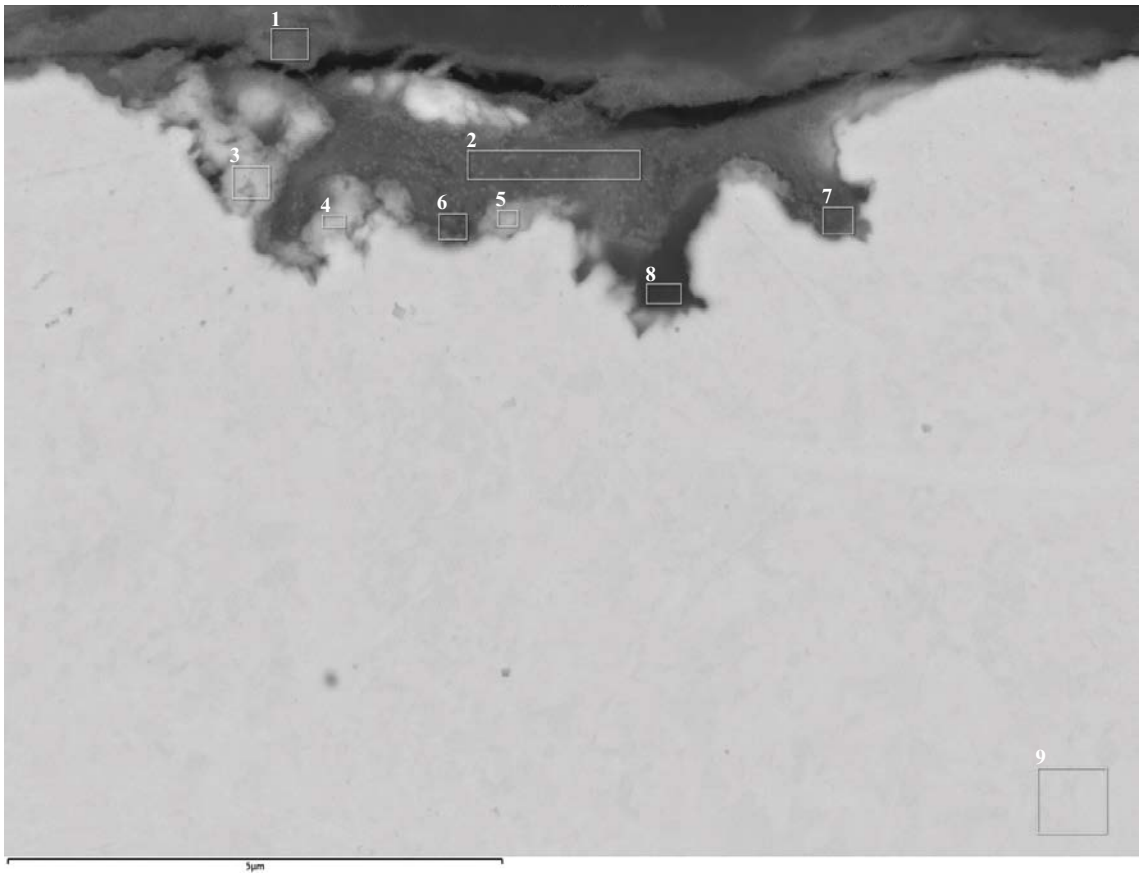

Element (At%)	1	2	3	4	5	6	7	8	9
O	49.86	55.48	37.92	38.63	39.59	56.20	44.19	30.56	0.79
Mg	1.20	1.74	0.84	0.49	0.58	1.25	1.08		
Al	4.63	6.65	3.16	2.17	3.01	3.84	3.75	2.46	0.57
Si	15.09	19.97	6.80	4.00	5.63	9.56	8.26	4.66	
S	2.00	0.18	0.18	0.17	0.19	0.29	0.63		
Cl	0.39	0.25	2.83	2.35	1.55	0.30	0.28	0.56	
K	0.14	0.13	0.07			0.06			
Ca	8.53	2.82	0.82	1.65	1.54	8.63	6.64	1.44	
Fe	0.35	0.69				0.36			
Cu	17.81	12.08	47.38	50.54	47.89	19.53	35.16	60.33	98.64
Total	100.00	100.00	100.00	100.00	100.00	100.00	100.00	100.00	100.00

Figure 3-19. *SEM image of pipe sample S2 in cross section, magnification ×12 000, with associated EDS analysis results.*

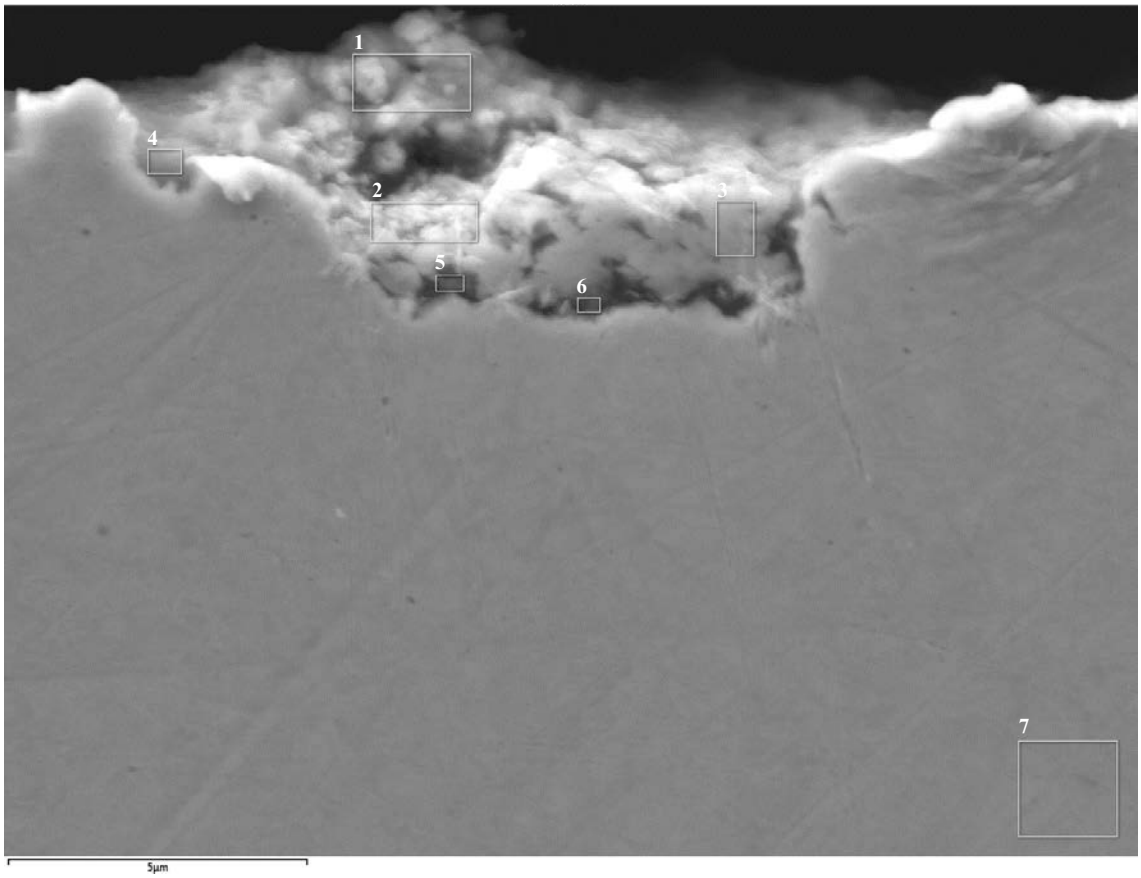

Element (At%)	1	2	3	4	5	6	7
O	20.42	12.58	7.32	37.23	22.02	22.35	0.76
Mg		0.22		1.33	0.57	0.57	
Al	0.78	0.37	0.70	4.61	2.72	2.88	
Si	5.08	2.44	2.19	10.34	6.30	6.00	
P					0.19		
S	20.80	23.17	26.26	2.20	17.86	16.09	
K				0.08		0.09	
Ca	0.20	0.19	0.12	0.29	0.24	0.24	
Fe	0.31	0.26	0.32	0.36	0.39	0.49	
Cu	52.41	60.77	63.09	43.57	49.72	51.29	99.24
Total	100.00	100.00	100.00	100.00	100.00	100.00	100.00

Figure 3-20. *SEM image of pipe sample S2 in cross section, magnification ×15 000, with associated EDS analysis results.*

3.4.2 Elemental composition of the pipe material

3.4.2.1 H content measured by melt extraction

Cross sections of the pipe samples from A3 and S2 were cut using a metallographic abrasive cutter. A cutting fluid (Cool 3, Buehler) was used to reduce the warming of the material. Samples for H-analysis (ca 5 × 5 × 5 mm) were cut from the pipe cross-sections using a precision metallographic abrasive cutter with water-free cutting fluid (Water-free Cutting Fluid, Struers). Thereafter the samples were rinsed in deionized water. In total, 18 samples (9 from each pipe) were obtained for the various surface conditions to be tested. The samples were analysed either *as received*, ground with SiC paper, or ground and filed using a clean file. The H contents measured through melt extraction of the samples are shown in Table 3-6. The purpose of applying different levels of surface cleaning was to further establish the sensitivity of the obtained total H content to the surface conditions of the samples, where surface deposits (e.g. bentonite particles) may have a considerably higher H content than the bulk material. In previous studies it was noted that sample preparation played an important role when attempting to obtain more uniform and reliable analyses (Granfors 2017). The samples should be prepared shortly prior to analysis, and only clean tools and equipment should be used.

When the melt extraction was made on samples in their *as received* surface condition, i.e. with corrosion products and surface deposits still present, the measured hydrogen content was 1.99 (± 0.19) wt-ppm for the samples from S2 and 3.22 (± 0.17) wt-ppm for A3. When the sample surfaces had instead been ground with SiC paper in order to remove corrosion products and deposits, the measured hydrogen content fell to on average 0.4 wt-ppm for both test parcels. Further mechanical cleaning of the surface using a file reduced the measured H content to very low levels in both test parcels.

Material from the reference pipe was also analysed (Table 3-6). The measured H content for the as-received samples was 1.87 (± 0.28) wt-ppm, which was reduced to ca 0.6 wt-ppm for the ground samples, and further to ca 0.2 wt-ppm for the ground and filed samples.

Table 3-6. Hydrogen analysis of pipe samples from LOT S2 and A3.

A3 samples	Mass (g)	H (wt-ppm)	S2 samples	Mass (g)	H (wt-ppm)	Reference samples	Mass (g)	H (wt-ppm)	Condition
A3-1	0.7221	3.46	S2-1	0.6817	2.19	Ref H-1	0.5935	1.78	As received
A3-2	0.7345	3.10	S2-2	0.7299	2.03	Ref H-2	0.6185	2.25	As received
A3-3	0.7515	3.09	S2-3	0.6962	1.74	Ref H-3	0.7037	1.57	As received
		3.22 (± 0.17)			1.99 (± 0.19)			1.87 (± 0.28)	
A3-4	0.7403	0.39	S2-4	0.6733	0.51	Ref H-4	0.5608	0.65	Ground
A3-5	0.7366	0.42	S2-5	0.6963	0.41	Ref H-5	0.652	0.37	Ground
A3-6	0.7599	0.40	S2-6	0.761	0.35	Ref H-6	0.6713	0.75	Ground
		0.40 (± 0.01)			0.42 (± 0.07)			0.59 (± 0.16)	
A3-7	0.5166	0.27	S2-7	0.6491	0.07	Ref H-7	0.7708	0.17	Ground and filed
A3-8	0.5134	0.09	S2-8	0.5612	0.06	Ref H-8	0.594	0.12	Ground and filed
A3-9	0.5428	0.09	S2-9	0.684	0.03	Ref H-9	0.4521	0.18	Ground and filed
		0.15 (± 0.08)			0.05 (± 0.02)			0.16 (± 0.03)	

3.4.2.2 O content measured by melt extraction

Since the O content of the pipe material (SS 5015-04) is not well described by the reference literature, this was analysed for the reference pipe using Leco (Table 3-7). The results show a similar pattern to the H analyses, where removal of the outer surface reduced the measured O concentration of the sample. Average values for *as received* samples was 65.7 (± 7.6) wt-ppm, for ground samples 33.7 (± 2.3) wt-ppm, and for ground and filed samples 30.3 (± 0.5) wt-ppm. Since there was no significant effect of filing the samples, as compared with ground samples, an extra test on material that had been filed but not ground was carried out, which resulted in an average value of 30.5 (± 1.2) wt-ppm, suggesting that perhaps it is unnecessary to include the abrasive paper step in future analyses, even for H analyses. It thus seems that the copper material of the pipes (SS 5015-04) had a higher O content (~ 30 wt-ppm) than SKB's canister material Cu-OFP (< 5 wt-ppm).

Table 3-7. Results of the O analyses.

Sample	Description	Oxygen bulk (wt-ppm)
Ref O-1	As received	73.1
Ref O-2	As received	65.9
Ref O-3	As received	58.0
Ref O-4	Ground	33.9
Ref O-5	Ground	35.8
Ref O-6	Ground	31.3
Ref O-7	Ground and filed	30.7
Ref O-8	Ground and filed	29.7
Ref O-9	Ground and filed	30.1
Ref O-10	Filed	31.3
Ref O-11	Filed	29.6

3.4.2.3 Elemental profiles near surface

The elemental composition of the pipe material from LOT S2 and A3 was further analysed using GDOES to obtain elemental depth profiles near the surface of the material (Figures 3-21, 3-22 and Appendix H). Some elements that were present at very low levels, e.g. H and S, are presented as 10 times the measured concentrations (denoted "× 10" in the legend) in order to make their distribution profiles more visible. The major element near the surface of the samples was O, which was enhanced up to a few µm into the material from the surface. Si followed a similar distribution profile but was present at lower concentrations. The level of S was slightly enhanced near the surface of the samples, albeit to much lower levels than O. The sample from the S2 pipe had generally lower levels of O and S near the surface than the A3 sample.

The level of H was generally very low and its distribution profile is difficult to see even though it is shown as ten times the measured level in the diagrams including all elements (Figures 3-21 and 3-22). In order to visualise the H distribution profile more clearly, the level of H for pipe A3 (analysis spot 1) is shown as enhanced by two orders of magnitude in Figure 3-23. As can be seen, the level of H is only enhanced within the outermost ca 1 µm, a depth range where other elements, e.g. O and Si, are also enhanced.

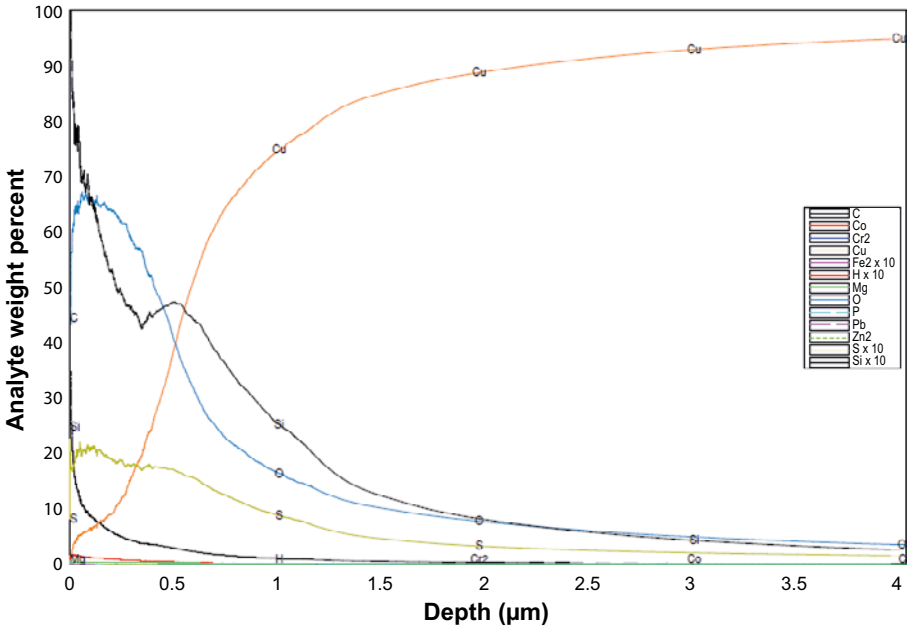

Figure 3-21. GDOES elemental analysis of the surface of pipe A3 (spot 1). Note that the levels of elements S, H, Fe and Si are shown as ten times their measured values.

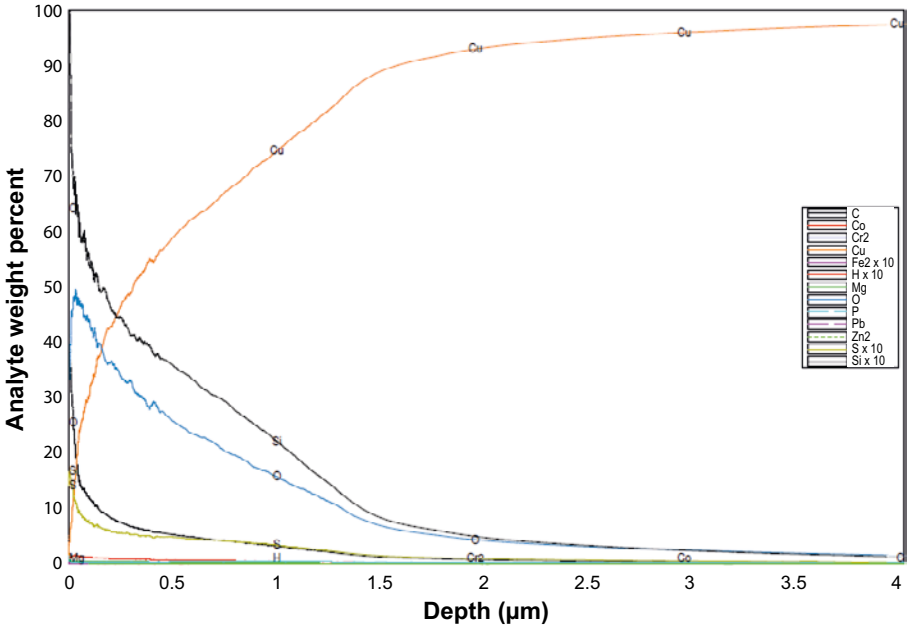

Figure 3-22. *GDOES elemental analysis of the surface of pipe S2 (spot 1).*

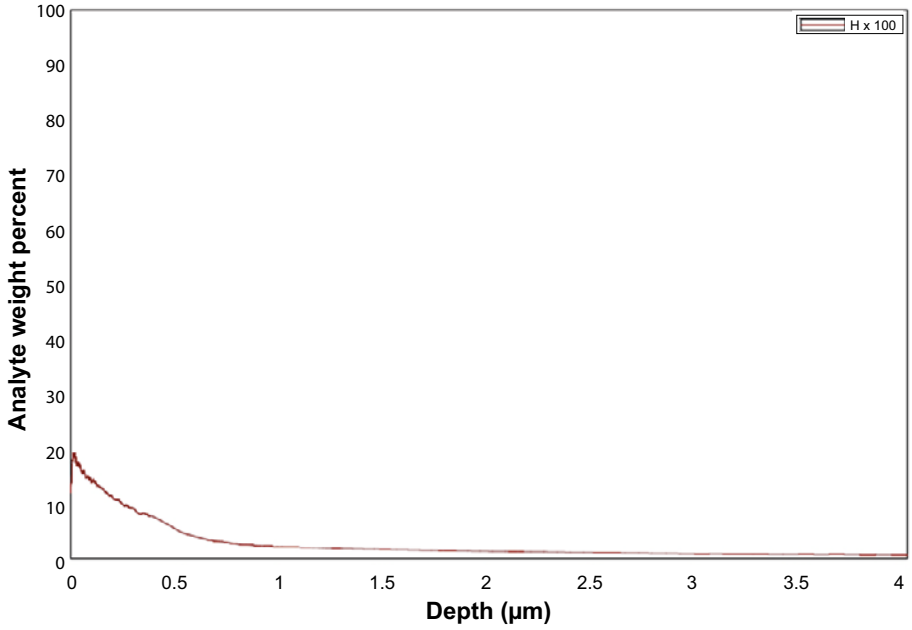

Figure 3-23. *Hydrogen distribution profile of the surface of pipe A3 (spot 1).*

3.5 Copper in the bentonite clay

The aim of analysing the copper content of the bentonite clay was to estimate the extent of corrosion (average corrosion depth) of the copper pipes. Corrosion of the copper pipes was estimated from profiles of the copper concentration in the bentonite near the copper surface. The copper concentrations were determined using XRF as described in Section 2.6.

With XRF the elements from sodium and higher atomic numbers are measured. Only the major elements were included in the analysis (i.e. no trace elements). For the quantification, the amounts of the identified elements are normalised to 100 wt% and expressed as oxides. No assignment of oxidation states is done in the XRF analysis and, hence, the notation "CuO" does not indicate the crystalline phase CuO (tenorite) or even a Cu(II) compound. The notation "CuO" is merely a way of expressing the element data for further calculations.

Since the determination of corrosion from the copper concentration profile in the clay is not a standardised method, the method was tested on the clay that had been in contact with the copper coupons, for which corrosion could be determined by standardised gravimetric methods.

3.5.1 Bentonite in contact with copper coupons

Some of the bentonite surfaces that had been in contact with the copper coupons had visible unevenly distributed corrosion products, primarily located in the corners, while others had no visible corrosion products (Figure 3-24).

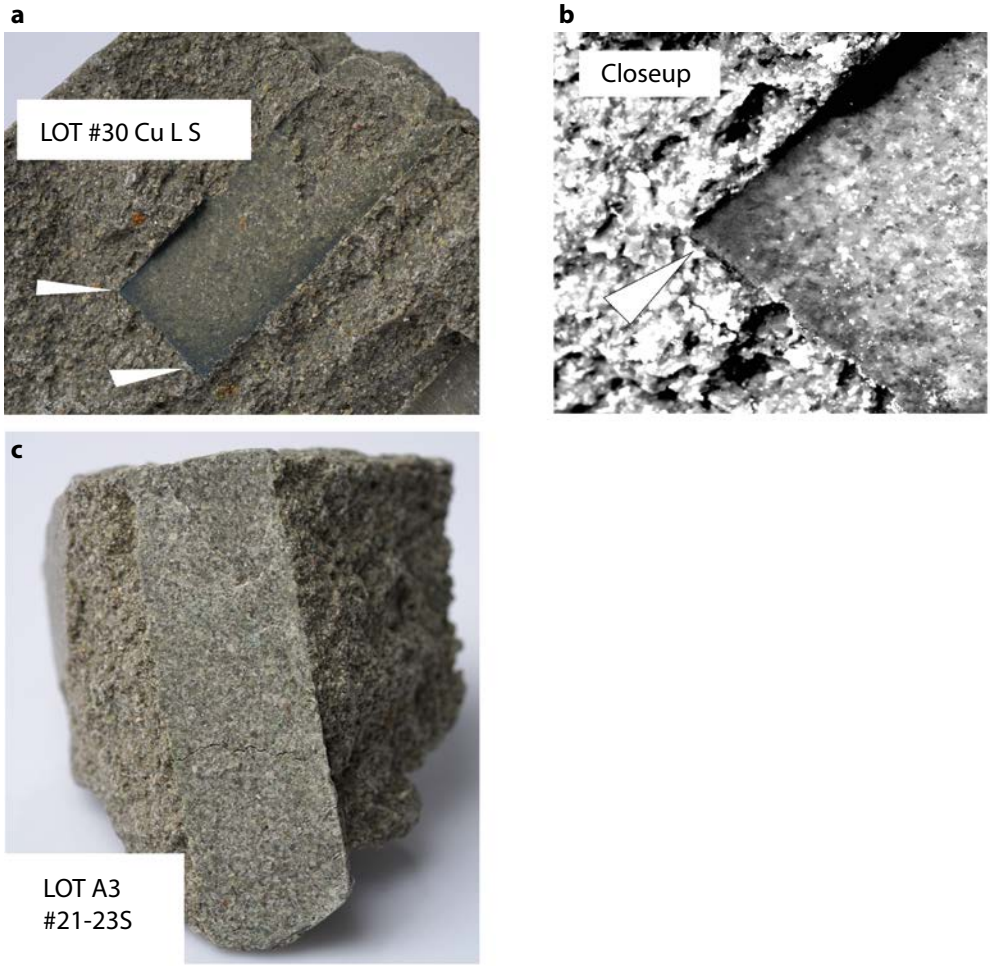

Figure 3-24. *(a) Example of bentonite with visible unevenly distributed corrosion products, primarily located in the corners. (b) Closeup of (a). (c) Example of bentonite with no visible corrosion products.*

Based on earlier experience, the copper in the bentonite was assumed to be present up to a distance of approximately 5 – 10 mm from the copper coupons. If the sampled interval was too small, some of the copper would be missed, and the estimation of corroded copper would have been underestimated. However, a larger sampled interval lowers the bulk copper concentration in the sample (as copper concentration decreases as a function of the distance from the coupon), and the quality of the measurement would drop, potentially below the detection limit of the method.

The first sample (Block 30; Cu K N) was sampled using the 0 – 10 mm interval (Figure 3-25). The resulting bulk sample obtained after grinding and compaction of the sample showed a copper concentration below detection limit. Hence it was decided to sample a smaller interval of 0 – 5 mm for the remaining samples (Figure 3-26). This means bulk samples were produced by milling all the bentonite that were within a 5 mm distance from the copper coupon. The 21 – 23 N Cu I sample was trimmed a little bit further after the photo was taken (on its right side).

Figure 3-25. *Sample "30 Cu K N" from block 30 of LOT A3, before and after trimming. All bentonite at 10 mm distance from the copper coupon was included in the final sample.*

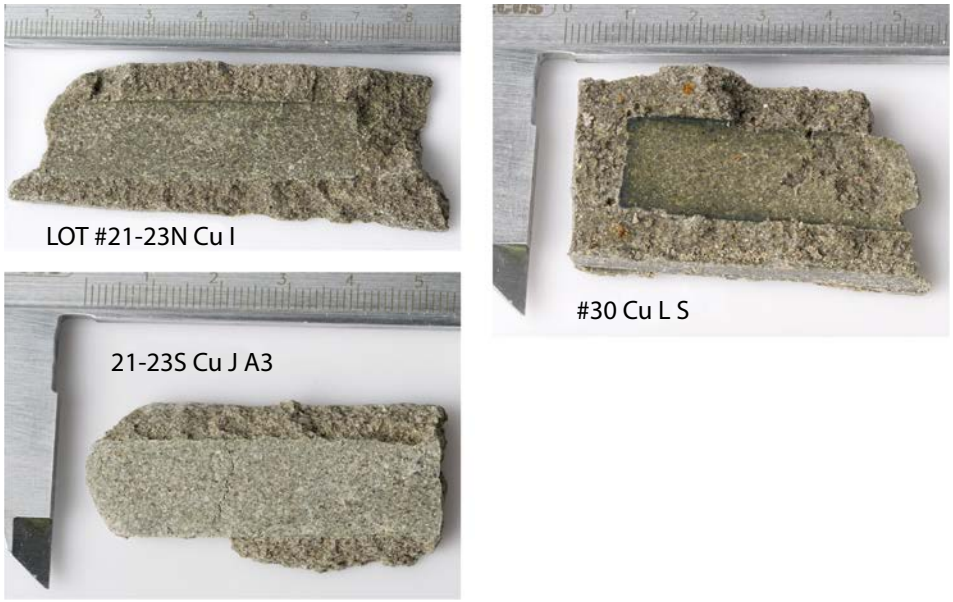

Figure 3-26. *Examples of trimmed samples with all bentonite at 5 mm distance from the copper coupon included.*

3.5.1.1 Chemical analysis (XRF) of bentonite from contact with coupons and estimation of corrosion

The sample “30 Cu K N” from block 30 of LOT A3, included all bentonite within a 10 mm distance from the copper coupon (Figure 3-25), and the resulting ”CuO” content was 0.008 wt% (Table 3-8), which is not a reliable quantification due to the very low concentration. This is not considered to be usable. Therefore, the other samples were instead trimmed using a 5 mm distance (Figure 3-26, Table 3-9). This resulted in higher ”CuO” levels in the range of 0.03 – 0.05 wt% (Table 3-8). The repeatability of the measurements was rather high (standard deviation SD was low, Table 3-8).

3.5.1.2 Method uncertainties

The method has previously been tested to work well at higher concentrations for standard elements (typically 2 – 20 %, Svensson et al. 2019). In this study, low levels of copper were important and hence the performance was tested by mixing milled bentonite (MX-80) with finely milled $CuCl_2 \times 2H_2O$ (Emsure ACS Reag. Merck, pro analysis) in different proportions (Table 3-10). The values obtained with XRF were very close to the calculated values (Table 3-10), and the bias error was regarded as very small and negligible in comparison to the assumption of the sample representativeness. Note that the standard deviation (SD) of these samples were significantly higher compared to the samples from the LOT experiment, hence the mixing of the copper salt with the bentonite was far from perfect (Table 3-11).

3.5.1.3 Mass loss of copper coupons into the bentonite

By using the mass of the samples (Table 3-9) and the concentration of “CuO” in the sample (Table 3-8) one can estimate the amount of Cu that corroded from the coupon and entered the bentonite. However, the bentonite samples were for practical reasons rather different in appearance, and only parts of the bentonite that covered the copper coupons were available. Hence, the relation in mass between the sample and the theoretical sample of 5 mm bentonite in all directions from the sample has to be estimated (sample representativeness). The 21 – 23 N sample (Figure 3-26) was close to 50 % of a perfect sample, some parts were missing on the left side so it was estimated that 43 % of the total sample was present. Based on that assumption, the total mass of a full sample would be 50 g (21.47 g/0.43), with a corresponding dry mass of 46 g using a water content of 7.5 wt% (average from Table 3-9).

The amount of ”CuO” leaving a coupon with around 0.05 wt% CuO (e.g. #22N and #21-23S) is given by 46 g × 0.05 % = 0.023 g ”CuO”. The molar mass of Cu is 63.55 g/mol and for ”CuO” it is 79.55 g/mol. Hence the amount of Cu lost from such a coupon was approximately (63.55/79.55) × 0.023 g = 0.018 g. While in the samples around 0.03 wt% CuO (#30 and #21-23N) the estimated amount is (0.03/0.05) × 0.018 = 0.011 g of Cu leaving the coupon into the bentonite.

Based on the assumptions above regarding the sample representativeness, the amount of copper leaving the coupons into the bentonite in the different samples is probably in the range of 0.01 – 0.02 g ± 20 %. It may be noted that this range, including the estimated uncertainty in the method, correspond to ca 0.5 – 1.2 µm of corrosion of the copper coupons (Table 3-2). The layer of corrosion products adherent to the surface were found to be thin (ca 360 nm thick on S2/N, Figure B-38, corresponding to ca 250 nm corrosion assuming Cu_2O), and thus the corrosion estimated by XRF is in fair agreement with the mass-losses determined by standardised gravimetric methods (Section 3.3.2).

Table 3-8. Composition of reference bentonite and bentonite in contact with coupons (wt%).

Sample	Na_2O	MgO	Al_2O_3	SiO_2	SO_3	Cl	K_2O	CaO	TiO_2	MnO	Fe_2O_3	CuO
LOT A2 MX-80 Reference block 4	1.7	2.3	20.5	67.5	0.7	0.0	0.7	1.7	0.2	0.0	4.6	0
LOT A2 MX-80 Reference block 4	1.6	2.4	20.6	67.8	0.7	0.0	0.5	1.6	0.2	0.0	4.6	0.001
LOT A2 MX-80 Reference block 29	1.7	2.4	20.5	67.6	0.7	0.0	0.7	1.7	0.2	0.0	4.6	0.001
LOT A2 MX-80 Reference block 29	1.7	2.3	20.5	67.7	0.7	0.0	0.7	1.7	0.2	0.0	4.5	0.001
LOT A2 MX-80 Reference block 24	1.7	2.3	20.5	67.7	0.7	0.0	0.6	1.7	0.2	0.0	4.5	0
LOT A2 MX-80 Reference block 24	1.7	2.3	20.4	67.6	0.8	0.0	0.7	1.7	0.2	0.0	4.6	0
Average	1.7	2.3	20.5	67.7	0.7	0.0	0.6	1.7	0.2	0.0	4.6	0.001
SD												0.001
LOT Block 30 Cu K Norr	1.1	2.3	21.0	67.7	0.3	0.1	0.6	2.1	0.2	0.0	4.6	0.008
LOT Block 30 Cu K Norr	1.1	2.3	21.0	67.8	0.4	0.1	0.6	2.0	0.2	0.0	4.6	0.008
LOT Block 30 Cu K Norr	1.1	2.3	20.9	67.8	0.4	0.1	0.6	2.0	0.2	0.0	4.6	0.007
LOT Block 30 Cu K Norr	1.1	2.3	21.0	67.7	0.4	0.1	0.6	2.0	0.2	0.0	4.6	0.008
Average	1.1	2.3	21.0	67.7	0.3	0.1	0.6	2.1	0.2	0.0	4.6	0.008
SD												0.001
LOT Bentonite-Cu coupon #22N CuP S2 M	1.6	2.3	20.3	68.3	0.6	0.2	0.5	1.4	0.2	0.0	4.6	0.052
LOT Bentonite-Cu coupon #22N CuP S2 M	1.6	2.3	20.2	68.3	0.6	0.1	0.5	1.4	0.2	0.0	4.5	0.048
Average	1.6	2.3	20.2	68.3	0.6	0.2	0.5	1.4	0.2	0.0	4.5	0.050
SD												0.003
LOT Bentonite-Cu coupon #21-23N Cu I	1.7	2.3	20.2	68.2	0.7	0.2	0.5	1.4	0.2	0.0	4.5	0.033
LOT Bentonite-Cu coupon #21-23N Cu I	1.6	2.3	20.3	68.2	0.8	0.1	0.6	1.4	0.2	0.0	4.5	0.031
Average	1.6	2.3	20.3	68.2	0.7	0.2	0.5	1.4	0.2	0.0	4.5	0.032
SD												0.001
LOT Bentonite-Cu coupon #21-23S A3	1.6	2.3	20.1	68.1	0.9	0.2	0.6	1.5	0.2	0.0	4.5	0.049
LOT Bentonite-Cu coupon #21-23S A3	1.6	2.3	20.4	67.7	1.0	0.1	0.5	1.5	0.2	0.0	4.5	0.049
Average	1.6	2.3	20.3	67.9	0.9	0.1	0.6	1.5	0.2	0.0	4.5	0.049
SD												0.000
LOT Bentonite-copper coupon #30 Cu L S	0.9	2.3	20.4	68.5	0.3	0.1	0.6	2.3	0.2	0.0	4.6	0.028
LOT Bentonite-copper coupon #30 Cu L S	0.9	2.3	20.5	68.4	0.3	0.1	0.5	2.2	0.2	0.0	4.5	0.032
Average	0.9	2.3	20.4	68.5	0.3	0.1	0.6	2.2	0.2	0.0	4.6	0.030
SD												0.003

Table 3-9. Mass of the bentonite samples taken from the 5 mm distance from copper coupons.

Sample	Weight (g)	Water content (wt%)	Dry weight (g)
LOT Bentonite-copper coupon #22N CuP S2 M	11.81	7.1	10.97
LOT Bentonite-copper coupon #21-23N Cu I	21.47	8	19.75
LOT Bentonite-copper coupon #21-23S A3	12	7.3	11.12
LOT Bentonite-copper coupon #30 Cu L S	14.81	8.1	13.61

Table 3-10. Comparison of observed (XRF) and calculated ”CuO” concentrations in bentonite-copper chloride mixtures. Bentonite water content assumed to be 10 wt%.

Sample	CuO_obs (wt%)	m_bentonite (g)	m_bentonite_dry (g)	m_cucl2_dihydrate (mg)	n_Cu (mmol)	CuO_equivalent (g)	CuO_calc (wt%)
Cu-b 1	0.517	8.5	7.65	86	0.504	0.0401	0.522
Cu-b 2	0.054	10.4	9.34	11.4	0.067	0.0053	0.057
Cu-b 3	0.252	8.34	7.51	35	0.205	0.0163	0.217
Ref	0.001						

Table 3-11. Chemical data (XRF) bentonite-copper chloride dihydrate mixtures. Wt%.

Sample	Na_2O	MgO	Al_2O_3	SiO_2	SO_3	Cl	K_2O	CaO	TiO_2	Fe_2O_3	CuO
Cu-b 1	1.8	2.5	22.0	65.1	0.7	0.4	0.6	1.4	0.2	4.7	0.51
Cu-b 1	1.7	2.5	22.0	65.2	0.7	0.4	0.7	1.4	0.2	4.7	0.524
										Average	0.517
										SD	0.0098
Cu-b 2	1.8	2.5	22.2	65.7	0.7	0.0	0.7	1.4	0.2	4.7	0.042
Cu-b 2	1.8	2.5	22.2	65.6	0.7	0.0	0.7	1.4	0.2	4.8	0.066
										Average	0.054
										SD	0.017
Cu-b 3	1.8	2.5	22.1	65.5	0.7	0.2	0.6	1.4	0.2	4.7	0.31
Cu-b 3	1.8	2.5	22.1	65.6	0.7	0.1	0.6	1.4	0.2	4.7	0.193
										Average	0.252
										SD	0.082
Reference MX-80	1.8	2.5	22.2	65.8	0.7	0.0	0.7	1.4	0.2	4.7	0.001
Reference MX-80	1.8	2.6	22.1	65.7	0.7	0.0	0.7	1.5	0.2	4.8	0.001
										Average	0.001
										SD	0

3.5.1.4 Microanalysis of bentonite in contact with coupons

The investigated sample that had been in contact with coupon L from the A3 parcel, is shown in Figure 3-26 (denoted "#30 Cu L S"). One corner visually rich in dark corrosion products in the bentonite was selected. The edge that looked dark visually in the sample looked very bright in backscatter mode in the SEM, indicating the presence of heavy atoms (Figure 3-27).

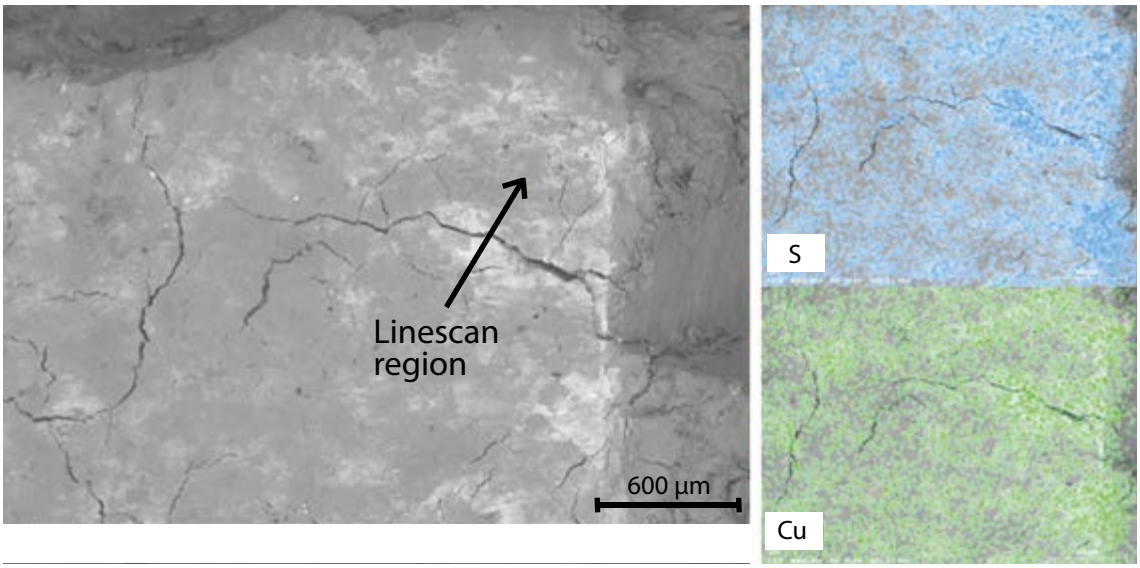

Figure 3-27. *Sample of bentonite ("30 Cu L S") from contact with a corner of coupon L from LOT A3. Left: BSE micrograph showing bright high scattering regions with elements of relatively higher atomic number. Upper right: EDS-map showing sulfur (S). Lower right: EDS-map showing copper (Cu).*

EDS mapping showed a presence of Cu and S more or less all over the sample, however, at the sites of the visible corrosion products they seemed enriched. However, quantification is difficult based on information from EDS-maps alone. In the region to the right, were Cu and S were enriched, other elements such as Mg, O, Si, Al seemed somewhat depleted (Figure 3-28).

Linescan EDS over the "corrosion product", showed the relative levels of Cu, S, O, Si and Al (Figure 3-29), and confirmed that both Cu and S had a maximum at the spot of the corrosion product, while the other elements were at a minimum. Hence, corrosion products are present over the entire surface, however enriched in some areas, and most likely the corrosion product is a copper sulfide.

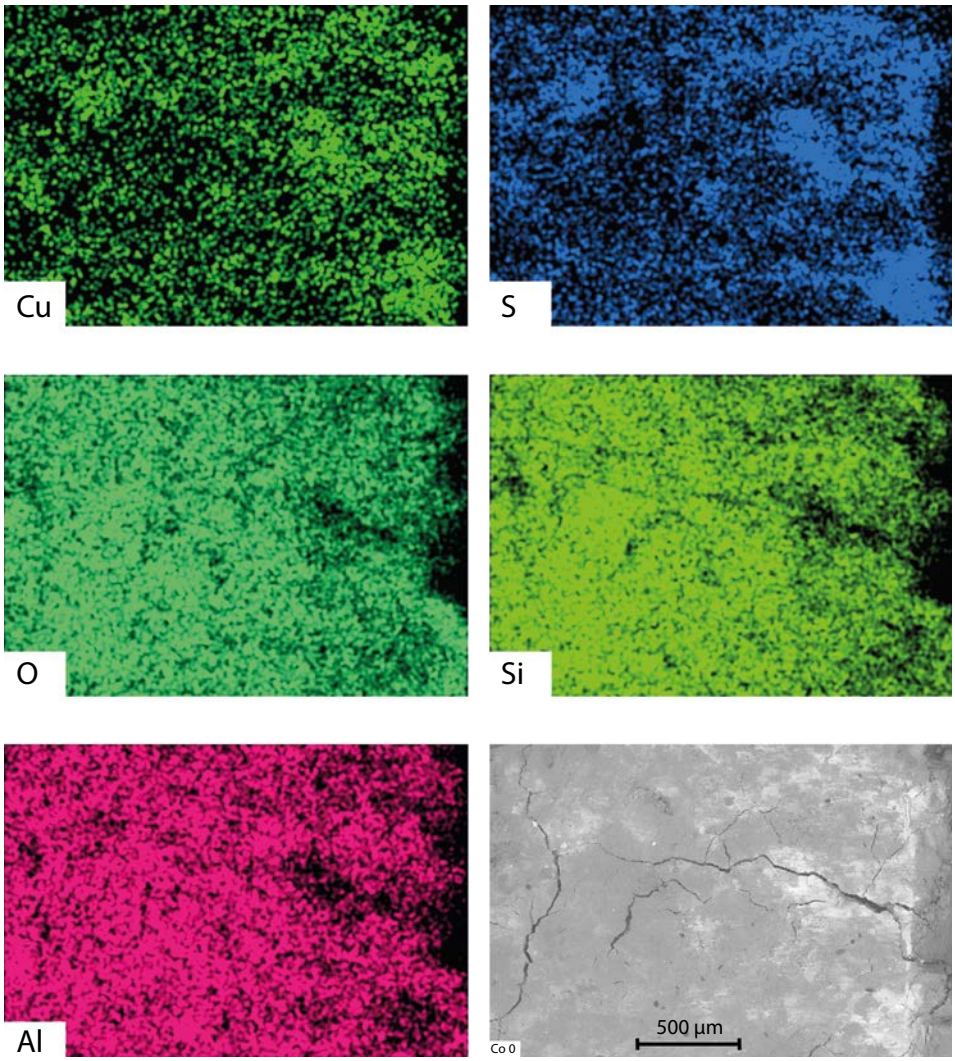

Figure 3-28. *Sample of bentonite ("30 Cu L S") from contact with a corner of coupon L from LOT A3. EDS-maps showing: Cu, S, O, Si, and Al.*

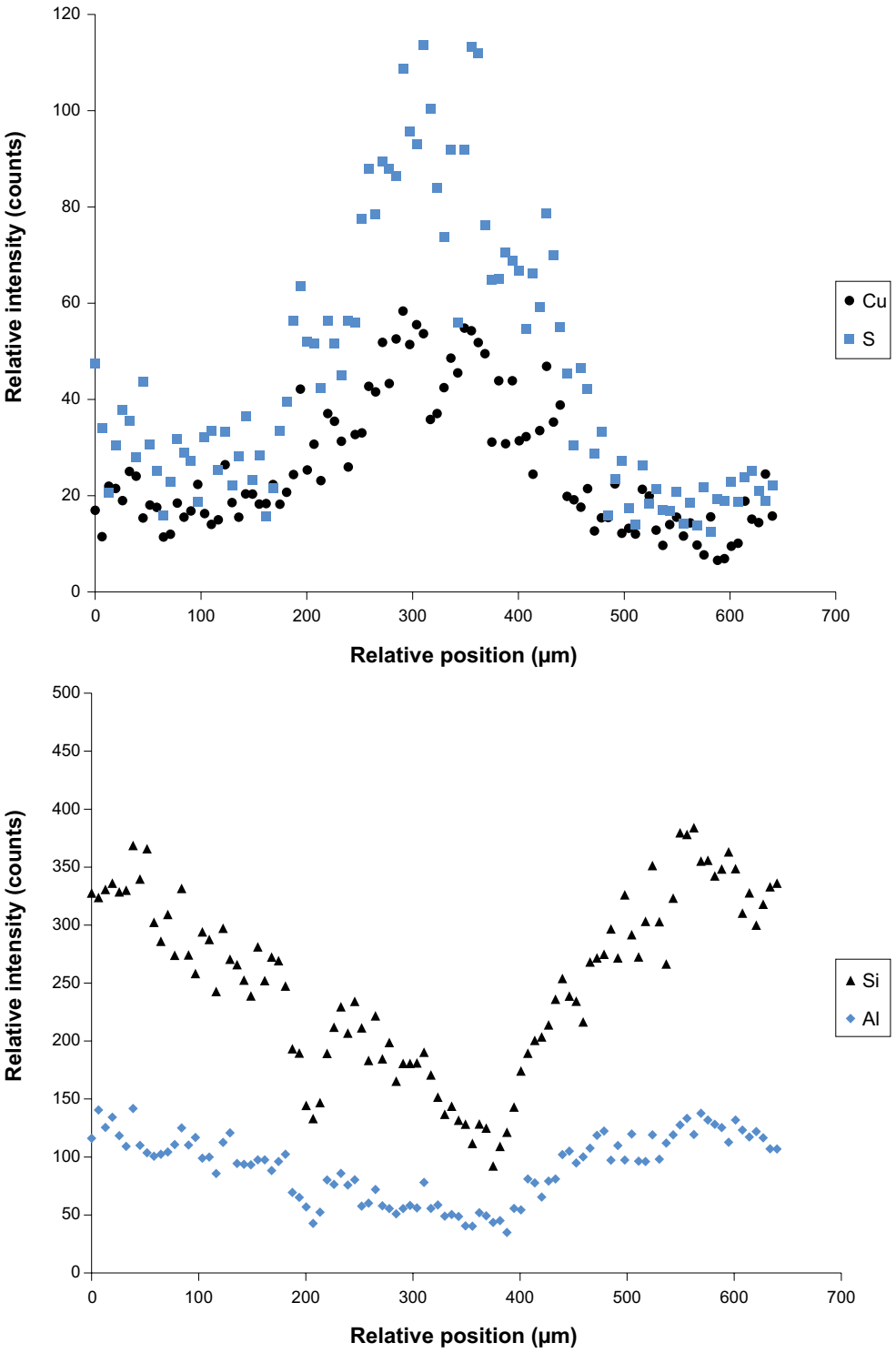

Figure 3-29. *EDS linescan over the bright section in Figure 3-27, showing relative levels of Cu, S, Si and Al.*

Spot analysis EDS on two sites were performed (Tables 3-12 and 3-13), and resulted in Cu/S atomic ratios of 13.03/7.77 = 1.7 and 10.37/5.73 = 1.8. This indicates that the visible corrosion product is a copper sulfide with a Cu/S ratio of around 2, including the possibility of e.g. digenite (1.8), djurleite (1.9) and chalcocite (2.0).

Table 3-12. SEM/EDS quantification of corrosion product site 1.

Element	Mass [%]	Mass Norm. [%]	Atom [%]	Abs. error [%] (1 sigma)	Rel. error [%] (1 sigma)
O	29.68	31.10	50.85	4.14	13.94
Si	14.67	15.38	14.32	0.66	4.46
Cu	30.21	31.66	13.03	1.11	3.67
S	9.09	9.53	7.77	0.37	4.03
C	2.73	2.86	6.22	0.98	35.93
Al	4.26	4.46	4.33	0.24	5.75
Ca	1.63	1.71	1.12	0.10	5.87
Cl	1.16	1.21	0.90	0.08	7.03
Mg	0.76	0.79	0.85	0.09	11.23
Fe	1.23	1.29	0.61	0.10	8.13
Sum	95.42	100.00	100.00		

Table 3-13. SEM/EDS quantification of corrosion product site 2.

Element [%]	Mass [%]	Mass Norm. [%]	Atom	Abs. error [%] (1 sigma)	Rel. error [%] (1 sigma)
O	32.71	35.08	53.91	4.47	13.65
Si	16.00	17.16	15.02	0.71	4.43
Cu	24.77	26.56	10.27	0.93	3.76
C	3.06	3.28	6.72	1.04	33.99
S	6.97	7.47	5.73	0.29	4.18
Al	5.44	5.84	5.32	0.30	5.48
Mg	0.81	0.87	0.88	0.09	10.72
Cl	1.07	1.14	0.79	0.08	7.28
Ca	1.16	1.25	0.77	0.08	6.83
Fe	1.25	1.34	0.59	0.10	8.03
Sum	93.25	100.00	100.00		

3.5.1.5 XRD analysis of bentonite and corrosion product from coupons contact

In an attempt to identify the copper sulfide phase, powder X-ray diffraction (XRD) was used for a sample of bentonite with copper corrosion product (“30 Cu L S” sample from LOT A3).

Chalcocite (Cu_2S) was not found in the sample (Figures 3-30 and 3-31) and no other CuS-phase could be identified. Hence, the corrosion product is likely amorphous or may have undetectable crystals (nanocrystalline) with no long-range order.

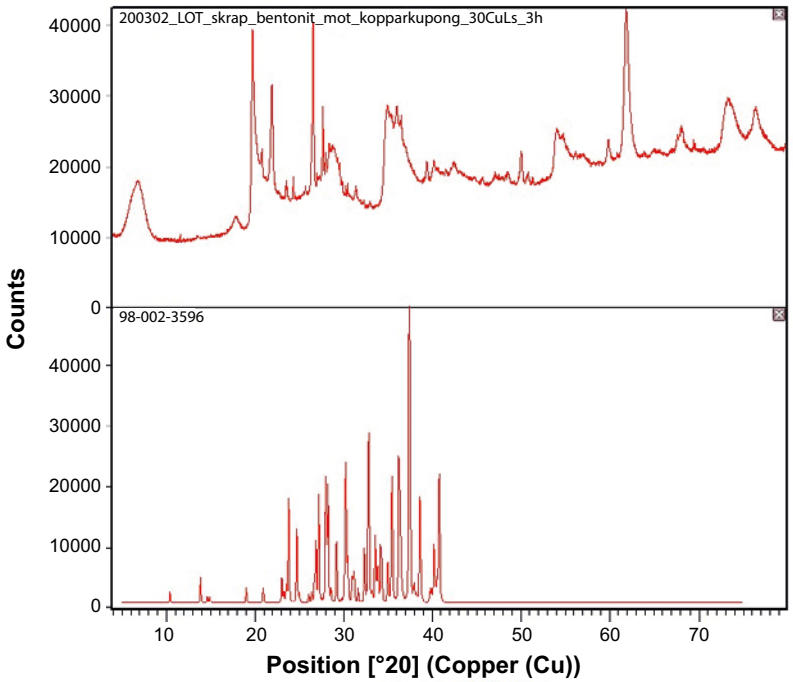

Figure 3-30. *X-ray diffractogram of a bentonite sample with visible corrosion product (30 Cu L S; top) compared to a calculated pattern of chalcocite (bottom). No chalcocite was visible in the sample.*

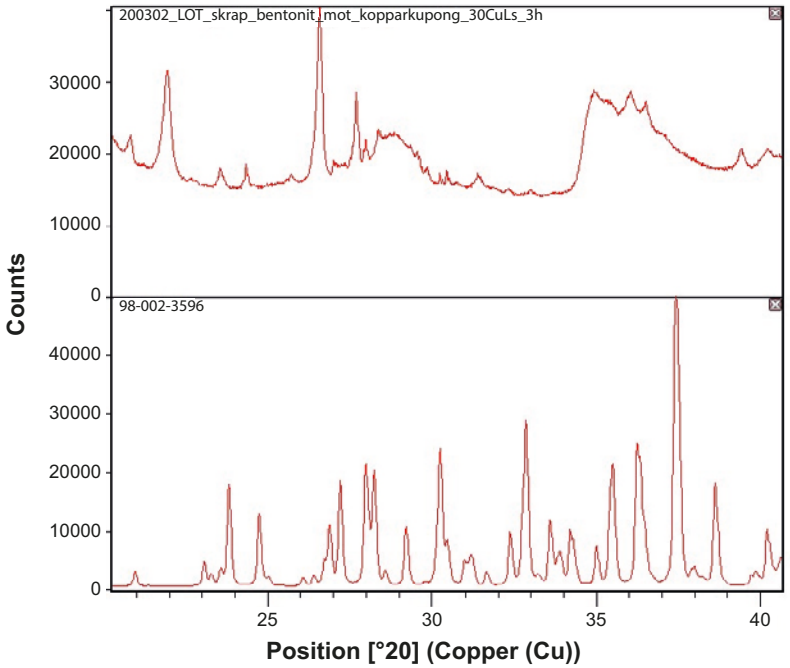

Figure 3-31. *Closeup of XRD pattern in previous figure. The bentonite sample with visible corrosion product (30 Cu L S; top) compared to a calculated pattern of chalcocite (bottom). No chalcocite was observed in the sample.*

3.5.2 Bentonite profiles from contact with the heaters

3.5.2.1 Sampling

The selected blocks were cut using a band saw to smaller pie-shaped pieces. The pie-shaped pieces were divided into six samples in the intervals: 0 – 2 mm, 2 – 10 mm, 10 – 20 mm, 20 – 50 mm and 70 – 100 mm, followed by drying, and milling using either an agate mortar (for samples in the 0 – 10 mm interval) or a ball mill (10 – 100 mm interval). After milling, samples for XRF were prepared by compaction of the milled bentonite.

3.5.2.2 Chemical analysis (XRF) of bentonite and estimation of corrosion

All data from the selected profiles in LOT A3 are listed in Tables 3-14 and 3-15, and all data from LOT S2 are presented in Table 3-16 and Table 3-17. Copper and sulfur are plotted for some selected data sets in Figure 3-32. Sulfur and calcium are typically redistributed within the bentonite to enrich towards the heater (as gypsum or anhydrite). This behaviour was expected and has been observed in several other field experiments at the Äspö laboratory. Sometimes gypsum is identified, sometimes anhydrite. This depends on the conditions during the experiment and the handling and storage of samples after the experiment.

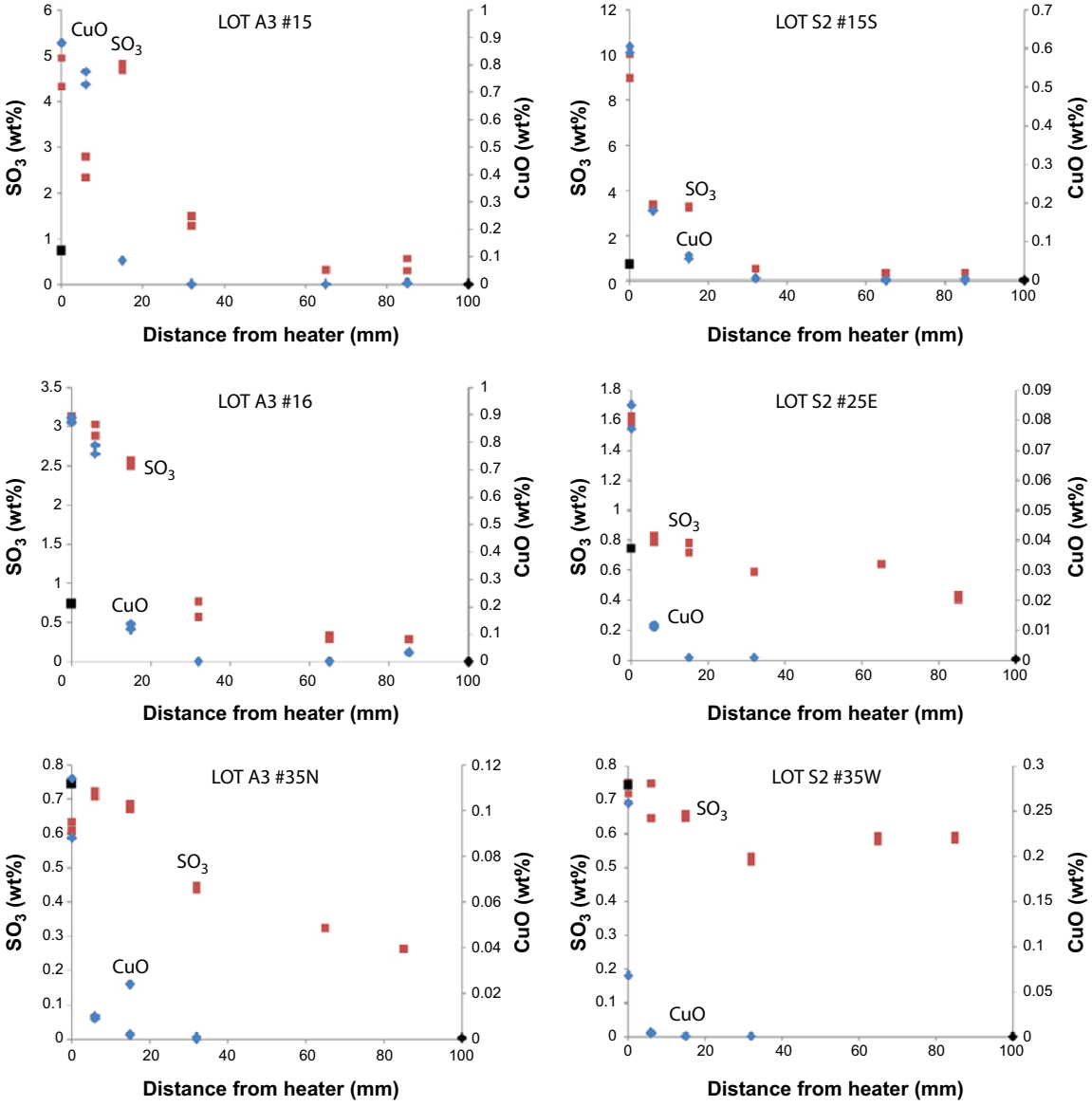

Figure 3-32. *Selected examples of elemental distribution data for LOT S2 and A3 (from Tables 3-14 to 3-17). No assignment of oxidation states is done. The oxide form is only a way of expressing the data for further quantitative calculations. Hence, the notations "CuO" and "SO_3" only give quantitative information about the amount of Cu and S in the samples, not the chemical forms or oxidation states of the elements.*

Another observation, also expected, is that the amount of copper was increased in the bentonite in the vicinity of the copper heater. An overview of the ”CuO” concentration as a function of the distance to the heater, can be seen in Figure 3-33 (LOT A3) and Figure 3-34 (LOT S2). In the LOT A3 experiment the ”CuO” concentrations were higher in the central part of the experiment (block #9–16; higher temperature) compared to the more peripheral blocks (#33–35; lower temperature). It was also observed that the ”CuO” concentrations in S2 were lower than in the warmer A3 (Figure 3-33 versus Figure 3-34).

These observations indicated that the ”CuO” concentrations were higher in bentonite that had a history of a higher temperature during the experiment. This could be interpreted as due to chemical kinetics, the corrosion reaction rate was higher at increased temperature, and hence hotter parts consumed a larger part of the installed oxygen in the experiment, resulting in more extensive corrosion in those areas. Additionally or alternatively, the hotter parts were desaturated for a longer time period compared to the colder parts, enabling more air corrosion.

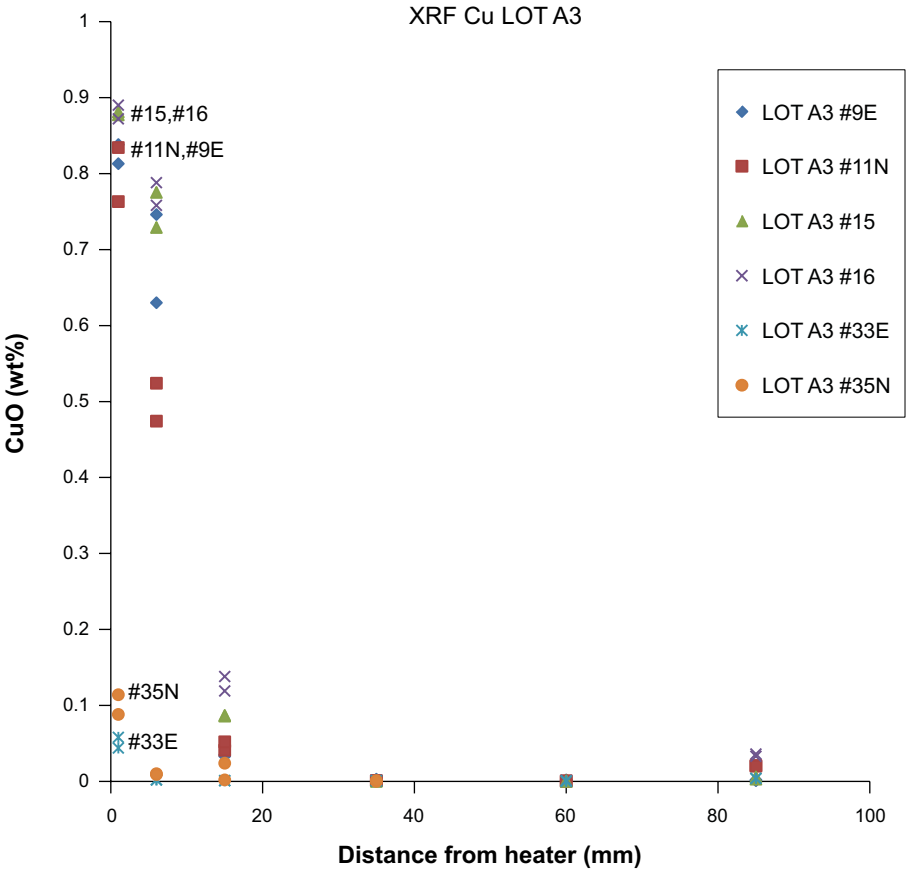

Figure 3-33. *”CuO” (wt%) as a function of the distance (mm) from the heater in LOT A3.*

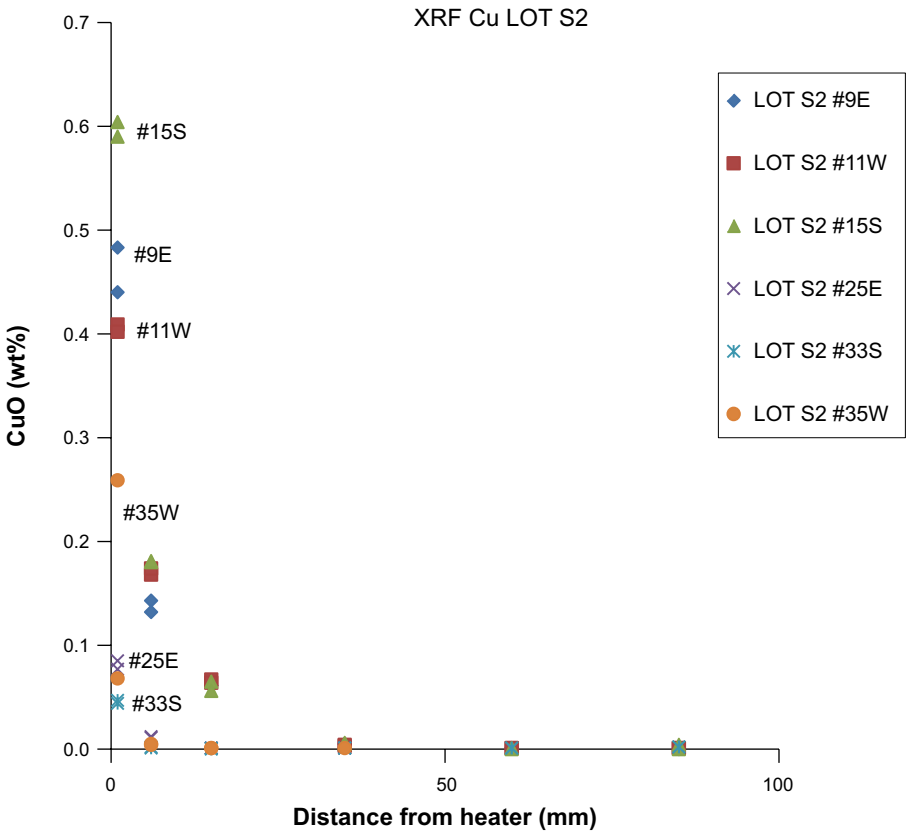

Figure 3-34. *"CuO" (wt%) as a function of the distance (mm) from the heater in LOT S2.*

Table 3-14. Chemical data (XRF) LOT A3 blocks #9, #11 and #15. Wt%. MnO and P_2O_5 were close to zero and excluded for improved visibility.

Sample	Na_2O	MgO	Al_2O_3	SiO_2	SO_3	Cl	K_2O	CaO	TiO_2	Fe_2O_3	CuO
LOT A3 #9E 0 – 2 mm d5c751	1.5	3.4	19.6	65.1	2.0	0.1	0.5	2.1	0.2	4.7	0.813
LOT A3 #9E 0 – 2 mm d5c751	1.5	3.3	19.5	64.6	2.5	0.1	0.6	2.3	0.2	4.6	0.838
LOT A3 #9E 2 – 10 mm d5c752	1.6	2.5	19.6	66.7	1.5	0.1	0.6	1.8	0.2	4.7	0.63
LOT A3 #9E 2 – 10 mm d5c752	1.5	2.6	20.0	66.2	1.4	0.1	0.6	1.7	0.2	4.9	0.746
LOT A3 #9E 10 – 20 mm d5c753	1.6	2.4	20.0	67.2	1.5	0.1	0.6	1.6	0.2	4.7	0.033
LOT A3 #9E 10 – 20 mm d5c753	1.6	2.4	20.1	67.1	1.5	0.1	0.5	1.6	0.2	4.7	0.035
LOT A3 #9E 20 – 50 mm d5c754	1.7	2.3	20.2	66.5	1.8	0.1	0.6	2.0	0.2	4.6	0.003
LOT A3 #9E 20 – 50 mm d5c754	1.7	2.3	20.3	66.5	1.8	0.1	0.6	2.0	0.2	4.5	0.001
LOT A3 #9E 50 – 70 mm d5c755	1.7	2.3	20.6	67.8	0.3	0.2	0.6	1.7	0.2	4.6	0.002
LOT A3 #9E 50 – 70 mm d5c755	1.7	2.3	20.6	67.8	0.3	0.2	0.6	1.7	0.2	4.6	0.001
LOT A3 #9E 70 – 100 mm d5c756	1.7	2.3	20.8	68.2	0.3	0.2	0.6	1.2	0.2	4.6	0.002
LOT A3 #9E 70 – 100 mm d5c756	1.7	2.3	20.8	68.3	0.3	0.2	0.6	1.2	0.2	4.6	0.001
LOT A3 #11N 0 – 2 mm d5c757	1.6	3.2	20.1	65.9	1.2	0.1	0.5	1.6	0.2	4.6	0.834
LOT A3 #11N 0 – 2 mm d5c757	1.6	3.2	20.0	66.1	1.2	0.1	0.6	1.7	0.2	4.6	0.763
LOT A3 #11N 2 – 10 mm d5c758	1.6	2.7	20.0	66.7	1.3	0.2	0.6	1.6	0.2	4.7	0.524
LOT A3 #11N 2 – 10 mm d5c758	1.6	2.7	20.0	66.6	1.5	0.1	0.5	1.7	0.2	4.7	0.474
LOT A3 #11N 10 – 20 mm d5c759	1.6	2.5	19.8	66.4	2.1	0.1	0.5	1.9	0.2	4.8	0.041
LOT A3 #11N 10 – 20 mm d5c759	1.6	2.5	19.8	66.5	2.0	0.1	0.6	1.8	0.2	4.7	0.052
LOT A3 #11N 20 – 50 mm d5c75a	1.7	2.4	20.4	67.0	1.3	0.2	0.5	1.8	0.2	4.6	0.001
LOT A3 #11N 20 – 50 mm d5c75a	1.7	2.4	20.5	66.9	1.2	0.2	0.6	1.8	0.2	4.6	0.001
LOT A3 #11N 50 – 70 mm d5c75b	1.7	2.3	20.8	67.8	0.3	0.2	0.6	1.5	0.2	4.6	0
LOT A3 #11N 50 – 70 mm d5c75b	1.7	2.3	20.8	67.8	0.3	0.2	0.6	1.6	0.2	4.6	0.001
LOT A3 #11N 70 – 100 mm d5c75c	1.7	2.3	20.7	68.2	0.3	0.2	0.6	1.1	0.2	4.7	0.021
LOT A3 #11N 70 – 100 mm d5c75c	1.7	2.3	20.8	68.2	0.3	0.2	0.6	1.1	0.2	4.7	0.02
LOT A3 #15 0 – 2 mm d5c745	1.4	3.2	18.6	62.1	4.9	0.1	0.5	3.3	0.2	4.7	0.88
LOT A3 #15 0 – 2 mm d5c745	1.4	3.1	18.8	62.9	4.3	0.1	0.5	3.0	0.2	4.8	0.88
LOT A3 #15 2 – 10 mm d5c746	1.5	2.6	19.3	65.6	2.3	0.1	0.6	2.2	0.2	4.9	0.78
LOT A3 #15 2 – 10 mm d5c746	1.5	2.5	19.3	65.1	2.8	0.1	0.5	2.3	0.2	4.9	0.73
LOT A3 #15 10 – 20 mm d5c747	1.5	2.2	18.8	63.8	4.7	0.2	0.6	3.1	0.2	4.8	0.09
LOT A3 #15 10 – 20 mm d5c747	1.5	2.2	18.8	63.6	4.8	0.2	0.5	3.1	0.2	4.8	0.09
LOT A3 #15 20 – 50 mm d5c748	1.6	2.2	19.7	67.7	1.3	0.2	0.6	1.7	0.2	4.8	0.00
LOT A3 #15 20 – 50 mm d5c748	1.6	2.3	19.6	67.4	1.5	0.2	0.6	1.7	0.2	4.9	0.00
LOT A3 #15 50 – 70 mm d5c749	1.7	2.3	20.1	68.3	0.3	0.2	0.5	1.6	0.2	4.8	0.00
LOT A3 #15 50 – 70 mm d5c749	1.6	2.2	20.0	68.7	0.3	0.2	0.6	1.3	0.2	4.8	0.00
LOT A3 #15 70 – 100 mm d5c750	1.6	2.2	20.0	68.7	0.3	0.3	0.6	1.3	0.2	4.9	0.00
LOT A3 #15 70 – 100 mm d5c750	1.6	2.2	19.9	68.5	0.6	0.3	0.6	1.4	0.2	4.8	0.01

Table 3-15. Chemical data (XRF) LOT A3 blocks #16, #33 and #35. Wt%. MnO and P_2O_5 were close to zero and excluded for improved visibility.

Sample	Na_2O	MgO	Al_2O_3	SiO_2	SO_3	Cl	K_2O	CaO	TiO_2	Fe_2O_3	CuO
LOT A3 #16 0 – 2 mm d5c74b	1.5	2.9	19.2	64.3	3.1	0.1	0.5	2.5	0.2	4.8	0.87
LOT A3 #16 0 – 2 mm d5c74b	1.5	3.0	19.2	64.1	3.1	0.1	0.5	2.5	0.2	4.9	0.89
LOT A3 #16 2 – 10 mm d5c74c	1.5	2.4	19.0	65.2	3.0	0.1	0.6	2.5	0.2	4.7	0.79
LOT A3 #16 2 – 10 mm d5c74c	1.5	2.4	19.3	65.0	2.9	0.1	0.5	2.4	0.2	4.8	0.76
LOT A3 #16 10 – 20 mm d5c74d	1.6	2.3	19.4	66.1	2.5	0.2	0.6	2.1	0.2	5.0	0.14
LOT A3 #16 10 – 20 mm d5c74d	1.6	2.3	19.1	66.3	2.6	0.1	0.6	2.2	0.2	4.8	0.12
LOT A3 #16 20 – 50 mm d5c74e	1.6	2.2	19.7	68.3	0.8	0.2	0.6	1.6	0.2	4.7	0.00
LOT A3 #16 20 – 50 mm d5c74e	1.6	2.3	20.2	68.1	0.6	0.2	0.6	1.3	0.2	4.9	0.00
LOT A3 #16 50 – 70 mm d5c74f	1.6	2.2	20.0	68.7	0.3	0.2	0.6	1.3	0.2	4.9	0.00
LOT A3 #16 50 – 70 mm d5c74f	1.7	2.2	19.9	68.5	0.3	0.2	0.6	1.6	0.2	4.8	0.00
LOT A3 #16 70 – 100 mm d5c74a	1.7	2.2	19.9	68.8	0.3	0.3	0.6	1.3	0.2	4.8	0.03
LOT A3 #16 70 – 100 mm d5c74a	1.7	2.2	19.9	68.7	0.3	0.2	0.6	1.3	0.2	4.8	0.04
LOT A3 #33E 0 – 2 mm d5c75d	0.8	2.3	20.5	67.5	0.6	0.1	0.5	2.8	0.2	4.7	0.058
LOT A3 #33E 0 – 2 mm d5c75d	0.8	2.2	20.4	67.9	0.5	0.1	0.6	2.6	0.2	4.6	0.044
LOT A3 #33E 2 – 10 mm d5c75e	0.8	2.2	20.3	68.1	0.6	0.1	0.6	2.6	0.2	4.6	0.002
LOT A3 #33E 2 – 10 mm d5c75e	0.8	2.3	20.5	67.9	0.6	0.1	0.5	2.5	0.2	4.6	0.002
LOT A3 #33E 10 – 20 mm d5c75f	0.8	2.2	20.3	68.1	0.6	0.1	0.6	2.5	0.2	4.6	0.001
LOT A3 #33E 10 – 20 mm d5c75f	0.8	2.2	20.3	68.0	0.6	0.1	0.6	2.6	0.2	4.6	0.001
LOT A3 #33E 20 – 50 mm d5c760	0.8	2.3	20.7	67.7	0.5	0.1	0.5	2.6	0.2	4.6	0.001
LOT A3 #33E 20 – 50 mm d5c760	0.8	2.3	20.8	67.6	0.5	0.1	0.6	2.5	0.2	4.6	0.001
LOT A3 #33E 50 – 70 mm d5c761	0.9	2.3	20.8	67.8	0.3	0.1	0.5	2.5	0.2	4.6	0
LOT A3 #33E 50 – 70 mm d5c761	0.8	2.3	20.8	67.9	0.3	0.1	0.6	2.5	0.2	4.6	0.001
LOT A3 #33E 70 – 100 mm d5c762	0.9	2.2	20.8	67.9	0.3	0.1	0.5	2.4	0.2	4.6	0.004
LOT A3 #33E 70 – 100 mm d5c762	0.8	2.3	20.9	67.9	0.3	0.1	0.5	2.4	0.2	4.6	0.004
LOT A3 #35N 0 – 2 mm	1.1	2.3	20.5	67.7	0.6	0.1	0.6	2.3	0.2	4.6	0.09
LOT A3 #35N 0 – 2 mm	1.1	2.3	20.4	67.6	0.6	0.1	0.6	2.4	0.2	4.5	0.11
LOT A3 #35N 2 – 10 mm	1.1	2.3	20.3	67.8	0.7	0.1	0.6	2.3	0.2	4.6	0.01
LOT A3 #35N 2 – 10 mm	1.1	2.3	20.2	68.1	0.7	0.1	0.6	2.2	0.2	4.5	0.01
LOT A3 #35N 10 – 20 mm	1.1	2.3	20.2	67.7	0.7	0.1	0.6	2.5	0.2	4.6	0.02
LOT A3 #35N 10 – 20 mm	1.1	2.2	20.2	67.9	0.7	0.1	0.6	2.4	0.2	4.6	0.00
LOT A3 #35N 20 – 50 mm	1.1	2.3	20.9	67.7	0.4	0.1	0.6	2.1	0.2	4.5	n/a
LOT A3 #35N 20 – 50 mm	1.2	2.3	20.8	67.7	0.4	0.1	0.6	2.1	0.2	4.5	0.00
LOT A3 #35N 50 – 70 mm	1.1	2.3	20.7	68.0	0.3	0.1	0.6	2.0	0.2	4.6	n/a
LOT A3 #35N 50 – 70 mm	1.1	2.3	20.7	68.0	0.3	0.1	0.6	2.1	0.2	4.6	n/a
LOT A3 #35N 70 – 100 mm	1.1	2.3	20.7	68.1	0.3	0.1	0.6	2.0	0.2	4.6	n/a
LOT A3 #35N 70 – 100 mm	1.1	2.3	20.7	68.1	0.3	0.1	0.6	2.0	0.2	4.6	n/a

Table 3-16. Chemical data (XRF) LOT S2 blocks #9, #11 and #15. Wt%. MnO and P_2O_5 were close to zero and excluded for improved visibility.

Sample	Na_2O	MgO	Al_2O_3	SiO_2	SO_3	Cl	K_2O	CaO	TiO_2	Fe_2O_3	CuO
LOT S2 #9E 0 – 2 mm d5c769	1.5	2.3	18.9	61.8	6.1	0.1	0.5	3.6	0.2	4.5	0.44
LOT S2 #9E 0 – 2 mm d5c769	1.5	2.2	18.2	59.3	7.9	0.1	0.6	5.0	0.2	4.5	0.48
LOT S2 #9E 2 – 10 mm d5c76a	1.6	2.4	20.1	66.3	1.9	0.1	0.5	1.8	0.2	4.8	0.14
LOT S2 #9E 2 – 10 mm d5c76a	1.6	2.3	19.8	66.5	2.0	0.1	0.6	1.9	0.2	4.7	0.13
LOT S2 #9E 10 – 20 mm d5c76b	1.7	2.4	20.5	67.1	1.2	0.1	0.6	1.6	0.2	4.6	0.06
LOT S2 #9E 10 – 20 mm d5c76b	1.7	2.4	20.5	67.1	1.1	0.1	0.6	1.6	0.2	4.6	0.06
LOT S2 #9E 20 – 50 mm d5c76c	1.7	2.3	20.5	67.1	1.2	0.1	0.6	1.7	0.2	4.6	0.01
LOT S2 #9E 20 – 50 mm d5c76c	1.7	2.3	20.6	67.1	1.2	0.1	0.6	1.7	0.2	4.6	0.01
LOT S2 #9E 50 – 70 mm d5c76d	1.7	2.3	20.7	68.1	0.3	0.1	0.6	1.4	0.2	4.6	0.00
LOT S2 #9E 50 – 70 mm d5c76d	1.7	2.3	20.7	68.1	0.4	0.1	0.6	1.4	0.2	4.6	0.00
LOT S2 #9E 70 – 100 mm d5c76e	1.7	2.3	20.7	68.2	0.3	0.1	0.6	1.3	0.2	4.6	0.00
LOT S2 #9E 70 – 100 mm d5c76e	1.7	2.3	20.7	68.2	0.3	0.1	0.6	1.3	0.2	4.6	0.00
LOT S2 #11W 0 – 2 mm d5c76f	1.6	2.4	19.4	64.0	4.0	0.1	0.5	2.7	0.2	4.8	0.41
LOT S2 #11W 0 – 2 mm d5c76f	1.6	2.3	19.1	63.9	4.2	0.1	0.6	2.9	0.2	4.6	0.40
LOT S2 #11W 2 – 10 mm d5c770	1.6	2.4	20.1	66.8	1.8	0.1	0.6	1.7	0.2	4.7	0.17
LOT S2 #11W 2 – 10 mm d5c770	1.6	2.4	19.9	66.5	1.8	0.1	0.6	1.9	0.2	4.8	0.17
LOT S2 #11W 10 – 20 mm d5c771	1.7	2.4	20.5	67.1	1.1	0.1	0.6	1.6	0.2	4.6	0.07
LOT S2 #11W 10 – 20 mm d5c771	1.7	2.4	20.5	67.1	1.1	0.1	0.6	1.6	0.2	4.6	0.06
LOT S2 #11W 20 – 50 mm d5c772	1.7	2.3	20.5	67.1	1.2	0.1	0.6	1.7	0.2	4.6	0.00
LOT S2 #11W 20 – 50 mm d5c772	1.7	2.3	20.5	67.2	1.2	0.1	0.6	1.7	0.2	4.6	0.00
LOT S2 #11W 50 – 70 mm d5c773	1.7	2.3	20.8	68.0	0.3	0.1	0.6	1.3	0.2	4.6	0.00
LOT S2 #11W 50 – 70 mm d5c773	1.7	2.3	20.8	68.0	0.3	0.1	0.6	1.3	0.2	4.6	0.00
LOT S2 #11W 70 – 100 mm d5c774	1.7	2.3	20.8	68.0	0.3	0.1	0.6	1.3	0.2	4.6	0.00
LOT S2 #11W 70 – 100 mm d5c774	1.7	2.3	20.8	68.0	0.3	0.1	0.6	1.3	0.2	4.6	0.00
LOT S2 #15S 0 – 2 mm	1.5	2.2	17.9	58.0	9.0	0.1	0.5	5.4	0.2	4.6	0.59
LOT S2 #15S 0 – 2 mm	1.4	2.1	17.4	57.1	10.0	0.1	0.5	5.9	0.2	4.5	0.60
LOT S2 #15S 2 – 10 mm	1.6	2.4	19.4	65.2	3.2	0.2	0.6	2.5	0.2	4.5	0.18
LOT S2 #15S 2 – 10 mm	1.6	2.4	19.5	65.1	3.4	0.2	0.5	2.5	0.2	4.6	0.18
LOT S2 #15S 10 – 20 mm	1.6	2.3	19.5	65.4	3.2	0.2	0.6	2.5	0.2	4.5	0.07
LOT S2 #15S 10 – 20 mm	1.6	2.3	19.6	65.1	3.3	0.2	0.5	2.4	0.2	4.6	0.06
LOT S2 #15S 20 – 50 mm	1.8	2.4	20.7	67.9	0.5	0.2	0.6	1.3	0.2	4.5	0.01
LOT S2 #15S 20 – 50 mm	1.8	2.4	20.7	67.9	0.5	0.2	0.6	1.3	0.2	4.5	0.01
LOT S2 #15S 50 – 70 mm	1.7	2.3	20.7	68.1	0.3	0.2	0.6	1.3	0.2	4.6	n/a
LOT S2 #15S 50 – 70 mm	1.7	2.3	20.7	68.1	0.3	0.2	0.6	1.3	0.2	4.6	0.00
LOT S2 #15S 70 – 100 mm	1.7	2.3	20.5	68.2	0.3	0.2	0.6	1.3	0.2	4.7	0.00
LOT S2 #15S 70 – 100 mm	1.7	2.3	20.6	68.2	0.3	0.2	0.6	1.3	0.2	4.7	n/a

Table 3-17. Chemical data (XRF) LOT S2 blocks #25, #33 and #35. Wt%. MnO and P_2O_5 were close to zero and excluded for improved visibility.

Sample	Na_2O	MgO	Al_2O_3	SiO_2	SO_3	Cl	K_2O	CaO	TiO_2	Fe_2O_3	CuO
LOT S2 #25E 0 – 2 mm	1.7	2.3	20.0	67.0	1.6	0.1	0.6	1.9	0.2	4.5	0.09
LOT S2 #25E 0 – 2 mm	1.7	2.3	20.1	66.8	1.6	0.1	0.6	2.0	0.2	4.6	0.08
LOT S2 #25E 2 – 10 mm	1.8	2.3	20.2	68.0	0.8	0.2	0.6	1.4	0.2	4.5	0.01
LOT S2 #25E 2 – 10 mm	1.8	2.3	20.3	67.8	0.8	0.2	0.5	1.4	0.2	4.5	0.01
LOT S2 #25E 10 – 20 mm	1.7	2.3	20.1	68.3	0.7	0.2	0.6	1.4	0.2	4.4	0.00
LOT S2 #25E 10 – 20 mm	1.7	2.4	20.2	67.9	0.8	0.2	0.6	1.4	0.2	4.6	0.00
LOT S2 #25E 20 – 50 mm	1.7	2.4	20.7	67.8	0.6	0.2	0.6	1.4	0.2	4.5	0.00
LOT S2 #25E 20 – 50 mm	1.7	2.4	20.7	67.8	0.6	0.2	0.6	1.4	0.2	4.5	0.00
LOT S2 #25E 50 – 70 mm	1.7	2.3	20.6	67.7	0.6	0.1	0.6	1.5	0.2	4.7	n/a
LOT S2 #25E 50 – 70 mm	1.7	2.3	20.6	67.7	0.6	0.1	0.6	1.5	0.2	4.6	n/a
LOT S2 #25E 70 – 100 mm	1.7	2.4	20.7	67.9	0.4	0.2	0.5	1.3	0.2	4.6	n/a
LOT S2 #25E 70 – 100 mm	1.7	2.4	20.7	68.0	0.4	0.2	0.6	1.3	0.2	4.6	n/a
LOT S2 #33S 0 – 2 mm d5c781	1.6	2.3	20.6	68.0	0.4	0.1	0.6	1.4	0.2	4.7	0.04
LOT S2 #33S 0 – 2 mm d5c781	1.6	2.3	20.6	68.0	0.4	0.1	0.6	1.5	0.2	4.7	0.05
LOT S2 #33S 2 – 10 mm d5c782	1.6	2.3	20.2	68.0	0.8	0.1	0.6	1.7	0.2	4.6	0.00
LOT S2 #33S 2 – 10 mm d5c782	1.6	2.3	20.2	67.7	0.8	0.1	0.6	1.8	0.2	4.7	0.00
LOT S2 #33S 10 – 20 mm d5c783	1.6	2.3	20.3	67.9	0.7	0.1	0.6	1.7	0.2	4.6	0.00
LOT S2 #33S 10 – 20 mm d5c783	1.6	2.3	20.3	68.1	0.7	0.1	0.6	1.5	0.2	4.7	0.00
LOT S2 #33S 20 – 50 mm d5c784	1.6	2.3	20.9	67.7	0.4	0.1	0.6	1.5	0.2	4.7	0.00
LOT S2 #33S 20 – 50 mm d5c784	1.6	2.3	20.9	67.7	0.4	0.1	0.6	1.5	0.2	4.6	0.00
LOT S2 #33S 50 – 70 mm d5c785	1.6	2.3	20.9	68.1	0.3	0.1	0.6	1.4	0.2	4.6	0.00
LOT S2 #33S 50 – 70 mm d5c785	1.6	2.4	20.8	68.0	0.3	0.1	0.6	1.4	0.2	4.6	0.00
LOT S2 #33S 70 – 100 mm d5c786	1.6	2.4	20.8	68.1	0.3	0.1	0.6	1.4	0.2	4.6	0.00
LOT S2 #33S 70 – 100 mm d5c786	1.6	2.3	20.8	68.2	0.3	0.1	0.6	1.4	0.2	4.5	0.00
LOT S2 #35W 0 – 2 mm	1.6	2.3	20.5	67.8	0.7	0.1	0.6	1.5	0.2	4.6	0.07
LOT S2 #35w 0 – 2 mm	1.7	2.3	20.3	67.7	0.8	0.1	0.6	1.6	0.2	4.5	0.26
LOT S2 #35w 2 – 10 mm	1.6	2.3	20.3	68.2	0.6	0.1	0.6	1.5	0.2	4.6	0.01
LOT S2 #35W 2 – 10 mm	1.6	2.3	20.3	67.7	0.7	0.1	0.6	1.7	0.2	4.7	0.00
LOT S2 #35W 10 – 20 mm	1.6	2.3	20.3	68.1	0.7	0.1	0.6	1.5	0.2	4.6	0.00
LOT S2 #35w 10 – 20 mm	1.7	2.3	20.2	68.3	0.6	0.1	0.6	1.5	0.2	4.5	0.00
LOT S2 #35w 20 – 50 mm	1.7	2.3	20.8	67.9	0.5	0.1	0.6	1.4	0.2	4.5	0.00
LOT S2 #35W 20 – 50 mm	1.7	2.4	20.8	67.8	0.5	0.1	0.6	1.4	0.2	4.5	n/a
LOT S2 #35W 50 – 70 mm	1.7	2.3	20.7	67.8	0.6	0.1	0.6	1.5	0.2	4.6	n/a
LOT S2 #35W 50 – 70 mm	1.7	2.3	20.7	67.8	0.6	0.1	0.6	1.5	0.2	4.6	n/a
LOT S2 #35W 70 – 100 mm	1.7	2.3	20.6	67.9	0.6	0.1	0.6	1.5	0.2	4.6	n/a
LOT S2 #35W 70 – 100 mm	1.7	2.3	20.6	67.9	0.6	0.1	0.6	1.4	0.2	4.6	n/a

Table 3-18. Chemical data (XRF) reference samples. Wt%. MnO and P_2O_5 were close to zero and excluded for improved visibility.

Sample	Na_2O	MgO	Al_2O_3	SiO_2	SO_3	Cl	K_2O	CaO	TiO_2	Fe_2O_3	CuO
LOT A2 MX-80 Referens block 4	1.7	2.3	20.5	67.5	0.7	0.0	0.7	1.7	0.2	4.6	0
LOT A2 MX-80 Referens block 4	1.6	2.4	20.6	67.8	0.7	0.0	0.5	1.6	0.2	4.6	0.001
LOT A2 MX-80 Referens block 29	1.7	2.4	20.5	67.6	0.7	0.0	0.7	1.7	0.2	4.6	0.001
LOT A2 MX-80 Referens block 29	1.7	2.3	20.5	67.7	0.7	0.0	0.7	1.7	0.2	4.5	0.001
LOT A2 MX-80 Referens block 29	1.6	2.4	20.8	67.3	0.9	0.0	0.5	1.7	0.2	4.6	n/a
LOT A2 MX-80 Referens block 29	1.6	2.4	20.8	67.3	0.7	0.0	0.5	1.8	0.2	4.7	n/a
LOT A2 MX-80 Referens block 24	1.7	2.3	20.5	67.7	0.7	0.0	0.6	1.7	0.2	4.5	0
LOT A2 MX-80 Referens block 24	1.7	2.3	20.4	67.6	0.8	0.0	0.7	1.7	0.2	4.6	0
LOT A2 MX-80 Referens block 24	1.6	2.4	20.8	67.5	0.8	0.0	0.5	1.7	0.2	4.6	n/a
LOT A2 MX-80 Referens block 24	1.6	2.4	21.0	66.7	0.9	0.0	0.5	1.9	0.2	4.6	n/a

3.5.2.3 Estimation of corrosion depths

The heater diameter was 10.8 cm, and the bentonite had approximately a dry density of 1 500 g/cm^3 (Sandén and Nilsson 2020). The copper found in the bentonite in the interval of 0 – 20 mm from the heater is included. Each block is assumed to be 10 cm high. This estimation of corrosion is based on the amount of copper in the bentonite, and the very thin oxide layer on the copper surface is hence not included in this estimation.

Calculation of the total mass representing the samples

The 0 – 2 mm, 2 – 10 mm and the 10 – 20 mm samples represents different volumes (and masses) in the blocks.

The 0 – 0.2 cm, 0.2 – 1 cm and the 1 – 2 cm samples represents different volumes (and masses) in the blocks. The volume of the central heater in one block is: $10\pi \times 5.4^2$ cm^3 = 916 cm^3.

The volume of the "0 – 0.2 cm bentonite" is $10\pi \times 5.6^2$ cm^3 − 916 cm^3 = 69 cm^3 (corresponding dry mass = 104 g). In the same way, the "0.2 – 1 cm bentonite" has a corresponding dry mass of 452 g, and the "1 – 2 cm bentonite" dry mass of 650 g.

The total mass of "CuO" from each block can then be calculated using the estimated masses from above together with the concentration values in Tables 3-14 to 3-17. The total amount of copper was calculated by multiplying with the ratio of the molar mass of Cu and "CuO" = 63.55/79.55. The volume of the corroded copper was calculated from the density of copper 8.96 g/cm^3. The circumference of the heater is 10.8 cm π = 33.9 cm. The corrosion depth is calculated as the volume of the corroded copper, divided by the circumference of the heater × 10 cm (block height). The estimated corrosion depthes are in the range of 0.2 – 13.8 µm for LOT A3 and in the range of 0.2 – 4.8 µm for LOT S2 (see Table 3-19, further details are given in Appendix J).

Table 3-19. Estimated corrosion depths on different positions of the copper heater pipes in LOT A3 and S2, based on the copper content in the bentonite.

Block	Estimated corrosion depth (µm)
LOT A3 #9E	11.02
LOT A3 #11N	8.91
LOT A3 #15	12.82
LOT A3 #16	13.80
Average hot region A3:	11.64
LOT A3 #33E	0.18
LOT A3 #35N	0.61
Average cold region A3:	0.40
LOT S2 #9E	3.94
LOT S2 #11W	4.26
LOT S2 #15S	4.81
Average hot region S2:	4.34
LOT S2 #25E	0.38
LOT S2 #33S	0.15
LOT S2 #35W	0.52
Average cold region S2:	0.35

3.5.2.4 Phase analysis (XRD) of bentonite

The analytical work of the bentonite buffer in LOT S2 and A3 is to be reported later separately, however, some example XRD data of the bentonite is included here to support the interpretation of the XRF data listed above. Most importantly, gypsum was identified in samples close to the heater (Figure 3-35) and is a source of Ca and S in the XRF data. Except from gypsum enrichment no other significant change could be seen to the bentonite (Figure 3-36 and Figure 3-37), however, the bentonite will be further evaluated in greater detail in a separate future report.

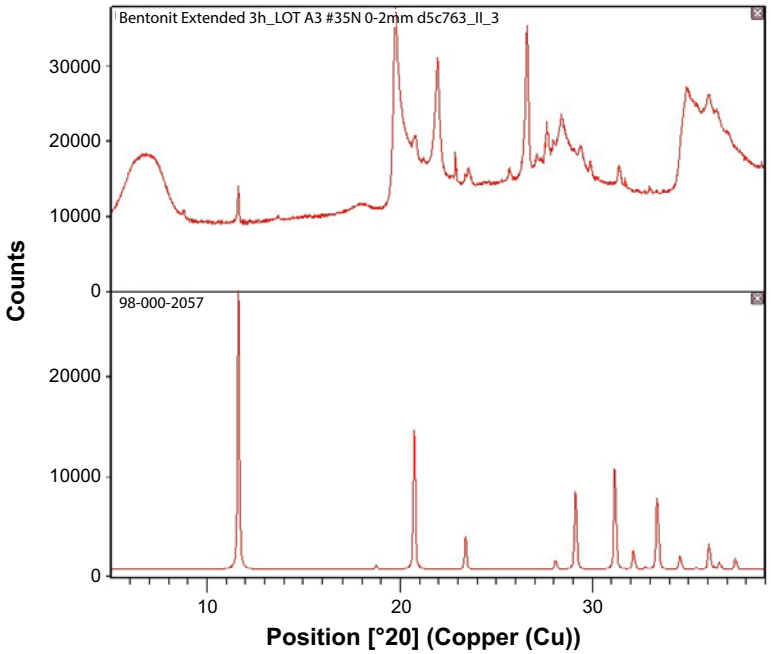

Figure 3-35. *X-ray diffractogram of a bentonite sample from the heater contact (LOT A3 #35N 0–2 mm; top) compared to a calculated pattern of gypsum (bottom). Gypsum is visible in the sample. The gypsum main reflection is at around 12 degrees two theta.*

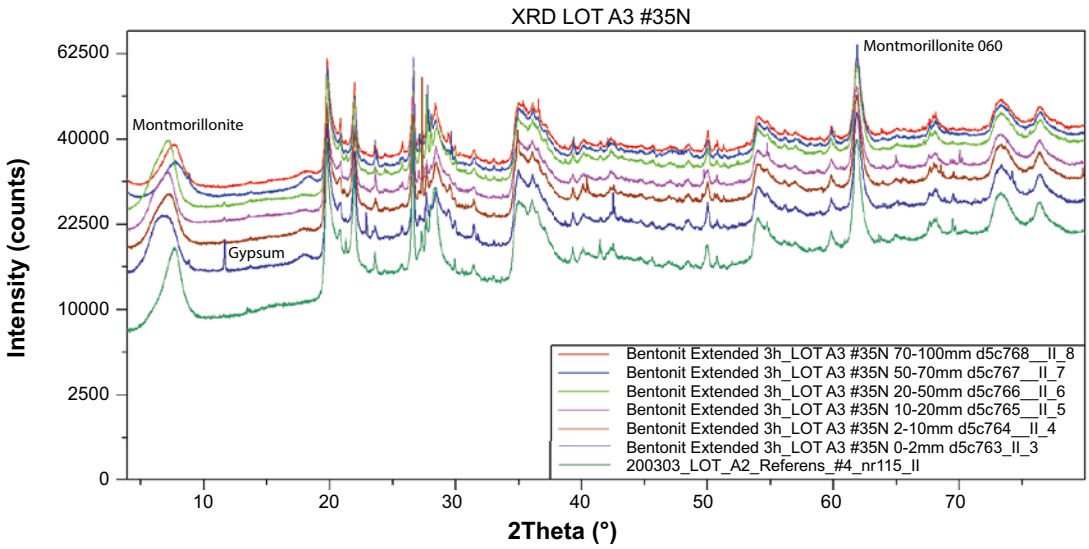

Figure 3-36. *Example of XRD data from a bentonite profile (LOT A3 #35N).*

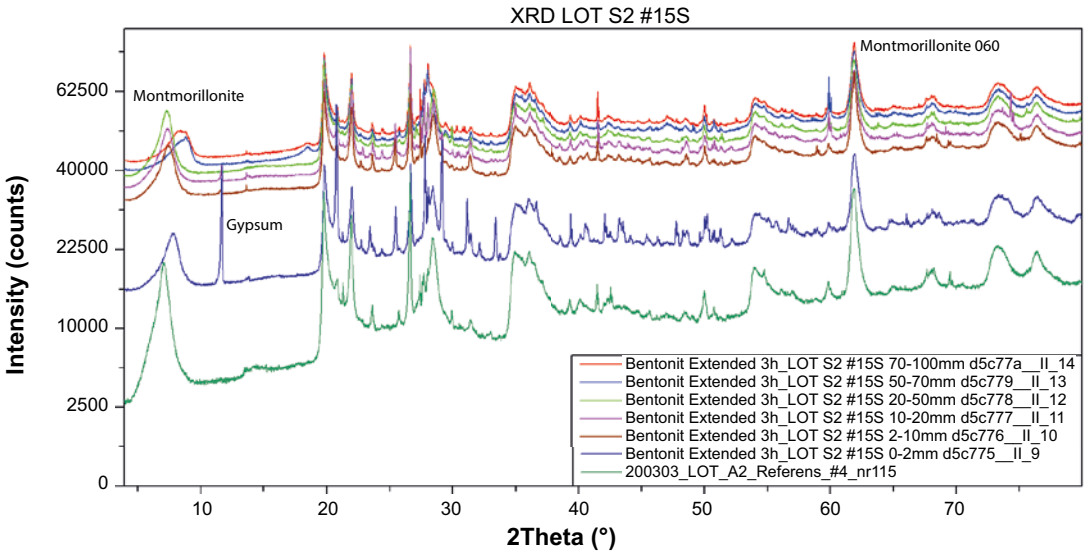

Figure 3-37. *Example of XRD data from a bentonite profile (LOT S2 #15S).*

4 Discussion

In this chapter the findings made during examination of copper and clay samples from LOT S2 and A3 are discussed in the context of copper corrosion in previously retrieved parcels from the LOT series, other repository-like field tests and the general knowledge of copper corrosion in repository-like environments. The discussion is divided in three parts; corrosion products, extent of corrosion, and corrosion morphology.

4.1 Corrosion products

Integrated elemental analysis with SEM-EDS over larger areas (a few mm^2) showed that in general the most common elements on the surfaces of copper coupons and pipes were Cu, O and Si. The level of O varied from 16 to 70 at%, while the level of Si was 3 – 17 at%. The origin of Si was most likely the SiO_2 component of bentonite clay, as some clay was still attached to the copper surfaces when the examination of corrosion products was made. This can also be seen in the level of Al (from the Al_2O_3 component of the bentonite), which was also enhanced in some areas. In areas where bentonite was present, the O signal in the EDS spectra may come from either SiO_2 and/or Al_2O_3 in the bentonite, as well as from copper corrosion products (e.g. Cu_2O) on the surface. In the EDS data for smaller spots on the surfaces using higher magnification, several observations were made where the level of Si was less than 1 at%, and still the level of O was found to be tens of at%, indicating the formation of copper oxide. Applying XRD to the surfaces of the copper coupons confirmed the formation of Cu_2O, which is the main oxide expected as a corrosion product under the initially oxygenated conditions.

The only surface adherent Cu^{2+} corrosion products detected in S2 and A3 were the blue-green deposits under the bottom plates, verified by XRD to contain $Cu_2(OH)_3Cl$ (paratacamite), a compound found on the coupons in the previously retrieved LOT A2, as well as in other intermediate or large-scale field tests (Karnland et al. 2009, Wersin and Kober 2017) and laboratory experiments (Huttunen-Saarivirta et al. 2017). A circumstance that could have affected the formation of Cu^{2+} corrosion products under the bottom plates, is that one of the Ti-tubes (Tube 7 in Figure 1-2) extended into the sand filled space just below the bottom plate, and since the Ti-tubes were open for about four months after installation of the test parcels, the bottom plates may have experienced atmospheric O_2 pressure during this period (and thereby a higher electrochemical potential than other parts of the copper pipe or the coupons). Furthermore, the bottom plate may have been exposed to O_2 for an extended period also after closing the Ti-tubes, since the sand filled hole below the test parcel may still have contained air. A possible explanation for the adherence of $Cu_2(OH)_3Cl$ under the bottom plate could be that there was no interaction between Cu^{2+} and bentonite at this part of the copper surface.

In general, the EDS analysis showed that the level of S on the corroded surfaces was much lower than the level of O. These results are in qualitative agreement with the near surface elemental profiles determined with GDOES. Peaks possibly matching with the diffraction pattern of Cu_2S, were found in the XRD analysis of the coupons. A few observations of enhanced levels of S in small areas were made in the SEM-EDS examination of both the copper coupons and pipes. For coupons A3/K and S2/N, such areas were examined further using HR-TEM and diffraction techniques, which confirmed the formation of an interfacial layer and nanoparticles rich in Cu and S at some locations. Analysis of the Cu:S ratio from EDS data together with the diffraction pattern, suggested that the corrosion product was Cu_2S.

It may be noted that although one coupon of each block (22 and 30) in LOT S2 had been immersed in a bacterial solution before installation (Figure 1-2), there was no obvious difference in the elemental compositions of these surfaces as compared with the other coupons in the same block (Table 3-1 and Appendix C).

In the previously retrieved LOT A2, the level of S on the copper coupons was less than 1 at%, however, only a few spots were analysed with SEM-EDS. Similar to the findings on the coupons in S2 and A3, a nano-particulate phase rich in Cu and S was identified with SEM-EDS in the bentonite close to the copper pipe in A2 (Karnland et al. 2009).

The low levels of S in the corrosion products and surface deposits on copper surfaces in LOT S2 and A3 are ultimately due to the low concentrations of sulfide in the groundwater and the slow diffusion through the compact bentonite clay. The composition of the water from the borehole which provided LOT S2 and A3 with groundwater was measured several times during the experiment. The highest sulfide concentration measured was 0.6 μM in 2001, since then the measured values have been even lower (Table 1-2).

In some of the cross-sectioned samples of coupons S2/N and A3/K, the level of S was too low to analyse its distribution. However, at some locations where the EDS showed higher levels of S, there was a tendency for higher levels of S in the outer parts of the corrosion products. An example from the A3/K coupon is shown in Figure 3-13, which is a detail of a wide pit shown in full in Figure B-17 (Appendix B). The EDS data suggests that the outer part of the surface deposit is a mixture of Cu_2O, Cu_2S, and bentonite, with an S content of 11 to 16 at%. It's possible that the enhanced S content is associated with the particles observed in the deposit, which is similar to what was found in the LOT A2 parcel (Karnland et al. 2009). The level of S decreases towards the copper surface, which can be seen by following the EDS observation spots 1–5, and 6–7 in Figure 3-13.

Another interesting observation was made on a FIB cut sample of coupon A3/K (Figure 3-15). The EDS maps show a clear correlation of Si and O, as expected due to the presence of bentonite clay. A pronounced overlap was also seen between the EDS maps for Cu and S, indicating the formation of a Cu-S phase. It may be noted that this overlap was found both in a layer of ca 250 nm thickness along the copper surface, as well as in particles of diameters < 100 nm in the bentonite clay near the surface. A detailed EDS analysis showed that the outer part of the deposit and the particles were composed of Cu, O and S (spots 54–60 in Figure 3-15), while the deposit near the copper surface was composed of mainly Cu and O (spots 61–67 in Figure 3-15).

Since bentonite contributes to the measured levels of both O (e.g. SiO_2) and S (e.g. $CaSO_4$), the presence of bentonite at many observation spots makes it difficult to analyse the relative distribution of O and S in the corrosion product. However, there are a few spots where the EDS analysis indicates a very low presence of bentonite (i.e. low levels of Si and Al), and where there is still a tendency of higher levels of S near the outer part of the corrosion product. An example of such a region can be seen in Figure C-35 in Appendix C. Examples of corrosion films with very low presence of bentonite and an overall low S:O ratio can also be found in for example Figures C-38 and C-39 (Appendix C).

Using SEM-EDS it was observed that Cu and S were present over more or less the entire surface of bentonite that had been in contact with the coupons, but that the elements did sometimes accumulate at the regions corresponding to the corners of the coupons. One source of S in the EDS spectrum is precipitated $CaSO_4$, which was identified with XRD on a bentonite surface that had been in contact with a copper pipe (Figure 3-35). Nevertheless, EDS line-scans confirmed that Cu and S were associated in stained areas near the corners of the coupons. The line-scans did not indicate any association of Cu and O, but instead showed a strong overlap of Si and O. Although it was not possible to identify any crystalline Cu-S phase with XRD, quantification of Cu and S in the EDS spectra of selected small areas indicated a Cu:S ratio of 1.7–1.8. This can be compared to Cu:S ratios in copper sulfides such as digenite ($Cu_{1.8}S$) djurleite ($Cu_{1.9}S$), and chalcocite (Cu_2S).

Although the oxidation state of the copper measured in the clay herein has not been verified, there are studies implying that the steep part of the copper profiles determined by XRF in the clay near the copper pipes indicate the presence of Cu^{2+}. King et al. (1992, 1997) studied the interaction of copper corrosion products with bentonite clay and showed that the Cu^{2+}:Cu^{+} ratio of the corrosion products depended on the O_2 concentration and the salinity of the pore water. It was suggested that because Na-bentonite clay is a cation-exchange material, positively charged Cu^{2+} species adsorb more strongly than the negatively charged $CuCl_2^-$ complexes formed by Cu^{+}, and therefore a steep copper profile is associated with Cu^{2+}, while the $CuCl_2^-$ complexes are transported further out in the clay. The presence of Cu^{2+} in the clay could mean that the environment in LOT have remained oxidising even after the depletion of O_2, since Cu^{2+} is capable of oxidising metallic copper via the comproportionation of Cu(s) and Cu^{2+} to Cu^{+} (Equation 6).

The observations of corrosion products and their distribution in the corrosion films on copper surfaces and in the bentonite clay, are consistent with the interpretation that the corrosion process at the time of retrieval was in a transient phase, progressing from O_2 driven corrosion to sulfidation. The initially

available O_2 has been the main oxidant behind the corrosion observed, however, that process has probably ceased many years before retrieval due to consumption of O_2 by copper corrosion and other chemical and/or microbial processes in the experimental environment. As a result of O_2 induced corrosion, Cu^{2+} may have prevailed as an intermediate oxidant after depletion of O_2 (Equations 4 to 6). Although the sulfidation of cuprite (Equation 10), and possibly also the sulfide induced corrosion of copper (Equations 7 to 9), has been in progress for several years, sulfur is observed in relatively small amounts on the surfaces and in the corrosion products.

The bulk hydrogen concentrations measured on samples *as received* were around 2.0 (± 0.2) wt-ppm for the S2 pipe and 3.2 (± 0.2) wt-ppm for the A3 pipe. It may be noted that the pipe sample from A3 was darker than the sample from S2, and that grey deposits (likely bentonite) were visible on the surface of the A3 pipe (Figure 2-1). Grinding of the sample surfaces with SiC paper prior to measurement reduced the hydrogen level to ca 0.4 wt-ppm for both S2 and A3, and filing the samples reduced the measured hydrogen below 0.3 wt-ppm. The reduction of the measured hydrogen level after grinding and filing, indicate that the major contribution to the higher levels measured on the samples *as received*, were hydrogen associated with deposits and corrosion products present on the sample surfaces. Similar effects of mechanical surface cleaning have been demonstrated by Granfors (2017). Material from a reference pipe was also analysed and showed similar trends as the experimental pipes. After grinding and filing the measured H level was very low for all samples and there was no significant difference between the H content of the pipes from LOT A3 and S2, as compared with the reference pipe (Table 3-6).

The elemental profiles of the pipe material obtained by GDOES showed slightly enhanced levels of hydrogen in the outer part of the material ca 0 – 2 µm from the surface. At this depth and a few µm deeper, O and Si were enhanced to much higher levels than hydrogen. This shows, in agreement with the interpretation of the bulk measurements, that hydrogen was not enhanced in the copper material itself (above the detection limits of the methods used), but was associated with corrosion products and surface deposits.

4.2 Extent of corrosion

4.2.1 Copper coupons

The mass-losses of the corrosion coupons in LOT S2 and A3 (20 years) corresponded to average corrosion depths of 0.6 – 1.3 µm (Table 3-2). This is slightly less than, but comparable with, what was found for the coupons in the previously retrieved test parcel A2 (6 years), 1.5 – 2.5 µm, which in turn was lower than for the coupons in the pilot test parcels A0 and S1 (ca 1 year), 3.7 – 4.8 µm (Karnland et al. 2009, Johansson 2019). These results can also be compared with ABM 5, a field test very similar to the LOT series, in which the mass-loss of copper specimens corresponded to corrosion depths of 2.3 – 5 µm, within the same test parcel (Gordon et al. 2018b). Analysis of the gravimetric data from LOT and ABM shows that the correlation of corrosion depth with temperature is very weak. For example, the variation in the corrosion depths of the coupons from LOT S2 and A3 is very small although the temperature varied from 25 to 55 °C, and the samples in ABM 5 all had a temperature of ca 80 °C and still their corrosion depths varied several µm. Thus, the variation in gravimetrically determined corrosion depth of coupons within and between the test parcels is probably a reflection of other environmental differences, e.g. regarding the bentonite saturation process and the availability of O_2.

The integrated corrosion rates calculated in the gravimetric analysis of the coupons in LOT S2 and A3 ranged from ca 0.02 to 0.07 µm/y (Table 3-2), which is one or two orders of magnitude lower than for the coupons in previously retrieved parcels from the LOT series, e.g. LOT A2 (Karnland et al. 2009, Johansson 2019). It should be noted that the integrated corrosion rates are calculated for an environment in which the corrosion process has changed over time, starting with O_2 driven corrosion and developing into sulfide induced corrosion. A decrease in the integrated corrosion rate with time is expected, since the major oxidant O_2 was most likely consumed already before the retrieval of the A2 parcel. However, the integrated corrosion rates were calculated by dividing the mass-loss with the whole exposure period of 20 years, and since most of the corrosion of the coupons occurred during the initially oxygenated conditions, these rates are not representative for the long-term corrosion, which is instead expected to be controlled by the diffusion of sulfide through the bentonite clay (SKB 2010b, 2019).

4.2.2 Copper pipes

The corrosion of the copper pipes was measured indirectly from profiles of the copper concentration in the bentonite near the copper surface. The copper concentrations were determined using XRF and the procedure used to estimate the corrosion depth is described in Sections 2.7 and 3.6. In the LOT S2 test parcel, the corrosion depths of hottest parts of the copper pipe (70 – 90 °C) were 3.9 – 4.8 µm, while the corrosion depths of the colder parts of the pipe (20 – 40 °C) were 0.2 – 0.5 µm (Table 3-19). In the LOT A3 test parcel, the corrosion depths of the hottest parts of the copper pipe (100 – 120 °C) were 8.9 – 13.8 µm, while the corrosion depths of the colder parts of the pipe (20 – 40 °C) were 0.2 – 0.6 µm.

In addition to the corrosion depths estimated from the copper concentration in the clay, corrosion products adherent to the copper surface should be accounted for. However, layers of adherent corrosion products on the pipes were less than 1 µm thick (Appendix F), which can be compared with the 350 nm measured on coupon S2/N (Appendix B, Figure B-38). Since the corrosion product has a lower density than the metallic copper, the actual corrosion depth corresponding to the thickness of these layers was even smaller (roughly 70 % of the layer thickness for Cu_2O), i.e. a minor addition to the estimated corrosion depth.

As discussed above for the coupons, integrated corrosion rates are not representative for the long-term corrosion process, simply because most of the corrosion in LOT occurred very early in the experiment when there was still O_2 present. It may be noted, however, that just as when comparing the coupons in A3 (20 years) and A2 (6 years), the integrated corrosion rate of the pipes is also decreasing with time. The hottest part of the pipe in A2 had a maximum corrosion depth of 9.6 µm, which gives an integrated corrosion rate of (9.6/6) 1.6 µm/y, while the hottest part of the pipe in A3 had a maximum corrosion depth of 13.8 µm, corresponding to a rate of (13.8/20) 0.7 µm/y. Turning to the colder parts of the pipes, the integrated corrosion rate in A2 was (0.6/6) 0.1 µm/y, while the corresponding rates for A3 and S2 were 0.01 – 0.03 µm/y. The decrease of the integrated corrosion rates with time is an expected behavior.

In Figure 4-1 the corrosion depths estimated for the copper pipes are plotted versus temperature. This trend is similar to what was found in the LOT A2 parcel, in which the estimated corrosion depth (also derived from the concentration of copper in clay) was 0.6 µm on cold parts of the pipe and varied from 2.2 to 9.6 µm on the hot parts (Wersin 2013). It may be noted that the lower value measured on the hot parts (2.2 µm) was estimated for a sample from which the innermost 1 mm of the clay that had been in contact with the copper pipe had been omitted, and thus, this value is probably underestimating the corrosion at that point. The remaining values varied from 6.7 to 9.6 µm corrosion on the hot part of the pipe in A2.

In this context it is important to recall that the corrosion of the copper coupons in A3 (and S2) was less than in A2, which in turn was less than in the A0 and S1 parcels. This is in itself an indication of that there were some differences in the (initial) conditions among the test parcels of the LOT series that makes it difficult to make direct comparison of the extent of corrosion between the test parcels. Comparison of the corrosion of the pipes from different test parcels, as estimated from the copper concentration in the clay, is further uncertain by the fact that the method is not standardised (as opposite to the gravimetric method) and the results may thus depend on the detailed procedure as well as the laboratory undertaking the measurements.

The copper pipe was initially in direct contact with the air-filled gaps, meaning that O_2 could be transported by gas-phase diffusion and/or convection within and between the gaps. The operation of such transport mechanisms during the unsaturated phase (before saturation and swelling of the clay) has been suggested in earlier studies of full-scale tests (Luterkort et al. 2017). In the LOT test parcels, gas transport between the gaps is further promoted by the sand filled spaces above and below the test parcels. Since this transport mechanism is faster than diffusion through the bentonite, it is likely that temperature dependent corrosion reactions (chemical kinetics) controlled the corrosion, occurring at different rates on colder and hotter parts of the copper surface. It is not known exactly how long it took before these initial gaps were closed, but reaching full saturation and swelling pressure of the bentonite clay took years. For blocks 8 and 14 in LOT A3, near the hottest part of the copper pipe, the process was particularly slow, taking 4 – 6 years to reach the final pressure (Sandén and Nilsson 2020). This can be compared with LOT A2, in which the saturation in blocks 8 and 14 took less than two years (Karnland et al. 2009). This could mean that the copper-bentonite gap closed earlier in A2 than in A3, which could be of importance for the extent of O_2 induced corrosion of the copper pipes, especially at the hot parts (near blocks 8 and 14).

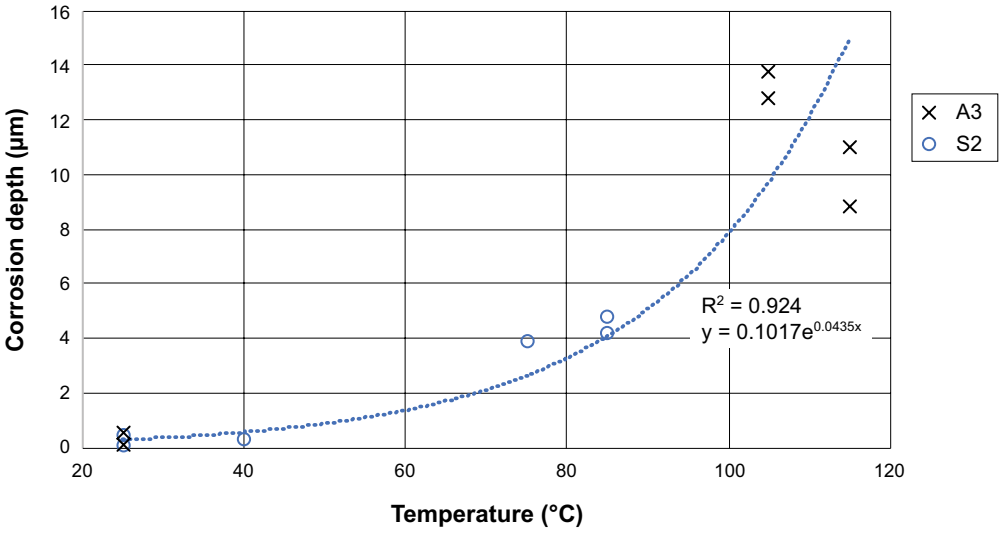

Figure 4-1. *Corrosion depth as a function of temperature for the copper pipes in LOT S2 and A3.*

The corrosion conditions for the two types of copper surfaces, coupons and pipes, were probably quite different, at least initially. While the pipes were in contact with the air-filled spatial gaps initially present at the copper-bentonite and bentonite-rock interfaces, the coupons were embedded in bentonite clay and were not in direct contact with the gas-phase. The corrosion of the coupons was therefore probably limited by diffusion of Cu^+ away from and/or O_2 towards the copper surface through the bentonite clay.

The theoretical limit of O_2 induced corrosion of copper in the LOT experiments can be analysed from a mass-balance perspective. While the groundwater is essentially free of O_2, some O_2 is entrapped in the pore volumes of bentonite clay and sand, as well as in macroscopic gaps in the experimental configuration, i.e. between the rock and bentonite blocks and between the bentonite and the copper pipe. An estimate of the initial O_2-inventory in a typical LOT test parcel is made in Table 4-1. The total air-filled volume is estimated to 69.6 dm^3, which corresponds to 0.65 mol O_2 (initially 15 °C and 1.05 atm pressure at 450 m depth). Under the assumption that the corrosion product is Cu_2O, 1 mole of O_2 consumes 4 moles of copper. With a copper pipe surface area of 1.38 m^2, this amount of O_2 corresponds to average corrosion depth of 13.2 µm for the whole pipe surface.

Table 4-1. Corrosion mass-balance based on estimates of the initial inventory of air volume and O_2 in LOT test parcels.

Air filled voids	Volume[a] (dm^3)	O_2 (mol)	Corrosion depth[b] (µm)
Rock-bentonite gap	36.3	0.34	6.9
Bentonite	19.4	0.18	3.7
Bentonite-copper gap	1.3	0.01	0.2
Sand	12.6	0.12	2.4
Total	69.6	0.65	13.2

[a] Values from Sandén and Nilsson (2020).
[b] Average corrosion depths calculated from mass-balance with O_2 and under the assumption of formation of Cu_2O and a copper surface area of 1.38 m^2.

It should be noted that the estimate above is based on the initial O_2 inventory. The total amount of O_2 available during the experiment is uncertain due to the fact that the seven Ti-tubes used to fill the gaps with groundwater when the measurements were started, were open during the period between installation and start, i.e. ca 4 months in the case of LOT S2 and A3. It is possible that some of the corrosion on the copper pipes occurred during this initial 4 month period in an aerated and humid environment.

After the initially aerated period of 4 month, the Ti-tubes were connected to the support borehole with the aim to fill up the air-filled voids with groundwater (and thus evacuate the gas-phase). Exactly how the water filling process of the rock-bentonite gap occurred is not known, however, the appearance of the bottom plates and the formation of $Cu_2(OH)_3Cl$, suggests that these were exposed to aerobic condi-

tions for a longer period of time. It may thus be that some of the air initially present in the gaps or in the sand porosity remained also after the initial 4 month period and that some of the O_2 was dissolved in the groundwater used to fill the voids. It is noted that when the experiments were started and the heating turned on, the copper pipes may have consumed the residual O_2 quickly since corrosion of copper under heated and aerated conditions in bentonite is rather rapid (Litke et al. 1992).

In LOT S2, the corrosion depths measured on the pipe were on average 4.3 µm on the hot parts and 0.4 µm on the cold parts (Table 3-19). The measured average depths for LOT A3 were 11.6 µm for the hot parts and 0.4 µm for the cold parts. In both test parcels ca 25 % of the pipe surface area was cold (20 – 40 °C), meaning that this part of the pipe surface consumed relatively little O_2. Using the temperature distribution at the pipe surfaces (Figure 1-3) and the temperature dependence of the corrosion depth (Figure 4-1), it is possible to estimate the integrated corrosion depth of the whole pipe surfaces (Appendix K). By this estimate, the average corrosion depth of the pipe in S2 was ca 1.5 µm, while the corresponding value for the pipe in A3 was ca 5.1 µm.

It may be noted that the average corrosion depths of the copper pipes are well supported by the initial O_2 inventory. If one would assume that the bentonite-rock gap and the sand porosity were perfectly filled with groundwater (which seems unlikely considering the observation of $Cu_2(OH)_3Cl$ under the bottom plates), there would still be ca 0.19 mole O_2 left in the bentonite porosity and in the copper-bentonite gap, plus ca 0.03 mole O_2 dissolved in the groundwater filling the air-filled gaps. This would correspond to a corrosion depth of ca 4.3 µm which, regarding the possibility of some corrosion of the pipes during the initial 4 months period, and the uncertainty in the measurements of the copper concentration in the clay, must be regarded as consistent with the interpretation that entrapped O_2 is the main oxidant behind the corrosion observed and measured.

In contrast to what is predicted by established science and thermodynamic data (Beverskog et al. 1997, Kubaschewski and Hopkins 1962, Landolt 2007, Pourbaix 1974, Wranglen 1985), it has been suggested that copper corrodes in pure O_2 free water, i.e. by reactions between copper and water molecules (Hultquist 1986, Hultquist et al. 2015). It is emphasized that this hypothesis can not be evaluated in a complex field test like LOT, first of all because the initially available amount of air (O_2) is of the same order of magnitude as the measured corrosion, but also, because groundwater is not pure water. This hypothesis has instead been thoroughly evaluated in careful laboratory experiments, which have been published in the scientific literature (Hedin et al. 2018, Ottosson et al. 2017).

4.3 Corrosion morphology

The corrosion morphology of copper components in the LOT S2 and A3 test parcels has been evaluated in several ways. The copper coupons have been examined by light optical microscopy (LOM), while selected coupons and pipe samples were cut and examined in cross-section in the SEM. LOM has the advantage that a larger surface area can be examined. Thus, a more representative description of the surface can be made than what is achieved by examination of cross-sections. A disadvantage with LOM is that in order to examine the topography of the underlying metal surface, corrosion products and surface deposits must be removed with chemical methods, which may affect the topography of the surface (Gordon et al. 2018a).

Examination of the coupons using LOM revealed surface defects up to 25 µm deep before removal of the corrosion products. After the removal of corrosion products the deepest defect found was 57 µm. In general, there was a tendency for more and deeper pits after removal of the corrosion products by the method described in Section 3.3.3 (Tables 3-3 and 3-4). It is possible that the pickling method affected the topography of the copper surface, however, it is also possible that before cleaning some pits may have been obscured by, or partially filled with, surface deposits, i.e. corrosion products and/or bentonite clay.

In this context it is important to note that surface defects of tens of µm, in both depth and width, have been observed on newly prepared and polished copper coupons in other experiments. For example, in Gordon et al. (2018a), Cu-OFP was used for the preparation of coupons which were cut from the bulk material using a bandsaw and electro-discharge machining. The coupons were then ground with abrasive paper to a fineness of P4000. Despite the polishing efforts, several defects of 10 – 20 µm depth and a few as deep as 50 – 60 µm, were found when the coupons were examined in LOM. These findings show that defects of this type could be related to cutting and machining the material, or possibly related

to internal defects in the material. Since no surface characterisation was carried out prior to exposure of the coupons in LOT, it is not possible to conclude with certainty how the pits found during examination with LOM are related to the corrosion of the coupons.

Examination of the cross-sectioned samples of coupons and pipes in the SEM, revealed rough interfaces with pits and surface defects densely distributed over the surfaces. This is particularly clear in micrographs taken at lower magnifications, where more extended cross-sections of the surface can be observed, see Figure 4-2 (which is a comparison of micrographs in Figures 3-11 and 3-17). As indicated by the micrographs, the corrosion process has not caused distinct pits in an otherwise unaffected (passive) copper surface, instead the corrosion has acted more or less everywhere on the surface.

The topography observed with SEM within the cross-sections of the coupons was found to be rough with pits and surface defects less than 10 µm deep (Appendix B). In the cross-sections of the pipes samples, pits up to 13 µm depth were found on S2, while pits up to 25 µm were found on the A3 sample (Appendix F). The observation of deeper pits on the A3 pipe could be related to the larger average corrosion depth of the pipe samples, which indicates that the morphology of the interface was caused or affected by the corrosion process. In LOT S2 the temperature at the pipe-clay interface in block 22 was 50 – 60 °C, while the corresponding temperature in LOT A3 was 70 – 80 °C. Although copper in the clay was not analysed for block 22, from which the cross-sectioned samples of the copper pipes were taken, interpolation of the data in Figure 4-1 suggests that the corrosion of the pipe at block 22 was ca 1 µm in S2 and ca 3 µm in A3.

Interpretation of the corrosion morphology observed in LOT S2 and A3 is not straight forward. First of all because, as discussed in the introduction, the experiments were not designed for detailed studies of copper corrosion and therefore the surfaces of the coupons and pipes were not characterised prior to the experimental exposure (Section 1.5).

Here it is appropriate to discuss the corrosion morphology observed in other repository-like field tests and laboratory experiments. In the full-scale Prototype Repository, two canisters were retrieved after 7 years exposure in the Äspö HRL. Analysis of corrosion products showed mainly cuprite (Cu_2O) and malachite ($Cu_2(OH)_2CO_3$) and only traces of sulfur (Taxén et al. 2012). In order to examine the canisters for localised corrosion, 240 cross-sections were made from samples taken at six heights of each canister and examined with SEM in order to count and measure pits and surface defects (Taxén et al. 2013). Among the hundreds of pits and defects observed and measured, the deepest pit found was less than 7 µm deep. The authors also made an extreme value analysis based on the data from the two canisters and estimated that pits up to ca 35 µm could be expected somewhere on the canister surfaces. Since the initial state surface topography of the experiment canisters had not been characterised prior to the start of the experiment, it was not possible to know to what degree the observed topography was related to the actual corrosion process. Metallographic examination of another copper canister, not exposed to the Äspö HRL environment, but stored at SKB's Canister Laboratory, revealed a surface topography that was similar to the Prototype canisters with frequently occurring pits and surface defects up to a few µm deep (Högberg et al. 2017). The surface topography of the canister material is probably due to machining of the surface in the canister manufacturing process, though the surfaces of the Prototype canisters could also have been affected by the subsequent corrosion during exposure in the Äspö HRL.

In the large-scale Febex experiment, two copper coupons were embedded next to each other in bentonite clay and were heated up to ca 100 °C for nearly 18 years (Wersin and Kober 2017). While the mass-loss of one coupon corresponded to an average corrosion depth of ca 9 µm, microscopic examination of another coupon revealed an area with several pit-like features on one side of the coupon. The pits found on cross-sectioned samples examined with SEM, were densely distributed and their lateral extension was comparable with their depths. The largest pit found was ca 100 µm deep and ca 400 µm wide, i.e. one order of magnitude deeper than the average corrosion of the other coupon. The origin of these pits is unclear but it can not be disregarded that they are related to the corrosion process.

In the 5 year long ABM 5 experiment, heated to circa 80 °C for the main period, copper samples were examined for weight-loss and surface topography using optical microscopy (Gordon et al. 2018b). The deepest pit found on a corrosion coupon was 21 µm, however, slightly deeper pits were found on reference specimens kept in a dry indoor environment during the experiment. Comparison of the deepest pits found revealed no statistically significant difference between the corroded and reference specimens. This comparison and microscopic inspection of the pit morphology suggested that the pits found were not caused primarily by the exposure in the Äspö HRL but are rather due to mechanical wear of the sample surfaces during preparation and machining of the samples.

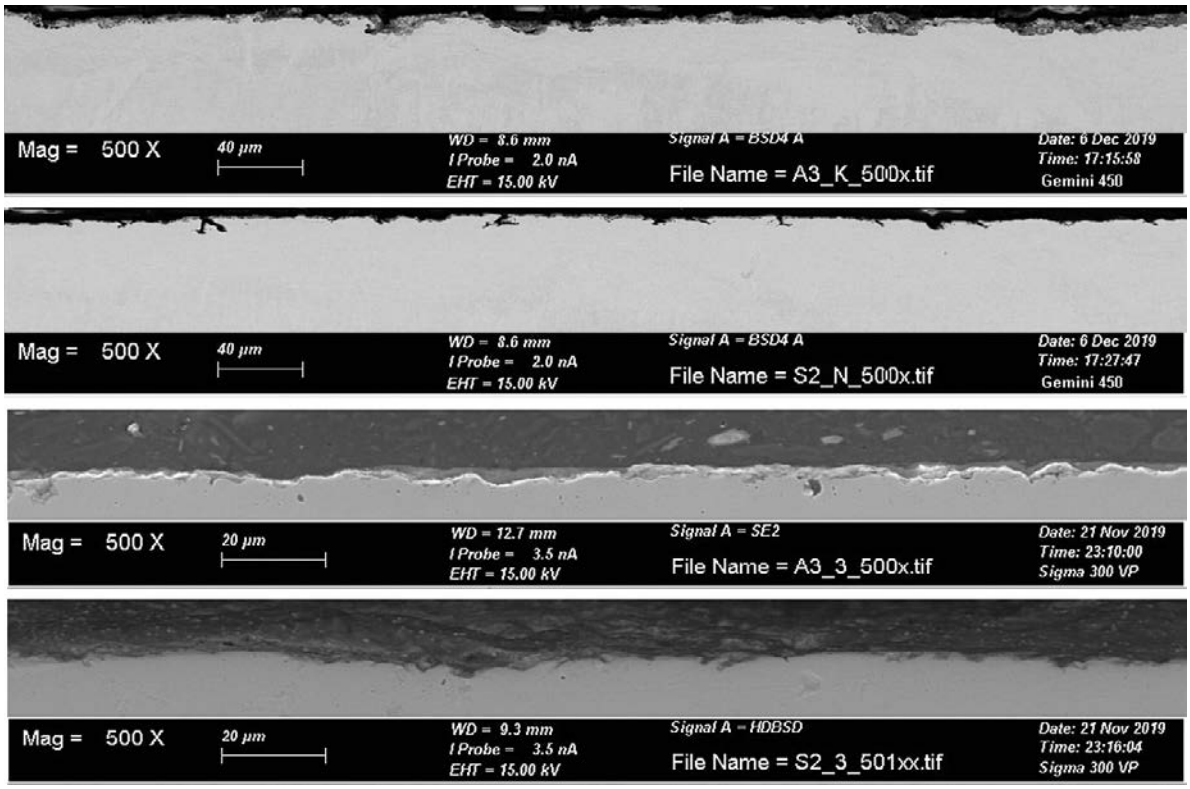

Figure 4-2. *Micrographs of cross-sectioned samples of coupon A3/K (top), coupon S2/N (second from top), pipe from A3 (third from top), and pipe from S2 (bottom).*

In all the field tests mentioned above, as in the test parcels examined herein, O_2 was the dominant oxidant, as evident from the analysis of corrosion products (Karnland et al. 2009, Wersin and Kober 2017, Taxén et al. 2012, Johansson 2019). The pits observed are thus, if at all caused by corrosion, related to the corrosion by O_2 and the formation of oxygen-containing corrosion products. Assessments of localised corrosion of copper in the initially oxygenated repository environment has been made in several steps, using studies of archeological artefacts, literature studies of electrochemical data, and theoretical models (SKB 2010a, King and Lilja 2014). The most recent probabilistic assessment of pit initiation and pit growth shows that the vast majority of pits that would form under (initially oxygenated) repository conditions would be less than 200 µm deep, while there is a small probability for pit growth up to ca 1 mm, depending on the environmental conditions (Briggs et al. 2020). The assessments thus cover any observations of pits made on copper specimens from various field tests, despite the uncertainty of their exact origin (corrosion and/or mechanical wear). In this context it is also important to remember that corrosion by O_2 is a finite process in a repository (SKB 2010b), as well as in repository-like field tests, and that the long-term corrosion behaviour of the copper material is instead determined by the sulfide corrosion of copper.

The corrosion morphology of copper in anoxic sulfide environments has been studied extensively over the years. A common experience is that the copper sulfide films formed are porous and non-protective (Sharma 1980), and thus support active and general corrosion of copper (Chen et al. 2010, 2011, Gordon et al. 2018a). Passivity, which is a requirement for pitting, is not achieved under natural corrosion conditions but requires applied potentials and high sulfide fluxes, which can only be upheld with a rotating electrode (Martino et al. 2014). Another mechanism for localised corrosion in sulfide solutions has been identified and attributed to micro-galvanic coupling between large Cu_2S grains and the copper surface, however, this mechanism requires very high sulfide fluxes that are not possible to uphold in compact bentonite clay (Chen et al. 2017, 2018, 2019, SKB 2019). It is thus unlikely that the minor copper sulfide formation observed in LOT S2 and A3 had any significant influence on the corrosion morphology in these experiments.

5 Conclusions

Corrosion of copper components from the experiment Long-term test of buffer materials (LOT), test parcels S2 and A3, have been examined after 20 years heating and exposure to the bentonite-groundwater environment at 450 m depth in the Äspö Hard Rock Laboratory. The experiments were aimed to study the long-term behaviour of bentonite clay in a heated repository-like environment, and are thus not ideally designed for detailed and quantitative evaluation of copper corrosion. For example, the development of the redox environment has not been monitored, and the copper surfaces were not characterised before exposure (see further Section 1.5). Nevertheless, two types of copper components were examined after retrieval of the LOT S2 and A3 test parcels, pipes which contained the heaters of the experiments, and coupons prepared for gravimetric analysis in order to quantify the extent of copper corrosion for the bentonite analysis. The bentonite clay in contact with the copper specimens has also been examined in order to make an indirect estimate of the corrosion of the pipe surfaces via the copper concentration profile in the clay. The following conclusions were made regarding the nature and extent of copper corrosion in these test parcels:

- Elemental analysis using SEM-EDS showed that Cu and O were the main constituents of the copper surfaces of both coupons and pipe samples. Elements from the bentonite clay (Si, Al) were also identified, as well as smaller amounts of S. Analysis with XRD confirmed that the main corrosion product on the copper coupons was Cu_2O (cuprite). However, weaker peaks, possibly corresponding with of Cu_2S (chalcocite), were also identified. Examination of cross-sectioned samples with SEM-EDS confirmed that the corrosion film had a generally low content of S. However, at some locations in the cross-sectioned samples of both coupons and pipes, EDS indicated higher levels of S (> 10 at%). Further examination of selected cross-sections of the coupons with TEM and EDS showed layers and nanoparticles with a Cu:S ratio close to Cu_2S. In the examination of bentonite clay that had been in contact with the coupons, some locations analysed with EDS were found to have a Cu:S ratio very close to Cu_2S, however, this could not be confirmed with XRD, possibly because the Cu_xS phase was amorphous. The examination of corrosion products suggests that the corrosion process, at the time of retrieval, was in a transient phase, in which corrosion by O_2 had ceased, while the sulfidation of Cu_2O was ongoing.
- The elemental distribution profile of the copper pipe material, as determined with GDOES, was dominated by O near the surface of the pipe samples. The levels of S and Si were also enhanced in the near surface profile, albeit to much lower levels than O. Both O and Si were enhanced to a depth of a few µm into the material. The level of H was also slightly enhanced near the surface, however, the enhancement of H occurred only within a depth where elements from corrosion products (O, S) and bentonite deposits (Si, O) were enhanced as well and to much higher levels than H. In agreement with the elemental profiles, measurements of the bulk hydrogen content of the pipe sample material showed very low H levels in samples where corrosion products and surface deposits were removed by grinding and/or filing. There was thus no indication of uptake of H in the copper material itself.
- The gravimetric analyses showed that the corrosion of the coupons was similar in the two test parcels, with an average mass loss corresponding to 1.0 (± 0.5) µm corrosion in S2 and 1.1 (± 0.2) µm in A3. Considering the variation found in mass loss of coupons from previously retrieved parcels from the LOT series (mass loss corresponding to 1.5 – 4.8 µm corrosion) and the similar ABM 5 experiment (2.3 – 5 µm), it is clear that there were differences in the experimental conditions both within and between the test parcels.
- Examination of the copper content of the bentonite clay that had been in contact with the heated copper pipes was used to estimate the corrosion depth of the pipe surfaces. The corrosion depths measured on the pipe from S2 were on average 4.3 µm on the hot parts and 0.4 µm on the cold parts. On average the corrosion of the whole S2 pipe surface may have been ca 2 µm. The corrosion depths measured on the pipe from A3 were on average 11.6 µm on the hot parts and 0.4 µm on the cold parts, and the A3 pipe surface may have had an average corrosion depth of ca 5 – 6 µm. Estimates of the initially available volume of air in macroscopic gaps and porous materials in the test parcels, were consistent with the interpretation that entrapped O_2 is the main oxidant behind the corrosion.

- Although the copper surfaces had not been characterised prior to the experiment, attempts were made to shed some light on the corrosion morphology. Examination using light optical microscopy over larger parts of the coupon surfaces revealed pits and surface defects of ca 10 – 60 µm after the removal of corrosion products during the gravimetric analysis. However, since the reference coupons also had plenty of pits reaching up to ca 30 µm in depth, and since surface defects up to ca 60 µm have been found on newly prepared copper coupons in earlier studies, the relation of these pits to the corrosion process in the LOT experiment is unclear. Micrographs of cross-sectioned samples of both the coupons and the pipes revealed rough interfaces, with shallow pits densely distributed over a generally corroded copper surface. The deepest pits found on the cross-sectioned coupons were ca 10 µm, while the deepest pit found on the pipes was ca 25 µm. Since the initial state of the copper surfaces was not characterised, it is unclear exactly how the observed morphology is related to the corrosion process. However, if interpreted as effects of localised corrosion, these observations are fully consistent with earlier studies and assessments of localised corrosion of copper under the initially oxygenated conditions in a repository environment.

References

SKB's (Svensk Kärnbränslehantering AB) publications can be found at www.skb.com/publications. SKBdoc documents will be submitted upon request to document@skb.se.

Beverskog B, Puigdomenech I, 1997. Revised Pourbaix diagrams for copper at 25 to 300 °C. Journal of The Electrochemical Society 144, 3476–3483.

Birgersson M, Goudarzi R, 2018. Investigations of gas evolution in an unsaturated KBS-3 repository. SKB TR-18-11, Svensk Kärnbränslehantering AB.

Briggs S, Lilja C, King F, 2020. Probabilistic model for pitting of copper canisters. Materials and Corrosion. doi:10.1002/maco.202011784

Chen J, Qin Z, Shoesmith D W, 2010. Kinetics of corrosion film growth on copper in neutral chloride solutions containing small concentrations of sulfide. Journal of the Electrochemical Society 157, C338–C345.

Chen J, Qin Z, Shoesmith D W, 2011. Long-term corrosion of copper in a dilute anaerobic sulfide solution. Electrochimica Acta 56, 7854–7861.

Chen J, Qin Z, Martino T, Shoesmith D W, 2017. Non-uniform film growth and micro/macro-galvanic corrosion of copper in aqueous sulfide solutions containing chloride. Corrosion Science 114, 72–78.

Chen J, Qin Z, Martino T, Guo M, Shoesmith D W, 2018. Copper transport and sulfide sequestration during copper corrosion in anaerobic aqueous sulfide solutions. Corrosion Science 131, 245–251.

Chen J, Guo M, Martino T, Ramamurthy S, Noël J J, Shoesmith D W, Lilja C, Johansson A J, 2019. The distribution of corrosion damage to copper surfaces exposed to aqueous sulfide solutions. SKBdoc 1706406 ver 1.0, Svensk Kärnbränslehantering AB.

Giroud N, 2014. FEBEX – assessment of redox conditions in phase 2 before dismantling. Nagra Arbeitsbericht NAB 14-55, Nagra, Switzerland.

Gordon A, Pahverk H, Börjesson E, Sjögren L, Karlsson O, Bergqvist H, Lindberg F, Johansson A J, 2018a. Corrosion morphology of copper in anoxic sulfide environments. SKB TR-18-14, Svensk Kärnbränslehantering AB.

Gordon A, Pahverk H, Börjesson E, Johansson A J, 2018b. Examination of copper corrosion specimens from ABM 45, package 5. SKB TR-18-17, Svensk Kärnbränslehantering AB.

Grandia F, Domènech C, Arcos D, Duro L, 2006. Assessment of the oxygen consumption in the backfill. Geochemical modelling in a saturated backfill. SKB R-06-106, Svensk Kärnbränslehantering AB.

Granfors M, 2017. Round-robin of hydrogen content in copper determined by melt extraction and gas analysis. SKB R-17-15, Svensk Kärnbränslehantering AB.

Hedin A, Johansson A J, Lilja C, Boman M, Berastegui P, Berger R, Ottosson M, 2018. Corrosion of copper in pure O_2-free water? Corrosion Science 137, 1–12.

Hollmark H M, Keech P G, Vegelius J R, Werme L, Duda L-C, 2012. X-ray absorption spectroscopy of electrochemically oxidized Cu exposed to Na_2S. Corrosion Science 54, 85–89.

Hultquist G, 1986. Hydrogen evolution in corrosion of copper in pure water. Corrosion Science 26, 173–177.

Hultquist G, Graham M J, Kodra O, Moisa S, Liu R, Bexell U, Smialek J L, 2015. Corrosion of copper in distilled water without O_2 and the detection of produced hydrogen. Corrosion Science 95, 162–167.

Huttunen-Saarivirta E, Rajala P, Bomberg M, Carpén L, 2017. EIS study on aerobic corrosion of copper in ground water: influence of micro-organisms. Electrochimica Acta 240, 163–174.

Högberg C-J, Karlsson O, Randelius M, Johansson A J, 2017. Surface morphology and elemental composition of copper canisters for disposal of spent nuclear fuel. SKB P-17-11, Svensk Kärnbränslehantering AB.

Johansson A J, 2019. Corrosion of copper in repository-like field tests: compilation and analysis of data. SKBdoc 1713264 ver 1.0, Svensk Kärnbränslehantering AB.

Karnland O, Sandén T, Johannesson L-E, Eriksen T, Jansson M, Wold S, Pedersen K, Motamedi M, Rosborg B, 2000. Long term test of buffer material. Final report on the pilot parcels. SKB TR-00-22, Svensk Kärnbränslehantering AB.

Karnland O, Olsson S, Dueck A, Birgersson M, Nilsson U, Hernan-Håkansson T, Pedersen K, Nilsson S, Eriksen T, Rosborg B, 2009. Long term test of buffer material at the Äspö Hard Rock Laboratory, LOT project. Final report on the A2 test parcel. SKB TR-09-29, Svensk Kärnbränslehantering AB.

Karnland O, Olsson S, Sandén T, Fälth B, Jansson M, Eriksen T, Svärdström K, Rosborg B, Muurinen A, 2011. Long term test of buffer material at the Äspö HRL, LOT project. Final report on the A0 test parcel. SKB TR-09-31, Svensk Kärnbränslehantering AB.

King F, Lilja C, 2014. Localised corrosion of copper canisters. Corrosion Engineering, Science and Technology 49, 420–424.

King F, Litke C D, Ryan S R, 1992. A mechanistic study of the uniform corrosion of copper in compacted Na-montmorillonite/sand mixtures. Corrosion Science 33, 1979–1995.

King F, Ryan S R, Litke C D, 1997. The corrosion of copper in compacted clay. AECL-11831, AECL, Canada.

King F, Lilja C, Pedersen K, Pitkänen P, Vähänen M, 2010. An update of the state-of-the-art report on the corrosion of copper under expected conditions in a deep geologic repository. SKB TR-10-67, Svensk Kärnbränslehantering AB.

King F, Lilja C, Vähänen M, 2013. Progress in the understanding of the long-term corrosion behaviour of copper canisters. Journal of Nuclear Materials 438, 228–237.

King F, Chen J, Qin Z, Shoesmith D, Lilja C, 2017. Sulfide-transport control of the corrosion of copper canisters. Corrosion Engineering, Science and Technology 52, 210–216.

Kristiansen P T, Massel F, Werme L, Lilja C, Duda L-C, 2015. Sulfidation of single-phase oxide on copper and as powder studied using soft x-ray spectroscopy. Journal of The Electrochemical Society 162, C785–C791.

Kubaschewski O, Hopkins B E, 1962. Oxidation of metals and alloys. 2nd ed. London: Butterworths.

Landolt D, 2007. Corrosion and surface chemistry of metals. Lausanne: EPFL Press.

Lazo C, Karnland O, Tullborg E-L, Puigdomenech I, 2003. Redox properties of MX-80 and Montigel bentonite-water systems. In Finch R J, Bullen D B (eds). Scientific Basis for Nuclear Waste Management XXVI. Warrendale, PA: Materials Research Society. (Materials Research Society Symposium Proceedings 757), II8.1.

Litke C D, Ryan S R, King F, 1992. A mechanistic study of the uniform corrosion of copper in compacted clay and soil. AECL-10397, AECL, Canada.

Luterkort D, Johannesson L-E, Eriksson P, 2017. Buffer design and installation method. Installation report. SKB TR-17-06, Svensk Kärnbränslehantering AB.

Martino T, Partovi-Nia R, Chen J, Qin Z, Shoesmith D W, 2014. Mechanisms of film growth on copper in aqueous solutions containing sulfide and chloride under voltammetric conditions. Electrochimica Acta 127, 439–447.

Muurinen A, Carlsson T, 2010. Experience of pH and Eh measurements in compacted MX-80 bentonite. Applied Clay Science 47, 23–27.

Ottosson M, Boman M, Berastegui P, Andersson Y, Hahlin M, Korvela M, Berger R, 2017. Copper in ultrapure water, a scientific issue under debate. Corrosion Science 122, 53–60.

Pourbaix M, 1974. Atlas of electrochemical equilibria in aqueous solutions. 2nd ed. Houston, TX: National Association of Corrosion Engineers.

Rosborg B, 2013. Post-test examination of a copper electrode from deposition hole 5 in the Prototype Repository. SKB R-13-14, Svensk Kärnbränslehantering AB.

Sandén T, Nilsson U, 2020. Installation, monitoring, dismantling and initial analyzes of material from LOT test parcel S2 and A3. Results from field test. SKB TR-20-11, Svensk Kärnbränslehantering AB.

Sandén T, Nilsson U, Andersson L, Svensson D, 2018. ABM45 experiment at Äspö Hard Rock Laboratory. Installation report. SKB P-18-20, Svensk Kärnbränslehantering AB.

Sharma S P, 1980. Reaction of copper and copper oxide with H_2S. Journal of The Electrochemical Society 127, 21–26.

SKB, 2010a. Fuel and canister process report for the safety assessment SR-Site. SKB TR-10-46, Svensk Kärnbränslehantering AB.

SKB, 2010b. Corrosion calculations report for the safety assessment SR-Site. SKB TR-10-66, Svensk Kärnbränslehantering AB.

SKB, 2019. Supplementary information on canister integrity issues. SKB TR-19-15, Svensk Kärnbränslehantering AB.

Smart N, Reddy B, Nixon D, Rance A, Johansson A J, 2015. A Miniature Canister (MiniCan) Corrosion experiment. Progress report 5 for 2008–2013. SKB P-14-19, Svensk Kärnbränslehantering AB.

Smith J, Qin Z, Shoesmith D W, King F, Werme L, 2004. Corrosion of copper nuclear waste containers in aqueous sulfide solutions. In Hanchar J M, Stroes-Gascoyne S, Browning L (eds). Scientific Basis for Nuclear Waste Management XXVIII: symposium held in San Francisco, California, USA, 13 – 16 April 2004. Warrendale, PA: Materials Research Society. (Materials Research Society Symposium Proceedings 824)

Smith J, Qin Z, King F, Werme L, Shoesmith D W, 2007a. Sulfide film formation on copper under electrochemical and natural corrosion conditions. Corrosion 63, 135–144.

Smith J, Wren J C, Odziemkowski M, Shoesmith D W, 2007b. The electrochemical response of preoxidized copper in aqueous sulfide solutions. Journal of The Electrochemical Society 154, C431–C438.

Stenlid J H, Johansson A J, Leygraf C, Brinck T, 2017. Computational analysis of the early stage of cuprous oxide sulfidation: a top-down process. Corrosion Engineering, Science and Technology 52, 50–53.

Svensson, D, Eriksson, P, Johannesson, L-E, Lundgren, C, Bladström, T, 2019. Development and testing of methods suitable for quality control of bentonite as KBS-3 buffer and backfill. SKB TR-19-25, Svensk Kärnbränslehantering AB.

Taxén C, Lundholm M, Person D, Jakobsson D, Sedlakova M, Randelius M, Karlsson O, Rydgren P, 2012. Analyser av koppar från prototypkapsel 5 och 6. SKB P-12-22, Svensk Kärnbränslehantering AB.

Taxén C, 2013. Ytprofiler på kopparkapslar från deponeringshål 5 och 6 i försöksserien Prototyp. SKB P-13-50, Svensk Kärnbränslehantering AB.

Wersin P, 2013. LOT A2 test parcel. Compilation of copper data in the LOT A2 test parcel. SKB TR-13-17, Svensk Kärnbränslehantering AB.

Wersin P, Kober F (eds), 2017. FEBEX-DP. Metal corrosion and iron-bentonite interaction studies. Nagra Arbeitsbericht NAB 16-16, Nagra, Switzerland.

Wranglén G, 1985. An introduction to corrosion and protection of metals. 2nd rev. ed. Dordrecht: Springer.

Åkesson M, Svensson D, Laitinen H, 2020. Gas phase composition during the unsaturated period – initial tests. SKB P-20-23, Svensk Kärnbränslehantering AB.

Appendix A

A1 As-received samples

A1.1 Corrosion coupons

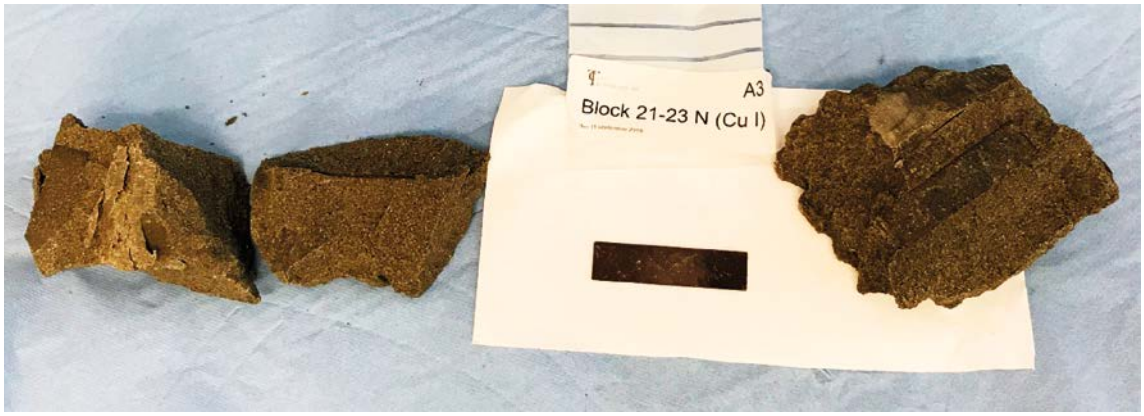

Figure A-1. *Corrosion coupon A3/I with surrounding bentonite clay.*

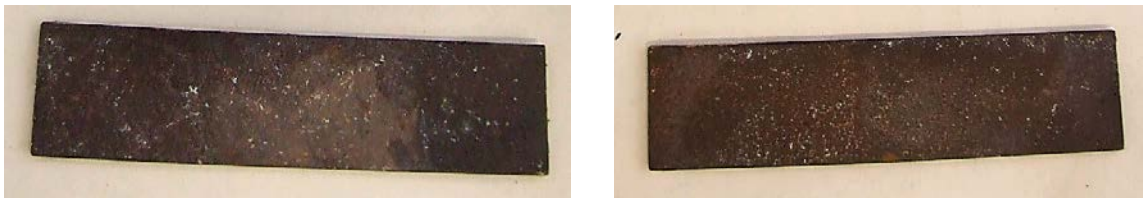

Figure A-2. *Corrosion coupon A3/I, left: milled side; right: polished side.*

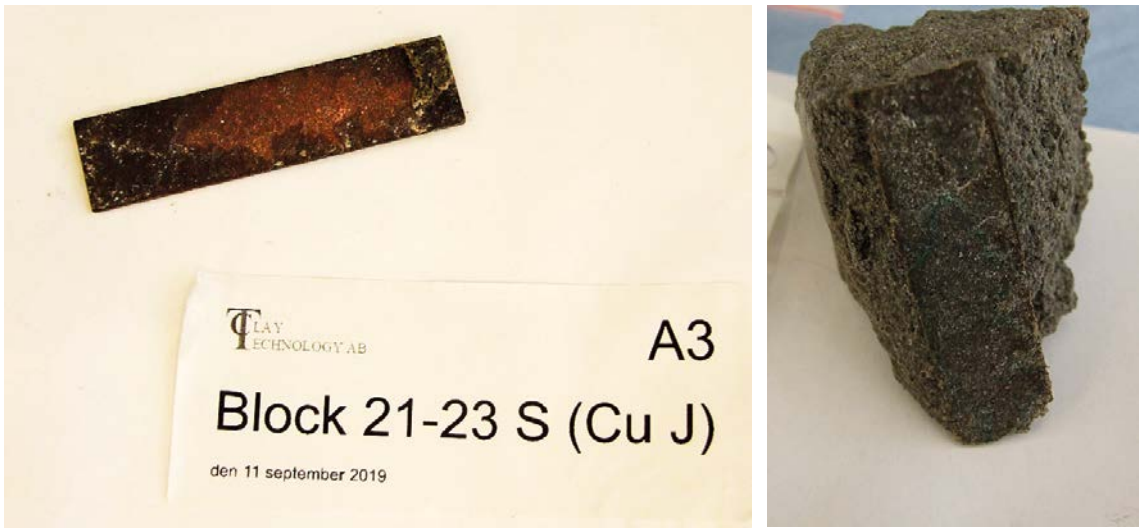

Figure A-3. *Corrosion coupon A3/J with surrounding bentonite clay.*

Figure A-4. *Corrosion coupon A3/K with surrounding bentonite clay.*

Figure A-5. *Corrosion coupon A3/L with surrounding bentonite clay.*

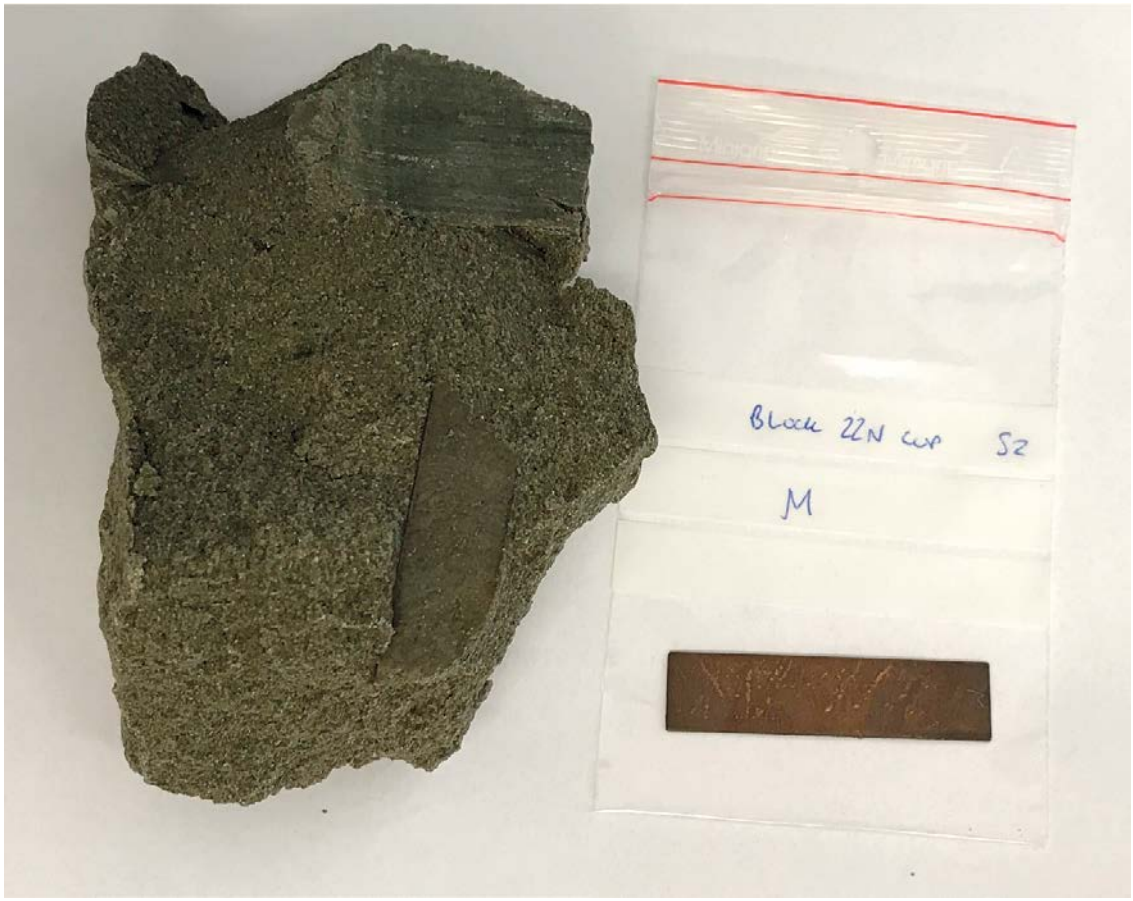

Figure A-6. *Corrosion coupon S2/M with surrounding bentonite clay.*

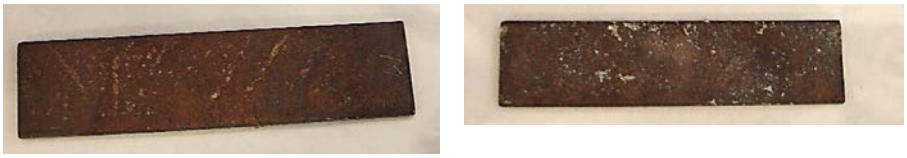

Figure A-7. *Corrosion coupon S2/M, left: milled side; right: polished side.*

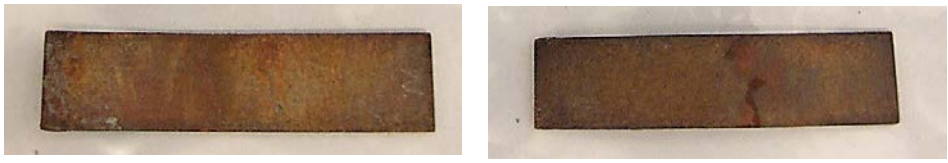

Figure A-8. *Corrosion coupon S2/N, left: milled side; right: polished side.*

Figure A-9. *Corrosion coupon S2/O, left: milled side; right: polished side.*

Figure A-10. *Corrosion coupon S2/P, left: milled side; right: polished side.*

Figure A-11. *Reference coupons K and L as-received, left: milled side, right: polished side.*

A1.2 Pipe samples

Figure A-12. *Pipe sample A3 as-received, photographed at 0º, 90º, 180º, 270º rotation.*

Figure A-13. *Pipe sample A3 inner surfaces as-received.*

Figure A-14. *Pipe sample S2 as-received, photographed at 0º, 90º, 180º, 270º rotation.*

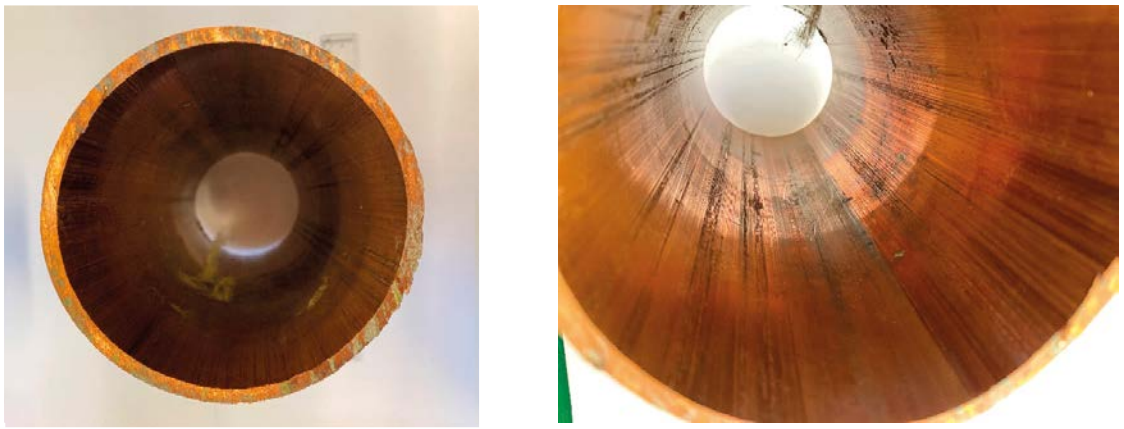

Figure A-15. *Pipe sample S2 inner surfaces as-received.*

Figure A-16. *Left: Condition of the reference pipe sample as received. Right: Positions of reference pipe samples that were extracted for H and O analysis.*

Appendix B

SEM images of corrosion coupons

The following images show the surfaces of the corrosion coupons examined under the SEM with varying magnifications. These are followed by micrographs showing the cross-sectioned samples of coupons A3/K and S2/N. Pits and defects observed in these micrographs were measured manually on the images. A second cross-section was examined for each of the coupons A3/K and S2/N in order to visualize the distribution of pits and defects over the coupon surfaces.

The images contain a file name in the lower right-hand corner, which denotes which test package they originate from (A3 or S2), which block they were located in (22 or 30) and a one letter identification for each coupon (e.g. Cu J). For example, A3_21-23N_Cu I_1000x denotes test parcel A3, block 22 (in between 21 and 23) direction north, coupon I, and magnification 1000x.

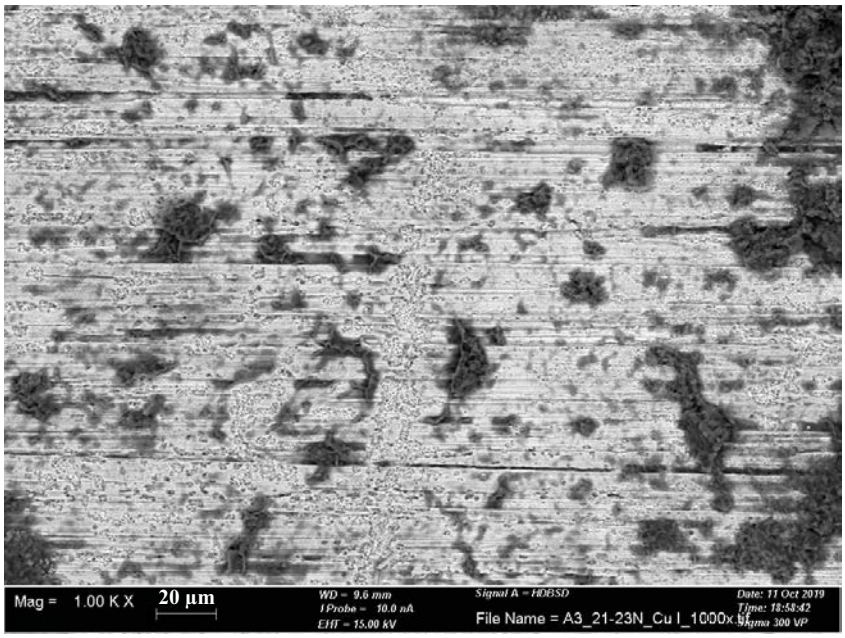

Figure B-1. *SEM image of coupon A3/I.*

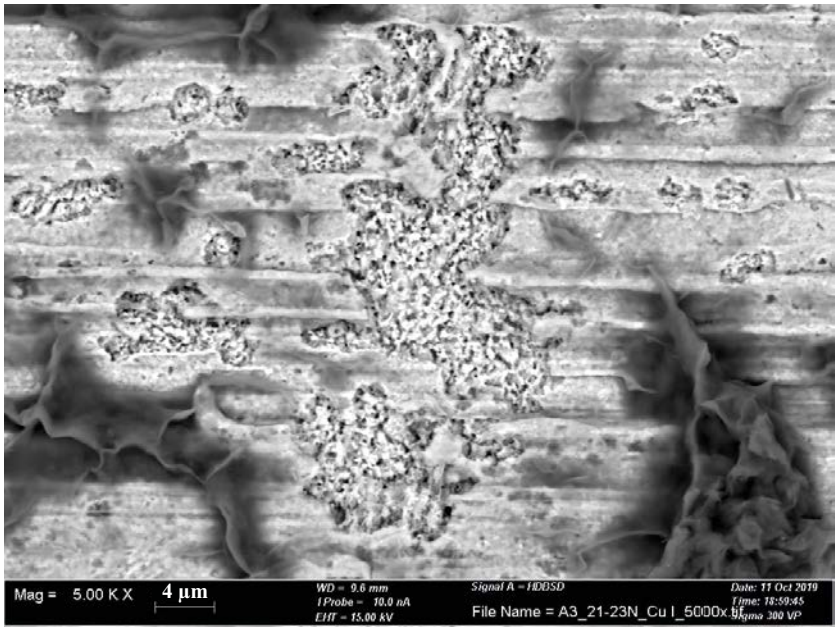

Figure B-2. *SEM image of coupon A3/I.*

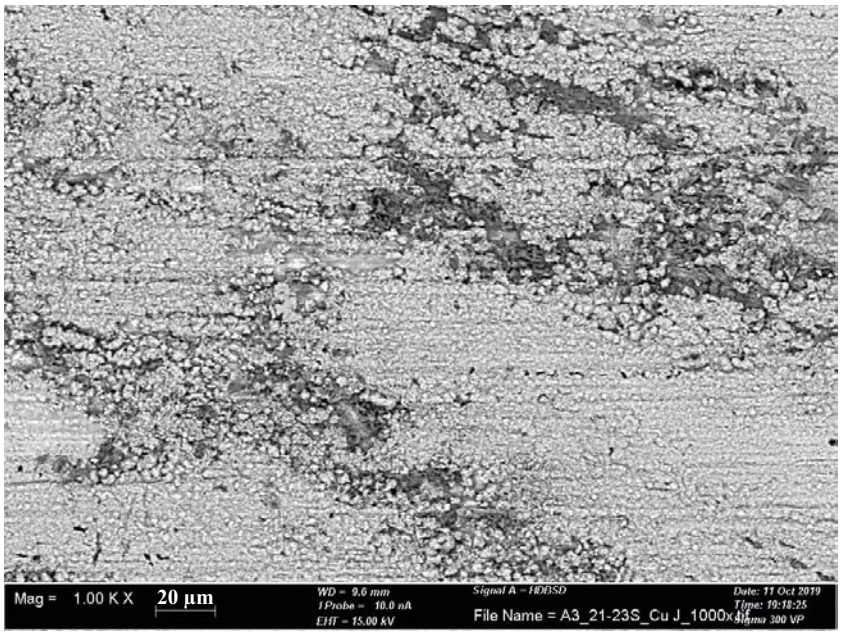

Figure B-3.
SEM image of coupon A3/J.

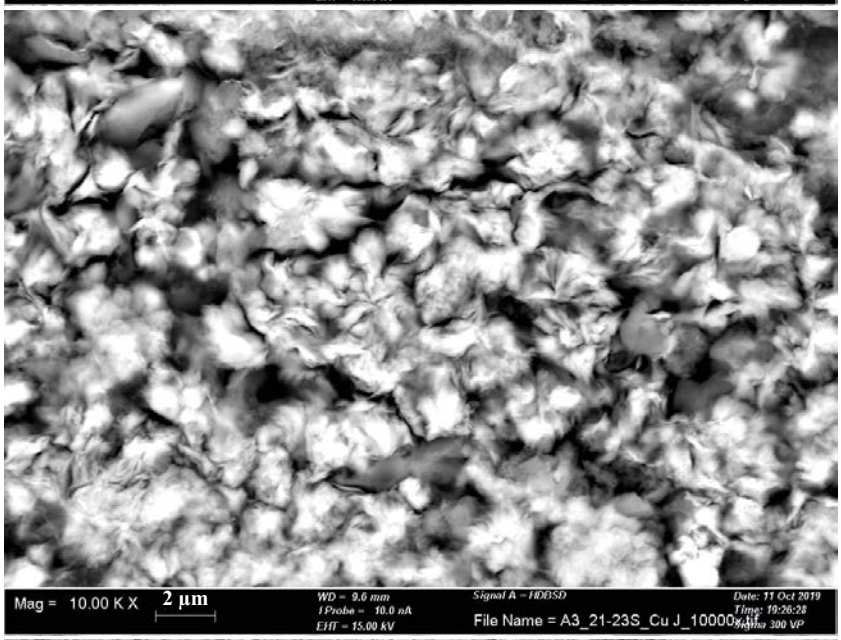

Figure B-4.
SEM image of coupon A3/J.

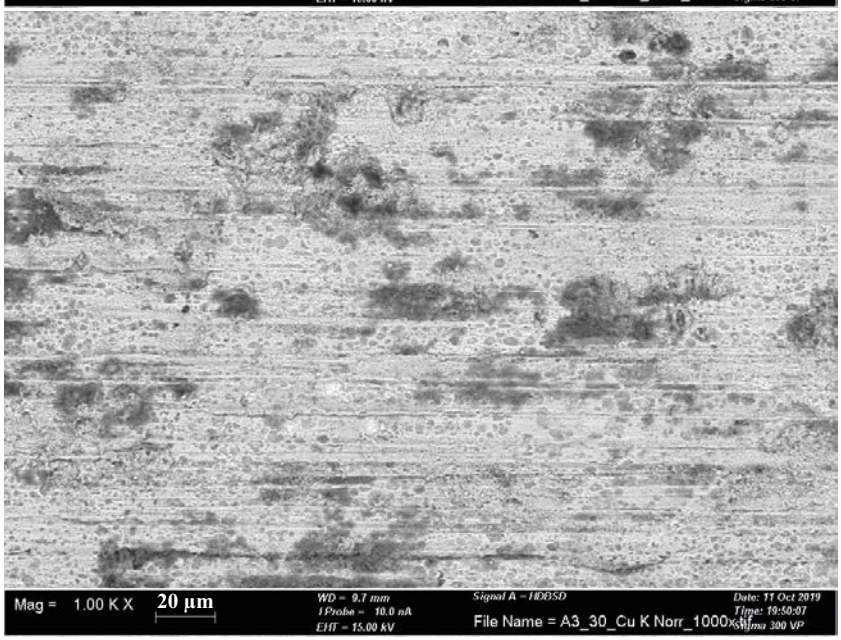

Figure B-5.
SEM image of coupon A3/K.

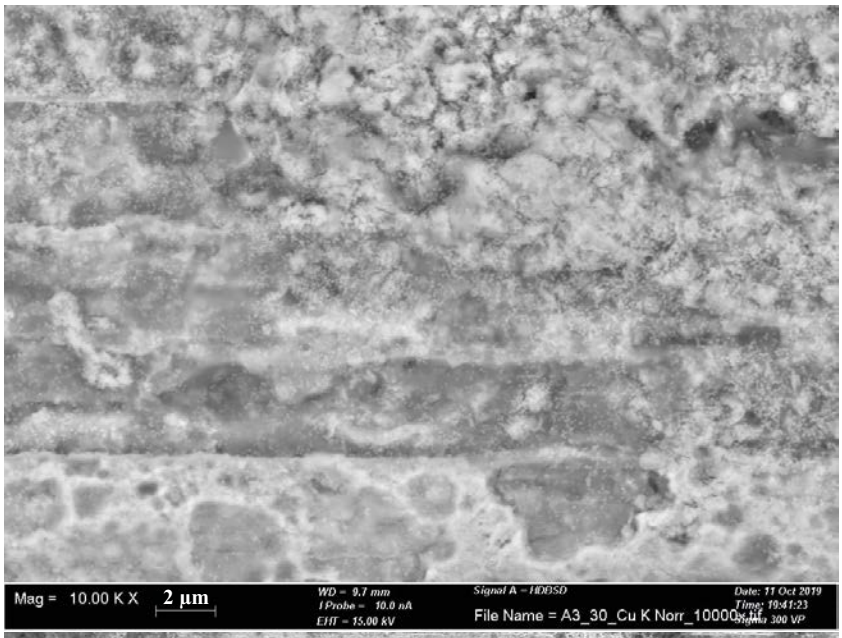

Figure B-6. *SEM image of coupon A3/K.*

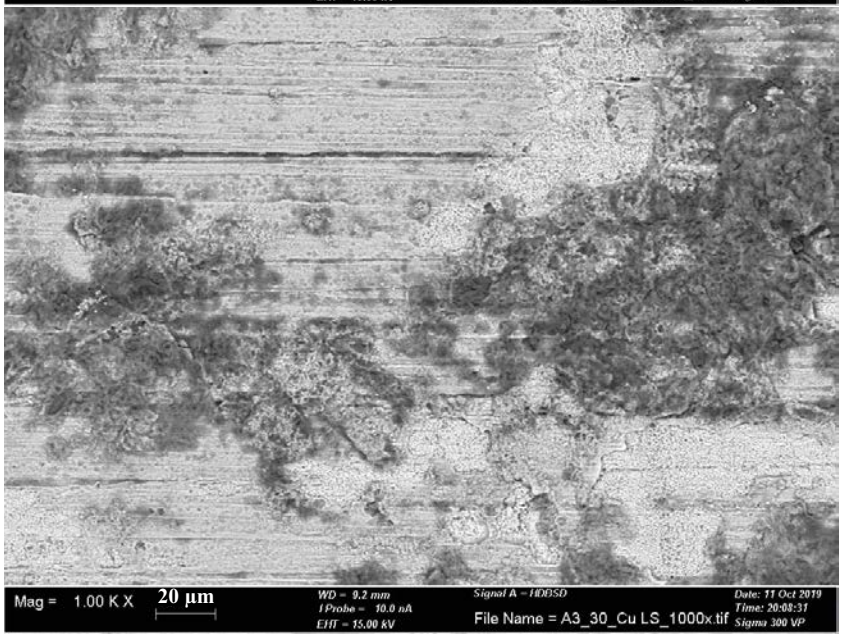

Figure B-7. *SEM image of coupon A3/L.*

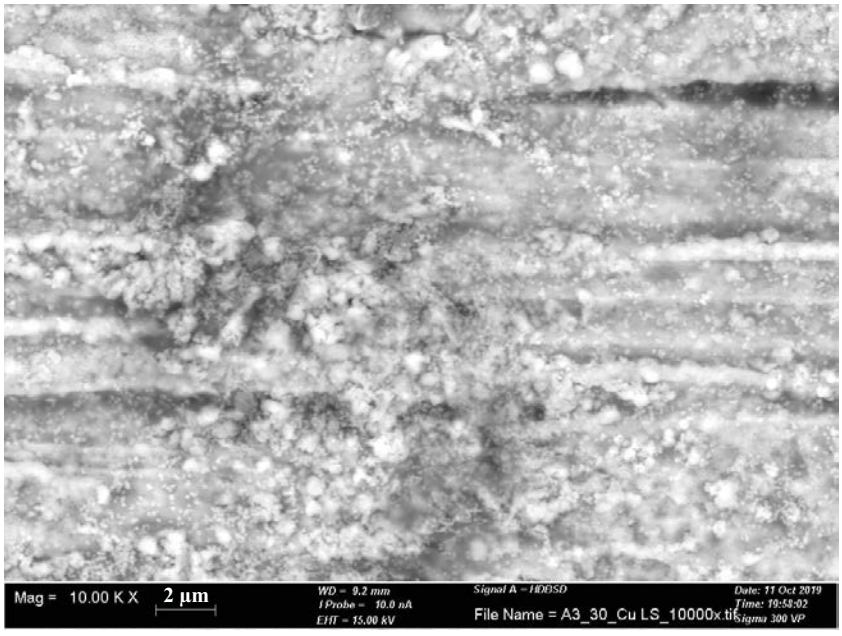

Figure B-8. *SEM image of coupon A3/L.*

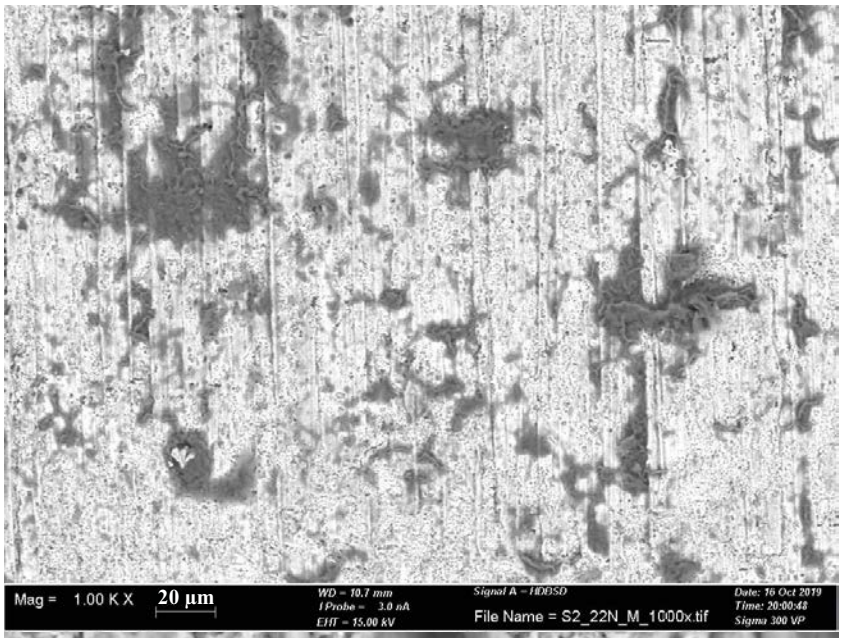

Figure B-9.
SEM image of coupon S2/M.

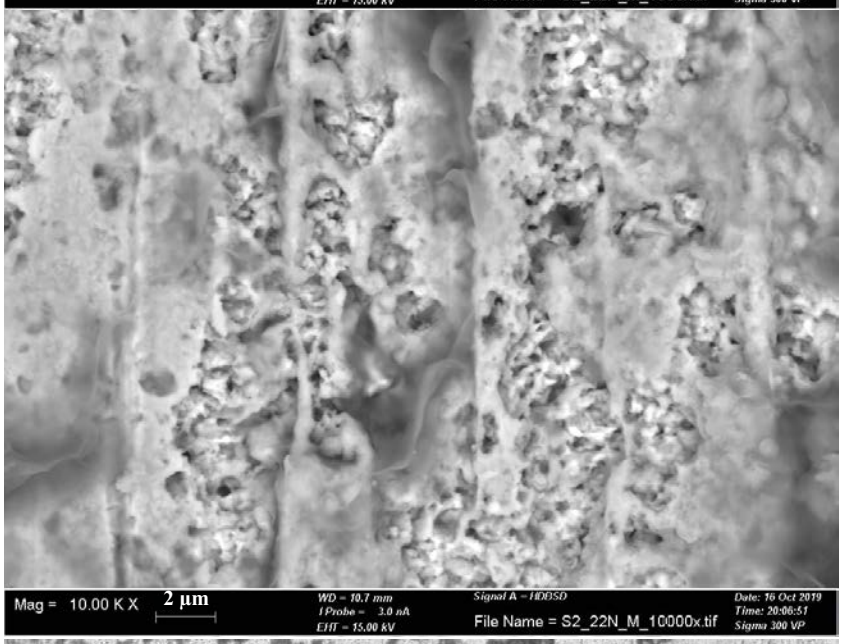

Figure B-10.
SEM image of coupon S2/M.

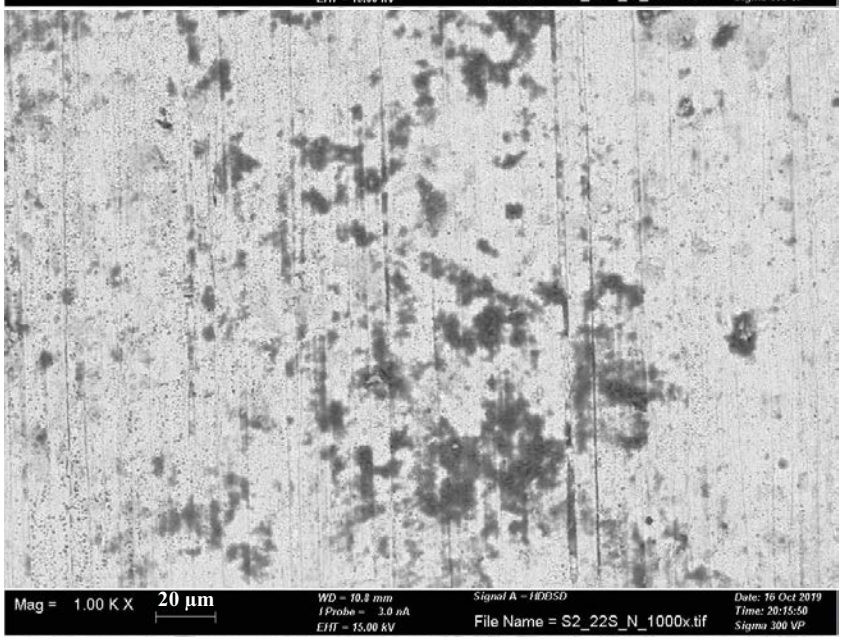

Figure B-11.
SEM image of coupon S2/N.

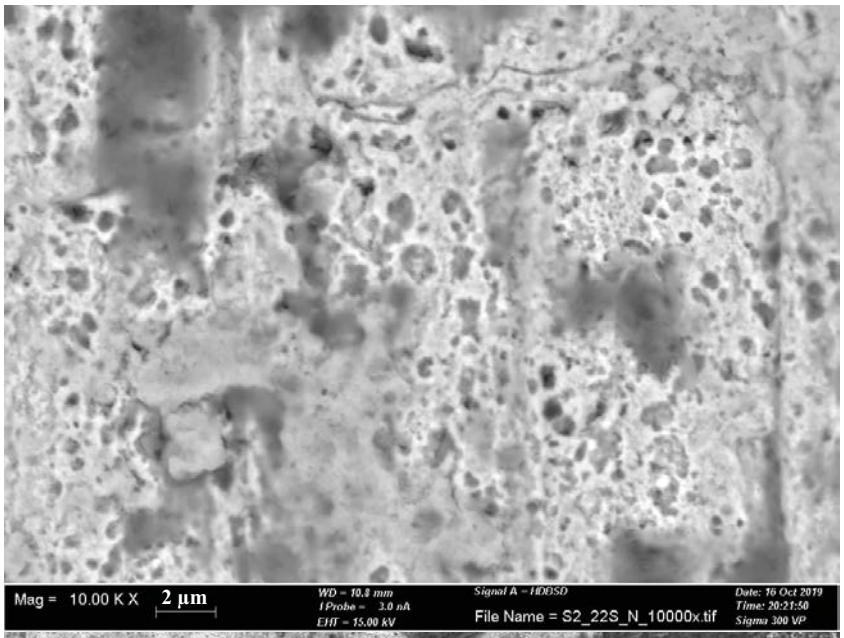

Figure B-12. *SEM image of coupon S2/N.*

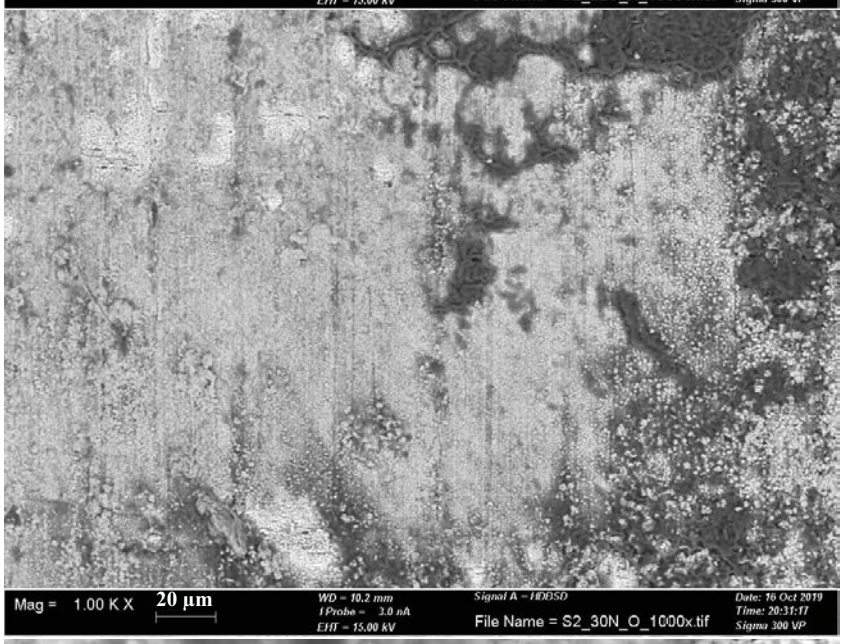

Figure B-13. *SEM image of coupon S2/O.*

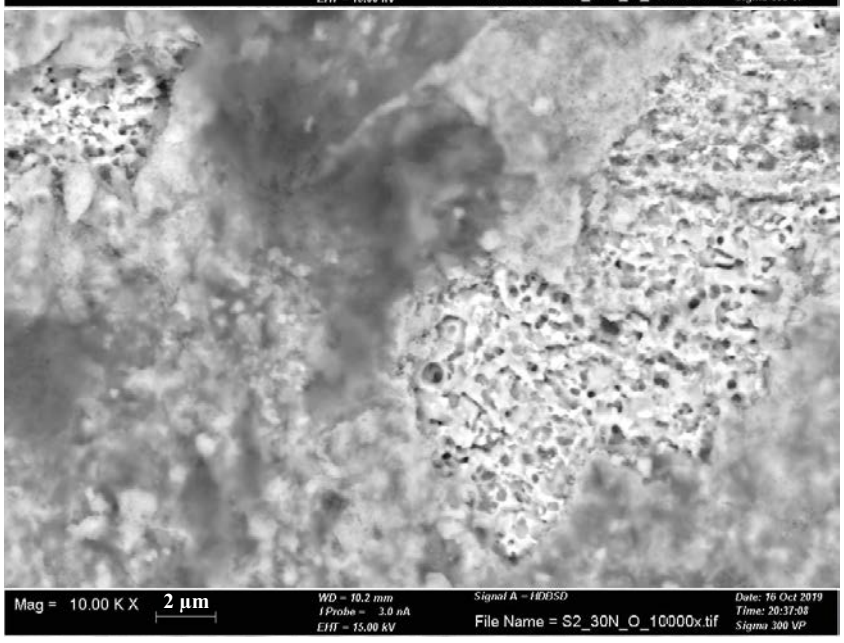

Figure B-14. *SEM image of coupon S2/O.*

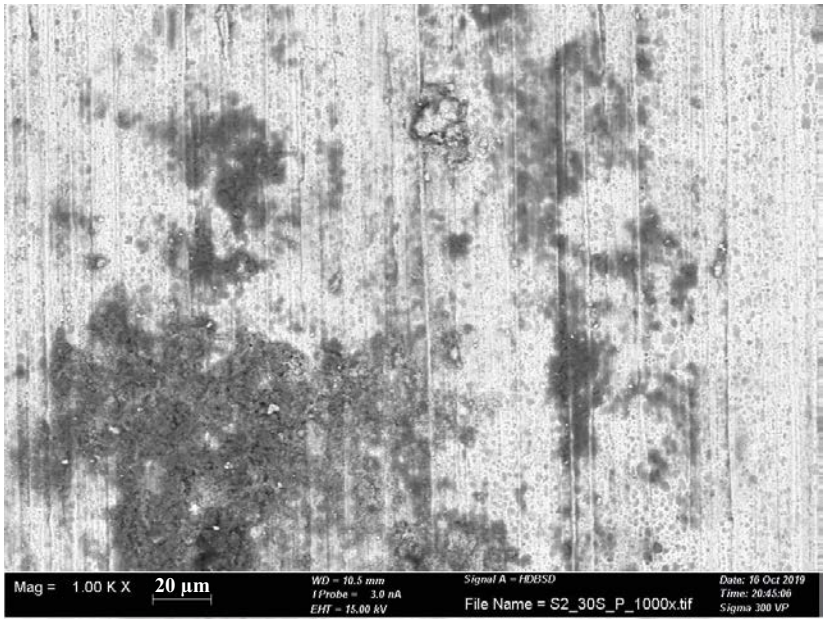

Figure B-15. *SEM image of coupon S2/P.*

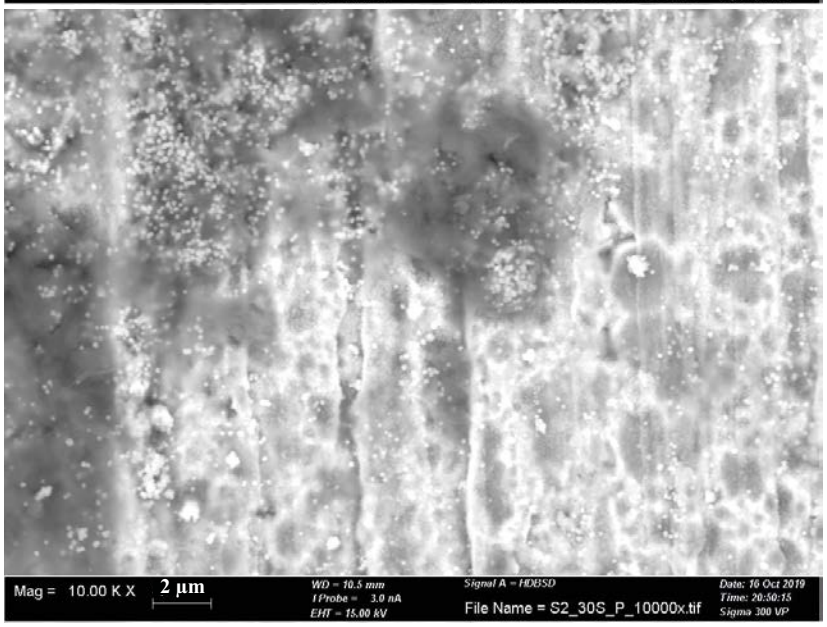

Figure B-16. *SEM image of coupon S2/P.*

A3/K – cross section 1

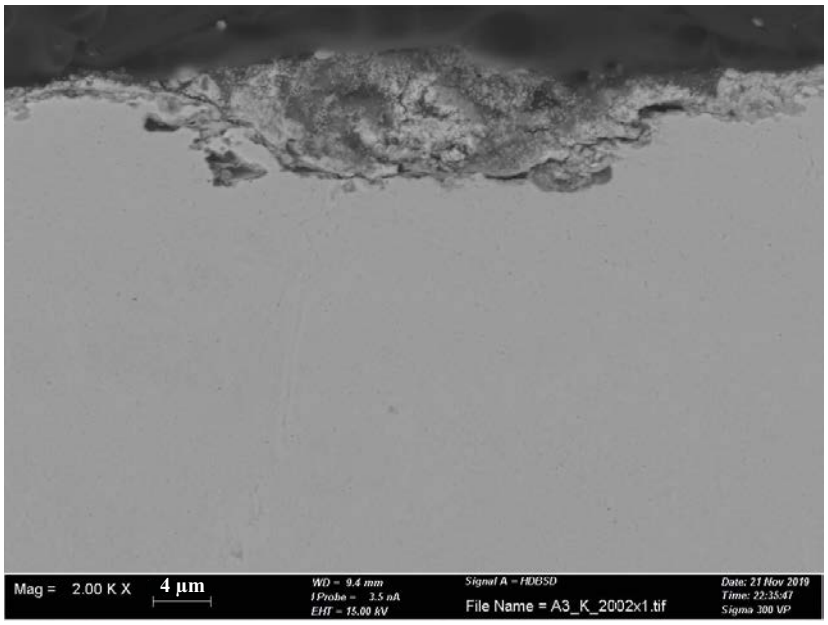

Figure B-17. *Cross-section SEM image of coupon A3/K.*

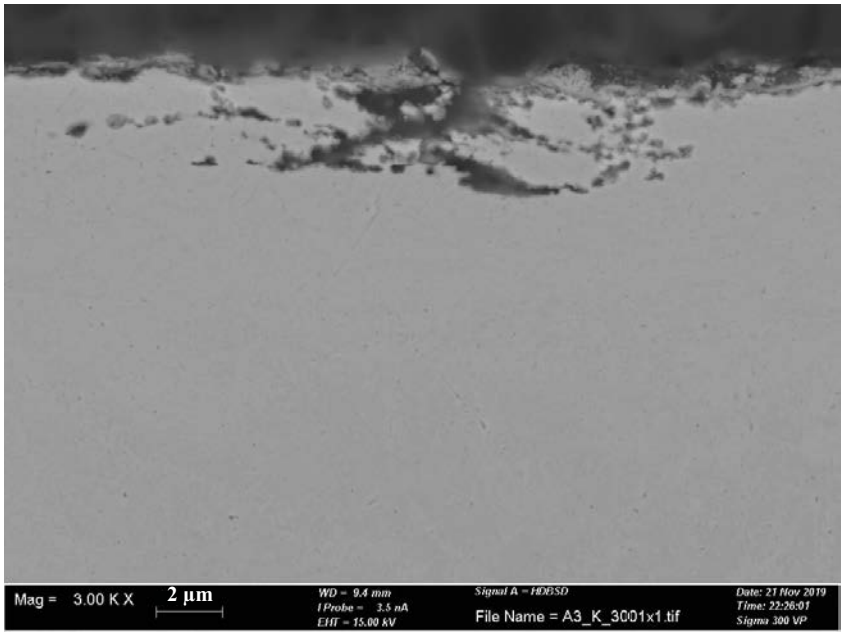

Figure B-18. *Cross-section SEM image of coupon A3/K.*

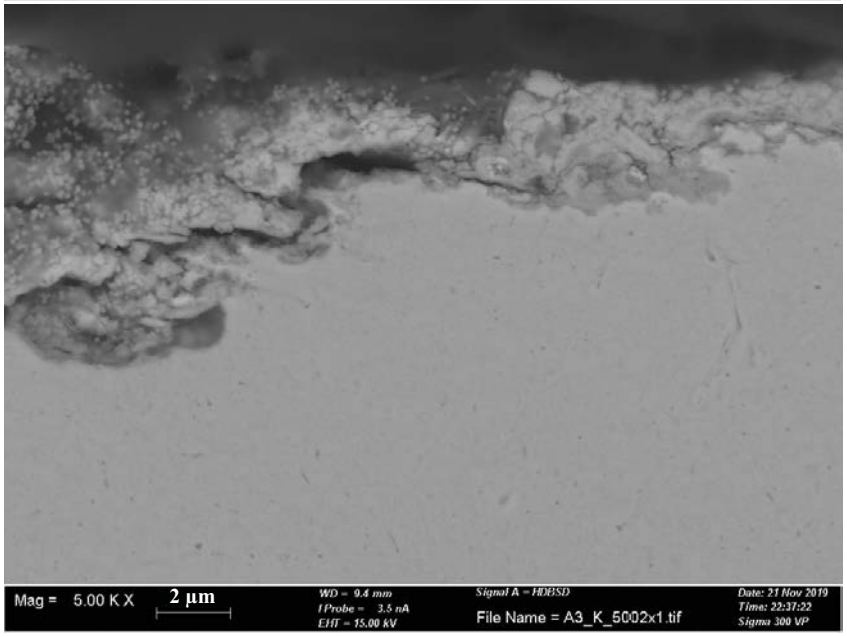

Figure B-19. *Cross-section SEM image of coupon A3/K.*

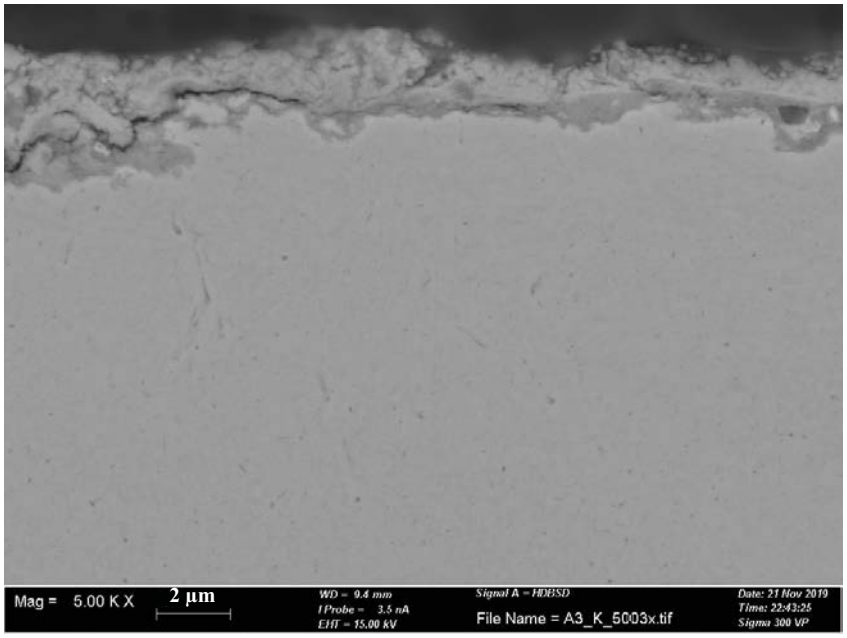

Figure B-20. *Cross-section SEM image of coupon A3/K.*

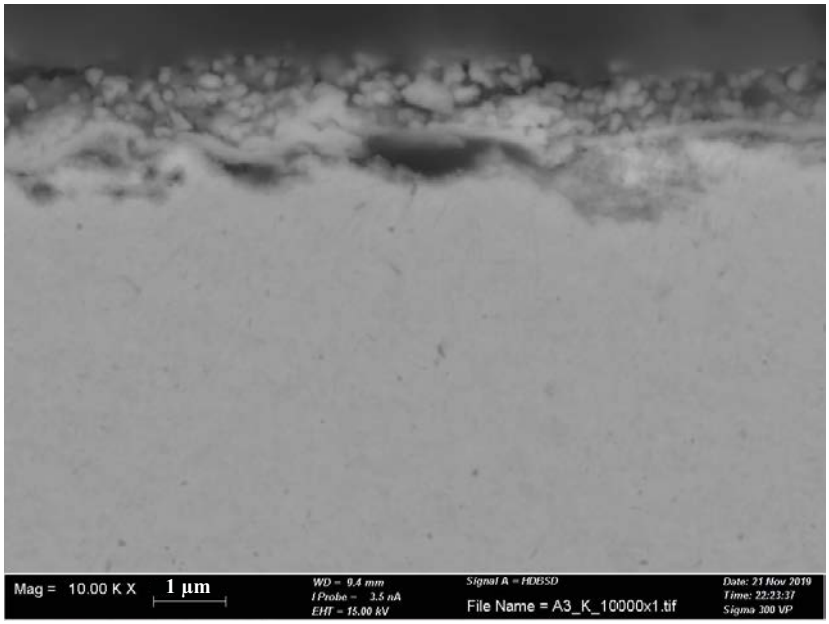

Figure B-21. *Cross-section SEM image of coupon A3/K.*

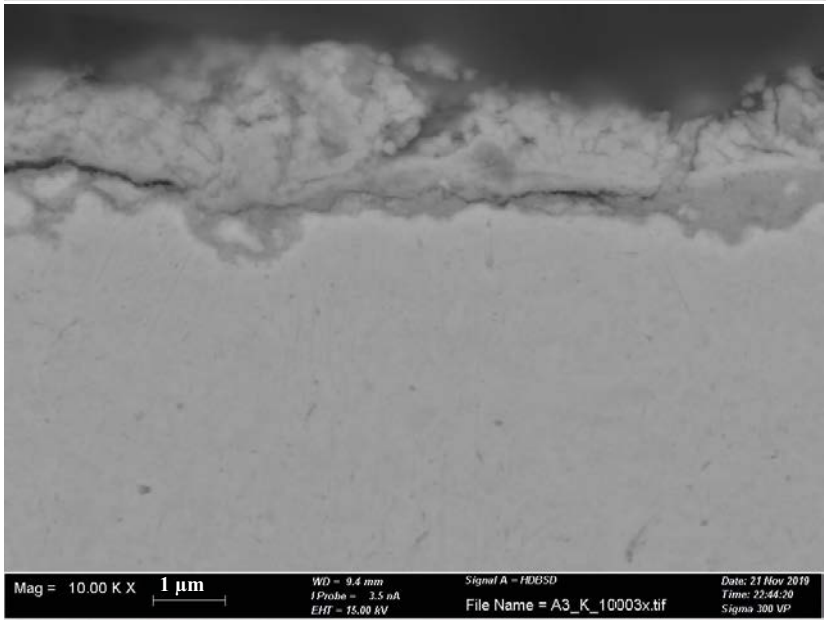

Figure B-22. *Cross-section SEM image of coupon A3/K.*

A3/K – cross section 2

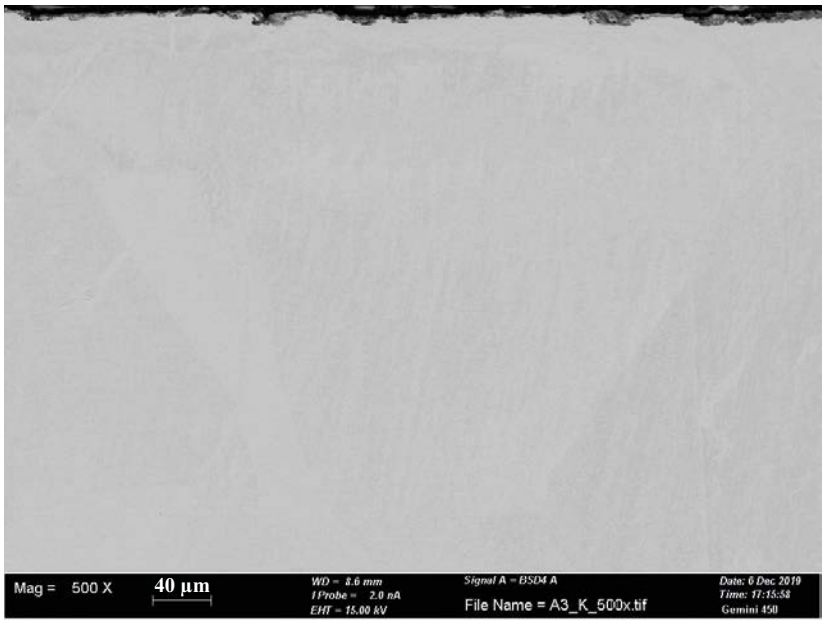

Figure B-23. *Cross-section SEM image of coupon A3/K.*

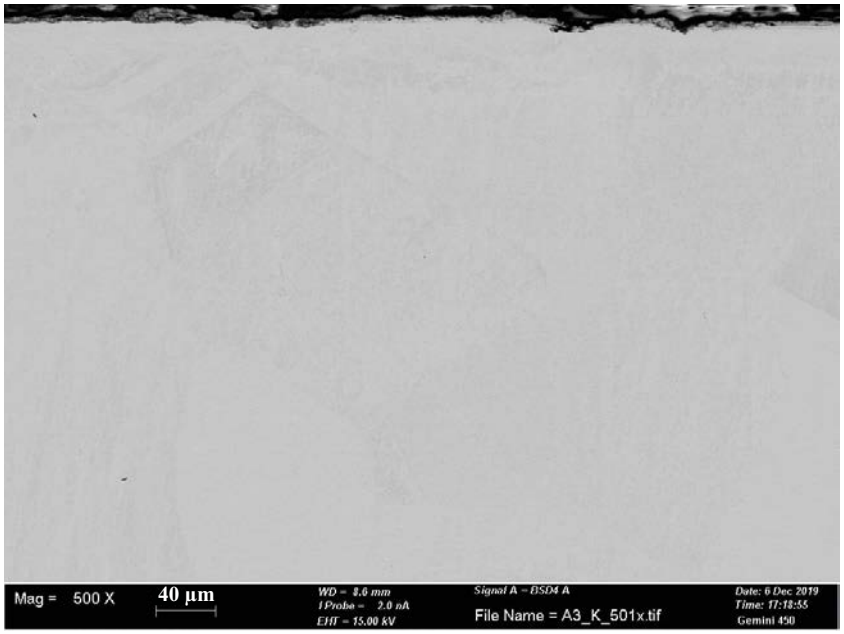

Figure B-24. *Cross-section SEM image of coupon A3/K.*

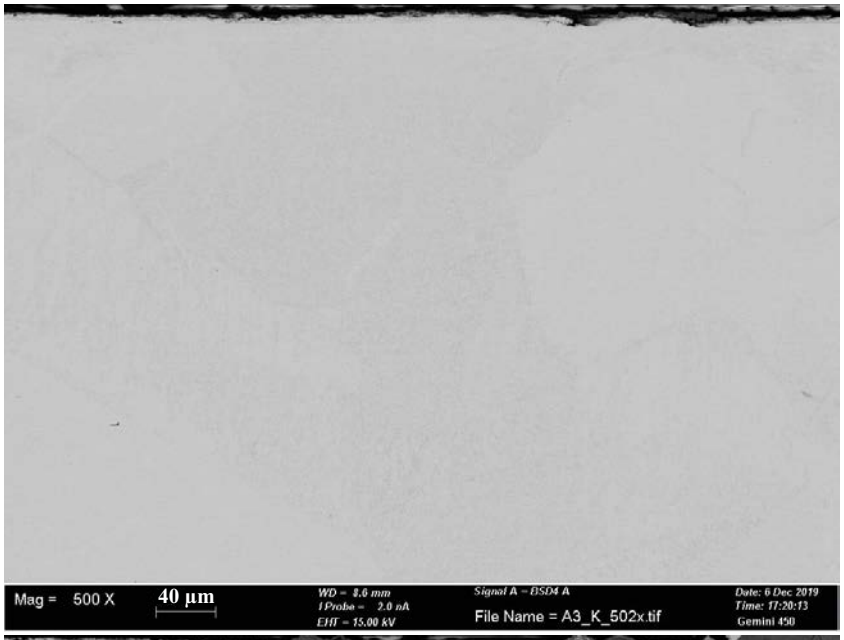

Figure B-25. *Cross-section SEM image of coupon A3/K.*

Figure B-26. *Cross-section SEM image of coupon A3/K.*

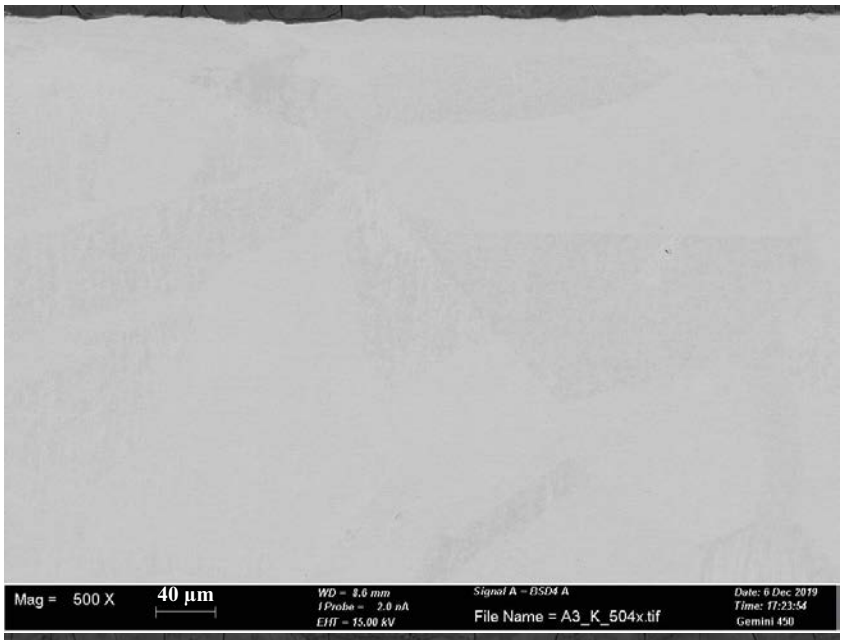

Figure B-27. *Cross-section SEM image of coupon A3/K.*

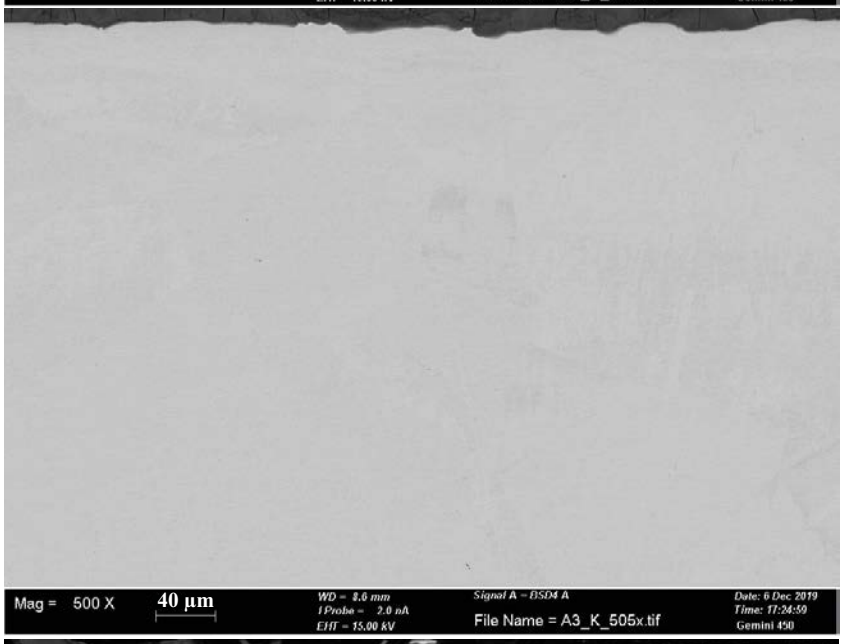

Figure B-28. *Cross-section SEM image of coupon A3/K.*

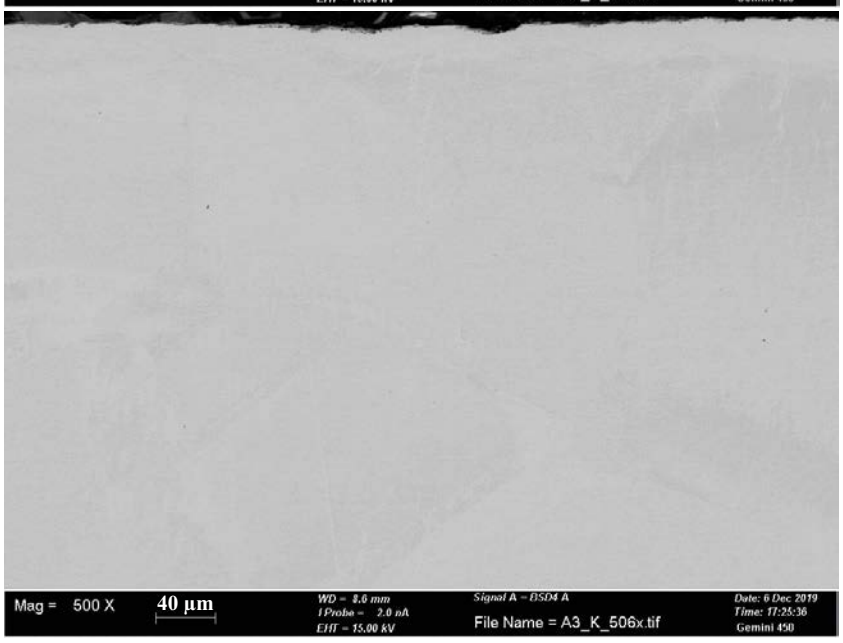

Figure B-29. *Cross-section SEM image of coupon A3/K.*

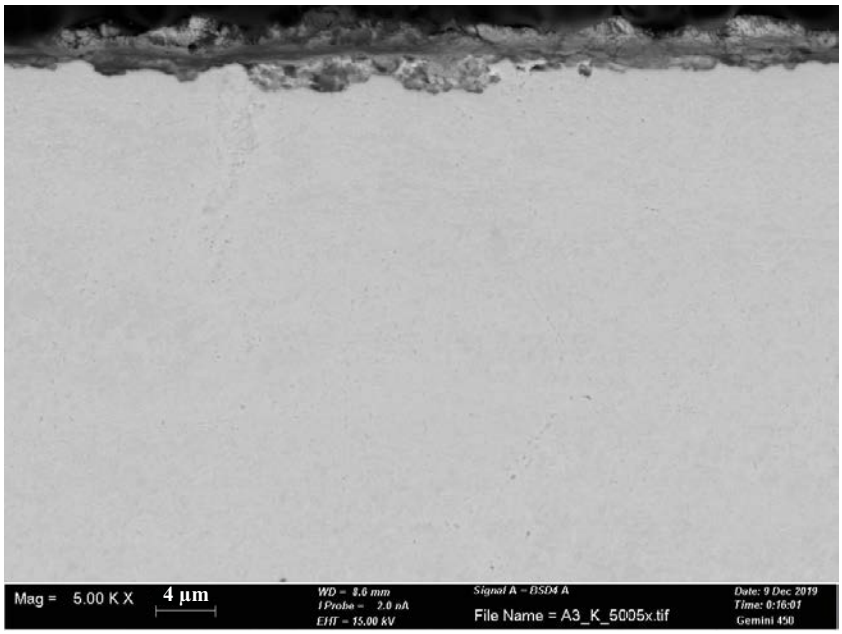

Figure B-30. *Cross-section SEM image of coupon A3/K.*

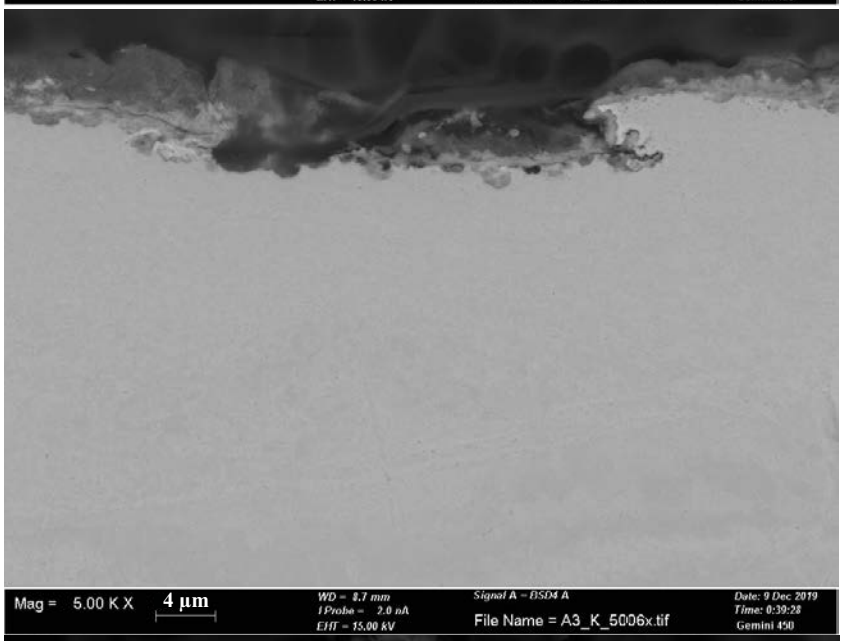

Figure B-31. *Cross-section SEM image of coupon A3/K.*

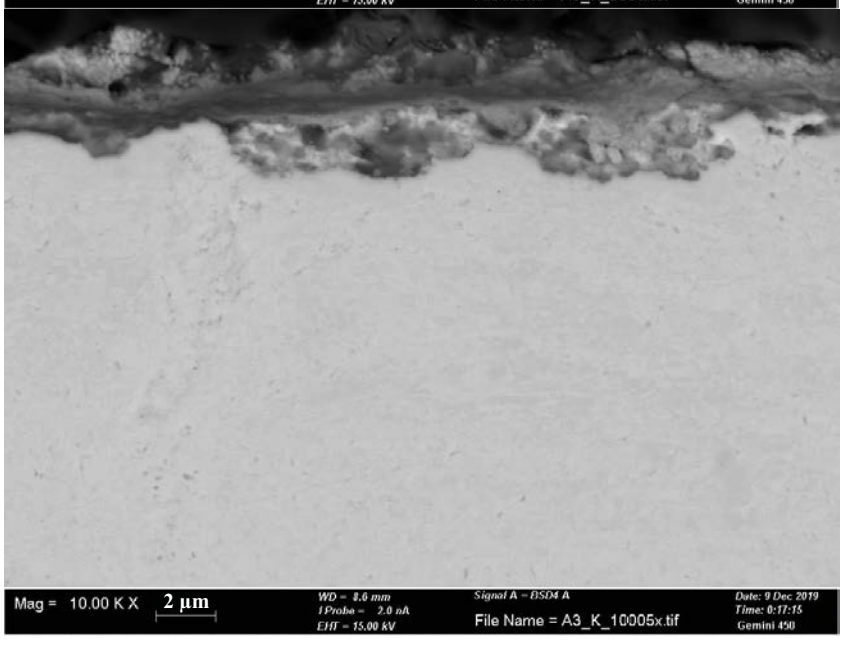

Figure B-32. *Cross-section SEM image of coupon A3/K.*

S2/N – cross section 1

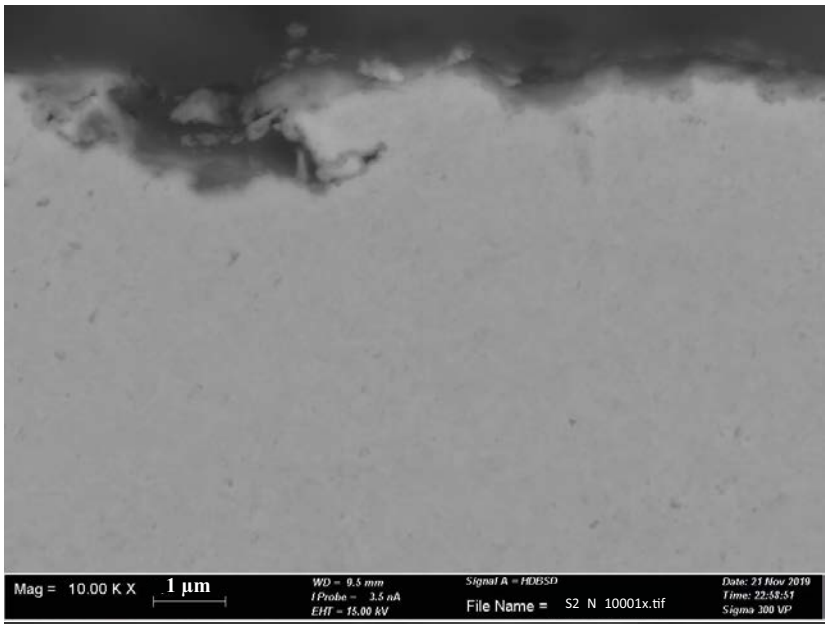

Figure B-33. *Cross-section SEM image of coupon S2/N.*

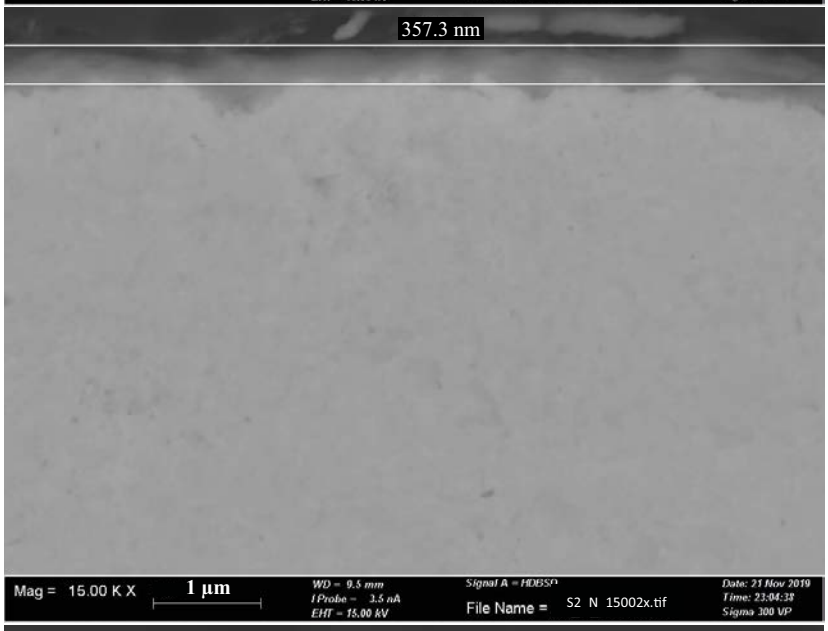

Figure B-34. *Cross-section SEM image of coupon S2/N.*

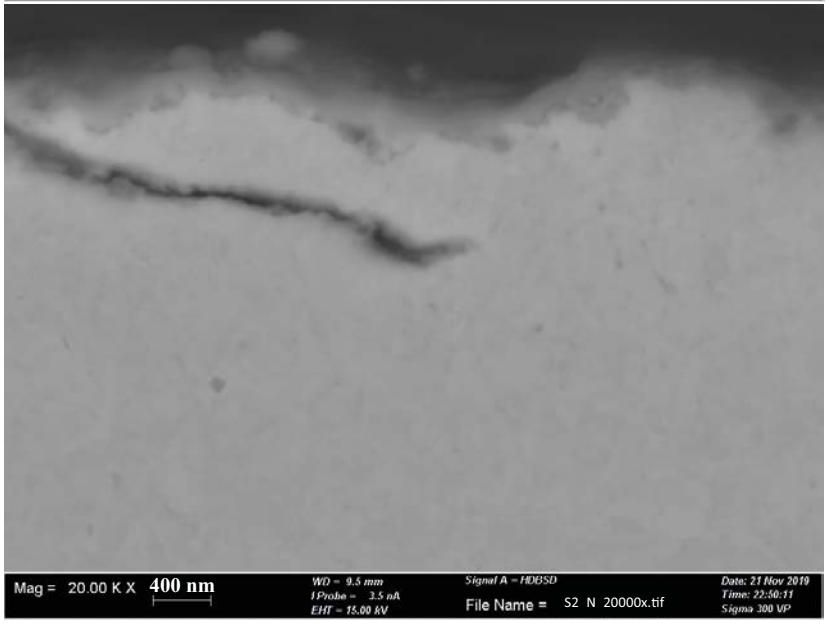

Figure B-35. *Cross-section SEM image of coupon S2/N.*

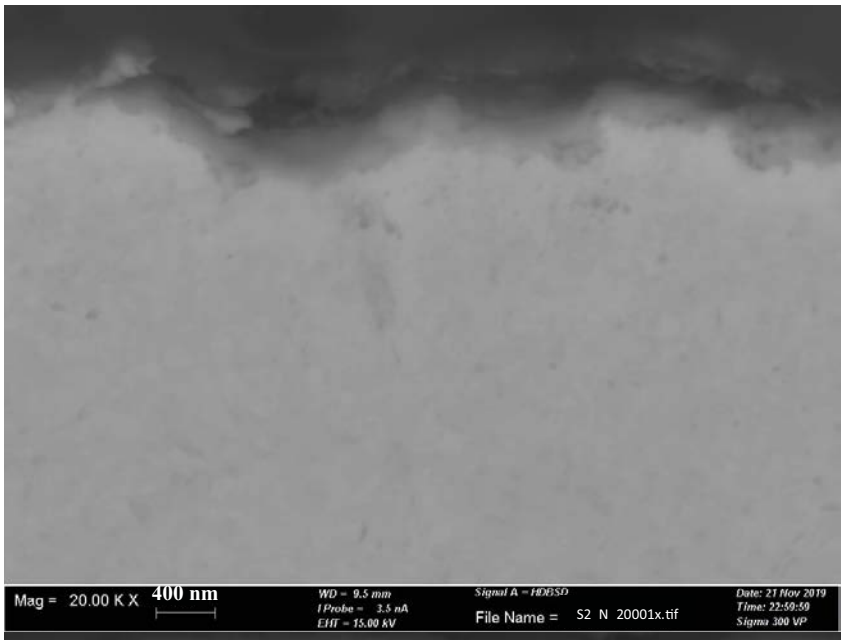

Figure B-36. *Cross-section SEM image of coupon S2/N.*

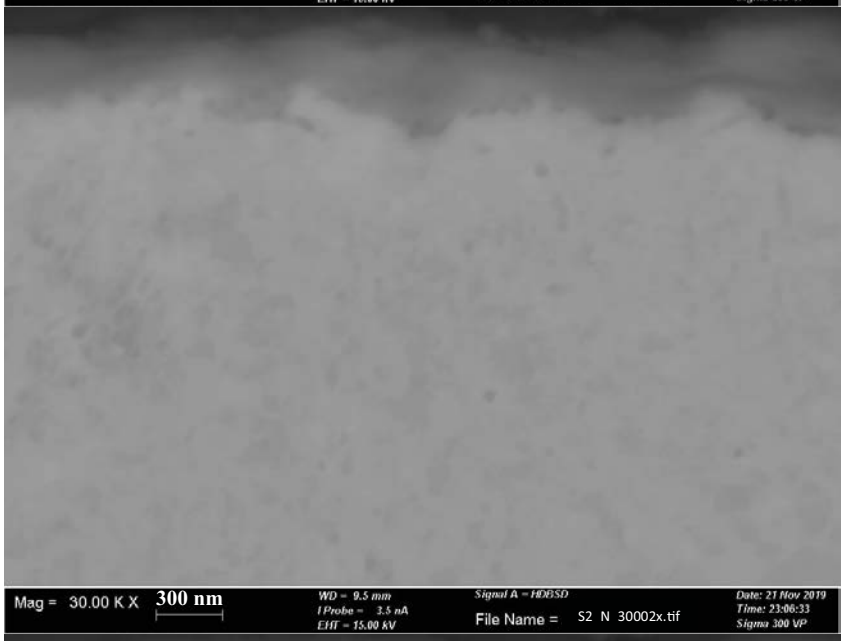

Figure B-37. *Cross-section SEM image of coupon S2/N.*

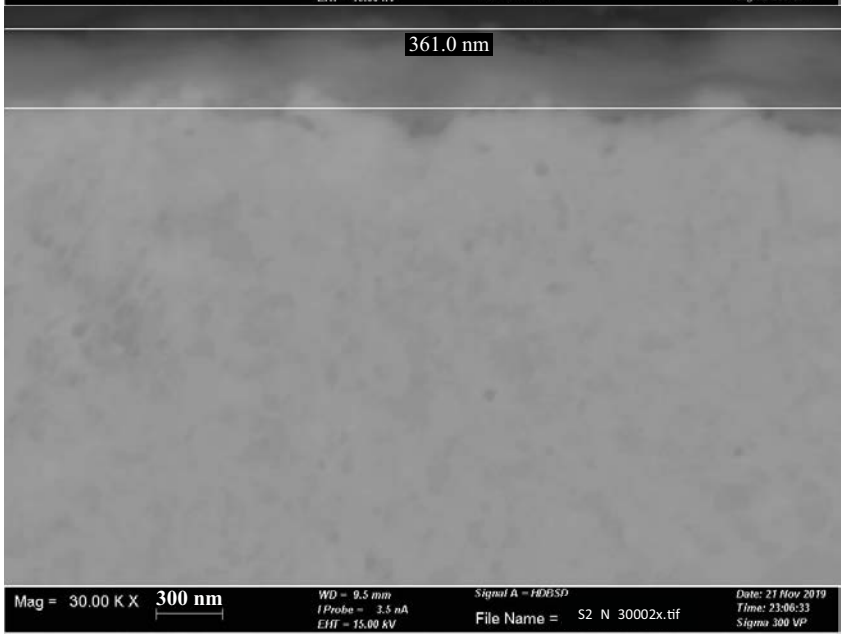

Figure B-38. *Cross-section SEM image of coupon S2/N.*

S2/N – cross section 2

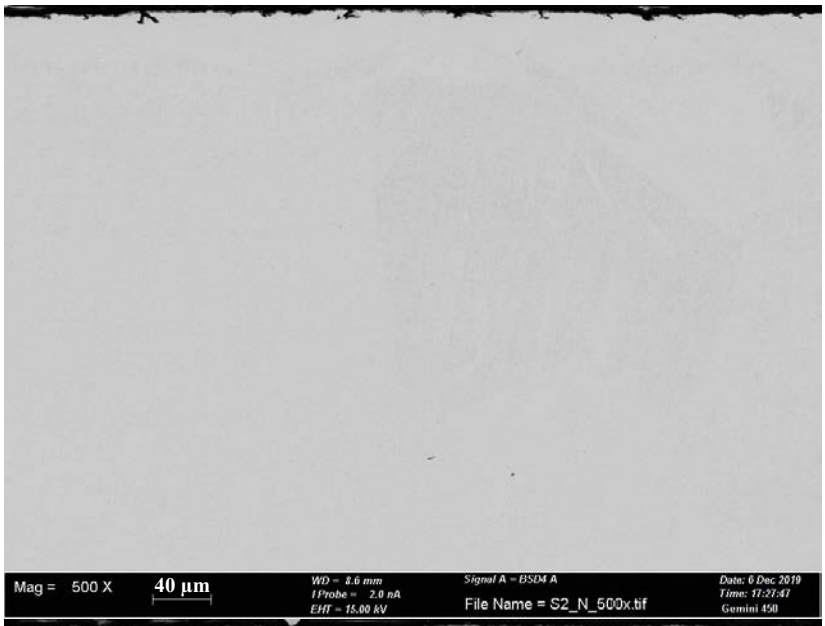

Figure B-39. *Cross-section SEM image of coupon S2/N.*

Figure B-40. *Cross-section SEM image of coupon S2/N.*

Figure B-41. *Cross-section SEM image of coupon S2/N.*

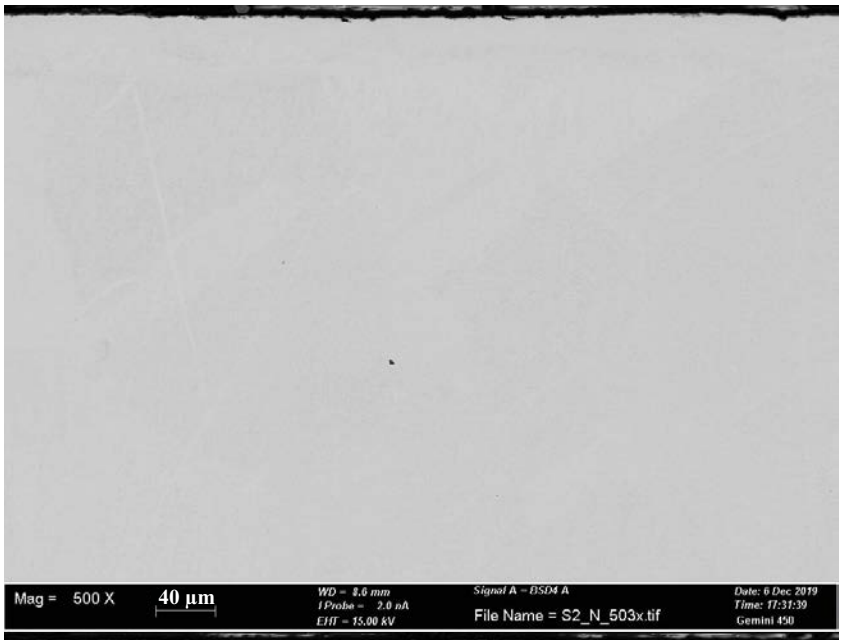

Figure B-42. *Cross-section SEM image of coupon S2/N.*

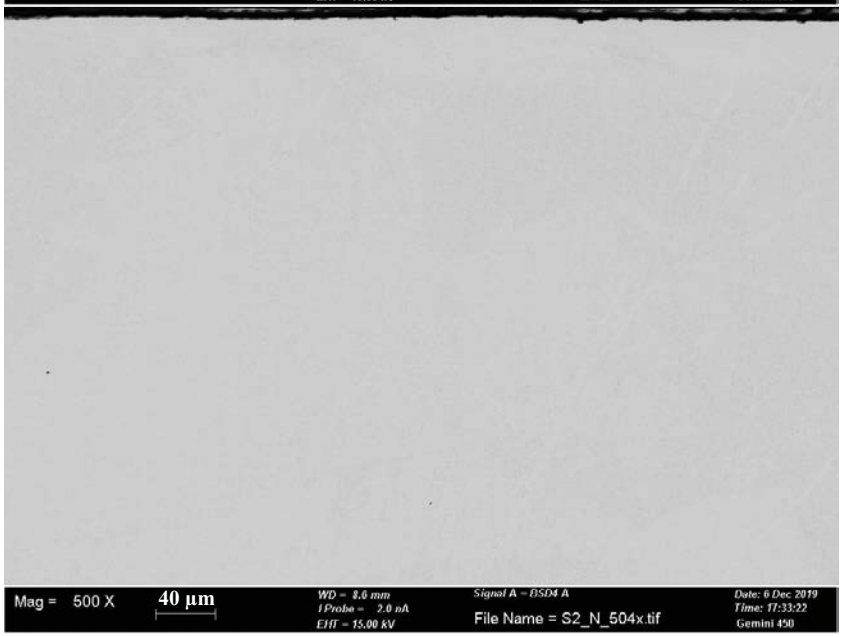

Figure B-43. *Cross-section SEM image of coupon S2/N.*

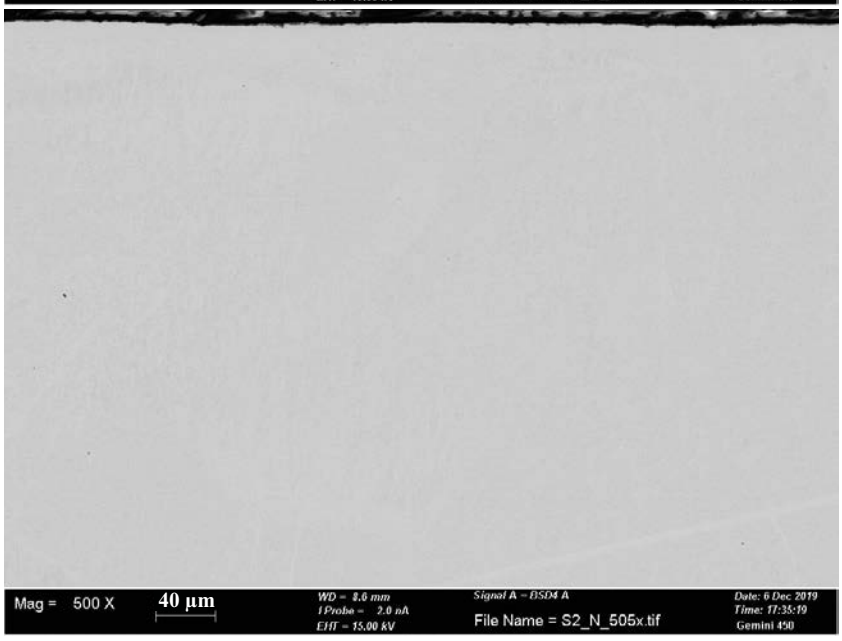

Figure B-44. *Cross-section SEM image of coupon S2/N.*

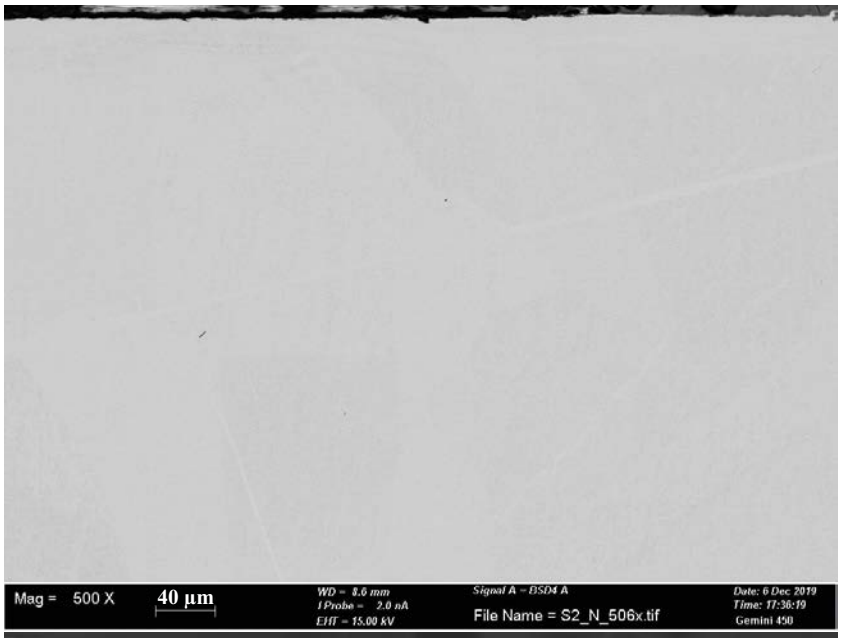

Figure B-45. *Cross-section SEM image of coupon S2/N.*

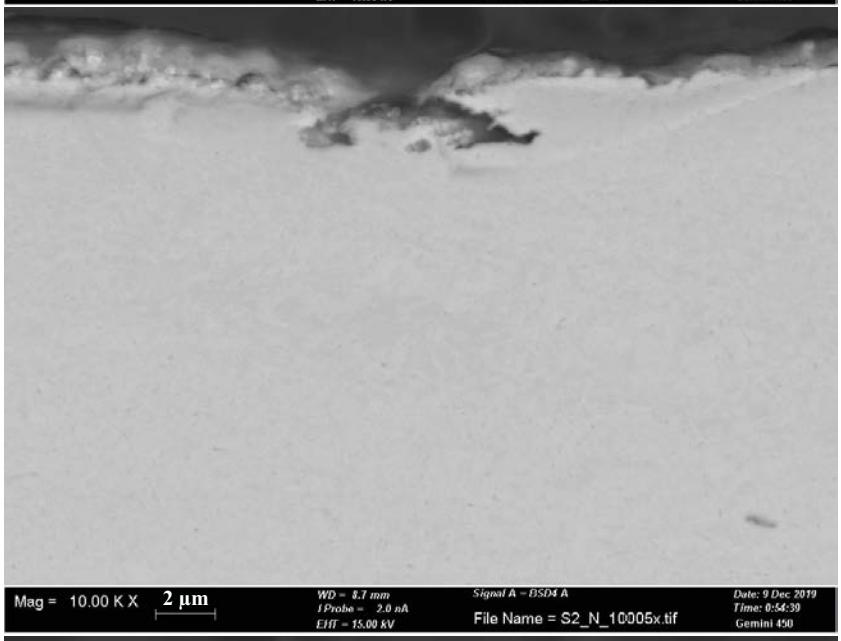

Figure B-46. *Cross-section SEM image of coupon S2/N.*

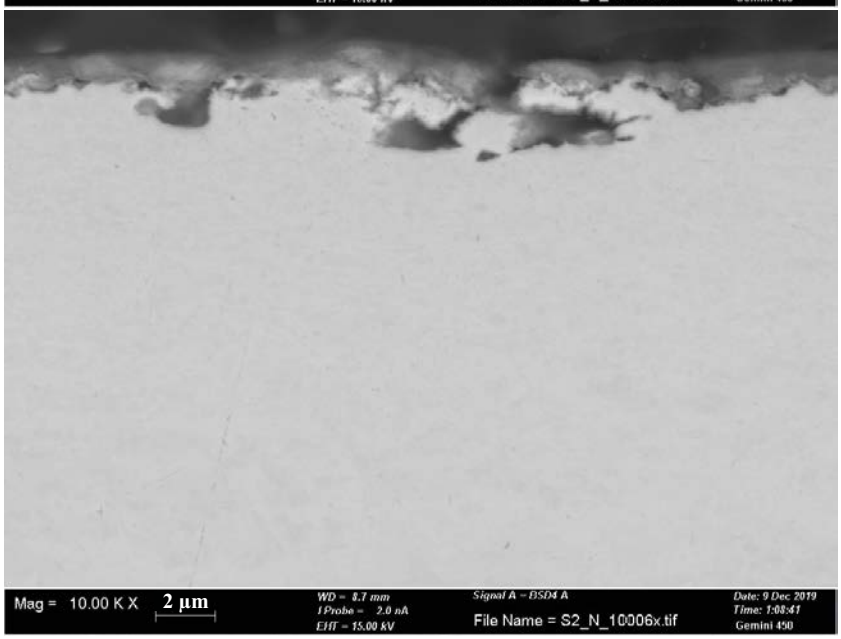

Figure B-47. *Cross-section SEM image of coupon S2/N.*

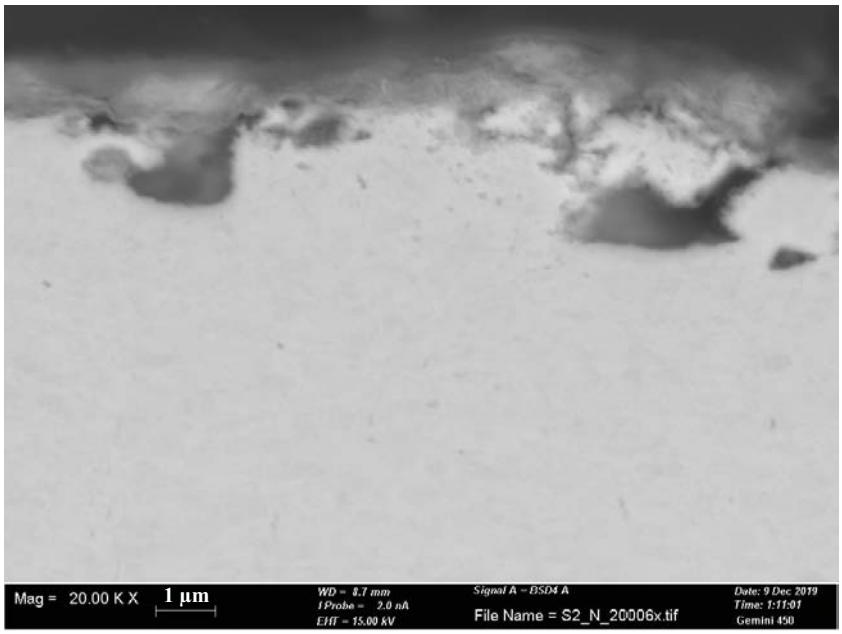

Figure B-48. *Cross-section SEM image of coupon S2/N.*

Appendix C

C1 XRD, EDS and TEM analysis of corrosion coupons

C1.1 Introduction

The first analyses carried out on the corrosion coupons was x-ray diffraction (XRD) to identify crystalline corrosion products on the surfaces. Thereafter the coupons were analysed in the SEM using energy dispersive spectroscopy (EDS) in order to investigate the elemental composition of the corrosion products.

Coupons A3/K and S2/N were not analysed for mass loss, instead they were cross sectioned so that their corrosion products could be analysed at depth in cross-section with SEM-EDS. Coupons A3/K and S2/N were also analysed using TEM. Several different analysis techniques were employed on these samples in order to verify what corrosion products that were present on the surfaces.

Reference coupons K and L were also analysed with XRD and EDS.

C1.2 XRD Results

XRD analysis of the corrosion coupons revealed strong peaks corresponding to metallic copper and cuprite (Cu_2O). Weaker peaks, possibly corresponding to chalcocite (Cu_2S), were also identified (Figure C-1). Other weak peaks observed in the analyses corresponded to components of bentonite clay and satellite peaks which come from reflected copper signals. These peaks can be seen at regular intervals from the strong copper peaks at 43 and 50 on the x-axis and can be thought of as a sort of reflectance from the material. The peaks for Cu_2S overlap somewhat the satellite peaks generated from the copper, which makes them difficult to see. This is perhaps clearest seen in Figure C-2 where the spectrum for A3/K is compared to the two reference coupons K and L, and at position 42 on the x-axis a Cu_2S peak can be seen for A3/K but not for the reference coupons.

The XRD analysis of the reference coupons revealed only copper and cuprite, along with the satellite peaks.

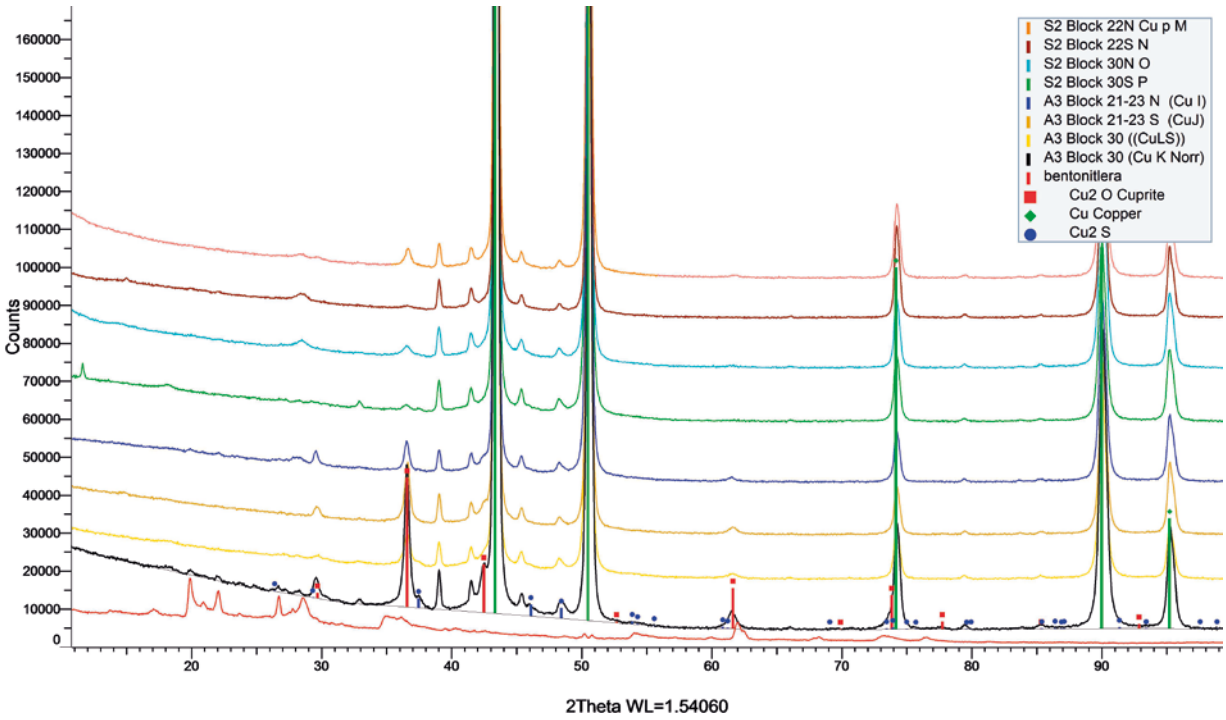

Figure C-1. *XRD spectra obtained for the corrosion coupons.*

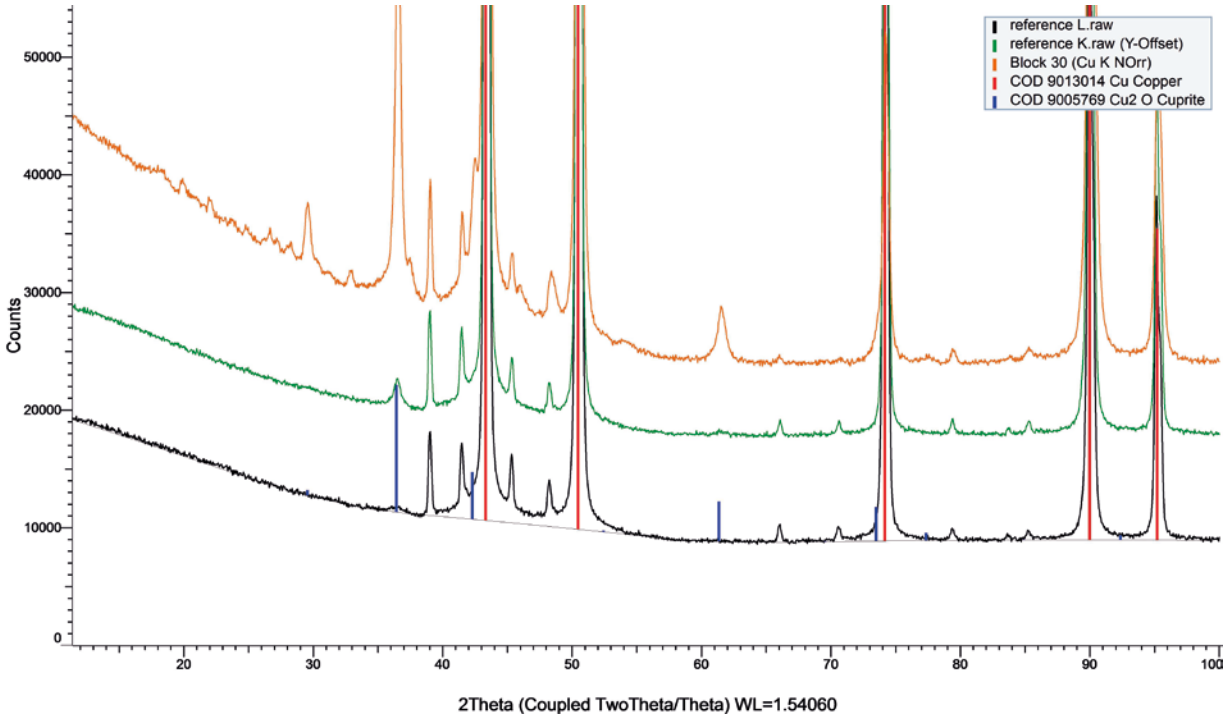

Figure C-2. *XRD spectra obtained for the reference coupons, with coupon A3/K for comparison.*

C1.3 EDS of the corrosion and reference coupons

The surfaces of the coupons were analysed with EDS with varying magnification at points deemed to be representative of the whole coupon surface (a more comprehensive selection of SEM images is presented in Appendix B). Traces of bentonite clay were identified (Al, Si, Na, Ca, K) as well as the expected copper and oxygen. Sulfur and chlorine were found in lower concentrations as were magnesium and iron, most likely from the groundwater and/or the bentonite clay. On the reference coupons several at % of zinc were found, of which the source is unknown at the time of writing.

The cross-section EDS analyses of corrosion coupons K and N revealed that the corrosion product was mainly comprised of copper oxides. Smaller amounts of copper sulfide were indicated, with a tendency for more sulfur further from the copper surface, and more oxygen closer to the copper surface.

C1.3.1 Coupon A3/I

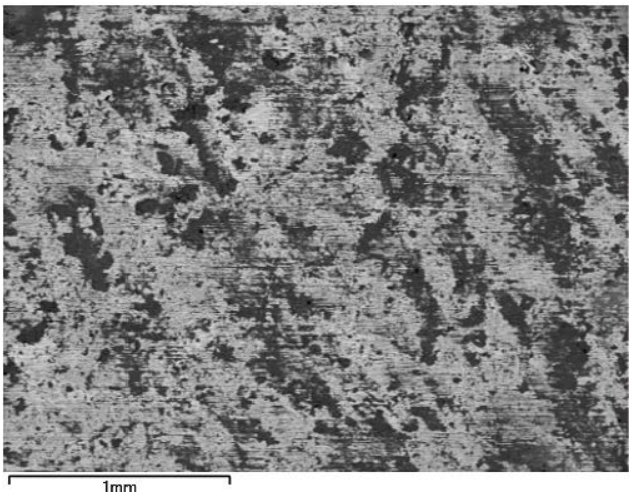

Element (At%)	1
O	50.82
Na	2.99
Mg	1.08
Al	5.00
Si	12.05
S	2.01
Ca	3.09
Fe	0.37
Cu	22.57
Total	100.00

Figure C-3. *EDS analysis of the surface of A3/I (100×).*

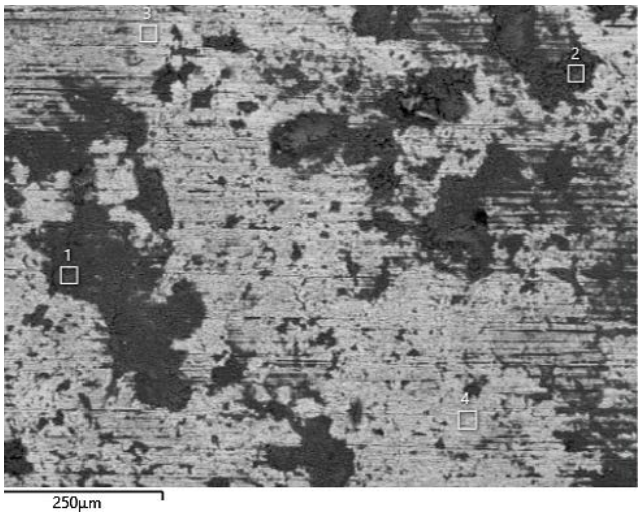

Element (At%)	1	2	3	4
O	61.90	61.58	28.00	31.34
Na	3.06	2.89	1.55	1.74
Mg	1.30	0.89	0.30	0.54
Al	8.73	5.30	1.44	1.62
Si	21.46	25.12	2.69	3.74
S	0.26	0.37	2.70	3.94
Cl		0.04	0.16	0.18
K	0.11	0.18		
Ca	0.42	0.16	0.20	0.38
Ti	0.03	0.08		
Fe	0.88	0.58		0.15
Cu	1.85	2.80	62.97	56.37
Total	100.00	100.00	100.00	100.00

Figure C-4. *EDS analysis of the surface of A3/I (300×).*

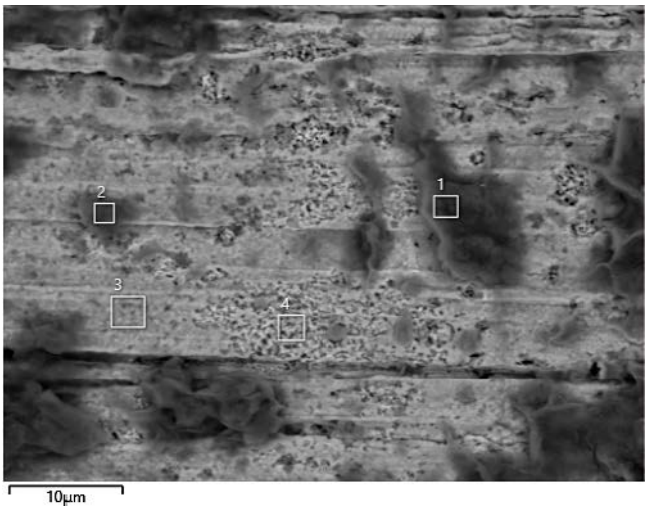

Element (At%)	1	2	3	4
O	62.07	66.84	27.22	26.70
Na	2.91	2.01	1.72	2.01
Mg	1.33	1.34	0.34	0.51
Al	7.57	2.18	1.54	0.36
Si	19.53	4.65	2.83	0.67
S	0.15	1.15	5.89	3.93
Cl	0.02	0.03	0.22	0.22
K	0.17			
Ca	0.13	12.88	0.08	0.16
Fe	0.92	0.21		
Cu	5.19	8.72	60.15	65.44
Total	100.00	100.00	100.00	100.00

Figure C-5. *EDS analysis of the surface of A3/I (5000×).*

C1.3.2 Coupon A3/J

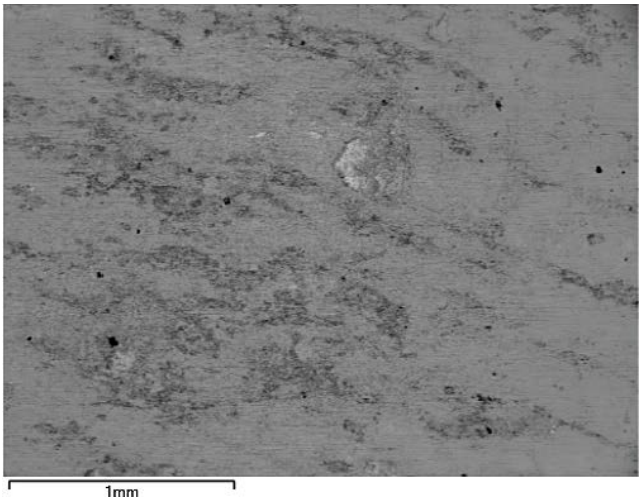

Element (At%)	1
O	68.72
Mg	0.42
Al	1.31
Si	3.24
S	0.71
Cl	0.05
K	0.05
Ca	1.64
Fe	0.17
Cu	23.70
Total	100.00

Figure C-6. *EDS analysis of the surface of A3/J (100×).*

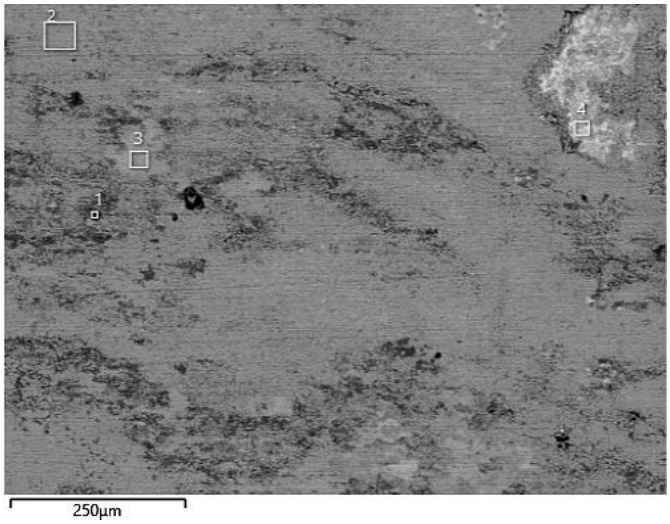

Element (At%)	1	2	3	4
O	71.86	67.81	65.40	55.39
Na	0.39			
Mg	1.11	0.34	0.27	0.26
Al	0.49	1.13	0.28	0.31
Si	1.02	2.75	0.69	0.74
S	1.53	0.72	0.69	0.50
Cl		0.06	0.07	0.20
Ca	19.88	0.35	0.40	0.20
Fe		0.13		
Cu	3.74	26.73	32.21	42.40
Total	100.00	100.00	100.00	100.00

Figure C-7. *EDS analysis of the surface of A3/J (300×).*

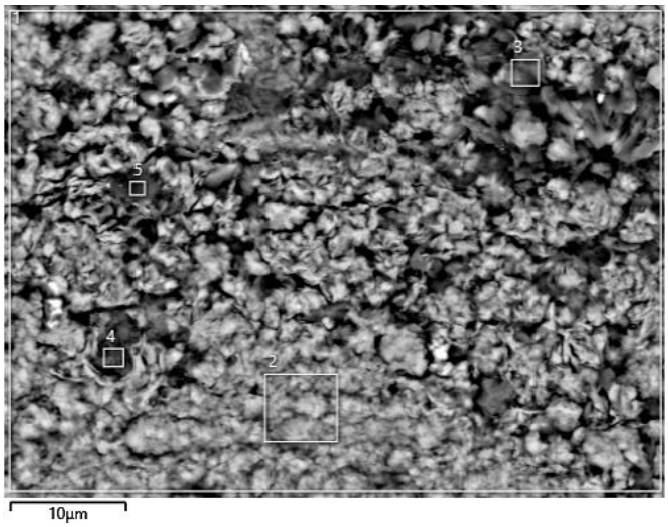

Element (At%)	1	2	3	4	5
O	68.60	68.27	67.81	69.64	65.78
Na			0.26		
Mg	0.60	0.43	0.66	0.76	1.09
Al	2.15	1.89	0.32	2.11	4.58
Si	5.27	4.69	0.74	4.83	10.75
S	1.05	0.13	4.03	0.60	0.26
Cl			0.04	0.03	0.04
Ca	5.19	0.66	17.50	12.62	2.61
Mn			0.07	0.09	
Fe	0.19	0.20		0.24	0.42
Cu	16.96	23.73	8.45	9.07	14.47
Sr			0.12		
Total	100.00	100.00	100.00	100.00	100.00

Figure C-8. *EDS analysis of the surface of A3/J (5000×).*

C1.3.3 Coupon A3/K

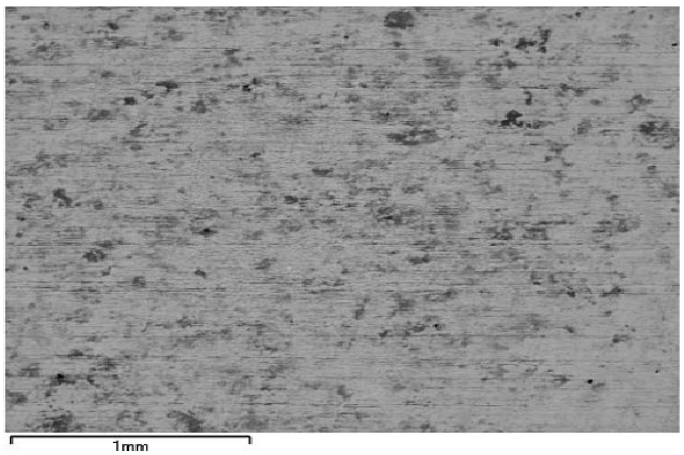

Element (At%)	1
O	28.65
Mg	0.61
Al	2.33
Si	5.72
S	7.79
Cl	0.41
Ca	0.34
Fe	0.24
Cu	53.91
Total:	100.00

Figure C-9. *EDS analysis of the surface of A3/K (100×).*

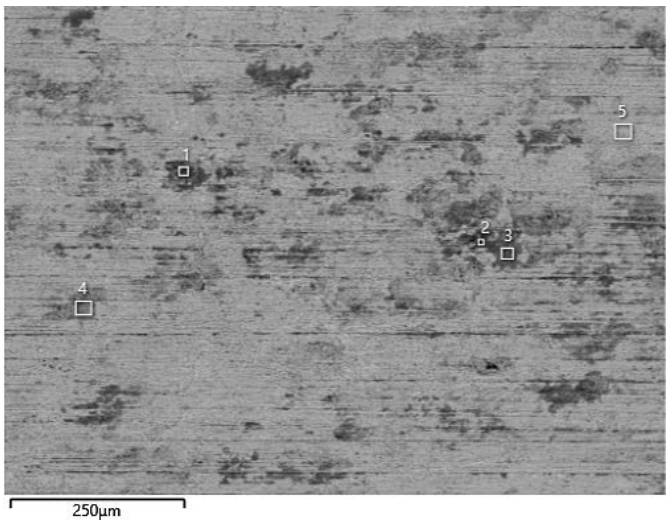

Element (At%)	1	2	3	4	5
O	55.67	44.87	49.99	37.84	13.03
Mg	1.13	0.84	1.17	1.01	
Al	6.22	8.89	6.44	5.01	0.41
Si	20.10	21.86	18.90	11.45	0.83
S	4.11	5.35	6.97	11.73	7.15
Cl	0.25	0.15		0.27	0.27
Ca	0.35	1.41	0.46	0.40	
Fe	0.65	0.42	0.72	0.45	
Cu	11.52	16.21	15.35	31.84	78.30
Total:	100.00	100.00	100.00	100.00	100.00

Figure C-10. *EDS analysis of the surface of A3/K (300×).*

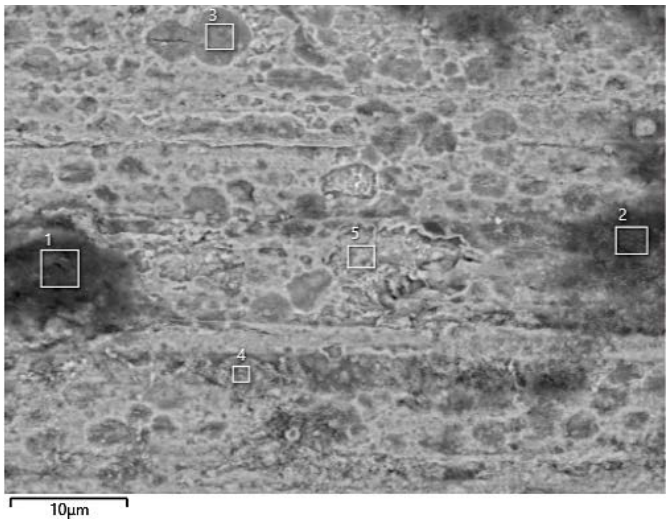

Element (At%)	1	2	3	4	5
O	59.62	57.72	18.13	29.79	19.91
Mg	1.10	1.48			0.37
Al	5.48	6.90	0.68	3.67	1.48
Si	19.40	16.07	1.27	7.88	3.16
S	1.33	2.42	5.42	11.69	7.73
Cl	1.02	0.24	0.33	0.36	0.13
Ca	0.33	0.31	0.10	0.24	0.07
Fe	0.49	0.59	0.09	0.36	
Cu	11.23	14.27	73.98	46.00	67.16
Total:	100.00	100.00	100.00	100.00	100.00

Figure C-11. *EDS analysis of the surface of A3/K (5000×).*

C1.3.4 Coupon A3/L

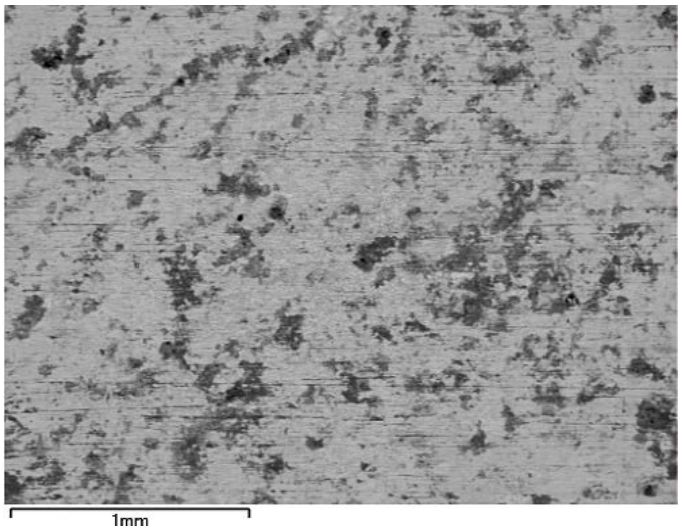

Element (At%)	1
O	34.85
Mg	0.84
Al	3.66
Si	8.66
S	8.66
Cl	0.33
Ca	0.35
Fe	0.26
Cu	42.40
Total	100.00

Figure C-12. *EDS analysis of the surface of A3/L (100×).*

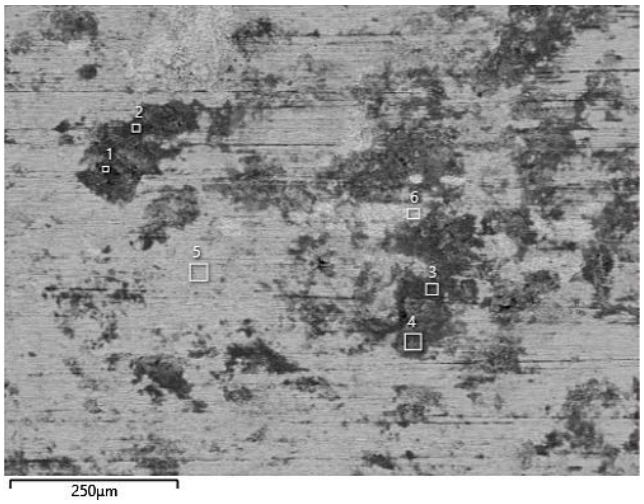

Element (At%)	1	2	3	4	5	6
O	42.10	61.74	59.22	54.25	13.44	11.78
Mg	1.50	1.19	1.43	1.07		
Al	7.61	6.43	7.90	5.71	0.33	0.37
Si	28.87	23.37	20.28	21.90	0.84	0.85
S	5.38	1.39	2.73	5.02	10.14	3.21
Cl	0.11	0.17	0.03	0.08	0.26	0.25
K	0.14		0.10			
Ca	0.81	0.46	0.57	0.52		
Ti	0.18					
Fe	0.50	0.64	0.80	0.61		
Cu	12.80	4.61	6.92	10.85	74.99	83.54
Total	100.00	100.00	100.00	100.00	100.00	100.00

Figure C-13. *EDS analysis of the surface of A3/L (300×).*

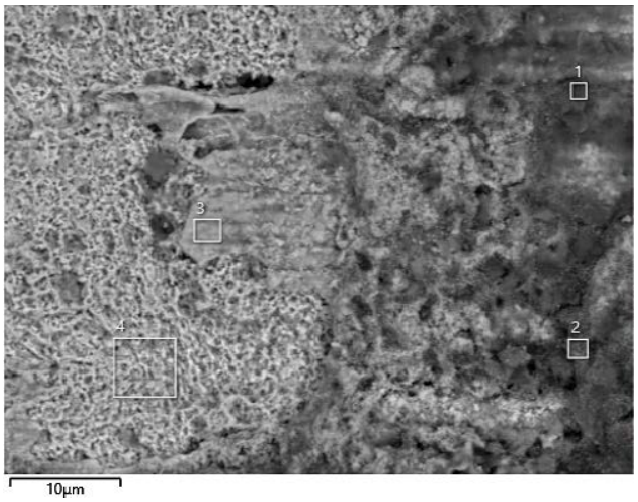

Element (At%)	1	2	3	4
O	60.30	53.21	9.66	12.97
Mg	1.41	1.07		
Al	7.62	5.58	0.24	0.19
Si	18.48	21.87	0.46	0.50
S	2.39	4.98	19.07	1.01
Cl	0.17	0.03	0.76	0.22
K		0.08		
Ca	0.45	0.56	0.10	
Fe	0.71	0.54		
Cu	8.47	12.08	69.72	85.10
Total	100.00	100.00	100.00	100.00

Figure C-14. *EDS analysis of the surface of A3/L (5000×).*

C1.3.5 Coupon S2/M

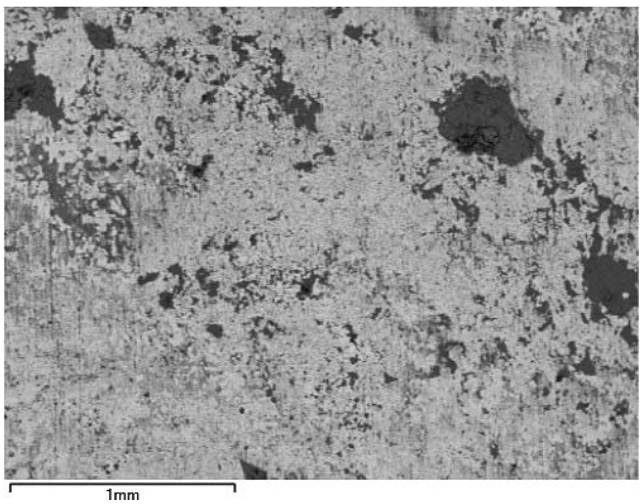

Element (At%)	1
O	40.22
Na	2.81
Mg	1.16
Al	4.69
Si	10.47
S	2.20
Cl	0.30
Ca	0.48
Fe	0.34
Cu	37.33
Total	100.00

Figure C-15. *EDS analysis of the surface of S2/M (100×).*

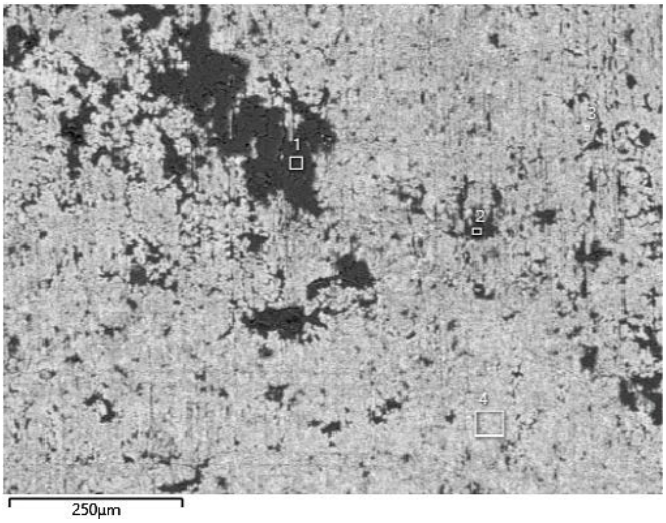

Element (At%)	1	2	3	4
O	65.32	63.20	5.91	22.95
Na	2.75	2.50		
Mg	1.28	1.38		
Al	7.99	8.40	0.41	0.96
Si	21.54	22.54	0.77	2.27
S	0.04	0.07	0.27	3.79
Cl			0.27	0.26
K	0.08	0.09		
Ca	0.05	0.27		
Fe	0.76	0.83		
Cu	0.19	0.71	92.38	69.78
Total	100.00	100.00	100.00	100.00

Figure C-16. *EDS analysis of the surface of S2/M (300×).*

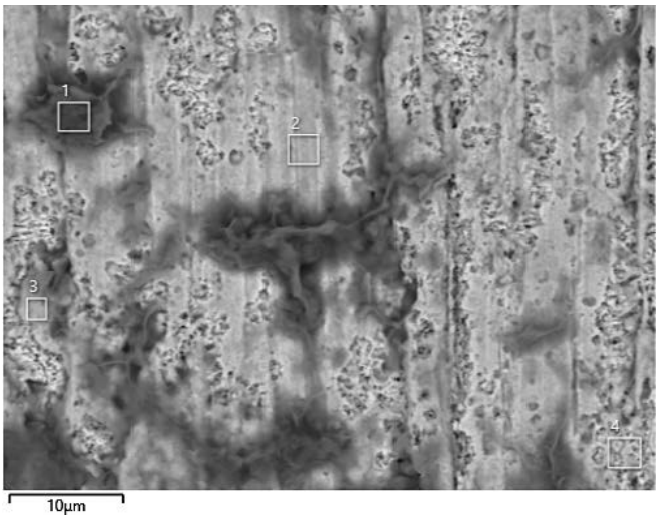

Element (At%)	1	2	3	4
O	61.32	25.21	37.25	15.10
Na	2.44		0.96	0.36
Mg	1.34	0.63	1.02	0.72
Al	9.79	1.82	3.91	1.61
Si	23.00	4.18	8.82	1.37
S	0.06	0.41	7.01	0.74
Cl	0.04	0.64	1.50	
K	0.11			
Ca	0.13			0.24
Fe	0.94		0.18	
Cu	0.83	67.11	39.34	79.85
Total	100.00	100.00	100.00	100.00

Figure C-17. *EDS analysis of the surface of S2/M (5000×).*

C1.3.6 Coupon S2/N

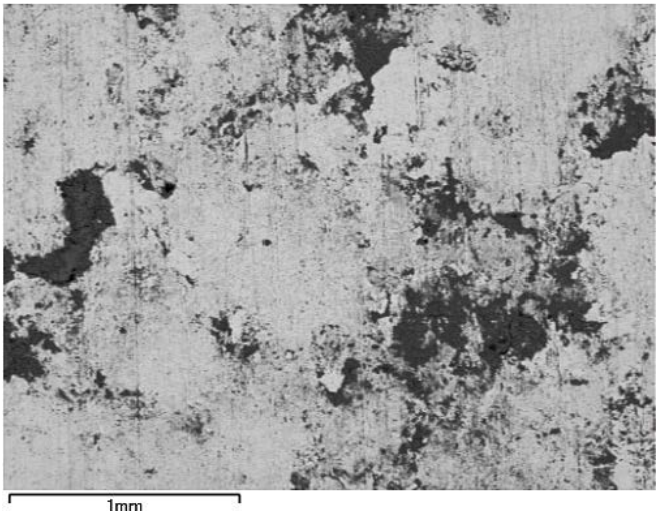

Element (At%)	1
O	37.25
Mg	0.96
Al	4.09
Si	10.28
S	1.54
Ca	1.37
Fe	0.25
Cu	44.26
Total	100.00

Figure C-18. *EDS analysis of the surface of S2/N (100×).*

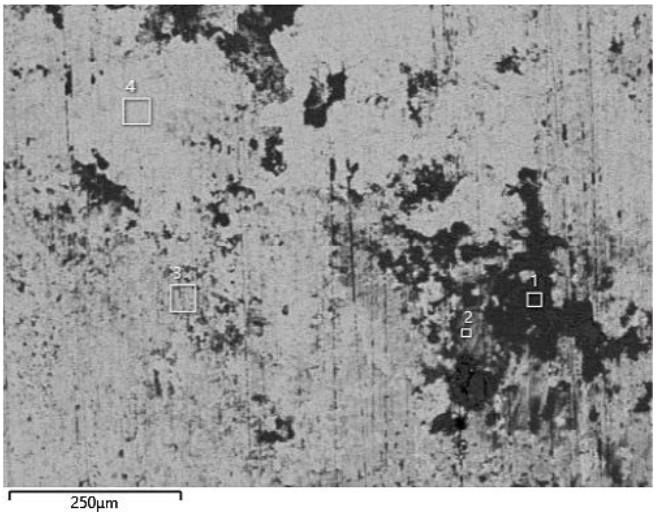

Element (At%)	1	2	3	4
O	75.12	56.29	26.79	12.96
Na	0.81	1.47		
Mg	0.59	1.31	0.60	
Al	3.44	6.20	1.31	
Si	7.66	12.62	2.72	0.43
S	0.29	0.99	2.69	2.24
Cl			0.12	0.18
K	0.04			
Ca	10.82	1.92	1.52	0.14
Fe	0.43	0.53		
Cu	0.78	18.65	64.25	84.04
Total	100.00	100.00	100.00	100.00

Figure C-19. *EDS analysis of the surface of S2/N (300×).*

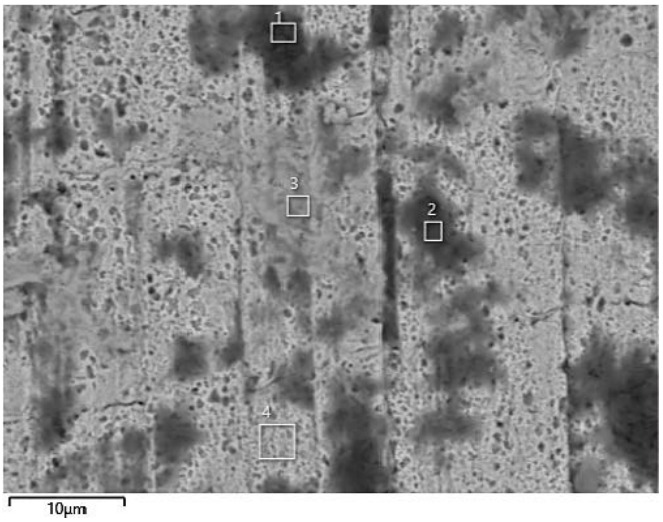

Element (At%)	1	2	3	4
O	65.25	59.67	34.33	15.13
Na	0.54	1.61		
Mg	0.59	1.30	0.74	
Al	2.79	6.95	3.09	0.38
Si	5.69	16.96	5.86	0.77
S	0.76	0.81	7.30	2.29
Cl	0.09	0.06		
K		0.13		
Ca	8.98	1.51	0.36	0.31
Fe	0.25	0.66	0.19	
Cu	15.06	10.34	48.11	81.11
Total	100.00	100.00	100.00	100.00

Figure C-20. *EDS analysis of the surface of S2/N (5000×).*

C1.3.7 Coupon S2/O

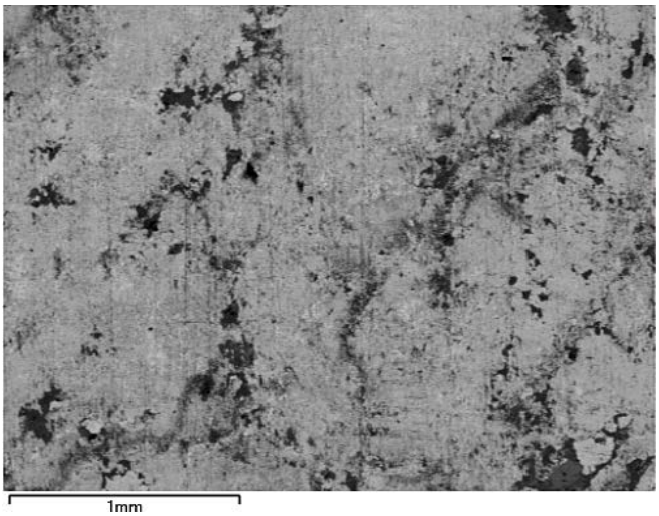

Element (At%)	1
O	38.70
Na	1.09
Mg	1.07
Al	4.58
Si	9.29
S	5.92
Ca	0.53
Fe	0.33
Cu	38.50
Total	100.00

Figure C-21. *EDS analysis of the surface of S2/O (100×).*

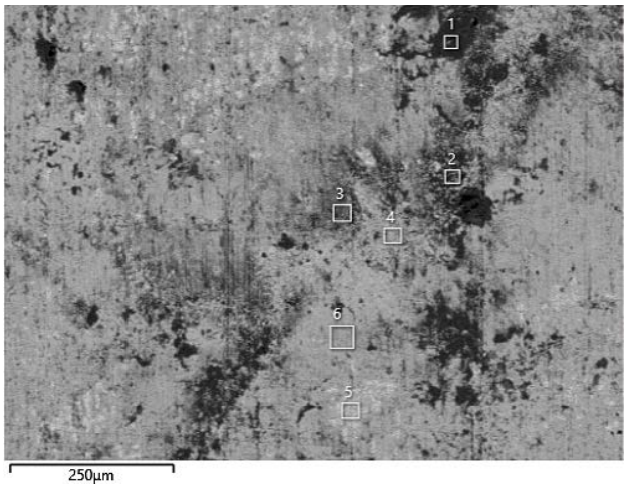

Element (At%)	1	2	3	4	5	6
O	60.78	53.22	50.72	23.14	10.40	32.39
Na	1.89	1.60	1.52			
Mg	1.40	1.43	1.16	0.31		0.82
Al	9.10	6.78	6.28	1.14	0.75	2.71
Si	20.85	15.80	13.01	2.23	1.30	5.15
S	1.09	3.83	5.56	14.15	3.61	7.84
Cl		0.09	0.13	0.24		0.14
K	0.11	0.07				
Ca	0.26	0.85	0.33	0.33		0.57
Fe	1.10	0.59	0.54			
Cu	3.42	15.74	20.75	58.45	83.94	50.37
Total	100.00	100.00	100.00	100.00	100.00	100.00

Figure C-22. *EDS analysis of the surface of S2/O (300×).*

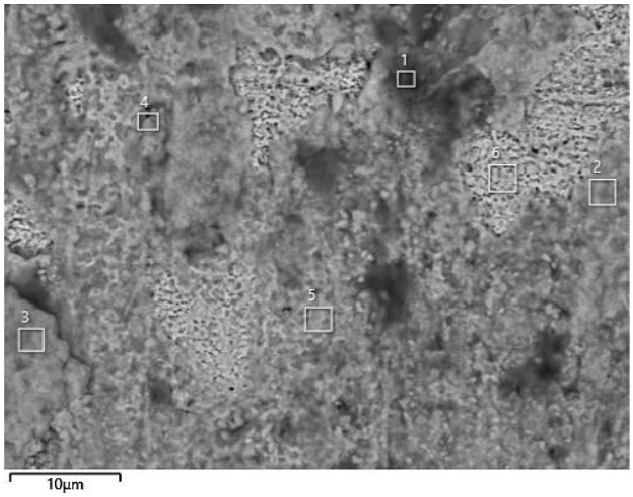

Element (At%)	1	2	3	4	5	6
O	66.77	32.08	37.87	28.62	21.60	2.85
Na	0.85	0.74				
Mg	0.51	0.79	0.91	0.82	0.27	
Al	2.05	3.29	3.61	2.78	1.47	
Si	4.35	6.48	8.28	5.60	2.72	0.48
S	3.21	7.36	10.05	6.30	6.51	0.41
Cl		0.13	0.24			
Ca	13.74	0.11	0.65		0.13	
Fe	0.14	0.28	0.36	0.17		
Cu	8.38	48.74	38.04	55.27	67.29	96.26
Total	100.00	100.00	100.00	100.00	100.00	100.00

Figure C-23. *EDS analysis of the surface of S2/O (5000×).*

C1.3.8 Coupon S2/P

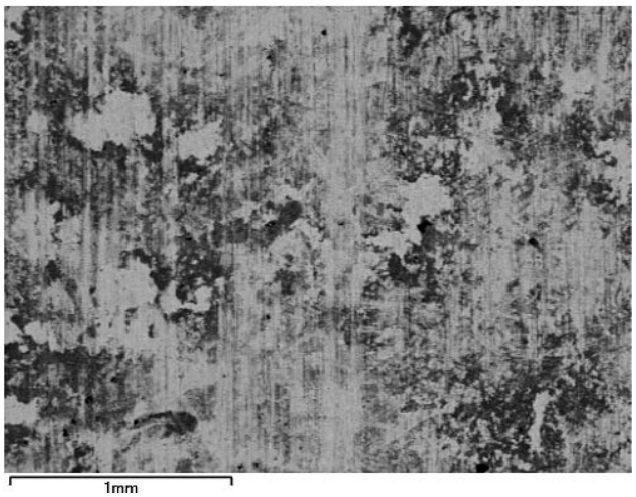

Element (At%)	1
O	40.92
Mg	1.13
Al	4.91
Si	11.46
S	7.32
Cl	0.12
Ca	0.43
Fe	0.37
Cu	33.34
Total	100.00

Figure C-24. *EDS analysis of the surface of S2/P (100×).*

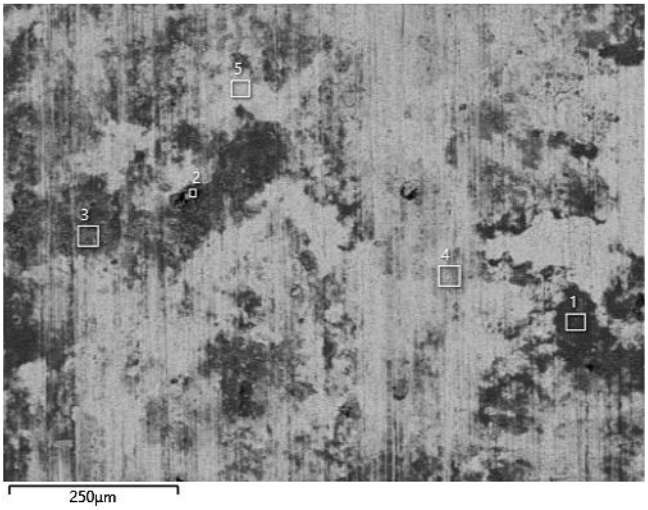

Element (At%)	1	2	3	4	5
O	61.78	51.58	53.07	35.29	11.44
Mg	1.36	1.33	1.25	0.80	
Al	7.57	7.89	6.15	3.60	0.59
Si	21.24	26.61	15.28	8.36	1.10
S	1.79	3.22	5.59	10.55	10.50
Cl	0.05		0.09	0.14	
K	0.05	0.15			
Ca	0.68	0.71	0.52	0.48	0.22
Fe	0.77	0.56	0.52	0.26	
Cu	4.69	7.94	17.54	40.51	76.15
Total	100.00	100.00	100.00	100.00	100.00

Figure C-25. *EDS analysis of the surface of S2/P (300×).*

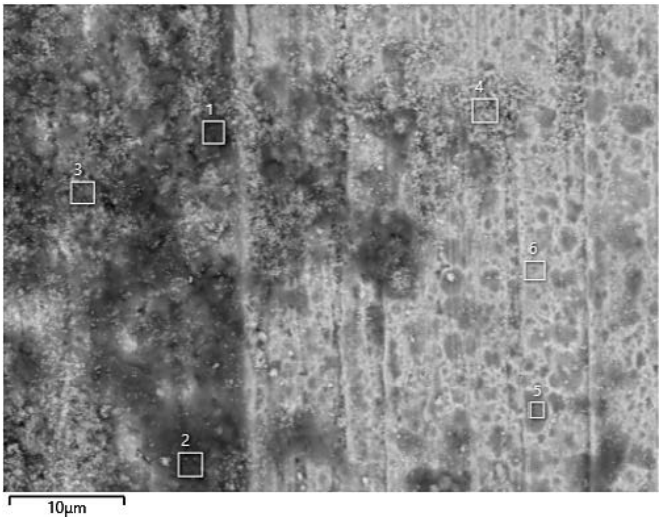

Element (At%)	1	2	3	4	5	6
O	57.90	58.00	48.72	30.43	7.34	8.98
Mg	1.28	1.10	1.13	0.70		
Al	8.24	6.32	5.65	2.91		0.56
Si	17.26	19.44	14.82	7.44	0.32	1.21
S	3.60	3.35	7.87	12.17	10.71	9.97
Cl	0.07		0.08	0.21		
K		0.06	0.07			
Ca	0.60	0.60	0.58	0.22		
Fe	0.78	0.53	0.56	0.28		
Cu	10.27	10.61	20.52	45.62	81.63	79.27
Total	100.00	100.00	100.00	100.00	100.00	100.00

Figure C-26. *EDS analysis of the surface of S2/P (5000×).*

C1.3.9 Reference coupon K

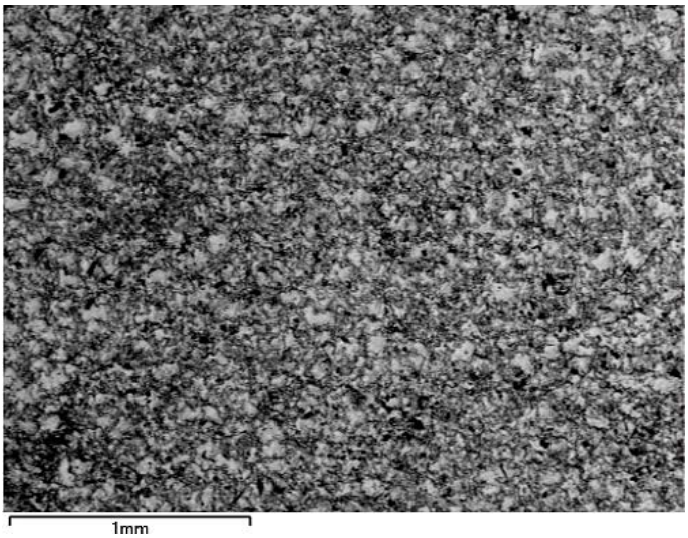

Element (At%)	1
O	30.36
Al	0.36
Si	0.49
Cl	1.13
Cu	63.05
Zn	4.61
Total	100.00

Figure C-27. *EDS analysis of the surface of reference coupon K (100×).*

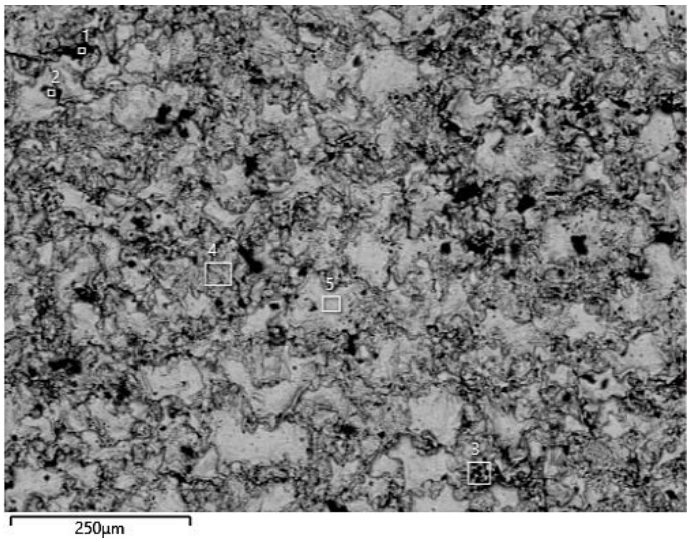

Element (At%)	1	2	3	4	5
O	63.28	44.14	39.72	22.85	11.32
Na	7.27	2.11			
Mg			1.44		
Al	0.74	0.48	1.23		
Si	0.87	0.70	1.93	0.53	
S	0.85		0.24		
Cl	1.45	1.82	1.23	0.76	0.49
K	4.99	0.79	0.51		
Ca	0.55		1.01		
Fe	0.27		0.42		
Cu	17.76	47.97	49.17	72.24	84.83
Zn	1.98	1.99	3.10	3.62	3.38
Total	100.00	100.00	100.00	100.00	100.00

Figure C-28. *EDS analysis of the surface of reference coupon K (300×).*

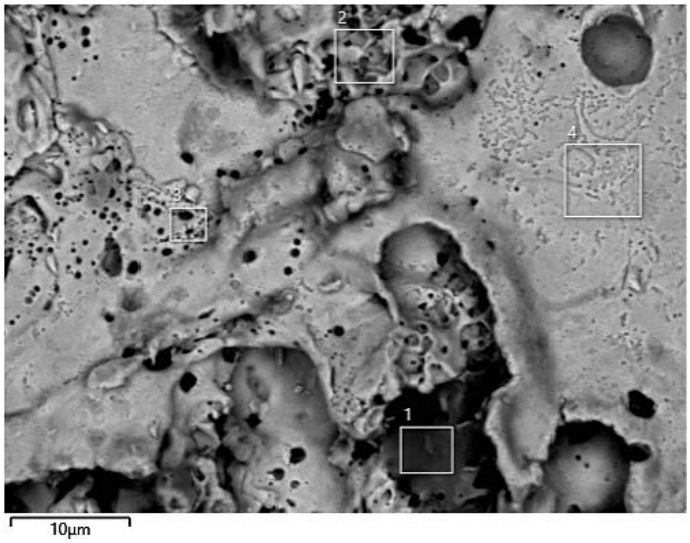

Element (At%)	1	2	3	4
O	50.81	17.64	13.63	9.36
Na	4.64			
Mg	0.50			
Al	7.26			
Si	15.56			
Cl	0.22	0.98	0.62	0.31
K	0.62	0.24		
Ca	0.73			
Cu	18.26	76.87	82.34	88.03
Zn	1.40	4.27	3.41	2.30
Total	100.00	100.00	100.00	100.00

Figure C-29. *EDS analysis of the surface of reference coupon K (5000×).*

C1.3.10 Reference coupon L

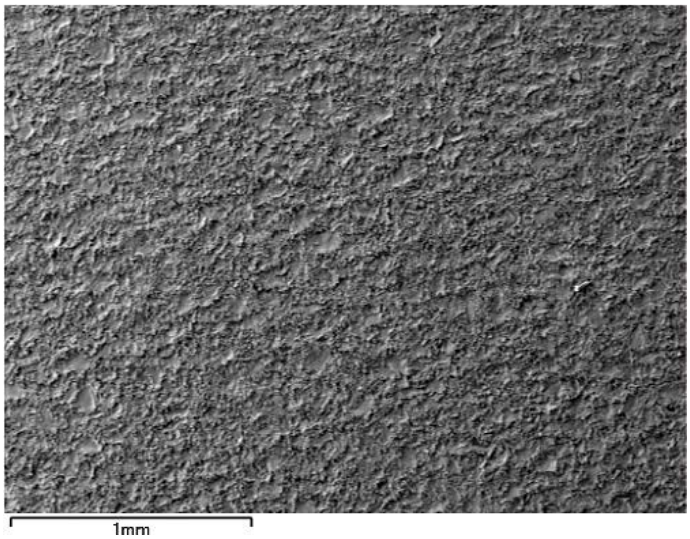

Element (At%)	1
O	14.47
Cu	81.33
Zn	4.21
Total	100.00

Figure C-30. *EDS analysis of the surface of reference coupon L (100×).*

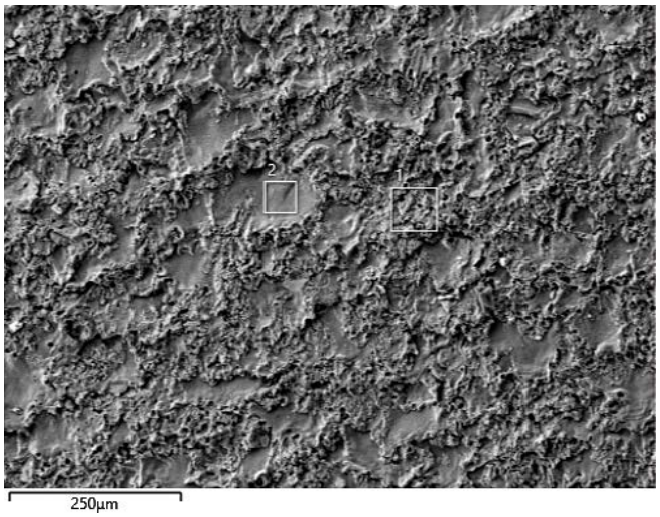

Element (At%)	1	2
O	12.30	8.40
Cu	83.54	88.86
Zn	4.16	2.73
Total	100.00	100.00

Figure C-31. *EDS analysis of the surface of reference coupon L (300×).*

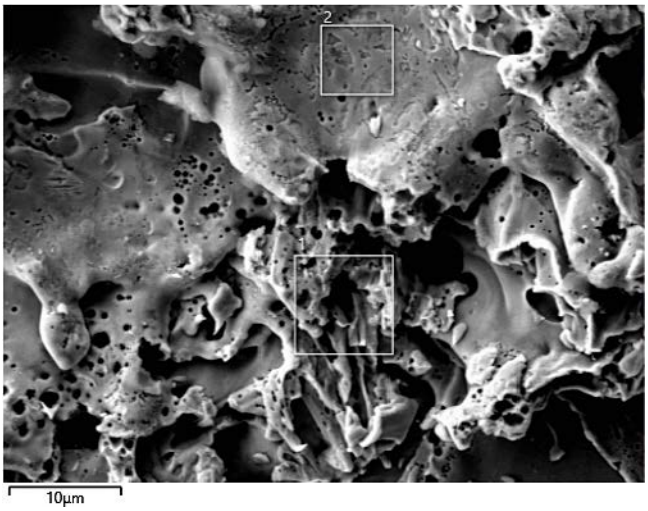

Element (At%)	1	2
O	14.16	5.01
Ca	0.57	
Cu	80.89	92.64
Zn	4.38	5.01
Total	100.00	100.00

Figure C-32. *EDS analysis of the surface of reference coupon L (5000×).*

C1.3.11 EDS analysis of cross section of sample A3/K

C1.3.11.1 Cross section 1

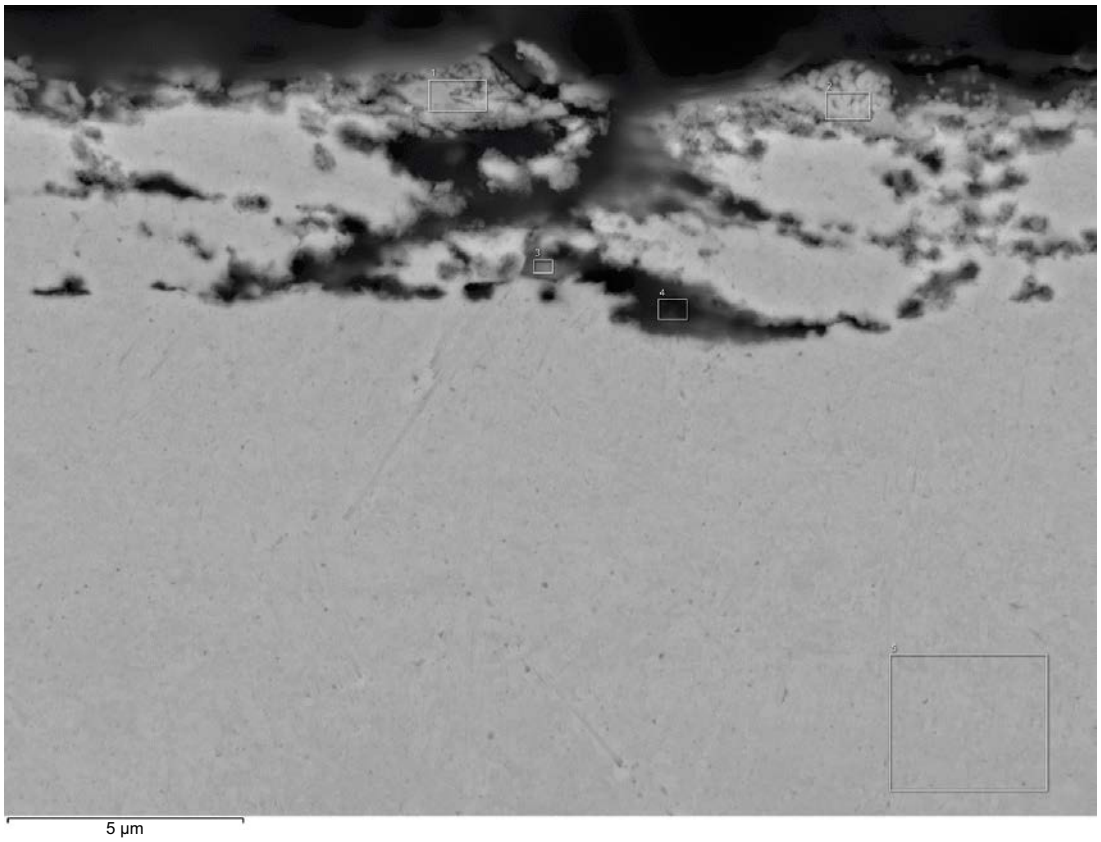

Element (At%)	1	2	3	4	5
O	6.33	8.17	7.50	8.81	0.87
Mg	0.67				
Al	0.39	0.31			
Si	1.18	0.80			
S	28.14	24.28			
Cl	0.38	0.42			
Ca	0.76	0.20			
Fe	1.12	0.95			
Cu	61.03	64.87	92.50	91.19	99.13
Total	100.00	100.00	100.00	100.00	100.00

Figure C-33. *EDS analysis of the cross-section of A3/K.*

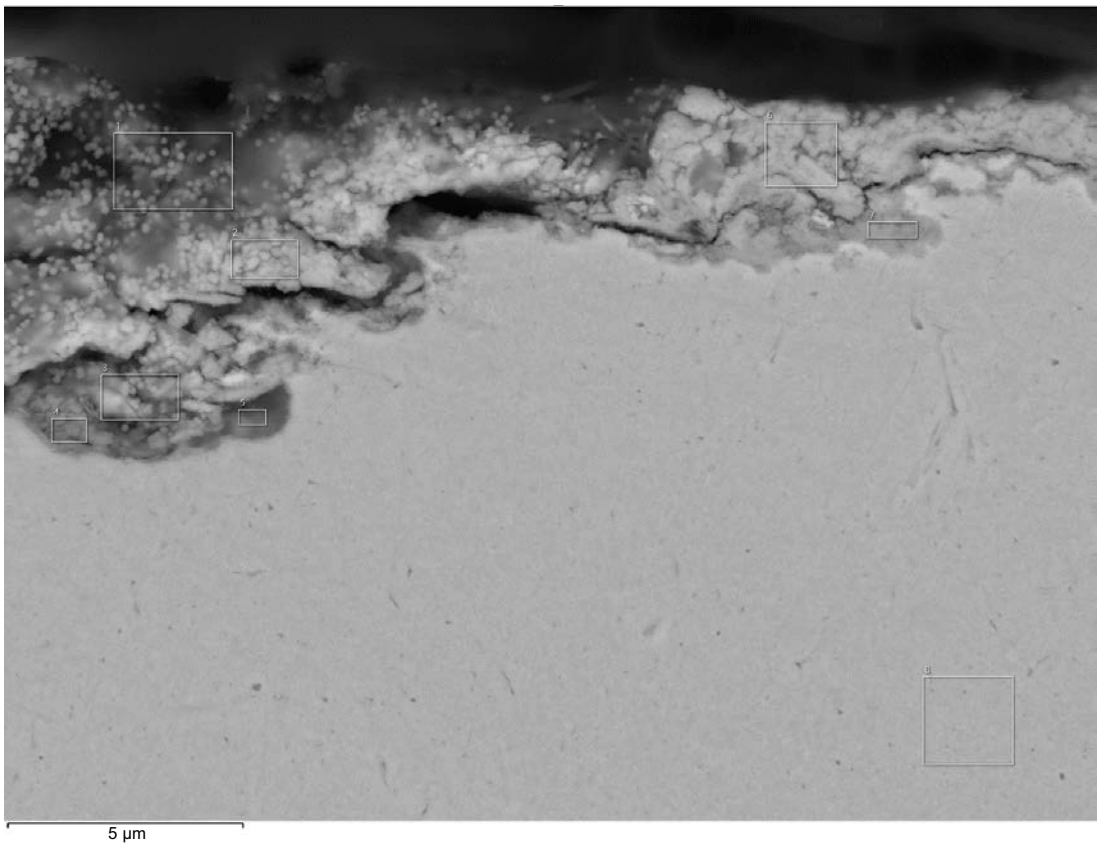

Element (At%)	1	2	3	4	5	6	7	8
O	37.48	22.01	25.20	18.03	12.26	13.93	4.65	0.45
Mg	1.88	0.38	0.62	0.34				
Al	7.88	1.68	1.90	0.71				
Si	20.12	3.98	4.58	1.75	0.52	1.99		
S	11.49	13.43	10.10	4.52	1.98	16.17	0.89	
Cl	0.10	0.26	0.30			0.22		
Ca	0.46							
Cu	20.59	58.27	57.29	74.66	85.25	67.69	94.46	99.55
Total	100.00	100.00	100.00	100.00	100.00	100.00	100.00	100.00

Figure C-34. *EDS analysis of the cross-section of A3/K.*

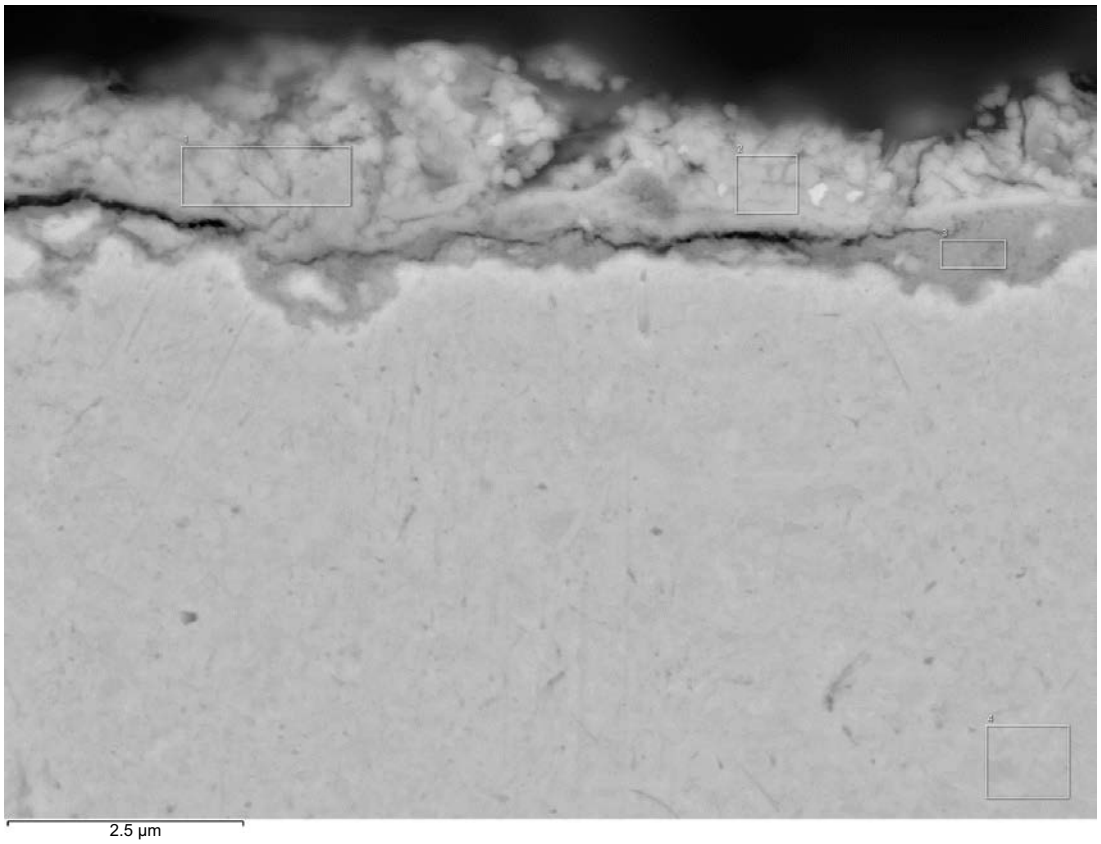

Element (At%)	1	2	3	4
O	14.62	12.77	14.39	0.51
Al	0.63	0.66		
Si	2.08	2.23	0.70	
S	17.71	17.27	5.32	
Cl	0.23	0.33	0.28	
Cu	64.73	66.72	79.31	99.49
Total	100.00	100.00	100.00	100.00

Figure C-35. *EDS analysis of the cross-section of A3/K.*

C1.3.11.2 Cross section 2

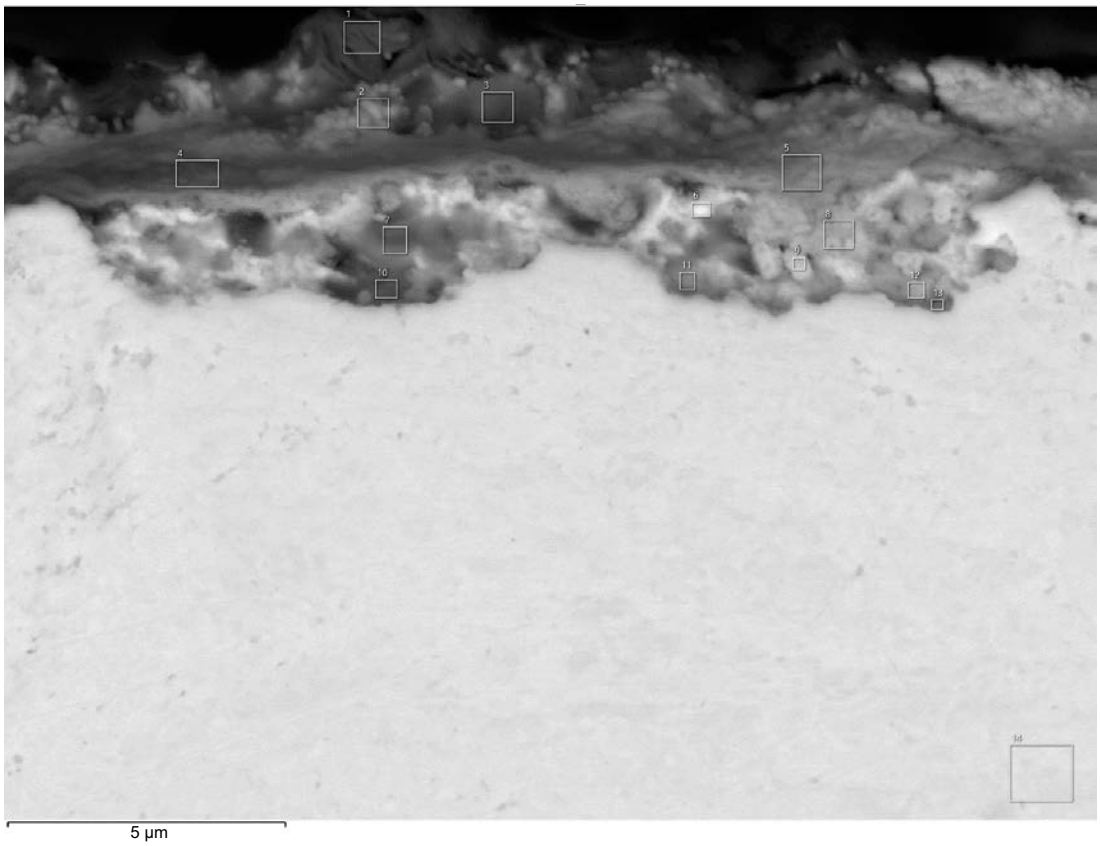

Element (At%)	1	2	3	4	5	6	7	8	9	10	11	12	13	14
O	41.32	47.90	58.46	22.27	21.16	15.49	29.73	17.68	20.77	19.49	20.41	14.40	18.01	0.91
Na	6.02	4.57	2.57											
Mg	3.61	1.40	0.63	0.69	0.55	0.74	0.39	0.50			0.46			
Al	9.22	4.66	2.34	1.72	1.58	0.93	0.28	0.70	0.71	0.41	0.73	0.89	0.55	0.64
Si	26.20	12.40	21.73	4.80	3.69	2.01	12.24	2.81	2.47	5.80	7.76	2.80	6.76	
S	3.21	6.02	3.11	15.91	13.69	3.92	1.50	9.31	3.28	0.45	0.59	6.07	2.55	
Cl		0.21	0.08	0.20	0.20	0.14		0.37	0.94			0.20		
Ca	0.78	0.32	0.14	0.15			0.22			0.27				
Fe	5.47	1.64	0.57	1.16	1.43	1.41	0.91	1.17	0.91	1.01	0.95	1.03	0.90	0.60
Cu	4.17	20.88	10.36	53.10	57.68	75.35	54.73	67.47	70.92	72.57	69.10	74.62	71.22	97.85
Total	100.00	100.00	100.00	100.00	100.00	100.00	100.00	100.00	100.00	100.00	100.00	100.00	100.00	100.00

Figure C-36. *EDS analysis of the cross-section of A3/K.*

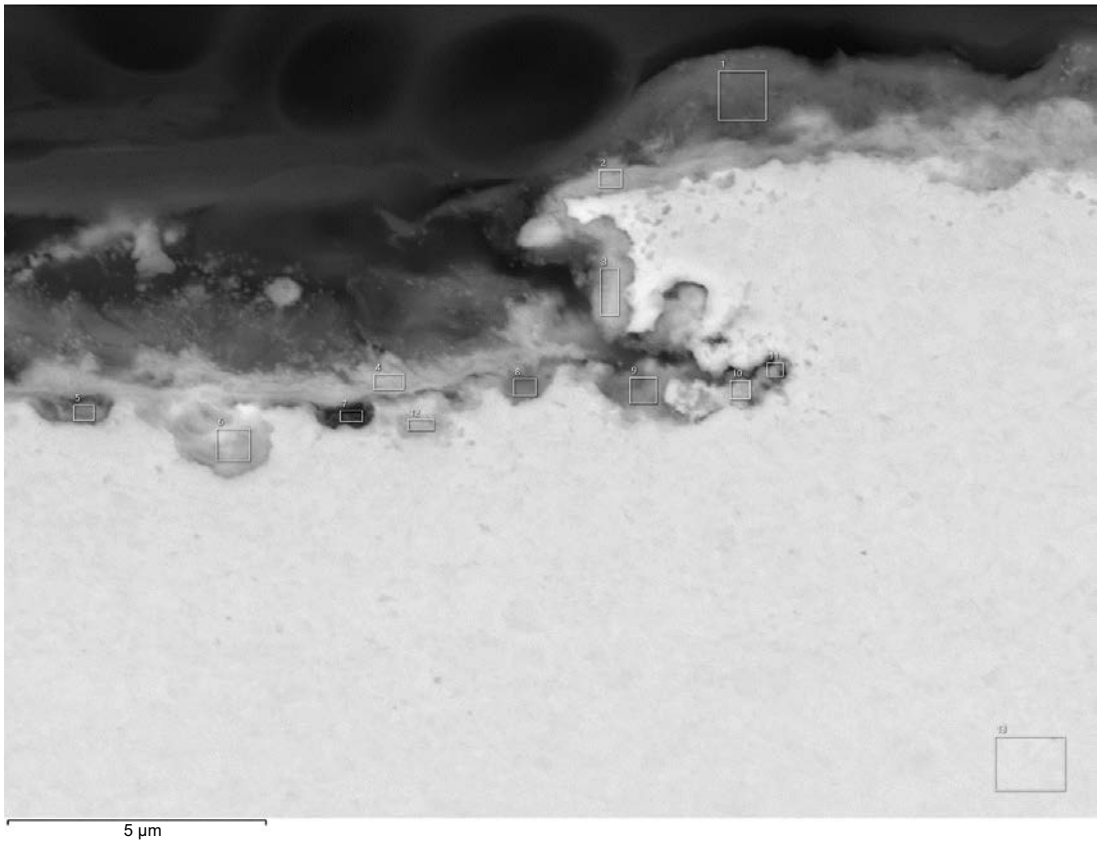

Element (At%)	1	2	3	4	5	6	7	8	9	10	11	12	13
O	59.18	31.54	31.98	36.35	27.91	11.00	23.67	22.25	13.06	7.22	3.93	16.33	0.88
Na	3.95	2.59	1.46	2.08	2.75		2.44	2.69	2.66				
Mg	1.32	0.75	0.93	1.51	1.12		1.09	0.69	0.39			0.73	
Al	6.48	3.37	3.08	2.51	1.13	0.68	2.10	1.39	0.96	0.96	0.76	0.61	0.84
Si	18.55	8.02	7.63	5.96	4.60	1.33	5.13	4.41	1.86	1.22	0.91	2.85	
P			0.13	0.17	0.28	0.14	0.45	0.20					
S	1.87	7.56	7.54	5.70	3.67	2.11	4.66	4.51	2.08	0.57	0.55	3.31	
Cl	0.05	0.34	1.17	0.38	0.13		0.22	0.20	0.16				
Ca	0.57	0.37	0.39	0.39	0.64	0.13	1.13	0.31				0.37	
Fe	1.95	0.96	0.82	0.72	1.06	0.51	0.43	0.53	0.44	0.91	1.00	0.91	0.41
Cu	6.09	44.50	44.88	44.24	56.72	84.10	58.69	62.82	78.38	89.12	92.85	74.90	97.87
Total	100.00	100.00	100.00	100.00	100.00	100.00	100.00	100.00	100.00	100.00	100.00	100.00	100.00

Figure C-37. *EDS analysis of the cross-section of A3/K.*

C1.3.12 EDS analysis on cross section of sample S2/N

C1.3.12.1 Cross section 1

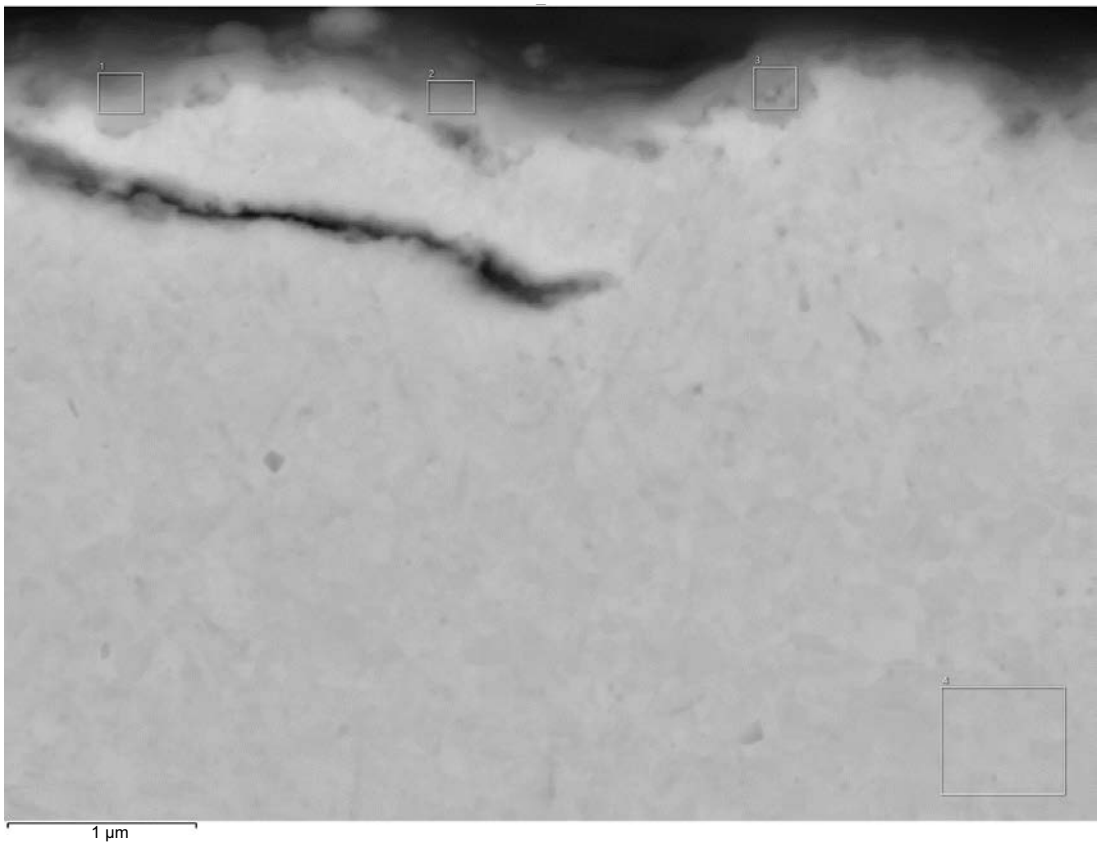

Element (At%)	1	2	3	4
O	12.50	14.29	8.29	0.96
Si	1.47		1.33	
S	4.10	1.46	4.13	
Cl		0.26	0.86	
Cu	81.93	83.98	85.37	99.04
Total	100.00	100.00	100.00	100.00

Figure C-38. *EDS analysis of the cross-section of S2/N.*

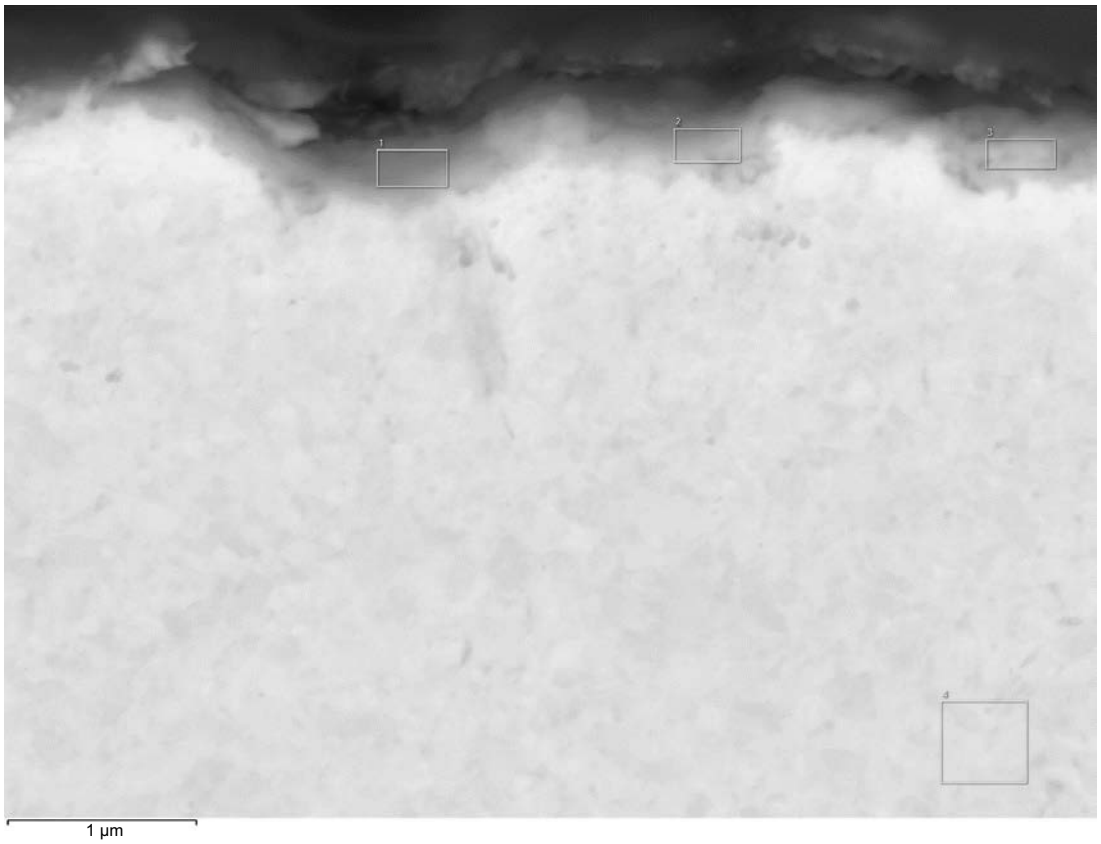

Element (At%)	1	2	3	4
O	17.00	13.88	12.02	0.80
Al	0.55			
Si	0.92	0.45	0.50	
S	3.04	1.31	1.12	
Cu	78.49	84.37	86.36	99.20
Total	100.00	100.00	100.00	100.00

Figure C-39. *EDS analysis of the cross-section of S2/N.*

C1.3.12.2 Cross section 2

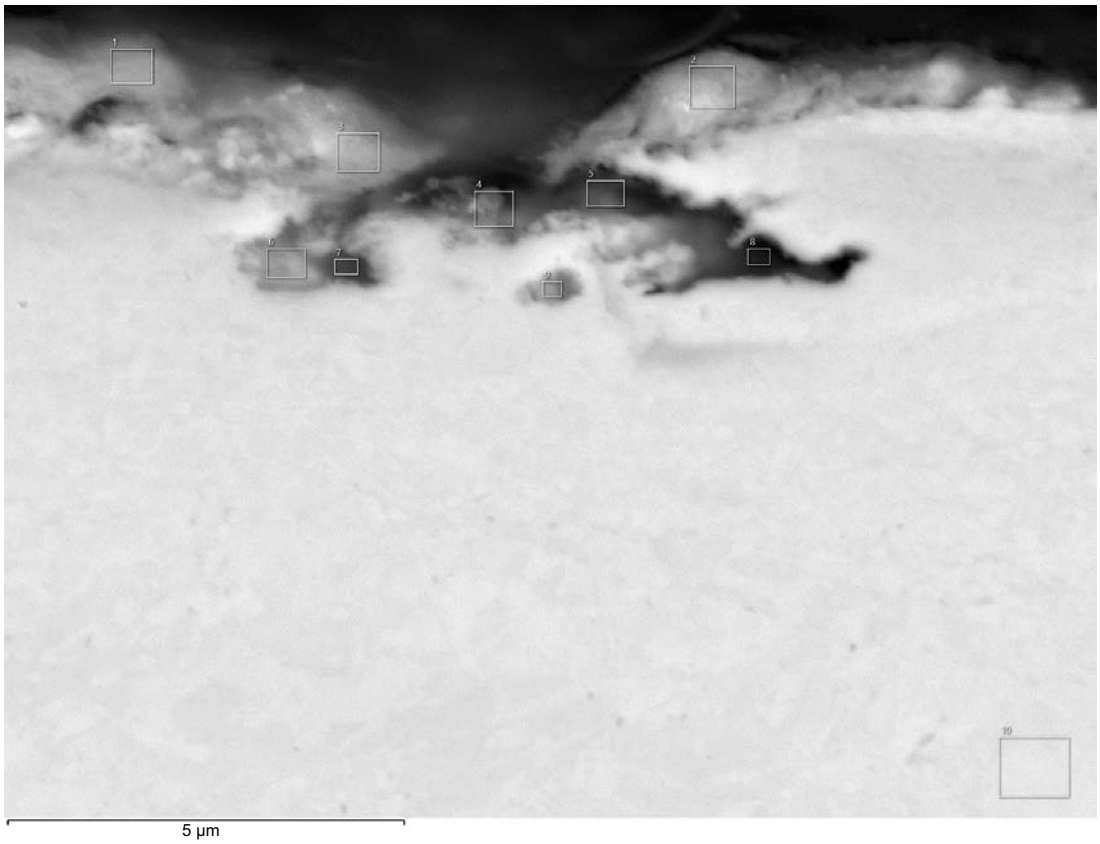

Element (At%)	1	2	3	4	5	6	7	8	9	10
O	37.64	32.12	31.60	21.05	19.35	7.58	11.64	8.31	2.04	1.09
Na	4.98	3.80	3.61	2.59	2.98					
Mg	1.37	1.98	0.94	1.10	0.80	0.41	0.36			
Al	2.45	2.04	2.72	1.66	1.36	0.73	0.79	0.26	0.43	0.66
Si	7.75	5.90	7.08	2.63	2.47	0.55	0.66	0.63		0.18
S	5.17	5.17	5.75	2.78	2.88	0.68	0.68	1.43	0.42	
Cl	0.07									
Ca	0.38	0.40	0.35	0.31	0.18					
Fe	2.04	2.24	2.68	1.51	1.46	1.34	1.39	2.46	1.81	0.83
Cu	38.14	46.35	45.27	66.39	68.51	88.71	84.48	86.92	95.30	97.24
Total	100.00	100.00	100.00	100.00	100.00	100.00	100.00	100.00	100.00	100.00

Figure C-40. *EDS analysis of the cross-section of S2/N.*

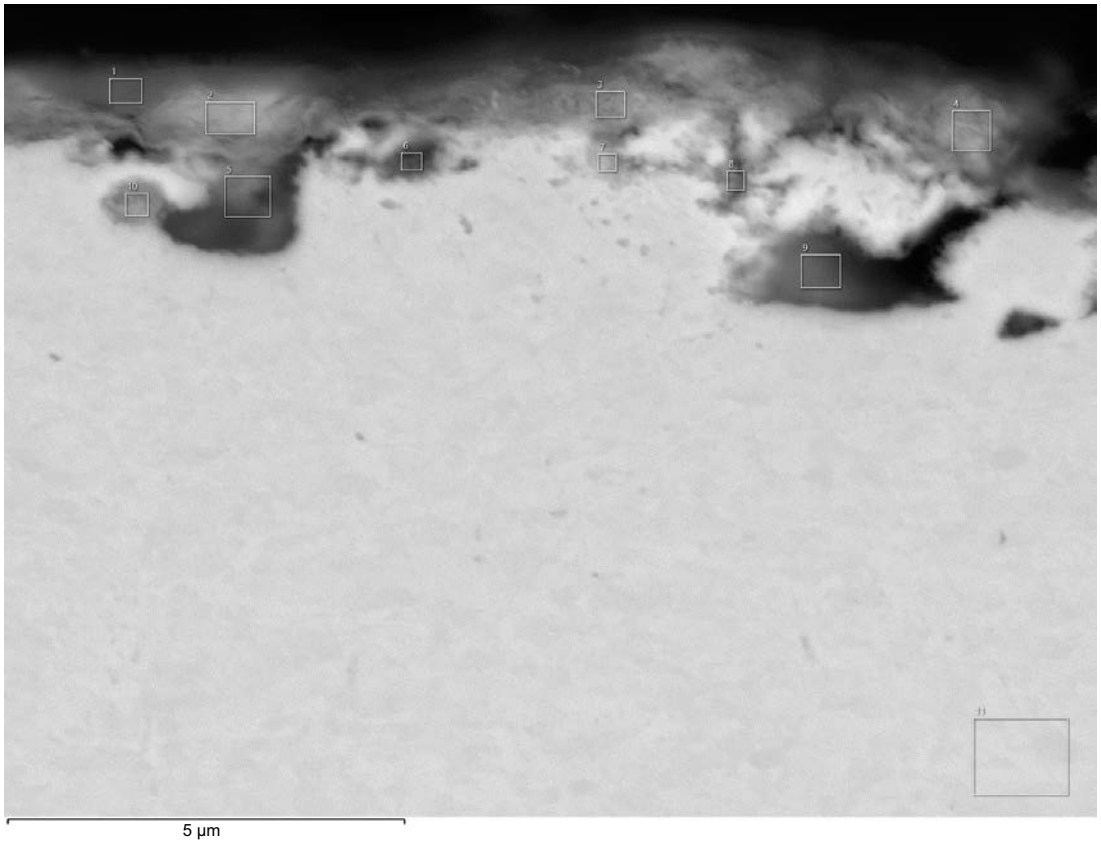

Element (At%)	1	2	3	4	5	6	7	8	9	10	11
O	47.32	38.93	31.44	39.03	12.34	14.36	15.14	17.62	9.34	5.59	0.89
Na	11.77	10.74	19.79	15.26	6.49	6.25	4.36	2.41			
Mg	3.77	3.37	0.80	2.86	0.33	0.62	0.39	0.44			
Al	3.34	2.04	0.59	1.57	0.32	0.53	0.89	0.65			0.99
Si	8.41	4.43	1.60	3.69	0.37	0.73	0.96	0.32	0.25		
S	4.41	5.36	7.57	6.99	1.66	2.06	2.54	3.65	1.88	0.58	
Cl	0.09	0.21	0.20	0.14			0.17	0.30			
Ca	0.30	0.15	0.08	0.21							
Fe	2.12	0.83	0.47	0.72	1.28	0.91	0.78	0.76	2.06	0.93	0.64
Cu	18.47	33.94	37.46	29.54	77.22	74.54	74.77	73.86	86.46	92.90	97.48
Total	100.00	100.00	100.00	100.00	100.00	100.00	100.00	100.00	100.00	100.00	100.00

Figure C-41. *EDS analysis of the cross-section of S2/N.*

C1.4 Examination of cross-sectioned samples of coupons A3/K and S2/N using transmission electron microscopy (TEM)

In total, 4 samples for TEM analysis (lamellae) were prepared using focused ion beam machining (FIB), 2 lamellae from each coupon. The lamellae were cut in the bottom of selected pits that had already been investigated using SEM and where the highest amount of sulfur had been found. Since the samples analysed were already cross-sections, the TEM lamellae are planar cuts, parallel to the surface, from the bottom of the pits. The lamellae from coupon A3/K are named 1 and 2, whilst the lamellae from coupon S2/N are named 3 and 4. Figure C-42, Figure C-48, and Figure C-57 show the positions of the lamellae taken from the cross section samples.

TEM lamellae were prepared using FIB with a FEI Strata DB235 instrument, using the in situ lift-out technique. A metal-organic precursor consisting of Pt and C was deposited using the electron beam to protect the area of interest from the high energy ions during milling and preparation of the lamellae. The lamellae were then transferred to special grids which are of the correct dimensions for analysis in the TEM, then polished to electron transparency with successively lower beam currents, to achieve a sharper ion beam and less surface damage on the final lamellae. During the final step of preparation, the lamellae were cleaned using low energy ions (5 keV) to remove the majority of affected layer on both sides of the lamellae. This method results in approximately 5 nm of amorphous layers on each side of the lamellae instead of ~20 – 30 nm.

The grids are typically made from Cu, but in this case when Cu was to be analysed, Ti grids are more suitable so that EDS analysis can be performed in the TEM without the unavoidable additional Cu signal from the grid. However, for the first lamella from each sample Cu grids were used since no Ti grids were available at the time.

The lamellae were investigated in A JEOL 2001F TEM equipped with an EDS detector from Oxford Instruments and a Gatan Trideum energy filter for Electron Energy-Loss Spectroscopy (EELS). When performing EDS and EELS, the TEM was run in STEM mode (scanning TEM) so that the beam is scanned over the sample and elemental information collected from each pixel separately. The STEM images exhibit compositional contrast, resulting in brighter areas in the image with a higher mean composition (or density). It should be noted that regions that are significantly thicker are also observed as brighter, for example areas closest to the grid for each lamella.

C1.4.1 Coupon A3/K lamella 1

Figure C-43 shows STEM images of almost the whole lamella 1. Notable are the bright particles that are present throughout the lamella. These particles have a round, but irregular shape and are typically 50 – 80 nm. Higher magnification also reveals a large number of smaller particles, see Figure C-44.

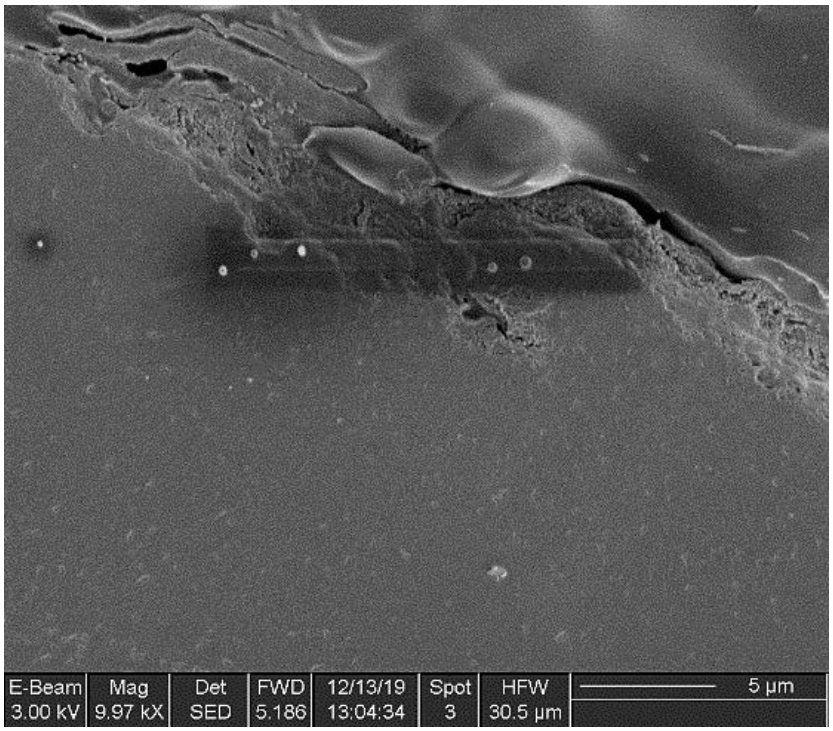

Figure C-42. *FIB SEM image showing the position from where lamella 1 was taken from sample A3/K. The rectangular box is the deposited Pt-precursor that protects the area of interest during milling.*

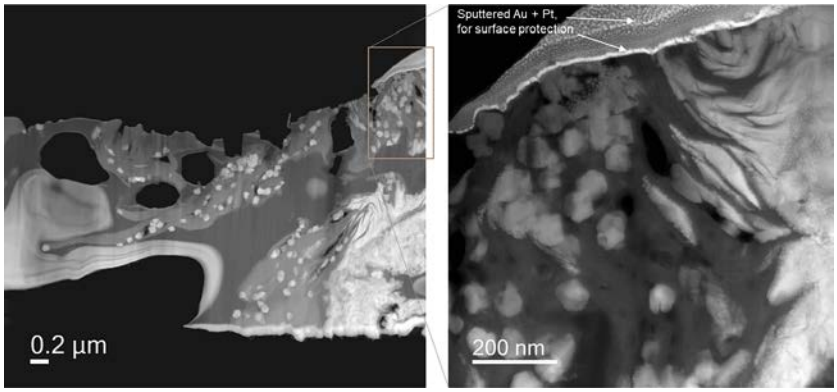

Figure C-43. *STEM images showing a lot of round particles in lamella 1.*

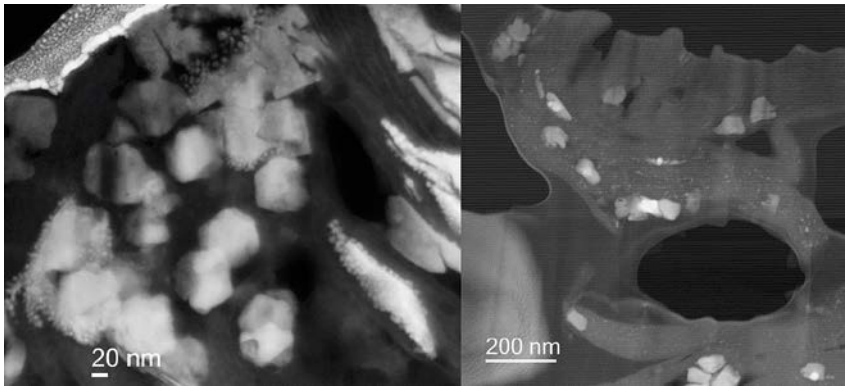

Figure C-44. *STEM images showing a high number of even smaller particles present in lamella 1.*

STEM EDS maps acquired from lamella 1 display that the larger particles consist of Cu and S, while the surrounding material is a mixture of mainly oxides from Cu, Si, Fe, Al, Ca, including also some Cl and C, which is most likely remaining bentonite clay, see Figure C-45.

Examples from quantitative EDS results acquired from selected areas are displayed in Figure C-46. The larger round particles (spectrum 3 and 7) consist mainly of Cu and S. The more compact bright area at the bottom of the image (spectrum 4) also seems to contain mainly Cu and S. There is one particle that except from Cu and O contains Na, Cl, and Ca (spectrum 2), which could be a salt crystal. The darker region in the centre of the image (spectrum 5) is likely clay. The bright streaks to the right of the image (spectrum 6) appear to be mainly Cu-oxide.

Since the lamella is about 100 nm thick and heterogeneous there will be some contributions from surrounding material in the spectra. The X-ray information of a single point typically originates from an area in the image with a radius up to ~ 50 – 100 nm, but most of the signal comes from the centre of that area. Therefore, where bentonite clay is present some contribution to the analysis result can be expected (bentonite clay has a typical composition of ~ 80 % SiO_2, 6 % Al, 1 % Mg, 0.5 % S, and 2 % Ca). Additionally, due to the expected Cu signal from the support grid, there will be an increased amount of background Cu signal in all analysis points. It is therefore doubtful if the areas corresponding to spectrum 5 and 8 contain any Cu.

In order to verify that the larger round particles (spectrum 3 in Figure C-46) were Cu-S, EELS was performed. EELS is more complicated and requires very thin areas, but the spatial resolution is much higher than EDS. The signal comes only from very close to the beam (< 1 nm). Figure C-47 shows the spectrum image and extracted maps of Cu, S, O, and C. Here the particles are a Cu-S phase, no other main elements were identified. However, for EELS the detection limit is less than EDS and elements present in less ~ 1 wt% are not be identified.

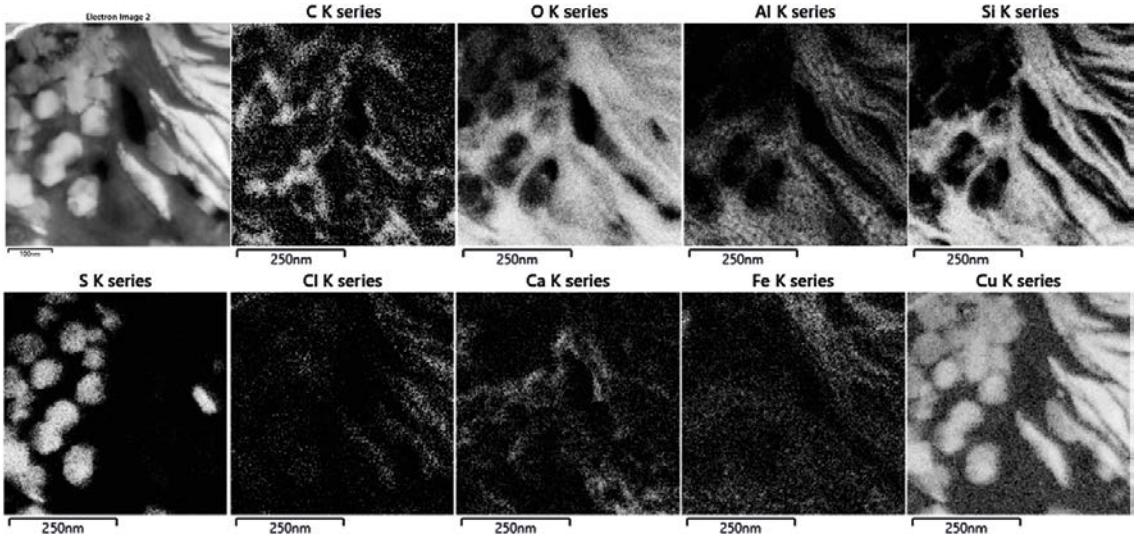

Figure C-45. *STEM EDS maps acquired from lamella 1. Note that the intensity scales apply only within the same map and cannot be compared to other maps. The intensity on one map may have a scale between 0 and 1 At%, and in another between 60 and 80 At%. The Cu map cannot be completely trusted quantitatively, since a certain amount of Cu comes from the support grid, but relative amounts should be accurate.*

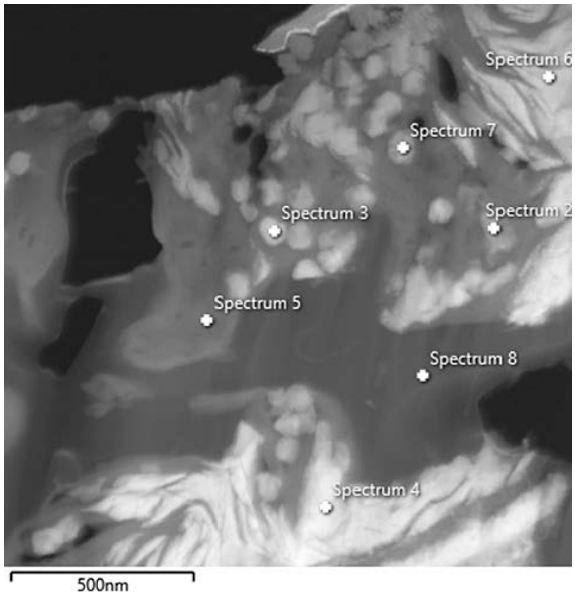

With C							
Element (At%)	**2**	**3**	**4**	**5**	**6**	**7**	**8**
C	9.14	14.09	2.54	14.87	1.80	24.67	89.7
O	31.79	5.79	3.05	51.04	38.18	11.28	5.74
Na	2.28	0.80	0	0	0	1.24	0.26
Mg	0.39	0.18	0	0.90	0.14	0.42	0
Al	0.27	0.28	0.17	1.83	0.71	0.63	0.02
Si	2.20	0.42	0	17.47	2.75	2.92	0.02
S	0	24.35	26.72	0.08	0	15.64	0.02
Cl	4.42	0	0.16	0	1.16	0.14	0.01
Ca	1.98	0.08	0	0.13	0	0.19	0
Fe	0.24	0.46	0.18	0.12	0.26	0.25	0.01
Cu	47.28	53.56	67.19	13.55	54.99	42.63	4.22
Total	100	100	100	100	100	100	100

Without C							
Element (At%)	**2**	**3**	**4**	**5**	**6**	**7**	**8**
O	34.99	6.74	3.13	59.96	38.88	14.97	55.71
Na	2.51	0.93	0	0	0	1.64	2.57
Mg	0.43	0.21	0	1.05	0.15	0.56	0
Al	0.30	0.32	0.18	2.15	0.72	0.84	0.15
Si	2.42	0.49	0	20.52	2.80	3.88	0.20
S	0	28.34	27.41	0.09	0	20.76	0.24
Cl	4.86	0	0.16	0	1.18	0.19	0.10
Ca	2.18	0.09	0	0.16	0	0.25	0
Fe	0.26	0.53	0.18	0.15	0.27	0.33	0.10
Cu	52.04	62.34	68.94	15.92	56.00	56.59	40.94
Total	100	100	100	100	100	100	100

Figure C-46. *Quantitative EDS results (At%) of selected areas in the lamella 1. In the second table, C has been removed since there will always be some C due to contamination, but in this case, the surrounding material probably also contains a high amount of C.*

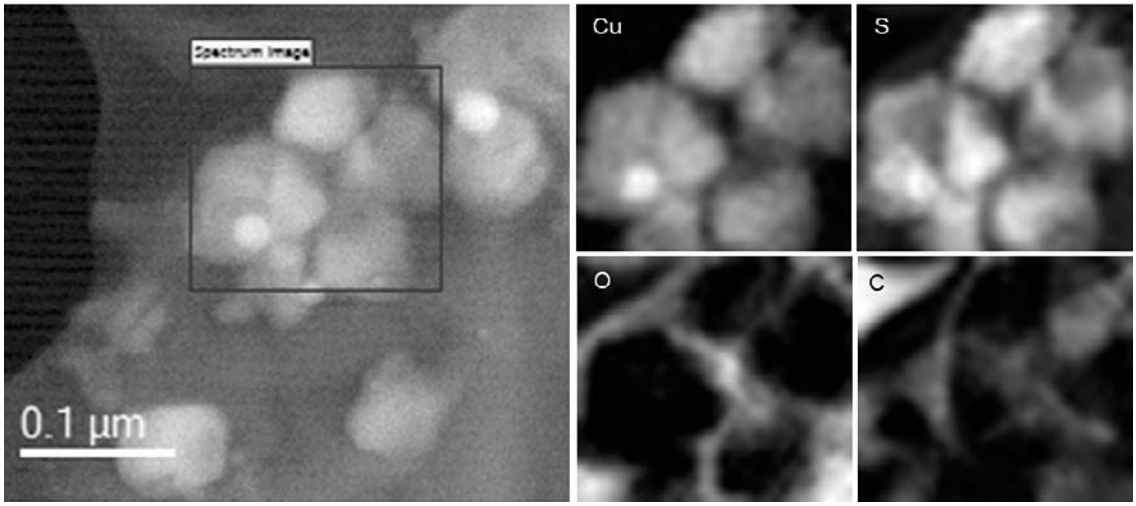

Figure C-47. *EELS maps from a region in lamella 1 where there are several larger Cu-S particles.*

C1.4.2 Coupon A3/K lamella 2

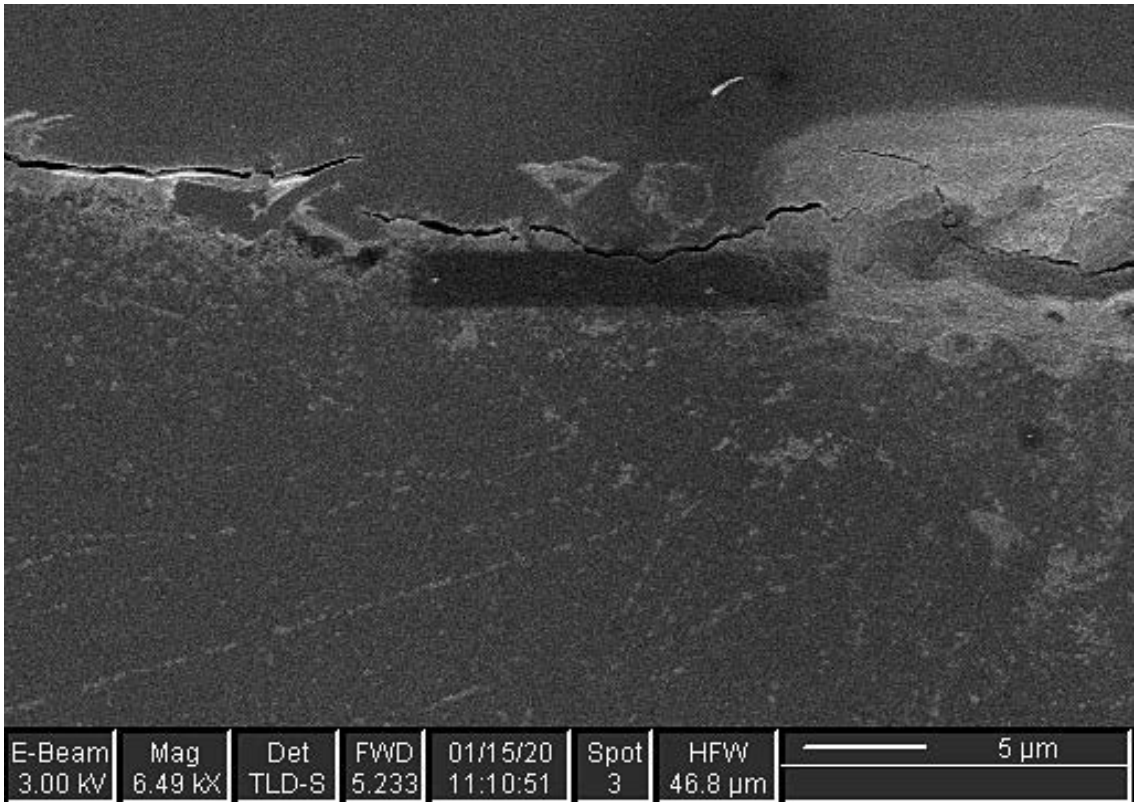

Figure C-48. *FIB SEM image showing the position from where lamella 2 was taken from sample A3/K. The rectangular box is the deposited Pt-precursor that protects the area of interest during milling.*

Figure C-49 shows the whole of lamella 2, including zoomed in images of two of the interesting areas. As with lamella 1, round particles of ca 50 – 80 nm were observed. EDS maps acquired over the region where the particles were observed can be seen in Figure C-50. Again, the particles appear to be Cu-S. They seem to be either compacted into or released from a larger and denser layer of Cu-S. in the surrounding areas Si- and Fe-oxides as well as C were observed. Small amounts of Na, Cl, Mg, and Ca were also found in the analyses.

Examples of quantitative EDS results from selected areas in lamella 2 are seen in Figure C-51. This lamella was mounted on a Ti grid, so no additional Cu signal is added into the results. The S-rich particles and layer (spectra 54–60) all appear to have the ratio Cu_2S. The surrounding dark regions (spectra 61–63), appear to be clay, but with higher amounts of Fe, likely Fe-oxide from the bedrock. The region closest to the Cu metal (spectra 64–67) shows high amounts of oxide, but also some Fe, S, and Si. However, it seems to be an oxide layer between the Cu and the thicker S layer. The results indicate that the Cu-oxide must have much more Cu than O, so the oxide is likely Cu_2O, as seen in the XRD analyses.

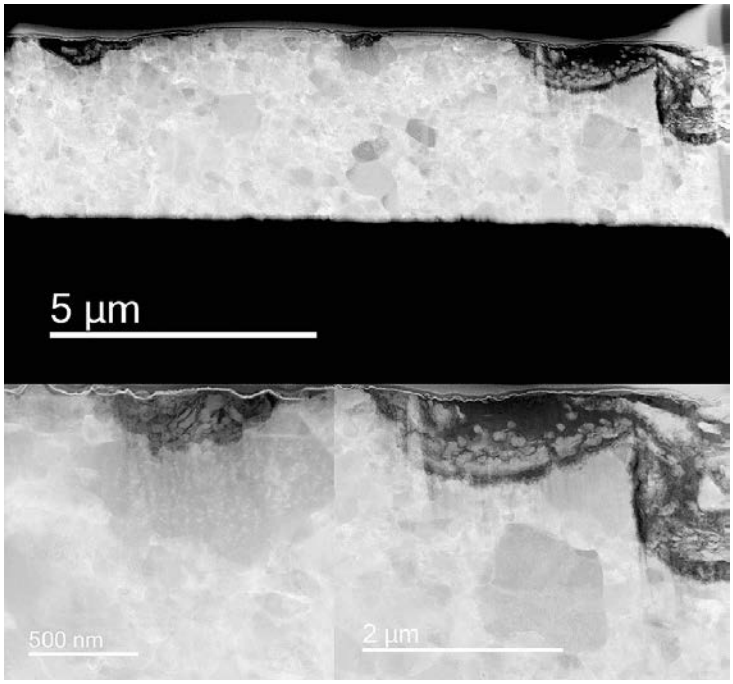

Figure C-49. *STEM images of lamella 2 and the two most interesting regions.*

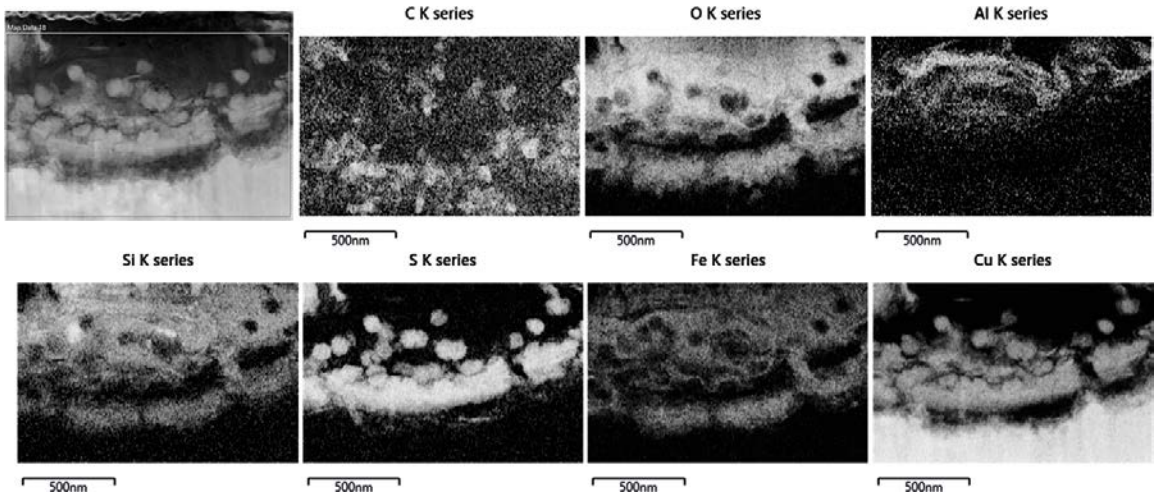

Figure C-50. *EDS maps from lamella 2.*

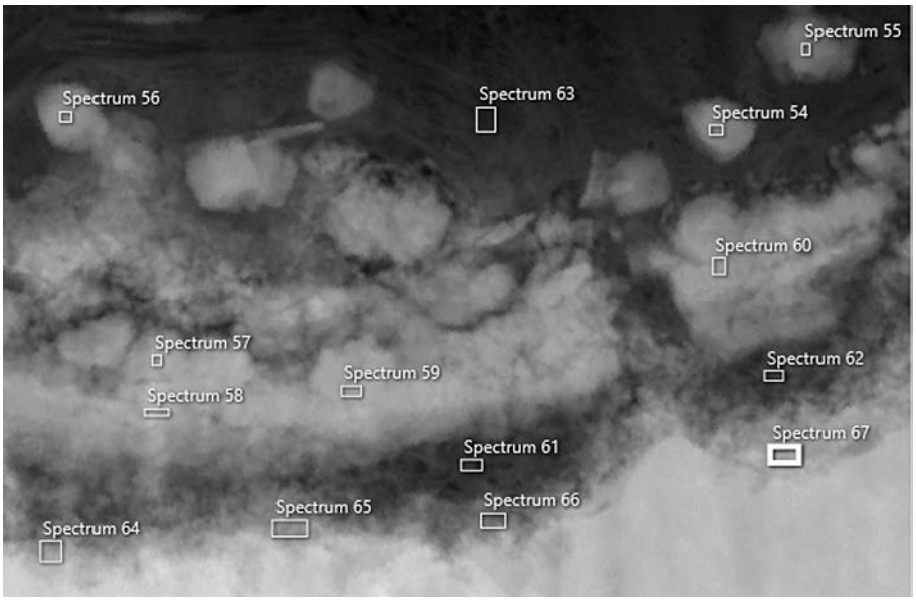

With C

Element (At%)	**54**	**55**	**56**	**57**	**58**	**59**	**60**	**61**	**62**	**63**	**64**	**65**	**66**	**67**
C	13.20	25.41	0	17.35	11.63	13.44	17.44	36.66	18.38	14.89	25.61	32.39	35.69	38.97
O	8.25	17.05	21.39	11.16	4.56	4.79	0	42.52	56.88	61.15	16.09	20.44	26.13	17.52
Na	0	0	0	0	0	0	0	2.09	2.39	1.49	0	0	0	0
Mg	0	0	0	0	0	0	0	0	0	0	0	0	0	0
Al	0	0	0	0	0	0	0	0	0	2.62	0	0	0	0
Si	1.55	2.19	1.97	2.22	0	0	0	5.14	5.54	11.88	0.75	1.13	2.10	0.83
S	28.15	18.21	25.06	22.11	27.06	25.63	28.42	0	1.06	0	1.03	0.56	1.44	0
Cl	0	0	0	0	0	0	0	0	0	0	0	0	0	0
Ca	0	0	0	0	0	0	0	0	0	0	0.47	0	0	0
Fe	0	1.44	3.31	1.28	0	0	0	12.10	13.06	7.13	2.09	1.84	5.09	1.50
Cu	48.84	35.7	48.27	45.89	56.75	56.14	54.14	1.49	2.69	0.83	53.97	43.63	29.55	41.18
Total	100	100	100	100	100	100	100	100	100	100	100	100	100	100

Without C

Element (At%)	**54**	**55**	**56**	**57**	**58**	**59**	**60**	**61**	**62**	**63**	**64**	**65**	**66**	**67**
O	9.51	22.86	21.39	13.5	5.16	5.53	0	67.12	69.69	71.86	21.63	30.24	40.63	28.7
Na	0	0	0	0	0	0	0	3.3	2.93	1.75	0	0	0	0
Mg	0	0	0	0	0	0	0	0	0	0	0	0	0	0
Al	0	0	0	0	0	0	0	0	0	3.08	0	0	0	0
Si	1.79	2.93	1.97	2.68	0	0	0	8.11	6.79	13.96	1.01	1.68	3.27	1.36
S	32.43	24.41	25.06	26.75	30.62	29.61	34.43	0	1.3	0	1.38	0.83	2.24	0
Cl	0	0	0	0	0	0	0	0	0	0	0	0	0	0
Ca	0	0	0	0	0	0	0	0	0	0	0.63	0	0	0
Fe	0	1.93	3.31	1.54	0	0	0	19.11	15.99	8.37	2.81	2.72	7.92	2.46
Cu	56.27	47.87	48.27	55.52	64.22	64.85	65.57	2.35	3.3	0.98	72.54	64.53	45.95	67.48
Total	100	100	100	100	100	100	100	100	100	100	100	100	100	100

Figure C-51. *Quantitative EDS results (At%) of selected areas in the lamella 2. In the second table, C has been removed since there will always be some C due to contamination. But in this case, the surrounding material probably also contains a high amount of C.*

C1.4.3 HR TEM images and diffraction

For improved spatial resolution, high resolution (HR) TEM is required. In such images, contrast mechanisms are more complicated. Figure C-52 shows some regions from lamella 1 where there are many Cu-S particles. The larger particles appear to be agglomerates of smaller particles and many small particles (5 – 10 nm) can be observed throughout the whole sample. Higher magnification of the smaller particles from lamella 1 can be seen in Figure C-53.

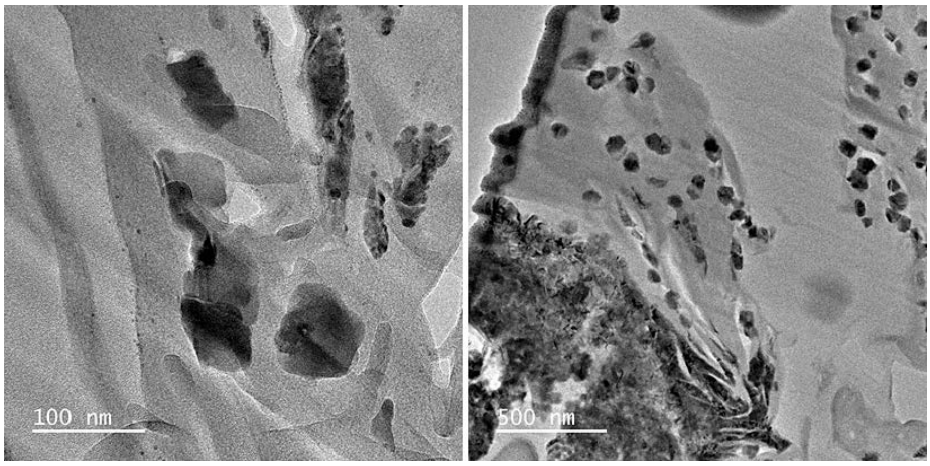

Figure C-52. *HR TEM images at medium magnification, showing that the Cu-S particles are not round, but agglomerates of several small particles.*

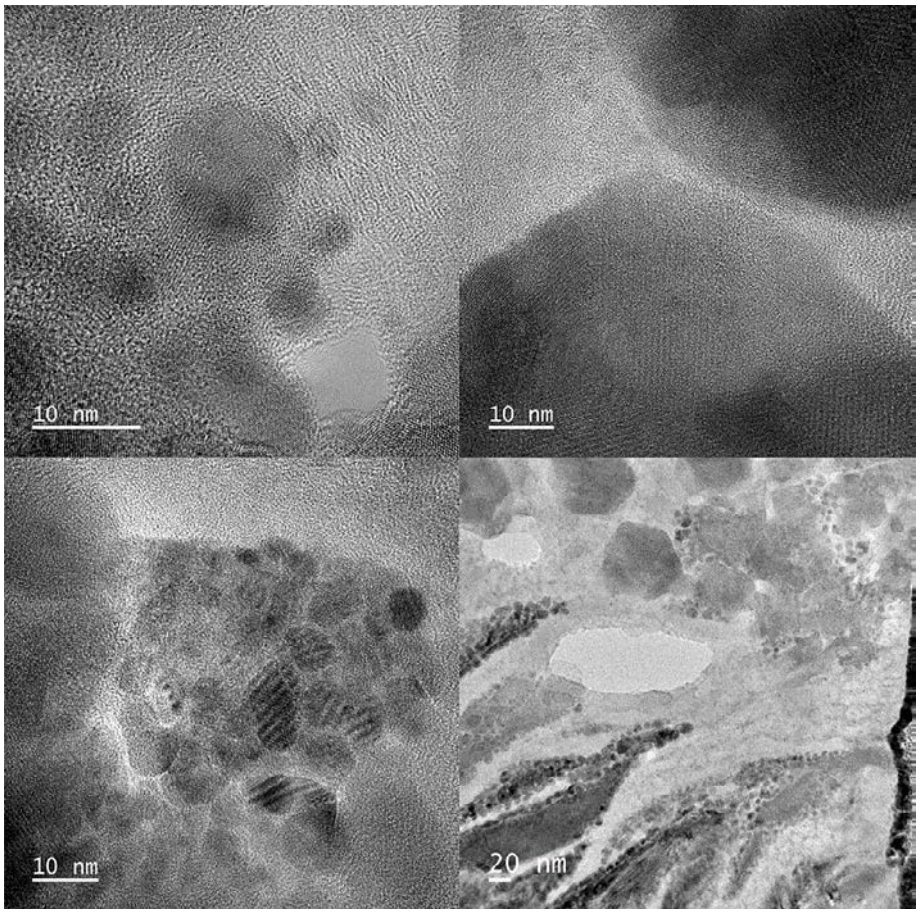

Figure C-53. *HR TEM images showing that the Cu-S particles observed with STEM consist of many small particles, agglomerated together.*

Acquiring selected area electron diffraction (SAED) from regions containing particles results in diffraction patterns that show that the sample is polycrystalline (many small particles), see Figure C-54. By rotating the pattern and summing all intensities it is possible to get the radial distances that most frequently occur, and then these can be recalculated to planar distances. Such information then is compared to experimental data in literature for different phases. In this case, the data was compared to phase descriptions of Cu_2S (Chalcocite), CuS (Covellite), Cu_2O (Cuprite), and CuO (Tenorite).

The SAED patterns were collected from an area of at least ~ 100 – 200 nm radius, which allows many reflections from surrounding material and particles to contribute to the diffraction patterns. To extract information from smaller areas it is possible to produce a Fast Fourier Transform (FFT) from a selected part of a HR TEM image. These are closely related to diffraction patterns, and similar information can be extracted. Examples of FFT's from small particles in lamella 1 can be seen in Figure C-55.

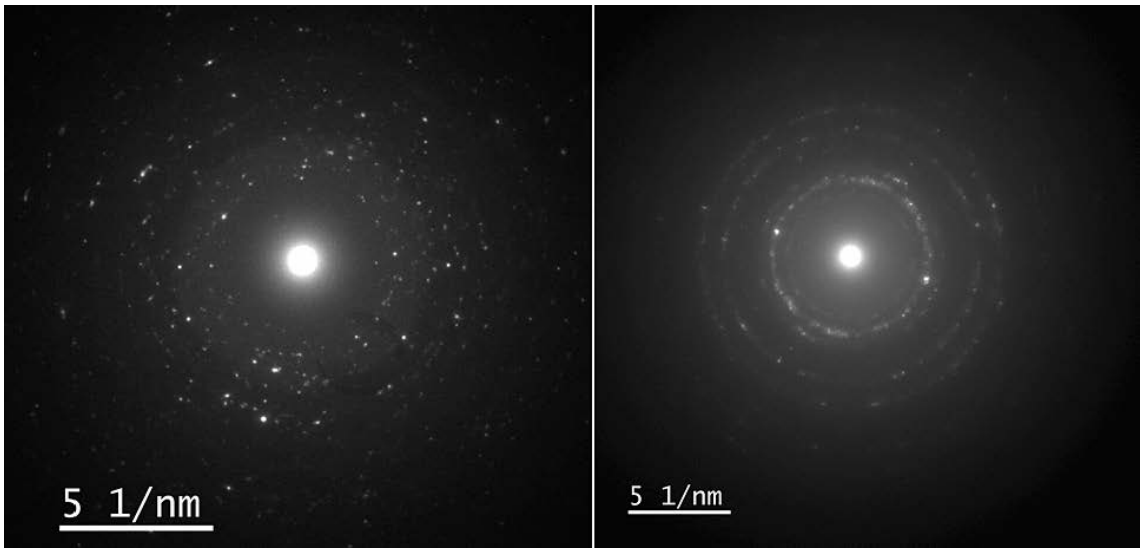

Figure C-54. *Typical SAED patterns from areas with Cu-S particles from lamellae 1 and 2. The ring-shaped patterns indicate that the sample is polycrystalline or contain many small particles.*

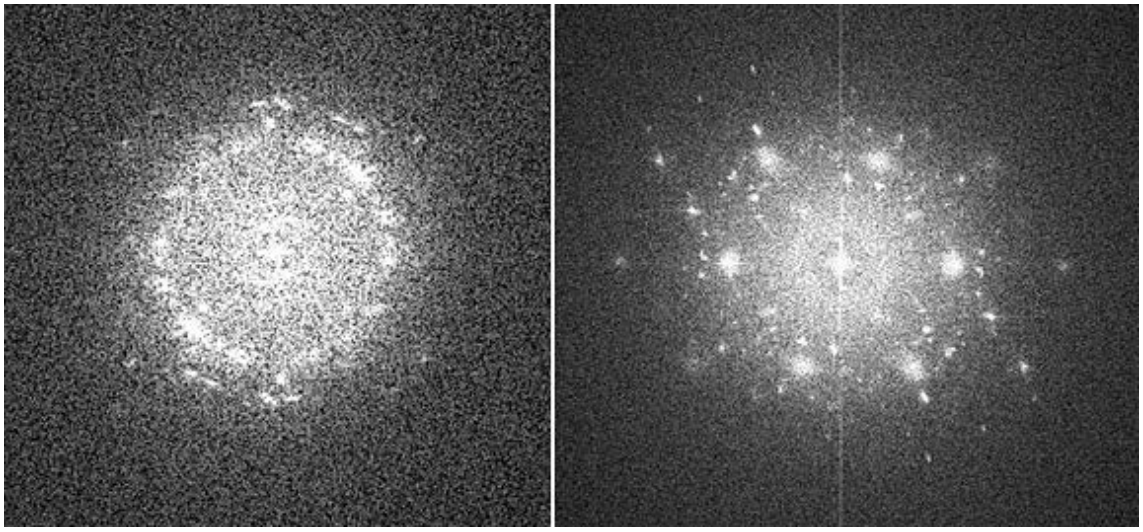

Figure C-55. *FFTs from small particles found on lamella 1.*

Table C-1 shows the planar distances that should be observed using diffraction. The numbers marked in darker green are the main reflections that occurs most for each phase, and the numbers marked in light green should also be occur frequently. The distance from the centre of the diffraction pattern to a reflection should equal 1/d for a phase to match. Calculating the radius of the rings and comparing for all patterns acquired from both lamellae 1 and 2 it was possible to verify that Cu_2S (chalcocite) matches many of the patterns for the particles. Also, some areas match well to Cu_2O. There are some areas that appear to contain both phases, and in one area it is possible that there is CuO. There may also be other phases, such as Fe_2O_3 or SiO_2 present. The matching of these phases or other oxides was outside the scope of this work. A few reflections found indicate that there may be something more present, but there may also be weaker reflections from e.g. Cu_2S. Since the d-values for the presented phases overlap it is far from easy to verify the phases and since the particles are very small (~10 nm) there may be particles of different phases present in the same area, contributing to the diffraction patterns.

Table C-1. Corresponding planar distances to the for some phases that are likely to be present.

	Cu_2S Chalchocite monoclinic	CuS Covelite hexagonal	Cu_2O cuprite cubic	CuO monoclinic	Cu cubic
d (Å)	3.7	3	2.45	2.51	2.1
	3.2	2.82	2.13	2.31	
	2.95	2.7	1.5		
	2.72	1.91			
	2.4	1.56			
	2.2–2.3				
	1.98				

From the SAED patterns it is also possible to select a specific reflection and construct a dark field (DF) image. In such images, the areas from which this reflection is collected becomes bright. It is then possible to verify that a reflection comes from a specific particle/area. Figure C-56 shows a few examples of DF images corresponding to reflections that should match Cu_2S. Here it is obvious that the information comes from many small particles and parts of larger particles, again corroborating that there are many small particles.

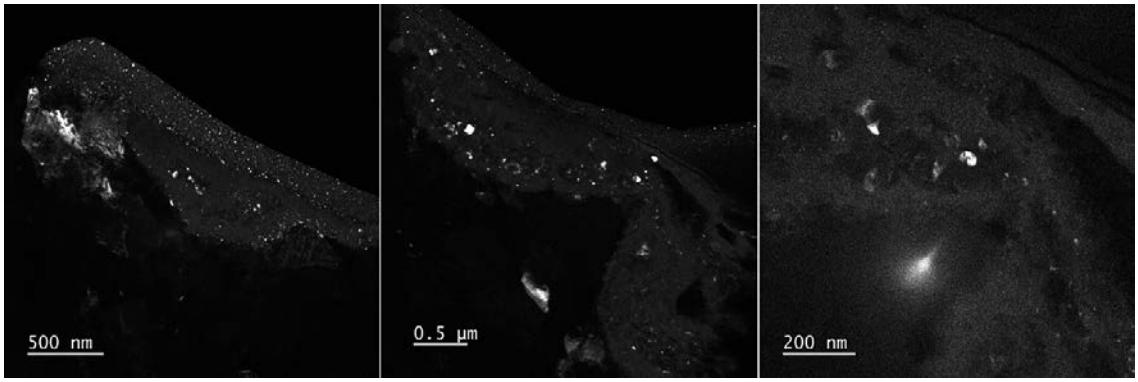

Figure C-56. *Dark field images formed from reflections in a diffraction pattern that was collected in the same area as EDS was acquired in Figure C-51.*

C1.4.4 Coupon S2/N lamellae 3 and 4

Two lamellae were produced using FIB from coupon S2/N. The selected areas are seen in Figure C-57.

Figure C-58 shows STEM image of the whole lamella 3 and of a particularly interesting region. In this lamella, several areas with particles (as seen on coupon A3/K) appear to protrude through the Cu. In the lower part of the right image particles are attached to the Cu surface. Figure C-59 shows more areas where similar reactions seem to have occurred.

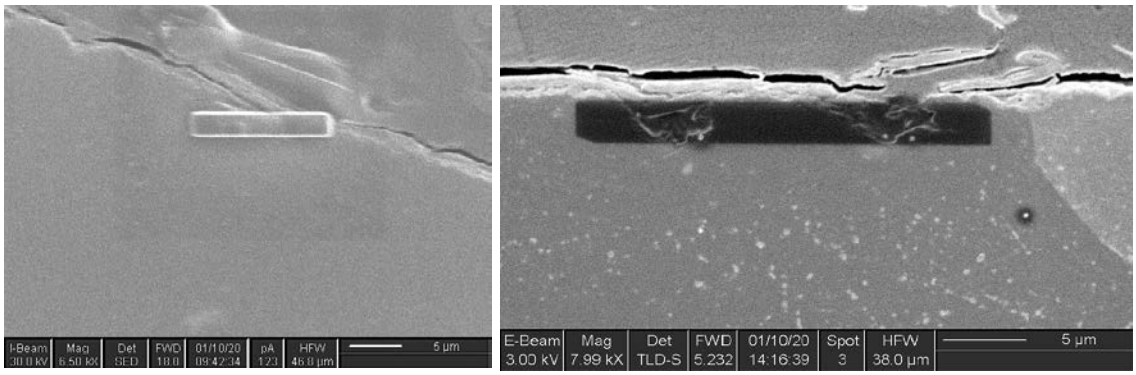

Figure C-57. *FIB SEM images showing the positions from where the lamellaes were taken from coupon S2/N; left is lamella 3 and right is lamella 4. The rectangular box is the deposited Pt-precursor that protects the area of interest during milling.*

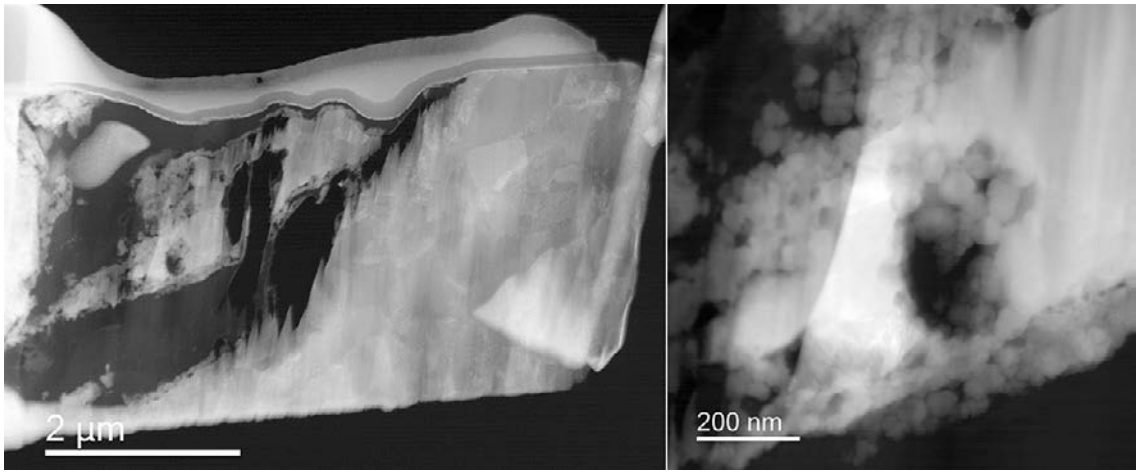

Figure C-58. *STEM image of the whole lamella 3 (left) and higher magnification of an interesting region slightly left of the centre of the lamella (right). The black regions in the centre are holes in the lamella from the final thinning.*

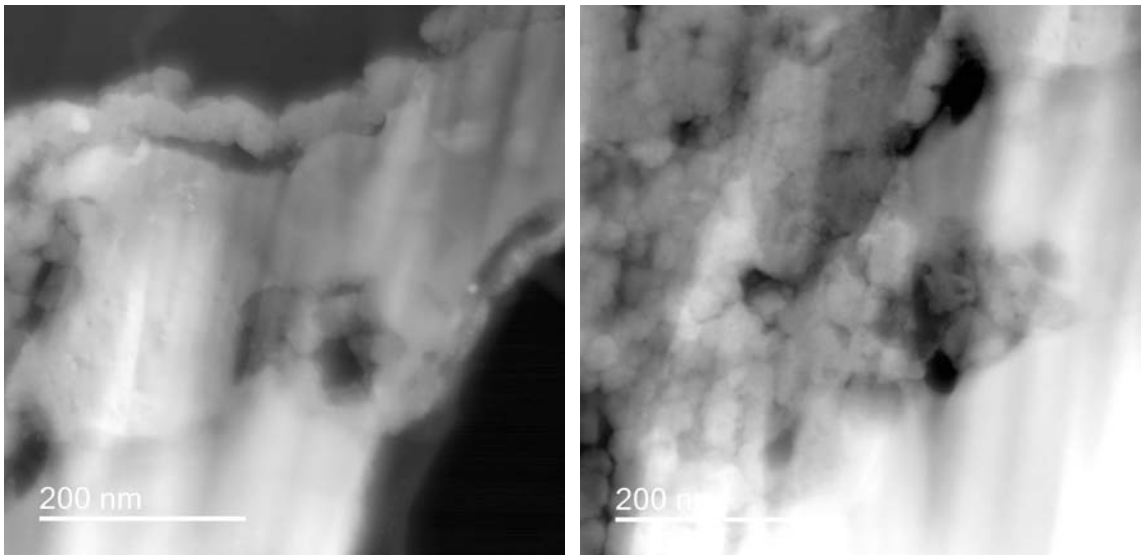

Figure C-59. *STEM images of more regions where particles appear to have penetrated the Cu and attached to the Cu (oxide) surface.*

STEM EDS maps acquired from lamella 3 show that the particles again consist of mainly Cu and S, but also a high amount of oxide and C is present. Most of the particles in the hole seem to be oxide with only very low amounts of other elements observed, see Figure C-60.

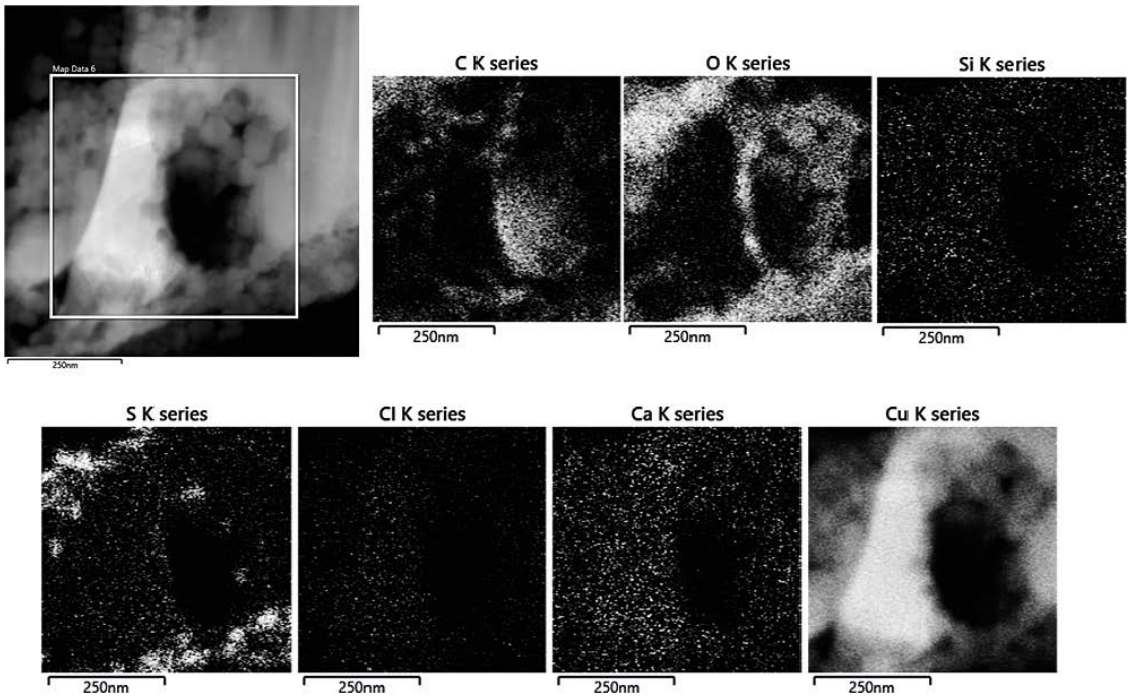

Figure C-60. *EDS maps of what appear to be a hole through the Cu. Note that this is a planar cut so the top surface is inward or outward in the images.*

Examples from quantitative EDS results acquired from selected areas inside the hole are displayed in Figure C-61. Here, the round particles consist mainly of Cu and O. This lamella was also mounted on a Cu grid and therefore there is additional Cu signal in the results. Not much S was observed here.

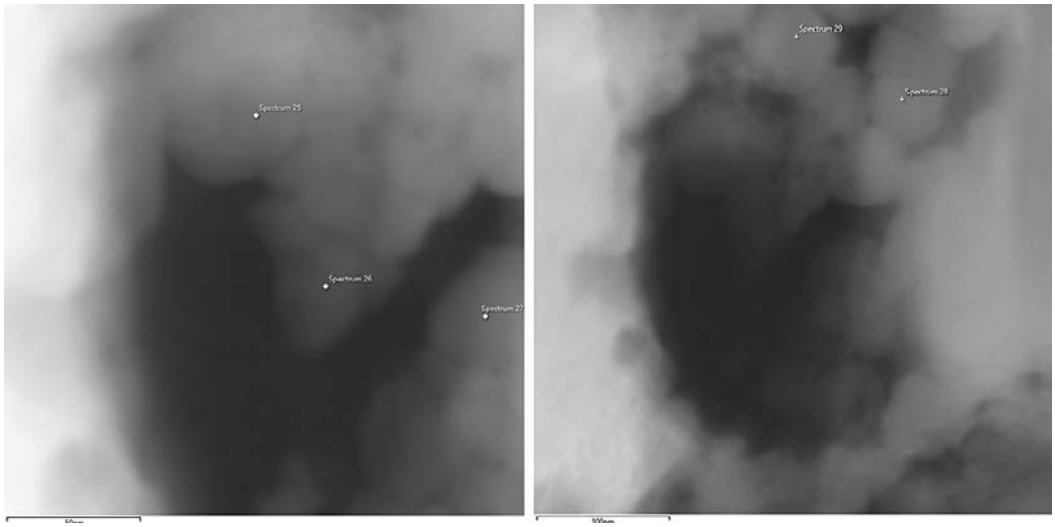

With C					
Element (At%)	**25**	**26**	**27**	**28**	**29**
C	40.92	71.52	45.68	10.24	1.45
O	13.2	6.26	14.63	14.67	23.69
Na	0.44	0	0	0	0
Mg	0.12	0	0	0	0
Al	0	0	0	0	0
Si	0.12	0	0.12	0	0
S	0	0	0.11	0.38	0.47
Cl	0	0	0	0	0
Ca	0	0	0	0.15	0
Fe	0.14	0.04	0.11	0.2	0
Cu	45.06	22.18	39.35	74.35	74.38
Total	100	100	100	100	100

Without C					
Element (At%)	**25**	**26**	**27**	**28**	**29**
O	22.34	22	26.94	16.35	24.04
Na	0.74	0	0	0	0
Mg	0.21	0	0	0	0
Al	0	0	0	0	0
Si	0.21	0	0.22	0	0
S	0	0	0.2	0.43	0.48
Cl	0	0	0	0	0
Ca	0	0	0	0.16	0
Fe	0.24	0.13	0.2	0.23	0
Cu	76.27	77.87	72.44	82.83	75.48
Total	100	100	100	100	100

Figure C-61. *Quantitative EDS results (At%) of selected areas in the lamella 3. In the second table, C has been removed (on request), since there will always be some C due to contamination. But in this case, the surrounding material probably also contains a high amount of C in all areas, except in spectra 28 and 29.*

Figure C-62 shows lamella 4. The left part of the image is zoomed in and the contrast changed in order to be able to see both parts due to large difference in contrast. It is probable that the left part has a much lower mean atomic number since it looks similar to the clay regions in coupon A3/K and the right part is mainly Cu.

STEM EDS maps acquired from lamella 4 show that most of the particles (here ca 20 – 80 nm) along the left side of the Cu surface consist of Cu and S, while the surrounding material is a mixture of mainly oxides of Cu, Si, Fe, Al, Mg, including also some Ca and C, see Figure C-63. This is likely some remaining bentonite clay. It is notable that there is more Fe on the right side of the sample than in the oxide region, this may be an artefact.

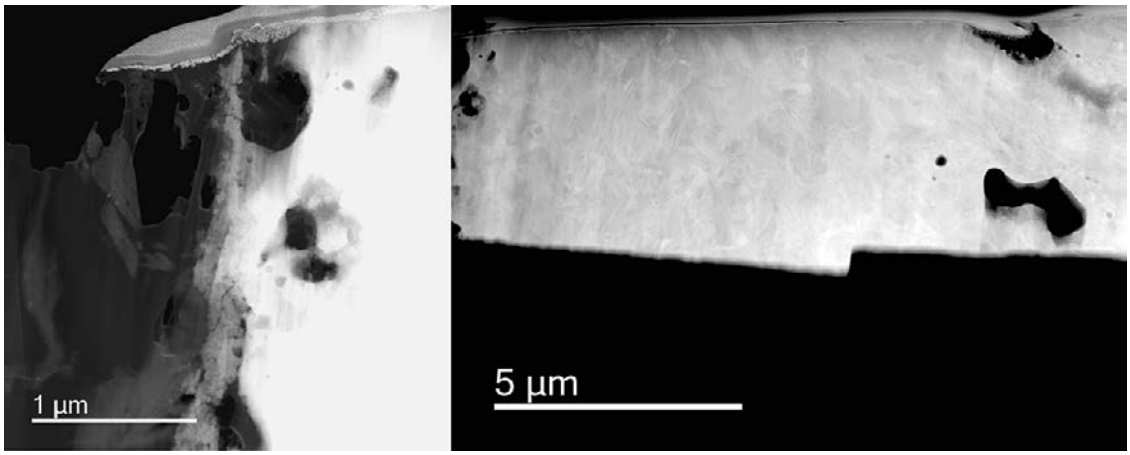

Figure C-62. *STEM image of the whole lamella 4 but in two images. The left part has lower mean atomic number and is therefore much darker.*

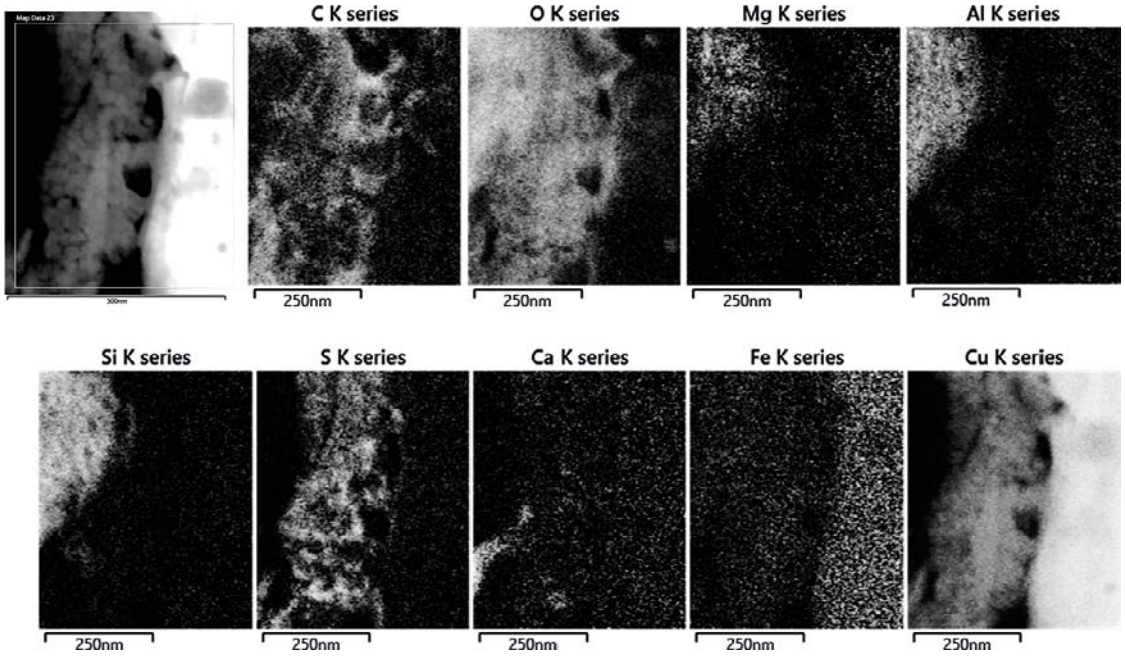

Figure C-63. *STEM EDS maps from lamella 4 acquired in a region with a lot of particles near the Cu (oxide) surface.*

Examples of quantitative EDS results from selected areas in lamella 4 are seen in Figure C-64. This lamella was mounted on a Ti grid, so no additional Cu signal is added into the results. The region outside the Cu surface (spectra 68–73) seems to be a mixture of oxides (mainly Cu) some S-rich particles/areas and clay. Also, a high amount of C is observed. The dark areas close to the Cu surface (spectra 74–75) show only Cu-oxide and C. Spectrum 76 from the left side of the image appears to be mainly clay. On the surface of the Cu (spectra 77–79) only C and Cu-oxide or pure Cu is observed. If C is removed from the quantification, the Cu:O ratio varies a lot, giving no clear indication of what phase is present. EELS was attempted in several areas but resulted in very poor-quality spectra. This may be due to the lamella being slightly too thick.

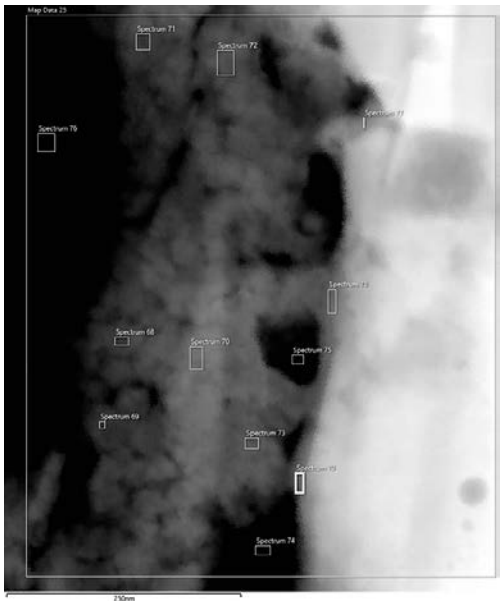

With C

Element (At%)	68	69	70	71	72	73	74	75	76	77	78	79
C	36.86	56.12	27.97	14.82	39.58	18.29	85.87	76.88	13.46	0	17.84	30.64
O	28	18.34	28.93	44.62	22.7	30.53	11.39	12.11	63.27	0	30.89	18.9
Na	0	0	0	0	0	0	0	0	0	0	0	0
Mg	0	0	0	1.41	0	0	0	0	1.73	0	0	0
Al	0	0	0	3.98	0	0	0	0	5.48	0	0	0
Si	0	1.42	0	5.28	0	0	0	0	12.56	0	0	0
S	4.09	0	2.6	1.75	3.18	4.81	0	0	0	0	0	0
Cl	0	0	0	0	0	0	0	0	0.25	0	0.6	0
Ca	0	0	0	0.34	0	0	0	0	0.27	0	0	0
Fe	0	0	0.53	0.37	0.44	0	0	0	0.54	0	0.61	0.46
Cu	31.05	24.12	39.97	27.42	34.09	46.38	2.75	11.01	2.44	100	50.05	50
Total	100	100	100	100	100	100	100	100	100	100	100	100

Without C

Element (At%)	68	69	70	71	72	73	74	75	76	77	78	79
O	44.34	41.8	40.16	52.38	37.57	37.36	80.56	52.38	73.11	0	37.6	27.24
Na	0	0	0	0	0	0	0	0	0	0	0	0
Mg	0	0	0	1.66	0	0	0	0	2	0	0	0
Al	0	0	0	4.67	0	0	0	0	6.33	0	0	0
Si	0	3.23	0	6.2	0	0	0	0	14.51	0	0	0
S	6.48	0	3.61	2.05	5.27	5.88	0	0	0	0	0	0
Cl	0	0	0	0	0	0	0	0	0.29	0	0.74	0
Ca	0	0	0	0.4	0	0	0	0	0.31	0	0	0
Fe	0	0	0.74	0.43	0.73	0	0	0	0.62	0	0.75	0.67
Cu	49.18	54.97	55.49	32.2	56.42	56.75	19.44	47.62	2.82	100	60.92	72.09
Total	100	100	100	100	100	100	100	100	100	100	100	100

Figure C-64. *Quantitative EDS results (At%) of selected areas in the lamella 4. In the second table, C has been removed since there will always be some C due to contamination. But in this case, there seems to be a lot of C present.*

HR TEM images and diffraction

Figure C-65 displays higher magnification HR TEM images of areas in lamella 3 containing particles in the range of 20 – 80 nm, most of them appearing to be Cu-S according to EDS, but some possibly being Cu-oxide.

Diffraction patterns and FFTs collected from areas containing particles, see Figure C-66, match Cu_2S the best, but some areas match Cu_2O better, and some match both. Since EDS also shows both O and S it is possible that both phases are present, but since they have several reflections that overlap it is not possible to say for sure. One thing that seems to differ from coupon A3/K is that no very small particles (~5 nm) are observed in lamellae 3 and 4, but that may be just a coincidence.

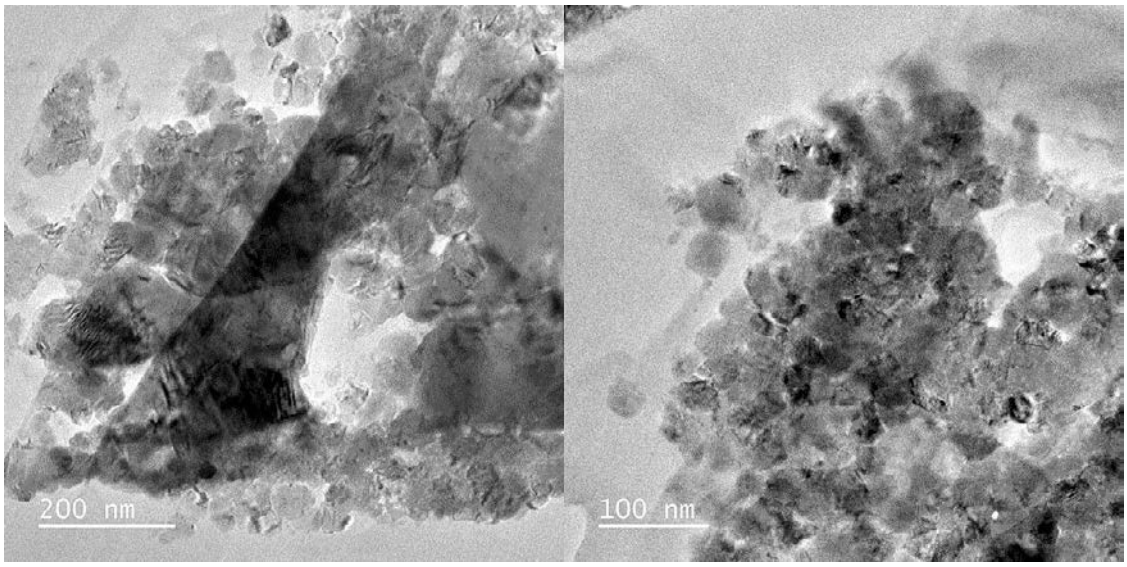

Figure C-65. *HR TEM images of lamella 3 at medium magnification, showing crystalline particles in the range of 20–80 nm, seeming to be agglomerated nears the Cu surface.*

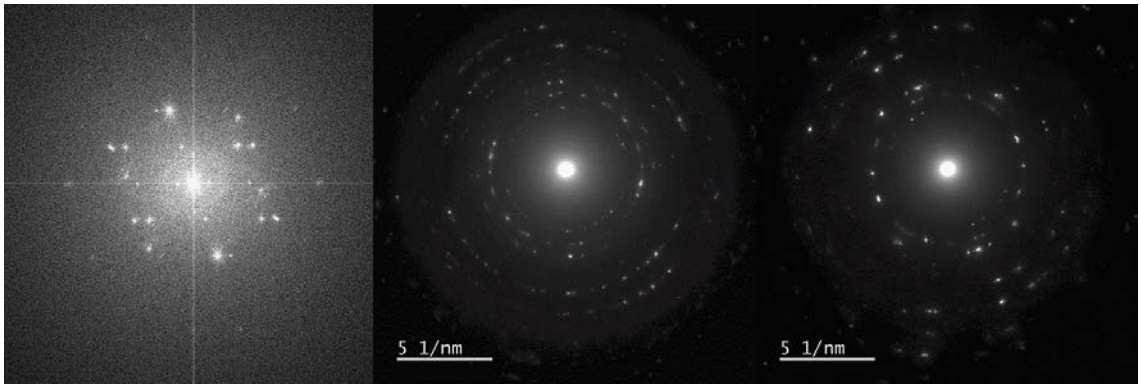

Figure C-66. *FFT and diffraction patterns collected from areas with particles in lamella 3.*

By selecting spots in the diffraction pattern lying on the inner rings and then producing dark field (DF) images the area where the information comes from is highlighted. Figure C-67 shows the area, the diffraction pattern and three such DF images. The reflections don't match exactly any of the phases, but it is the relative distances between the reflections that is more important than the absolute, because during acquisition it is easy to get an error of ~5 % just due to focusing. Note that for each DF image, only one spot on the ring is selected. If another spot were to be chosen, other particles or parts of particles would likely be highlighted. As mentioned above, it is probable that both Cu_2O and Cu_2S are present, as EDS analysis from Figure C-60 and Figure C-61 of the same area also shows.

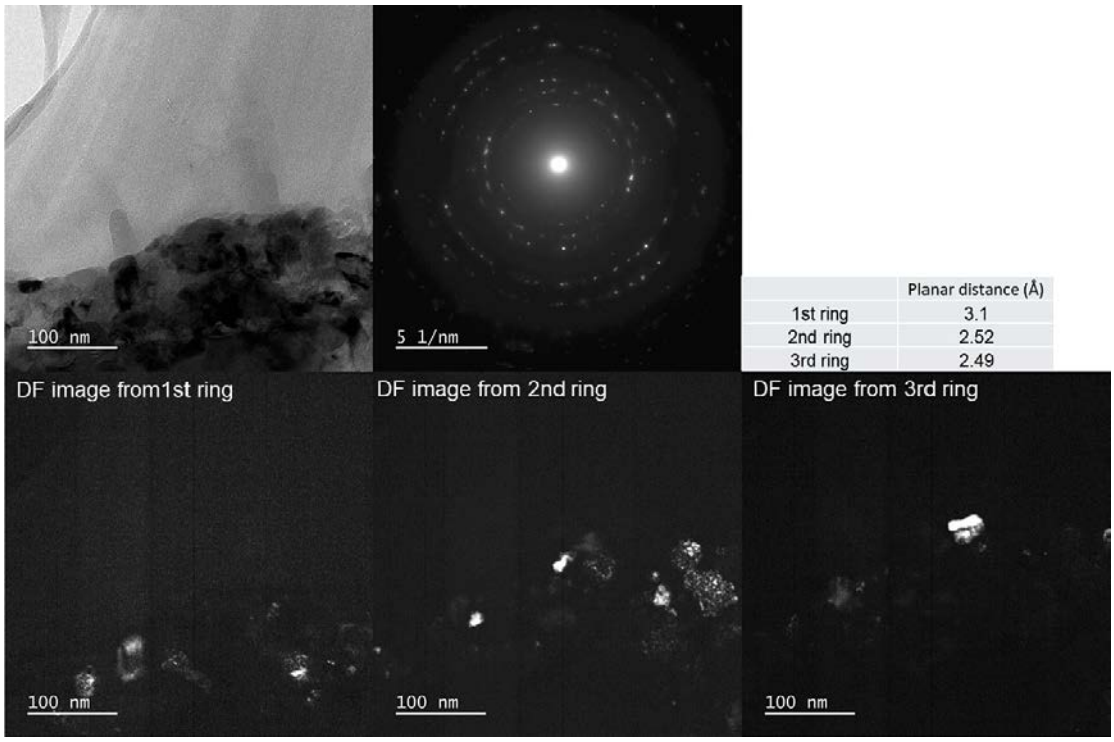

Figure C-67. *Bright field image, diffraction pattern and three DF images corresponding to reflections from the three inner rings.*

C2 Summary

The investigation has shown that there are a lot of small particles attached to the Cu surfaces in the pits. On coupon A3/K, the particles, first appearing to be 50 – 80 nm, seem to consist of many even smaller particles (5 – 10 nm) that are agglomerated. There may be even smaller particles, but such are very hard to find. On coupon S2/N, the particles seemed to be slightly larger, with no particles smaller than 20 nm found during the analyses. Such particles were found in the clay outside the Cu surfaces, but closer to the Cu surfaces or possibly in direct contact with the copper oxide a more compact layer was found, consisting of Cu_2S on coupon A3/K and Cu_2S and Cu_2O on coupon S2/N. This layer consists of many smaller particles, possibly formed by reaction in the copper oxide – clay interface which leads to some particles then being released into the clay, either by natural movement in the clay or by mass transport through the clay. On coupon S2/N, what appears to be holes through the Cu was observed, with particles inside and attached to the Cu walls. Since the lamellae were produced as planar cuts, i.e. parallel to the surface of the coupons, these holes probably extend up to the surface.

EDS analyses showed that the particles on coupon A3/K mainly consist of Cu-S and on coupon S2/N of both Cu-O and Cu-S. Identifying the exact phase is very difficult due to several reasons:

i) The samples are a mixture of many phases, with many elements present in the same areas.

ii) It is hard to manually collect diffraction information from such small particles and compare to phase descriptions, since there are several phases that contribute to the diffraction patterns.

iii) The most likely phases have overlapping reflections.

To overcome this situation and clearly identify the particles, an automated method that can compare the diffraction patterns to phase templates for each phase would be very useful, for example the method called Precession Electron Diffraction (PED). Today, we have no access to such a method, but hope to have one in the future.

The collective information from EDS and diffraction suggests that the particles found on coupon A3/K are Cu_2S, meanwhile on coupon S2/N it is less clear, but most probably a mixture of Cu_2O and Cu_2S. The lamellae from coupon A3/K were also more successfully produced, resulting in thinner sample with areas containing mainly one type of particle.

Appendix D

D1 Gravimetric analysis of corrosion coupons

Gravimetric analysis, or mass loss analysis, was used to quantify the extent of corrosion that had occurred to the test specimens. The corroded specimens were chemically cleaned, removing the corrosion products by pickling. Repeated pickling is typically needed to remove all corrosion products. The specimen is weighed after each cleaning treatment and the procedure is repeated until the mass loss between two treatments is very small, and comparable to mass loss on an unexposed reference specimen. Both the metal and the corrosion products determine what chemical cleaning solution is suitable to use.

Initial weights of each coupon were obtained prior to exposure by SKB. After analysis with XRD and EDS is was thought that the corrosion products on the coupons consisted mainly of cuprite (Cu_2O) and so a pickling solution of sulfamic acid (5 %wt) was selected in accordance with SS-EN ISO 8407:2014, with a cleaning interval of 1 minute. The results of the mass loss analysis and appearance of coupons after pickling indicated that the corrosion closer to the copper surface had a different composition and/or morphology than the outer corrosion product, since it was less sensitive to the original pickling solution, see Figure D-1 to Figure D-6.

Figure D-1. *Coupon A3/I after pickling for 5 minutes in sulfamic acid.*

Figure D-2. *Coupon A3/J after pickling for 5 minutes in sulfamic acid.*

Figure D-3. *Coupon A3/L after pickling for 5 minutes in sulfamic acid.*

Figure D-4. *Coupon S2/M after pickling for 5 minutes in sulfamic acid.*

Figure D-5. *Coupon S2/O after pickling for 5 minutes in sulfamic acid.*

Figure D-6. *Coupon S2/P after pickling for 5 minutes in sulfamic acid.*

Further XRD analysis on the pickled coupon S2/P revealed weak signals of chalcocite (Cu_2S), see Figure D-7. Therefore, a second pickling step was added to complete the mass loss analysis with hydrochloric acid. The solution was de-aerated through purging with purified nitrogen to minimize base metal removal due to oxygen driven corrosion, in accordance with SS-EN ISO 8407:2014 with cleaning intervals of 5 minutes.

This procedure was first tested on coupon S2/P with 3.5 %wt HCl in 1-minute intervals, but this was found to be ineffective and thus the data points from these cleaning steps are disregarded in the analysis (the coupon mass loss was = 0 g). Therefore, the concentration of the HCl was increased to 50 %wt (for 20 min) and tested before being implemented on the remaining coupons to confirm the efficiency of the method and to ensure no adverse effects on the base material. This was confirmed by measuring the pit depths before and after pickling. Ref K was used as a pickling reference for coupon S2/P, whilst a separate piece of copper plate was used as a pickling reference for the remaining coupons.

Coupon S2/P was further pickled in 9.5 %wt H_2SO_4 for a total of 14 minutes (in intervals of initially 1 minute then 2 minutes) in order to try and remove all remaining surface deposits. This was in accordance with what had been used in previous LOT studies for removal of corrosion products. This method was also unsuccessful in completely removing the staining of the surface, as can be seen in Figure D-14 which shows the appearance of the coupon after pickling. However, the pickling curves imply the removal of corrosion products to be complete as the mass loss of the coupon during the later pickling steps matches that of the bare copper reference pickling sample.

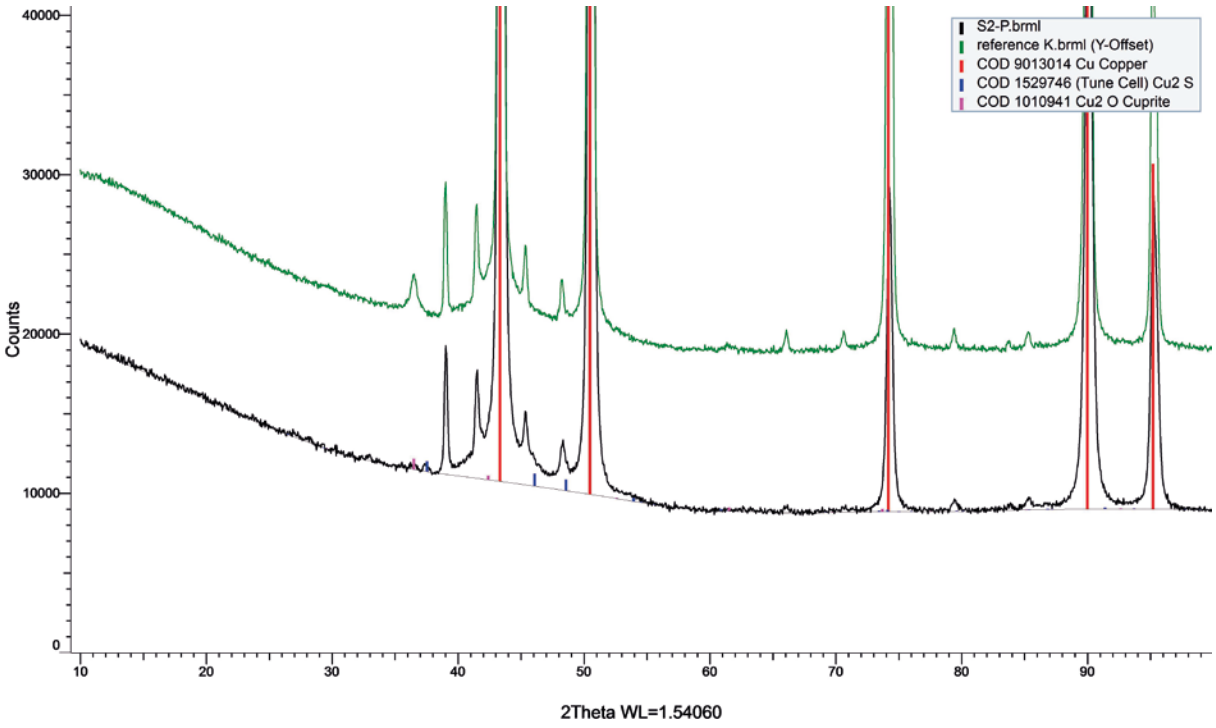

Figure D-7. *XRD spectra for coupon S2/P after pickling in sulfamic acid for 5 minutes.*

Figure D-8. *Coupon A3/I after pickling for 5 minutes in sulfamic acid and 20 minutes in hydrochloric acid.*

Figure D-9. *Coupon A3/J after pickling for 5 minutes in sulfamic acid and 20 minutes in hydrochloric acid.*

Figure D-10. *Coupon A3 L after pickling for 5 minutes in sulfamic acid and 20 minutes in hydrochloric acid.*

Figure D-11. *Coupon S2/M after pickling for 5 minutes in sulfamic acid and 20 minutes in hydrochloric acid.*

Figure D-12. *Coupon S2/O after pickling for 5 minutes in sulfamic acid and 20 minutes in hydrochloric acid.*

Figure D-13. *Coupon S2/P after pickling for 5 minutes in sulfamic acid and 20 minutes in hydrochloric acid.*

Figure D-14. *Coupon S2/P after pickling for 5 minutes in sulfamic acid, 20 minutes in hydrochloric acid, and 14 minutes in sulfuric acid.*

A final attempt was made to completely clean coupon S2/P back to a shiny copper surface by electrolytic cleaning in a solution of KCl with an applied cathodic current of 100 A/m^2. This was in accordance with SS-EN ISO 8407:2014 E3.1. Each side of the coupon was cleaned for 12 minutes, and a slight improvement in appearance could be seen but no significant mass loss was measured (Figure D-15 and Figure D-23).

The summarised results of the mass loss analysis can be seen in Table D-1, where the average corrosion rates for the exposure period are also given.

Table D-1. Mass loss and corrosion of the coupons.

Coupon	Mass loss	Corrosion			
	g	g/m^2	g/m^2, yr	µm/yr	µm
Pickling ref.	0.0006	0.2094	-	-	-
Ref L	0.0016	0.6458	0.0323	0.0036	0.072
Ref K	0.0035	1.3945	0.0697	0.0078	0.156
A3/I	0.0172	8.4885	0.4244	0.0477	0.954
A3/J	0.0234	11.5041	0.5752	0.0646	1.292
A3 L	0.0181	8.9252	0.4463	0.0501	1.002
S2/M	0.0217	10.7183	0.5359	0.0602	1.204
S2/O	0.0238	11.7589	0.5879	0.0661	1.322
S2/P	0.0088	4.3310	0.2165	0.0243	0.486
S2/P*	0.0105	5.2037	0.2602	0.0292	0.584
S2/P**	0.0120	5.9307	0.2965	0.0333	0.666

* Coupon S2/P was further pickled in H_2SO_4 for 14 minutes.
** Coupon S2/P was further electrolytically cleaned for 12 minutes in KCl according to E3.1 in SS-EN ISO 8407:2014.

Figure D-15. *Coupon S2/P after pickling for 5 minutes in sulfamic acid, 20 minutes in hydrochloric acid, 14 minutes in sulfuric acid, and 12 minutes in electrolytic cleaning.*

Pickling curves and data

The following figures show the pickling curves obtained when cleaning the corrosion products from the coupons, with mass loss in grams on the Y-axis and pickling duration in minutes on the X-axis. Table D-2 to Table D-4 show the data from the pickling procedure.

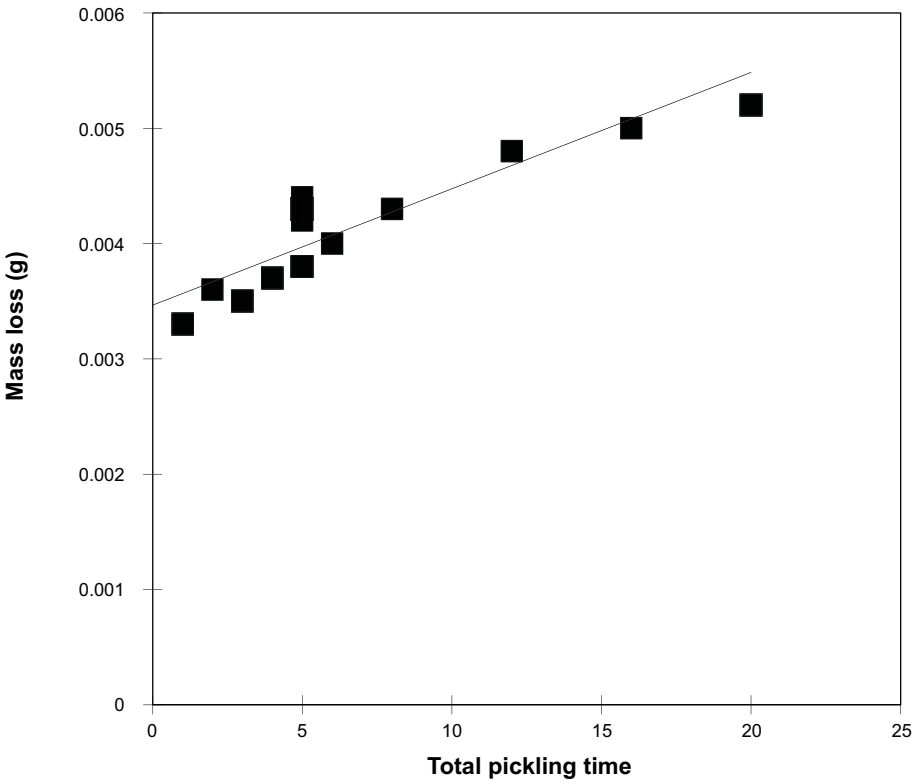

Figure D-16. *Pickling curve for coupon Ref K.*

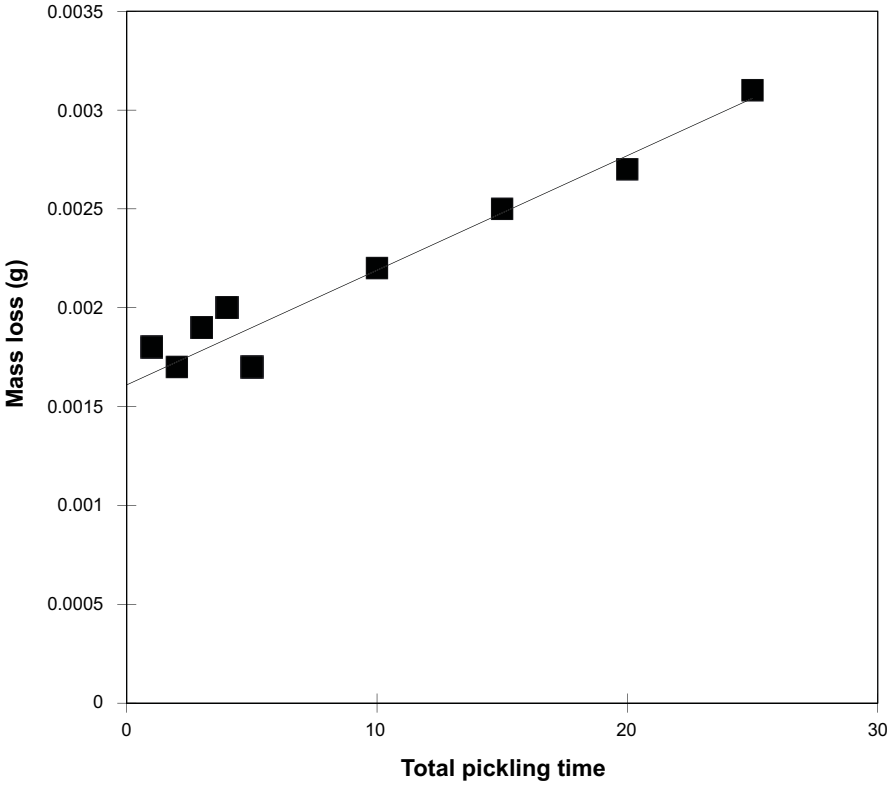

Figure D-17. *Pickling curve for coupon Ref L.*

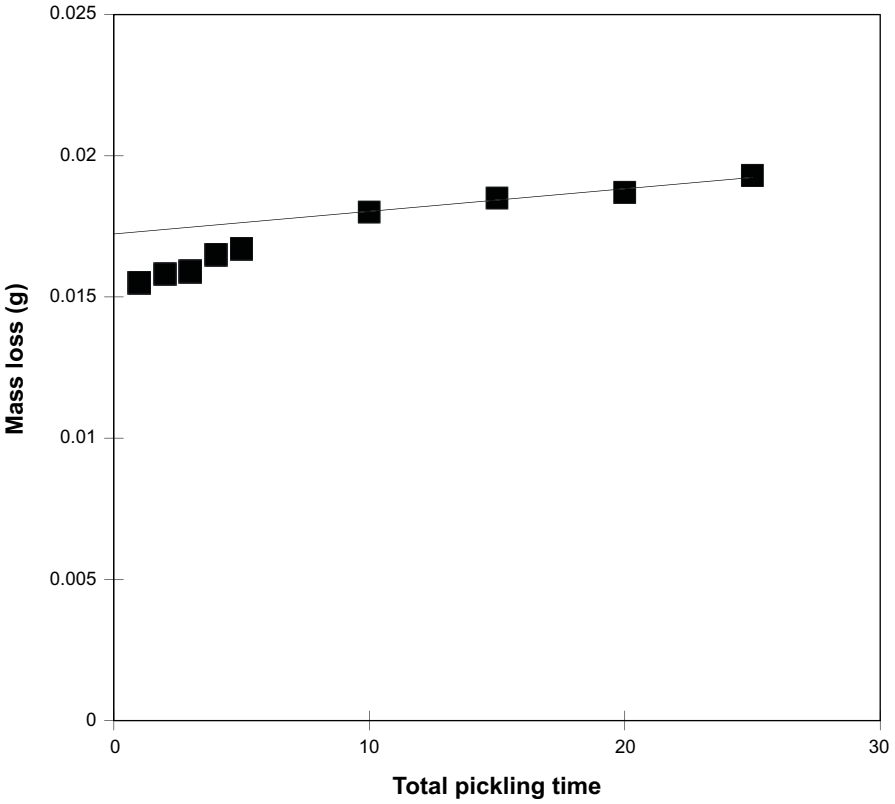

Figure D-18. *Pickling curve for coupon A3/I.*

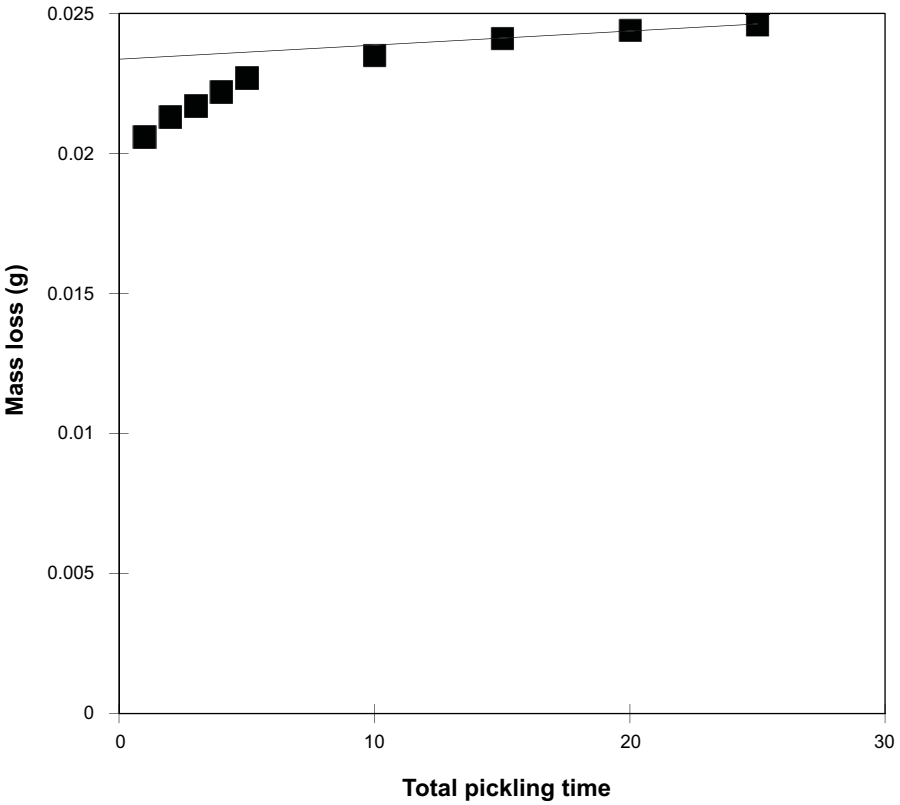

Figure D-19. *Pickling curve for coupon A3/J.*

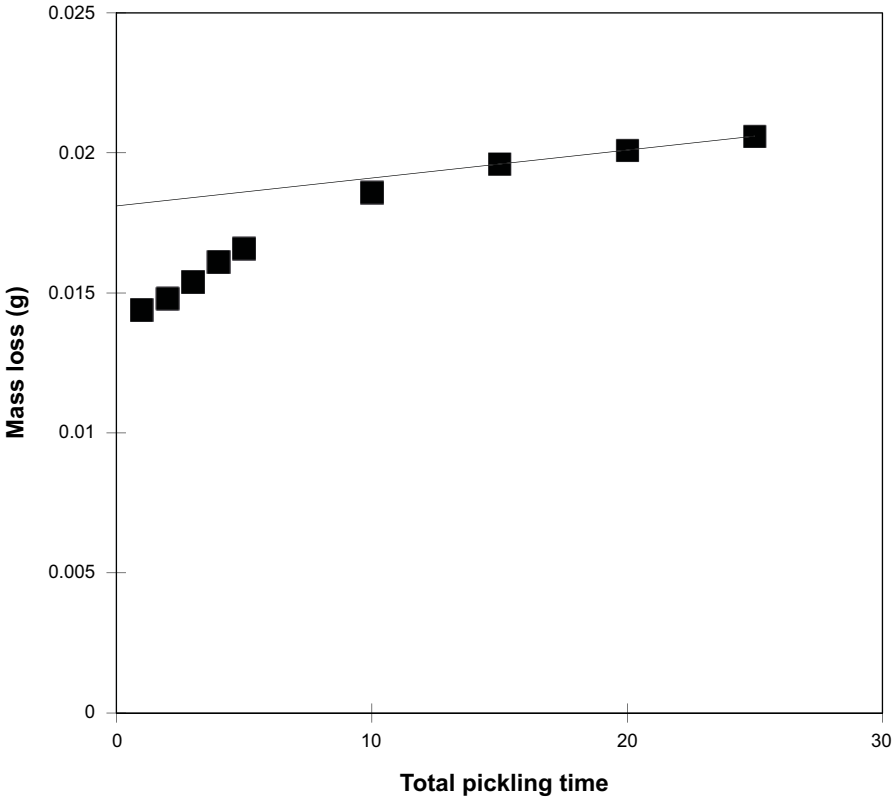

Figure D-20. *Pickling curve for coupon A3/L.*

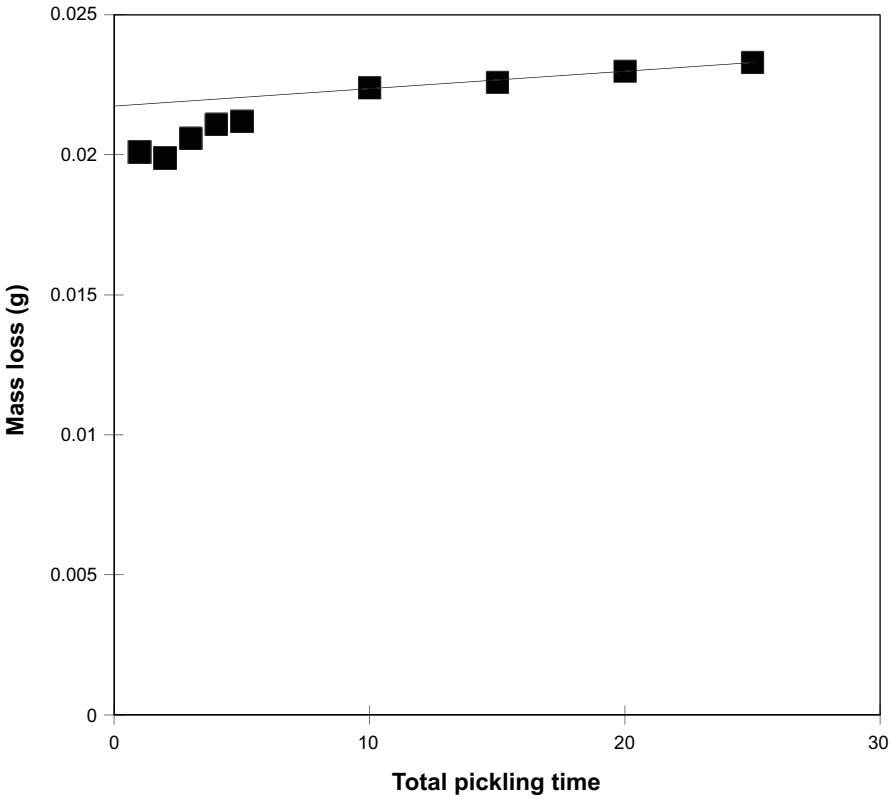

Figure D-21. *Pickling curve for coupon S2/M.*

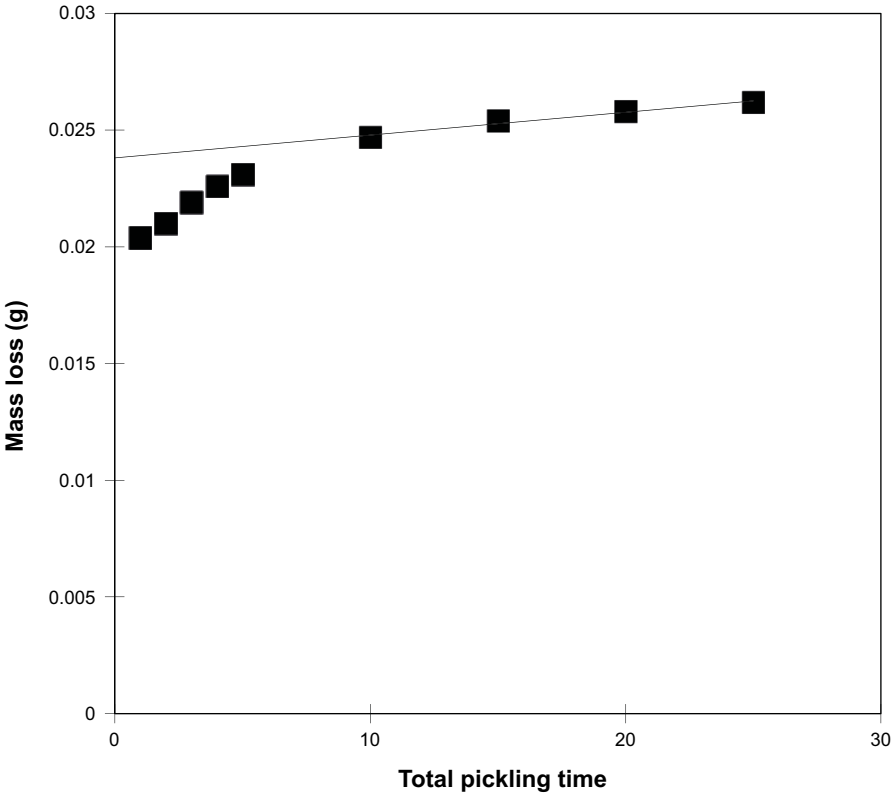

Figure D-22. *Pickling curve for coupon S2/O.*

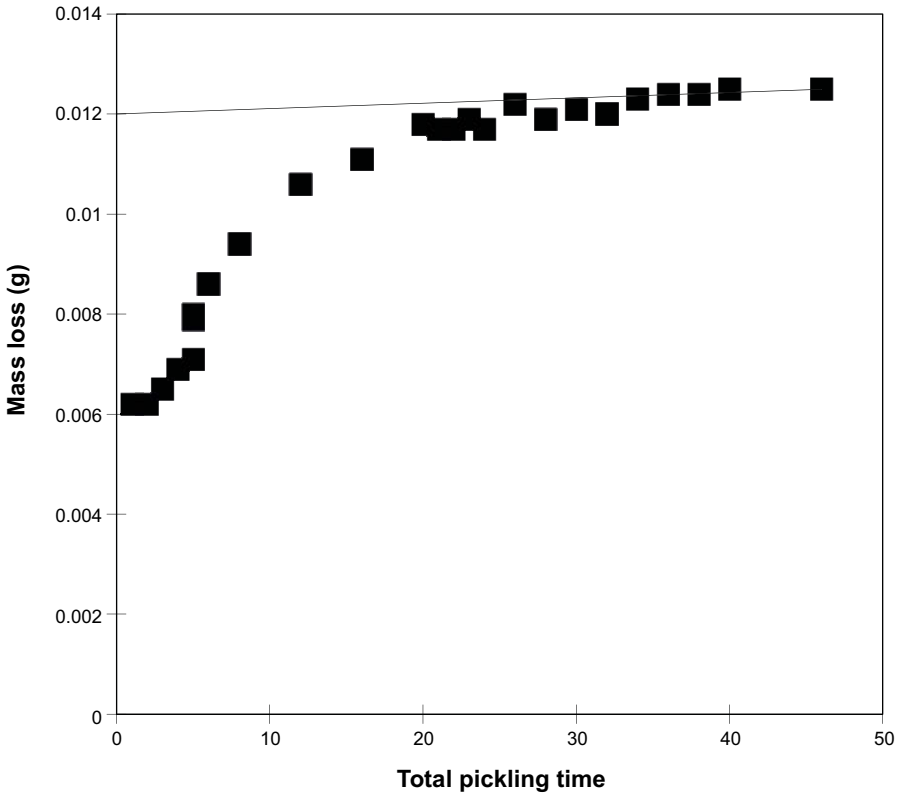

Figure D-23. *Pickling curve for coupon S2/P.*

Table D-2. Pickling data for coupons Ref K and S2/P.

				Pickling in 5 % sulfamic acid then in 3.5 % HCl then in HCl:H_2O (1:1)												
Specimen	Density	Exposure Duration		Sulfamic acid					3.5 % HCl			HCl:H_2O (1:1)				
				Pickling # 1	Pickling # 2	Pickling # 3	Pickling # 4	Pickling # 5	Pickling # 6	Pickling # 7	Pickling # 8	Pickling # 9	Pickling # 10	Pickling # 11	Pickling # 12	Pickling # 13
			Duration (min)	1	1	1	1	1	0	0	0	1	2	4	4	4
			Total Pickling time	1	2	3	4	5	5	5	5	6	8	12	16	20
	g/cm^3	years	Initial weight [g]	weight after pickling # 1	weight after pickling # 2	weight after pickling # 3	weight after pickling # 4	weight after pickling # 5	weight after pickling # 6	weight after pickling # 7	weight after pickling # 8	weight after pickling # 9	weight after pickling # 10	weight after pickling # 11	weight after pickling # 12	weight after pickling # 13
Ref K	8.9	20	12.303	12.2997	12.2994	12.2995	12.2993	12.2992	12.2987	12.2986	12.2988	12.299	12.2987	12.2982	12.298	12.2978
S2/P	8.9	20	11.7604	11.7542	11.7542	11.7539	11.7535	11.7533	11.7525	11.7524	11.7525	11.7518	11.751	11.7498	11.7493	11.7486

Table D-3. Pickling data for coupon S2/P in H_2SO_4 and KCl with 100 A/m^2.

				Pickling in H_2SO_4									Electrolyctic cleaning in KCl with 100 A/m^2			
Specimen	Density	Exposure Duration		Pickling # 14	Pickling # 15	Pickling # 16	Pickling # 17	Pickling # 18	Pickling # 19	Pickling # 21	Pickling # 22	Pickling # 23	Pickling # 24	Pickling # 25	Pickling # 26	Pickling # 27
			Duration (min)	1	1	1	1	2	2	2	2	2	2	2	2	6
			Total Pickling time	1	2	3	4	6	8	10	12	14	36	38	40	46
	g/cm^3	years	Initial weight [g]	weight after pickling # 14	weight after pickling # 15	weight after pickling # 16	weight after pickling # 17	weight after pickling # 18	weight after pickling # 19	weight after pickling # 20	weight after pickling # 21	weight after pickling # 22	weight after pickling # 12	weight after pickling # 12	weight after pickling # 12	weight after pickling # 12
S2/P	8.9	20	11.7486	11.7487	11.7487	11.7485	11.7487	11.7482	11.7485	11.7483	11.7484	11.7481	11.7480	11.7480	11.7479	11.7479
Pickling ref	8.9	-	4.2184	4.2186	4.218	4.2183	4.2182	4.2180	4.2178	4.2179	4.2179	4.2180	4.2178	4.2177	4.2178	4.2178

Table D-4. Pickling data for coupons Ref L, A3/I/J/L and S2/M/O.

Pickling in 5 % sulfamic acid, then in HCl:H_2O (1:1)												
Specimen	Density	Exposure Duration		Sulfamic acid					HCl			
				Pickling # 1	Pickling # 2	Pickling # 3	Pickling # 4	Pickling # 5	Pickling # 6	Pickling # 7	Pickling # 8	Pickling # 9
			Duration (min)	1	1	1	1	1	5	5	5	5
			Total Pickling time	1	2	3	4	5	10	15	20	25
	g/cm^3	years	Initial weight [g]	weight after pickling # 1	weight after pickling # 2	weight after pickling # 3	weight after pickling # 4	weight after pickling # 5	weight after pickling # 6	weight after pickling # 7	weight after pickling # 8	weight after pickling # 9
Pickling ref	8.9	20	8.4068	8.4068	8.4068	8.4068	8.4068	8.4068	8.406	8.4058	8.4055	8.4054
Ref L	8.9	20	12.1421	12.1403	12.1404	12.1402	12.1401	12.1404	12.1399	12.1396	12.1394	12.139
A3I	8.9	20	11.9518	11.9363	11.936	11.9359	11.9353	11.9351	11.9338	11.9333	11.9331	11.9325
A3J	8.9	20	11.9373	11.9167	11.916	11.9156	11.9151	11.9146	11.9138	11.9132	11.9129	11.9127
A3L	8.9	20	11.9451	11.9307	11.9303	11.9297	11.929	11.9285	11.9265	11.9255	11.925	11.9245
S2M	8.9	20	11.8978	11.8777	11.8779	11.8772	11.8767	11.8766	11.8754	11.8752	11.8748	11.8745
S2O	8.9	20	11.9175	11.8971	11.8965	11.8956	11.8949	11.8944	11.8928	11.8921	11.8917	11.8913

Appendix E

Topographic examination of coupon surfaces

Pits and surface defects were analysed on the corrosion coupons before and after removal of corrosion products by pickling. All pits deeper than 6 µm were measured and the five deepest pits for are shown in the tables below. The density of pits/defects for an area of 0.5 cm^2 is also shown. Images of some of the surface defects found under microscope are also presented.

Table E-1. Topographic examination of copper coupons before removal of corrosion products.

	5 deepest pits (µm)					**Pit density**		
Coupon	1	2	3	4	5	Area (cm^2)	No. of pits	Pits/cm²
Ref K	25	19				0.5	2	4
Ref L	22	18	11			0.5	1	2
A3/I	8					0.5	1	2
A3/J	13	12	11	10	9	0.5	7	14
A3/K	7	6				0.5	1	2
A3/L	17	9	8	8	7	0.5	6	12
S2/M	12	8	6			0.5	2	4
S2/N	9	5	5	4		0.5	1	2
S2/O	16	14	13	13	12	0.5	7	14
S2/P	14	13	13	10	9	0.5	6	12

Table E-2. Topographic examination of copper coupons after removal of corrosion products.

	5 deepest pits (µm)					**Pit density**		
Coupon	1	2	3	4	5	Area (cm^2)	No. of pits	Pits/cm²
Ref K	28	28	25	24	23	0.5	20	40
Ref L	25	23	23	22	22	0.5	18	36
A3/I	16	12	11	10	10	0.5	5	10
A3/J	39	22	13	10	10	0.5	11	22
A3/L	9	8	8	7	7	0.5	5	10
S2/M	57	26	15	13	12	0.5	14	28
S2/O	20	16	14	14	12	0.5	12	24
S2/P	39	14	12	8	8	0.5	5	10

A3/I coupon before pickling

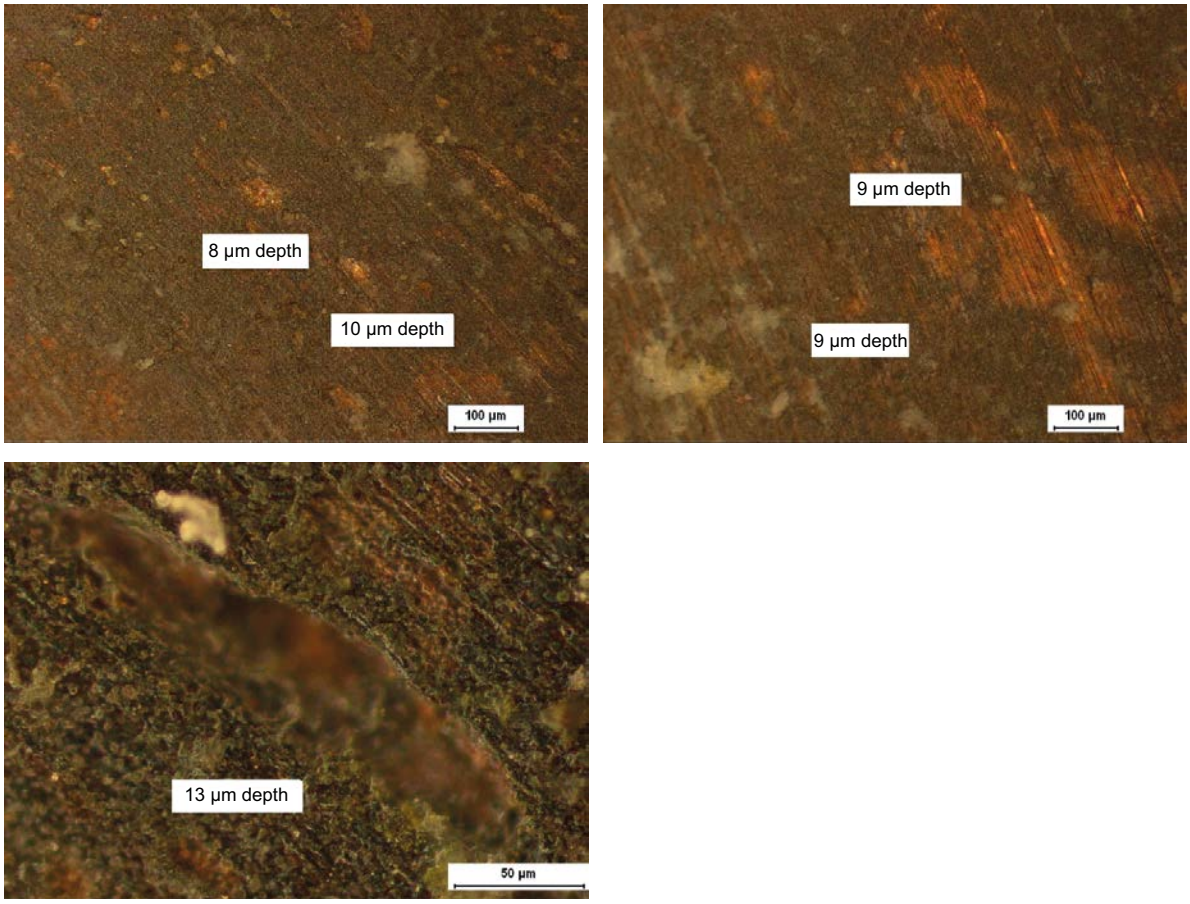

Figure E-1. *Microscope images of the deepest defects found on coupon A3/I before pickling.*

A3/J coupon before pickling

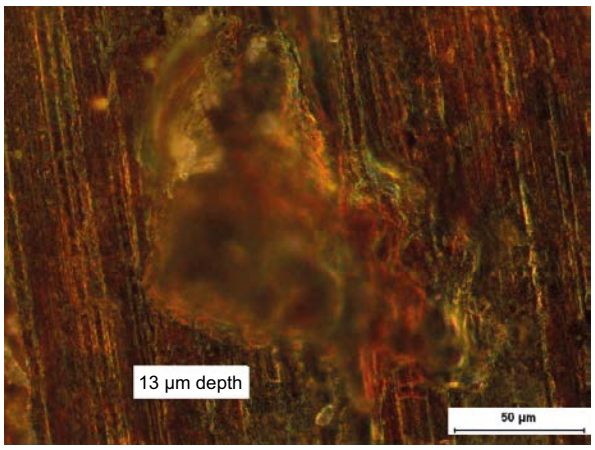

Figure E-2. *Microscope images of the deepest defects found on coupon A3/J before pickling.*

A3/K coupon before pickling

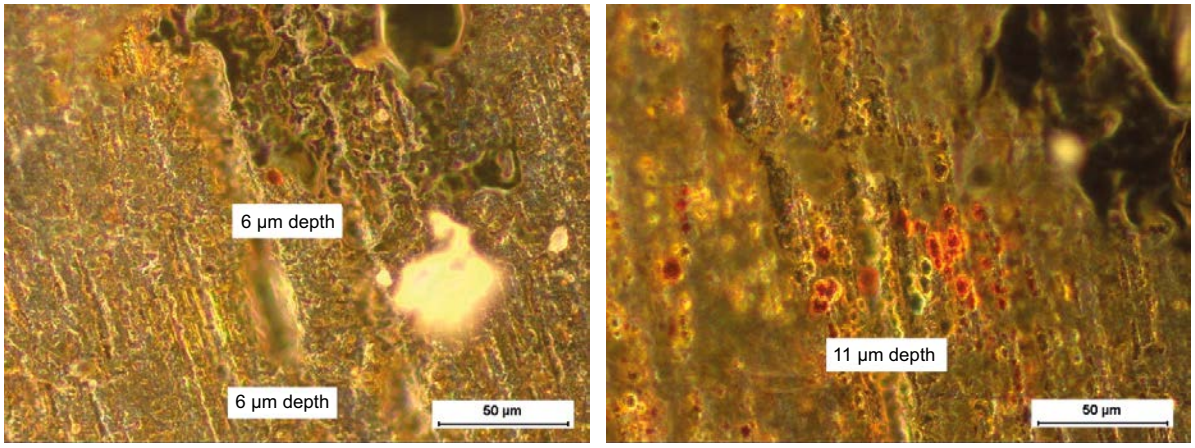

Figure E-3. *Microscope images of the deepest defects found on coupon A3/K before pickling.*

A3/L coupon before picking

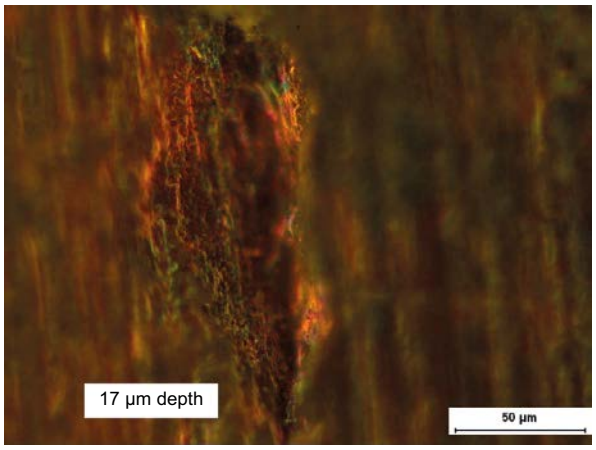

Figure E-4. *Microscope images of the deepest defects found on coupon A3/L before pickling.*

S2/M coupon before pickling

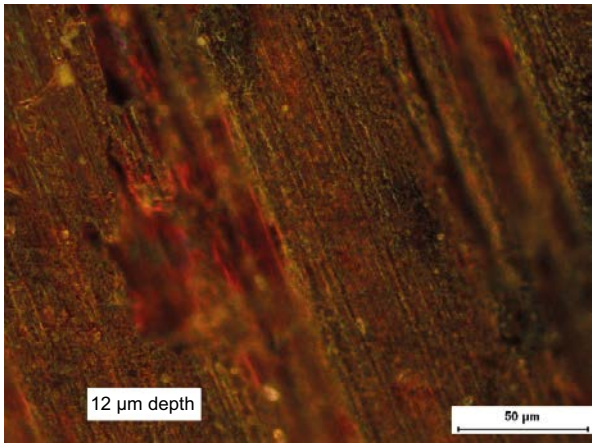

Figure E-5. *Microscope images of the deepest defects found on coupon S2/M before pickling.*

S2/N coupon before pickling

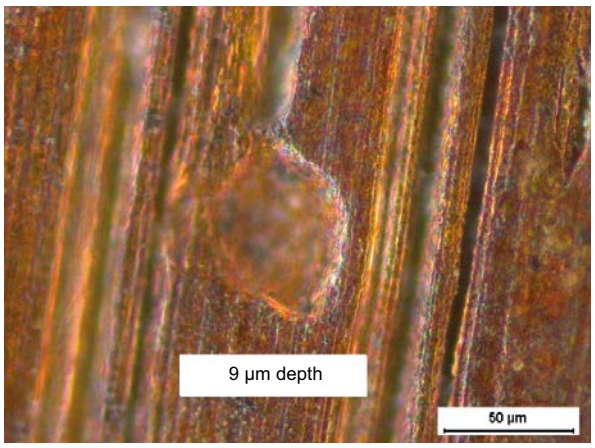

Figure E-6. *Microscope images of the deepest defects found on coupon S2/N before pickling.*

S2/O coupon before pickling

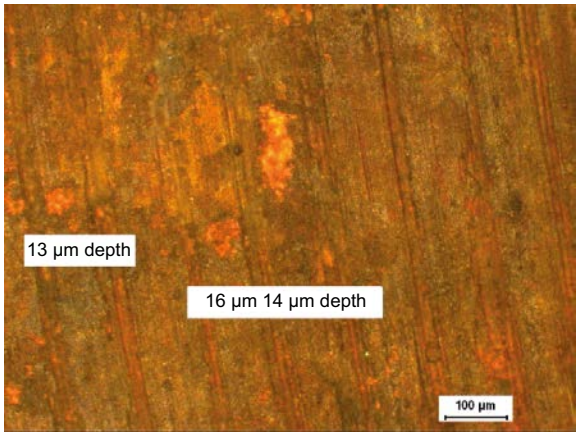

Figure E-7. *Microscope images of the deepest defects found on coupon S2/O before pickling.*

S2/P coupon before pickling

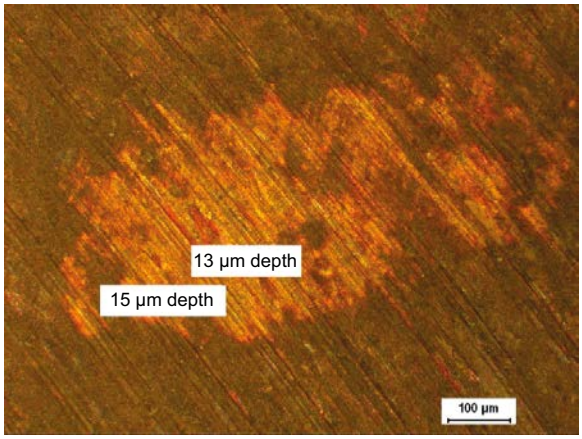

Figure E-8. *Microscope images of the defects found on coupon S2/P before pickling.*

Ref K coupon before pickling

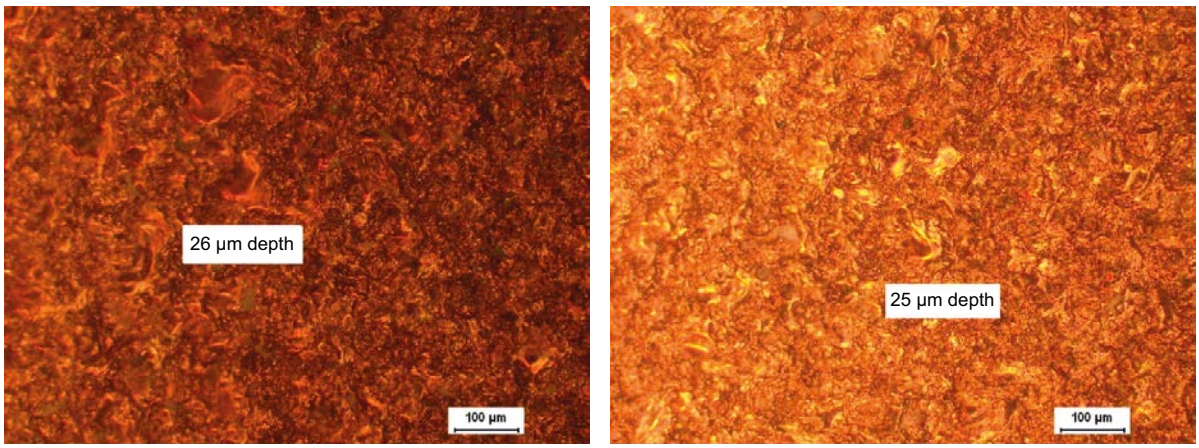

Figure E-9. *Microscope images of the deepest defects found on coupon Ref K before pickling.*

Ref L coupon before pickling

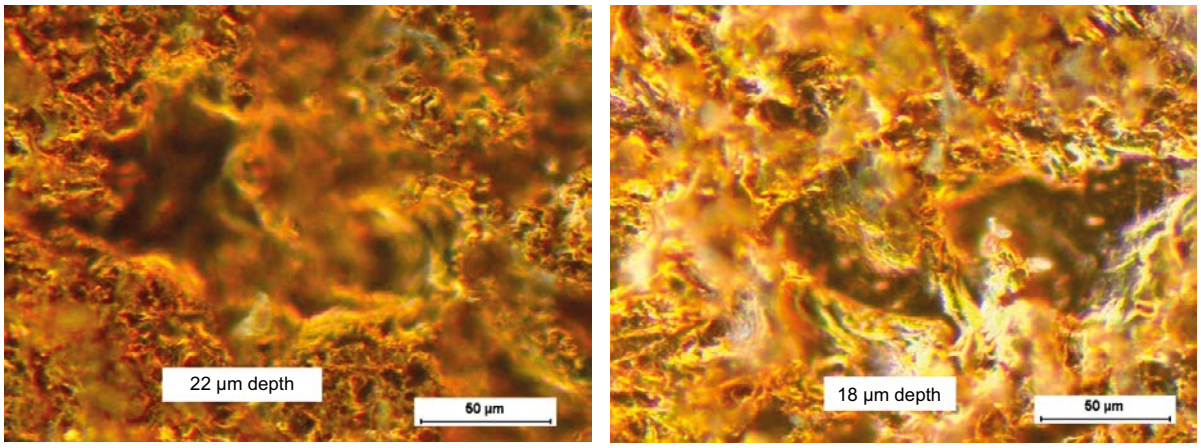

Figure E-10. *Microscope images of the deepest defects found on coupon Ref L before pickling.*

A3/I coupon after pickling

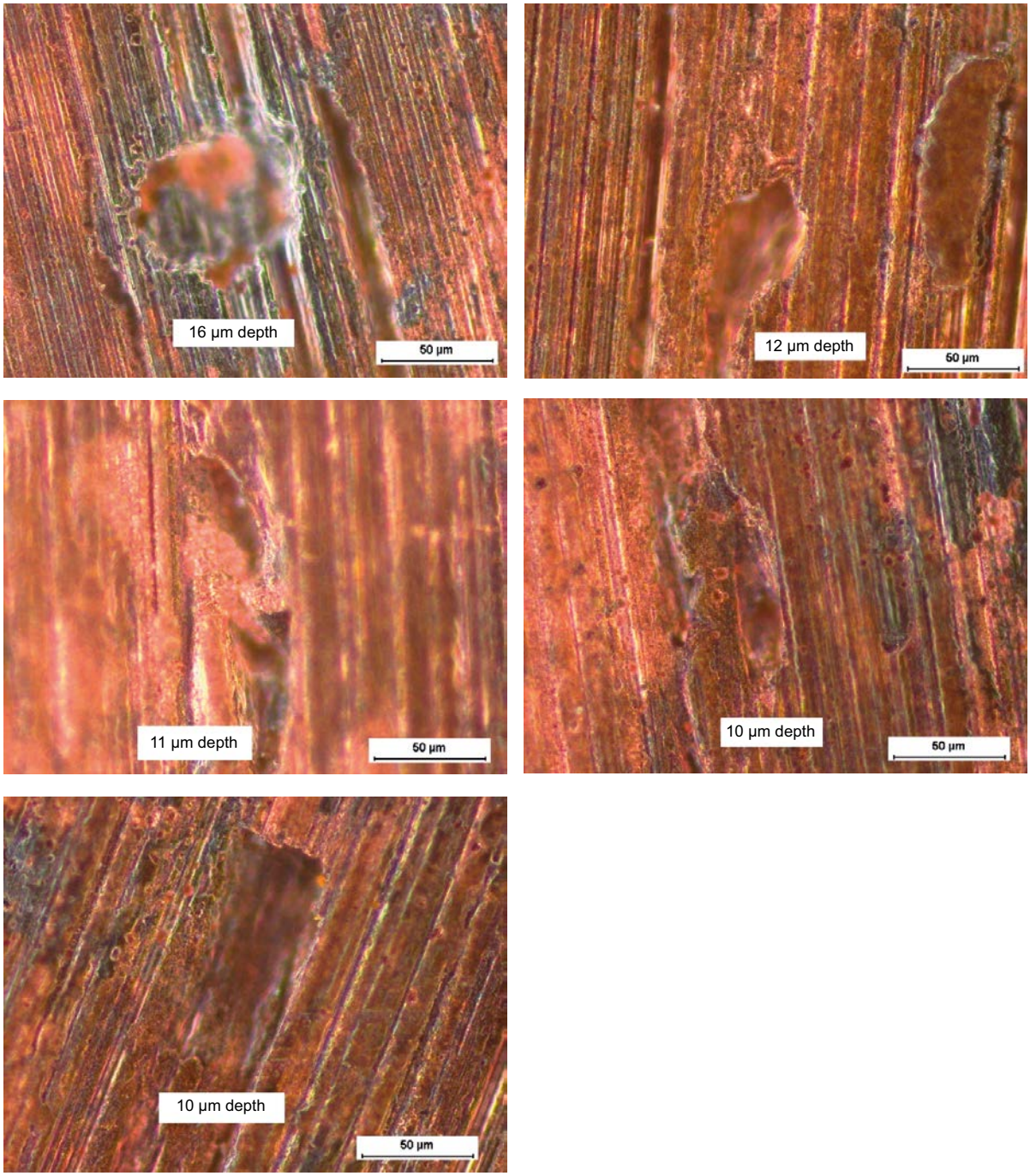

Figure E-11. *Microscope images of the deepest defects found on coupon A3/I after pickling.*

A3/J coupon after pickling

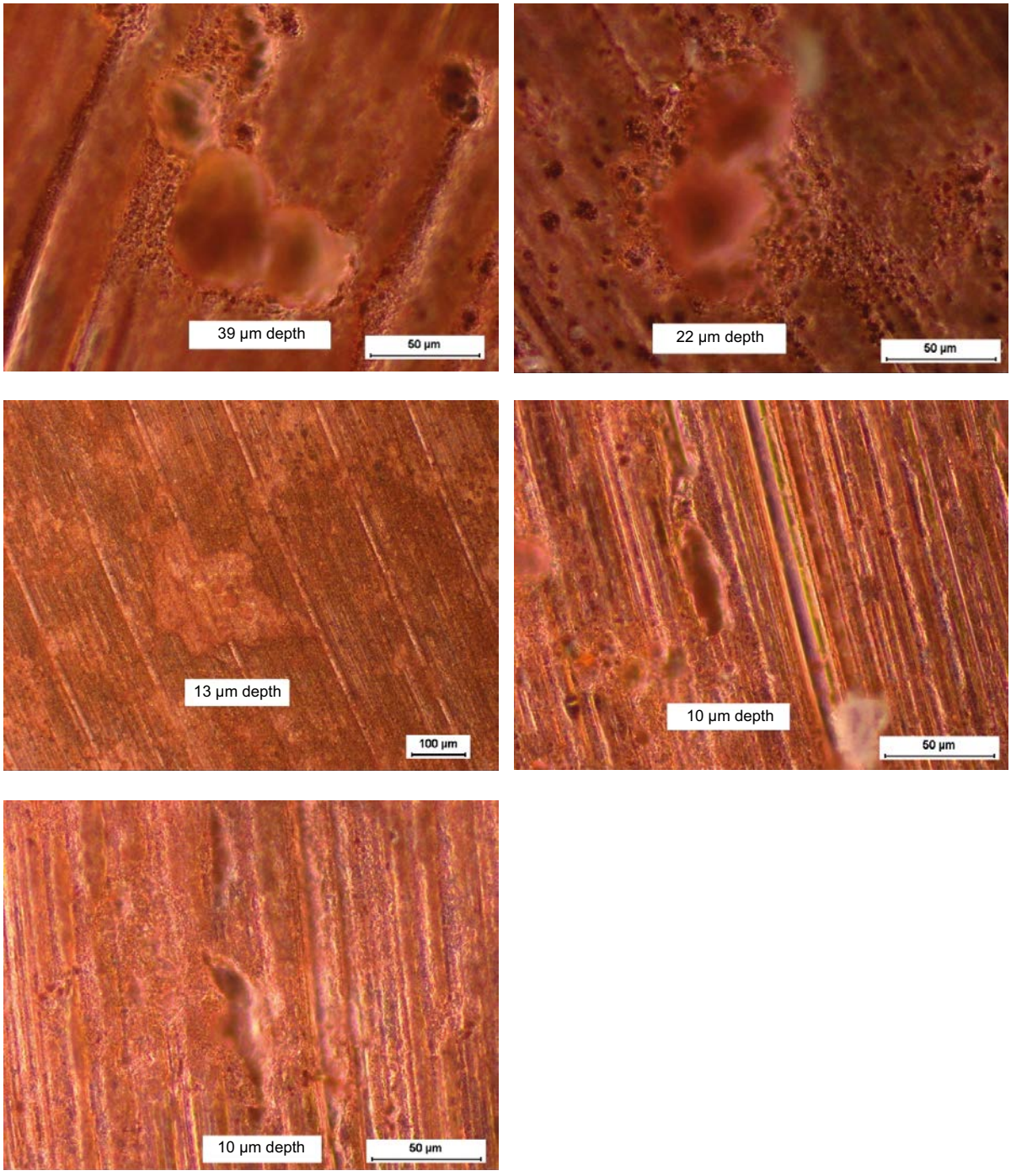

Figure E-12. *Microscope images of the deepest defects found on coupon A3/J after pickling.*

A3/L coupon after pickling

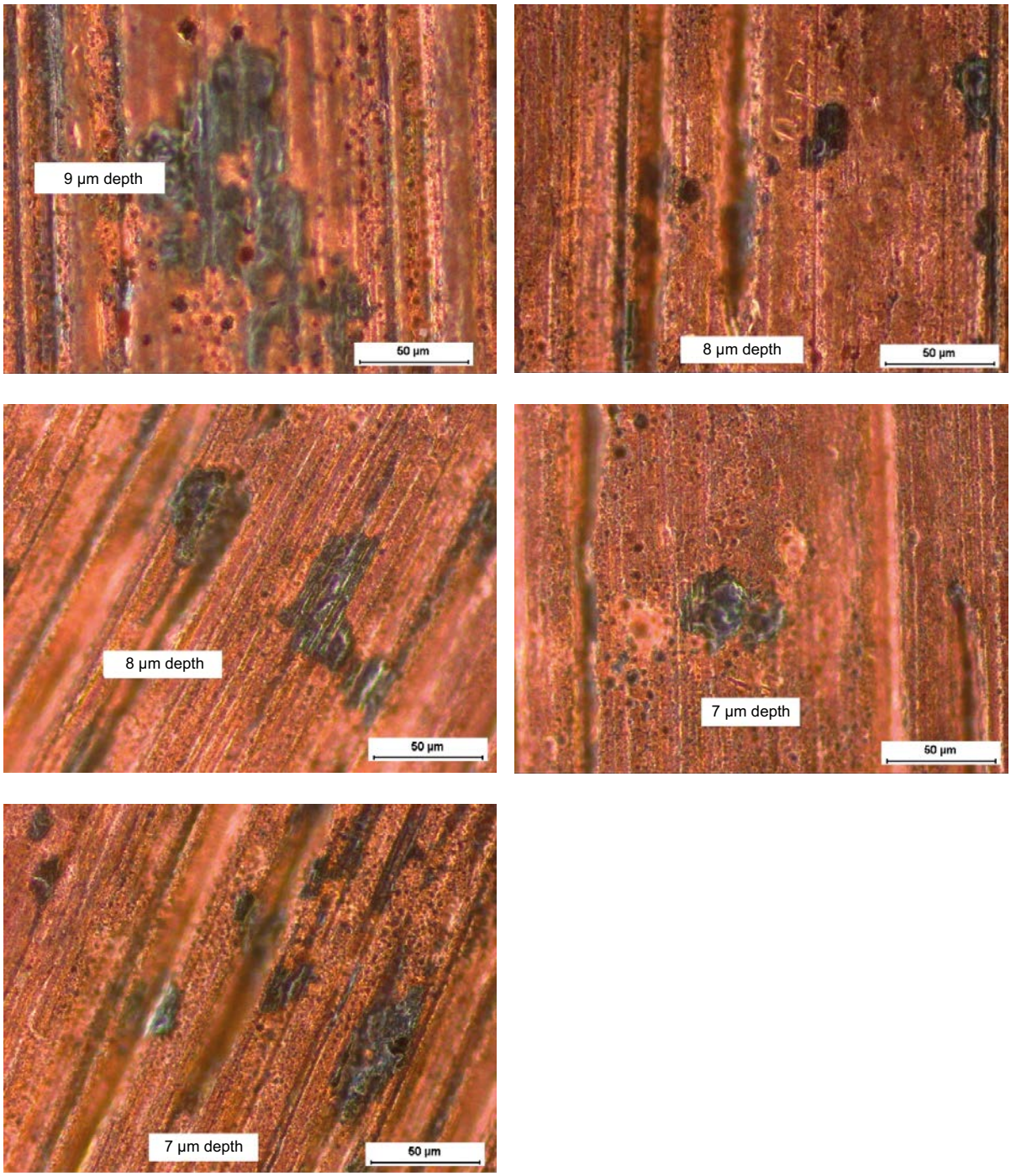

Figure E-13. *Microscope images of the deepest defects found on coupon A3/L after pickling.*

S2/M coupon after pickling

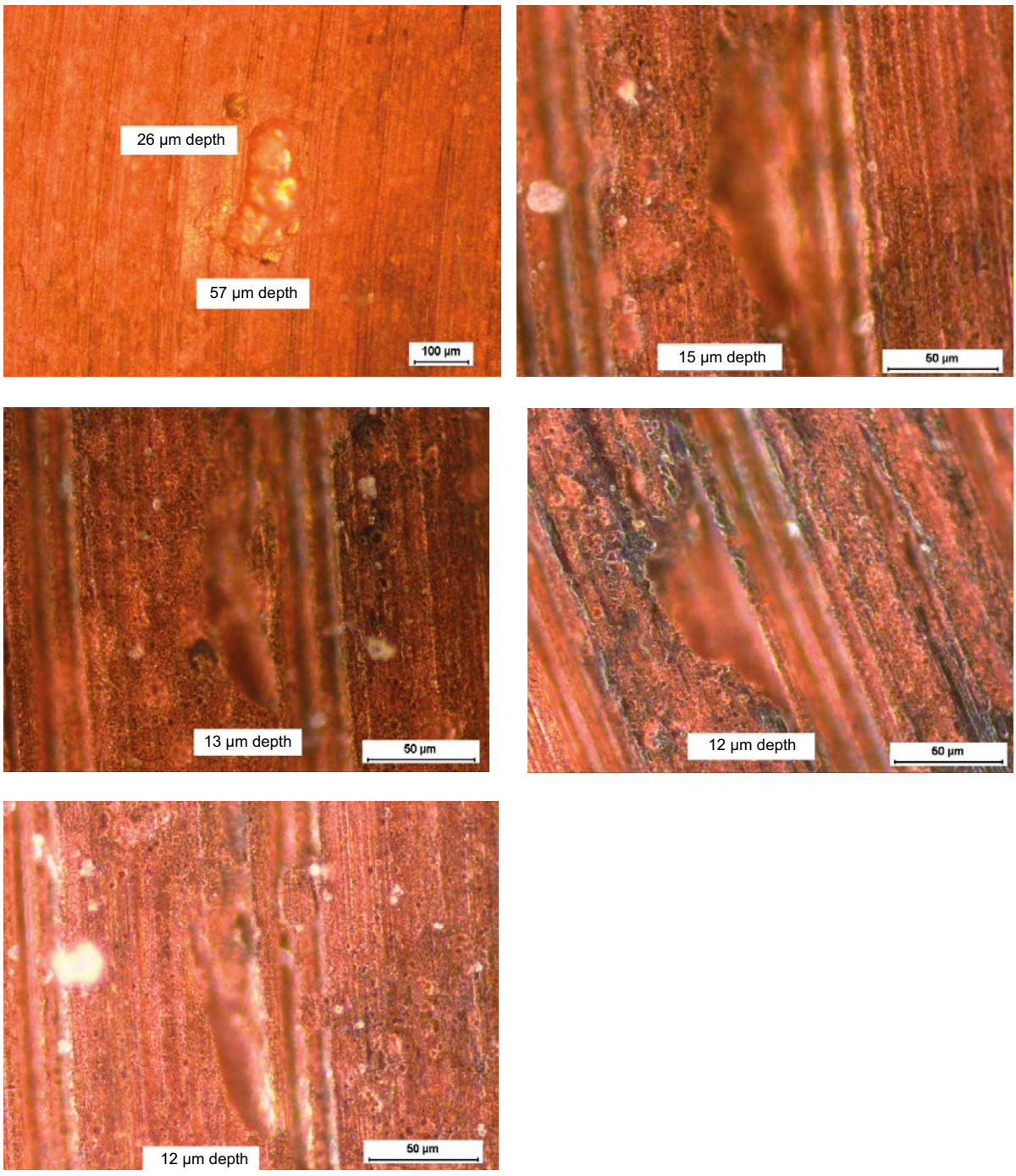

Figure E-14. *Microscope images of the deepest defects found on coupon S2/M after pickling.*

S2/O coupon after pickling

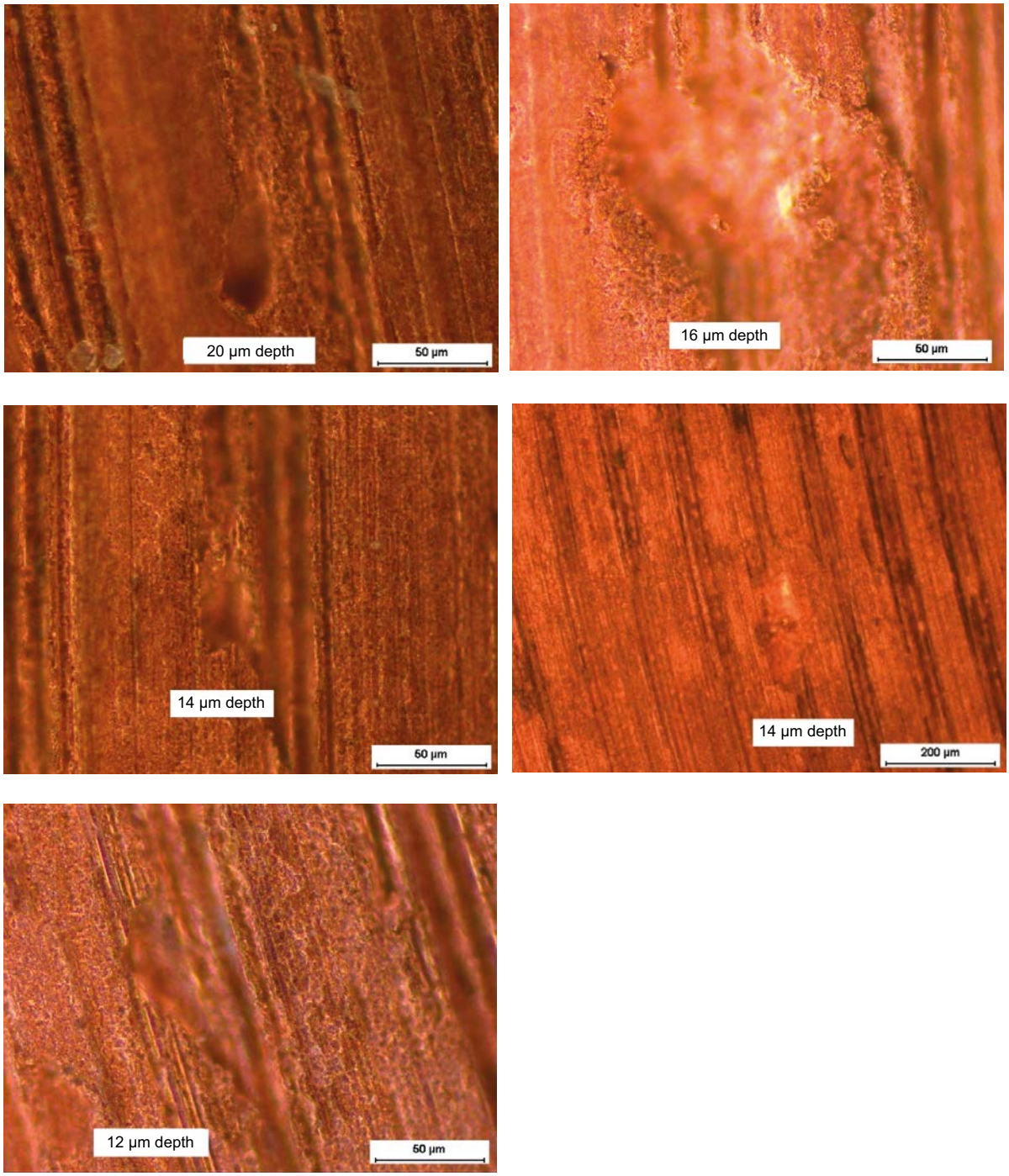

Figure E-15. *Microscope images of the deepest defects found on coupon S2/O after pickling.*

S2/P coupon after pickling

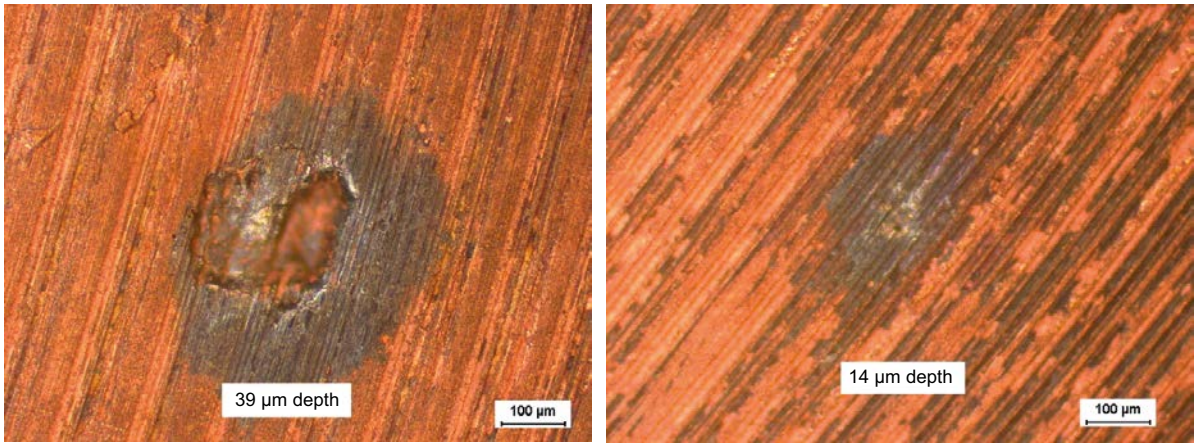

Figure E-16. *Microscope images of the deepest defects found on coupon S2/P after pickling.*

Ref L coupon after pickling

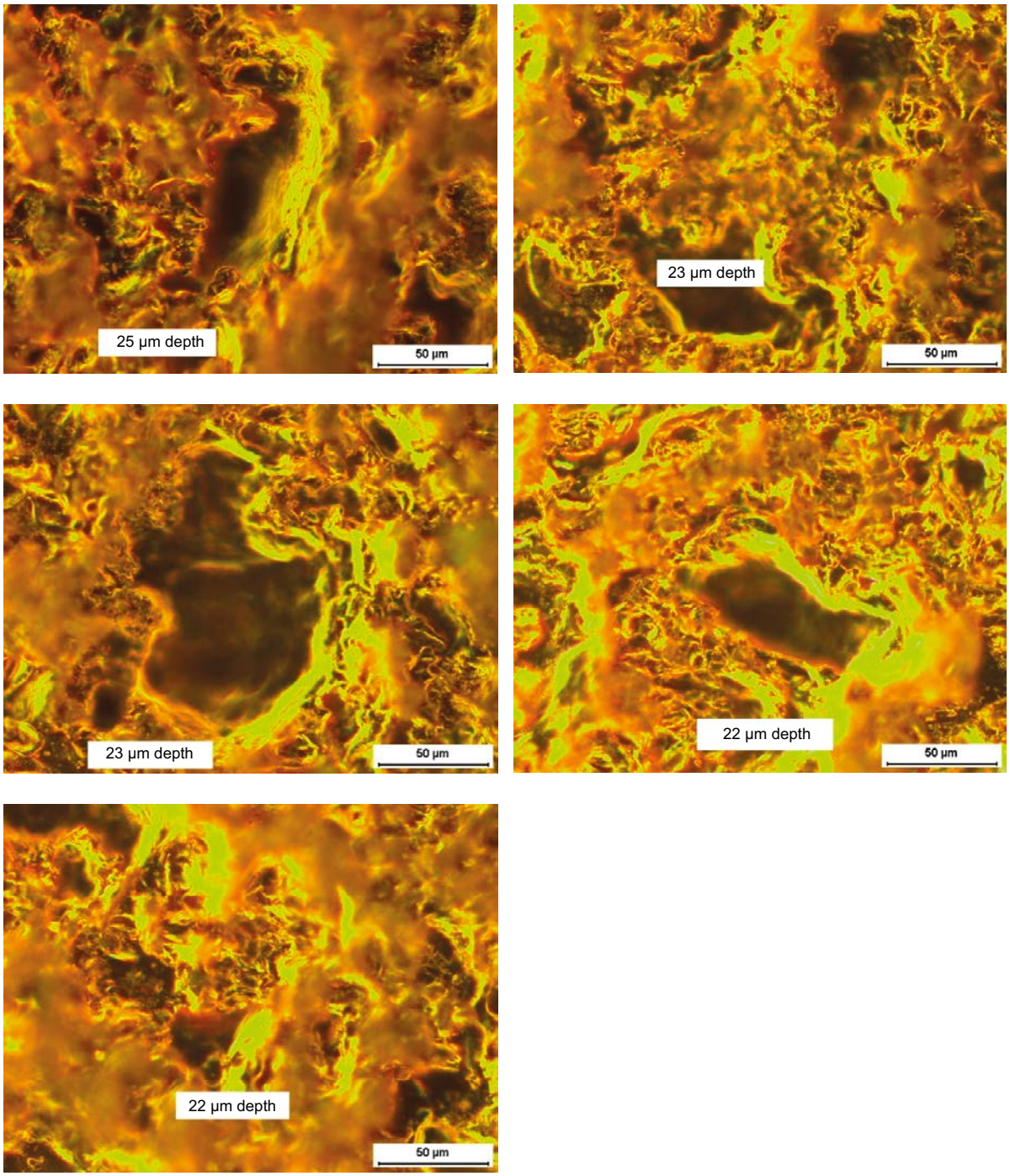

Figure E-17. *Microscope images of the deepest defects found on coupon Ref L after pickling.*

Ref K coupon after pickling

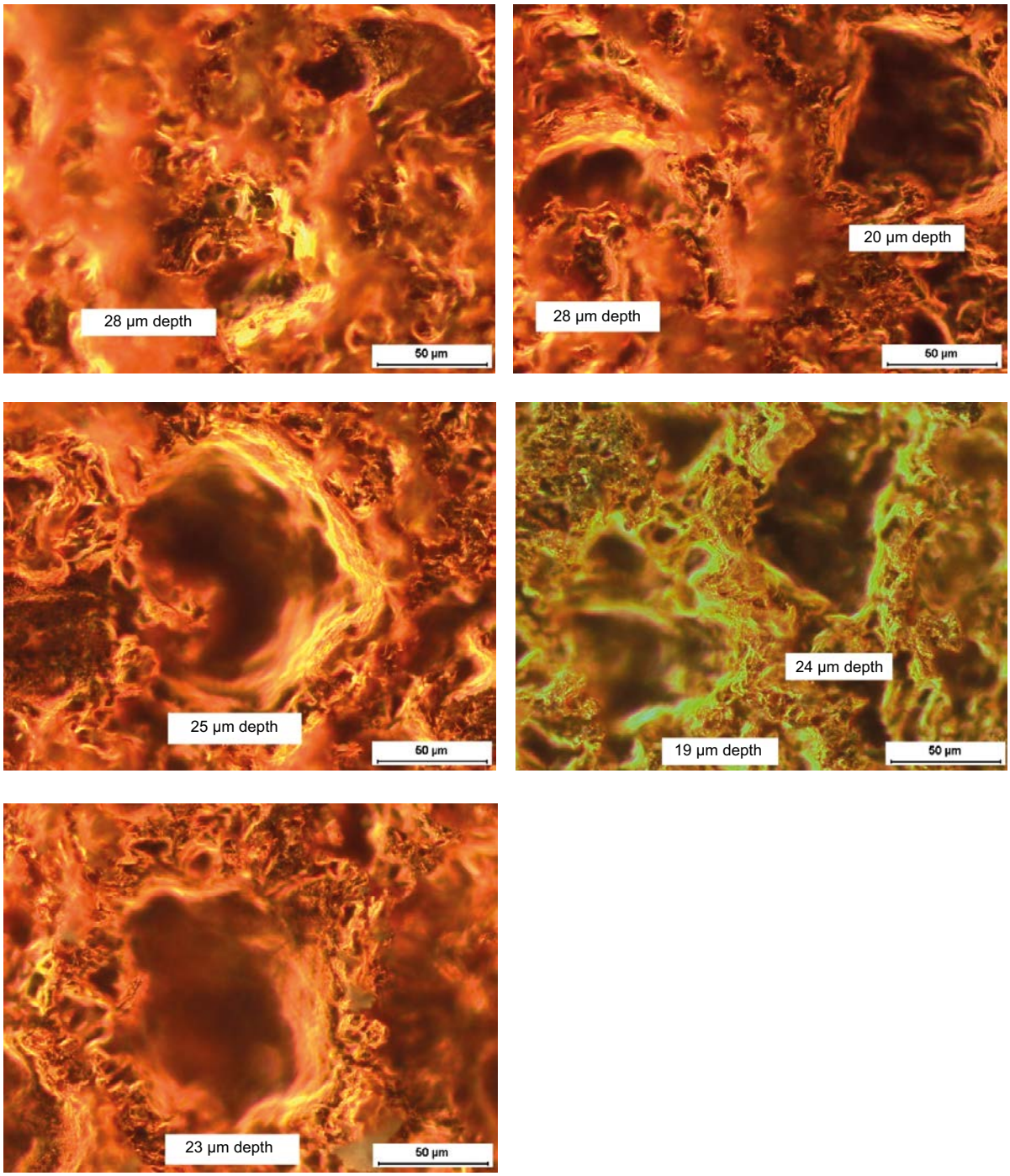

Figure E-18. *Microscope images of the deepest defects found on coupon Ref K after pickling.*

Vickers indentation mark on coupon A3/K

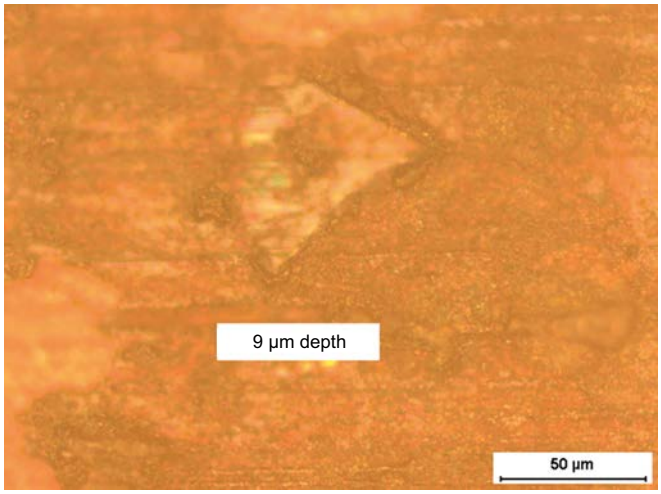

Figure E-19. *Vickers hardness indentation mark found on coupon A3/K.*

Appendix F

SEM images of pipe cross sections

The following images show the surfaces of the pipe cross sections examined under the SEM with varying magnifications. Three samples areas from pipe A3 were analysed and two sample areas from pipe S2. For each sample multiple sites were examined for the outer surface of the pipe, i.e. the surface that was in contact with the bentonite clay, and one site for the inner surfaces of the pipe, i.e. the surface that was in contact with air. Surface defects observed in the cross-sections at lower magnifications (< ×5 000 for pipe A3, and < ×8 000 for pipe S2) were measured and are tabulated in Table F-1. These measurements were taken between the lowest point of a defect and the adjacent outer surface of the pipe sample.

The images contain a file name in the lower right-hand corner, which denotes which pipe, which sample area and which site is contained within the image. For example, A3_1-1 denotes pipe A3, sample area 1, site 1. The magnification is also displayed in the images in the lower left corner, "Mag = 1.50 K X" denotes ×1 500 magnification, for example.

Table F-1. Measured depths of defects found during examination of pipe cross sections.

Sample	Depth of defects (µm)																		Max depth	Average depth
A3-1	25	16	14	12	12	12	11	10	10	10	9	8	8	8	6	5	5	5	25	10
A3-2	6	5																	6	6
A3-3	18	16	9	9	4														18	11
S2-1	13	12	8	5	5	3													13	8
S2-2	8	7	7	5															8	7

Pipe A3 sample 1

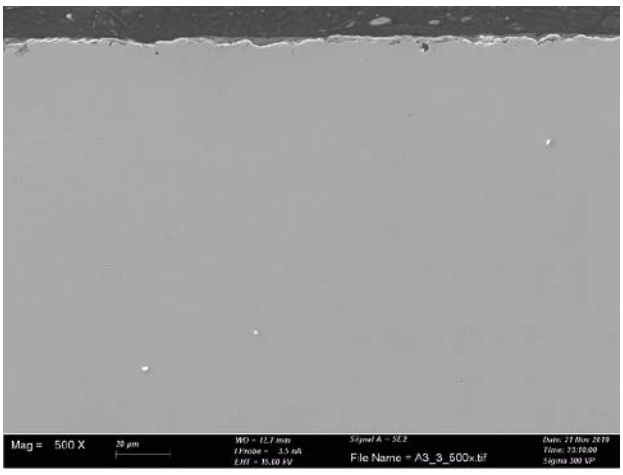

Figure F-1. *Cross-section of pipe A3 sample area 1.*

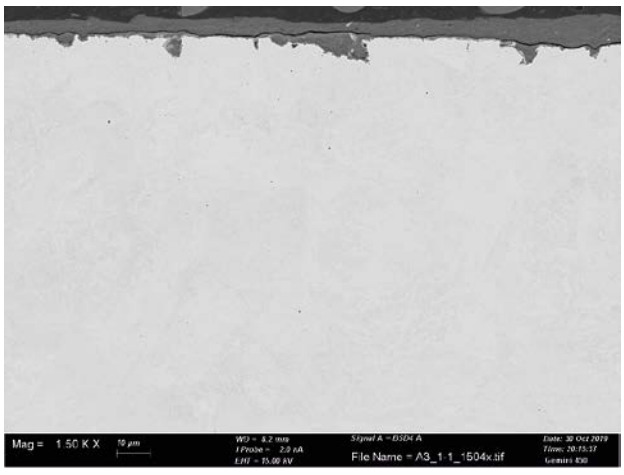

Figure F-2. *Cross-section of pipe A3 sample area 1.*

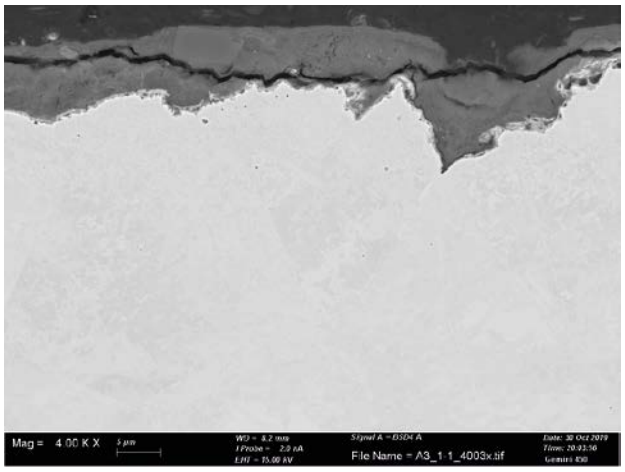

Figure F-3. *Cross-section of pipe A3 sample area 1.*

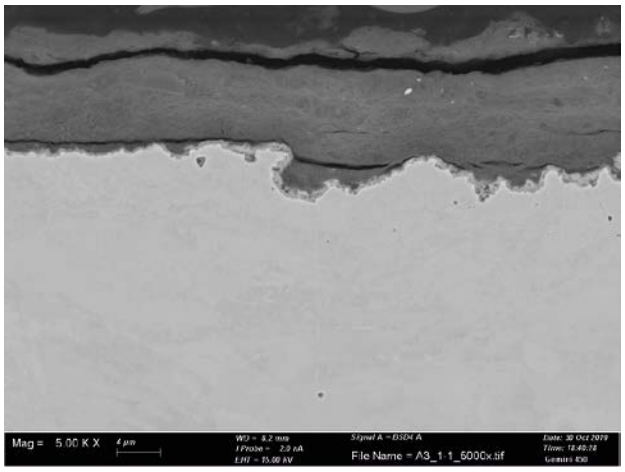

Figure F-4. *Cross-section of pipe A3 sample area 1.*

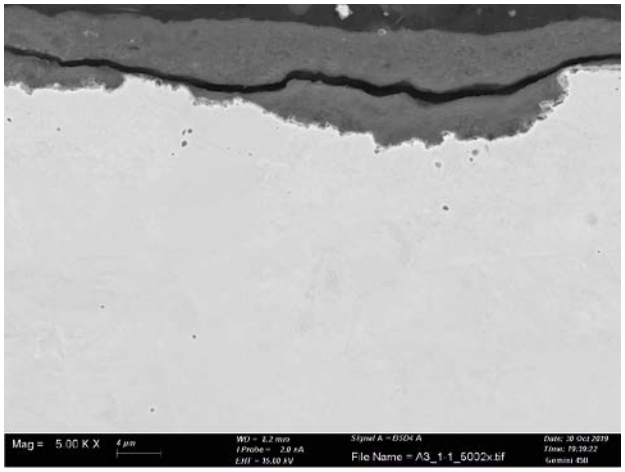

Figure F-5. *Cross-section of pipe A3 sample area 1.*

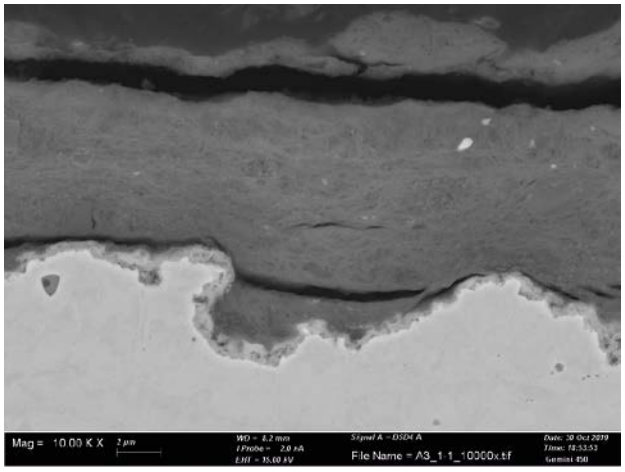

Figure F-6. *Cross-section of pipe A3 sample area 1.*

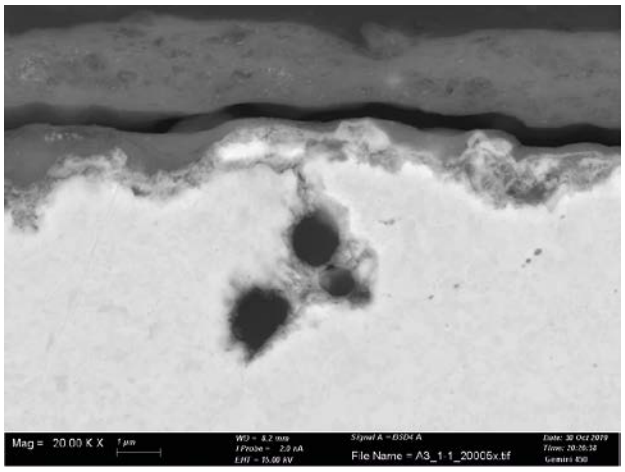

Figure F-7. *Cross-section of pipe A3 sample area 1.*

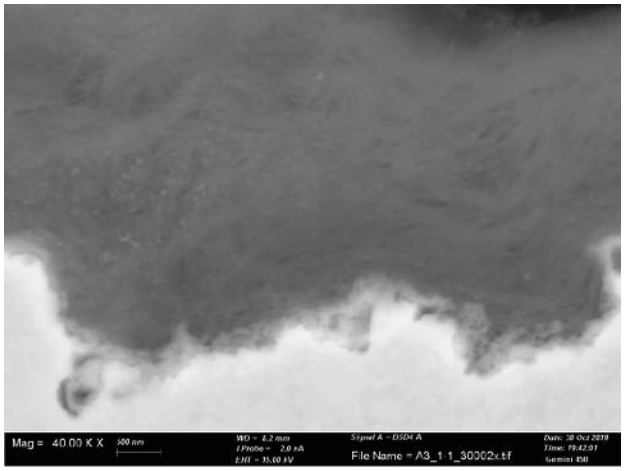

Figure F-8. *Cross-section of pipe A3 sample area 1.*

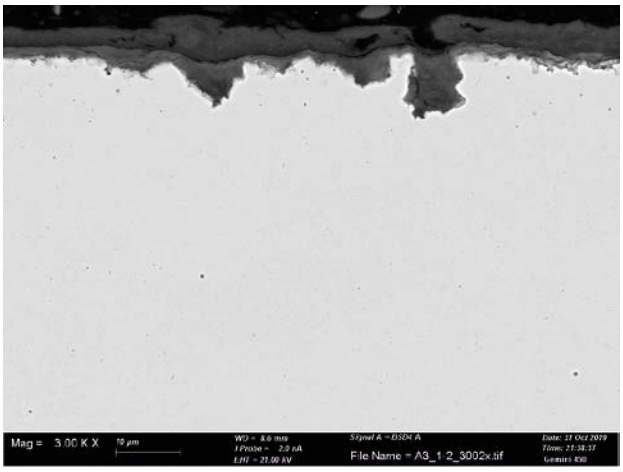

Figure F-9. *Cross-section of pipe A3 sample area 1.*

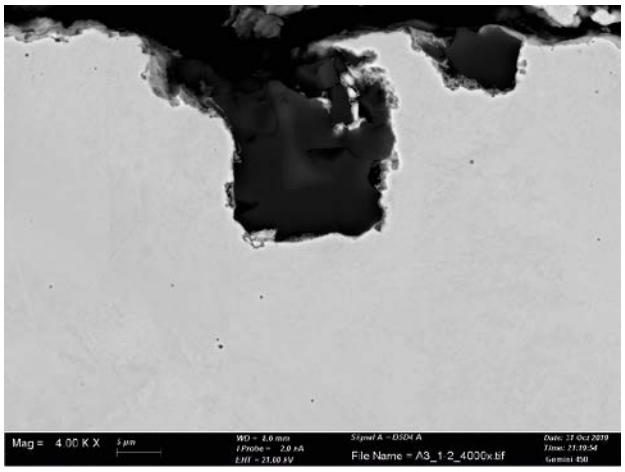

Figure F-10. *Cross-section of pipe A3 sample area 1.*

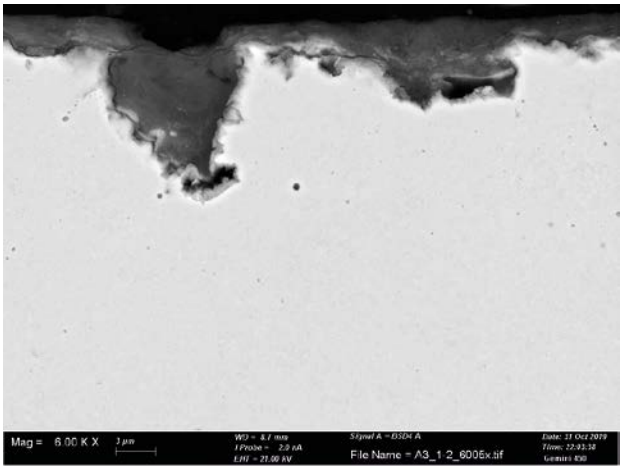

Figure F-11. *Cross-section of pipe A3 sample area 1.*

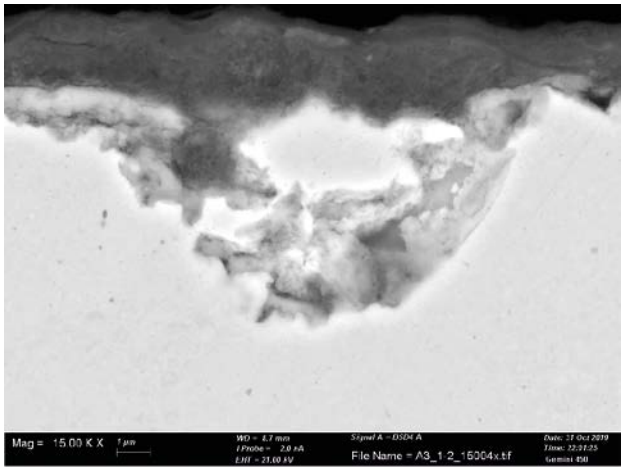

Figure F-12. *Cross-section of pipe A3 sample area 1.*

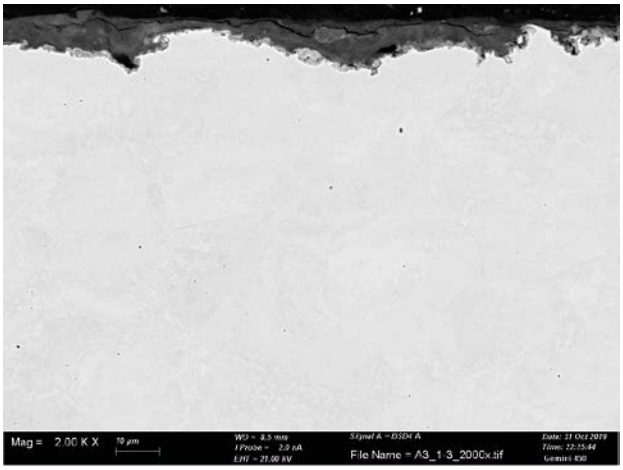

Figure F-13. *Cross-section of pipe A3 sample area 1.*

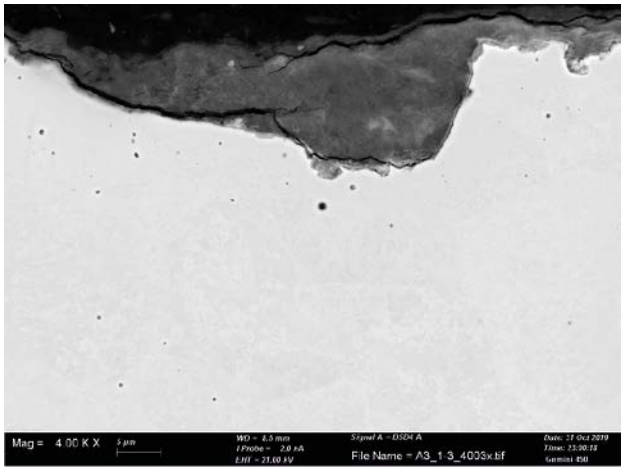

Figure F-14. *Cross-section of pipe A3 sample area 1.*

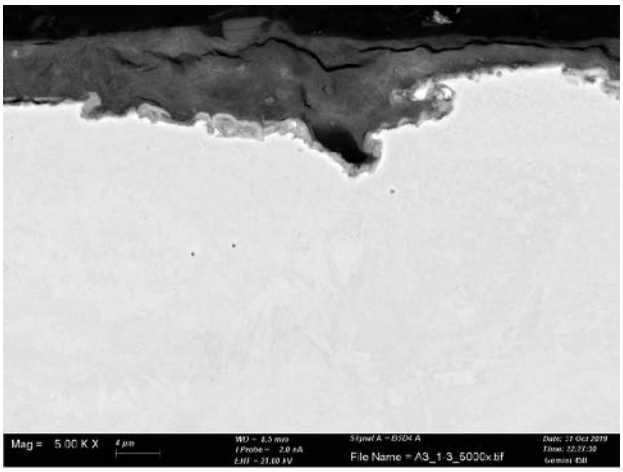

Figure F-15. *Cross-section of pipe A3 sample area 1.*

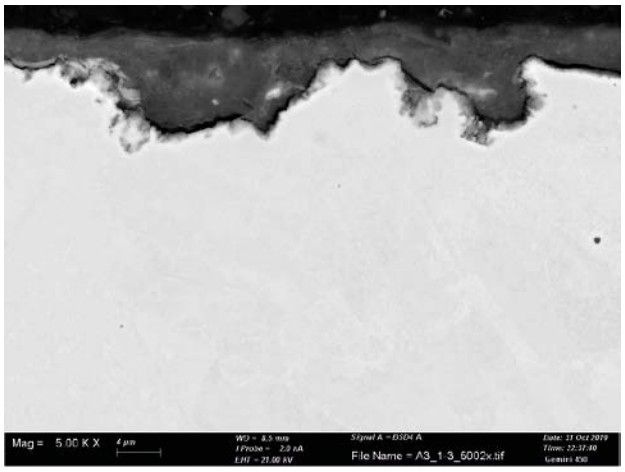

Figure F-16. *Cross-section of pipe A3 sample area 1.*

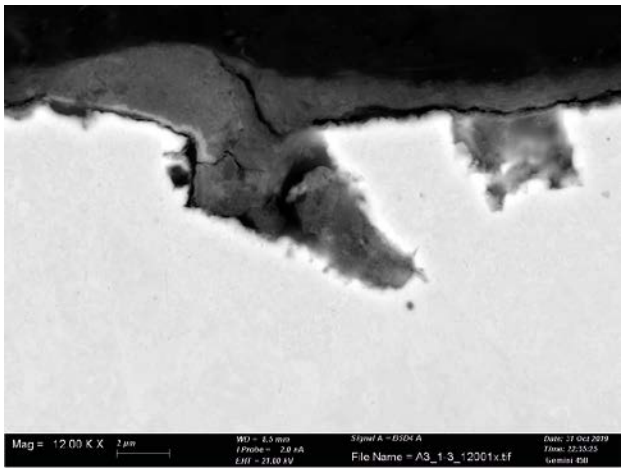

Figure F-17. *Cross-section of pipe A3 sample area 1.*

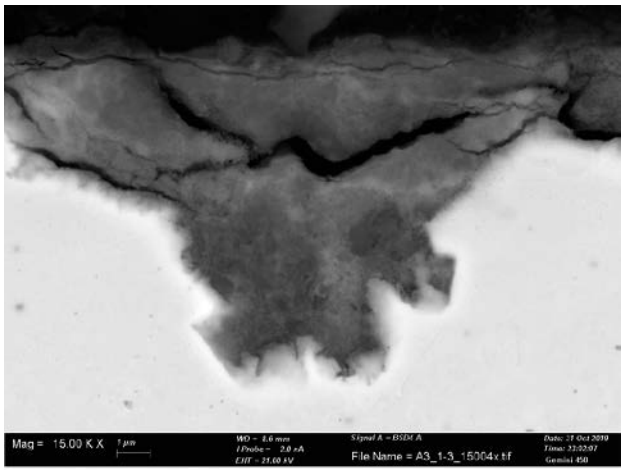

Figure F-18. *Cross-section of pipe A3 sample area 1.*

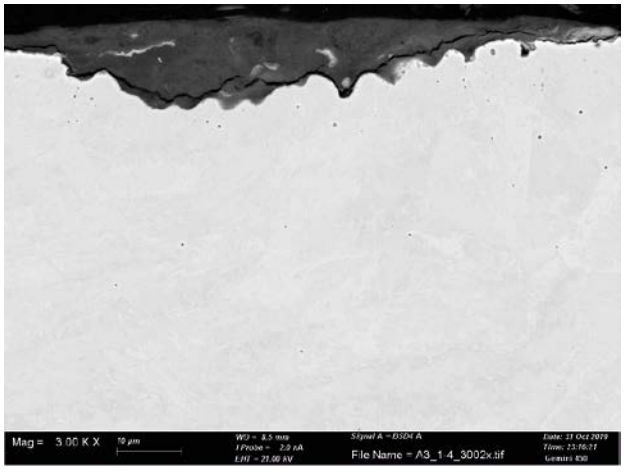

Figure F-19. *Cross-section of pipe A3 sample area 1.*

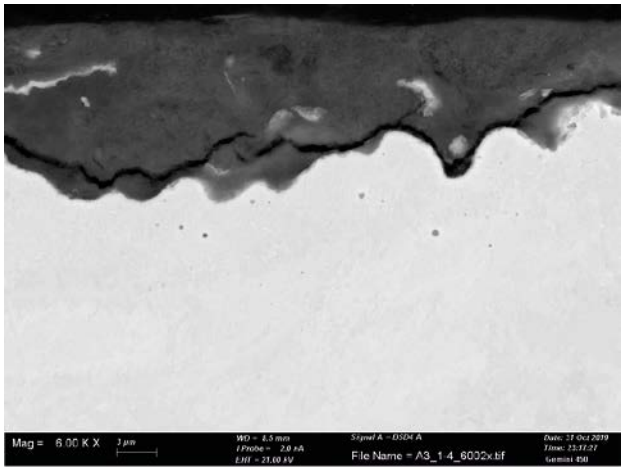

Figure F-20. *Cross-section of pipe A3 sample area 1.*

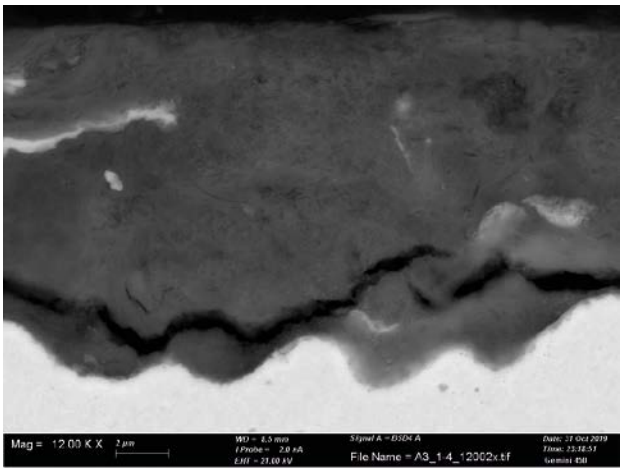

Figure F-21. *Cross-section of pipe A3 sample area 1.*

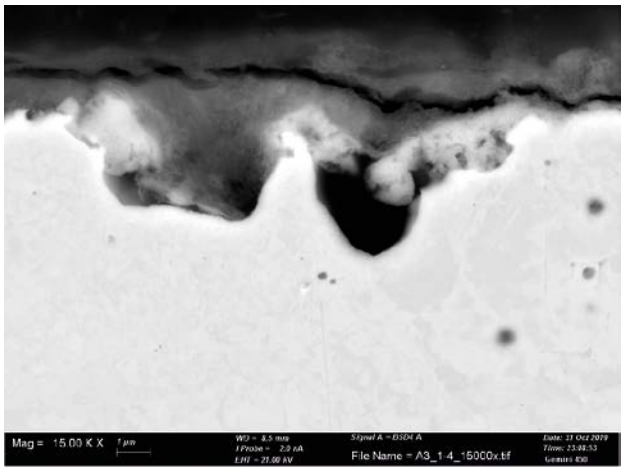

Figure F-22. *Cross-section of pipe A3 sample area 1.*

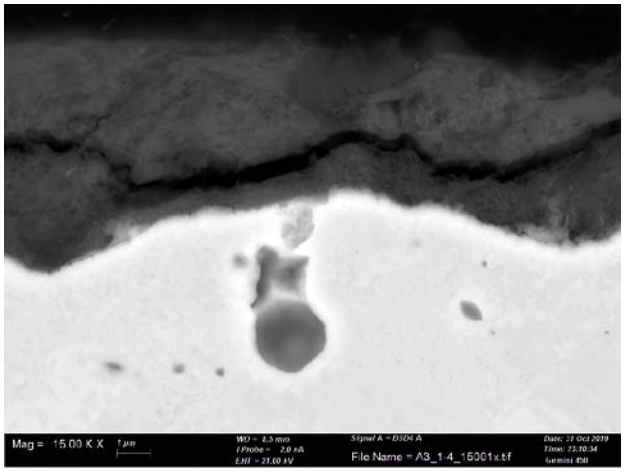

Figure F-23. *Cross-section of pipe A3 sample area 1.*

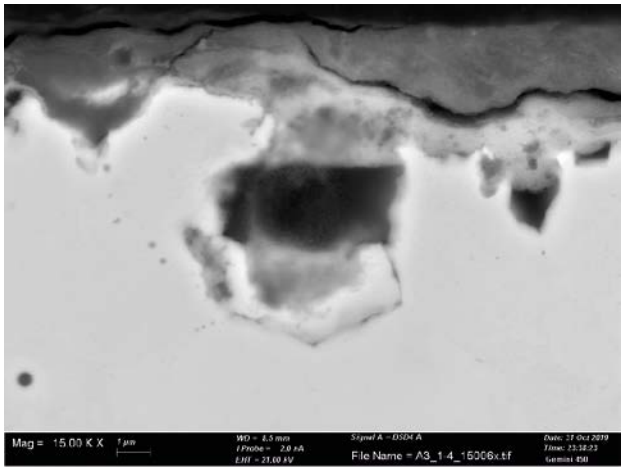

Figure F-24. *Cross-section of pipe A3 sample area 1.*

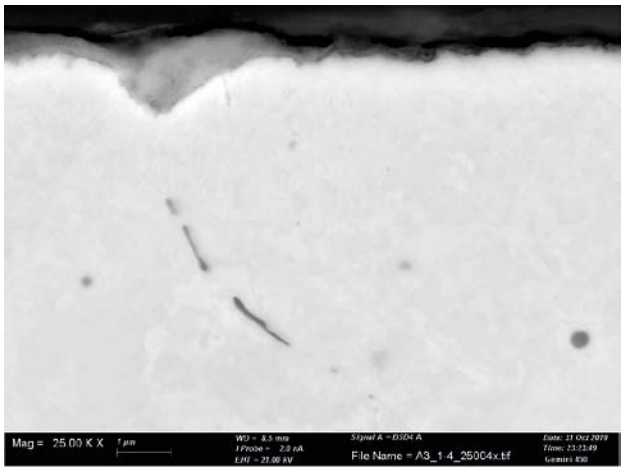

Figure F-25. *Cross-section of pipe A3 sample area 1.*

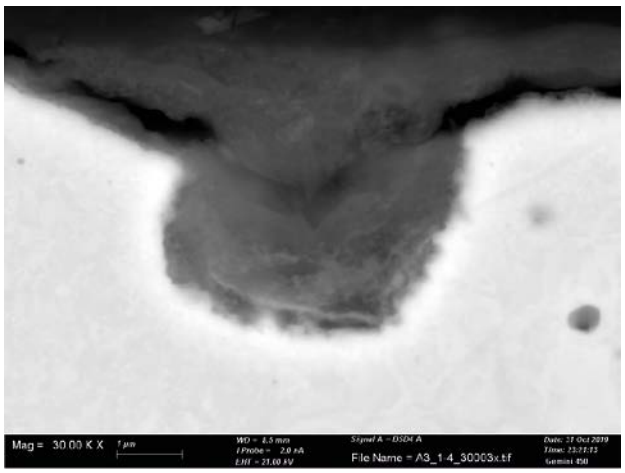

Figure F-26. *Cross-section of pipe A3 sample area 1.*

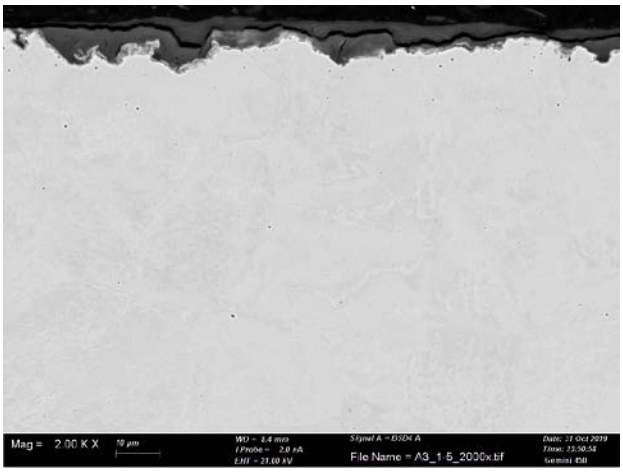

Figure F-27. *Cross-section of pipe A3 sample area 1.*

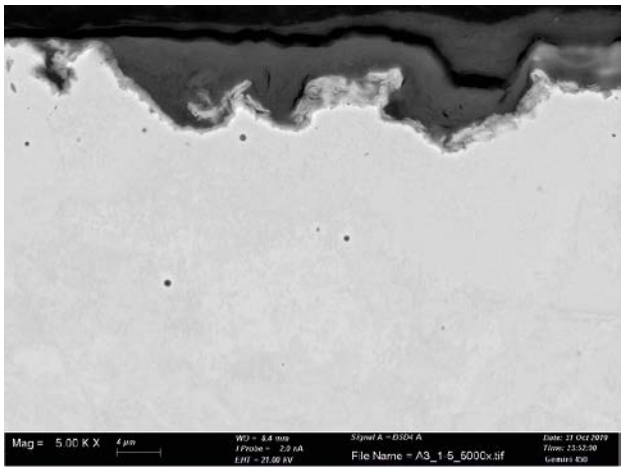

Figure F-28. *Cross-section of pipe A3 sample area 1.*

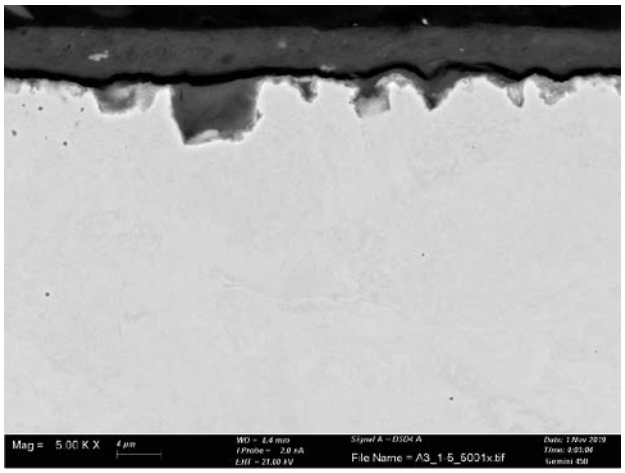

Figure F-29. *Cross-section of pipe A3 sample area 1.*

Inner surface of pipe A3

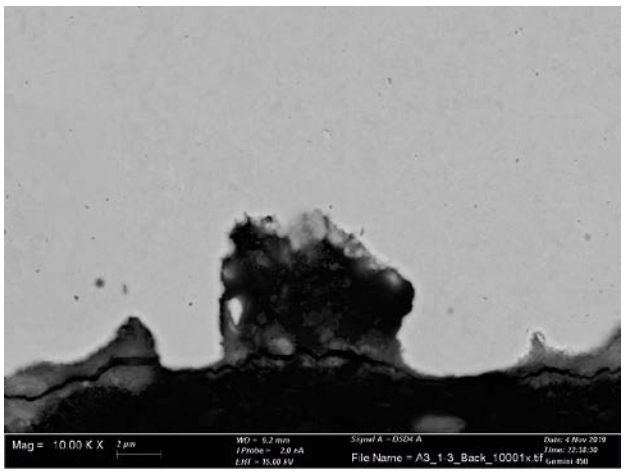

Figure F-30. *Cross-section of pipe A3 inner surface.*

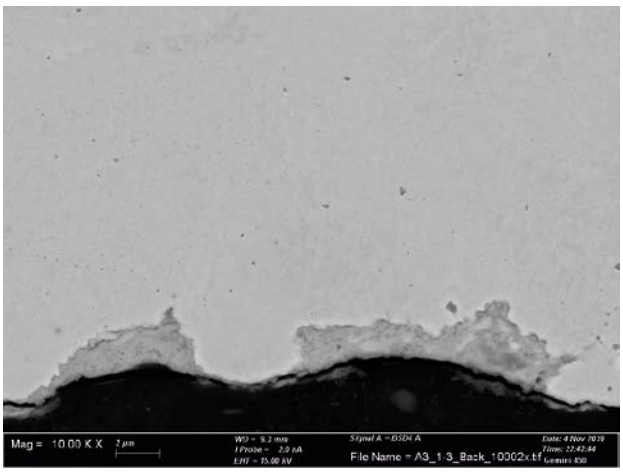

Figure F-31. *Cross-section of pipe A3 inner surface.*

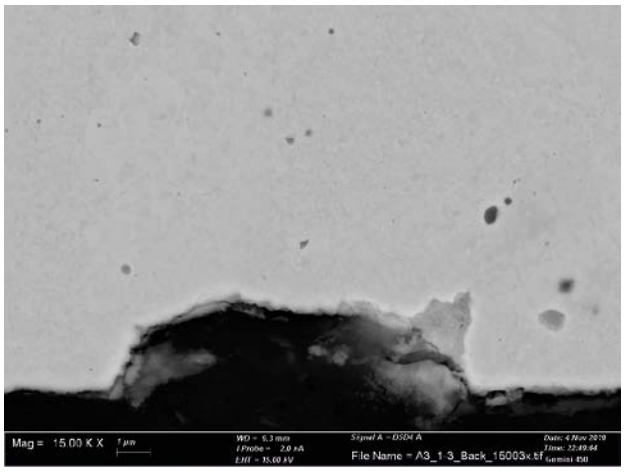

Figure F-32. *Cross-section of pipe A3 inner surface.*

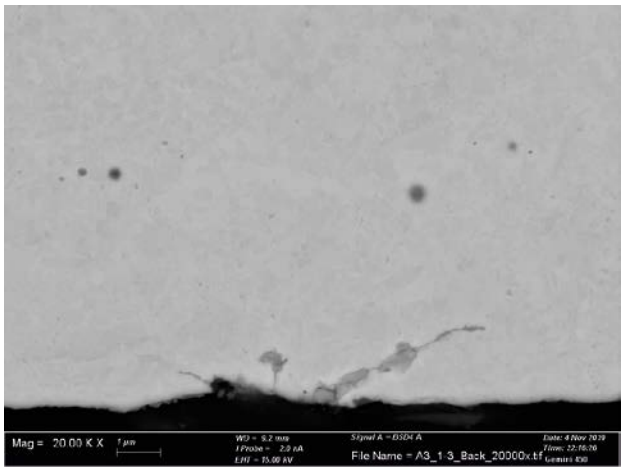

Figure F-33. *Cross-section of pipe A3 inner surface.*

Pipe A3 sample 2

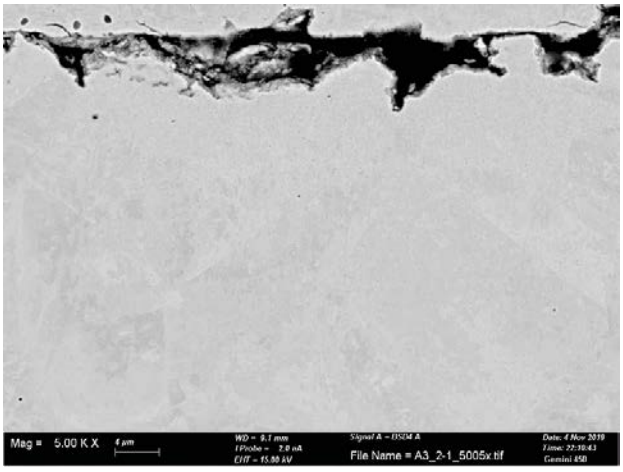

Figure F-34. *Cross-section of pipe A3 sample area 2.*

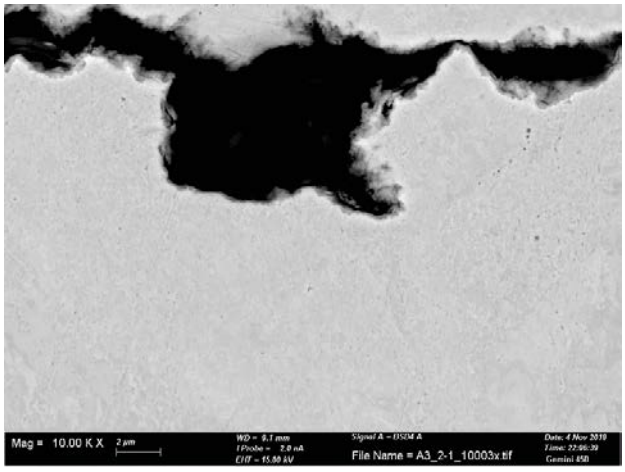

Figure F-35. *Cross-section of pipe A3 sample area 2.*

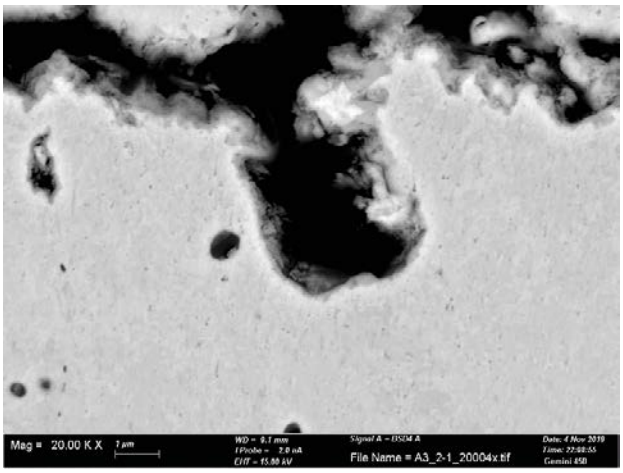

Figure F-36. *Cross-section of pipe A3 sample area 2.*

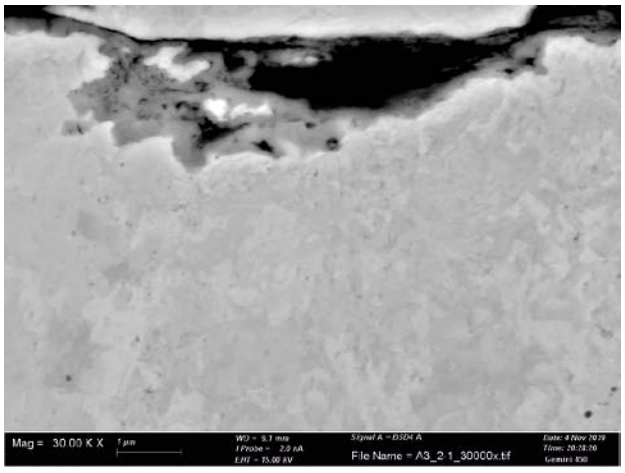

Figure F-37. *Cross-section of pipe A3 sample area 2.*

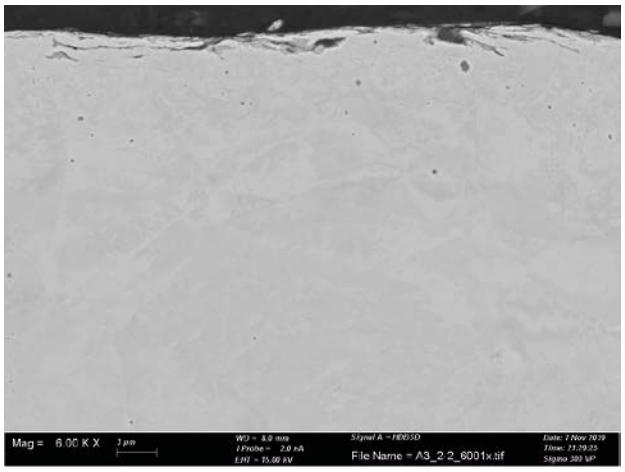

Figure F-38. *Cross-section of pipe A3 sample area 2.*

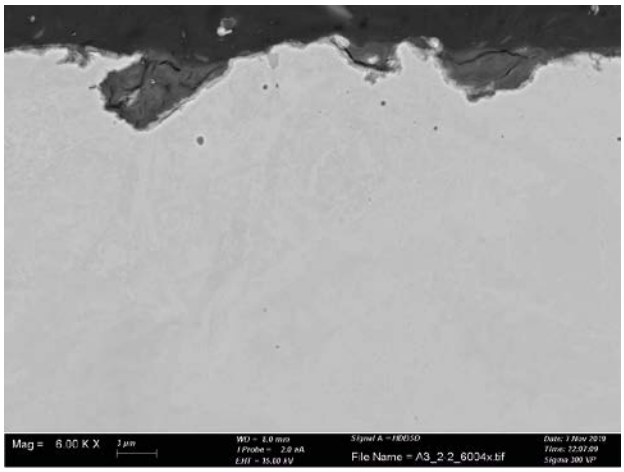

Figure F-39. *Cross-section of pipe A3 sample area 2.*

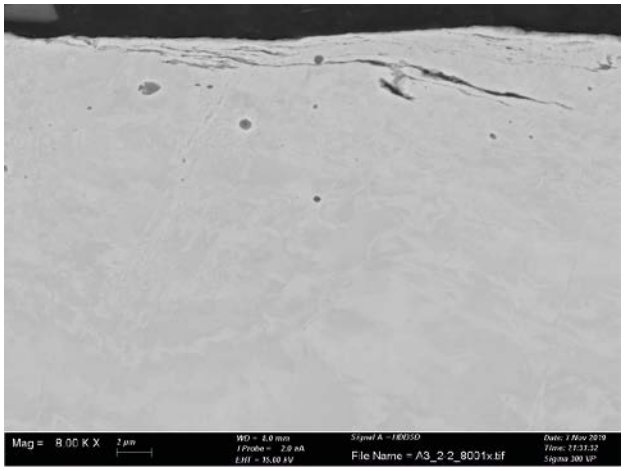

Figure F-40. *Cross-section of pipe A3 sample area 2.*

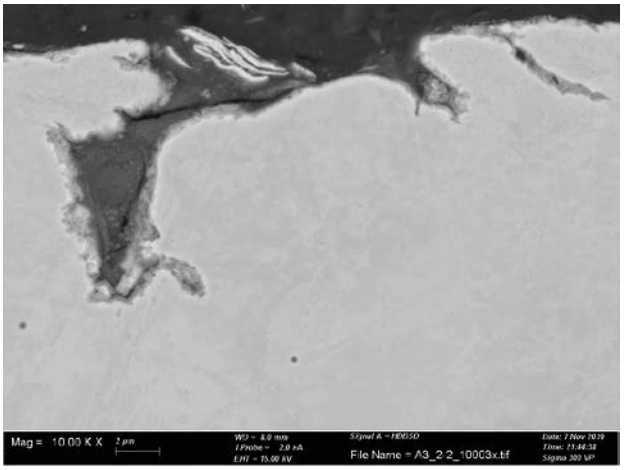

Figure F-41. *Cross-section of pipe A3 sample area 2.*

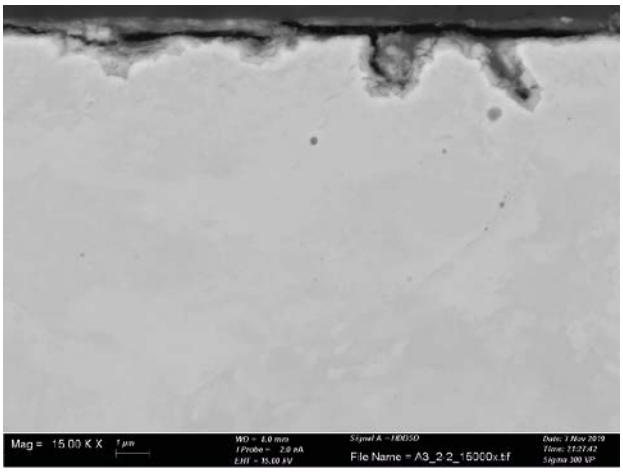

Figure F-42. *Cross-section of pipe A3 sample area 2.*

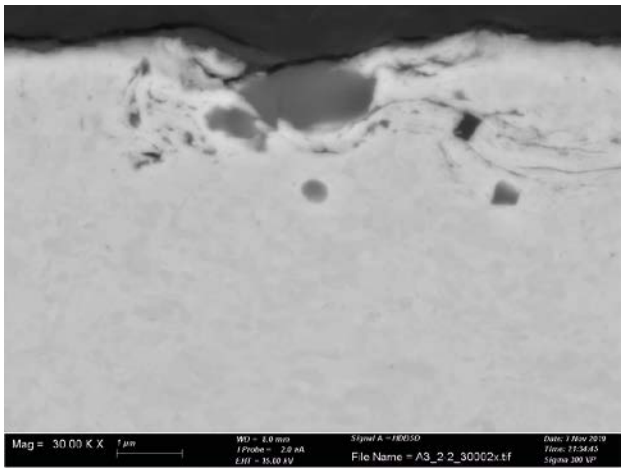

Figure F-43. *Cross-section of pipe A3 sample area 2.*

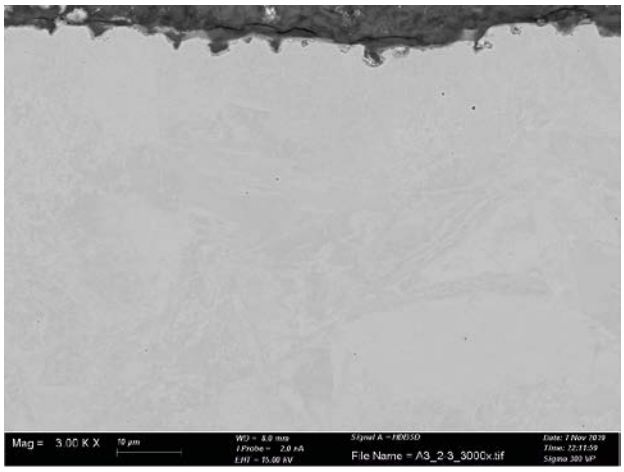

Figure F-44. *Cross-section of pipe A3 sample area 2.*

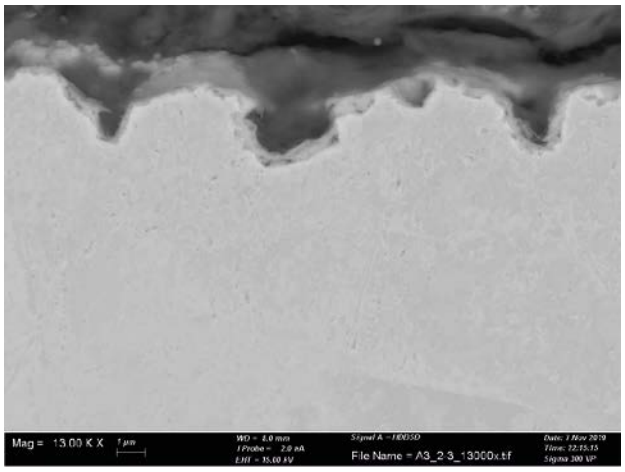

Figure F-45. *Cross-section of pipe A3 sample area 2.*

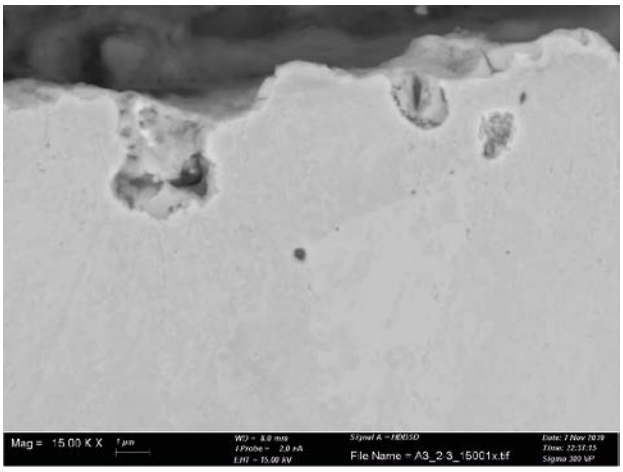

Figure F-46. *Cross-section of pipe A3 sample area 2.*

Pipe A3 sample 3

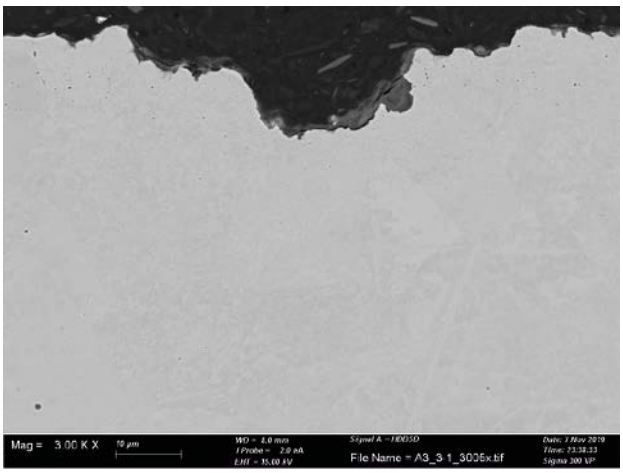

Figure F-47. *Cross-section of pipe A3 sample area 3.*

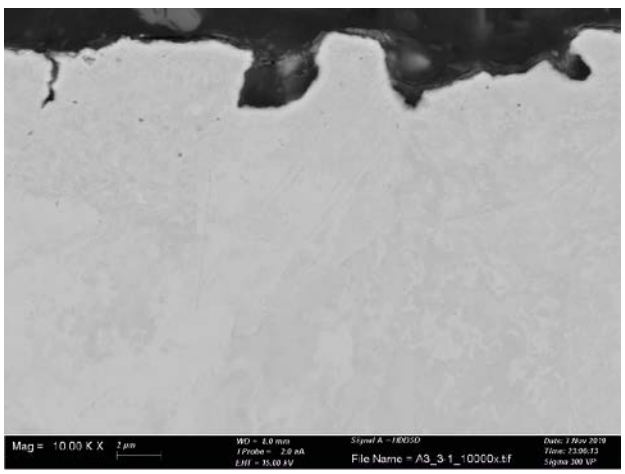

Figure F-48. *Cross-section of pipe A3 sample area 3.*

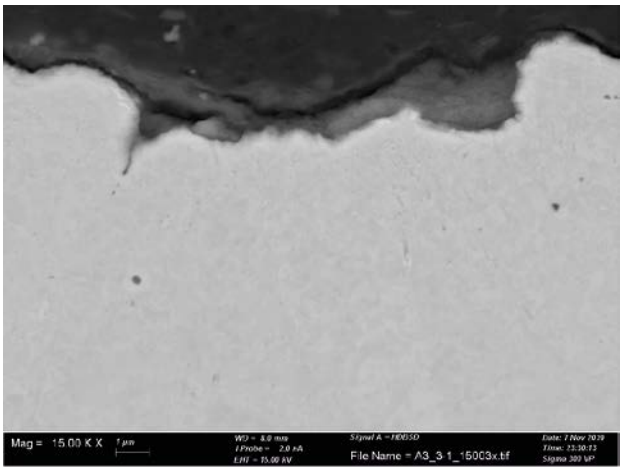

Figure F-49. *Cross-section of pipe A3 sample area 3.*

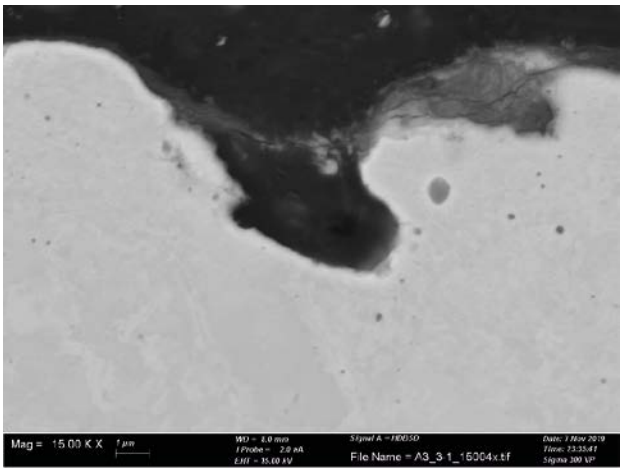

Figure F-50. *Cross-section of pipe A3 sample area 3.*

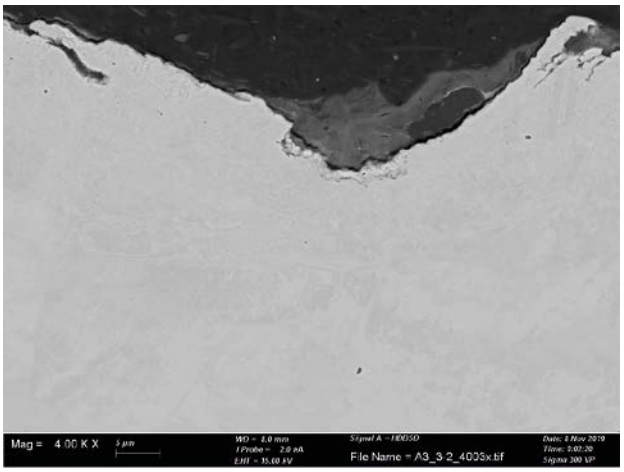

Figure F-51. *Cross-section of pipe A3 sample area 3.*

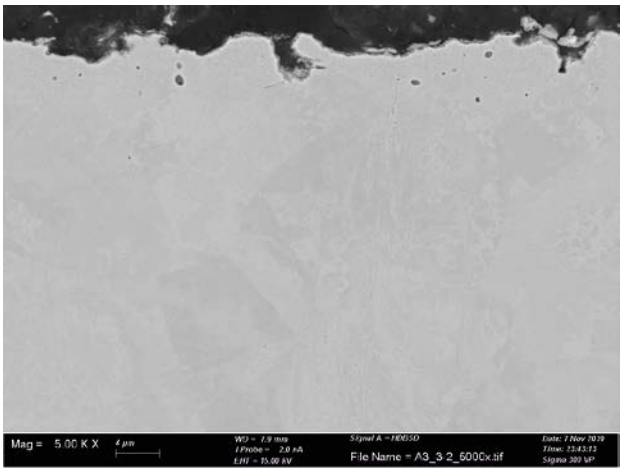

Figure F-52. *Cross-section of pipe A3 sample area 3.*

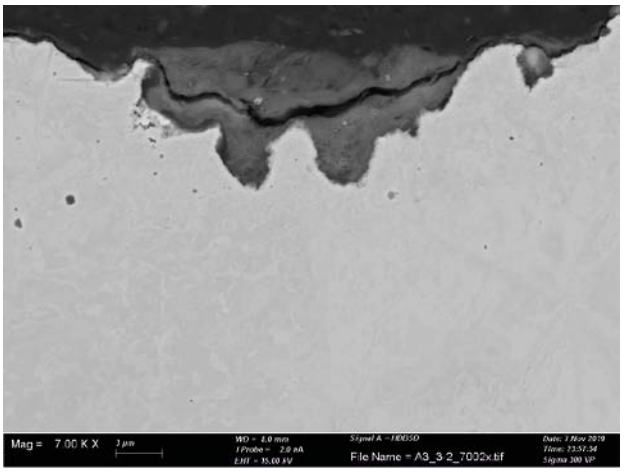

Figure F-53. *Cross-section of pipe A3 sample area 3.*

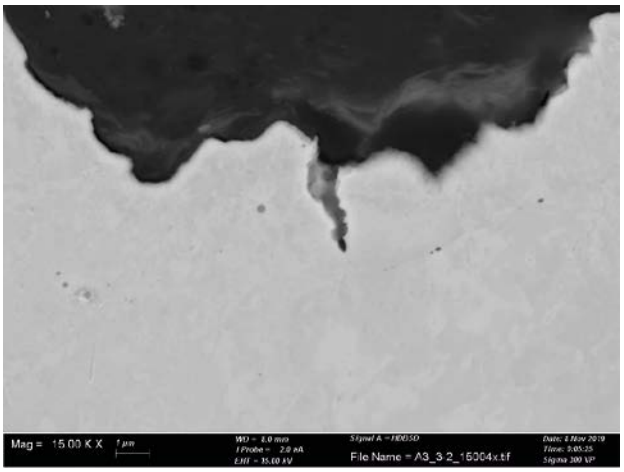

Figure F-54. *Cross-section of pipe A3 sample area 3.*

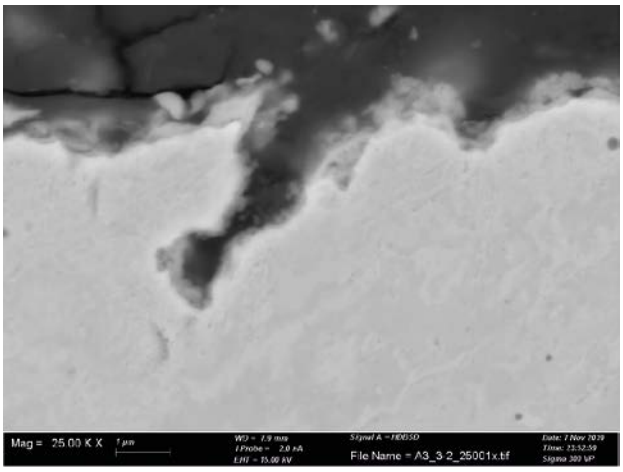

Figure F-55. *Cross-section of pipe A3 sample area 3.*

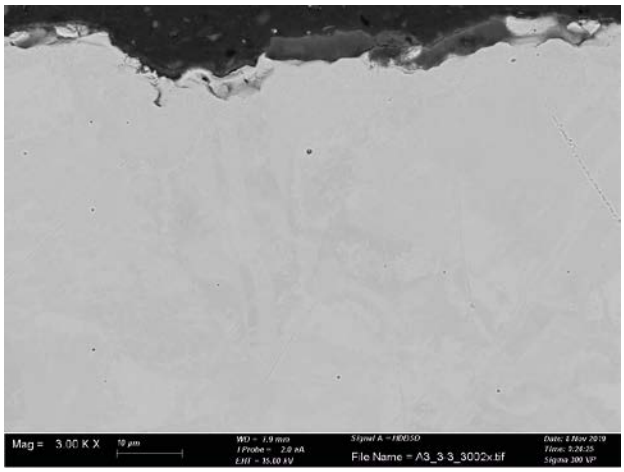

Figure F-56. *Cross-section of pipe A3 sample area 3.*

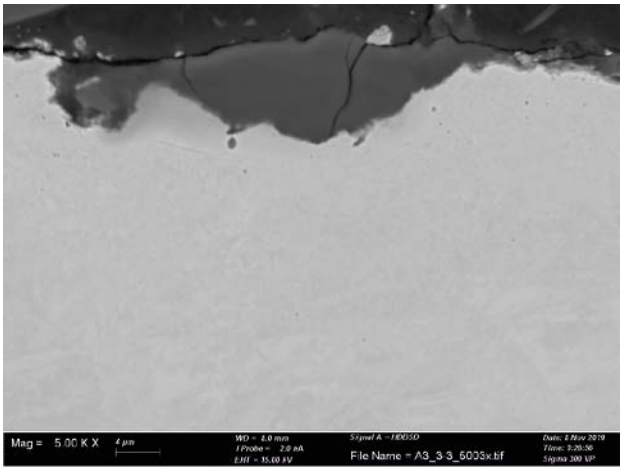

Figure F-57. *Cross-section of pipe A3 sample area 3.*

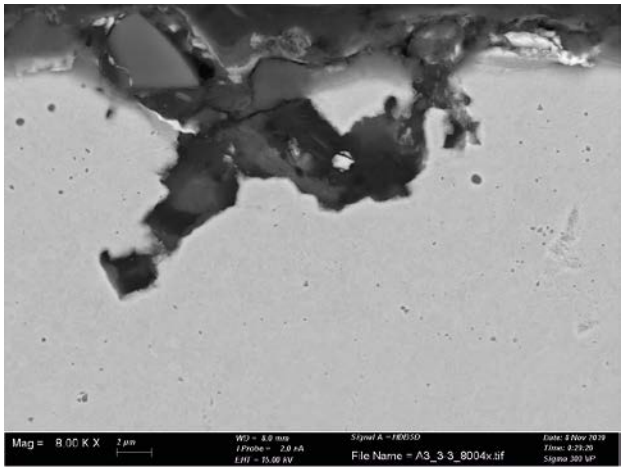

Figure F-58. *Cross-section of pipe A3 sample area 3.*

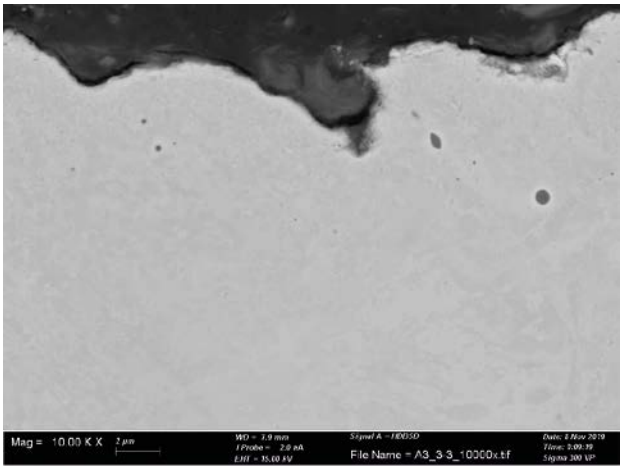

Figure F-59. *Cross-section of pipe A3 sample area 3.*

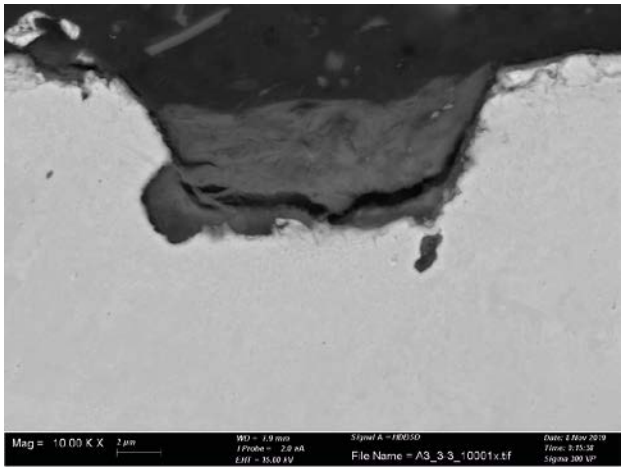

Figure F-60. *Cross-section of pipe A3 sample area 3.*

Pipe S2 sample 1

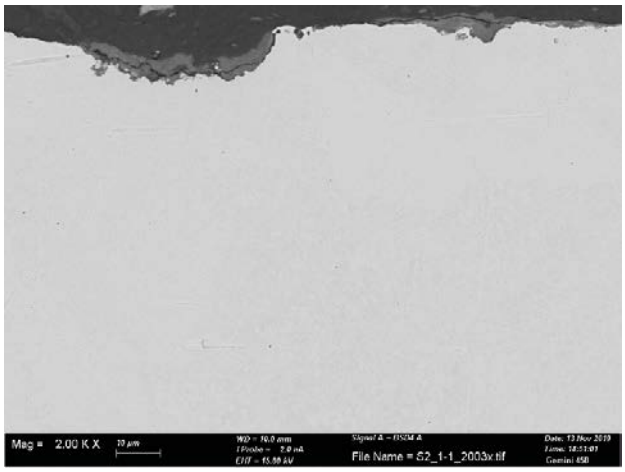

Figure F-61. *Cross-section of pipe S2 sample area 1.*

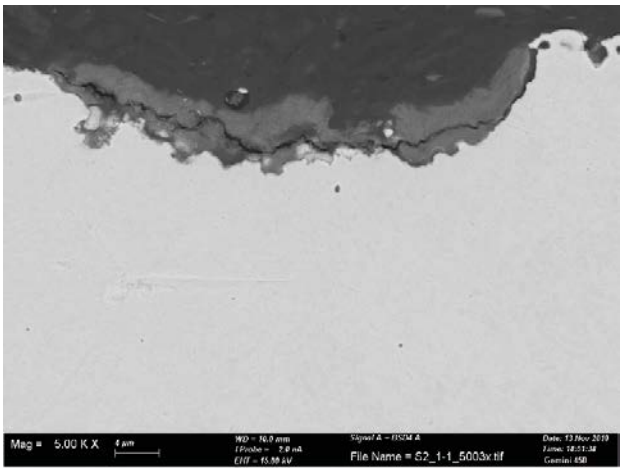

Figure F-62. *Cross-section of pipe S2 sample area 1.*

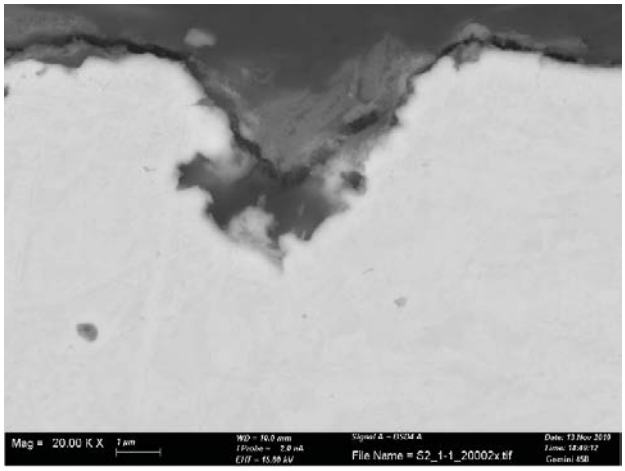

Figure F-63. *Cross-section of pipe S2 sample area 1.*

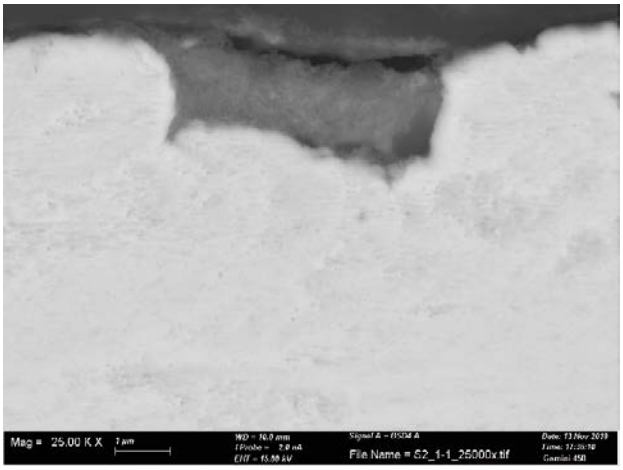

Figure F-64. *Cross-section of pipe S2 sample area 1.*

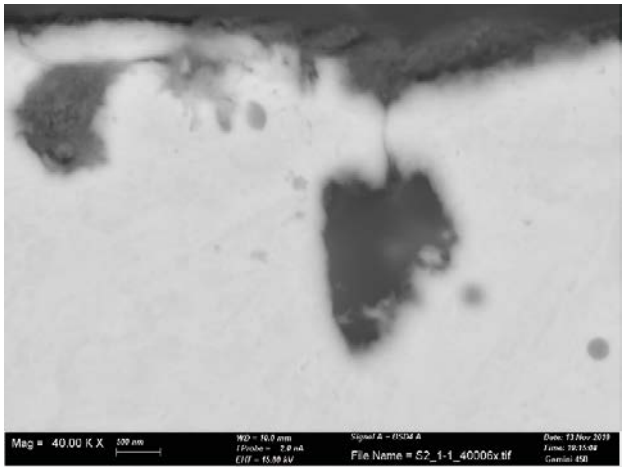

Figure F-65. *Cross-section of pipe S2 sample area 1.*

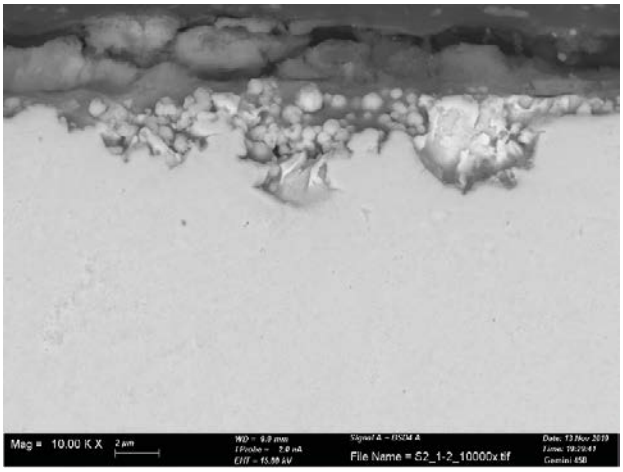

Figure F-66. *Cross-section of pipe S2 sample area 1.*

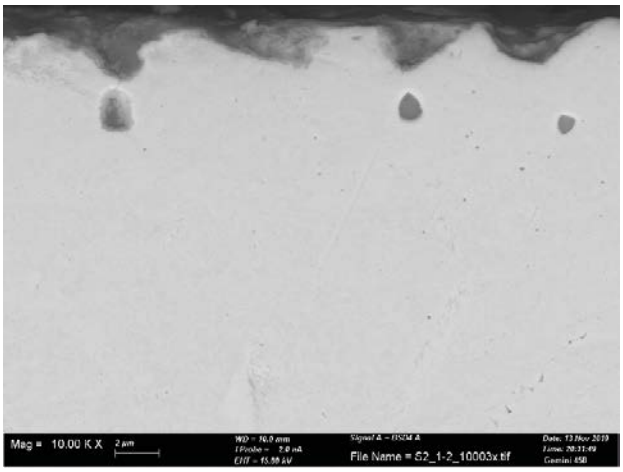

Figure F-67. *Cross-section of pipe S2 sample area 1.*

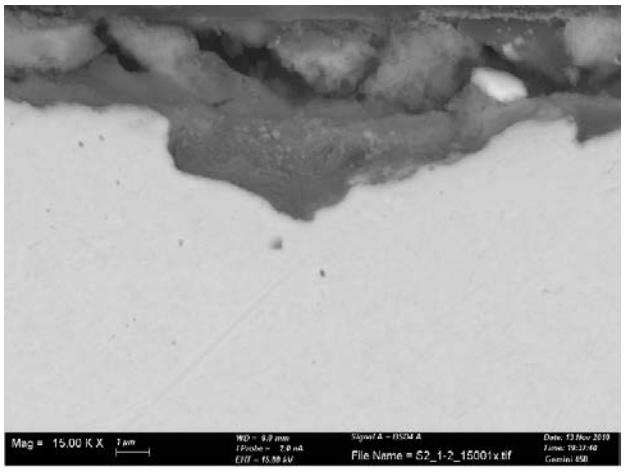

Figure F-68. *Cross-section of pipe S2 sample area 1.*

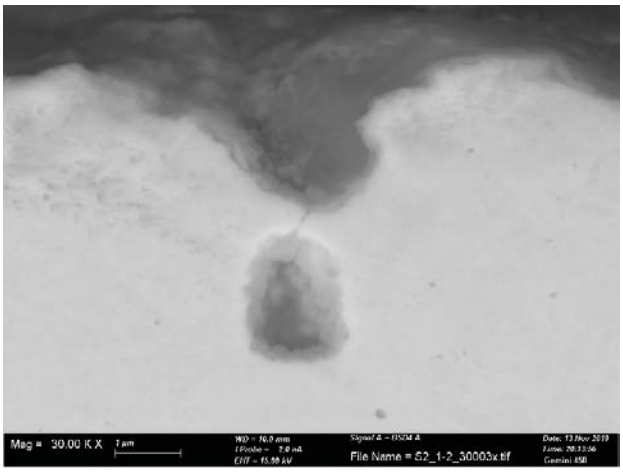

Figure F-69. *Cross-section of pipe S2 sample area 1.*

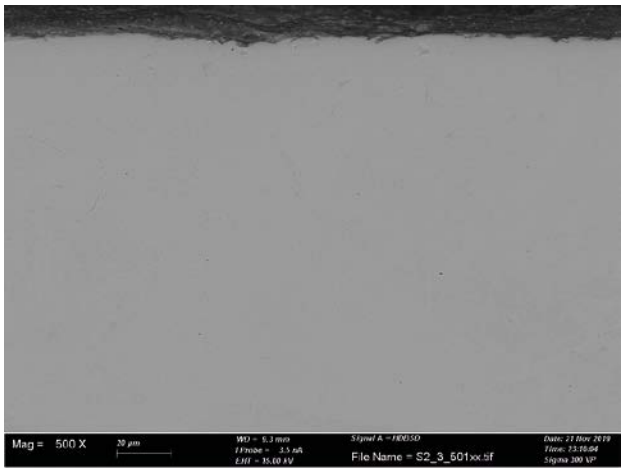

Figure F-70. *Cross-section of pipe S2 sample area 1.*

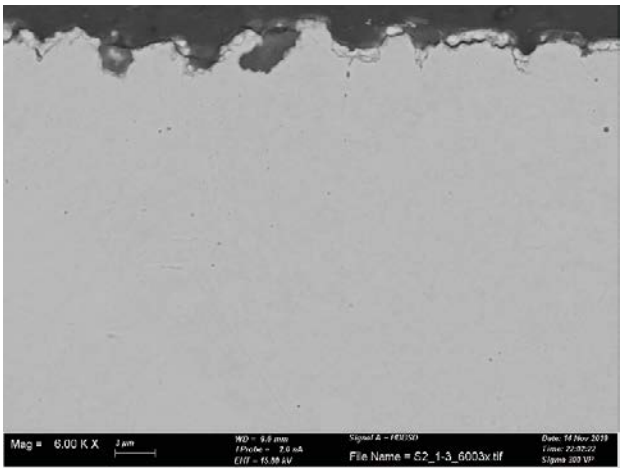

Figure F-71. *Cross-section of pipe S2 sample area 1.*

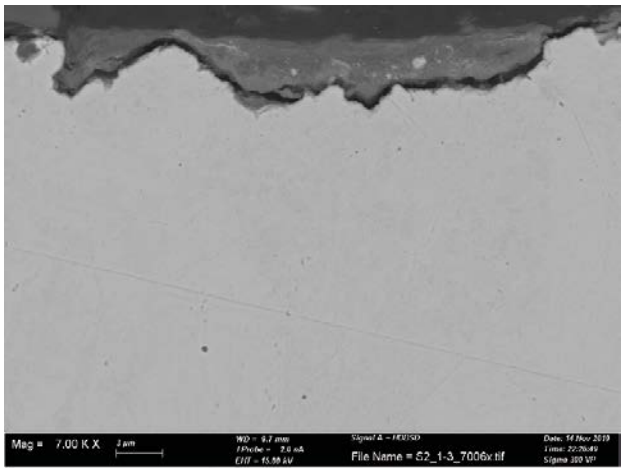

Figure F-72. *Cross-section of pipe S2 sample area 1.*

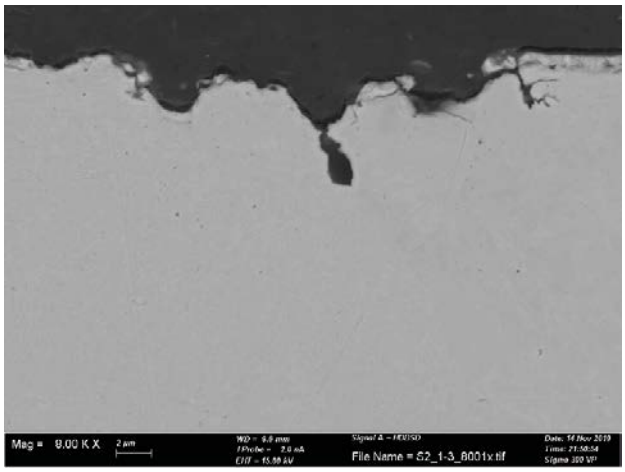

Figure F-73. *Cross-section of pipe S2 sample area 1.*

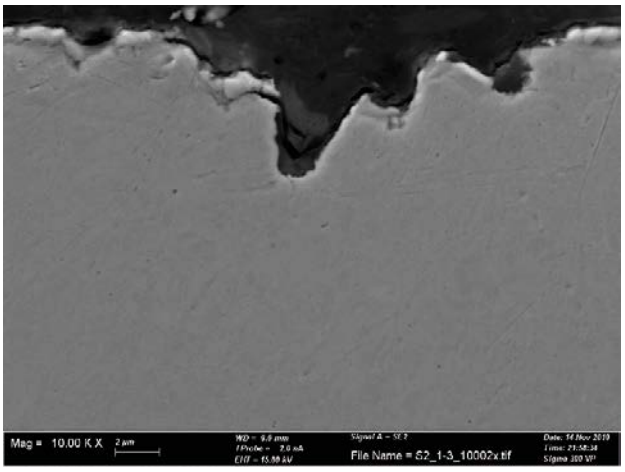

Figure F-74. *Cross-section of pipe S2 sample area 1.*

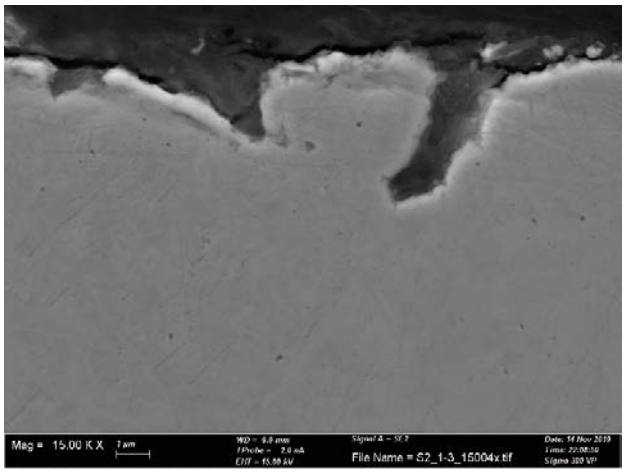

Figure F-75. *Cross-section of pipe S2 sample area 1.*

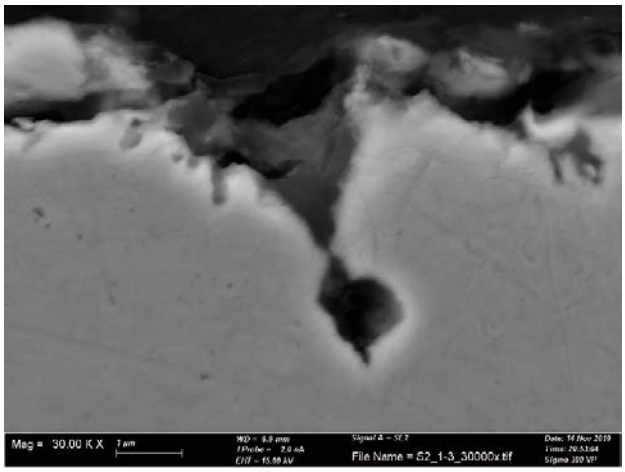

Figure F-76. *Cross-section of pipe S2 sample area 1.*

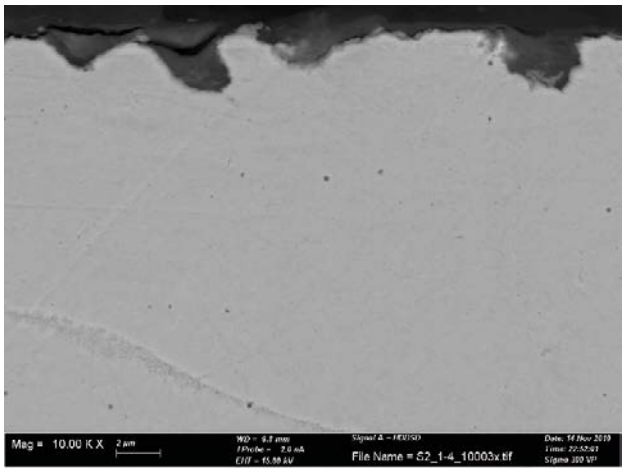

Figure F-77. *Cross-section of pipe S2 sample area 1.*

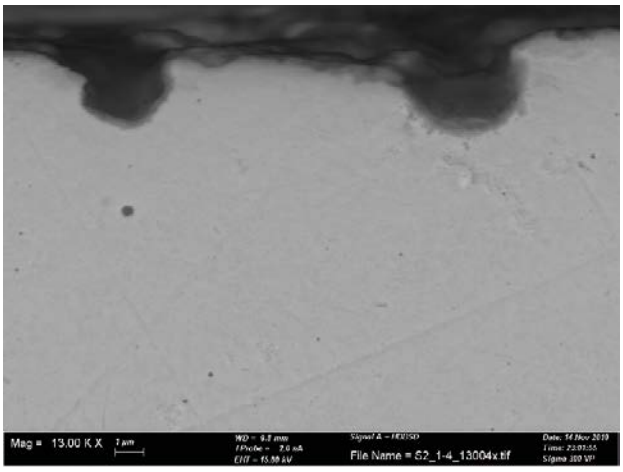

Figure F-78. *Cross-section of pipe S2 sample area 1.*

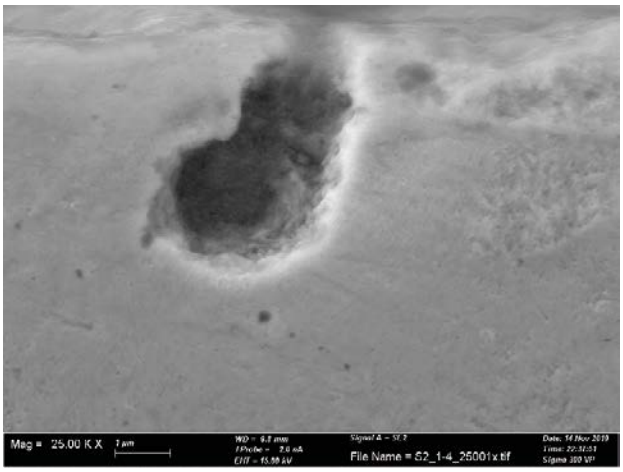

Figure F-79. *Cross-section of pipe S2 sample area 1.*

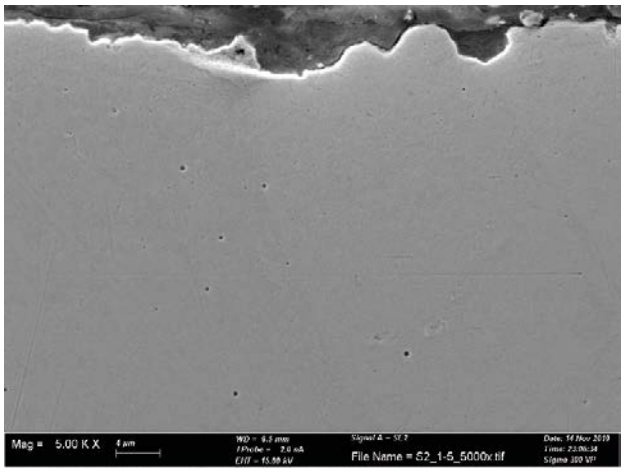

Figure F-80. *Cross-section of pipe S2 sample area 1.*

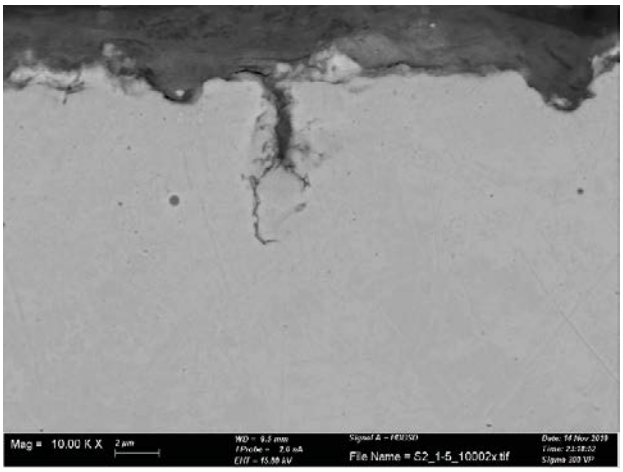

Figure F-81. *Cross-section of pipe S2 sample area 1.*

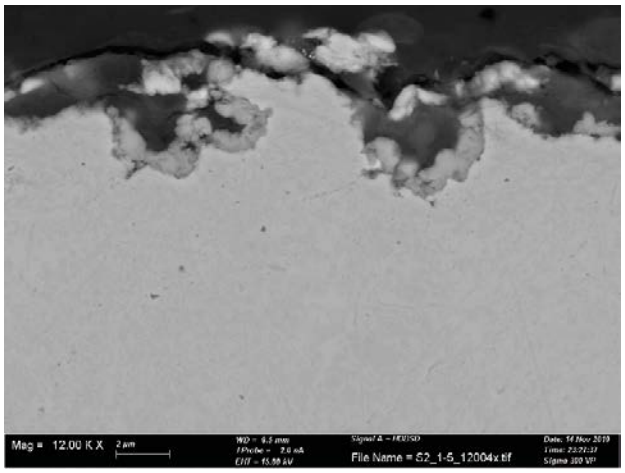

Figure F-82. *Cross-section of pipe S2 sample area 1.*

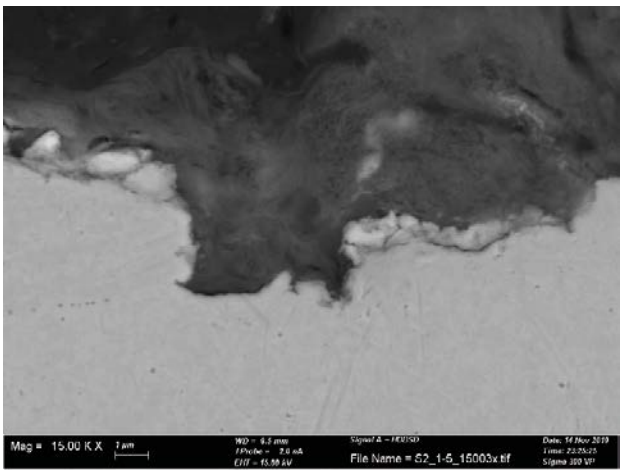

Figure F-83. *Cross-section of pipe S2 sample area 1.*

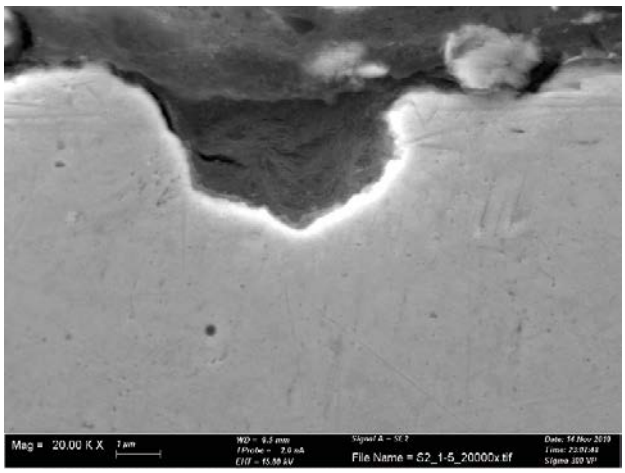

Figure F-84. *Cross-section of pipe S2 sample area 1.*

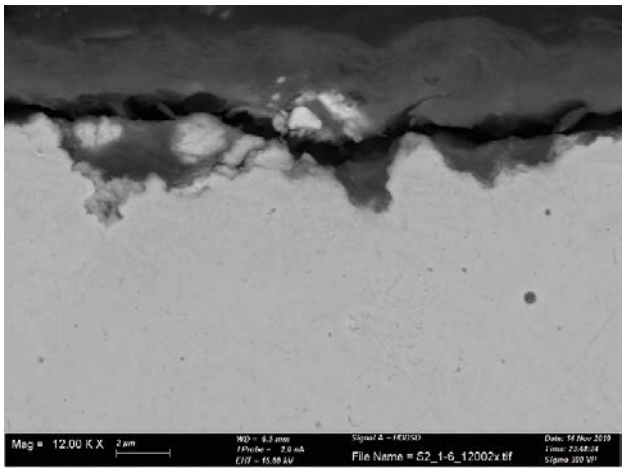

Figure F-85. *Cross-section of pipe S2 sample area 1.*

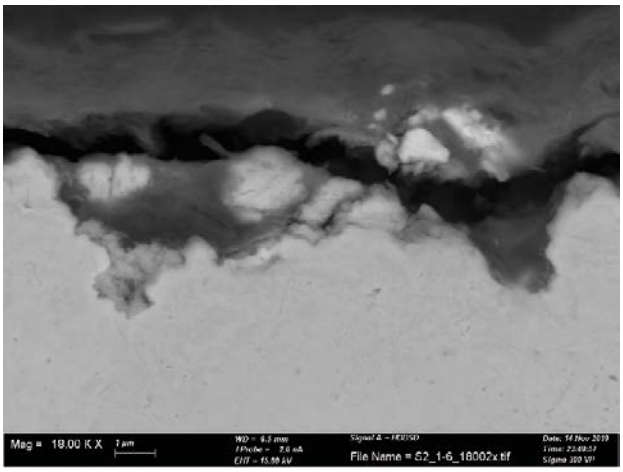

Figure F-86. *Cross-section of pipe S2 sample area 1.*

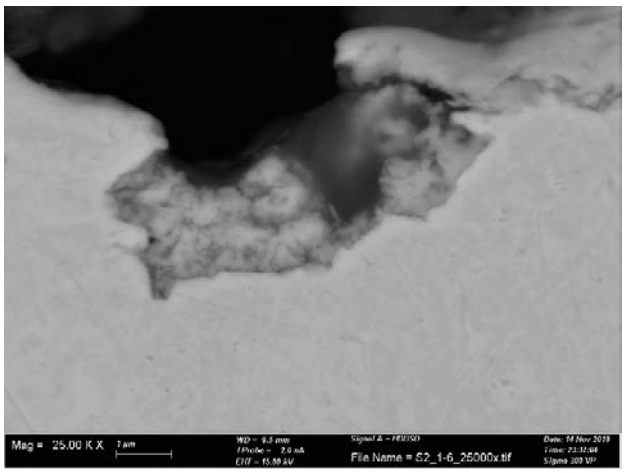

Figure F-87. *Cross-section of pipe S2 sample area 1.*

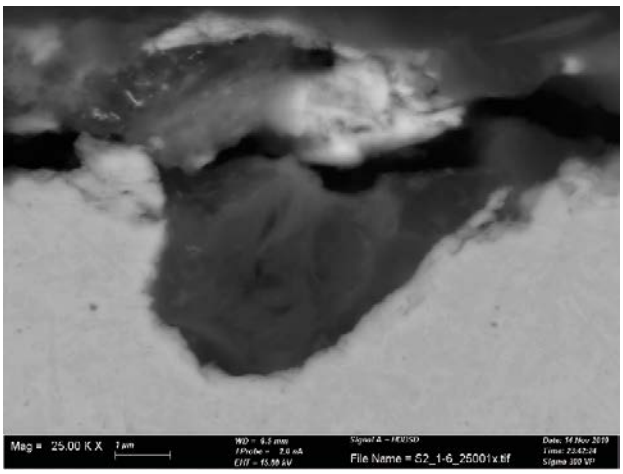

Figure F-88. *Cross-section of pipe S2 sample area 1.*

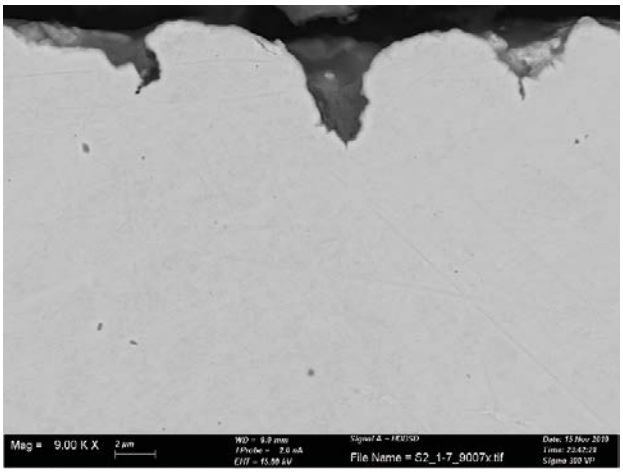

Figure F-89. *Cross-section of pipe S2 sample area 1.*

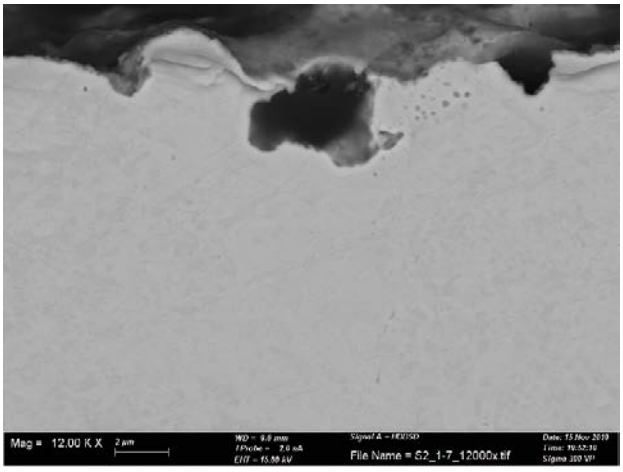

Figure F-90. *Cross-section of pipe S2 sample area 1.*

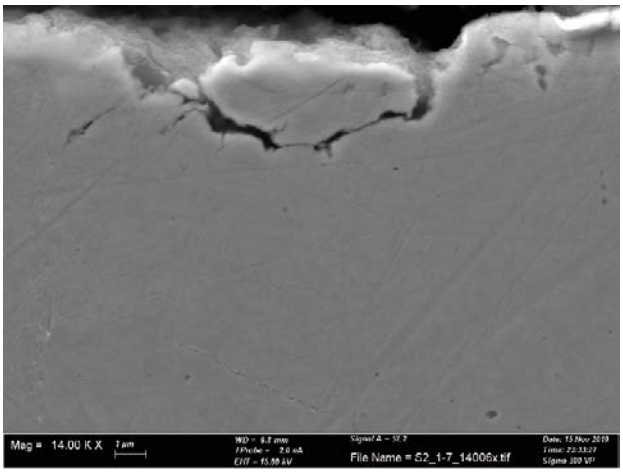

Figure F-91. *Cross-section of pipe S2 sample area 1.*

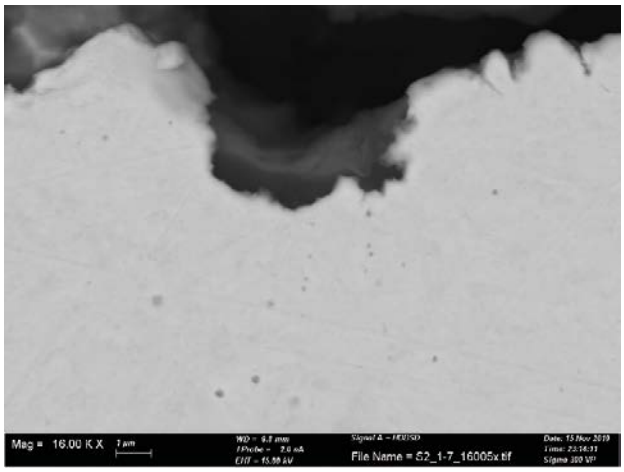

Figure F-92. *Cross-section of pipe S2 sample area 1.*

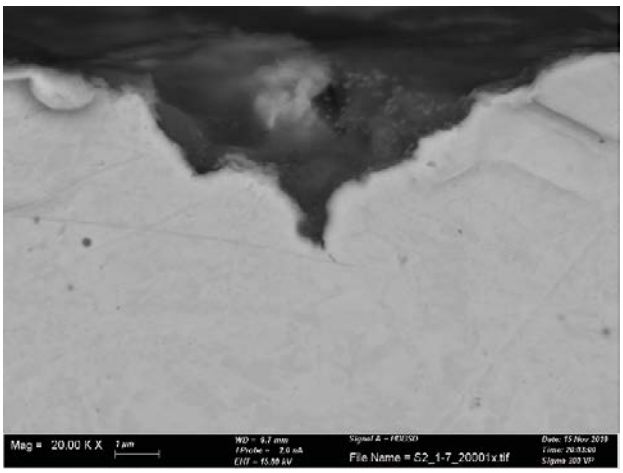

Figure F-93. *Cross-section of pipe S2 sample area 1.*

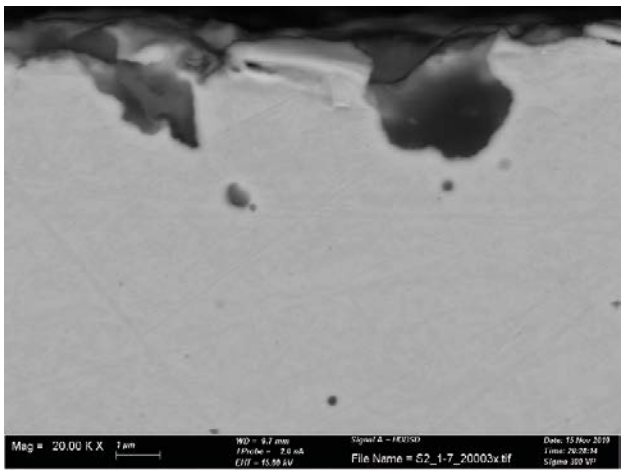

Figure F-94. *Cross-section of pipe S2 sample area 1.*

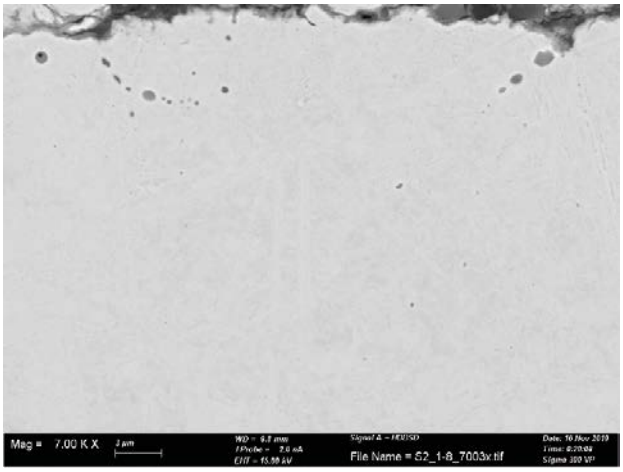

Figure F-95. *Cross-section of pipe S2 sample area 1.*

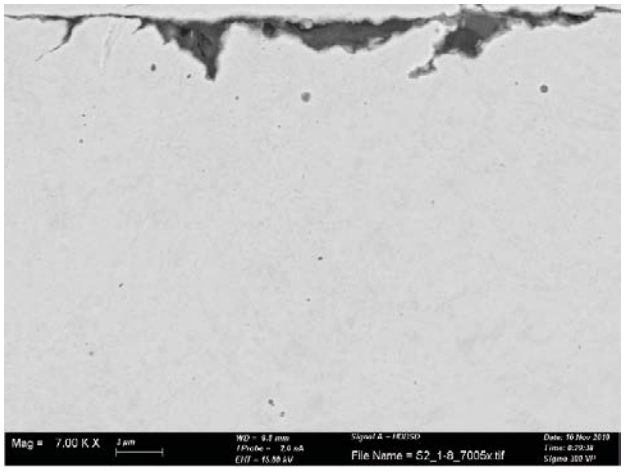

Figure F-96. *Cross-section of pipe S2 sample area 1.*

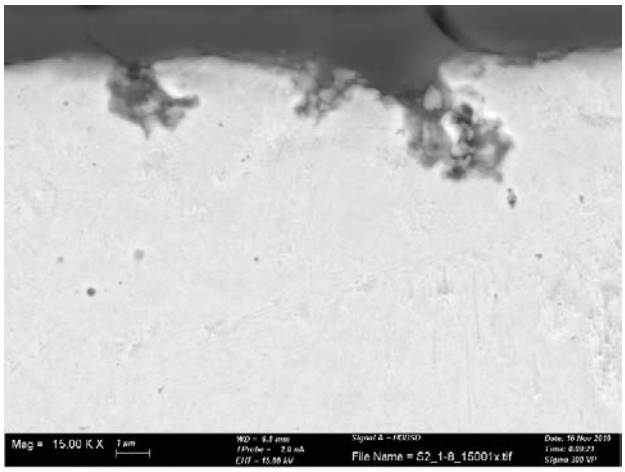

Figure F-97. *Cross-section of pipe S2 sample area 1.*

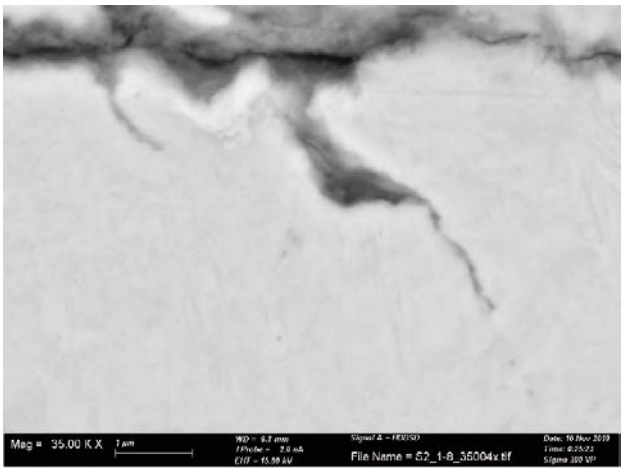

Figure F-98. *Cross-section of pipe S2 sample area 1.*

Inner surface pipe S2

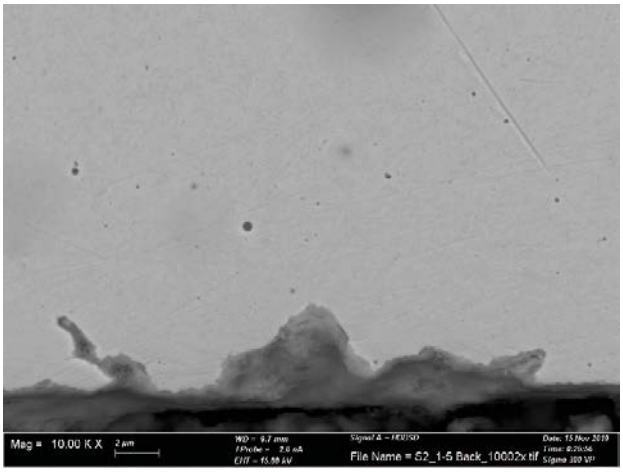

Figure F-99. *Cross-section of pipe S2 inner surface.*

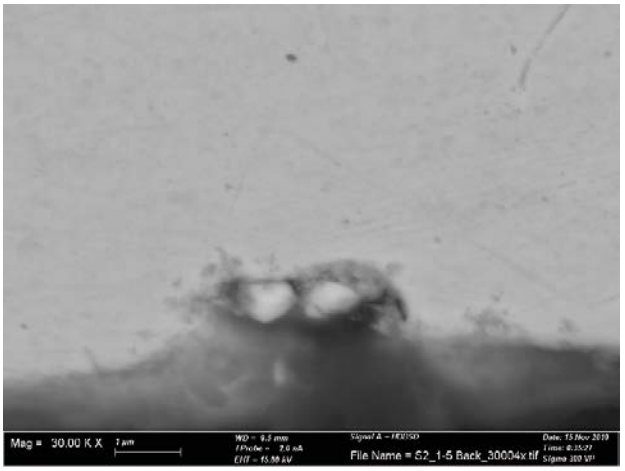

Figure F-100. *Cross-section of pipe S2 inner surface.*

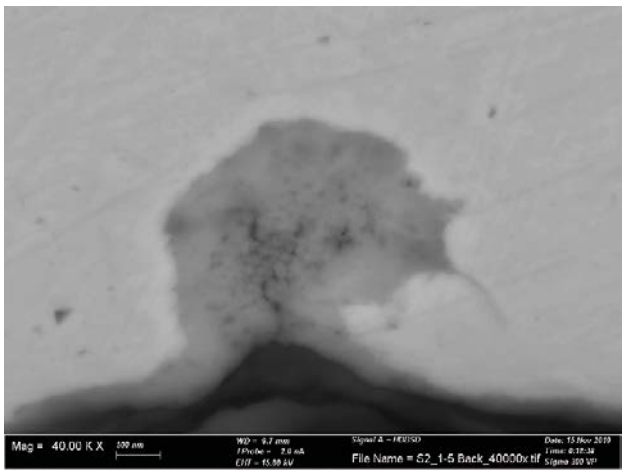

Figure F-101. *Cross-section of pipe S2 inner surface.*

Pipe S2 sample 2

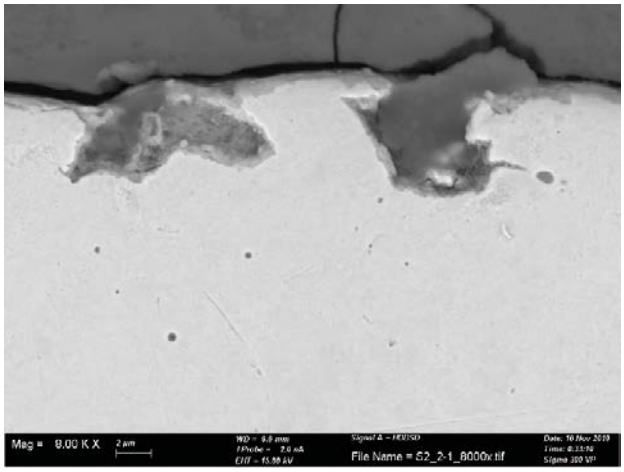

Figure F-102. *Cross-section of pipe S2 sample area 2.*

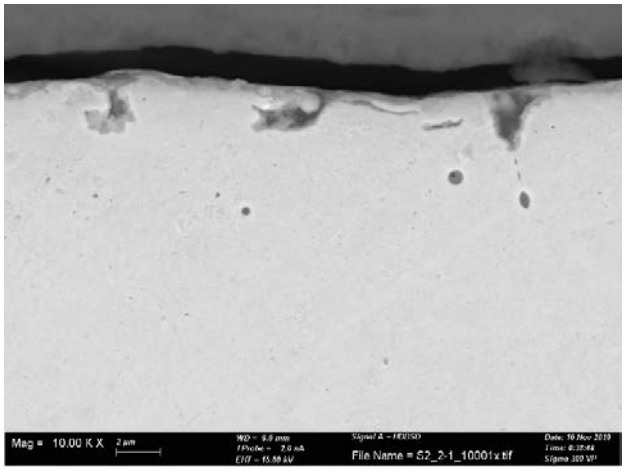

Figure F-103. *Cross-section of pipe S2 sample area 2.*

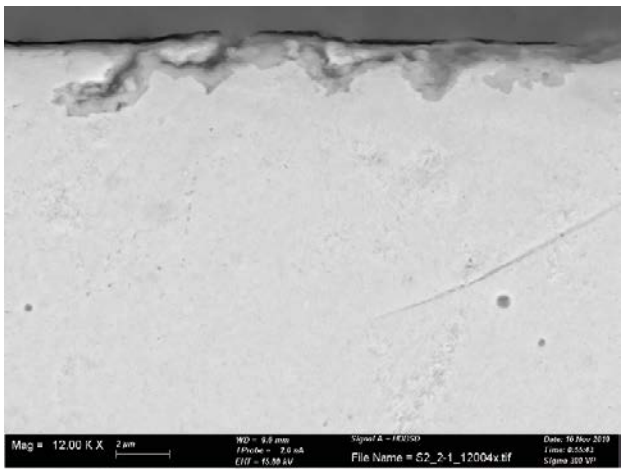

Figure F-104. *Cross-section of pipe S2 sample area 2.*

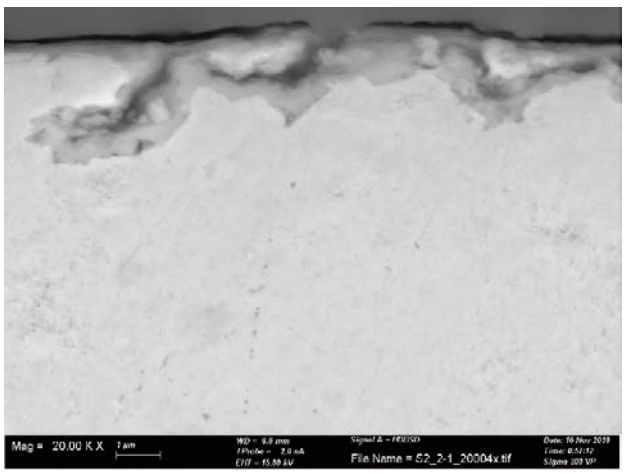

Figure F-105. *Cross-section of pipe S2 sample area 2.*

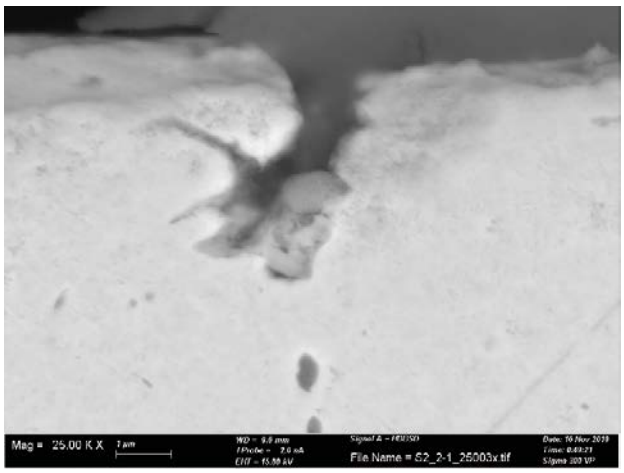

Figure F-106. *Cross-section of pipe S2 sample area 2.*

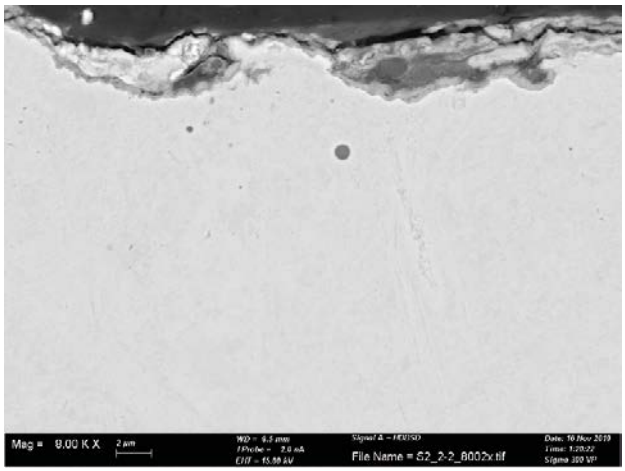

Figure F-107. *Cross-section of pipe S2 sample area 2.*

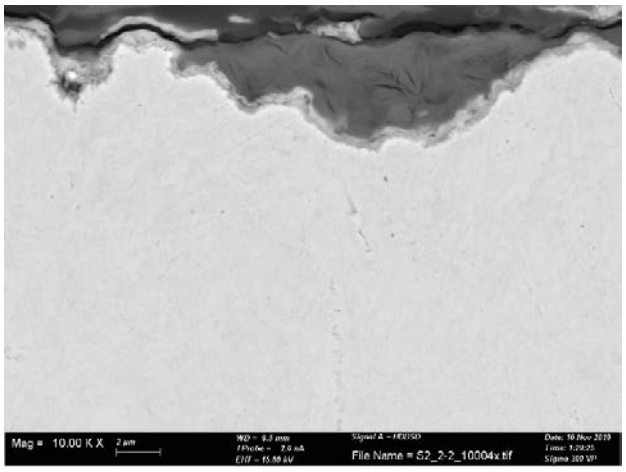

Figure F-108. *Cross-section of pipe S2 sample area 2.*

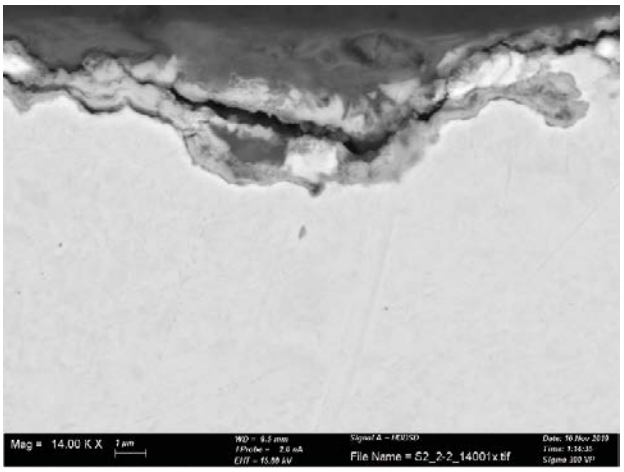

Figure F-109. *Cross-section of pipe S2 sample area 2.*

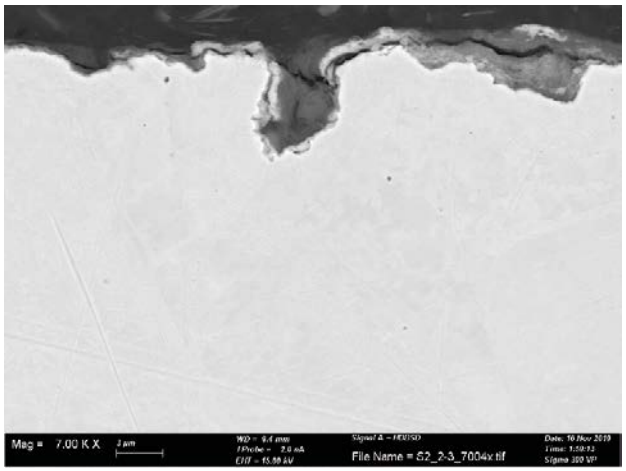

Figure F-110. *Cross-section of pipe S2 sample area 2.*

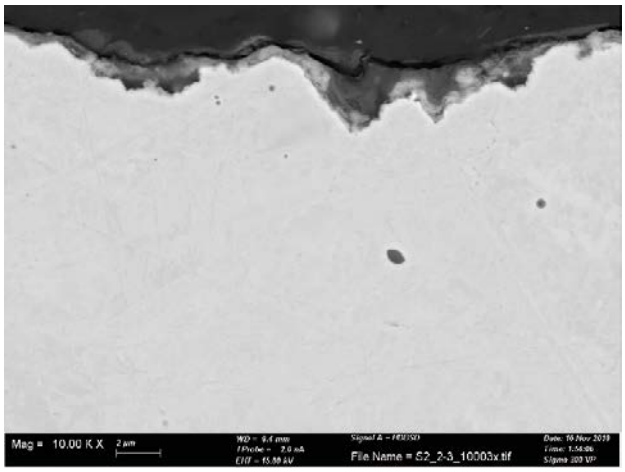

Figure F-111. *Cross-section of pipe S2 sample area 2.*

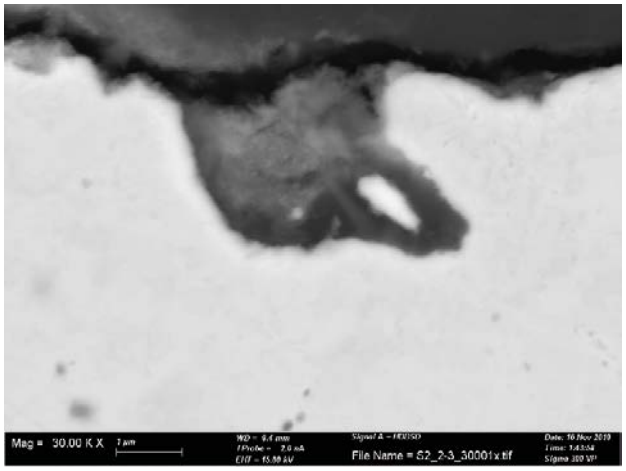

Figure F-112. *Cross-section of pipe S2 sample area 2.*

Appendix G

EDS analyses of pipe cross sections

Pipe samples A3 and S2 were sectioned for preparation of cross section samples for EDS analysis. Areas perceived are representative were chosen for analysis. For pipe A3 three areas were selected, and for pipe S2 two areas were selected. The selected areas were then cross sectioned using a bandsaw without cutting fluid. In total 10 cross section samples of each pipe were prepared, and EDS analysis was performed on all external surfaces, plus two internal surfaces for each pipe (24 analyses in total). The cross sections were cast into epoxy resin before grinding with P4000 SiC paper and polishing in a 3 µm diamond paste. The samples were washed in DI water and dried with ethanol prior to analysis. There results of the EDS analysis are shown below, and in summary it was found that the layers on the external surfaces of the pipe consisted mainly of Cu, O, Cl, S, Si and Al.

Figure G-1. *Sample area 1 from pipe A3.*

Figure G-2. *Sample area 2 from pipe A3.*

Figure G-3. *Sample area 3 from pipe A3.*

Figure G-4. *Sample area 1 from pipe S2.*

Figure G-5. *Sample area 2 from pipe S2.*

Figure G-6. Cross section samples from pipe A3 sample area 1.

Pipe A3 surface analysis – darker and lighter areas

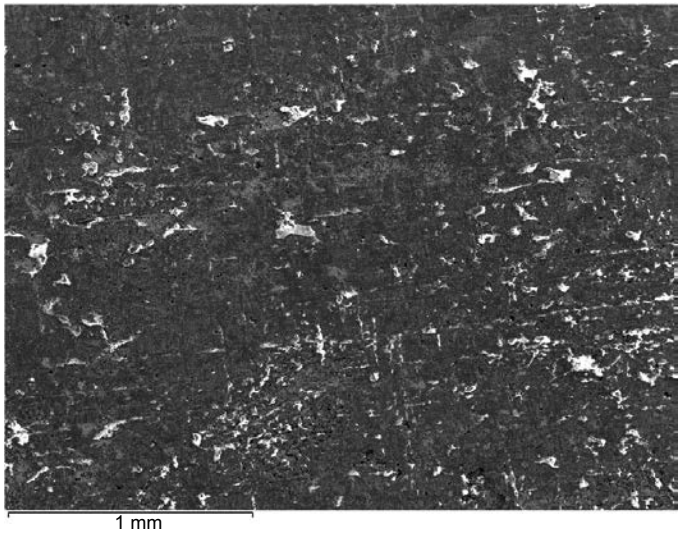

Element (At%)	1
O	29.14
Na	0.63
Mg	1.31
Al	7.13
Si	16.94
S	4.19
Cl	0.09
K	0.11
Ca	1.21
Fe	1.06
Cu	38.20
Total	100.00

Figure G-7. EDS analysis of pipe A3 surface with darker appearance.

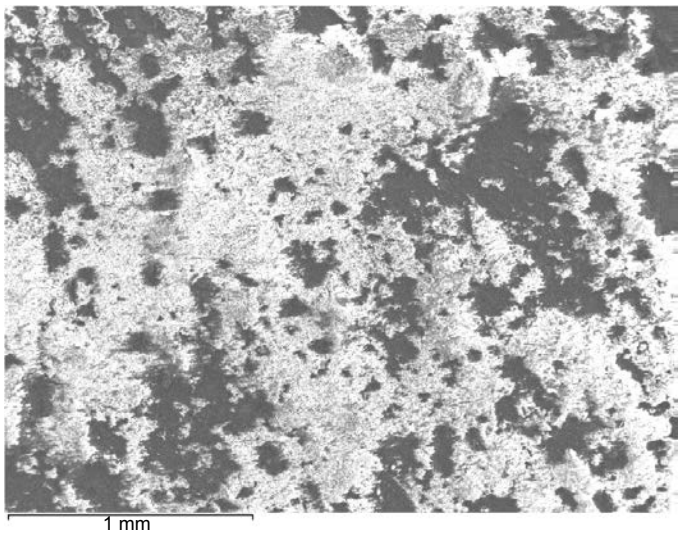

Element (At%)	1
O	46.16
Na	0.39
Mg	0.59
Al	3.99
Si	10.49
S	12.33
Cl	0.13
K	0.19
Ca	21.11
Fe	1.09
Cu	3.53
Total	100.00

Figure G-8. EDS analysis of pipe A3 surface with lighter (white) appearance.

Pipe A3 sample 1

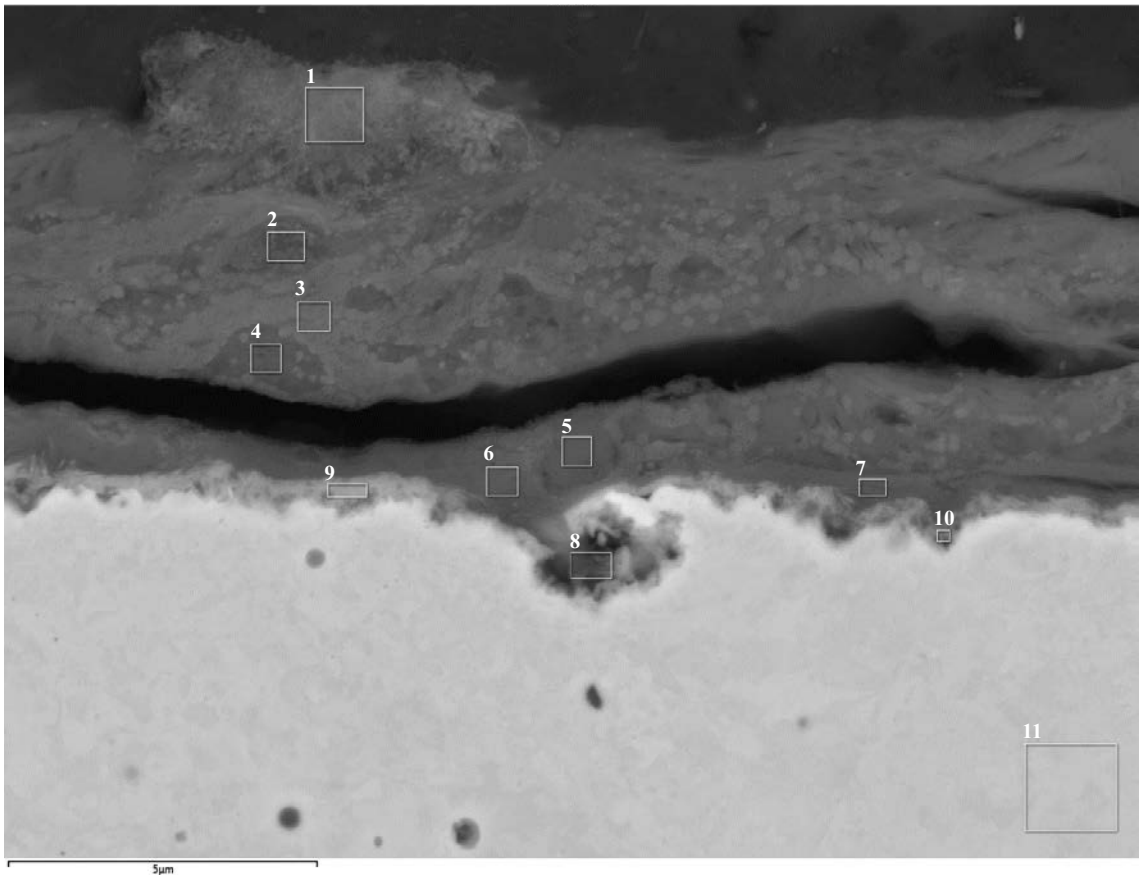

Element (At%)	1	2	3	4	5	6	7	8	9	10	11
O	53.97	58.03	61.29	64.70	64.46	59.06	57.22	42.11	47.79	36.33	1.35
Mg	0.89	1.16	1.28	1.09	0.79	1.36	1.64	1.11	1.25	1.28	
Al	4.25	6.37	6.81	4.99	4.32	8.02	9.09	6.19	6.07	5.89	0.75
Si	22.22	23.89	18.10	13.30	24.45	20.39	20.79	13.45	12.44	12.32	
S	0.25	0.51	0.31	0.35	0.19	0.32	0.16	1.60	2.41	0.93	
Cl	0.19	0.04	0.06	0.06	0.06	0.16	0.12	0.74	0.46	0.42	
K		0.04	0.08	0.09	0.07	0.07				0.09	
Ca	3.60	2.15	4.48	10.78	0.78	0.77	0.50	0.32	1.07	0.86	
Ti							0.50				
Fe	0.43	0.57	0.67	0.43	0.28	0.75	0.77	0.62	0.34	0.37	
Cu	14.20	7.24	6.91	4.22	4.61	9.09	9.21	33.87	28.18	41.50	97.90
Total	100.00	100.00	100.00	100.00	100.00	100.00	100.00	100.00	100.00	100.00	100.00

Figure G-9. *EDS analysis of pipe A3 sample area 1.*

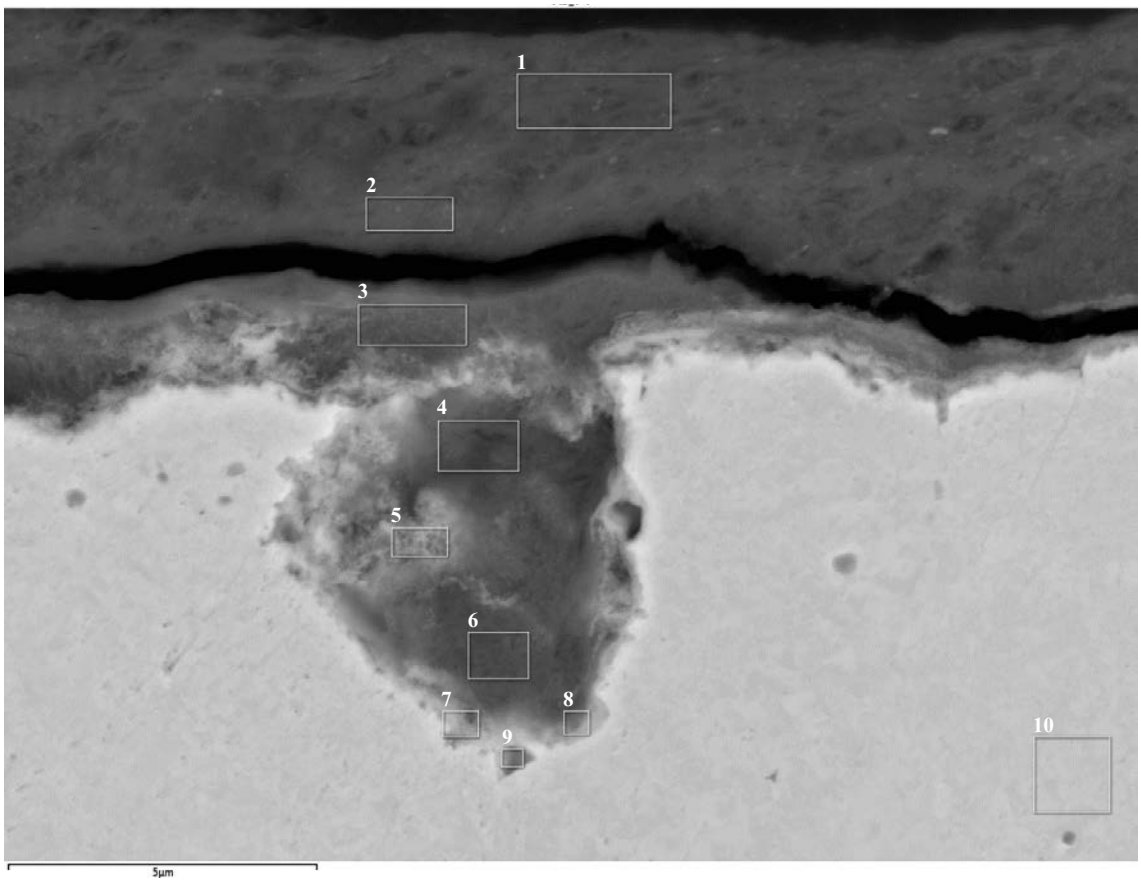

Element (At%)	1	2	3	4	5	6	7	8	9	10
O	56.80	62.43	65.47	57.25	45.87	59.63	24.87	30.27	9.99	2.30
Mg	1.63	1.51	1.19	1.27	0.85	1.04	0.63	0.64		
Al	8.81	7.67	2.69	3.38	1.65	1.06	1.46	1.04	0.57	0.80
Si	23.26	19.46	6.45	8.77	3.98	2.69	2.24	1.68	0.52	0.46
P			0.07			0.10				
S	0.40	0.47	2.09	1.34	3.71	0.97	2.23	0.57	0.16	
Cl			0.06	0.22	0.68	0.15	0.47	1.04	0.17	
K	0.10	0.08								
Ca	3.66	2.58	12.18	11.18	8.00	15.31	1.92	1.45	0.19	
Mn			0.13	0.14		0.26				
Fe	0.87	0.68	0.18	0.40						
Cu	4.46	5.12	9.50	16.06	35.26	18.79	66.18	63.31	88.39	96.44
Total	100.00	100.00	100.00	100.00	100.00	100.00	100.00	100.00	100.00	100.00

Figure G-10. *EDS analysis of pipe A3 sample area 1.*

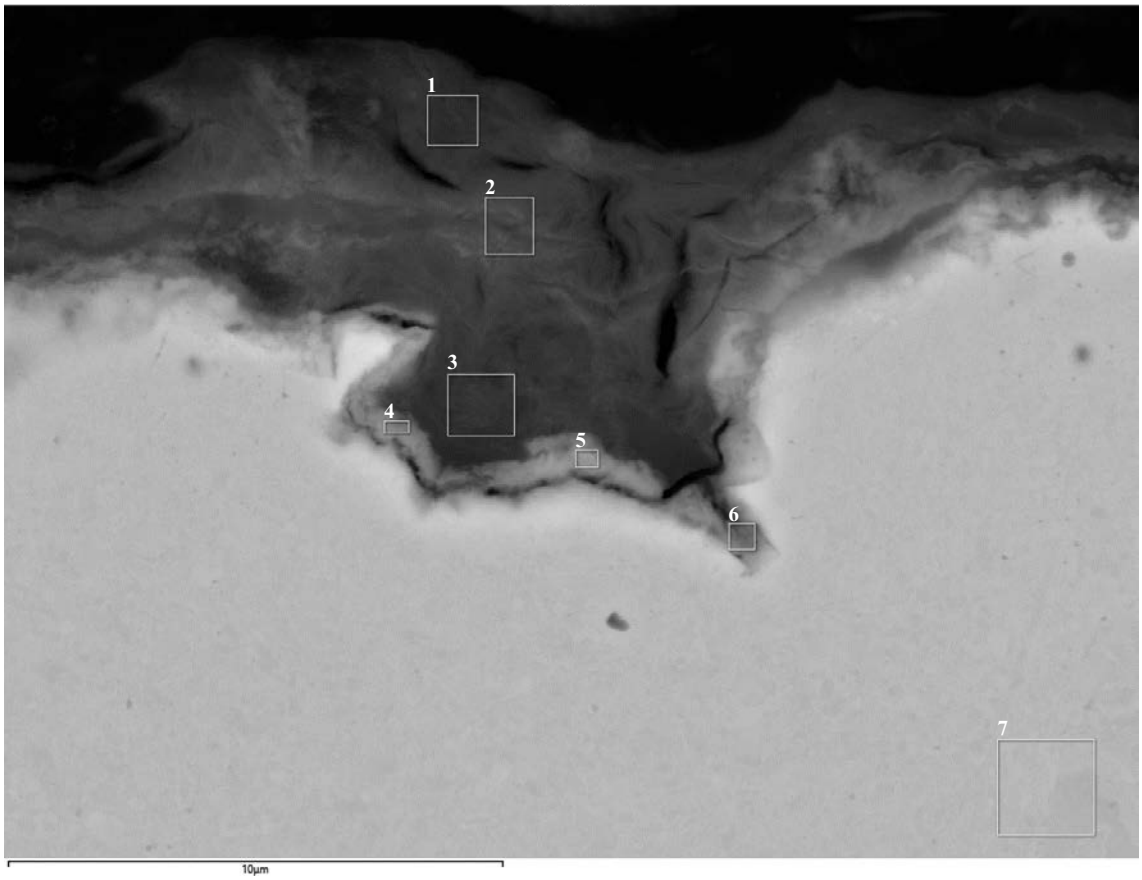

Element (At%)	1	2	3	4	5	6	7
O	55.82	57.00	54.52	40.62	39.80	27.93	1.22
Na	2.37	4.46	1.53	1.94			
Mg	1.69	1.16	1.12	1.27	1.27	0.88	
Al	8.72	6.52	7.17	6.50	6.26	4.07	1.35
Si	22.22	20.34	24.63	15.14	16.05	8.66	
S	1.09	2.54	1.20	1.31	6.58	1.17	
Cl	0.05	0.06	0.09	0.64	0.34	0.59	
K	0.09	0.07	0.16	0.06	0.27	0.08	
Ca	0.93	0.37	0.10	0.14	0.12	0.06	
Ti	0.04	0.03	0.04				
Fe	0.79	0.55	0.72	0.42	0.33	0.22	
Cu	6.18	6.88	8.72	31.94	29.00	56.34	97.43
Total	100.00	100.00	100.00	100.00	100.00	100.00	100.00

Figure G-11. *EDS analysis of pipe A3 sample area 1.*

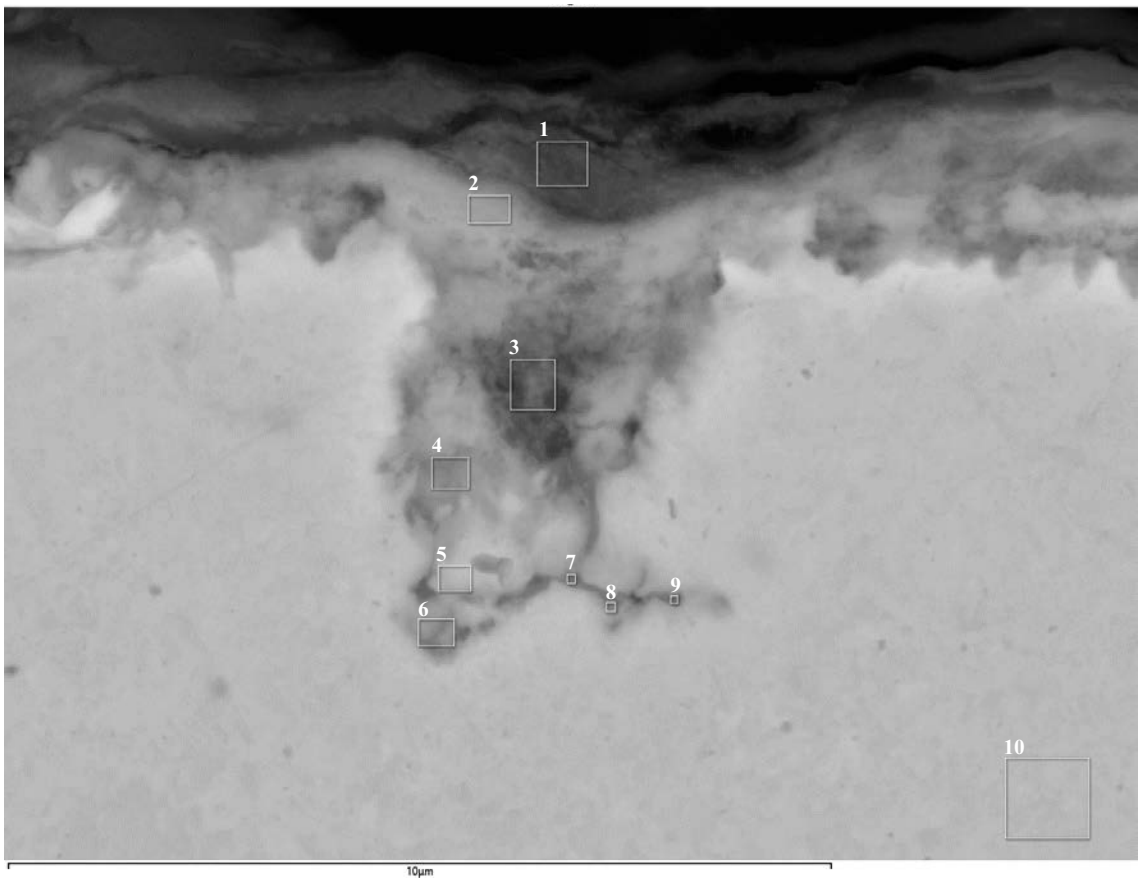

Element (At%)	1	2	3	4	5	6	7	8	9	10
O	48.27	36.00	38.47	20.36	7.41	8.25	17.09	13.50	11.47	1.65
Na	8.47	6.12	2.30							
Mg	1.30	1.09	0.86							
Al	6.75	5.44	3.23	1.36	1.38	1.36	1.52	1.45	1.73	1.17
Si	16.91	12.12	10.21	2.07	1.17	1.44	2.17	2.10	2.74	
S	4.11	8.23	9.21	13.71	3.31	2.51	6.17	4.28	3.08	
Cl	0.16	0.24	0.20	0.40	0.32	0.41	0.41	0.39	0.38	
K	0.09	0.08								
Ca	0.73	0.90	4.61	1.06	0.70	0.82	1.73	1.48	1.44	
Fe	0.48	0.28	0.39	0.09	0.09	0.12	0.17	0.15	0.16	
Cu	12.73	29.50	30.51	60.95	85.62	85.09	70.74	76.64	79.00	97.19
Total	100.00	100.00	100.00	100.00	100.00	100.00	100.00	100.00	100.00	100.00

Figure G-12. *EDS analysis of pipe A3 sample area 1.*

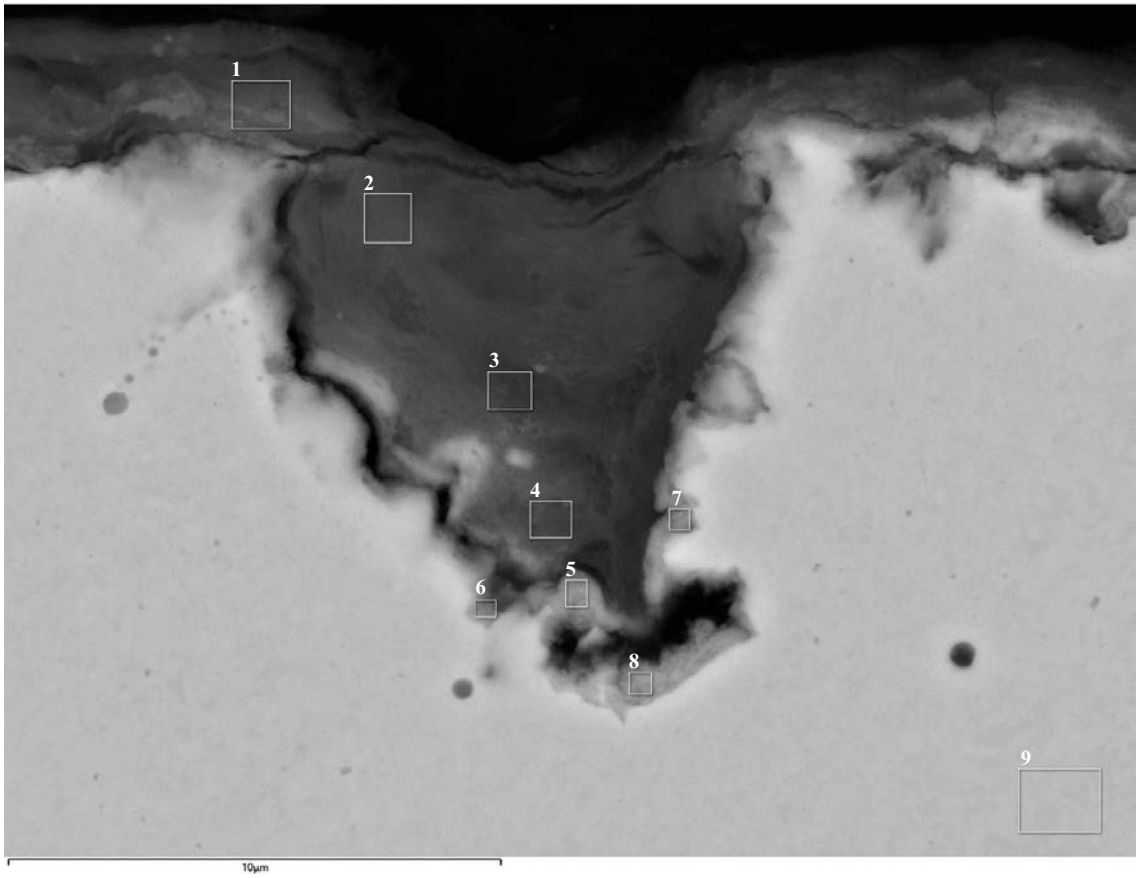

Element (At%)	1	2	3	4	5	6	7	8	9
O	51.49	56.25	53.48	51.08	42.07	25.73	34.88	32.11	1.06
Na	5.71	3.57	1.27	1.71					
Mg	1.52	1.43	1.55	1.33	1.47	0.75	1.37	0.63	
Al	6.04	8.09	8.69	6.23	7.22	3.80	6.72	2.80	1.22
Si	15.13	20.72	21.17	15.04	14.48	7.11	13.79	3.44	
S	4.41	1.79	2.00	3.97	2.10	2.59	1.05	0.52	
Cl	0.08	0.04	0.06	0.12	0.80	1.15	0.80	1.11	
K	0.07	0.09	0.10	0.08	0.05				
Ca	3.03	0.93	2.72	5.37	0.83	1.19	0.39	0.17	
Fe	0.46	0.71	0.83	0.54	0.41	0.26	0.32	0.09	
Cu	12.05	6.38	8.14	14.53	30.57	57.41	40.68	59.13	97.72
Total	100.00	100.00	100.00	100.00	100.00	100.00	100.00	100.00	100.00

Figure G-13. *EDS analysis of pipe A3 sample area 1.*

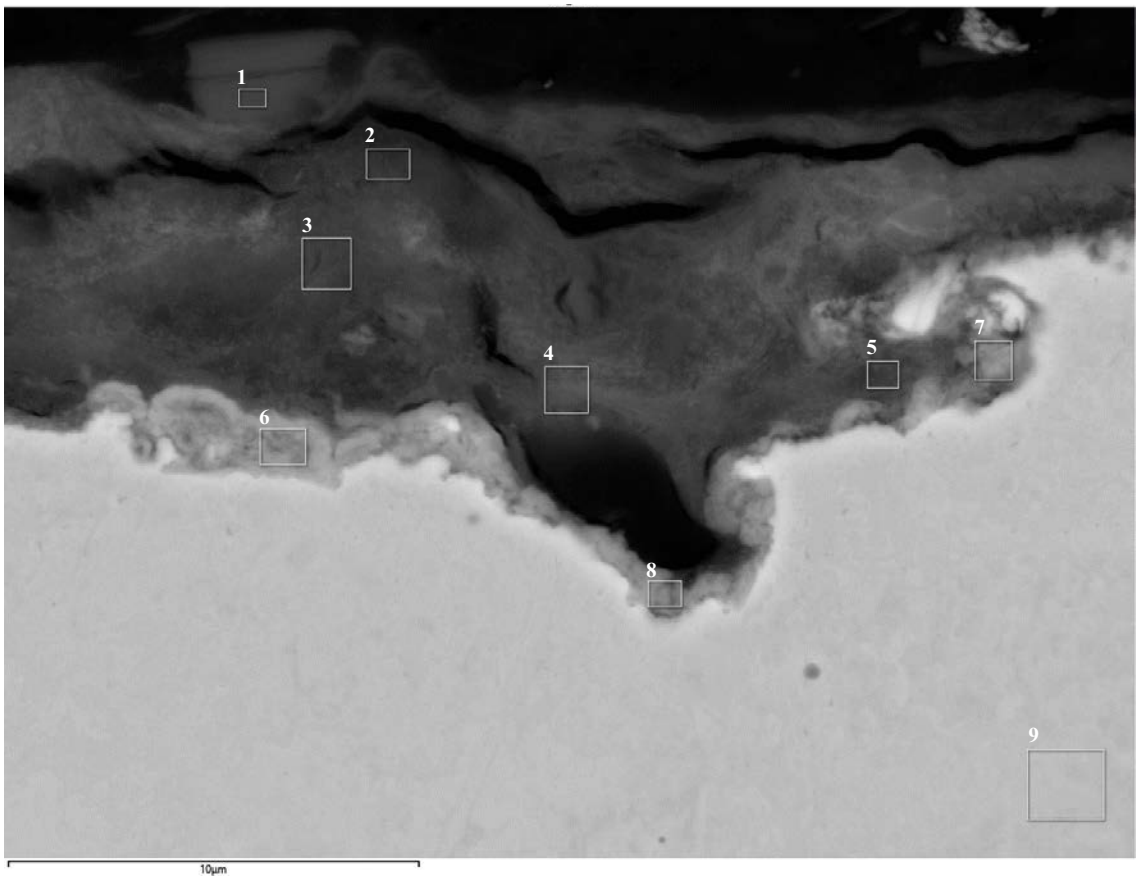

Element (At%)	1	2	3	4	5	6	7	8	9
O	55.77	56.70	51.88	51.10	43.80	39.13	22.82	36.43	1.46
Na	0.38	0.30	0.38						
Mg	2.96	3.49	2.53	1.71	1.49	1.02	0.64	1.05	
Al	14.09	8.10	9.14	8.29	6.87	4.23	3.12	3.35	1.22
Si	19.69	23.84	24.48	23.36	18.28	7.83	7.06	7.12	
S	0.63	0.60	2.15	3.36	5.91	1.49	9.00	1.42	
Cl	0.05	0.04	0.08	0.07	0.27	1.48	0.91	1.96	
K	3.51	0.12	0.12	0.17	0.11				
Ca	0.26	1.38	0.37	0.38	0.45	0.06	0.32	0.43	
Ti							0.12		
Fe	0.23	0.79	0.86	0.68	0.61	0.18	0.26	0.16	
Cu	2.43	4.63	8.00	10.89	22.21	44.58	55.76	48.07	97.33
Total	100.00	100.00	100.00	100.00	100.00	100.00	100.00	100.00	100.00

Figure G-14. *EDS analysis of pipe A3 sample area 1.*

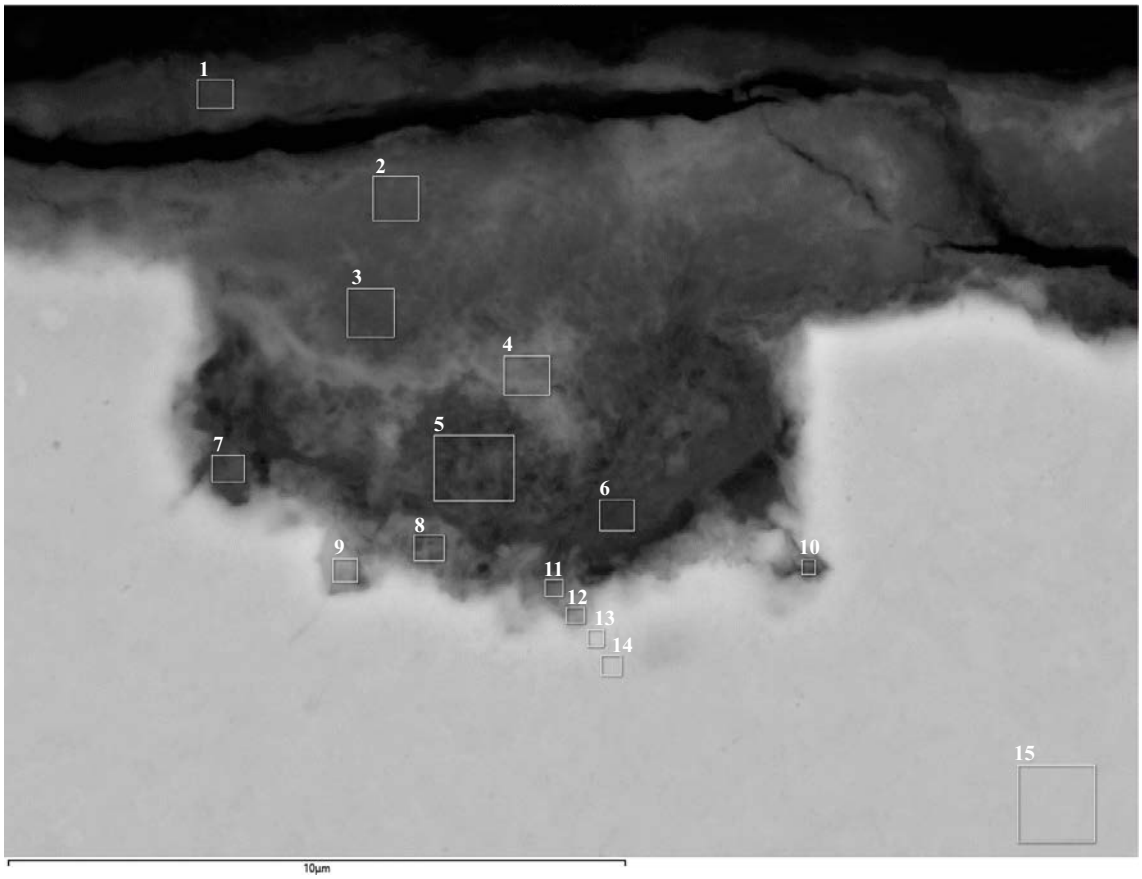

Element (At%)	1	2	3	4	5	6	7	8	9	10	11	12	13	14	15
O	60.97	66.32	65.12	61.29	62.49	54.52	46.88	54.97	34.48	16.87	44.33	26.39	14.80	6.20	4.97
Na	0.93	1.33	1.41	0.77	0.98	0.68	1.79								
Mg	1.34	1.09	0.78	0.63	0.55	0.92	0.55	0.71	0.57		1.02	0.65	0.56		
Al	5.11	4.41	2.79	1.95	1.68	5.65	2.19	2.32	2.40	1.76	4.75	3.74	2.52	1.43	1.26
Si	14.32	12.82	8.88	5.52	4.85	11.58	8.54	5.64	5.07	2.95	9.15	6.21	3.71	1.64	1.43
P		0.04	0.07	0.09	0.17	0.34	1.47	0.29	0.18	0.53	0.35	0.25	0.18		
S	1.62	1.38	2.01	1.15	1.43	2.44	3.50	1.27	0.92	2.67	1.65	1.80	0.80	0.14	
Cl	0.16	0.11	0.14	0.33	0.26	0.17	0.33	0.54	1.26	0.54	0.62	0.47	0.16		
Ca	6.78	6.38	12.33	16.48	17.59	7.89	8.11	12.32	4.21	1.63	5.28	3.55	1.27	0.24	
Mn	0.06	0.06	0.10	0.19	0.19	0.07		0.13							
Fe	0.40	0.32	0.24	0.11	0.12	0.39	0.15	0.14	0.14	0.13	0.22	0.13			
Cu	8.32	5.73	6.11	11.49	9.69	15.34	26.49	21.67	50.77	72.92	32.62	56.81	76.01	90.35	92.34
Total	100.00	100.00	100.00	100.00	100.00	100.00	100.00	100.00	100.00	100.00	100.00	100.00	100.00	100.00	100.00

Figure G-15. *EDS analysis of pipe A3 sample area 1.*

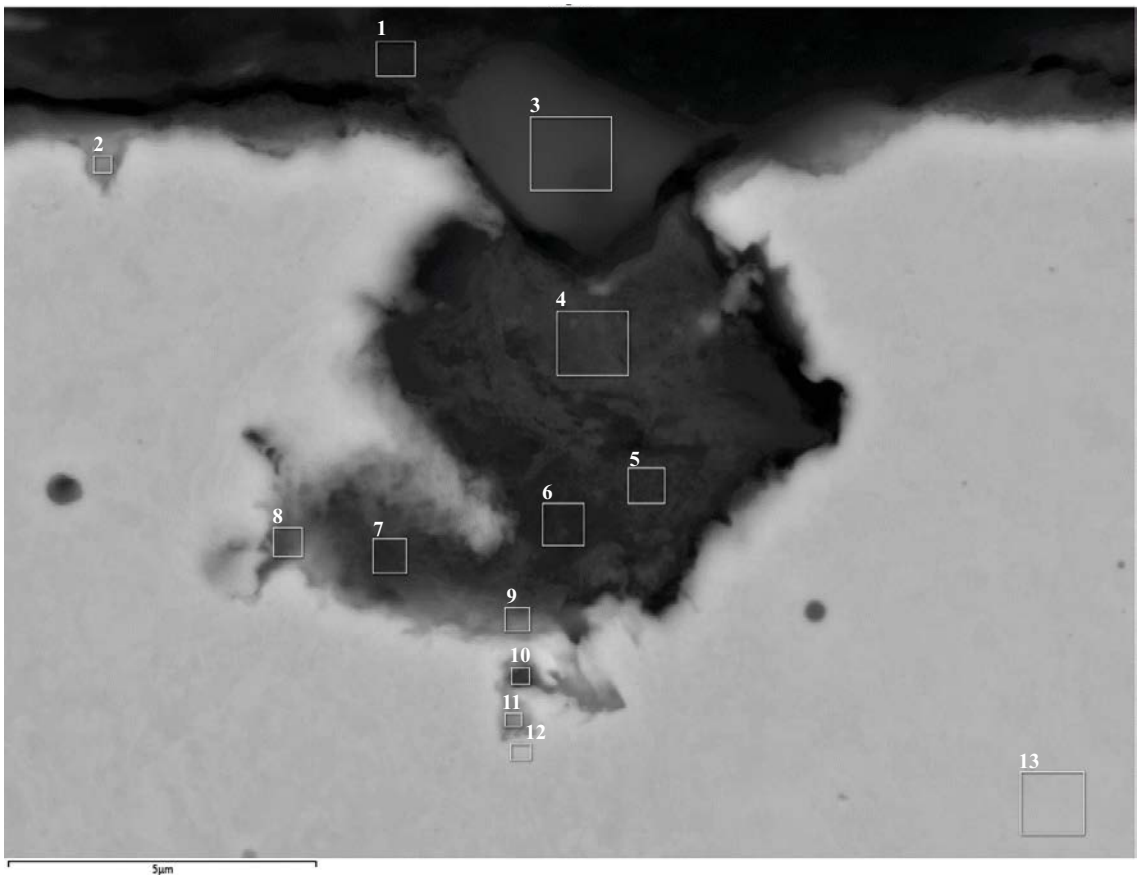

Element (At%)	1	2	3	4	5	6	7	8	9	10	11	12	13
O	57.41	21.31	59.28	53.14	49.08	43.46	37.87	21.62	39.55	12.40	10.03	2.99	1.46
Na	0.58		3.93	0.29									
Mg	1.70	0.95	0.55	1.53	1.94	1.77	1.49	0.65	1.29				
Al	6.65	3.20	9.23	7.02	9.18	8.41	6.17	2.55	5.45	1.84	2.13	1.96	1.12
Si	15.16	4.37	17.47	17.88	20.27	18.77	12.07	4.64	10.18	2.89	2.15	0.53	0.20
P						0.28	0.27	0.26	0.74				
S	1.06	7.39	0.83	0.67	0.41	0.39	0.47	0.88	0.57				
Cl	0.09	0.10	0.04	0.07	0.07	0.12	0.17	0.17	0.29				
K	0.17		0.20										
Ca	8.32	0.46	3.38	5.67	1.88	1.48	2.17	1.41	1.31	0.16			
Fe	0.34	0.10	0.26	0.39	0.59	0.40	0.28	0.10	0.21				
Cu	8.51	62.11	4.81	13.33	16.60	24.92	39.03	67.71	40.40	82.72	85.68	94.53	97.22
Total	100.00	100.00	100.00	100.00	100.00	100.00	100.00	100.00	100.00	100.00	100.00	100.00	100.00

Figure G-16. *EDS analysis of pipe A3 sample area 1.*

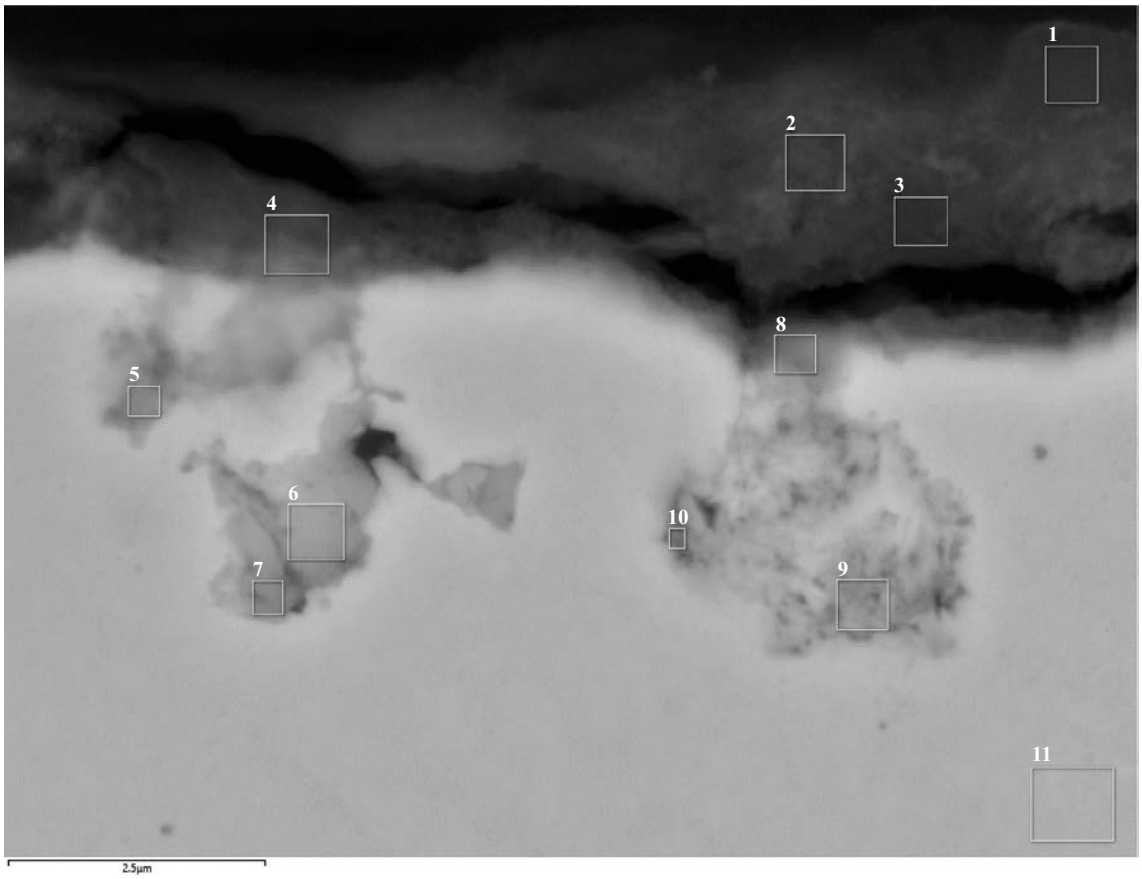

Element (At%)	1	2	3	4	5	6	7	8	9	10	11
O	59.81	56.58	56.23	54.25	27.51	25.38	22.59	39.69	15.98	16.32	5.28
Mg	1.00	1.41	1.18	1.45				1.18			
Al	5.34	6.21	5.37	6.53	1.01	1.02	1.15	4.27	1.01	1.08	1.16
Si	24.63	17.77	19.30	17.82	6.21	3.33	3.26	10.45	2.47	2.29	1.35
S	0.77	1.41	1.31	0.55	0.10			1.72	0.57	0.57	
Cl	0.08	0.13	0.11	0.25	0.42	0.88	0.71	0.36	0.66	0.81	
K	0.07										
Ca	3.16	6.23	4.28	1.49	0.16	0.15	0.09	2.39	0.52	0.42	0.13
Fe	0.50	0.52	0.40	0.38	0.09	0.08	0.07	0.18	0.08		
Cu	4.63	9.75	11.82	17.28	64.51	69.17	72.14	39.75	78.71	78.50	92.08
Total	100.00	100.00	100.00	100.00	100.00	100.00	100.00	100.00	100.00	100.00	100.00

Figure G-17. *EDS analysis of pipe A3 sample area 1.*

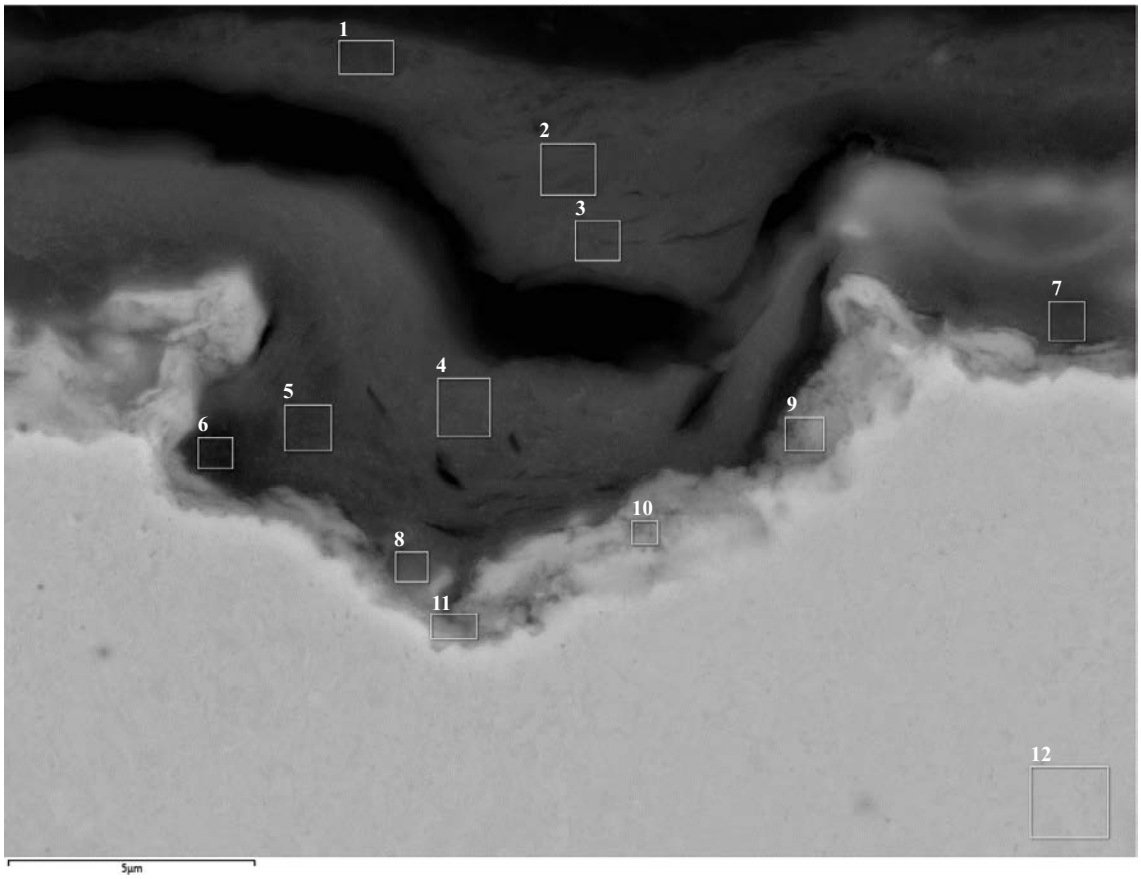

Element (At%)	1	2	3	4	5	6	7	8	9	10	11	12
O	53.12	56.08	56.58	60.34	54.55	39.03	47.71	45.75	35.36	37.25	33.40	1.39
Na	0.20		0.21									
Mg	1.30	1.67	1.62	1.69	1.75	1.46	1.63	1.68	1.32	1.22	0.82	
Al	7.81	9.81	9.75	8.97	9.00	6.76	6.49	6.62	6.48	5.32	3.51	1.15
Si	29.57	25.14	24.25	22.15	22.75	16.02	12.92	15.17	12.61	9.48	5.45	0.25
P								0.12				
S	0.60	0.39	0.66	0.85	1.08	1.34	4.18	3.47	6.92	6.01	2.35	
Cl			0.04		0.12	0.32	0.19	0.42	0.45	0.67	0.80	
K	0.08		0.04		0.05		0.09		0.09			
Ca	1.54	1.07	0.15	0.09	0.57	0.59	1.90	1.39	1.33	1.46	0.73	
Fe	0.69	0.87	0.82	0.70	0.81	0.47	0.27	0.35	0.35	0.18	0.13	
Cu	5.10	4.96	5.87	5.22	9.33	34.01	24.62	25.02	35.09	38.40	52.81	97.21
Total	100.00	100.00	100.00	100.00	100.00	100.00	100.00	100.00	100.00	100.00	100.00	100.00

Figure G-18. *EDS analysis of pipe A3 sample area 1.*

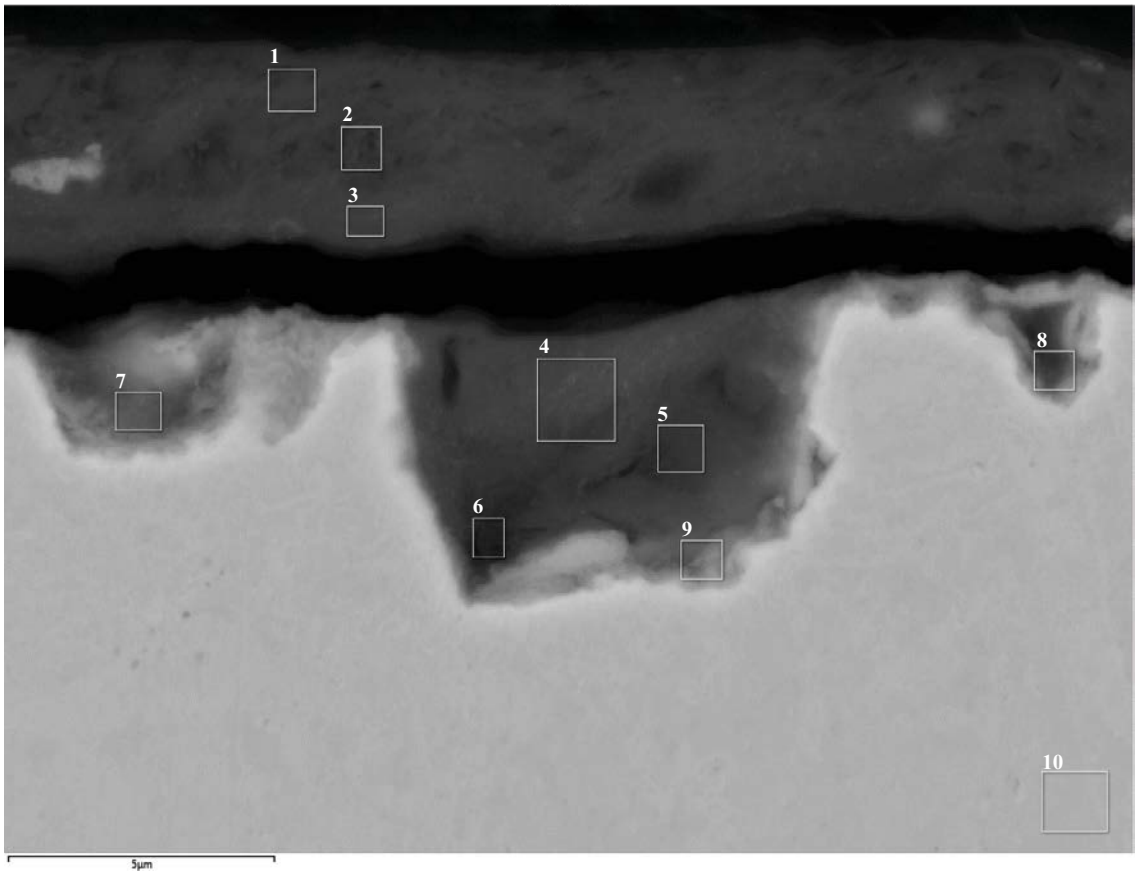

Element (At%)	1	2	3	4	5	6	7	8	9	10
O	53.22	52.87	53.36	58.55	49.21	39.96	37.35	37.49	38.39	1.50
Na	0.22	0.26	0.33							
Mg	1.76	1.52	1.69	1.61	1.74	1.52	1.14	1.25	1.25	
Al	8.90	8.32	8.01	8.27	9.06	6.65	2.35	5.64	5.00	1.28
Si	25.74	24.42	21.34	20.63	19.04	15.29	6.19	10.92	8.31	
S	0.80	1.29	1.94	1.20	1.23	1.17	2.81	1.39	2.17	
Cl			0.13	0.11	0.11	0.30	0.38	0.55	0.08	
K	0.08	0.09					0.08			
Ca	3.04	3.77	1.16	0.46	0.39	0.46	3.07	0.18	1.21	
Fe	0.74	0.73	0.54	0.57	0.52	0.32	0.11	0.26	0.14	
Cu	5.49	6.72	11.51	8.60	18.70	34.34	46.52	42.32	43.45	97.21
Total	100.00	100.00	100.00	100.00	100.00	100.00	100.00	100.00	100.00	100.00

Figure G-19. *EDS analysis of pipe A3 sample area 1.*

Pipe A3 – inner surface

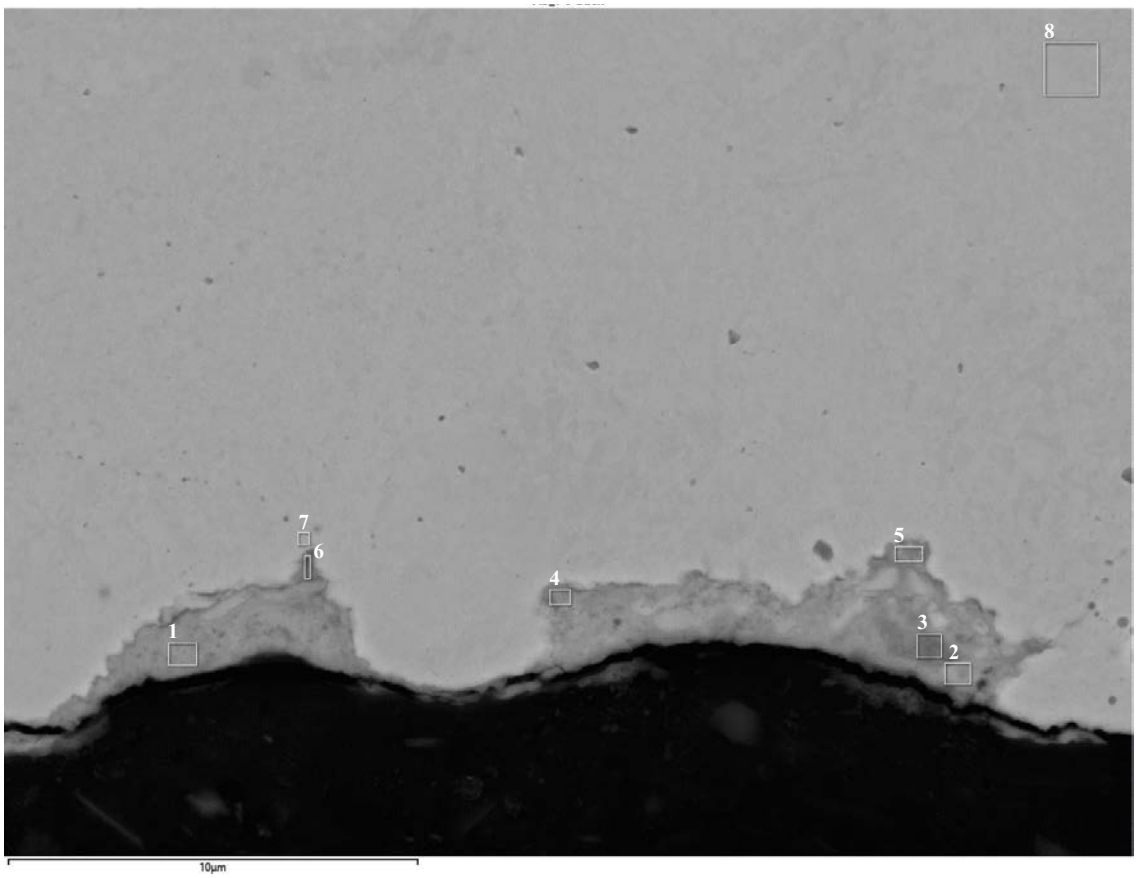

Element (At%)	1	2	3	4	5	6	7	8
O	30.27	35.48	35.26	24.06	23.99	22.65	2.61	0.92
Mg		0.28						
Al	0.62	0.66	0.33	0.57	0.42	0.60	0.64	0.56
Si	0.65	1.62	6.75			0.26	0.24	
S	0.61	1.38	1.25	0.13				
Cl	2.90	2.69	2.83	3.62	2.51	3.28	0.36	
K	0.40	1.11	0.86					
Ca		0.26	0.23					
Cu	64.55	56.54	52.49	71.63	73.08	73.21	96.15	98.52
Total	100.00	100.00	100.00	100.00	100.00	100.00	100.00	100.00

Figure G-20. *EDS analysis of pipe A3 inner surface.*

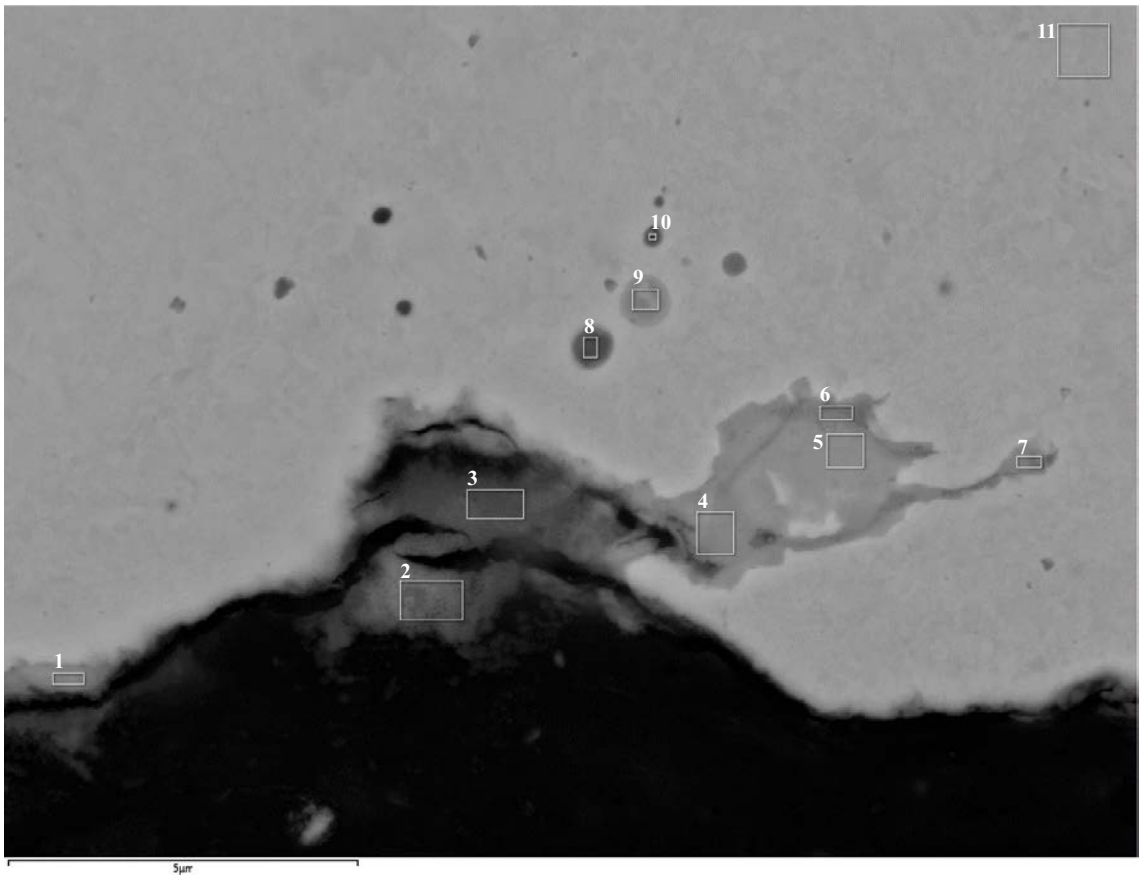

Element (At%)	1	2	3	4	5	6	7	8	9	10	11
O	29.44	49.65	48.38	27.07	26.13	23.74	18.65	28.28	11.92	7.06	0.73
Na		1.86	1.18								
Mg	0.22	0.73	1.63								
Al	0.86	2.49	5.66	0.43	0.41	0.38	0.60	0.37	0.41	0.26	0.55
Si	2.10	14.40	16.27						0.21	2.44	
P			0.09					7.83	2.12	0.32	
S		0.58	0.50					0.51		0.24	
Cl	2.70	1.14	0.77	2.77	2.87	2.61	0.22				
K	0.24	0.40	0.43		0.10						
Ca	0.12	0.19									
Fe		0.19	0.65								
Cu	64.31	28.36	24.44	69.73	70.49	73.28	80.54	63.00	85.35	89.68	98.72
Total	100.00	100.00	100.00	100.00	100.00	100.00	100.00	100.00	100.00	100.00	100.00

Figure G-21. *EDS analysis of pipe A3 inner surface.*

Pipe A3 sample 2

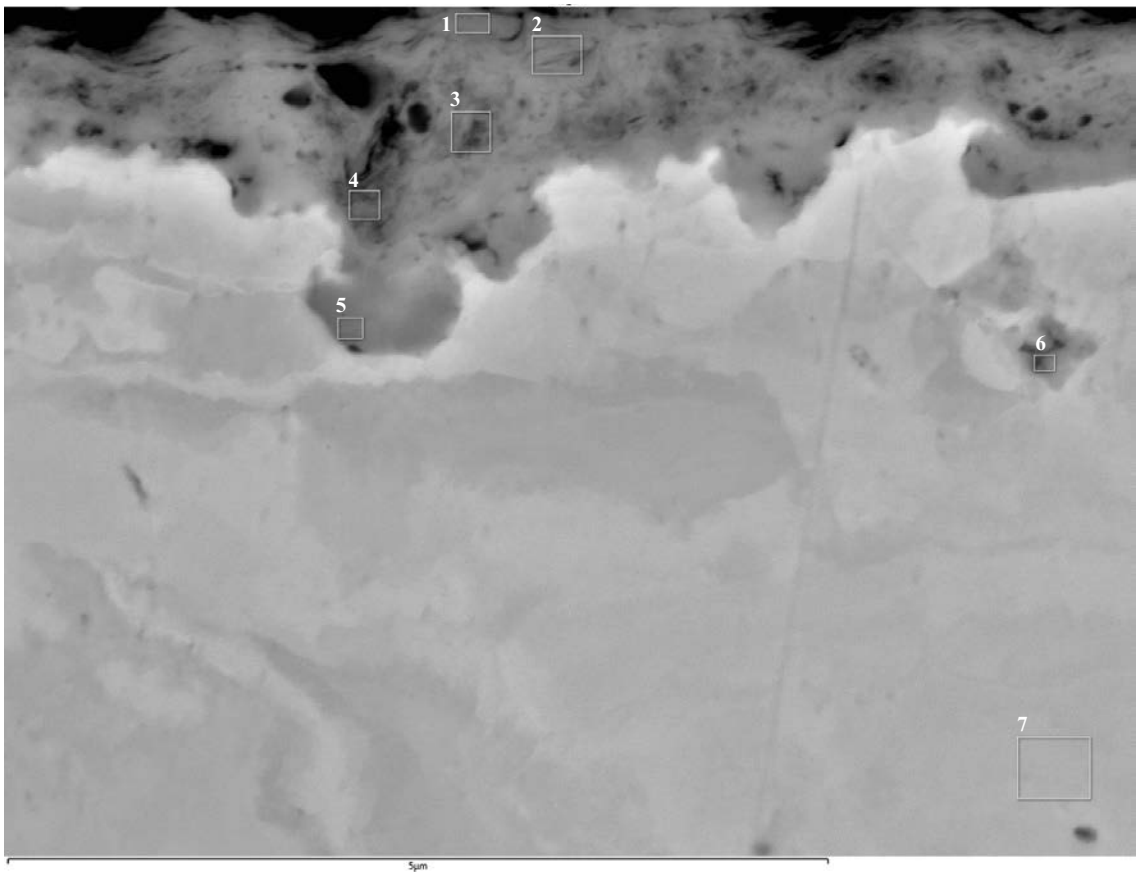

Element (At%)	1	2	3	4	5	6	7
O	8.09	9.36	8.30	7.67	5.82	3.31	0.22
Mg	0.13	0.12	0.18	0.11			
Al	0.66	0.86	1.04	0.81	0.18	0.24	0.30
Si	1.56	1.75	2.44	2.01	0.07	0.42	
S	1.59	3.01	7.52	6.15	0.20	0.07	
Cl	1.34	1.28	0.23	0.10			
Fe	0.23						
Cu	86.40	83.63	80.30	83.15	93.72	95.95	99.48
Total	100.00	100.00	100.00	100.00	100.00	100.00	100.00

Figure G-22. *EDS analysis of pipe A3 sample area 2.*

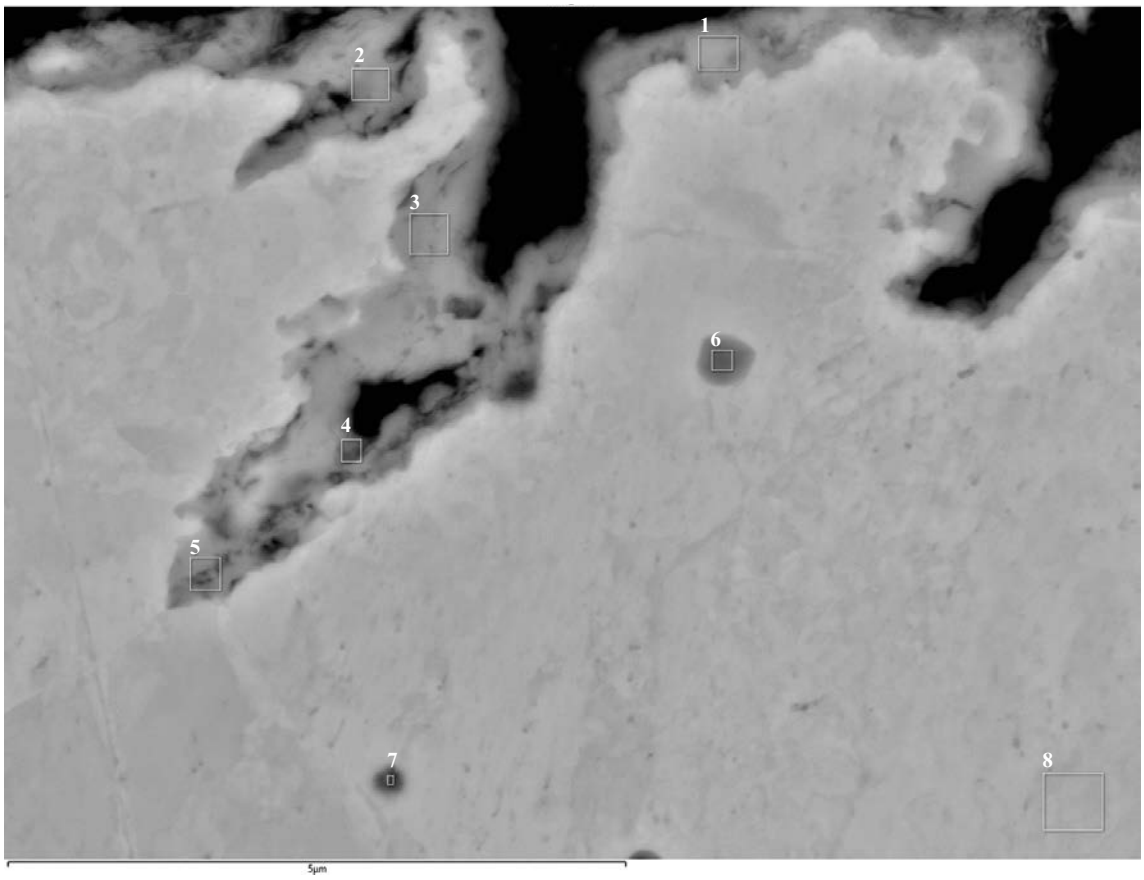

Element (At%)	1	2	3	4	5	6	7	8
O	8.95	8.12	7.99	7.88	5.53	7.20	6.06	0.22
Al	0.40	0.34	0.24	0.66	0.29	0.17	0.18	0.27
Si	0.34	0.54	0.19	1.12	0.18			
P						2.97	3.48	
S	0.43	1.15	1.87	0.35	0.20			
Cl	0.11	0.34	0.49	0.17	0.15			
Ca		0.39	0.13					
Cu	89.78	89.11	89.08	89.82	93.66	89.66	90.28	99.51
Total	100.00	100.00	100.00	100.00	100.00	100.00	100.00	100.00

Figure G-23. *EDS analysis of pipe A3 sample area 2.*

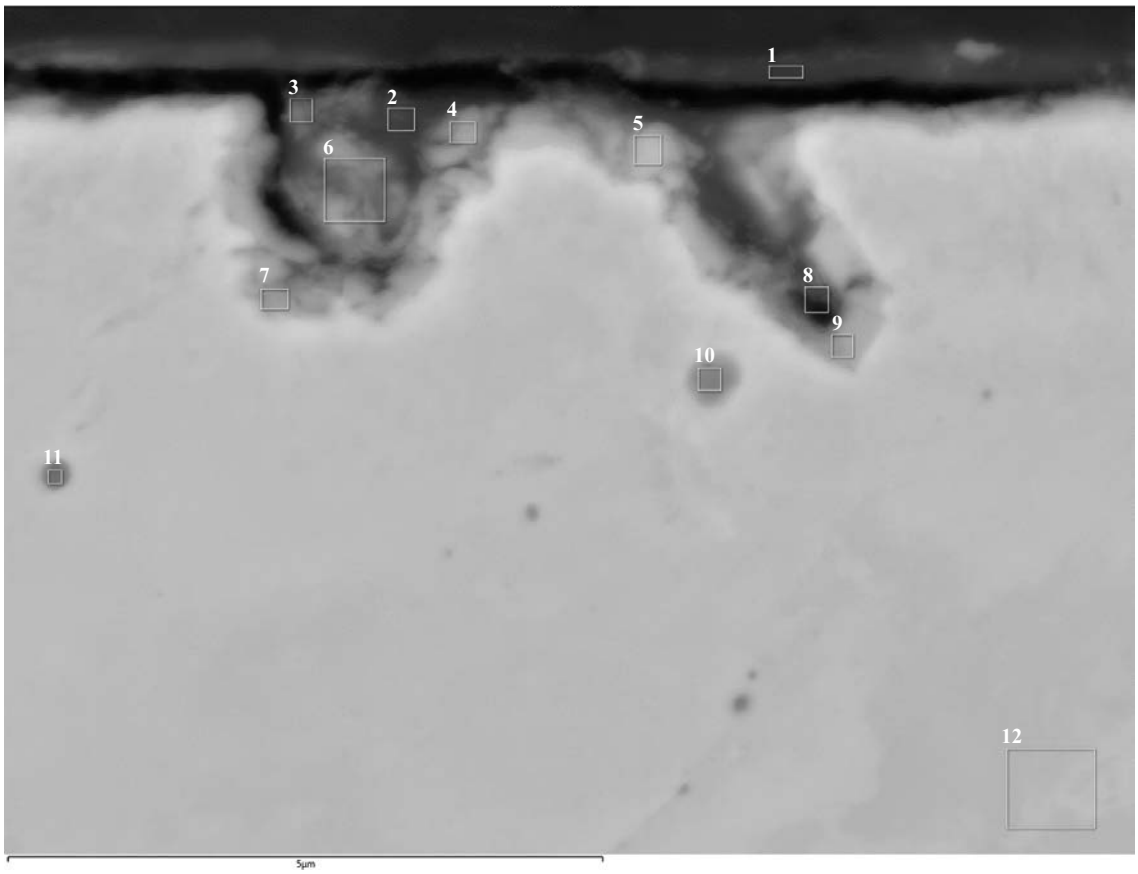

Element (At%)	1	2	3	4	5	6	7	8	9	10	11	12
O	20.83	26.58	16.13	17.86	15.06	17.64	9.06	9.37	6.97	6.27	6.26	0.10
Na	0.74	2.09	1.10	0.93								
Mg	1.36	1.24	0.69	0.64	0.46	0.70		0.24				
Al	6.36	6.08	2.73	2.88	1.89	3.07	0.56	1.11	0.25			
Si	17.55	19.37	13.37	8.28	4.97	10.36	2.07	2.95	0.48			
P	0.34	0.14				0.15		0.38		2.38	2.90	
S	1.16	1.38	2.28	0.93	0.75	2.82	0.94	0.99	0.47			
Cl	0.25	0.21	0.24	0.11		0.11	0.11					
K	0.20	0.17	0.13	0.09								
Ca	0.38	0.50	0.63	0.41	0.17	0.49	0.19	0.53		0.14	0.11	
Fe	1.04	1.05	0.42	0.44		0.35						
Cu	49.77	41.19	62.27	67.43	76.70	64.31	87.06	84.42	91.84	91.21	90.72	99.90
Total	100.00	100.00	100.00	100.00	100.00	100.00	100.00	100.00	100.00	100.00	100.00	100.00

Figure G-24. *EDS analysis of pipe A3 sample area 2.*

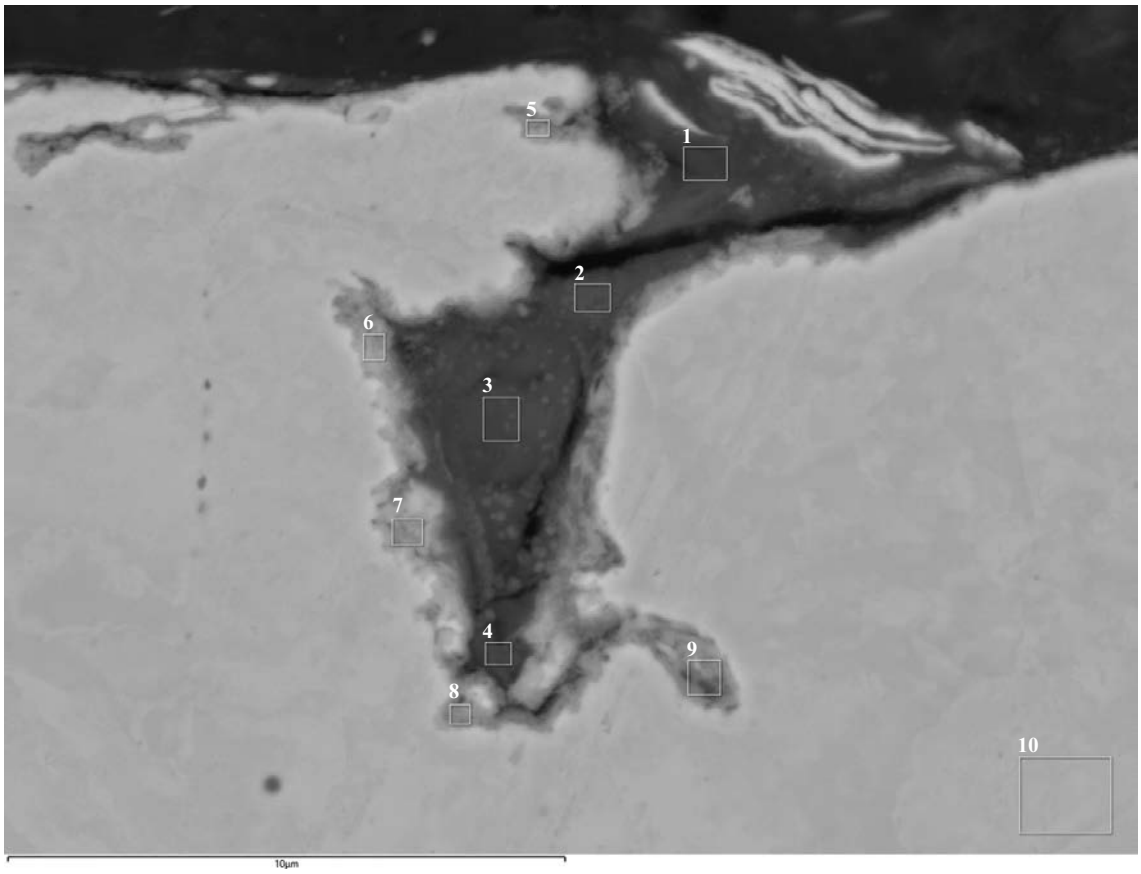

Element (At%)	1	2	3	4	5	6	7	8	9	10
O	26.98	37.87	38.88	27.17	6.81	7.48	8.93	6.66	6.82	0.16
Na				0.82						
Mg	1.42	1.30	1.52	1.23	0.12	0.14	0.12			
Al	8.52	9.26	10.95	6.83	0.61	0.26	0.59	0.35		
Si	20.77	21.95	26.63	17.32	1.33	0.69	1.33	0.82		
S	0.80	0.25	0.16	0.43	0.52	0.66	0.91	0.91	2.04	
Cl	0.15	0.09		0.13	0.13	0.14	0.12	0.08		
K	0.64	0.10	0.12	0.09						
Ca	0.51	0.91	0.26	0.29	0.16	0.16			0.13	
Fe	1.89	2.24	2.75	1.48						
Cu	38.32	26.03	18.74	44.20	90.32	90.45	88.01	91.19	91.00	99.84
Total	100.00	100.00	100.00	100.00	100.00	100.00	100.00	100.00	100.00	100.00

Figure G-25. *EDS analysis of pipe A3 sample area 2.*

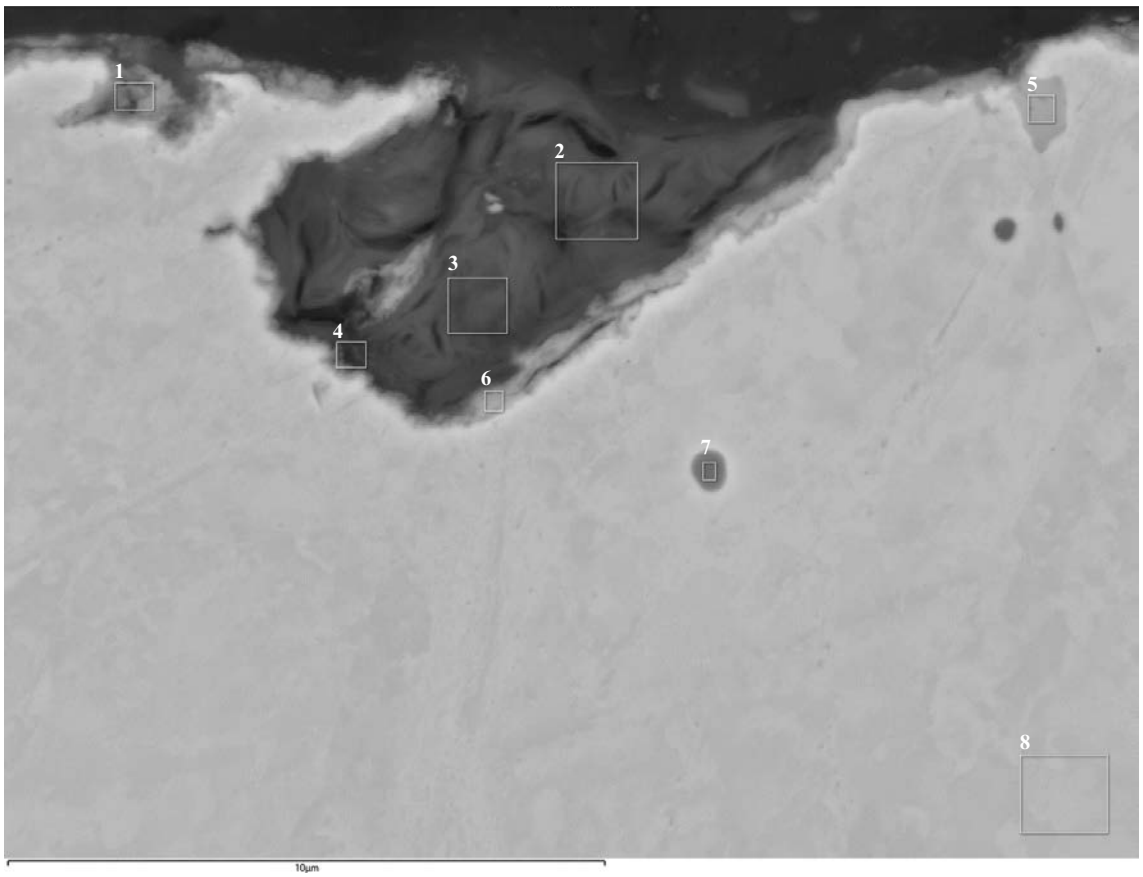

Element (At%)	1	2	3	4	5	6	7	8
O	15.92	36.29	38.46	26.19	8.49	15.08	12.08	0.16
Mg	0.81	1.87	1.70	1.42	0.13	0.61		
Al	3.88	11.31	9.11	6.93	0.25	2.31		
Si	8.78	31.23	29.19	22.72	0.54	6.17		
P							6.49	
S	3.20	0.44	0.61	1.01	0.36	2.34	0.14	
Cl	0.12					0.15		
Ca	0.12	0.49	0.51	0.30		0.11		
Fe	0.79	2.39	1.99	1.61		0.33	0.39	
Cu	66.37	15.97	18.44	39.82	90.23	72.89	79.94	99.84
Sn							0.97	
Total	100.00	100.00	100.00	100.00	100.00	100.00	100.00	100.00

Figure G-26. *EDS analysis of pipe A3 sample area 2.*

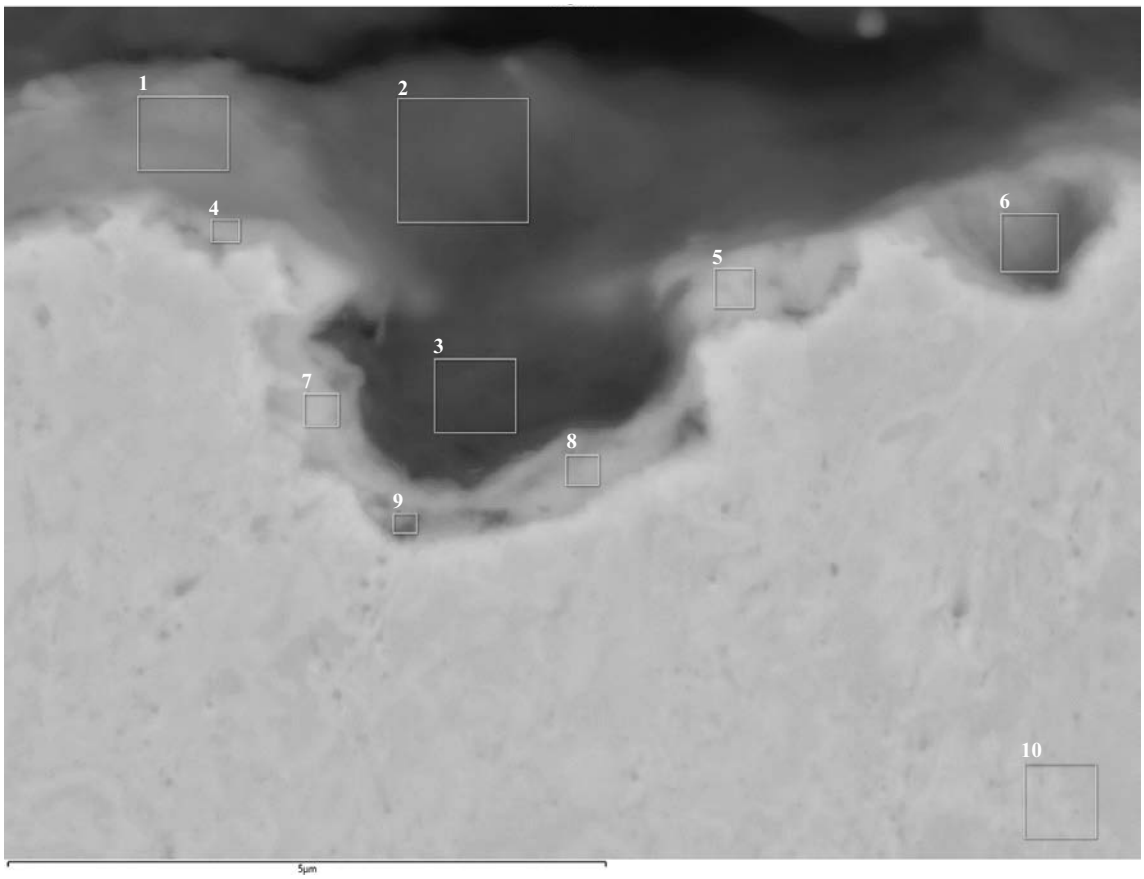

Element (At%)	1	2	3	4	5	6	7	8	9	10
O	11.64	36.18	35.15	11.60	12.21	11.78	11.92	12.80	10.10	0.14
Mg	0.24	1.36	1.25	0.17	0.11	0.35	0.18	0.35	0.30	
Al	1.09	7.63	7.34	0.82	0.64	1.36	1.04	1.47	1.38	
Si	2.80	20.15	18.60	1.95	1.49	2.99	2.29	3.26	3.06	
S	2.17	1.28	2.20	0.22	0.81	0.47	3.64	4.78	2.01	
Cl	0.07			0.13		0.14				
K		0.21	0.18							
Ca		0.23	0.33							
Fe		1.37	1.12							
Cu	81.98	31.58	33.82	85.11	84.73	82.93	80.93	77.34	83.15	99.86
Total	100.00	100.00	100.00	100.00	100.00	100.00	100.00	100.00	100.00	100.00

Figure G-27. *EDS analysis of pipe A3 sample area 2.*

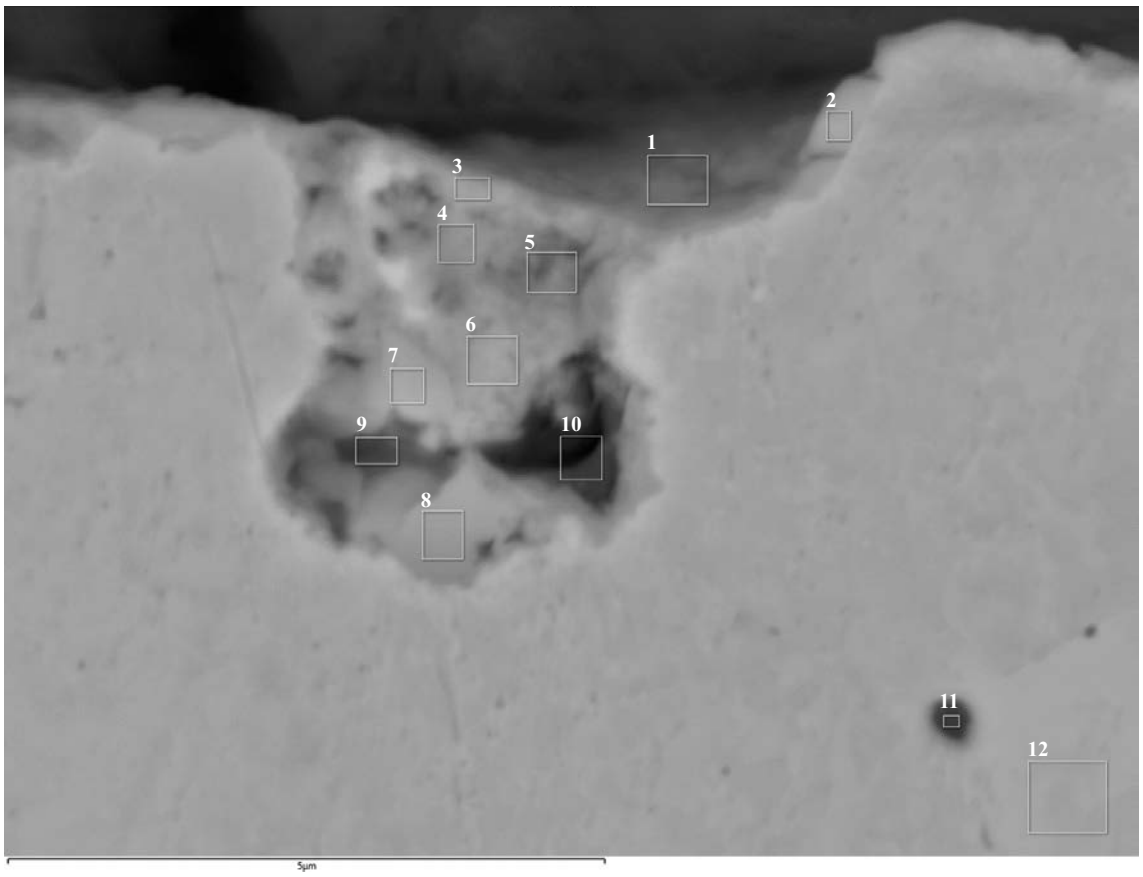

Element (At%)	1	2	3	4	5	6	7	8	9	10	11	12
O	16.92	9.99	13.65	8.73	9.77	8.91	10.06	9.69	10.41	14.87	10.86	0.19
Mg	0.42	0.24	0.21							0.42		
Al	2.15	0.87	0.86		0.30	0.21	0.09			1.91		
Si	5.14	2.76	2.81	0.55	0.76	0.53	0.28	0.20	0.26	4.88		
P											7.36	
S	1.13	0.22	0.75	2.28	2.00	2.90	0.67	0.19	0.39	1.03		
Cl					0.22	0.07	0.09	0.12				
Ca										0.20		
Fe	0.19									0.65	0.77	
Cu	74.05	85.93	81.71	88.45	86.95	87.37	88.81	89.80	88.94	76.04	72.20	99.81
Zn											3.03	
Sn											3.17	
Total	100.00	100.00	100.00	100.00	100.00	100.00	100.00	100.00	100.00	100.00	100.00	100.00

Figure G-28. *EDS analysis of pipe A3 sample area 2.*

Pipe A3 sample 3

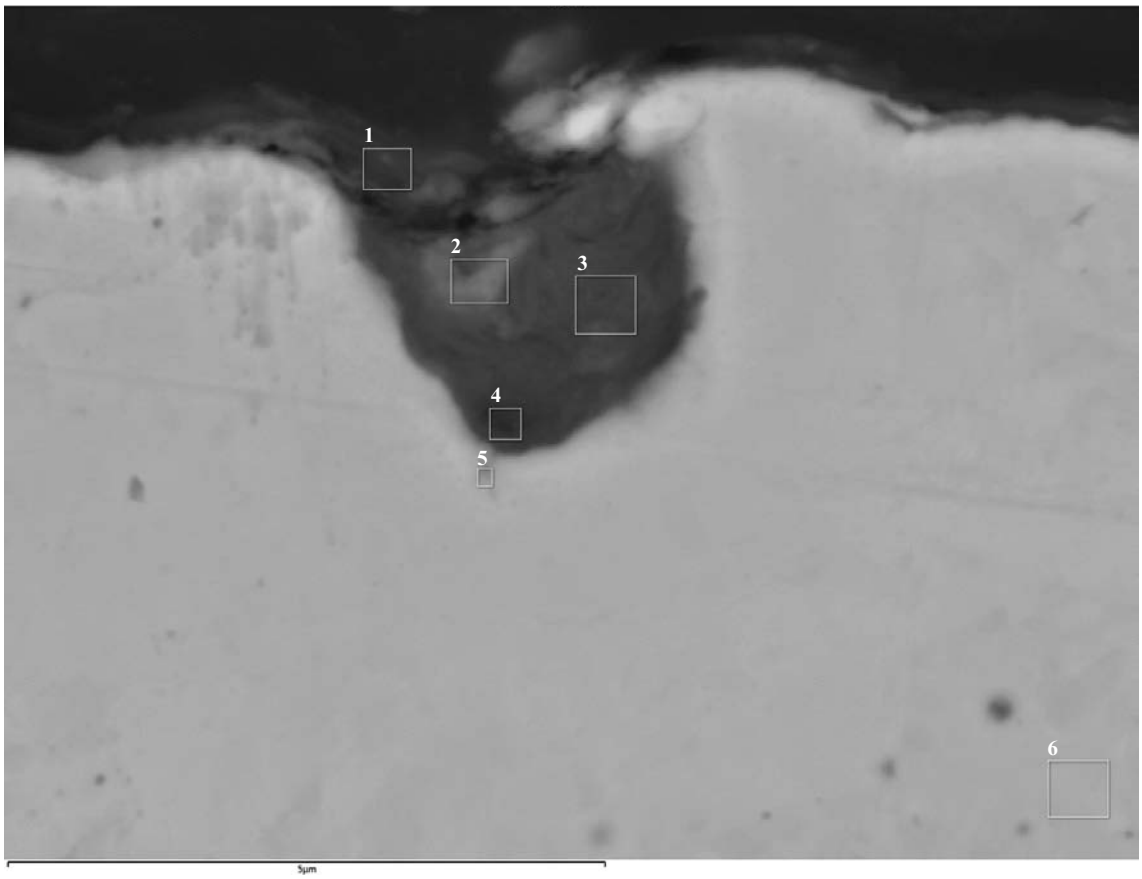

Element (At%)	1	2	3	4	5	6
O	27.58	27.71	35.31	28.67	13.37	0.14
Na	4.66	1.19		0.33		
Mg	1.61	1.25	1.50	1.20	0.59	
Al	9.34	5.94	7.55	6.04	2.73	
Si	13.78	14.41	20.02	17.62	6.16	
P					0.09	
S	3.74	4.07	1.07	1.42	0.55	
Cl	0.13	0.11	0.09		0.07	
K	0.34	0.21	0.39	0.14	0.08	
Ca	1.60	0.77	0.45	0.77	0.31	
Fe	0.67	1.06	1.73	1.04	0.33	
Cu	36.55	43.30	31.87	42.77	75.70	99.86
Total	100.00	100.00	100.00	100.00	100.00	100.00

Figure G-29. *EDS analysis of pipe A3 sample area 3.*

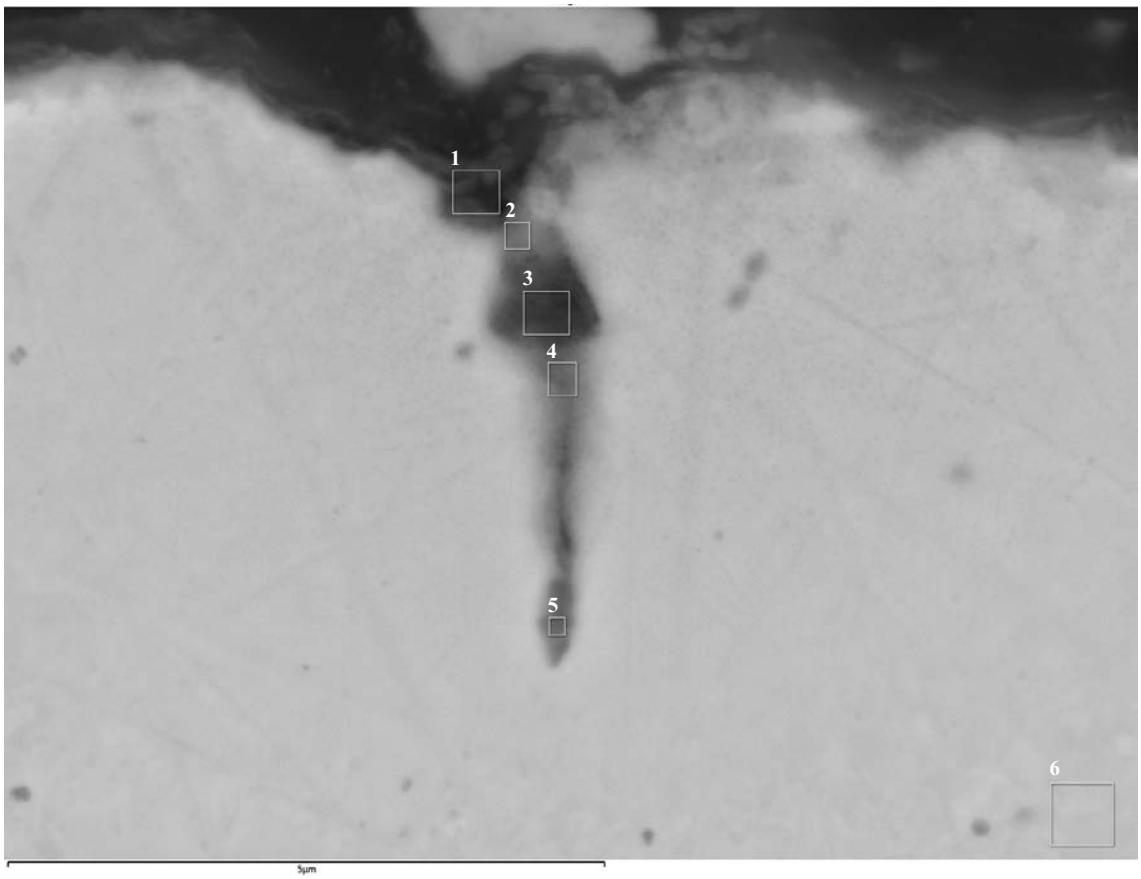

Element (At%)	1	2	3	4	5	6
O	17.03	15.40	9.82	14.17	9.58	0.16
Na	5.56	3.76		1.44		
Mg	0.51	0.43		0.19	0.37	
Al	1.54	0.96	0.52			
Si	4.13	3.97	3.77	2.71	0.78	
P		0.80	0.34	1.93	2.15	
S	6.23	3.01	1.87	1.40	0.23	
Cl	0.31	0.41	0.26	0.23	0.11	
K	2.58	1.28	0.76	0.25		
Ca	1.27	1.80	0.95	4.34	2.79	
Cu	60.84	66.21	81.72	71.33	82.73	99.84
Pb		1.98		2.00	1.26	
Total	100.00	100.00	100.00	100.00	100.00	100.00

Figure G-30. *EDS analysis of pipe A3 sample area 3.*

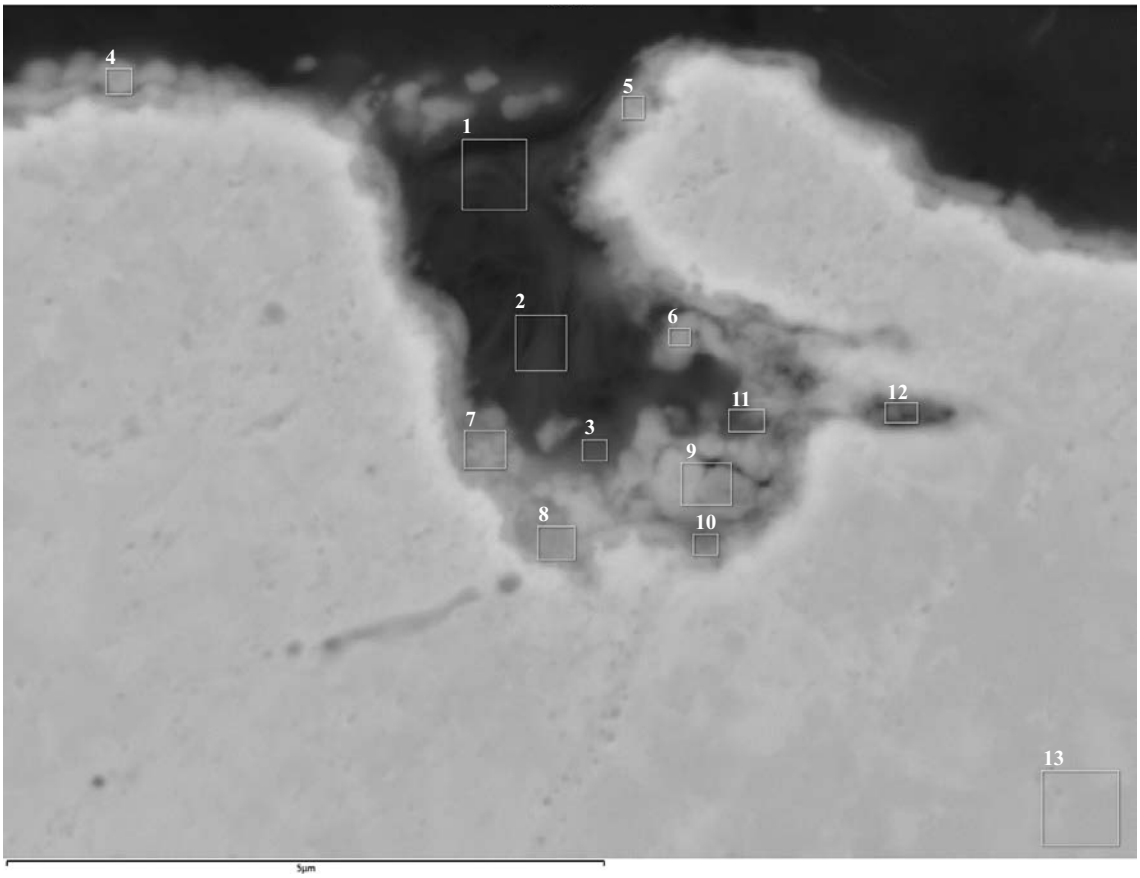

Element (At%)	1	2	3	4	5	6	7	8	9	10	11	12	13
O	18.67	22.31	13.90	7.39	8.41	12.44	10.14	5.08	9.61	7.14	10.09	4.67	0.14
Mg	1.76	1.21	0.59	0.37	0.56		0.29				0.21		
Al	6.84	5.93	2.83	0.00	1.18	1.18	0.96	0.10	0.20	0.10	0.51		
Si	16.88	12.90	5.73	0.15	2.64	3.96	1.85	0.19	0.86	0.30	1.69		
P							0.27				0.36		
S	1.62	0.98	0.53	0.69	0.99	0.66	0.67	0.67	0.40	0.57	1.11	0.53	
Cl	0.24	0.23	0.22	0.23	0.27	0.27	0.24	0.15	0.25	0.24	0.30	0.36	
K	0.32	0.24											
Ca	5.61	3.40	0.51		0.27	0.79	0.29		0.17	0.18	1.05	0.76	
Fe	1.88	1.44	0.46										
Cu	46.18	51.36	75.24	91.17	85.68	80.69	85.29	93.82	88.51	91.47	84.67	93.67	99.86
Total	100.00	100.00	100.00	100.00	100.00	100.00	100.00	100.00	100.00	100.00	100.00	100.00	100.00

Figure G-31. *EDS analysis of pipe A3 sample area 3.*

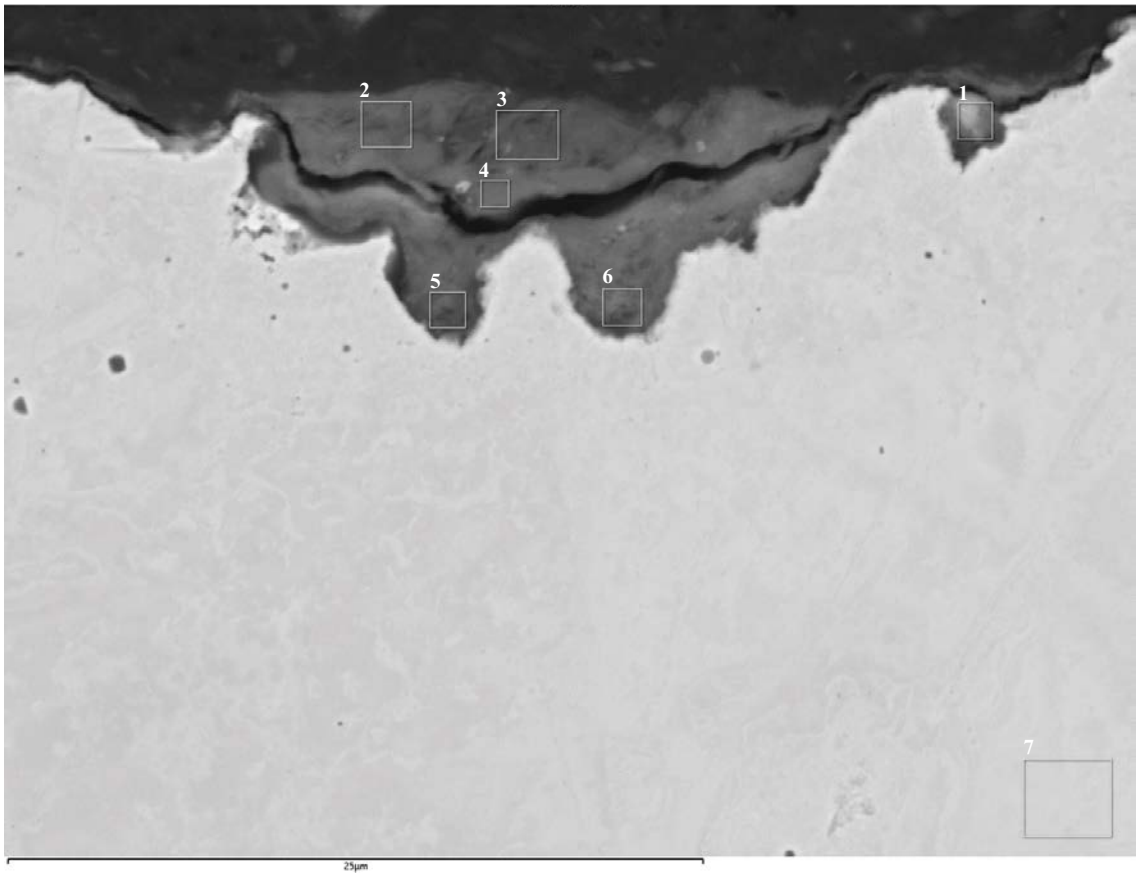

Element (At%)	1	2	3	4	5	6	7
O	19.68	33.84	36.99	34.29	30.79	24.38	0.13
Mg	0.29	1.36	1.65	1.53	1.27	1.12	
Al	0.82	7.80	9.42	8.37	5.65	4.39	
Si	13.78	27.82	28.50	23.71	16.14	11.91	
S	8.13	3.52	2.56	2.92	3.98	5.62	
Cl			0.09				
K		0.21	0.19		0.16	0.13	
Ca	2.17	0.57	0.88	1.76	5.76	6.96	
Ti		1.17					
Fe		1.63	1.97	1.58	1.22	0.89	
Cu	55.12	22.06	17.75	25.84	35.03	44.61	99.87
Total	100.00	100.00	100.00	100.00	100.00	100.00	100.00

Figure G-32. *EDS analysis of pipe A3 sample area 3.*

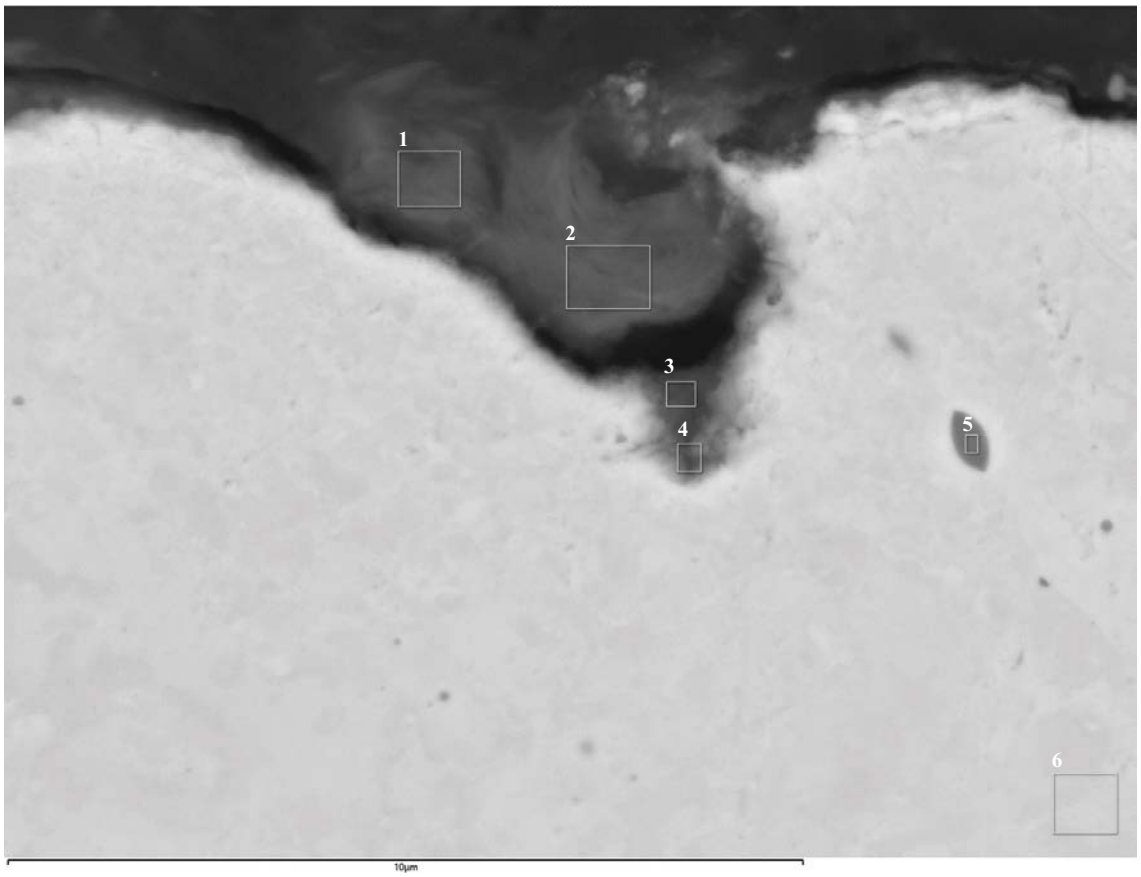

Element (At%)	1	2	3	4	5	6
O	32.69	38.18	35.64	16.79	11.26	0.12
Na	3.47	0.29	0.77			
Mg	0.82	1.52	1.13	0.74		
Al	11.79	6.29	1.36	0.61		
Si	27.89	15.70	6.02	2.76		
P					6.02	
S	0.23	1.25	0.91	1.86	0.61	
K	0.22	0.22	0.16			
Ca	2.48	9.55	17.61	11.47		
Mn			0.35			
Fe	1.02	1.15	0.27			
Cu	19.39	25.84	35.77	65.76	82.11	99.88
Total	100.00	100.00	100.00	100.00	100.00	100.00

Figure G-33. *EDS analysis of pipe A3 sample area 3.*

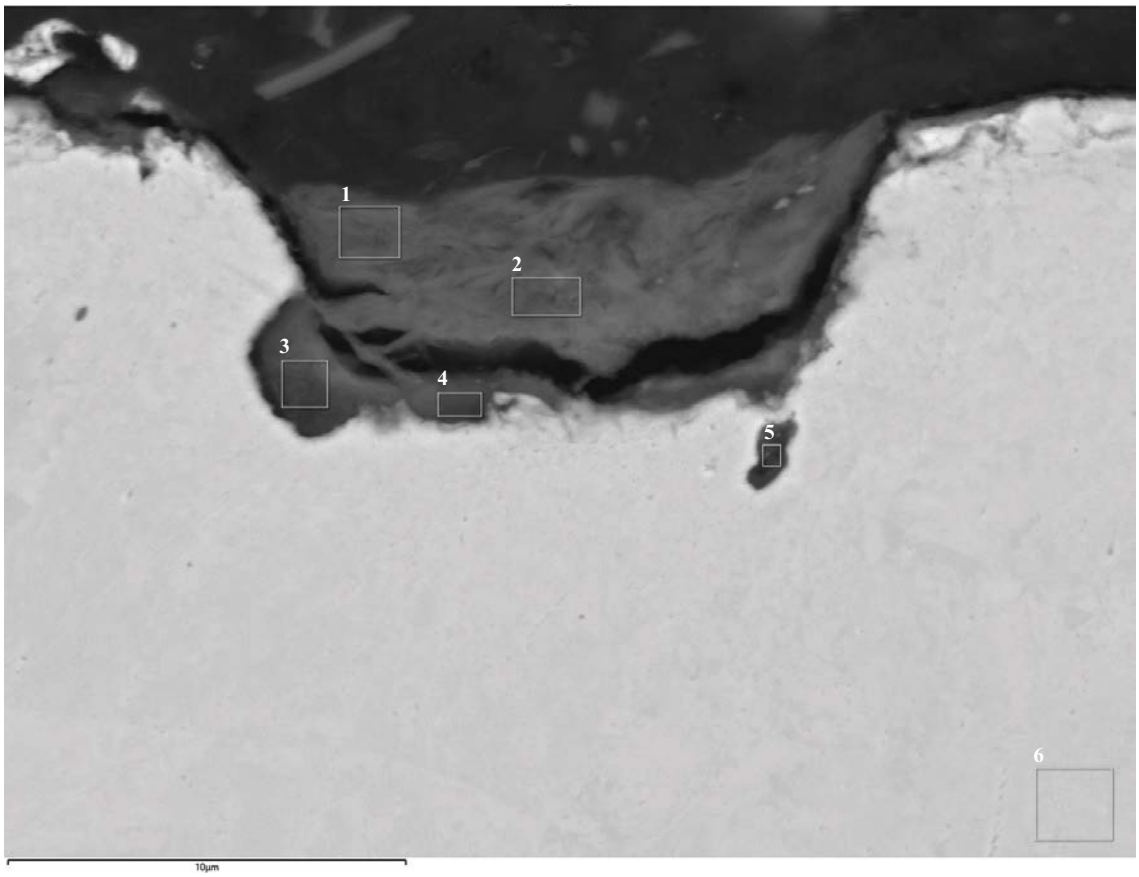

Element (At%)	1	2	3	4	5	6
O	37.32	40.27	34.47	33.66	22.16	0.14
F					0.61	
Na	0.24	0.21	0.28	0.67	1.67	
Mg	1.63	1.64	1.26	1.15	0.28	
Al	10.74	9.04	6.72	5.94	0.37	
Si	31.06	29.78	28.12	24.67	1.15	
P					7.39	
S	0.98	1.05	0.56	1.57	1.33	
Cl					0.12	
K	0.33	0.33	0.32	0.25	0.14	
Ca	0.65	0.74	0.78	0.75	20.29	
Fe	2.11	1.95	1.35	1.07		
Cu	14.93	15.01	26.15	30.27	44.47	99.86
Total	100.00	100.00	100.00	100.00	100.00	100.00

Figure G-34. *EDS analysis of pipe A3 sample area 3.*

PIpe S2 surface analysis – lighter and darker areas

Element (At%)	1
O	16.41
Na	4.16
Mg	0.67
Al	4.04
Si	7.90
S	1.30
Cl	1.04
K	0.08
Ca	2.09
Fe	0.68
Cu	61.64
Total:	100.00

Figure G-35. *EDS analysis of pipe S23 surface with lighter appearance.*

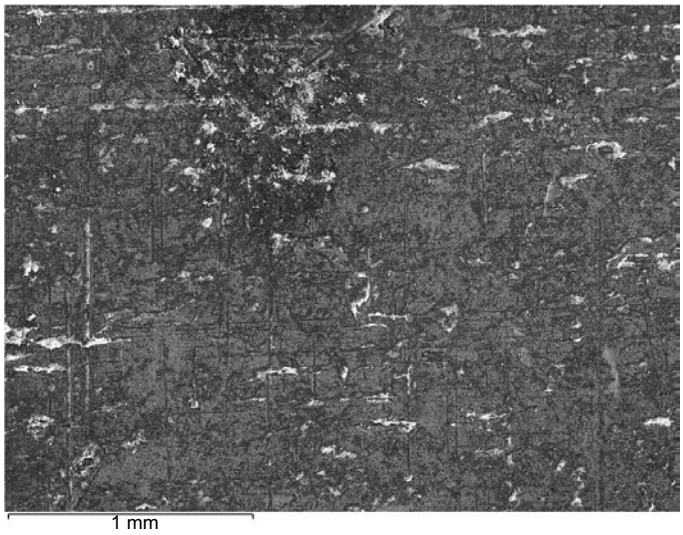

Element (At%)	1
O	23.44
Na	3.45
Mg	1.16
Al	6.77
Si	16.01
S	3.69
Cl	0.92
K	0.18
Ca	1.19
Fe	1.36
Cu	41.84
Total:	100.00

Figure G-36. *EDS analysis of pipe S23 surface with darker appearance.*

PIpe S2 sample 1

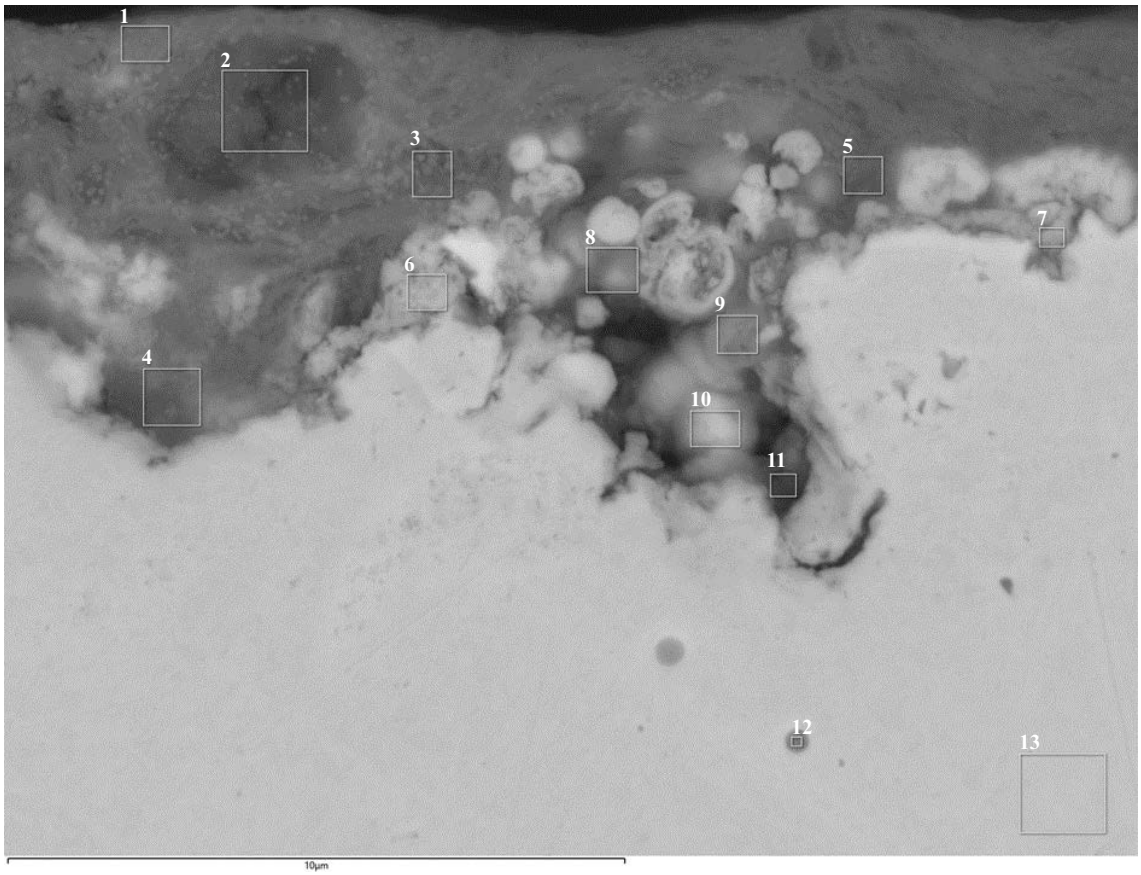

Element (At%)	1	2	3	4	5	6	7	8	9	10	11	12	13
O	60.36	58.70	56.21	42.43	52.70	30.48	25.71	44.21	37.02	36.14	40.04	20.60	0.82
Mg	1.36	0.68	1.33	1.34	1.52	0.40	0.18	1.08		0.54	0.67		
Al	6.65	4.13	6.81	3.92	8.29	1.80	1.25	6.04	3.30	2.61	2.53		0.84
Si	18.52	27.25	17.13	10.08	19.88	3.66	2.09	15.13	12.09	6.03	11.74		
P												5.91	
S	0.53	0.44	0.80	4.34	0.48	1.03	2.01	0.08		0.18	0.21		
Cl			0.22		0.75	2.17	1.97	2.31	2.83	3.40	2.36		
Ca	2.22	3.47	4.88	4.49	0.67	1.60	0.28	0.43		0.17	0.22		
Fe	0.66	0.45	0.63	0.25	0.82			0.86	0.53		0.46		
Cu	9.69	4.87	11.99	33.15	14.89	58.86	66.51	29.86	44.23	50.93	41.77	72.88	98.33
Sn												0.33	
Pb												0.28	
Total	100.00	100.00	100.00	100.00	100.00	100.00	100.00	100.00	100.00	100.00	100.00	100.00	100.00

Figure G-37. *EDS analysis of pipe S2 sample area 1.*

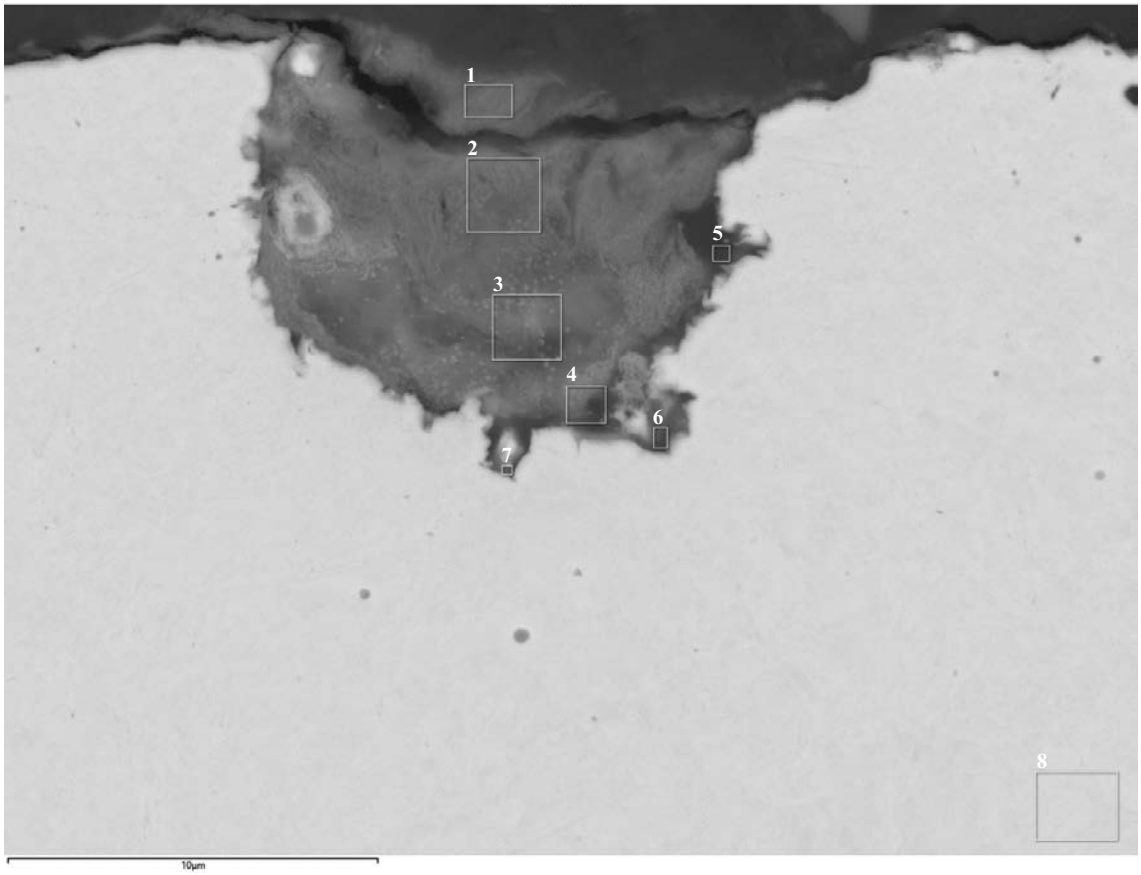

Element (At%)	1	2	3	4	5	6	7	8
O	54.13	58.98	58.48	49.58	46.74	34.29	18.22	0.87
Mg	1.84	1.38	1.68	1.44	1.26	0.83		
Al	8.54	6.97	6.71	4.82	3.32	3.99	1.74	0.93
Si	22.54	17.93	16.04	10.06	7.82	8.77	2.60	
P					1.03			
S	0.40	0.67	1.48	1.49	2.62	0.51	0.69	
Cl	0.10	0.11		0.22	0.51	0.48		
K		0.11						
Ca	2.10	3.43	3.52	2.68	4.01	1.29	0.21	
Fe	0.93	0.71	0.61	0.40		0.37		
Cu	9.41	9.72	11.48	29.30	32.70	49.46	76.53	98.20
Total	100.00	100.00	100.00	100.00	100.00	100.00	100.00	100.00

Figure G-38. *EDS analysis of pipe S2 sample area 1.*

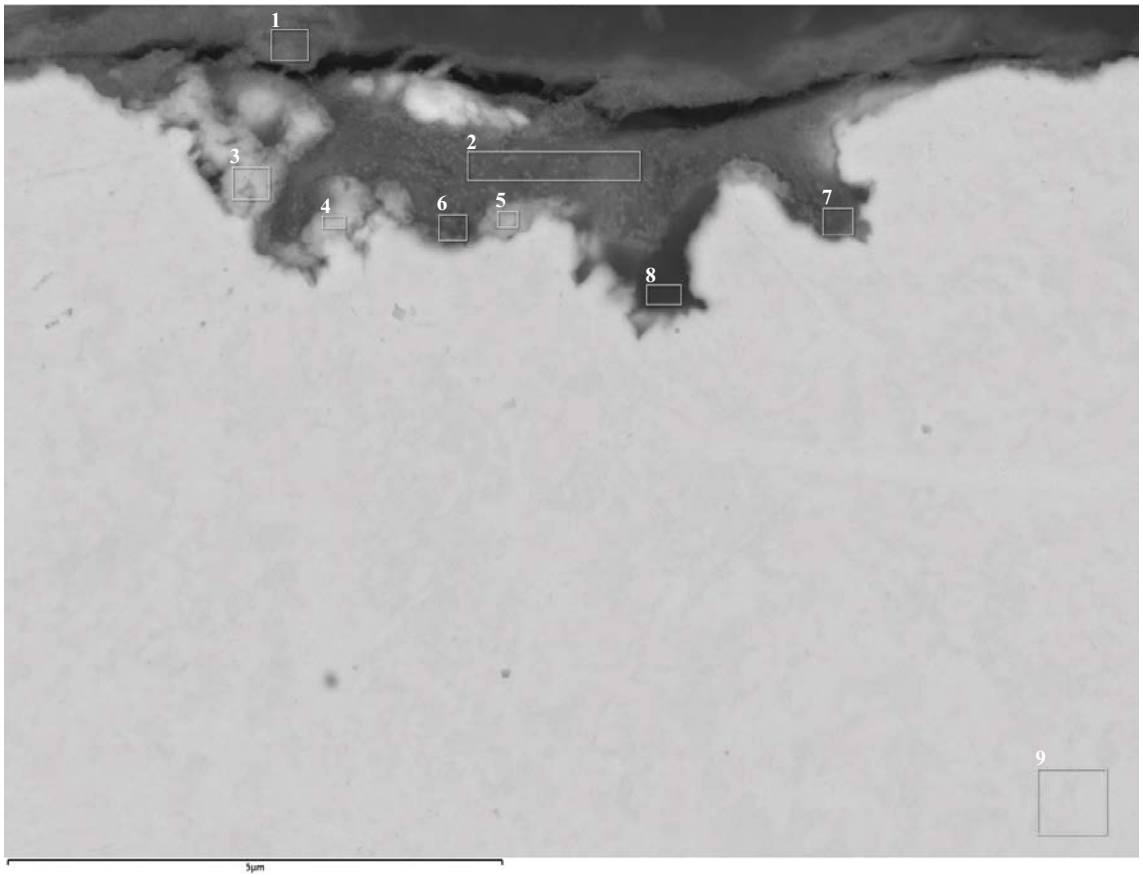

Element (At%)	1	2	3	4	5	6	7	8	9
O	49.86	55.48	37.92	38.63	39.59	56.20	44.19	30.56	0.79
Mg	1.20	1.74	0.84	0.49	0.58	1.25	1.08		
Al	4.63	6.65	3.16	2.17	3.01	3.84	3.75	2.46	0.57
Si	15.09	19.97	6.80	4.00	5.63	9.56	8.26	4.66	
S	2.00	0.18	0.18	0.17	0.19	0.29	0.63		
Cl	0.39	0.25	2.83	2.35	1.55	0.30	0.28	0.56	
K	0.14	0.13	0.07			0.06			
Ca	8.53	2.82	0.82	1.65	1.54	8.63	6.64	1.44	
Fe	0.35	0.69				0.36			
Cu	17.81	12.08	47.38	50.54	47.89	19.53	35.16	60.33	98.64
Total	100.00	100.00	100.00	100.00	100.00	100.00	100.00	100.00	100.00

Figure G-39. *EDS analysis of pipe S2 sample area 1.*

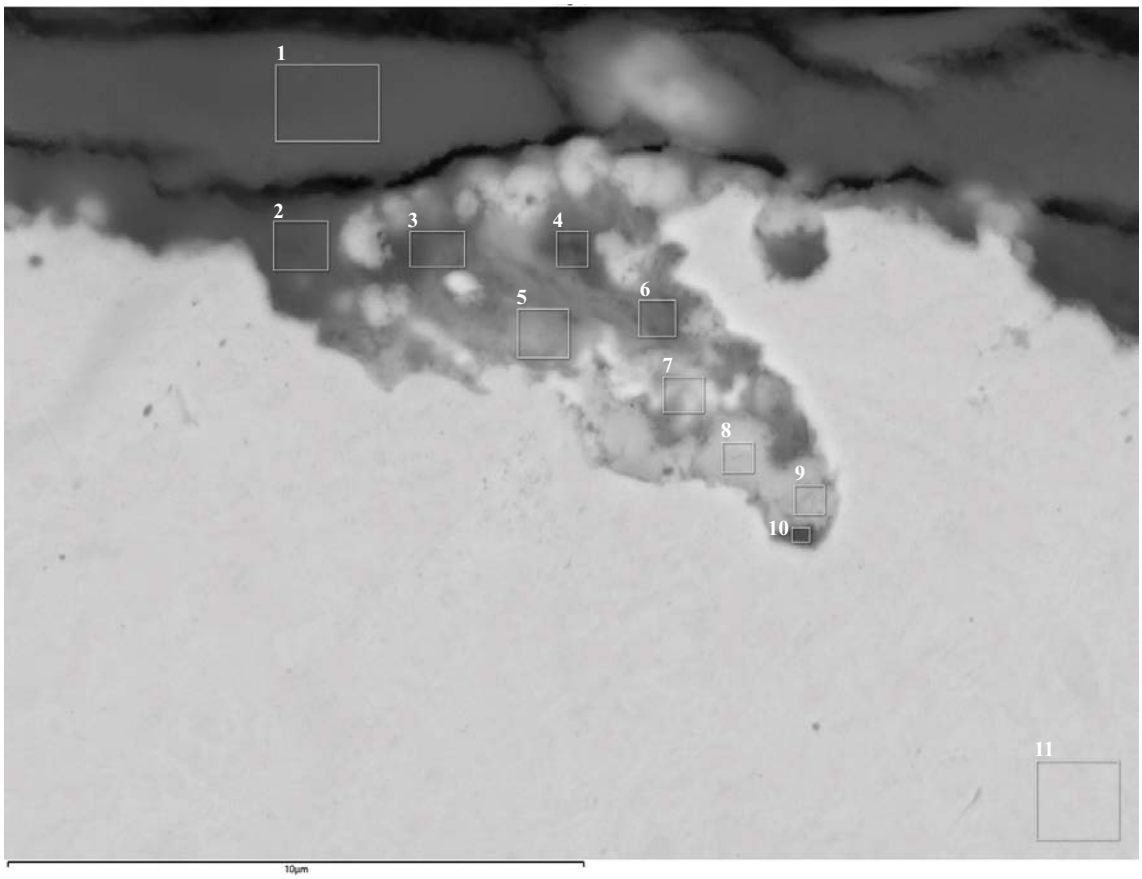

Element (At%)	1	2	3	4	5	6	7	8	9	10	11
O	59.08	56.92	52.96	51.77	49.85	51.10	34.37	30.67	29.19	29.13	1.27
Na	0.77	0.40									
Mg		1.14	0.86	0.48		0.49				0.46	
Al	0.40	5.74	3.81	2.70	0.92	2.64	1.07	0.95	1.20	2.02	0.95
Si	33.71	18.49	11.47	7.68	1.74	4.92	0.54	0.80	2.43	5.37	0.23
S	0.20	0.21	0.29	0.34	0.15	0.20					
Cl	0.11	0.19	0.95	1.20	1.57	1.17	0.71	4.04	3.02	0.89	
Ca	0.16	0.37	0.47	0.50	0.28	0.38					
Fe		0.40	0.28			0.22					
Cu	5.57	16.14	28.90	35.34	45.49	38.88	63.31	63.55	64.17	62.14	97.55
Total	100.00	100.00	100.00	100.00	100.00	100.00	100.00	100.00	100.00	100.00	100.00

Figure G-40. *EDS analysis of pipe S2 sample area 1.*

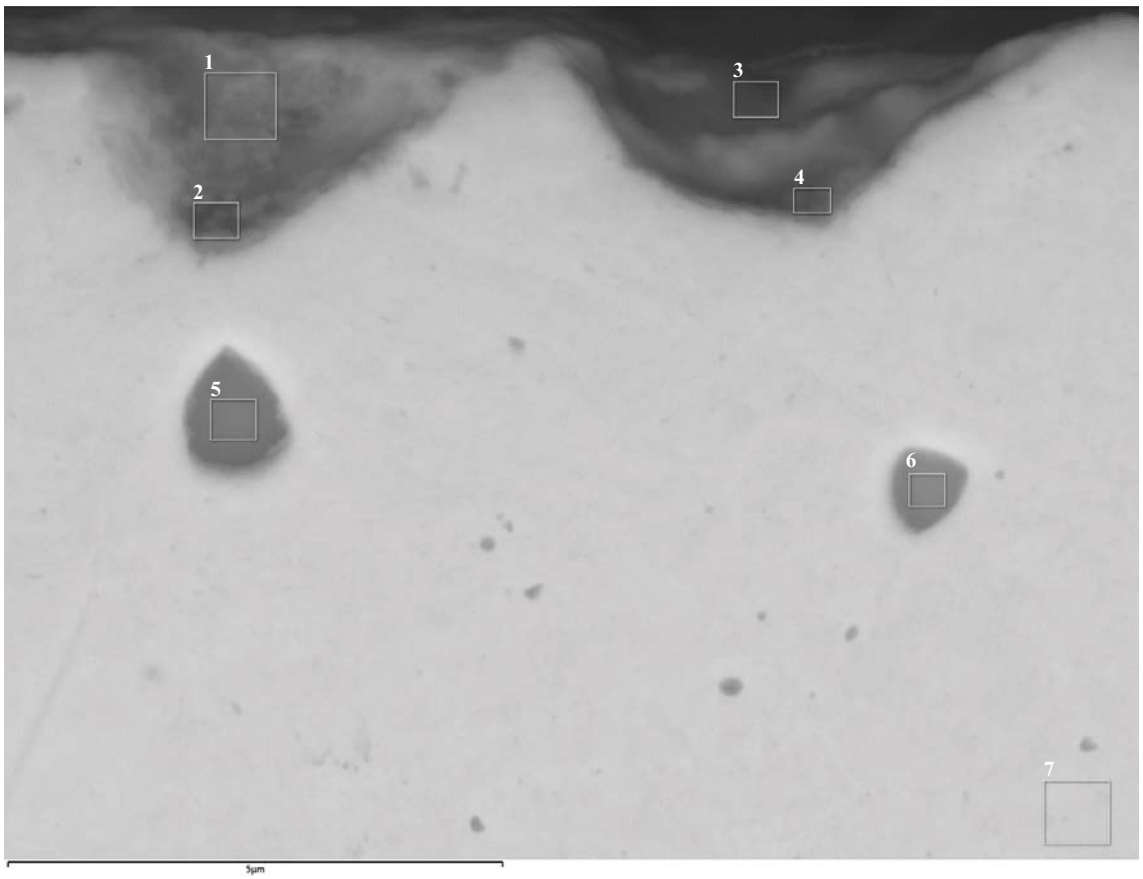

Element (At%)	1	2	3	4	5	6	7
O	55.09	46.79	53.47	39.74	48.41	38.80	
Mg	0.84	0.70					
Al	3.76	3.62	0.86	2.19	0.22	0.42	0.93
Si	12.40	6.98	13.44	4.12	2.31		
P	0.03				12.50	10.04	
S	0.10		0.08		0.24	0.45	
Cl	0.11	0.09	0.11	0.16			
Ca	0.29	0.28	0.57	0.58			
Ti				2.01			
Fe	0.48						
Cu	26.91	41.56	31.47	51.20	36.32	50.30	99.07
Total	100.00	100.00	100.00	100.00	100.00	100.00	100.00

Figure G-41. *EDS analysis of pipe S2 sample area 1.*

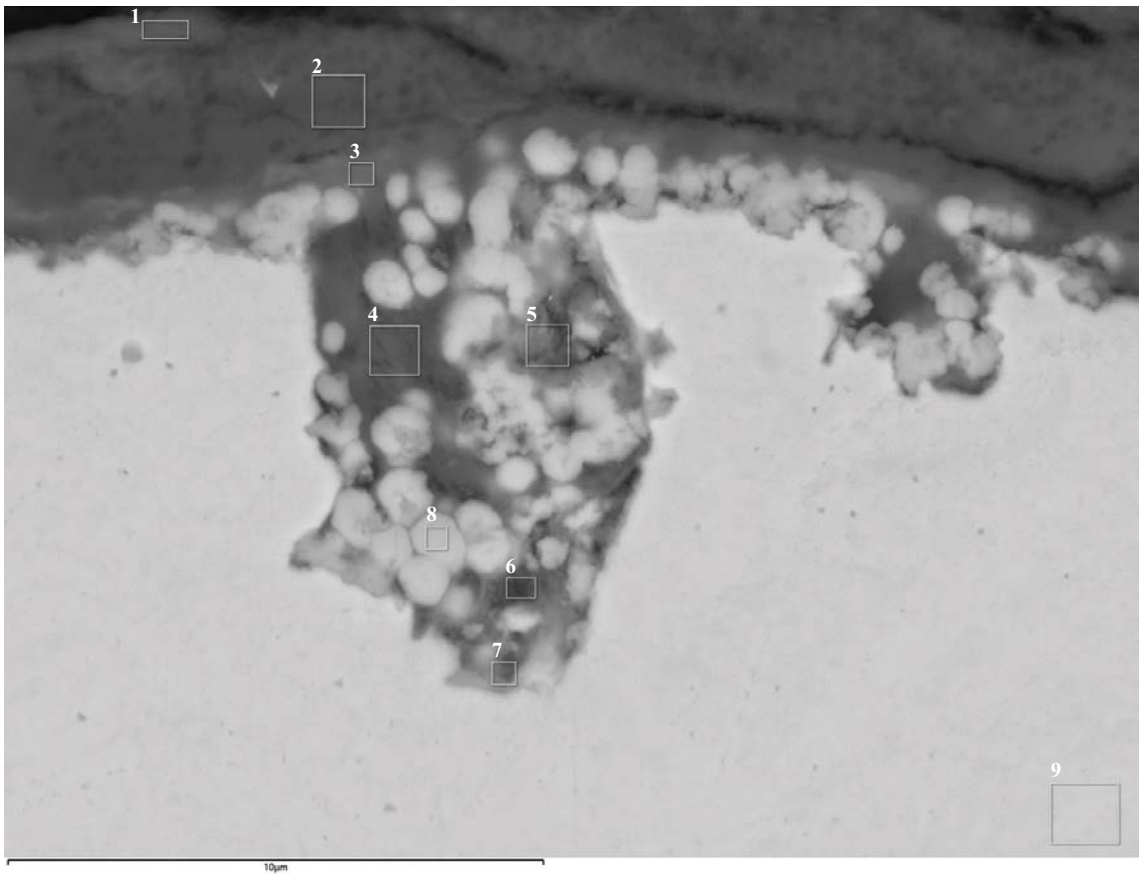

Element (At%)	1	2	3	4	5	6	7	8	9
O	61.84	56.43	58.82	54.89	51.26	41.38	37.08	32.83	1.07
Na	6.26	1.05			6.32	12.87	1.80		
Mg			0.61	1.22				0.26	
Al	0.22	0.26	2.91	7.24	1.13	0.69	0.71	1.41	0.84
Si	22.55	34.42	14.92	17.44	2.78	3.62	2.80	1.55	
P					0.15				
S	2.94	0.15	0.20	0.19	1.74	4.88	0.66		
Cl	0.09	0.12	0.48	0.79	1.29	1.74	1.95	3.29	
Ca	1.76	0.62	1.23	1.46	0.57	0.96	0.18	0.25	
Fe			0.30	0.66					
Cu	4.34	6.95	20.54	16.11	34.76	33.87	54.80	60.39	98.09
Total	100.00	100.00	100.00	100.00	100.00	100.00	100.00	100.00	100.00

Figure G-42. *EDS analysis of pipe S2 sample area 1.*

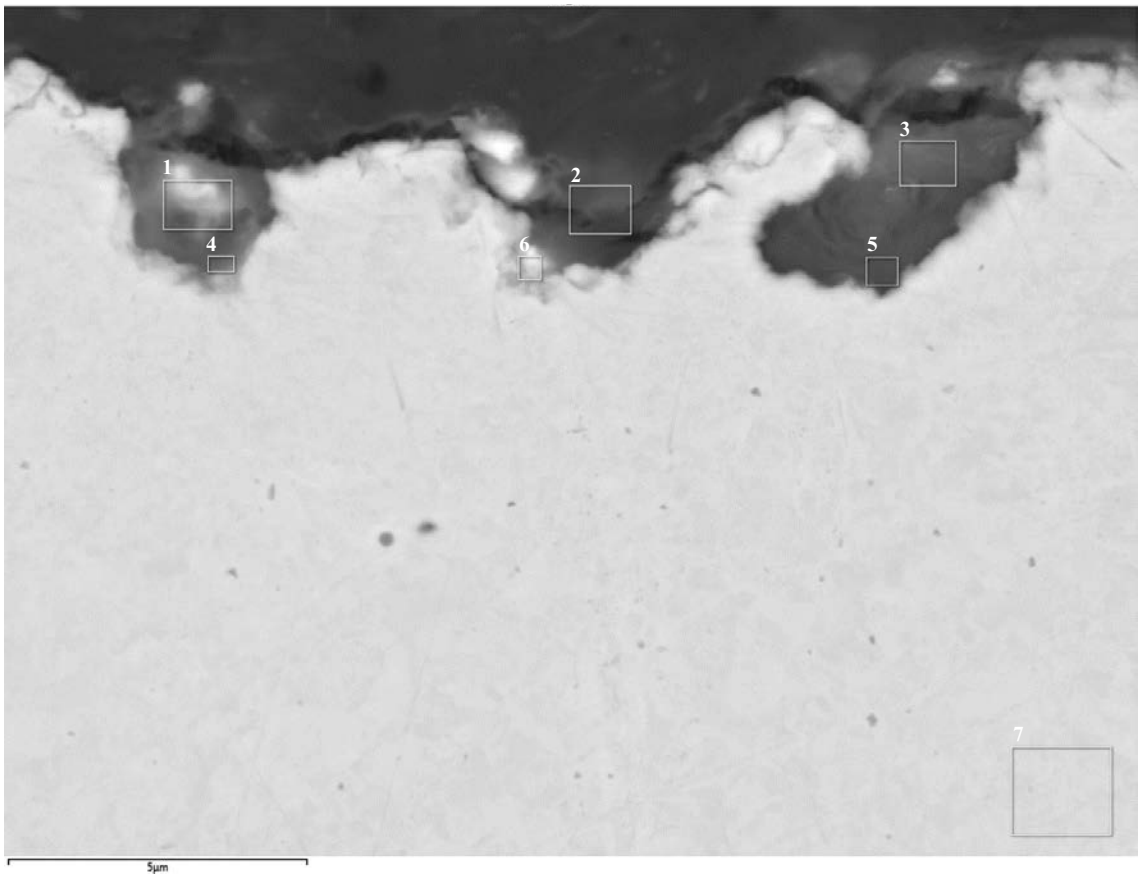

Element (At%)	1	2	3	4	5	6	7
O	31.48	26.53	53.22	31.56	53.74	14.25	1.01
Mg	0.98	1.24	1.64	1.27	1.55		
Al	2.47	2.75	6.88	3.91	7.31	0.52	
Si	6.60	11.91	19.37	8.21	20.88	2.03	
S	1.57	0.91	0.48	1.13	0.41	0.41	
Cl		0.30					
K					0.10		
Ca	0.38	0.45	0.36	0.26	0.20		
Fe			0.56	0.32	0.71		
Cu	56.51	55.93	17.48	53.34	15.10	82.80	98.99
Total	100.00	100.00	100.00	100.00	100.00	100.00	100.00

Figure G-43. *EDS analysis of pipe S2 sample area 1.*

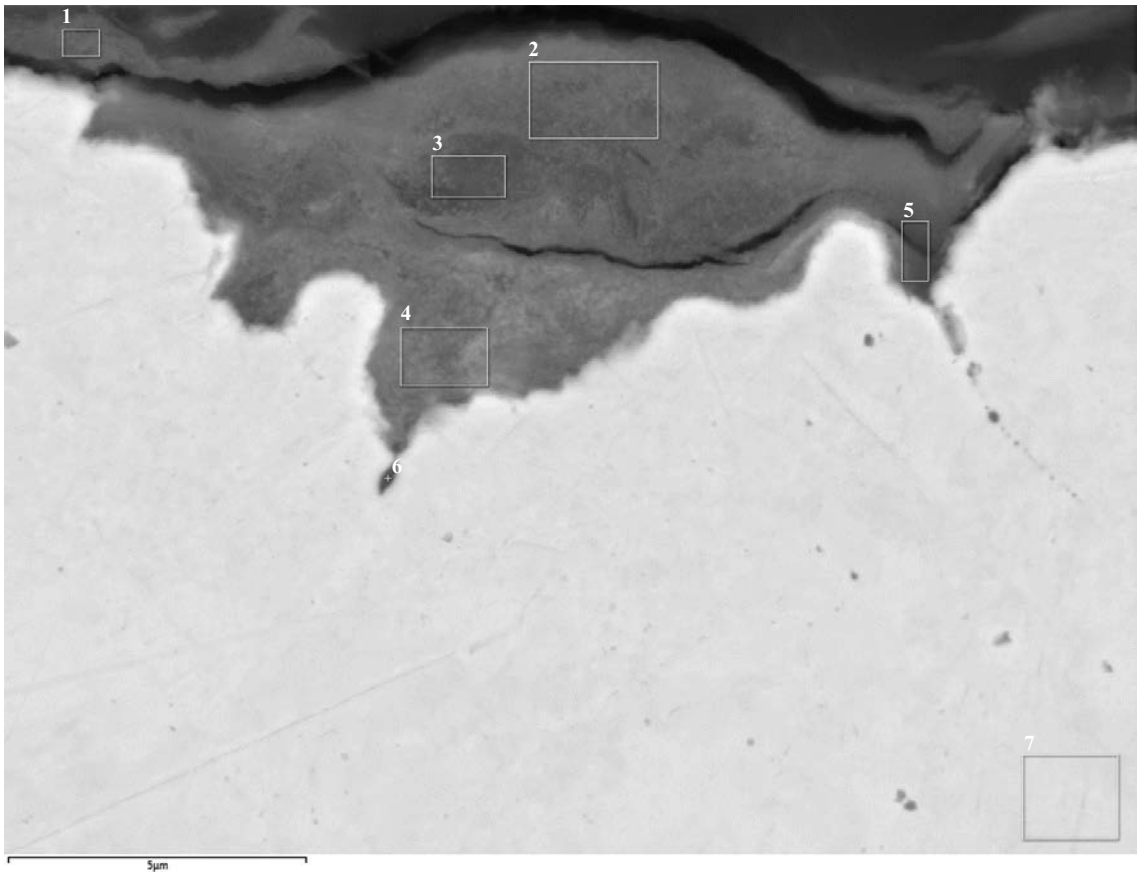

Element (At%)	1	2	3	4	5	6	7
O	45.83	57.40	56.19	42.83	44.04	20.42	1.00
Mg	1.58	1.54	1.50	1.97	1.51	0.81	
Al	7.86	9.73	9.85	5.57	7.41		
Si	23.49	22.88	23.56	14.68	16.81	0.53	
P						3.86	
S	1.38	0.35	0.58	5.22	1.94	2.74	
Ca	2.21	0.30	0.08	0.33	0.12	7.12	
Fe	0.51	0.91	0.92	0.51	0.69		
Cu	17.14	6.90	7.32	28.90	27.48	64.52	99.00
Total	100.00	100.00	100.00	100.00	100.00	100.00	100.00

Figure G-44. *EDS analysis of pipe S2 sample area 1.*

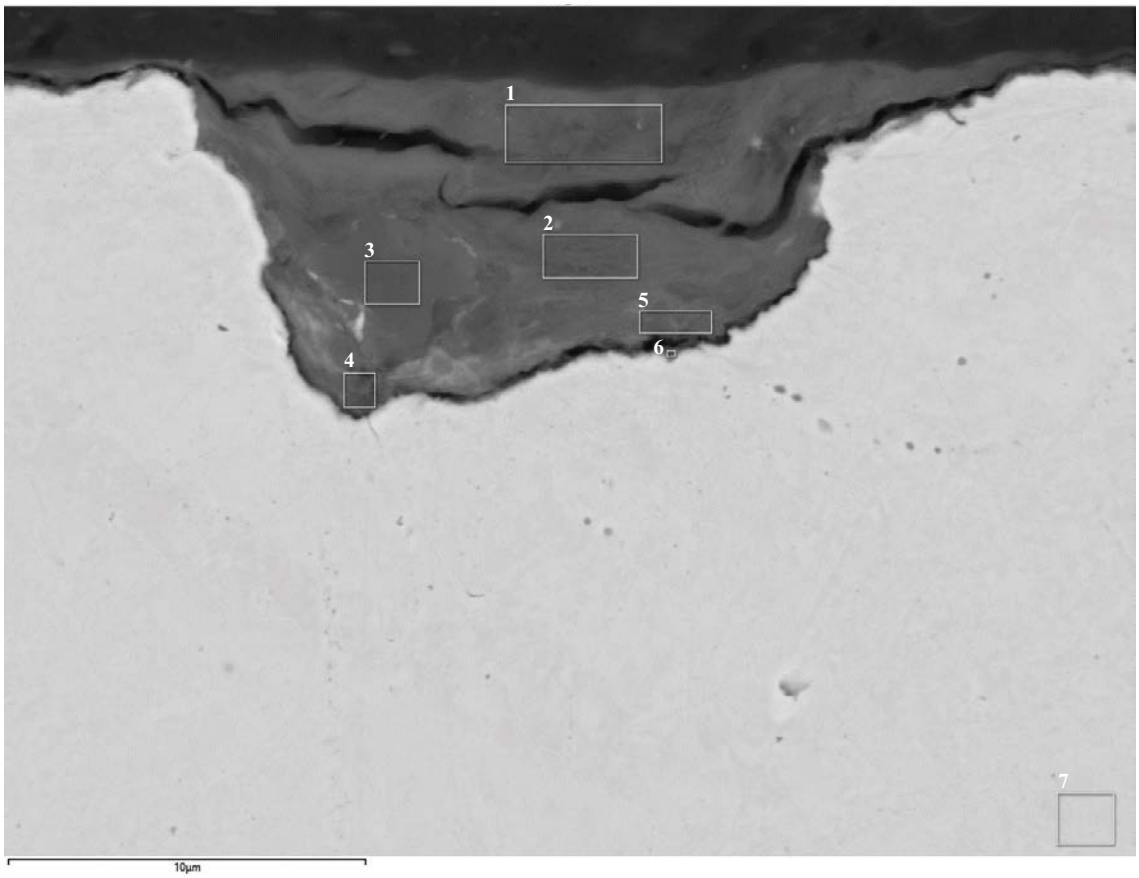

Element (At%)	1	2	3	4	5	6	7
O	54.94	60.76	65.16	48.64	48.49	29.74	1.15
Na			1.17				
Mg	1.07	1.44	0.08	1.47	1.62	0.93	
Al	6.19	8.47	2.32	6.15	8.40	4.65	
Si	30.67	21.86	29.46	17.13	18.45	9.84	
S	0.25	0.21	0.24	3.17	1.69	1.42	
Cl				0.07		0.15	
K	0.08	0.09	0.12	0.09			
Ca	0.13	0.14	0.31	0.79	0.16	0.18	
Fe	0.61	0.77		0.57	0.65	0.26	
Cu	6.05	6.27	1.15	21.92	20.56	52.84	98.85
Total	100.00	100.00	100.00	100.00	100.00	100.00	100.00

Figure G-45. *EDS analysis of pipe S2 sample area 1.*

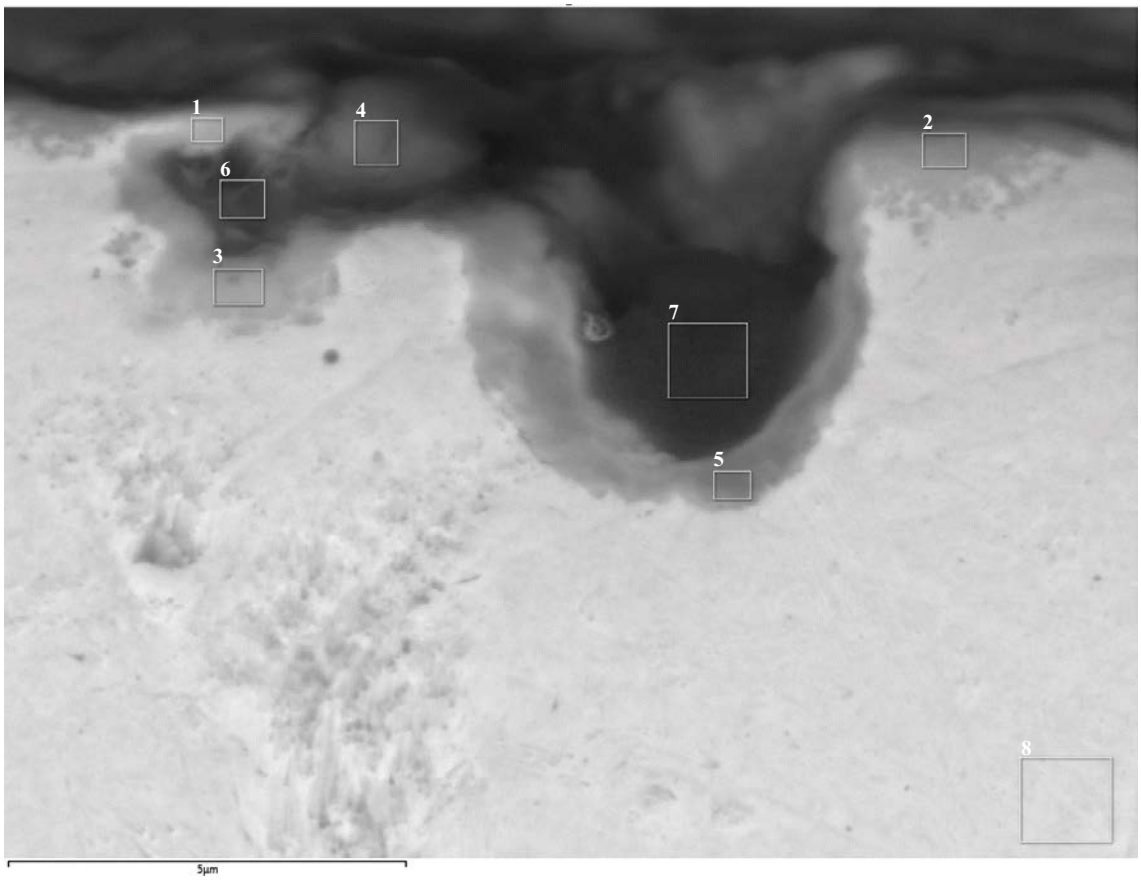

Element (At%)	1	2	3	4	5	6	7	8
O	47.65	35.38	45.52	59.94	51.43	55.59	64.58	1.47
Mg	0.38			0.31		1.05		
Al	1.18			0.95		4.44		
Si	3.21	0.51	0.74	15.51	5.71	10.45	21.73	
S	0.61	0.43	0.19	0.20	0.34	0.33	0.12	
Cl	0.10	0.35			0.06			
Fe						0.38		
Cu	46.88	63.32	53.55	23.11	42.45	27.77	13.58	98.53
Total	100.00	100.00	100.00	100.00	100.00	100.00	100.00	100.00

Figure G-46. *EDS analysis of pipe S2 sample area 1.*

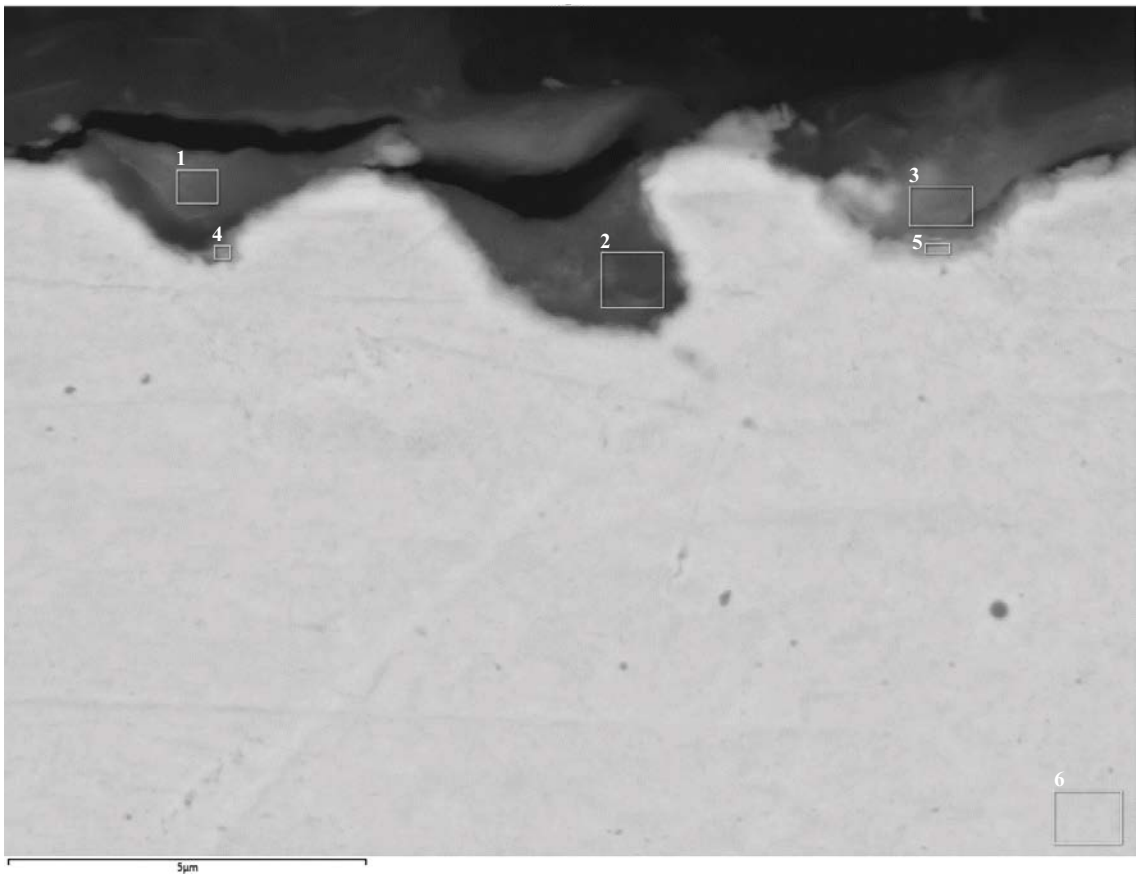

Element (At%)	1	2	3	4	5	6
O	49.48	49.46	37.85	28.77	26.98	0.99
Mg	1.54	1.36	1.21	0.64	0.57	
Al	7.42	6.36	5.16	2.92	2.24	
Si	16.58	18.14	11.38	6.14	5.71	
S	2.88	3.16	1.92	1.45	1.44	
Cl	0.08	0.09	0.24	0.16	0.30	
Ca	0.13	0.19				
Fe	0.66	0.45	0.33			
Cu	21.22	20.80	41.91	59.92	62.76	99.01
Total	100.00	100.00	100.00	100.00	100.00	100.00

Figure G-47. *EDS analysis of pipe S2 sample area 1.*

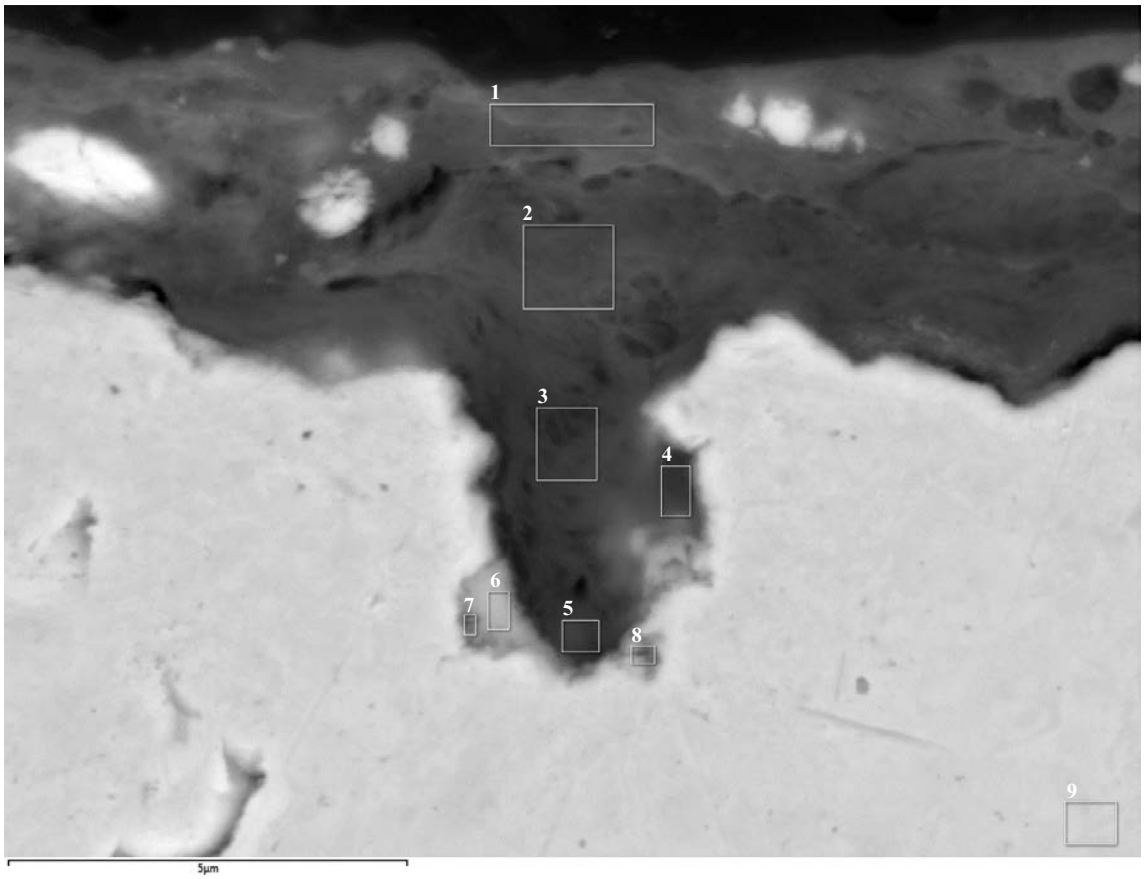

Element (At%)	1	2	3	4	5	6	7	8	9
O	47.50	59.46	56.49	43.36	44.28	38.63	29.20	28.71	0.74
Mg	1.65	1.37	1.63	1.34	1.31	0.79	0.38	0.72	
Al	8.24	6.28	7.43	5.51	5.81	3.48	1.94	2.26	
Si	21.37	16.59	20.16	13.57	11.99	6.87	4.11	5.03	
S	0.79	0.65	0.53	0.44	0.38	0.23	0.25	0.58	
Cl	0.22	0.13	0.32	0.36	0.37	1.92	1.88	0.70	
K	0.13	0.09	0.08						
Ca	2.24	4.62	0.41						
Ti			0.06						
Fe	0.84	0.56	0.70	0.50	0.48				
Cu	17.04	10.25	12.21	34.92	35.38	48.07	62.23	62.01	99.26
Total	100.00	100.00	100.00	100.00	100.00	100.00	100.00	100.00	100.00

Figure G-48. *EDS analysis of pipe S2 sample area 1.*

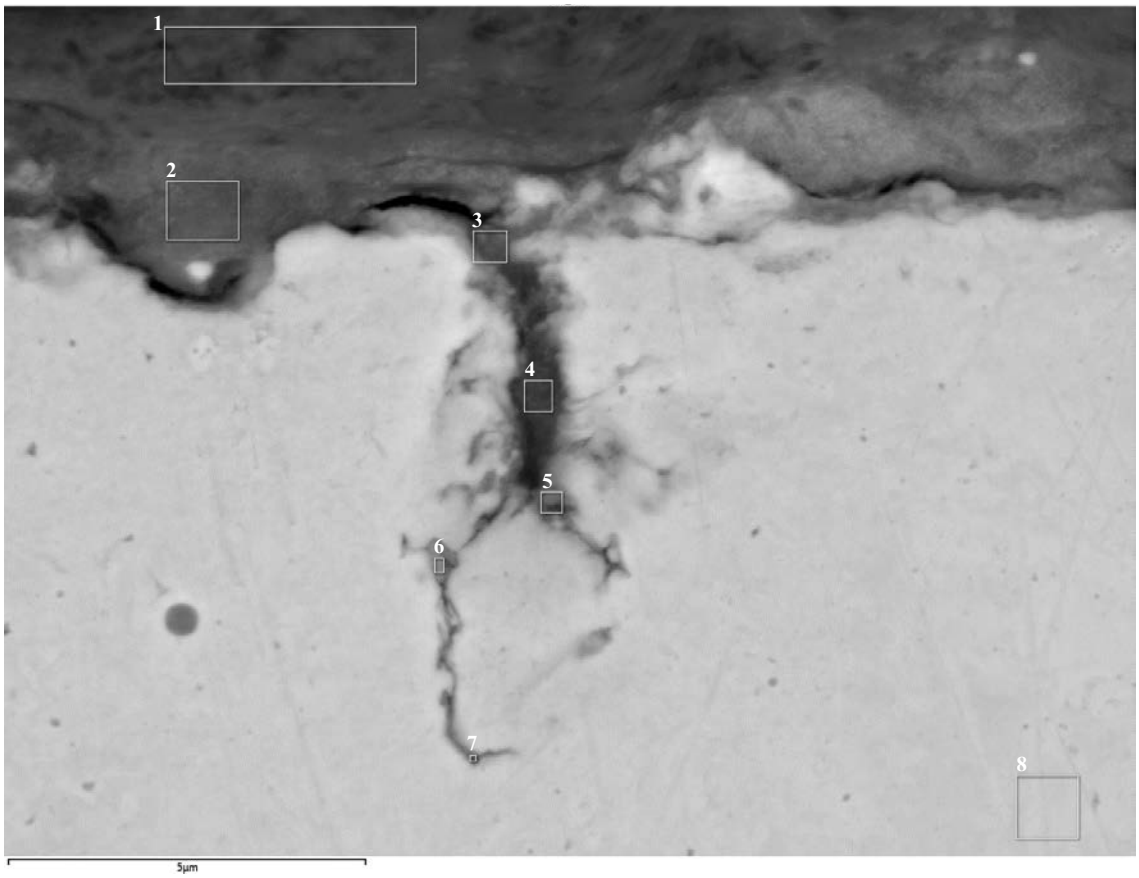

Element (At%)	1	2	3	4	5	6	7	8
O	67.23	48.16	36.24	41.80	38.14	24.33	9.91	0.64
Mg	1.07	1.35	1.25	1.38	0.87			
Al	3.56	5.48	4.90	5.87	5.32	0.94	0.58	
Si	8.43	18.61	12.85	15.90	13.21	2.17	1.60	
S	0.58	4.92	8.24	6.13	2.39	0.55	0.96	
Cl	0.07	0.18	0.31	0.27	0.79	2.23	0.84	
Ca	14.04	0.86	0.36	0.21				
Ti			0.30					
Mn	0.20							
Fe	0.73	0.51	0.39	0.68	0.64			
Cu	4.07	19.92	35.17	27.77	38.64	69.79	86.11	99.36
Total	100.00	100.00	100.00	100.00	100.00	100.00	100.00	100.00

Figure G-49. *EDS analysis of pipe S2 sample area 1.*

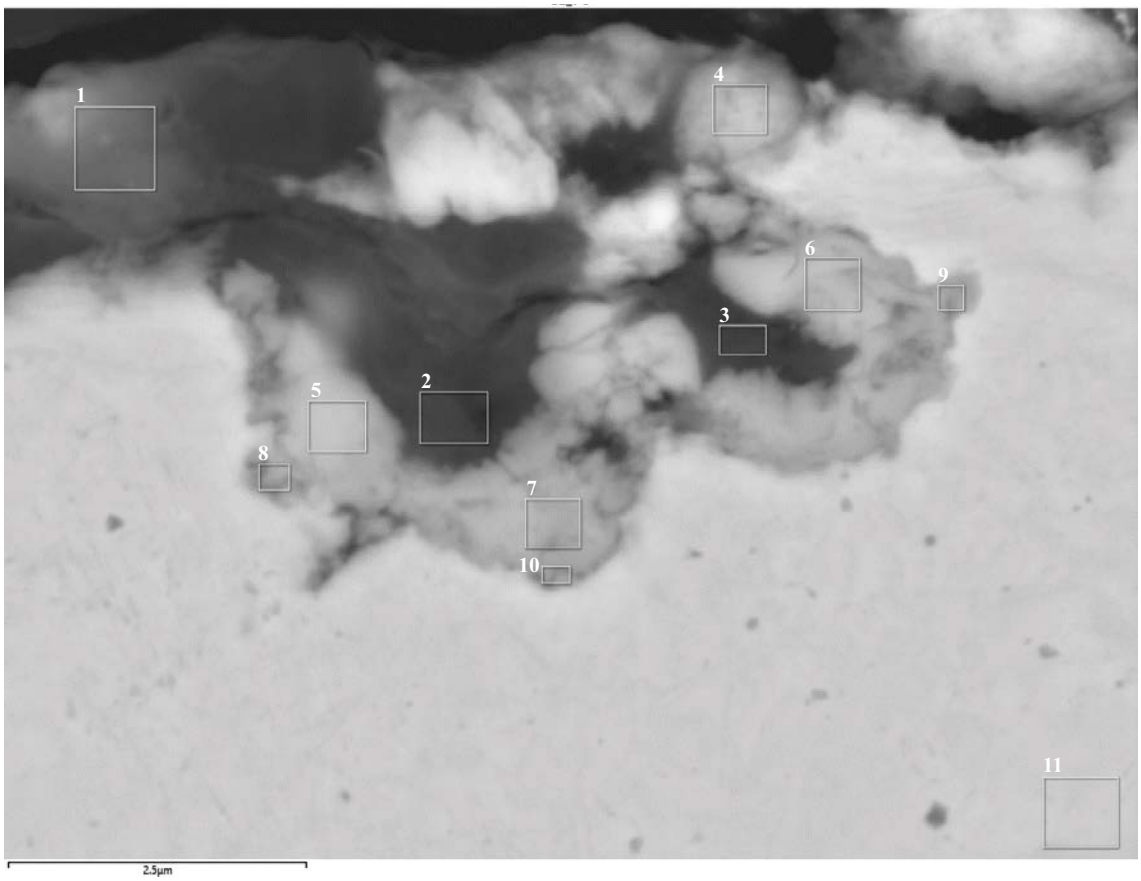

Element (At%)	1	2	3	4	5	6	7	8	9	10	11
O	48.58	50.11	48.10	36.79	35.64	32.53	34.23	25.11	18.53	26.17	0.93
Mg	1.02	0.91	1.02	0.38	0.43	0.30					
Al	3.30	3.52	5.39	0.89	1.11	1.54	0.93	0.56	0.35	0.29	
Si	19.46	21.71	20.82	4.78	4.91	3.98	5.27	1.71	1.10	1.70	
S	0.32	0.18	0.15	0.17		0.16			0.13		
Cl	0.30	1.28	1.10	2.74	3.08	3.20	2.94	2.70	1.62	2.91	
K	0.07										
Ca	0.45	0.26	0.23	0.22							
Fe	0.22	0.29	0.79								
Cu	24.84	21.74	22.41	54.03	54.84	58.29	56.64	69.93	78.27	68.93	99.07
Zn	1.45										
Total	100.00	100.00	100.00	100.00	100.00	100.00	100.00	100.00	100.00	100.00	100.00

Figure G-50. *EDS analysis of pipe S2 sample area 1.*

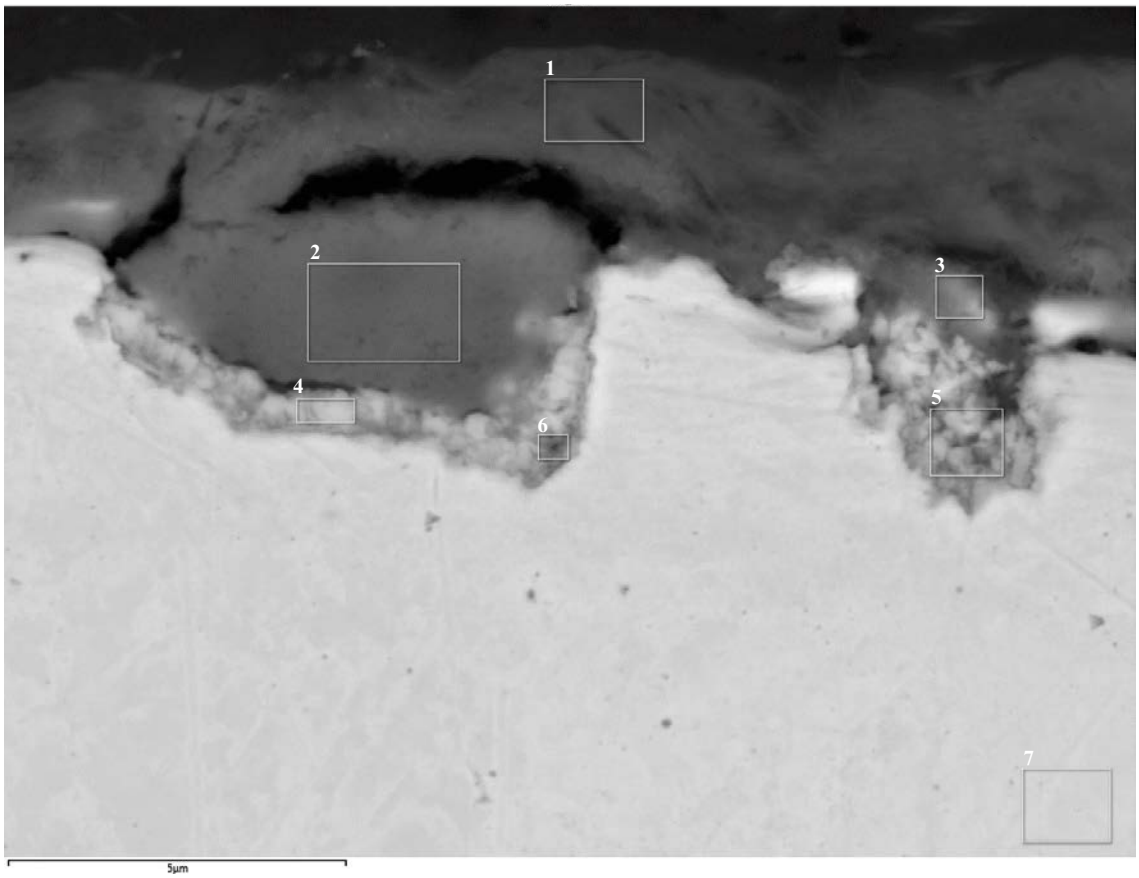

Element (At%)	1	2	3	4	5	6	7
O	49.69	53.71	43.85	38.25	35.87	26.96	1.11
Mg	1.87	0.26	1.19		0.49		
Al	10.26	0.45	4.96	0.76	1.40	0.60	
Si	28.11	23.46	12.90	5.64	3.78	1.45	
P				0.14		0.17	
S	0.83	1.45	3.26	0.30	1.08	0.27	
Cl		0.48	1.35	2.36	2.71	2.66	
K	0.36		0.19				
Ca	0.53	0.72	1.71	0.25	0.79	0.48	
Fe	1.02		0.28				
Cu	7.34	19.47	30.32	52.29	53.87	67.42	98.89
Total	100.00	100.00	100.00	100.00	100.00	100.00	100.00

Figure G-51. *EDS analysis of pipe S2 sample area 1.*

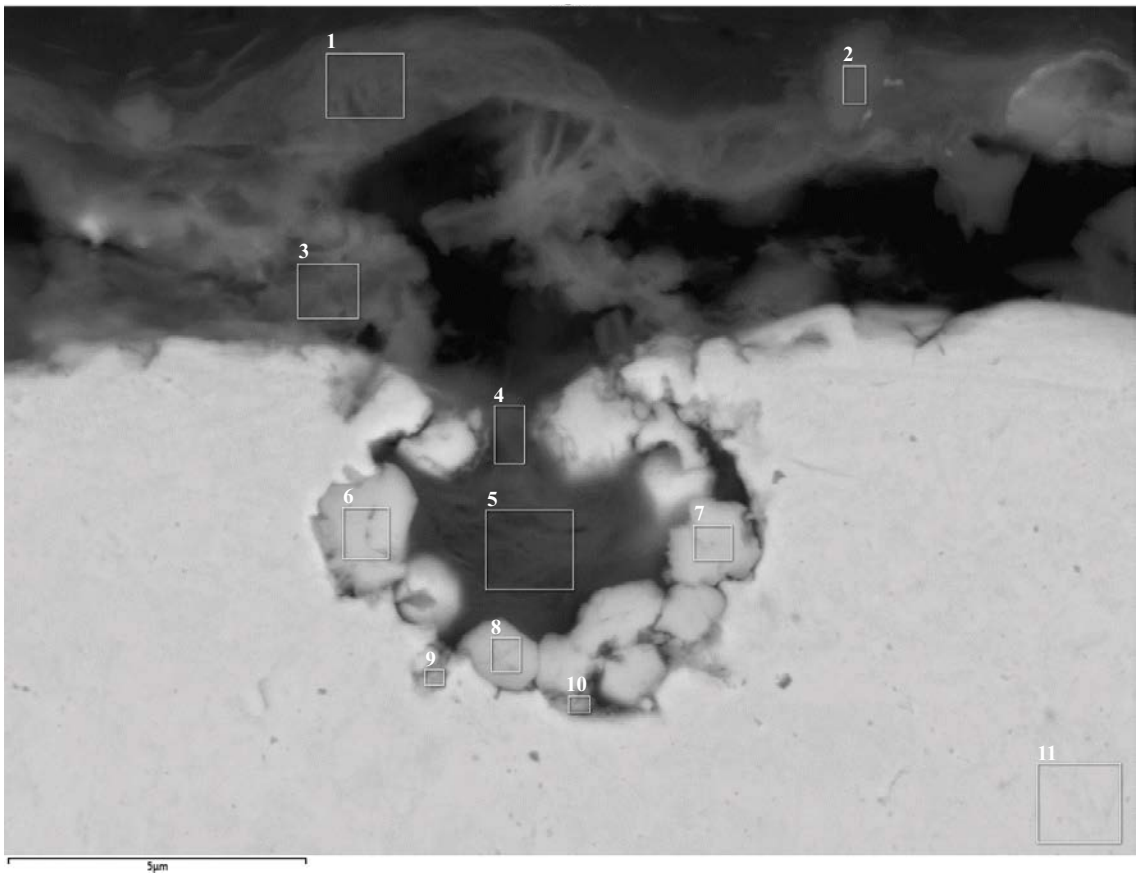

Element (At%)	1	2	3	4	5	6	7	8	9	10	11
O	46.43	60.53	54.09	54.35	58.82	30.35	33.13	38.25	24.92	33.74	0.77
Na	0.39		2.97								
Mg	1.88	1.06	0.25	1.23	1.63		0.32	0.62	0.51	0.68	
Al	10.47	4.68	1.28	5.46	8.02	0.76	1.29	2.36	1.71	2.68	
Si	28.29	28.78	3.99	14.97	20.62	1.28	2.49	4.71	3.54	6.14	
S	2.06	0.20	12.02	1.76	0.32		0.12		0.14	0.16	
Cl	0.17		0.09	0.59	0.36	3.84	3.44	2.55	0.85	1.90	
K	0.49	0.12	0.67	0.19	0.26						
Ca	2.15	0.25	10.75	1.39	0.42		0.13	0.10		0.22	
Fe	1.33	0.51	0.15	0.53	0.82					0.32	
Cu	6.35	3.88	13.76	19.51	8.74	63.78	59.08	51.40	68.33	54.16	99.23
Total	100.00	100.00	100.00	100.00	100.00	100.00	100.00	100.00	100.00	100.00	100.00

Figure G-52. *EDS analysis of pipe S2 sample area 1.*

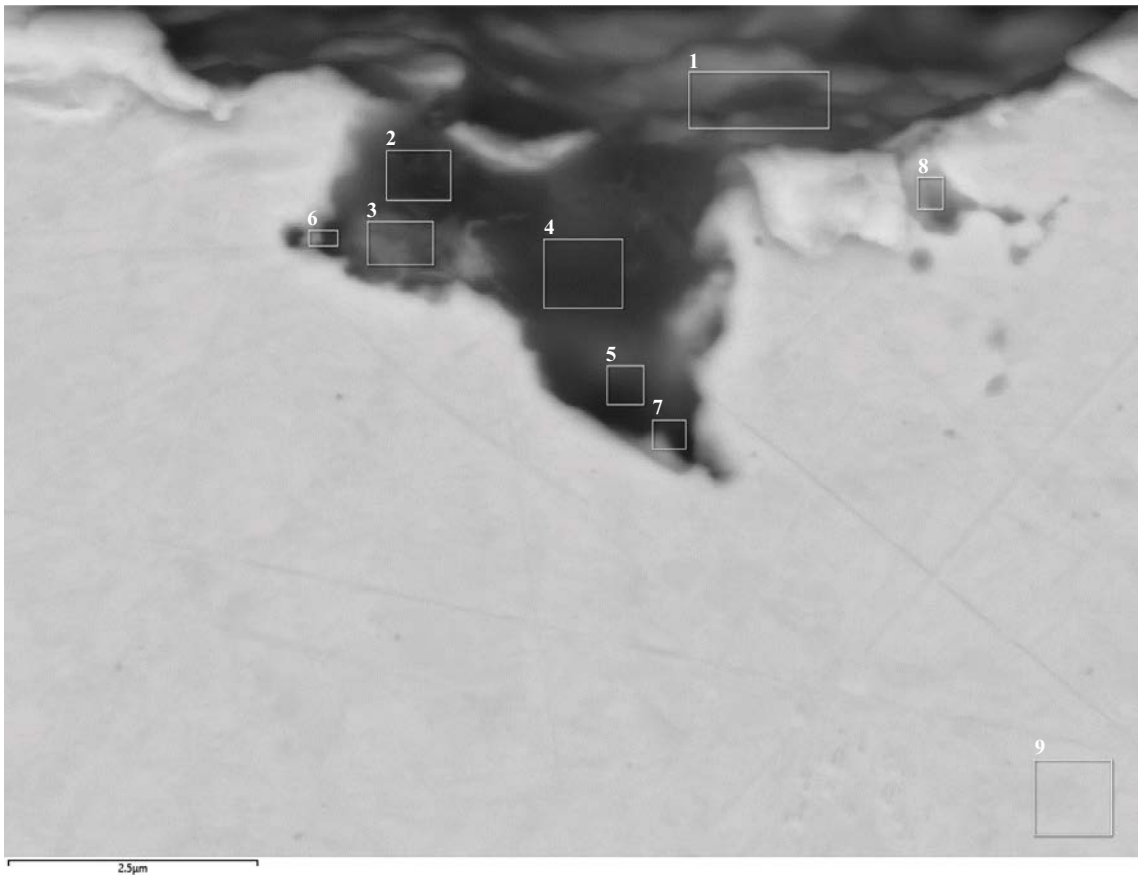

Element (At%)	1	2	3	4	5	6	7	8	9
O	12.04	32.00	42.33	27.43	21.73	26.87	17.28	6.65	0.70
Mg	0.65	0.86	1.04	0.98	0.86	0.56			
Al	1.22	1.65	0.55	4.91	0.59	0.43			
Si	3.54	5.89	1.39	6.08	0.96	0.59	0.36	0.29	
P		0.71	6.47	0.82	0.51	3.82	0.48		
S	1.84	1.42	2.76	1.87	0.55	1.44	0.55	0.65	
Cl		0.16	0.15						
K		0.14		0.36					
Ca	0.29	0.74	5.52	0.51	0.34	3.80	0.49	0.18	
Cu	80.42	56.43	39.79	57.03	74.47	62.48	80.84	92.23	99.30
Total	100.00	100.00	100.00	100.00	100.00	100.00	100.00	100.00	100.00

Figure G-53. *EDS analysis of pipe S2 sample area 1.*

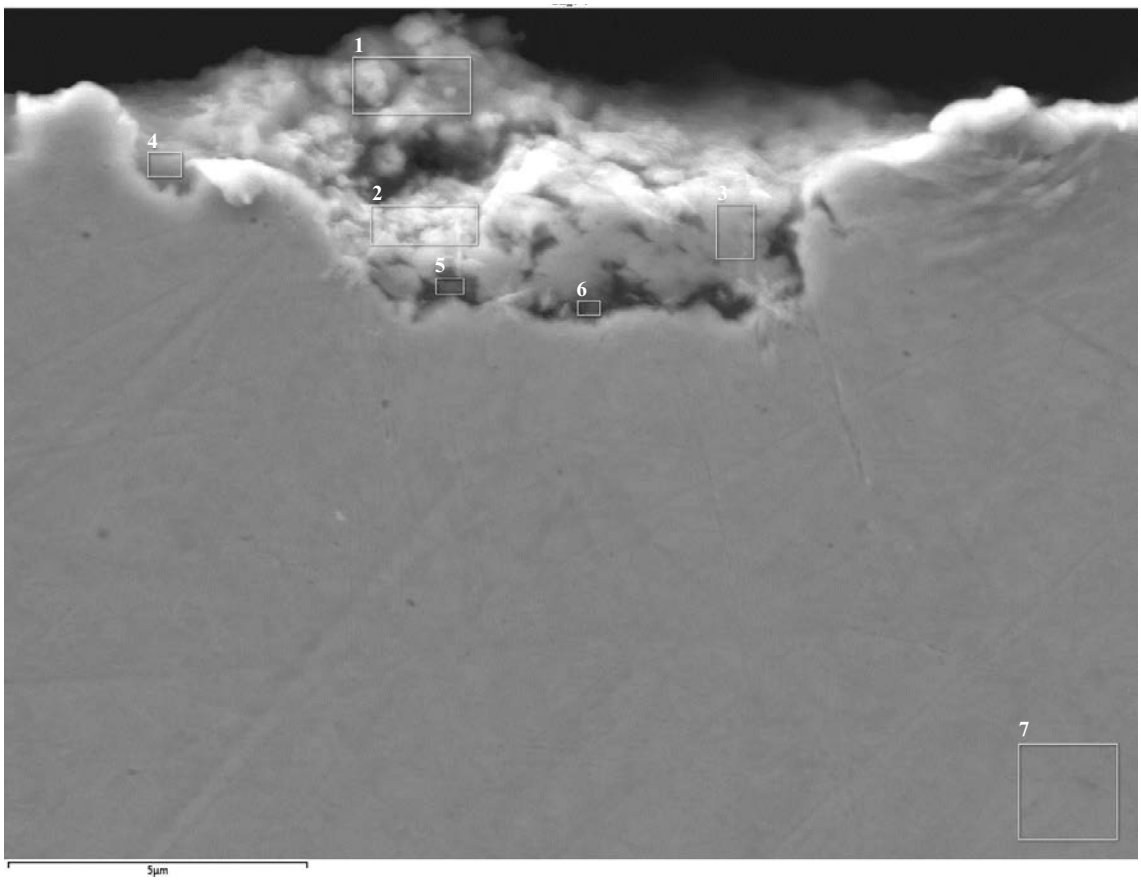

Element (At%)	1	2	3	4	5	6	7
O	20.42	12.58	7.32	37.23	22.02	22.35	0.76
Mg		0.22		1.33	0.57	0.57	
Al	0.78	0.37	0.70	4.61	2.72	2.88	
Si	5.08	2.44	2.19	10.34	6.30	6.00	
P					0.19		
S	20.80	23.17	26.26	2.20	17.86	16.09	
K				0.08		0.09	
Ca	0.20	0.19	0.12	0.29	0.24	0.24	
Fe	0.31	0.26	0.32	0.36	0.39	0.49	
Cu	52.41	60.77	63.09	43.57	49.72	51.29	99.24
Total	100.00	100.00	100.00	100.00	100.00	100.00	100.00

Figure G-54. *EDS analysis of pipe S2 sample area 1.*

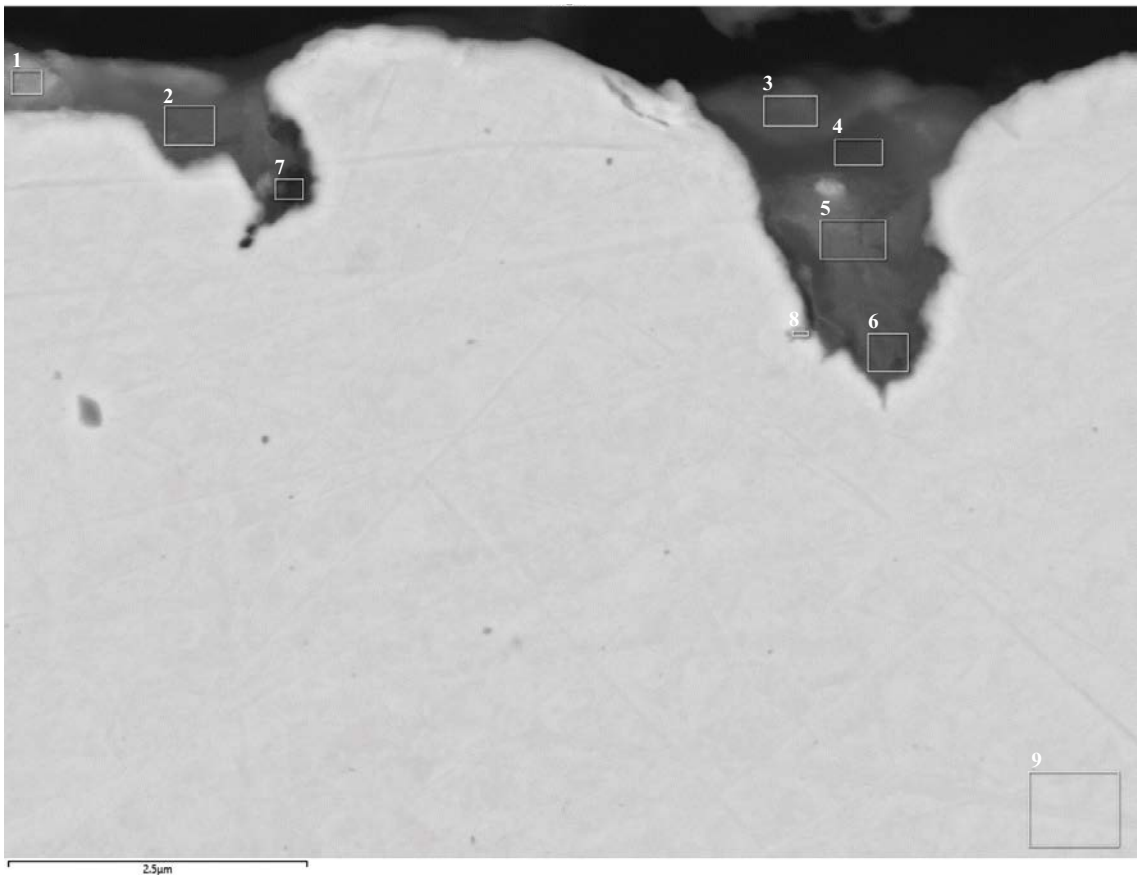

Element (At%)	1	2	3	4	5	6	7	8	9
O	25.83	52.03	43.32	59.63	55.42	42.25	38.52	11.68	0.90
Mg	0.65	1.31	1.88	0.92	1.33	1.42	0.93		
Al	2.65	5.81	5.52	3.51	6.80	7.03	3.10	1.21	
Si	5.73	14.52	16.86	20.11	17.92	14.45	6.64	2.66	
S	8.90	1.82	5.49	0.71	0.50	0.94	3.27	0.75	
Cl		0.08					0.10		
Ca	0.22	0.25	0.75	0.27	0.39	0.36	6.72	0.13	
Fe	0.29	0.39	0.62	0.26	0.55	0.51			
Cu	55.73	23.79	25.57	14.59	17.10	33.05	40.72	83.58	99.10
Total	100.00	100.00	100.00	100.00	100.00	100.00	100.00	100.00	100.00

Figure G-55. *EDS analysis of pipe S2 sample area 1.*

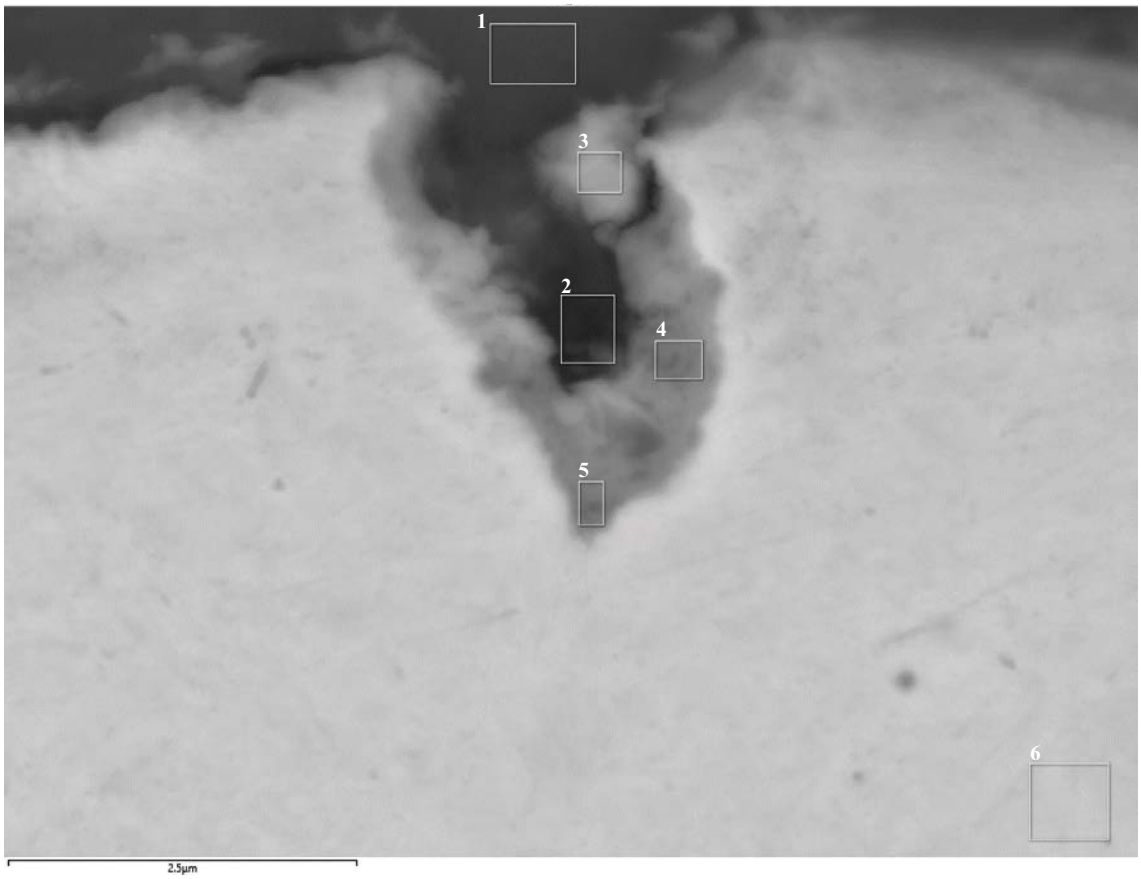

Element (At%)	1	2	3	4	5	6
O	66.58	57.56	50.05	46.81	41.47	1.85
Mg	0.17	0.94	0.43	0.45	0.23	
Al	0.66	6.77	1.64	2.46	0.34	
Si	23.50	15.96	8.23	5.83	0.59	0.53
P		0.12	0.12	0.75	0.58	
S	0.38	1.32	2.80	2.71	1.99	
Cl	0.07	0.06	0.07	0.08	0.13	
Ca	2.43	0.41	0.29	0.90	0.71	
Fe		0.64				
Cu	6.21	16.22	36.38	40.01	53.95	97.62
Total	100.00	100.00	100.00	100.00	100.00	100.00

Figure G-56. *EDS analysis of pipe S2 sample area 1.*

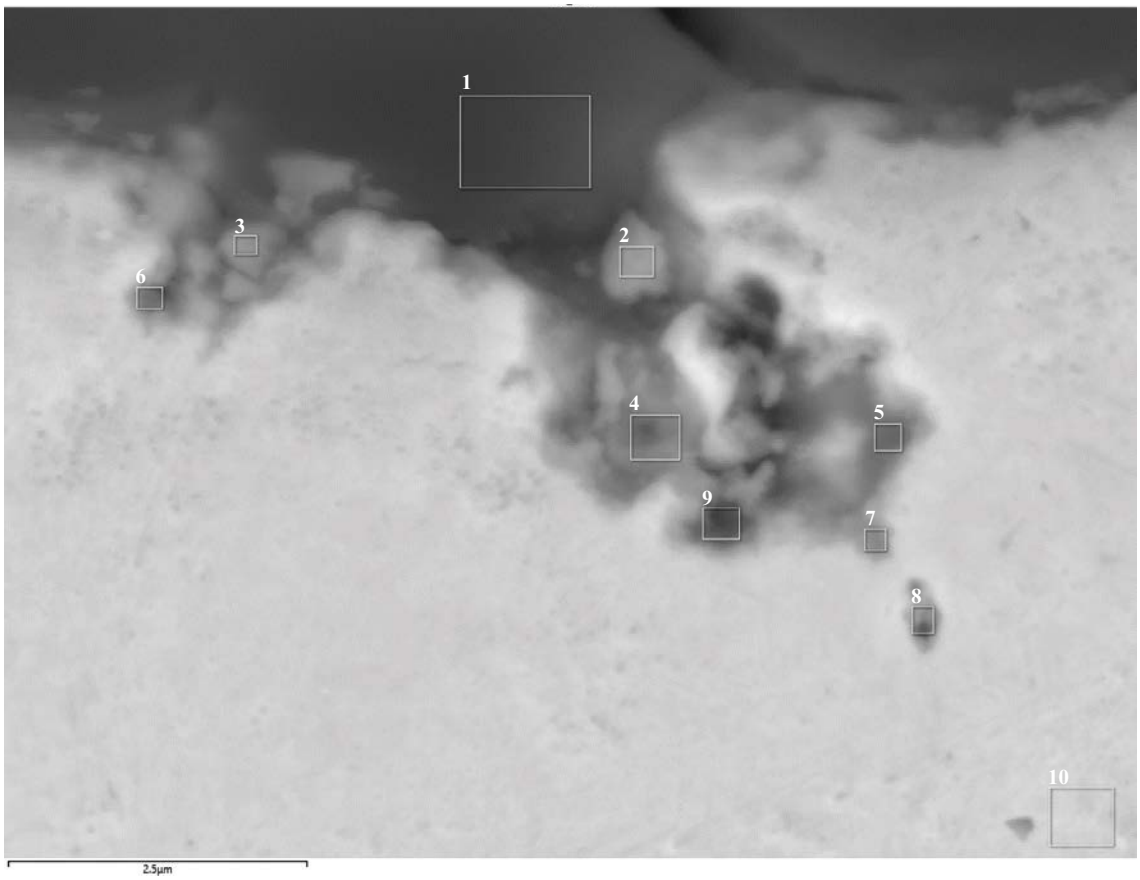

Element (At%)	1	2	3	4	5	6	7	8	9	10
O	67.85	47.37	36.11	42.76	26.41	21.44	17.96	10.92	34.18	2.73
Mg	0.22	0.32		0.65	0.41				0.75	
Al	0.85	0.65		0.16						
Si	16.17	4.74	2.39	1.12	0.78	1.71	0.46	0.29	0.35	0.89
P							1.00	0.33		
S	0.25	0.87	1.23	1.22	0.65	0.59	0.70	0.14	0.90	
Cl	0.06	0.34	0.25	0.11					0.11	
Ca	2.88	0.96	0.31	0.97	0.94	0.38	0.16	0.35	1.23	
Cu	11.73	44.76	59.72	53.00	70.80	75.89	79.72	87.97	62.48	96.38
Total	100.00	100.00	100.00	100.00	100.00	100.00	100.00	100.00	100.00	100.00

Figure G-57. *EDS analysis of pipe S2 sample area 1.*

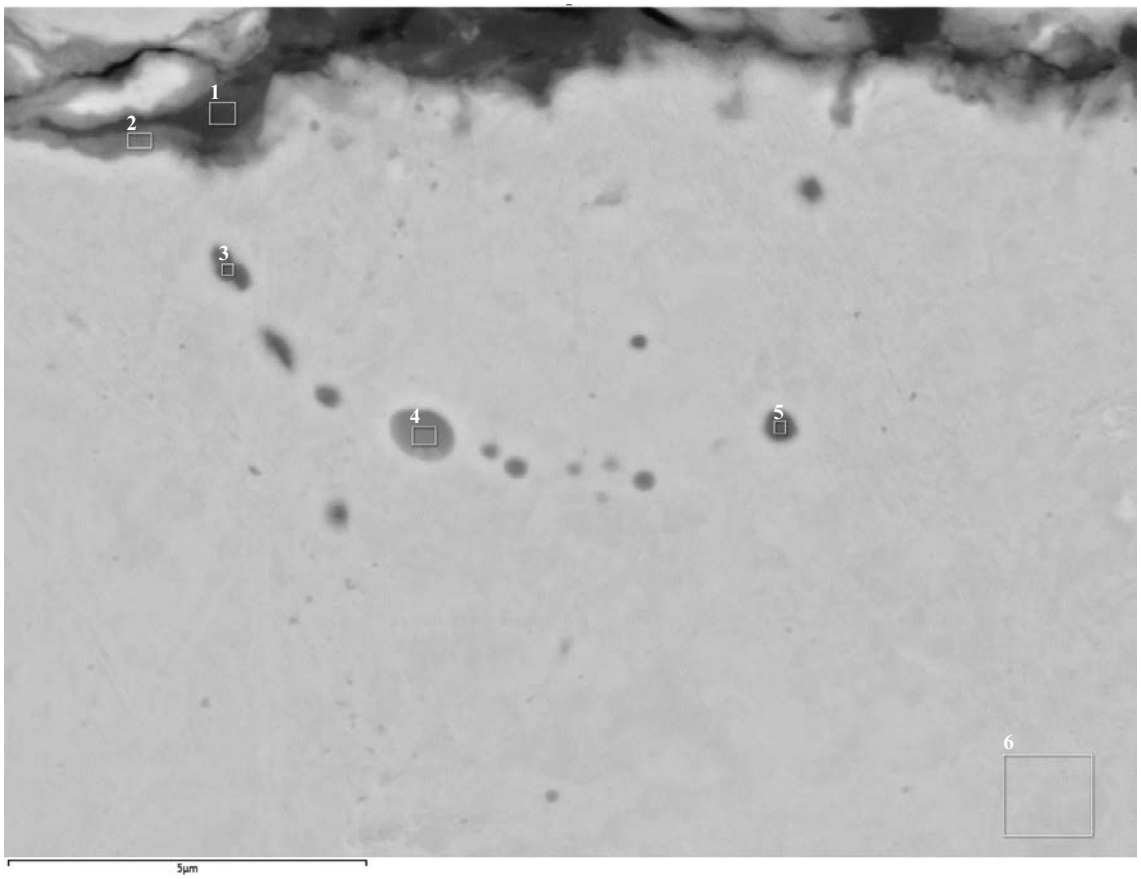

Element (At%)	1	2	3	4	5	6
O	55.84	43.23	29.52	35.28	36.40	0.83
Mg	1.22	0.33				
Al	6.28	1.45				
Si	15.09	4.20	0.22			
P			1.64	7.87	10.13	
S	0.35	0.34	0.31	0.41		
Cl	0.09	0.14	0.13			
Ca	0.86		2.69			
Fe	0.94					
Cu	19.33	50.32	65.48	56.44	53.47	99.17
Total	100.00	100.00	100.00	100.00	100.00	100.00

Figure G-58. *EDS analysis of pipe S2 sample area 1.*

Pipe S2 – inner surface

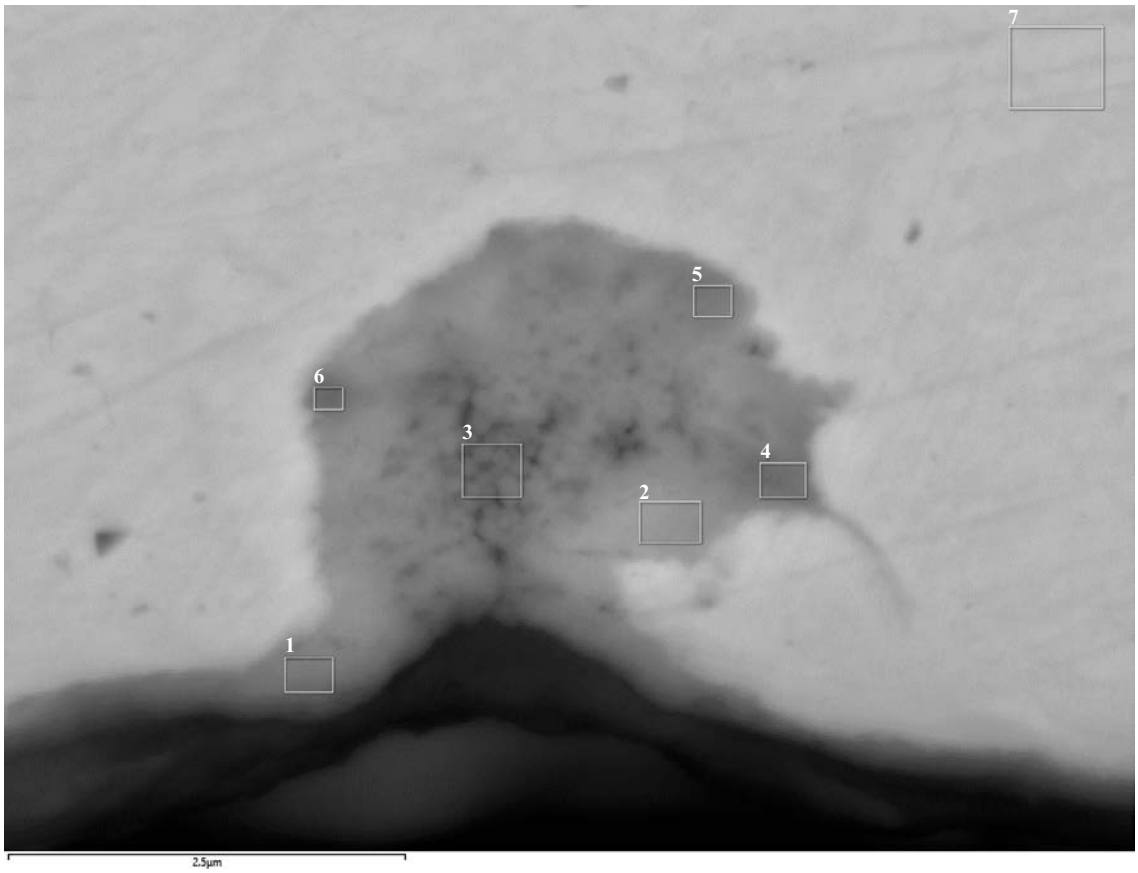

Element (At%)	1	2	3	4	5	6	7
O	43.87	46.89	47.45	40.56	32.73	33.16	0.79
Al	0.76						
Si	2.71		1.17				
S		0.12	0.33				
Cl	0.53	0.63	0.64	0.58	0.51	0.56	
Cu	52.13	52.37	50.42	58.85	66.76	66.28	99.21
Total	100.00	100.00	100.00	100.00	100.00	100.00	100.00

Figure G-59. *EDS analysis of pipe S2 inner surface.*

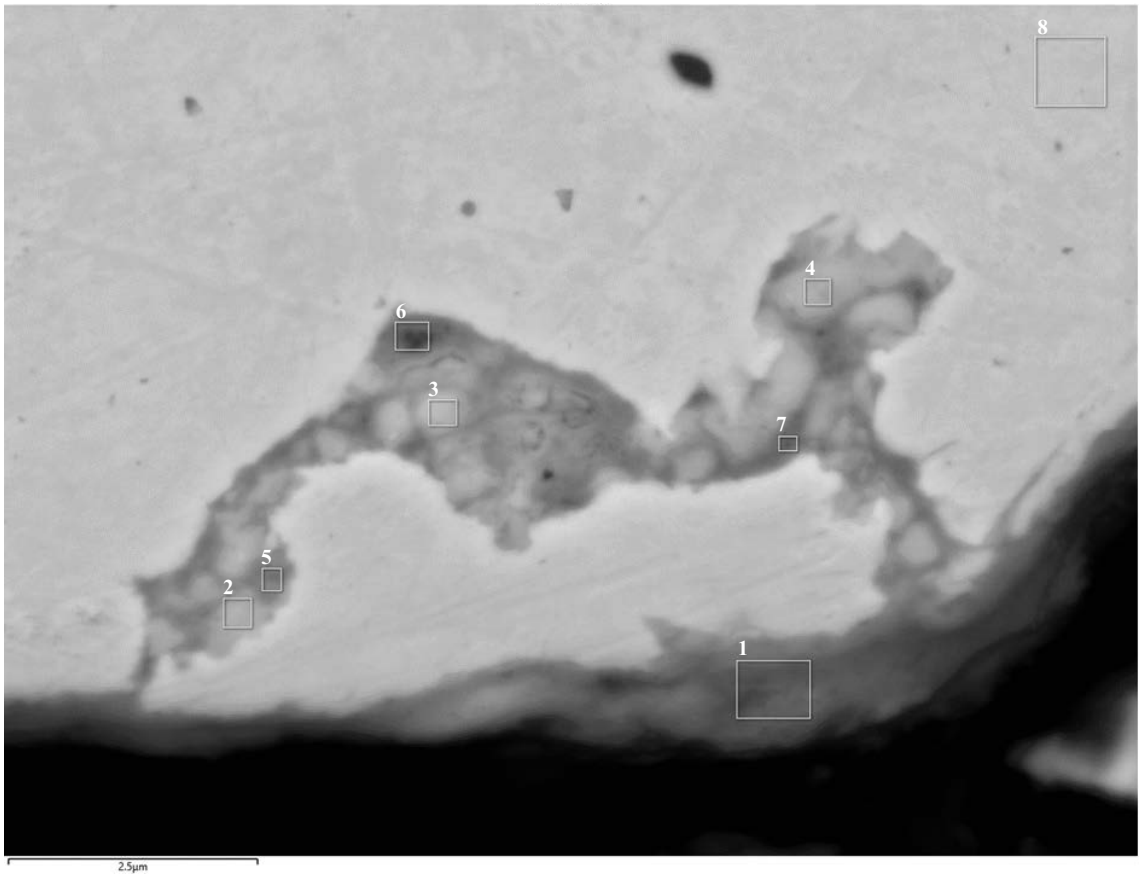

Element (At%)	1	2	3	4	5	6	7	8
O	52.51	33.80	40.86	32.84	34.79	33.77	38.21	0.99
Al	1.39							
Si	6.43							
Cl		0.48	0.35	0.27	0.48	0.52	0.58	
Cu	39.67	65.72	58.79	66.89	64.73	65.71	61.21	99.01
Total	100.00	100.00	100.00	100.00	100.00	100.00	100.00	100.00

Figure G-60. *EDS analysis of pipe S2 inner surface.*

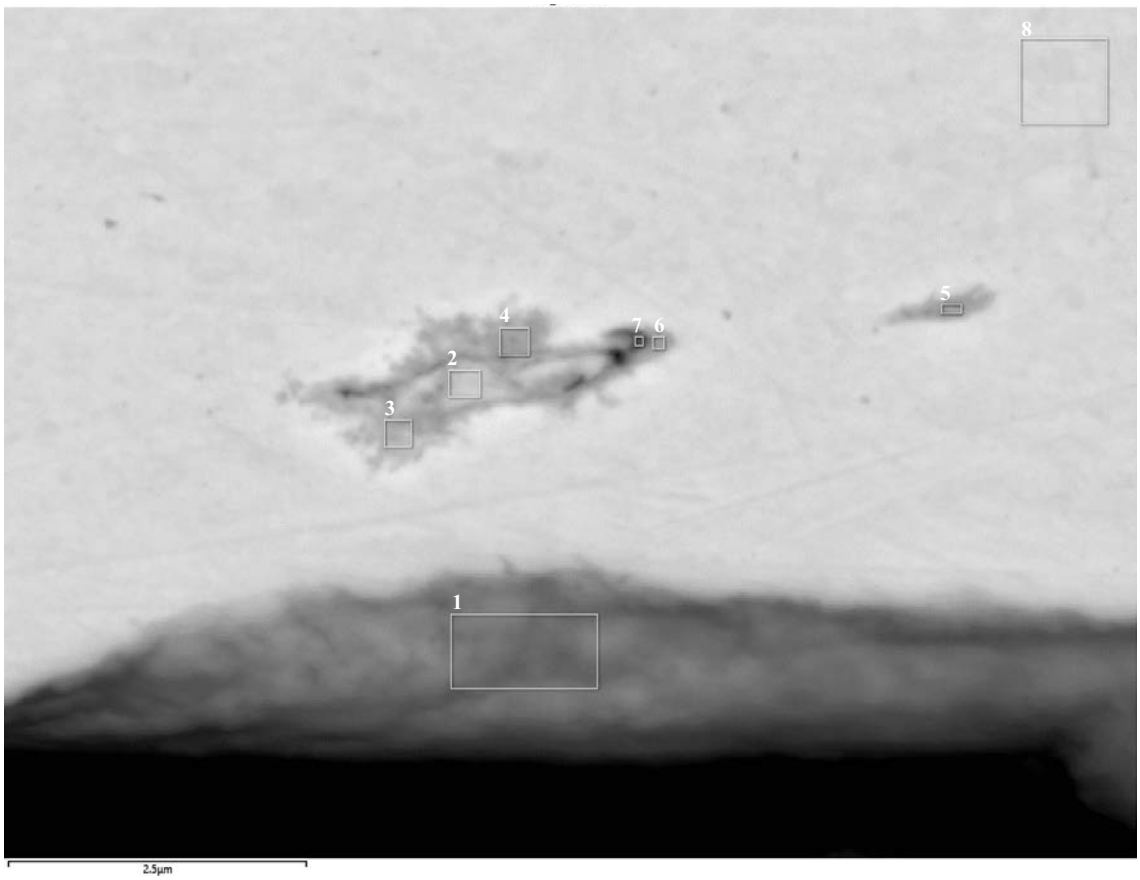

Element (At%)	1	2	3	4	5	6	7	8
O	44.58	15.02	16.83	19.05	12.02	15.76	12.06	0.77
Mg	1.84							
Al	3.34							
Si	8.54	0.37		0.22				
Cl		0.20	0.19	0.26				
Ca	2.61		0.14			0.21	0.31	
Cu	39.09	84.42	82.84	80.46	87.98	84.04	87.63	99.23
Total	100.00	100.00	100.00	100.00	100.00	100.00	100.00	100.00

Figure G-61. *EDS analysis of pipe S2 inner surface.*

PIpe S2 sample 2

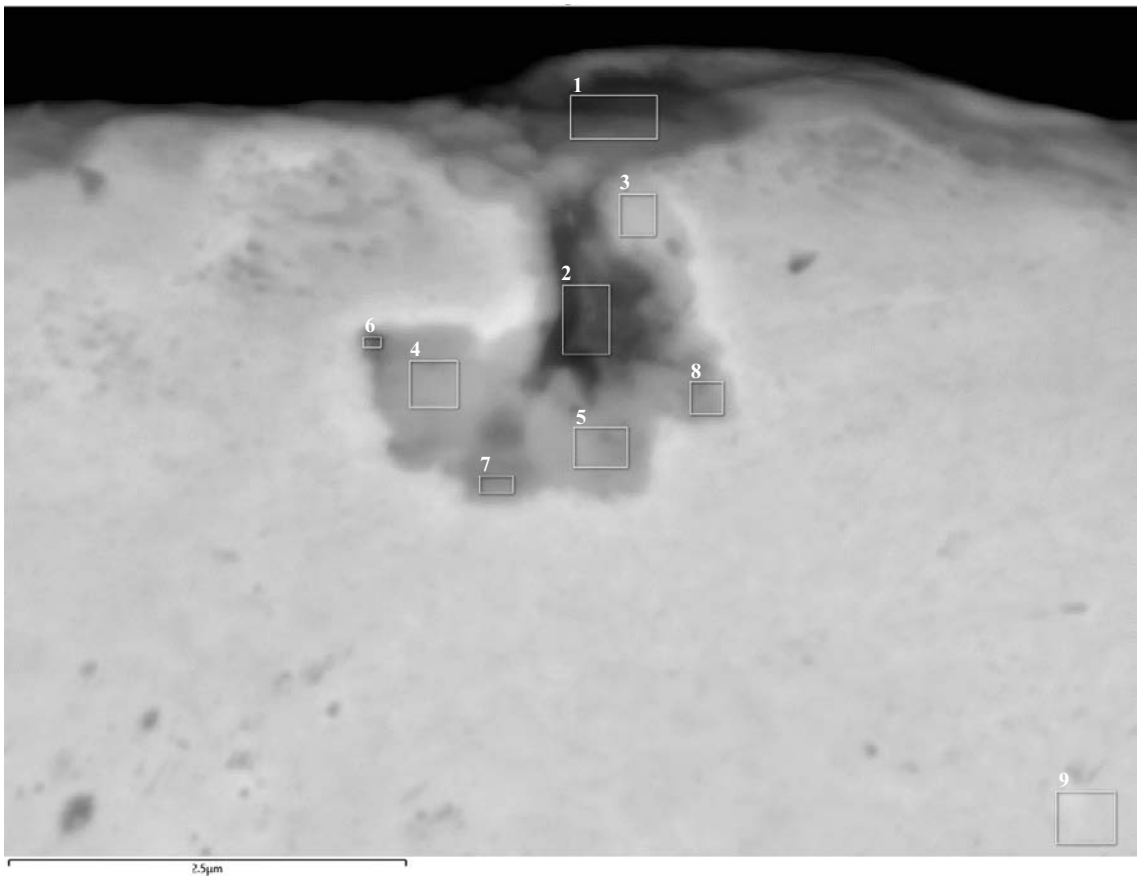

Element (At%)	1	2	3	4	5	6	7	8	9
O	58.44	45.33	29.33	27.98	30.45	19.01	30.10	23.28	0.82
Mg	0.48	0.23							
Al	1.18	5.56	0.66	0.19	0.81			0.30	
Si	13.04	6.00	1.74	0.31	0.79	0.54	0.24	0.85	
S	3.04	2.29	1.21	0.58	0.80	0.16	1.00	0.59	
Cl	0.04	0.36	0.31	3.33	2.13	1.22	1.14	0.40	
Ca	0.39				0.15				
Cu	23.39	40.23	66.76	67.60	64.88	79.08	67.52	74.58	99.18
Total	100.00	100.00	100.00	100.00	100.00	100.00	100.00	100.00	100.00

Figure G-62. *EDS analysis of pipe S2 sample area 2.*

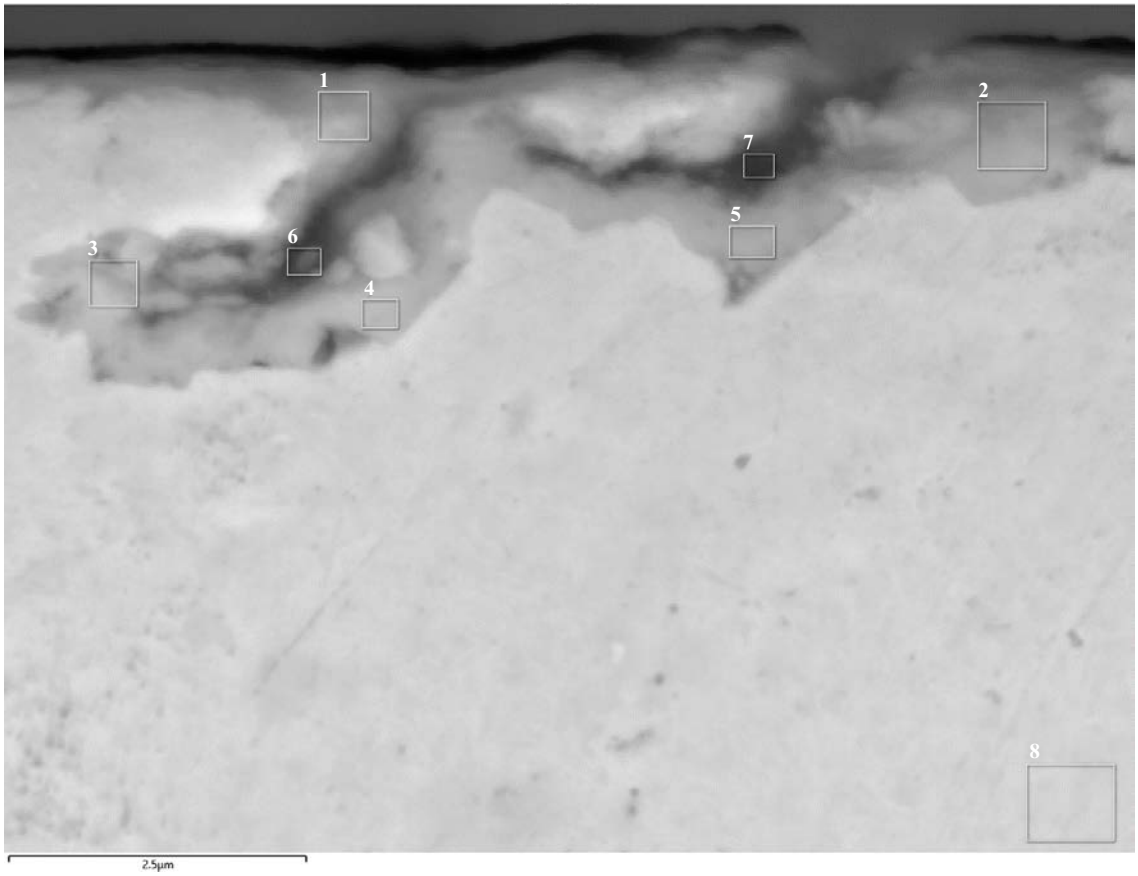

Element (At%)	1	2	3	4	5	6	7	8
O	33.29	31.62	25.52	25.75	29.96	34.59	44.36	0.87
Mg					0.36	0.60	1.06	
Al	0.36		0.48	0.30	0.55	2.88	4.09	
Si	3.91	2.25	2.51	0.52	1.33	7.76	10.78	
S	0.80	0.49	2.25	0.96	1.83	3.75	2.80	
Cl	0.30	0.90	0.61	0.62	1.55	0.98	0.50	
Ca						0.14	0.91	
Fe						0.30	0.43	
Cu	61.34	64.73	68.63	71.84	64.42	48.99	35.08	99.13
Total	100.00	100.00	100.00	100.00	100.00	100.00	100.00	100.00

Figure G-63. *EDS analysis of pipe S2 sample area 2.*

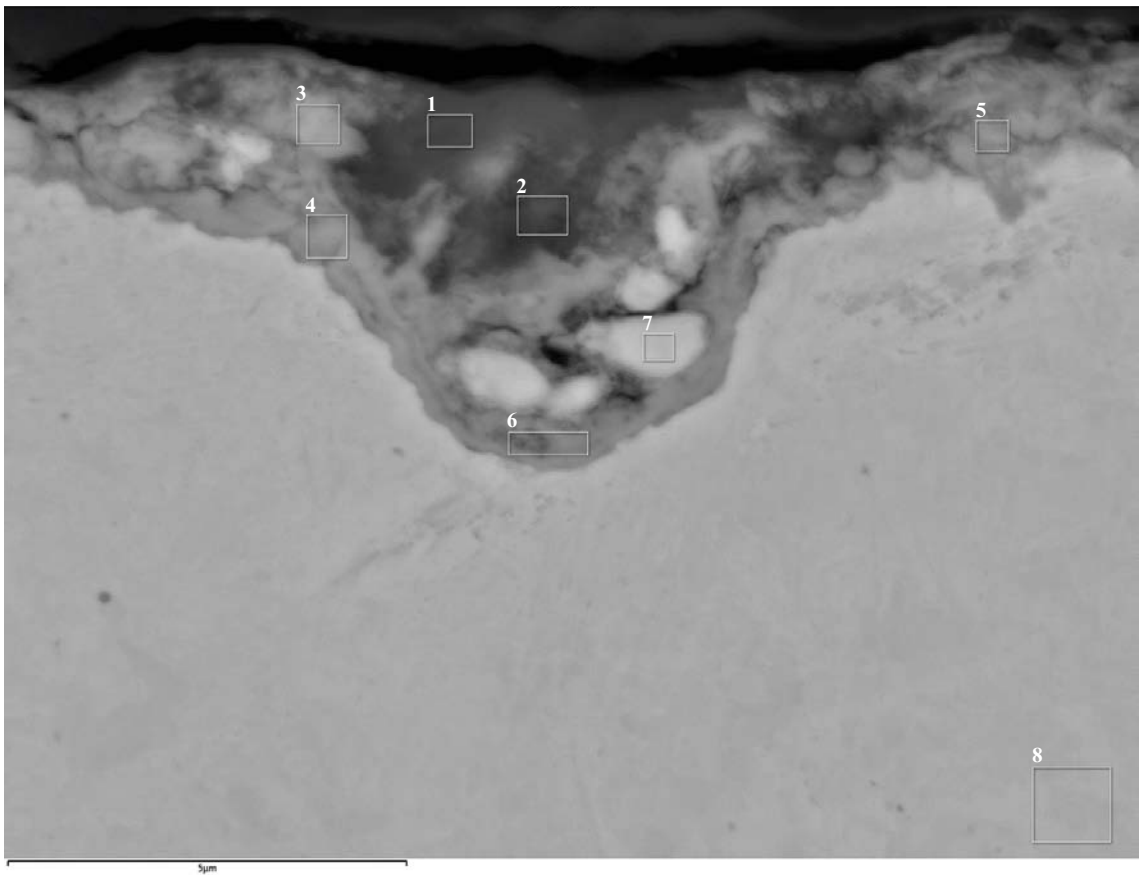

Element (At%)	1	2	3	4	5	6	7	8
O	57.29	52.09	43.46	42.56	49.62	40.23	10.75	0.80
Mg	1.62	1.51	0.64	0.60	0.44			
Al	7.53	5.66	2.20	1.05	1.55			
Si	18.97	15.24	5.56	3.34	5.00	2.29	1.27	
S	1.77	2.72	6.09	0.57	0.26	0.43		
Cl				0.25	0.09	0.15		
K	0.32	0.07	0.12					
Ca	0.73	1.95	0.58	0.42	0.79	0.41		
Fe	0.79	0.58						
Cu	10.98	20.18	41.36	51.21	42.26	56.49	87.98	99.20
Total	100.00	100.00	100.00	100.00	100.00	100.00	100.00	100.00

Figure G-64. *EDS analysis of pipe S2 sample area 2.*

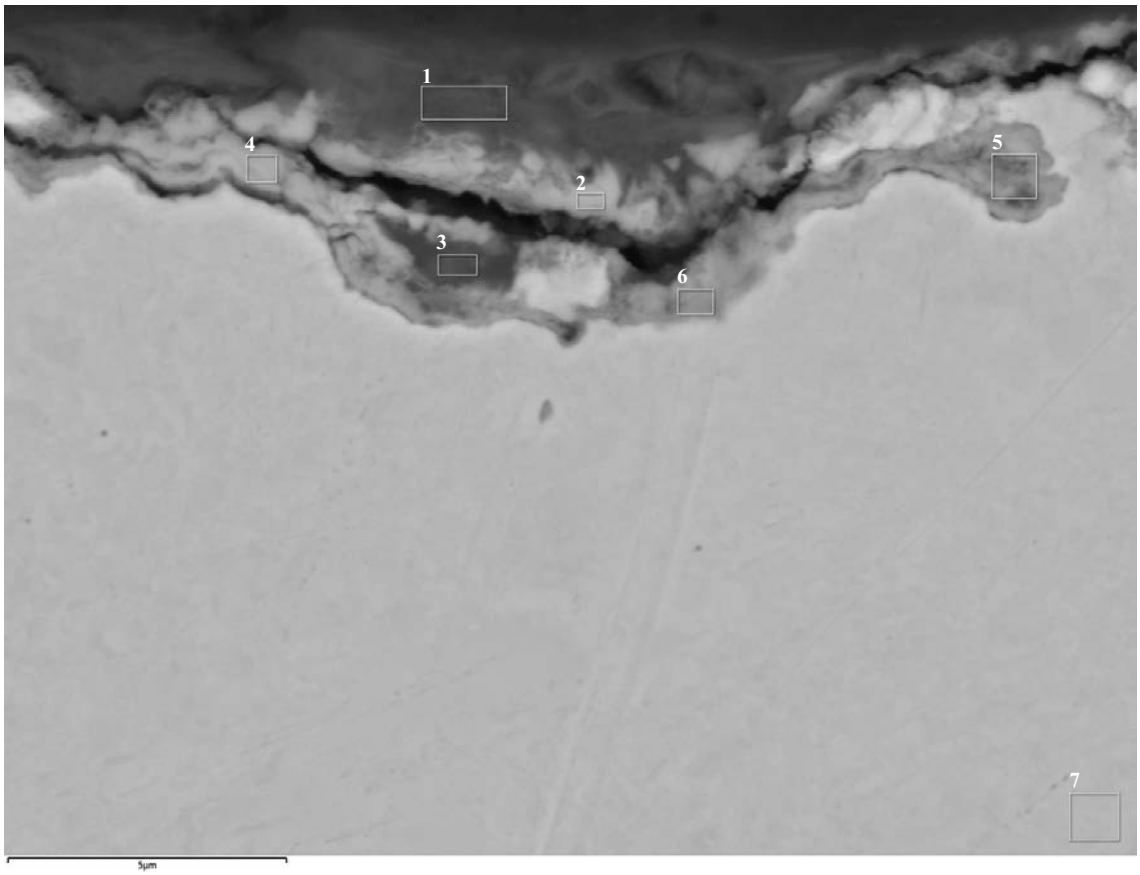

Element (At%)	1	2	3	4	5	6	7
O	54.28	52.89	52.18	46.49	43.87	45.91	1.15
Mg	1.51	0.31	0.29			0.31	
Al	9.39	0.99	2.05	0.44	0.46	0.45	
Si	18.93	3.15	9.64	1.75	2.23	2.88	
S	0.27	0.31	0.48	0.40	0.26	0.44	
Cl				0.18	0.14	0.18	
K	0.10		0.09	0.09			
Ca	2.91	1.02	2.80	0.33	1.40	1.79	
Fe	0.61						
Cu	12.00	41.33	32.46	50.31	51.63	48.04	98.85
Total	100.00	100.00	100.00	100.00	100.00	100.00	100.00

Figure G-65. *EDS analysis of pipe S2 sample area 2.*

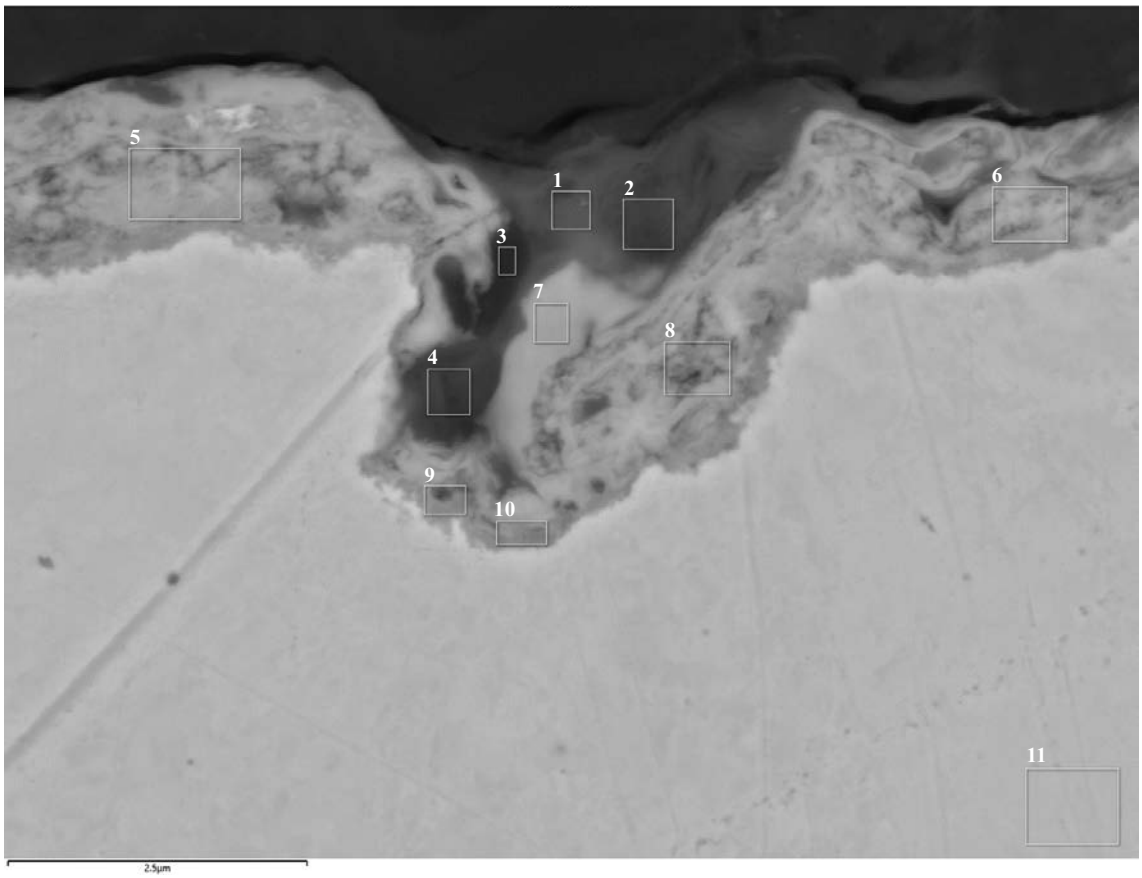

Element (At%)	1	2	3	4	5	6	7	8	9	10	11
O	56.90	59.55	45.43	55.79	27.19	24.61	47.75	26.01	30.49	27.06	1.08
Na	0.42	0.45									
Mg	1.54	1.53	1.14	1.08	0.29	0.59	0.44	0.36	0.42		
Al	4.66	5.82	5.04	7.26	1.75	1.58	1.30	1.76	0.77	0.63	
Si	22.95	19.61	14.33	19.66	4.72	4.19	3.53	5.03	2.87	1.21	
P							0.14		0.12		
S	0.48	0.50	1.70	0.24	12.55	15.10	0.28	16.32	0.96	1.35	
Cl	0.06		0.57	0.38	0.62	0.16	0.14	0.23	0.89	0.68	
K				0.20							
Ca	0.23	0.23	0.31	0.51	0.13	0.19	0.10	0.26			
Fe	0.46	0.55	0.48	0.61							
Cu	12.30	11.76	31.00	14.29	52.74	53.57	46.31	50.04	63.50	69.07	98.92
Total	100.00	100.00	100.00	100.00	100.00	100.00	100.00	100.00	100.00	100.00	100.00

Figure G-66. *EDS analysis of pipe S2 sample area 2.*

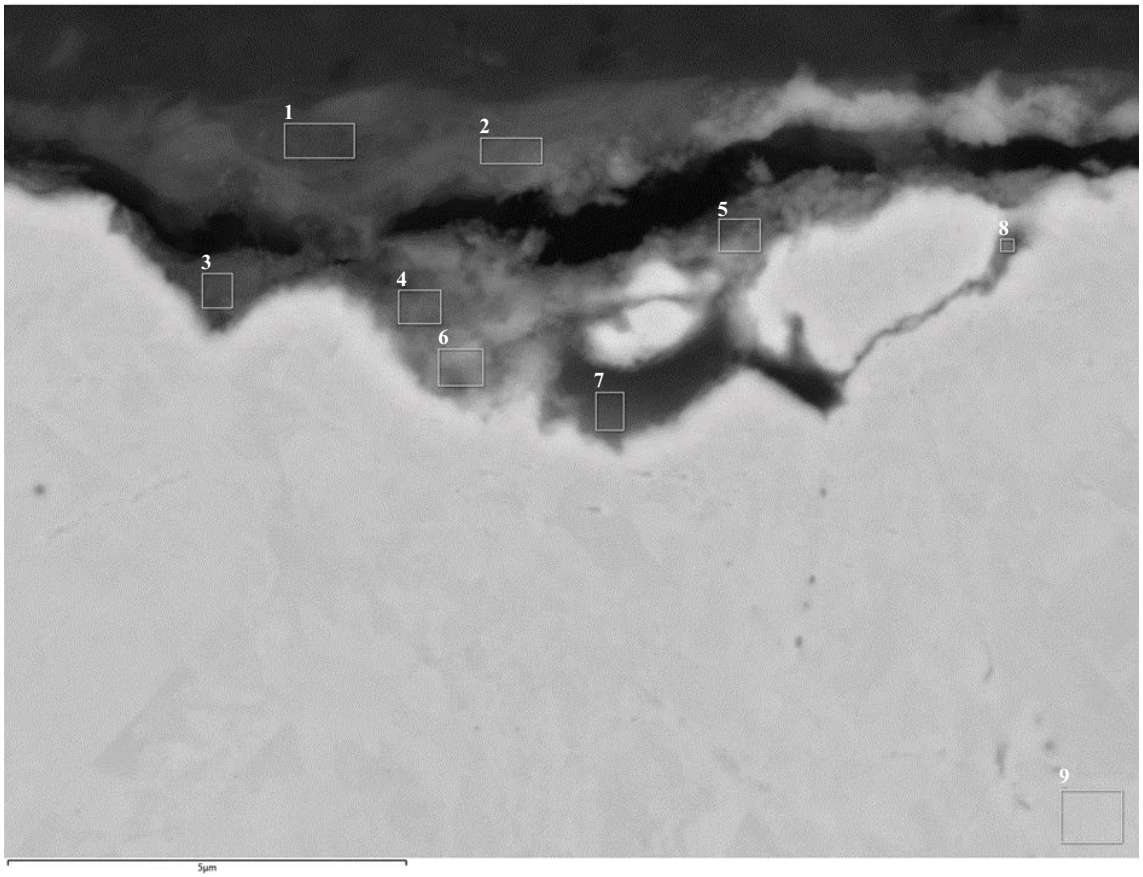

Element (At%)	1	2	3	4	5	6	7	8	9
O	53.57	52.86	54.12	49.07	40.99	35.57	20.75	31.10	1.19
Na			4.79						
Mg	1.17	1.52	0.72	0.88	0.79	0.73		0.40	
Al	5.97	6.03	6.24	3.08	1.60	2.05		0.46	
Si	27.29	14.68	15.98	12.14	5.57	5.59	0.51	1.52	
P								2.08	
S	0.38	1.40	0.25	0.93	3.59	0.84	0.51	1.93	
Cl	0.09	0.12		0.09	0.09	0.22		0.16	
Ca	2.13	5.34	1.36	1.10	3.79	0.58	0.39	2.69	
Fe	0.49	0.64	0.17	0.24		0.32		0.38	
Cu	8.91	17.41	16.38	32.46	43.57	54.10	77.84	58.30	98.81
Sn								0.97	
Total	100.00	100.00	100.00	100.00	100.00	100.00	100.00	100.00	100.00

Figure G-67. *EDS analysis of pipe S2 sample area 2.*

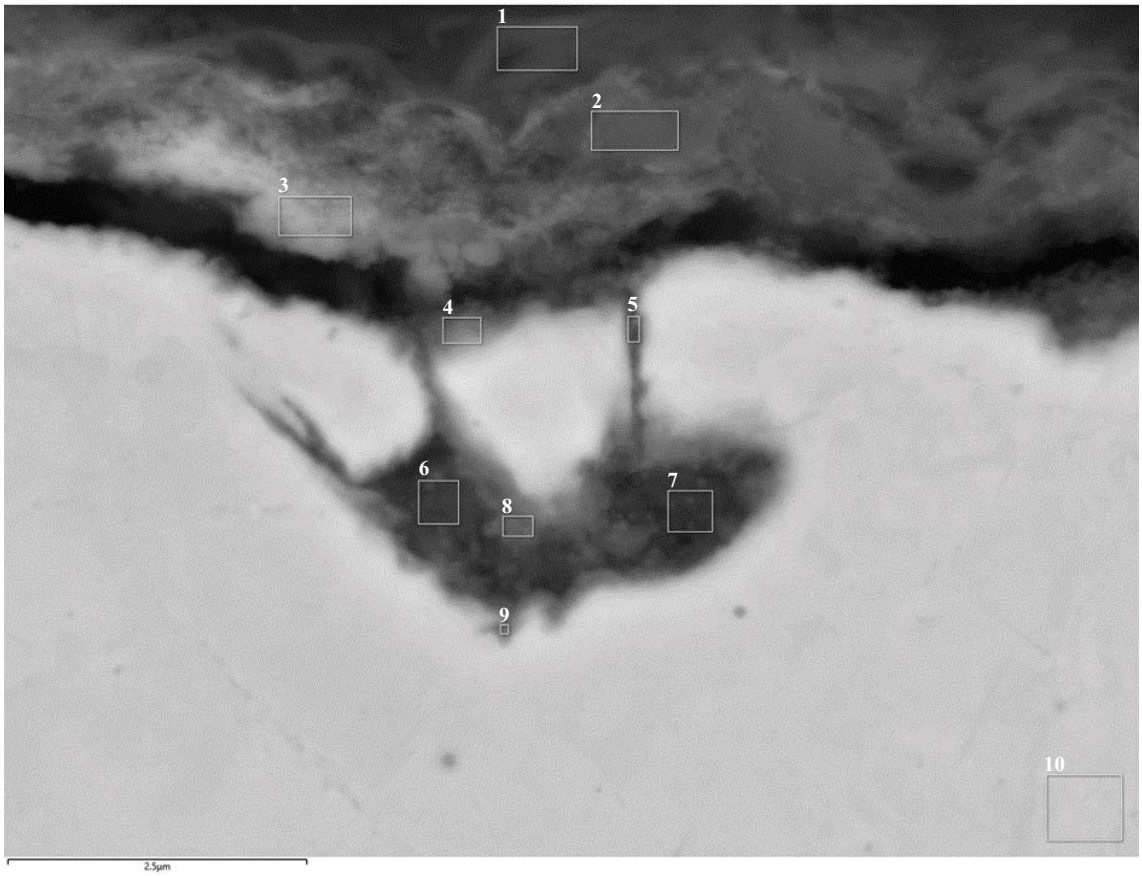

Element	1	2	3	4	5	6	7	8	9	10
O	50.91	58.23	26.92	29.09	33.48	50.94	54.09	47.38	31.17	0.95
Mg	1.94	0.96	0.76	0.99	1.01	0.31	0.56	0.43	0.29	
Al	10.44	4.66	2.51	3.91	3.31	0.66	1.12	0.87	0.23	
Si	26.39	23.33	5.41	11.17	16.62	5.62	4.88	4.43	1.22	
S	0.59	1.63	14.36	4.70	2.42	0.86	0.69	0.78	0.73	
Cl	0.09		0.07		0.16	0.07	0.06	0.09	0.12	
Ca	1.23	3.17	2.59	3.54	5.32	13.96	17.82	13.43	6.56	
Fe	1.15	0.38	0.29	0.56	0.32		0.29			
Cu	7.25	7.64	47.08	46.05	37.35	27.59	20.48	32.59	59.68	99.05
Total	100.00	100.00	100.00	100.00	100.00	100.00	100.00	100.00	100.00	100.00

Figure G-68. *EDS analysis of pipe S2 sample area 2.*

Appendix H

H1 GDOES analysis of pipe samples

H1.2 Technique and method

The samples were analysed using a LECO GDS 850A glow discharge technique. A circular area of 4 mm in diameter is continuously being sputtered in a small argon plasma (glow discharge). The optical emission coming from the various elements in the sample is the registered with an optical spectrometer – giving the elemental composition. Calibration has in this investigation has been done using reference samples (RM and CRF) with a known composition and content. Examples of used certified reference samples are steel samples from Jernkontoret (JK) and samples from the American National Institute of Standards and Technology, NIST. The GD-OES could be equipped with either a DC or RF lamp, and in this case the samples were analysed using the RF-lamp due to versatility and ability to analyse non-conducting samples.

In Glow Discharge Optical Emission Spectrometry, GD-OES, the sample is as a cathode in the glow discharge lamp. A plasma is formed by electric discharge in an argon atmosphere at low pressure. The sample is then sputtered by the argon ions in the plasma and the sputtered atoms diffuse out in the plasma. The optical emission of the plasma, i.e. the light from the de-excited atoms from the various ingoing elements from the sample and Argon, is detected for elemental composition by an optical spectrometer. Each element has a characteristic "finger print" determined by a certain number of wavelengths. The amount of light for a specific wavelength for each element is measured and converted to percentage of the sample.

During sputtering a crater is formed with a flat bottom (see Figure H-1). The analysed surface is circular in shape with a diameter of 4 mm, see Figure H-2.

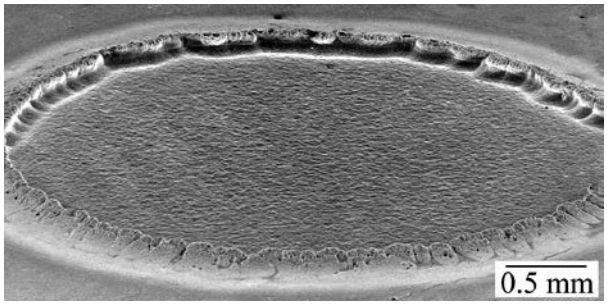

Figure H-1. *A crater formed after analysis with GD-OES.*

Figure H-2. *The pipe sections (left: A3, right: S2) and corresponding samples for GDOES analysis.*

The sputtering rate is well known by calibrations against reference materials (RM, CRF), normally around 20 – 100 nm/s. The method is therefore suitable for qualitative and quantitative depth profiling analysis. The results are given as a weight-percentage curve plotted against sputtered depth. This feature makes GD-OES useful by being able to quickly measure thickness and elemental composition of thin films and coatings. The analysis gives an average value of the film thickness and elemental composition over the sputtered area, with the smallest information depth of around 1 nm. For many elements the smallest detectable amount is in the order of a thousandth weight percent.

H1.3 Results

Before measurement each sample was cut without any cutting fluid or other additives – in order to preserve the surface. To be able to analyse using GDOES a flat surface is needed between the sample and instrument. To flatten the samples a vice was used (with clean paper between the sample and instrument). Each sample was analysed in triplicates. The corresponding depth profiles for each sample and measured spot can be seen in Figure H-3 to Figure H-16. Some elements are presented at × 10 the measured concentrations in order to make the figures easier to read and are denoted with "× 10" in the legend. Separate figures for hydrogen content of each sample are also shown, with the results presented × 100 in order to make them visible on the scale.

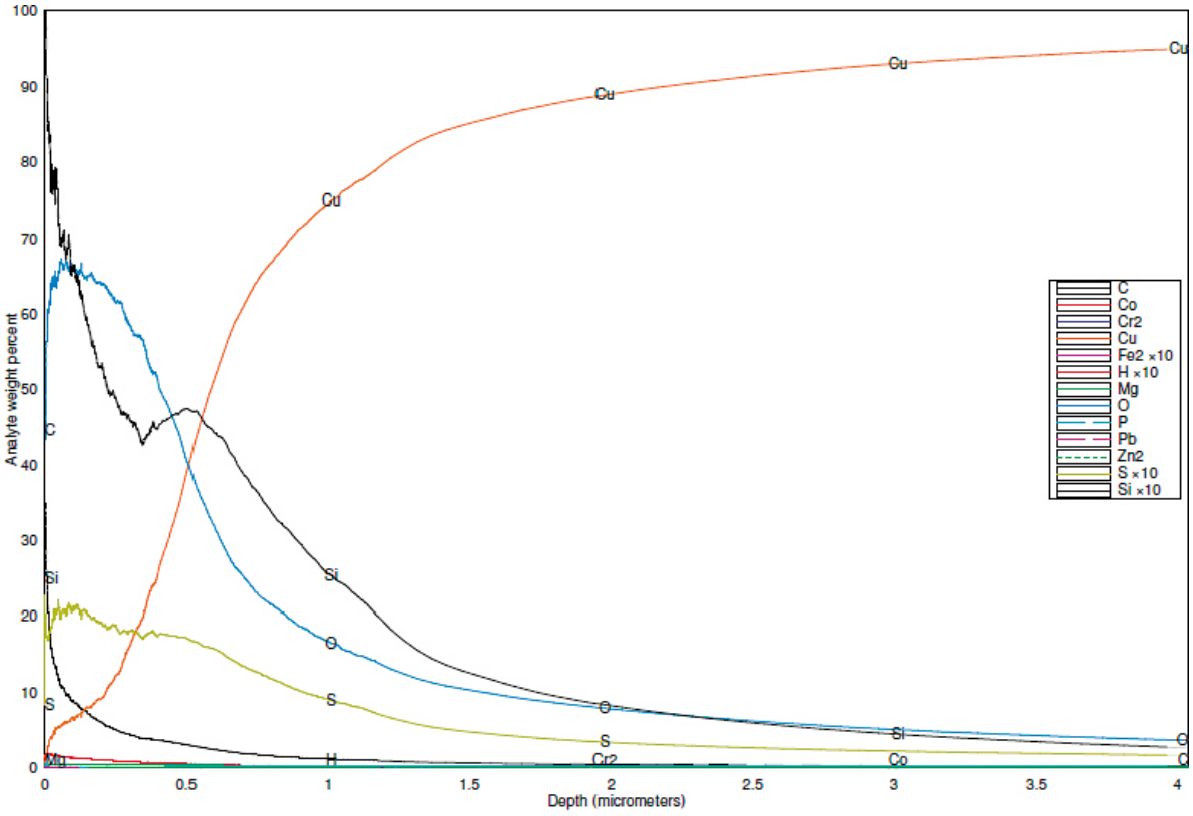

Figure H-3. *Sample A3 analysis 1.*

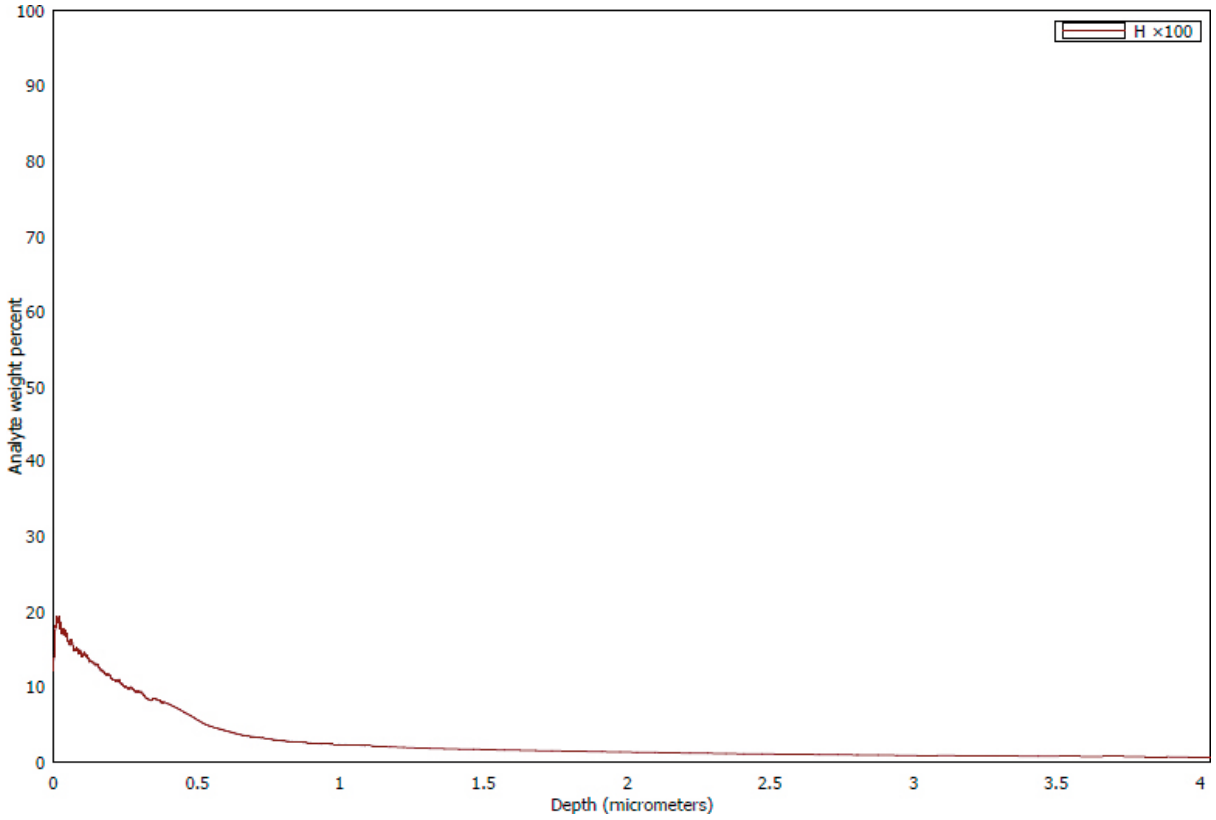

Figure H-4. *Hydrogen content (×100) sample A3 analysis 1.*

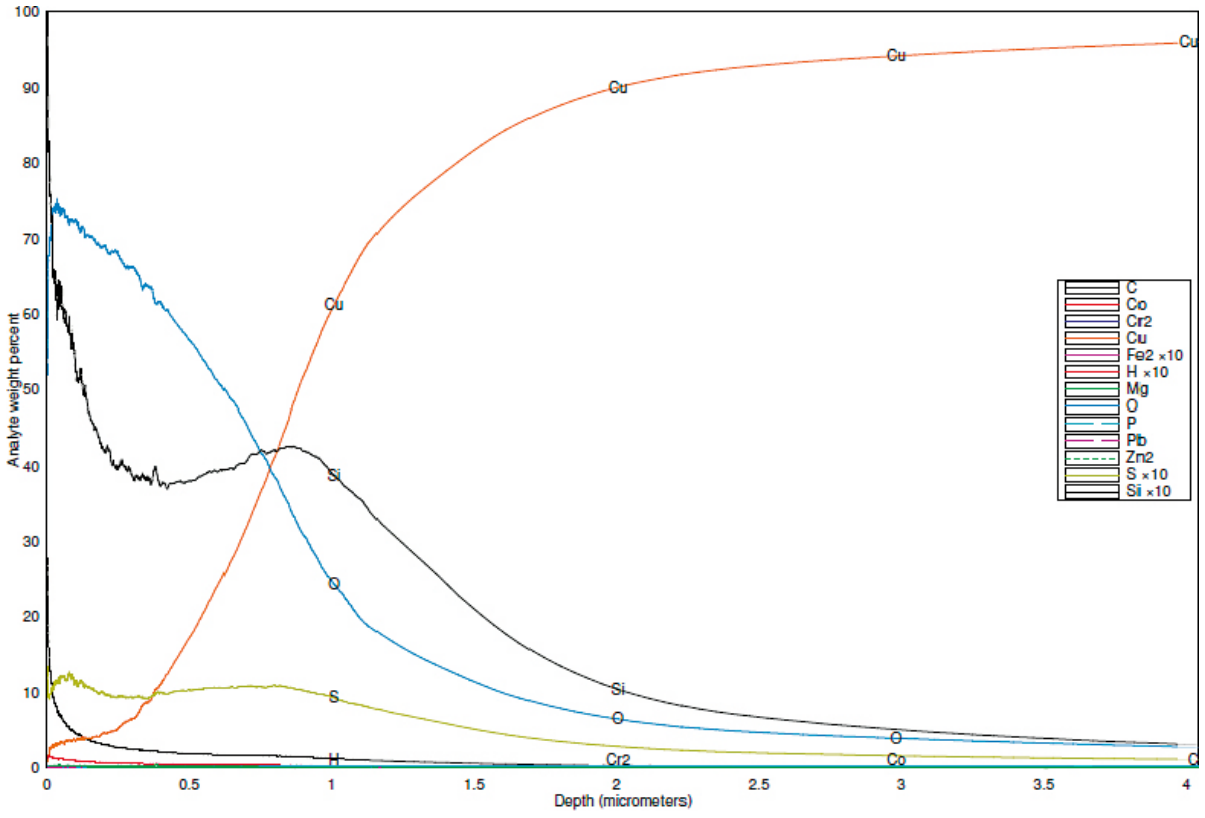

Figure H-5. *Sample A3 analysis 2.*

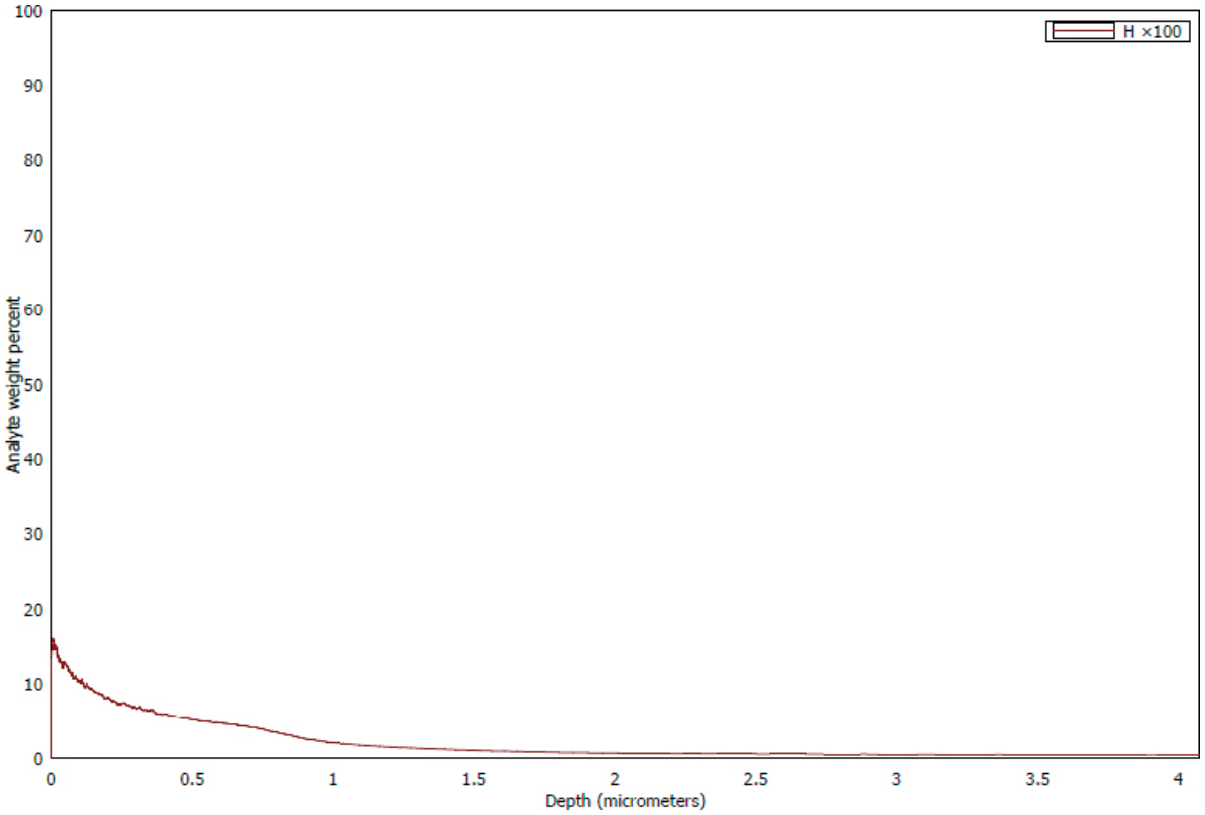

Figure H-6. *Hydrogen content (×100) sample A3 analysis 2.*

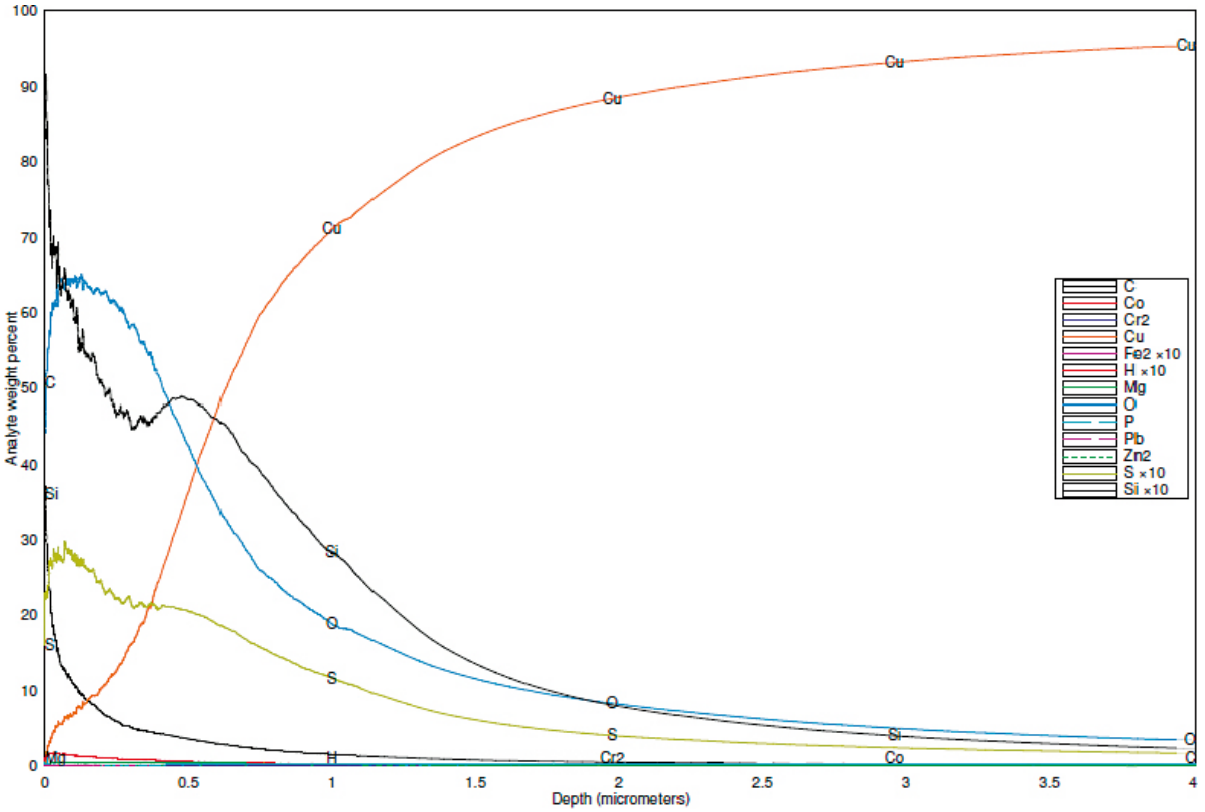

Figure H-7. *Sample A3 analysis 3.*

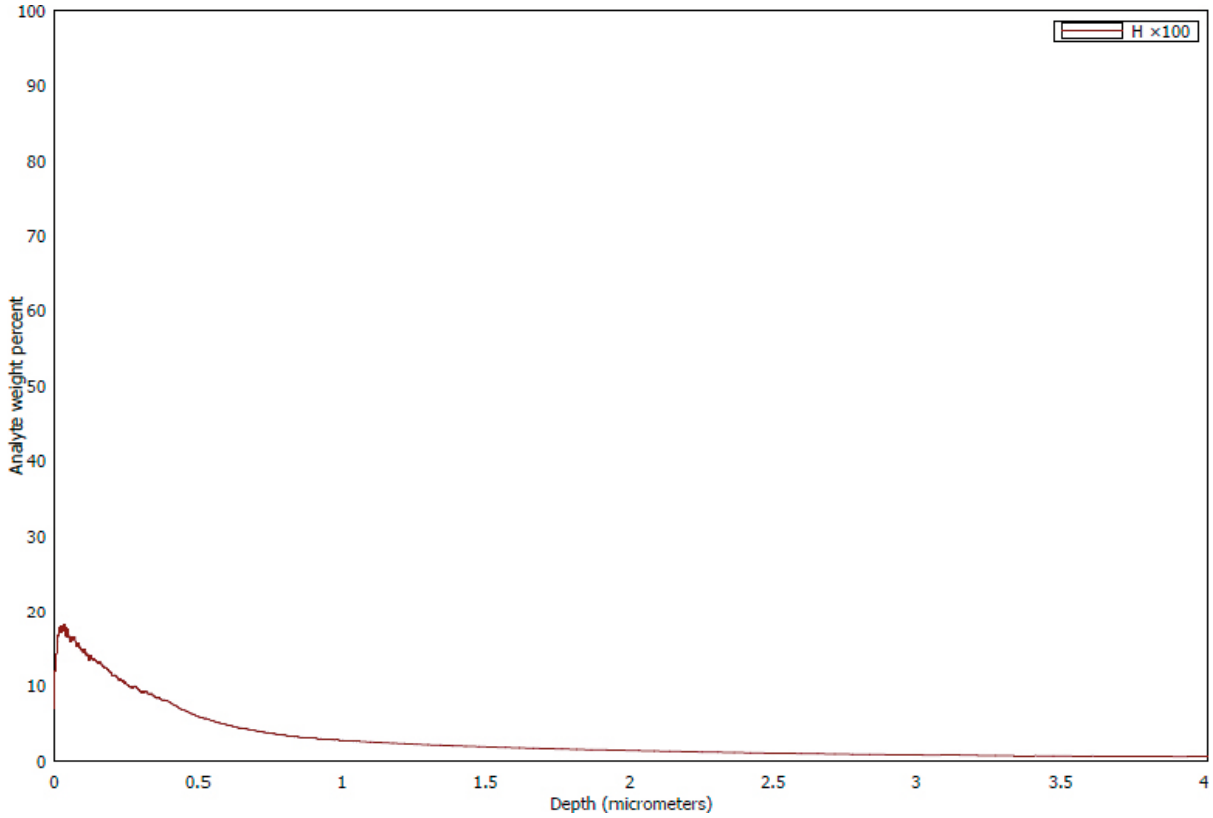

Figure H-8. *Hydrogen content (×100) sample A3 analysis 3.*

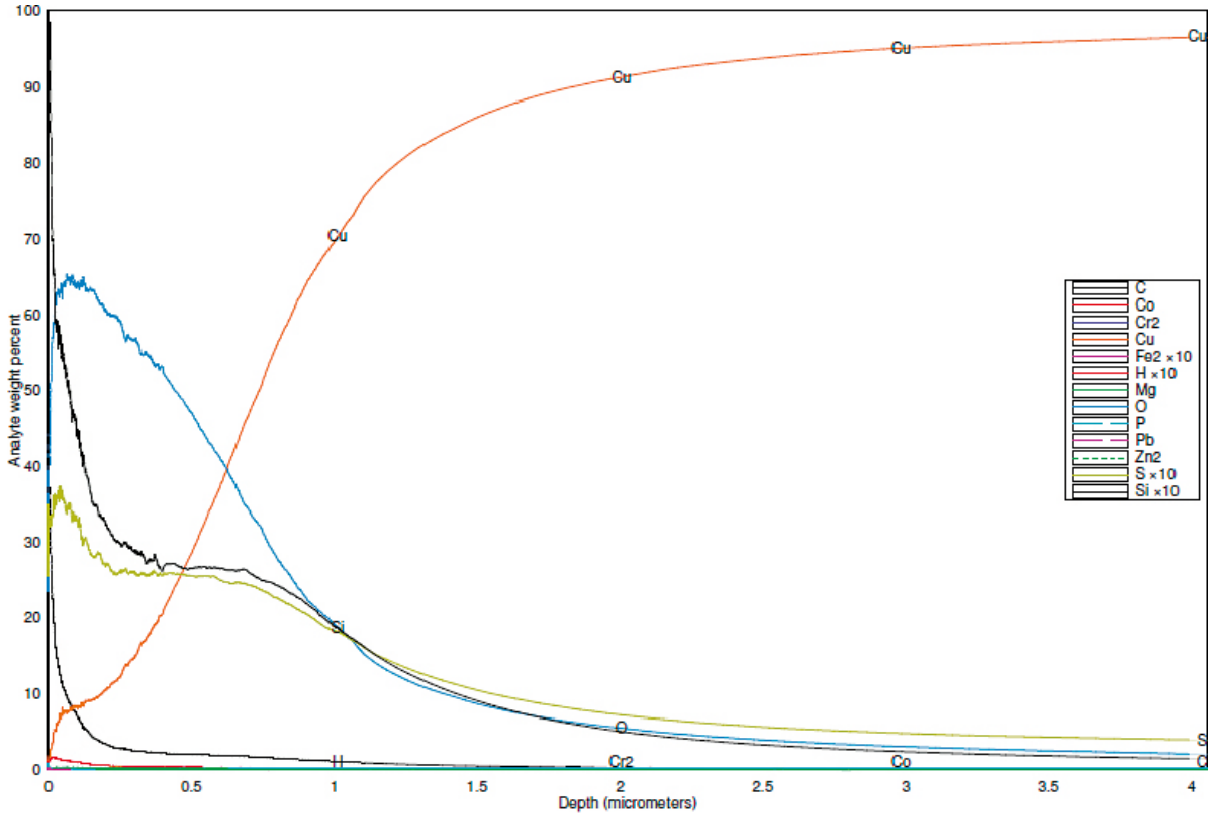

Figure H-9. *Sample A3 analysis 4.*

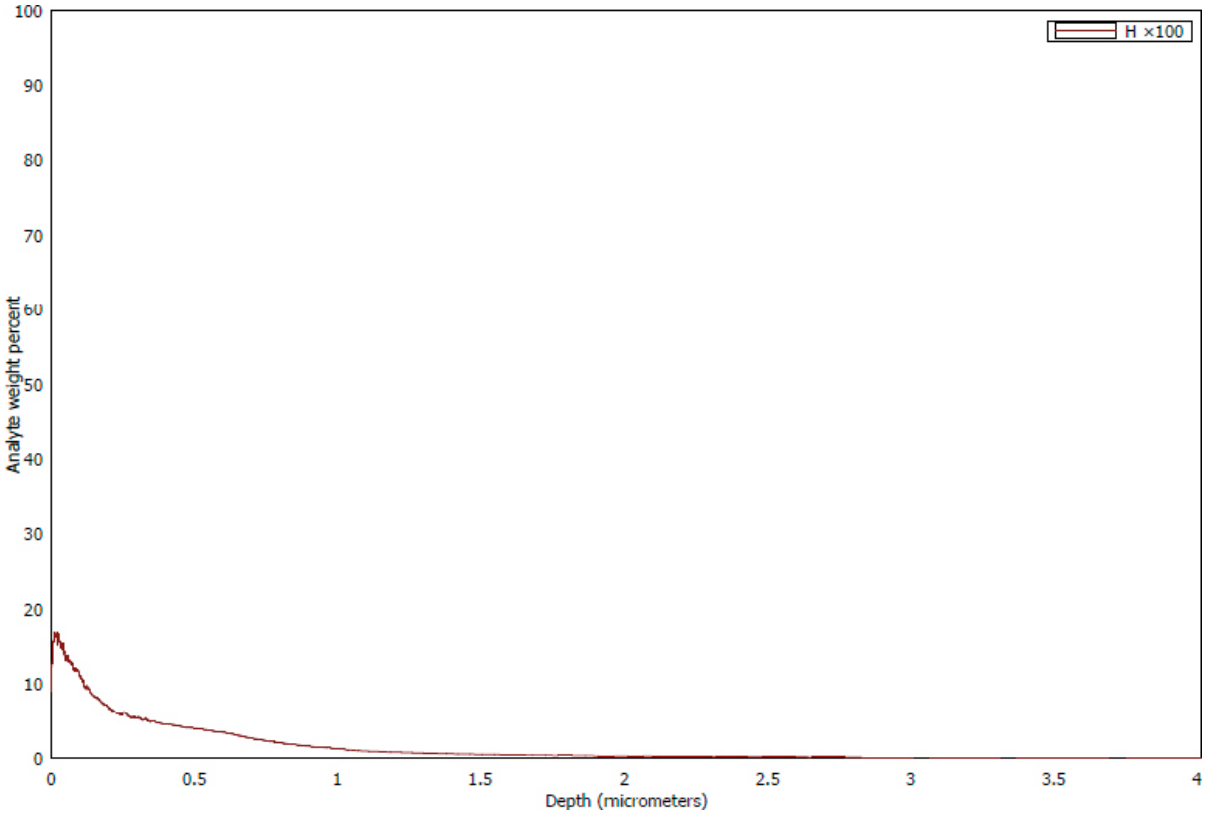

Figure H-10. *Hydrogen content (×100) sample A3 analysis 4.*

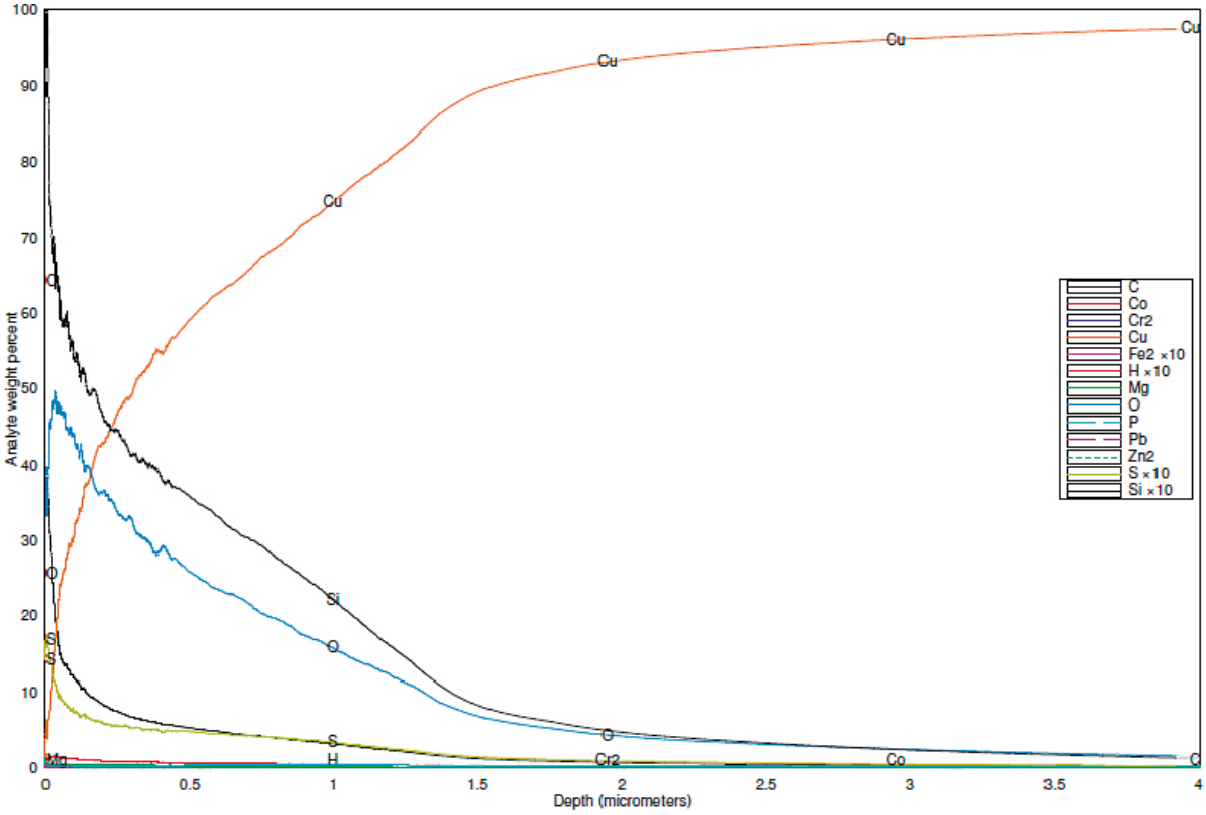

Figure H-11. *Sample S2 analysis 1.*

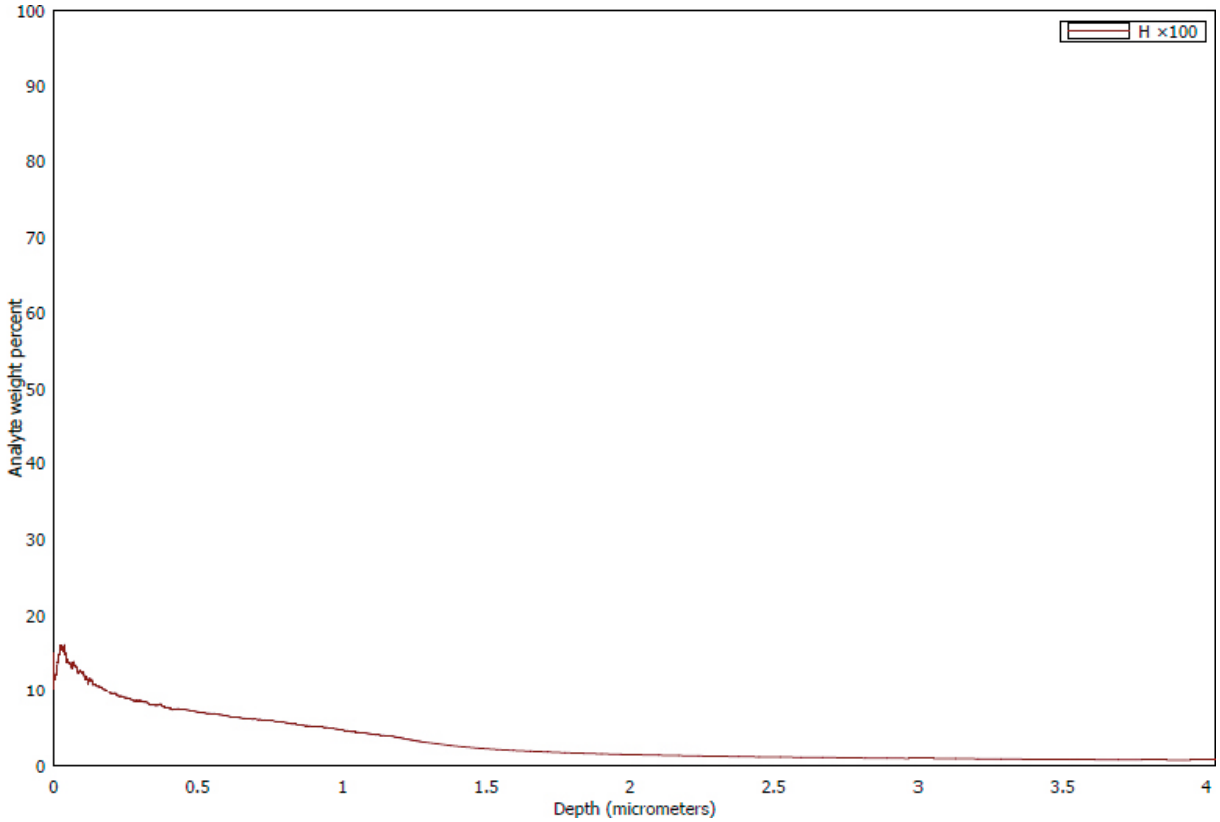

Figure H-12. *Hydrogen content (×100) sample S2 analysis 1.*

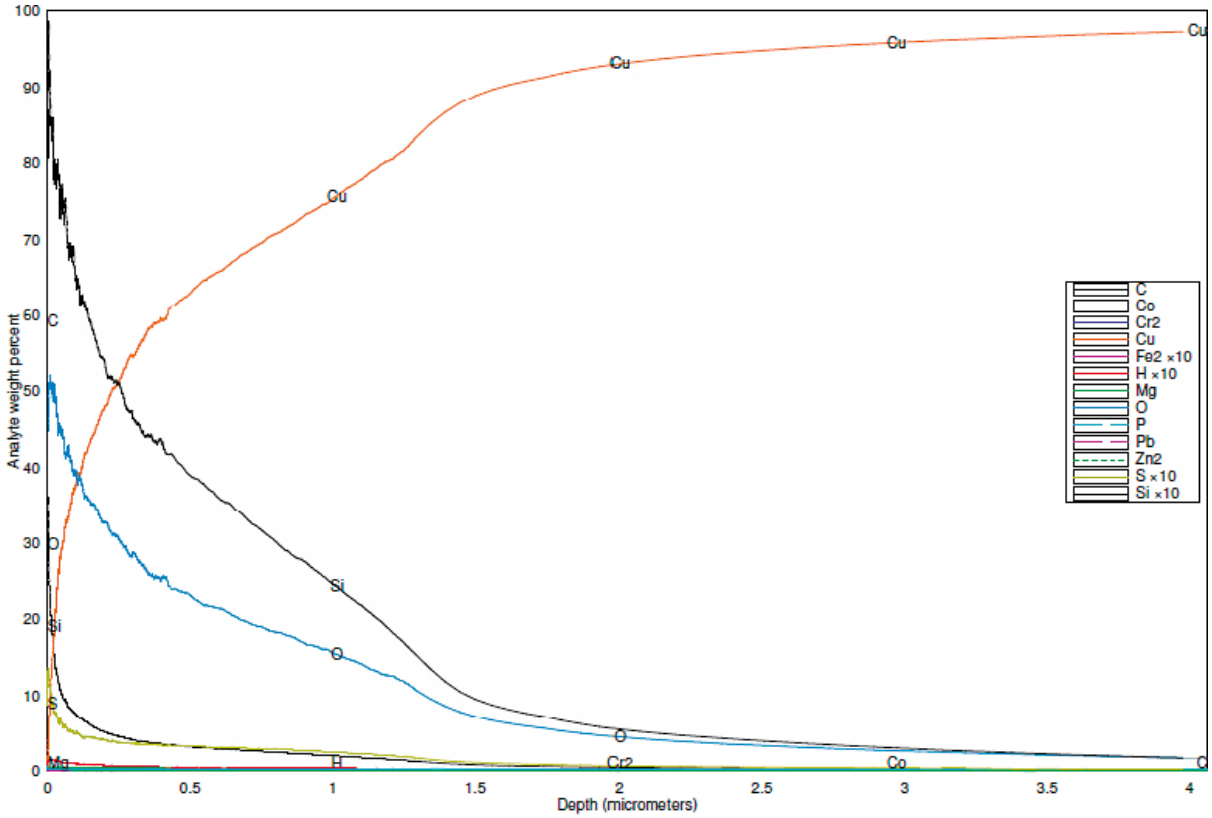

Figure H-13. *Sample S2 analysis 2.*

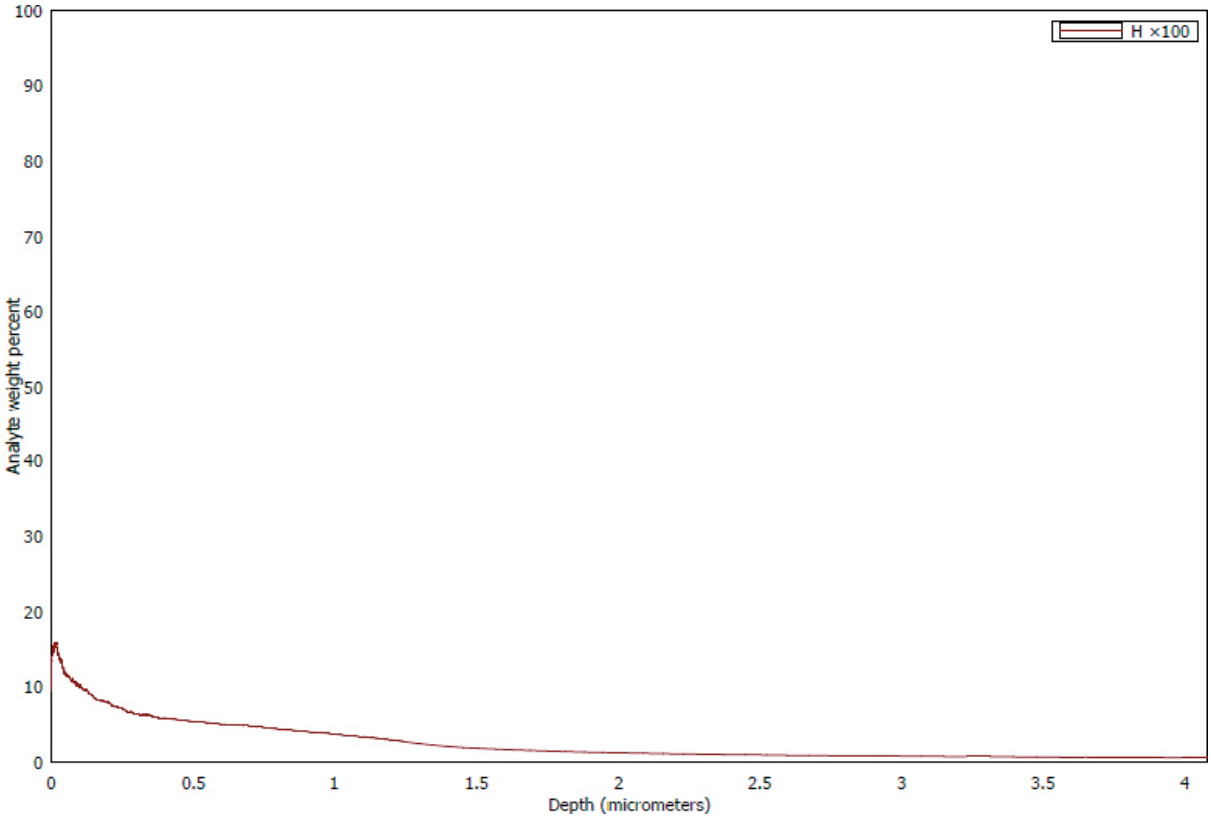

Figure H-14. *Hydrogen content (×100) sample S2 analysis 2.*

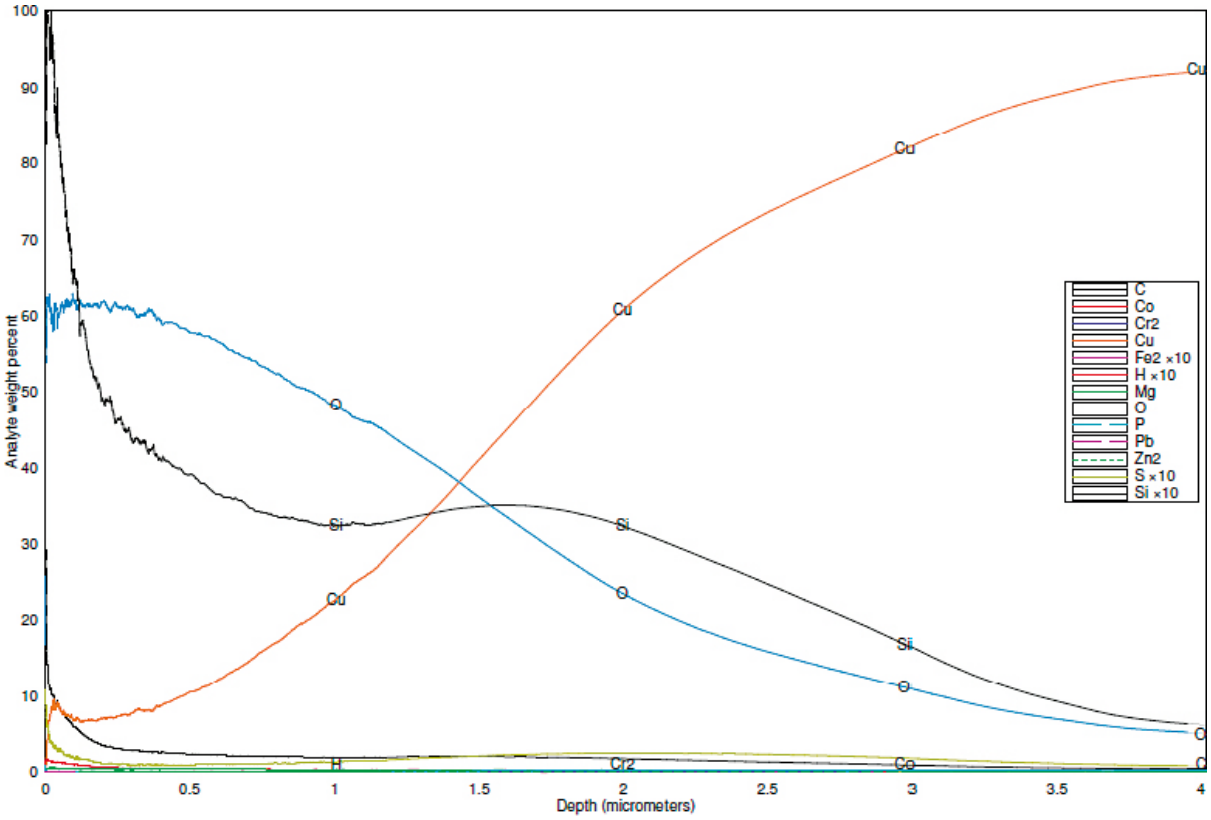

Figure H-15. *Sample S2 analysis 3.*

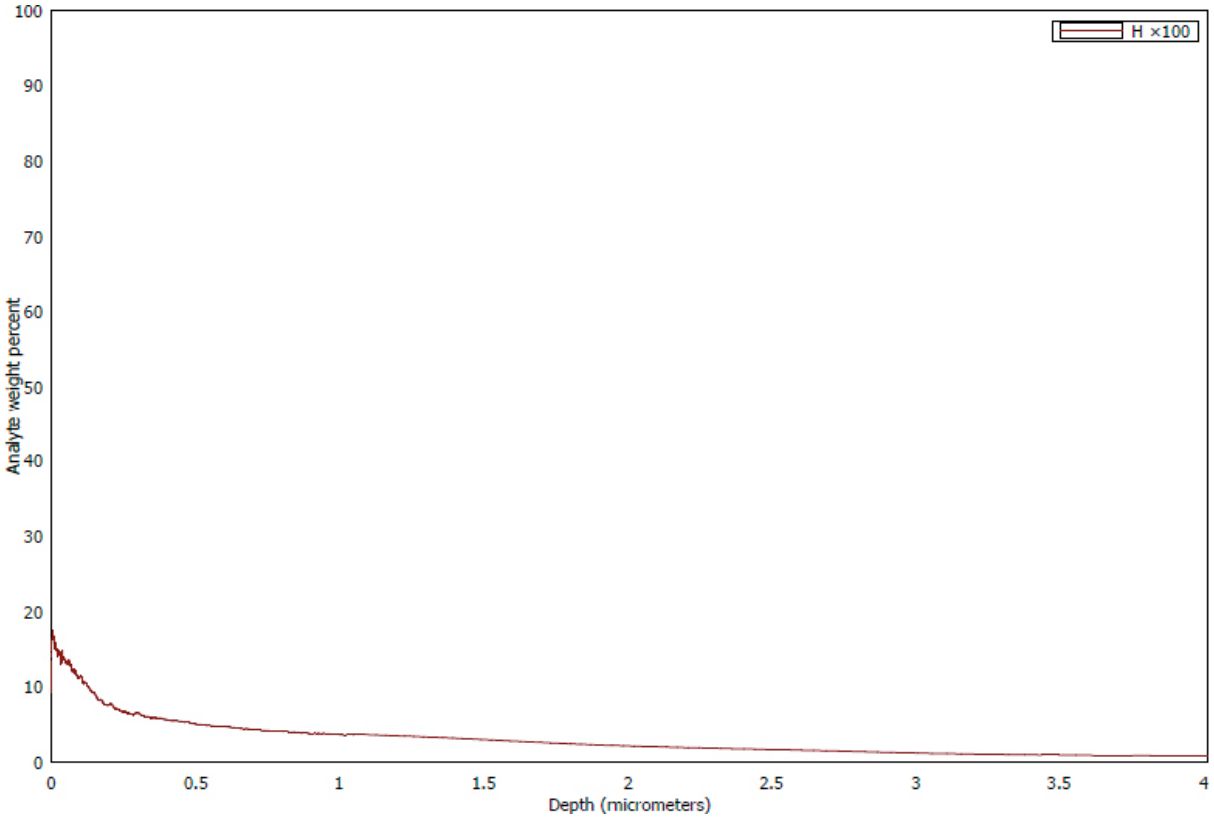

Figure H-16. *Hydrogen content (×100) sample S2 analysis 3.*

Appendix I

Analysis of corrosion products from a bottom plate

I.1 Introduction

A sample of blue-green deposits found under the copper bottom plate of the LOT A3 package was analysed first using SEM-EDS and subsequently powder XRD. Analysis with XRD required that the sample was ground to a fine powder before being analysed in the instrument as it was received as a mixture of particles of various sizes.

I.1.1 EDS analysis

Figure I-1 shows the surface of the sample analysed with EDS and Table I-1 provides the results in weight %. The main constituents were found as being O, Na, Si and Cl, with lower concentrations of Cu, Al, Mg, Ca, Fe, S and Rh, as well as traces of K and Nd.

Table I-1. Results of EDS analysis, on several parts of the sample.

Spectrum label/wt%	O	Na	Mg	Al	Si	S	Cl	K	Ca	Fe	Cu	Rh	Nd
1	34.1	14.6	1.2	4.5	13.2	2.8	17.6	0.3	2.2	2.2	4.9	2.4	
2	40.1	5.0	1.7	7.2	20.9	1.0	7.0	0.4	2.8	3.0	10.9		
3	32.1	11.7	1.3	5.5	15.2	0.8	18.1	0.2	2.3	3.0	8.4	1.5	
4	24.2	25.0	0.4	1.3	3.8	6.1	32.0		0.9	0.5	1.1	4.1	0.7

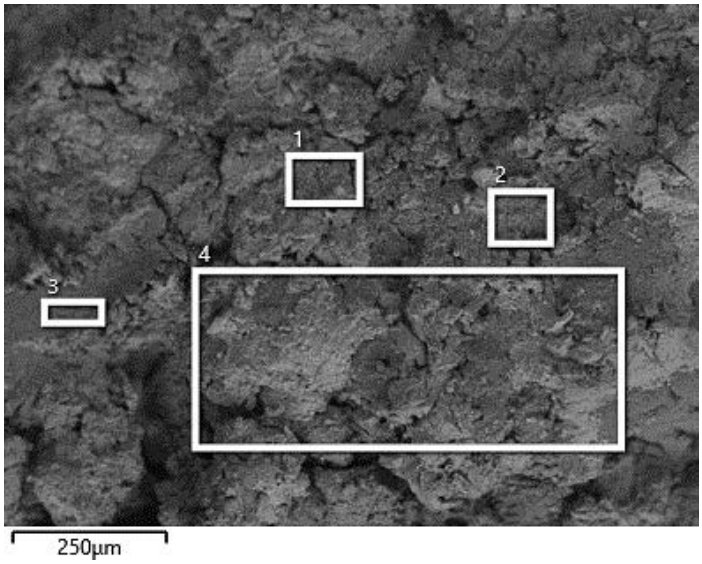

Figure I-1. *SEM image of the surface of the sample with areas where EDS analyses were performed marked on the image.*

I.1.2 X-ray diffraction analysis

Diffraction patterns obtained from the ground powder are displayed in Figure I-2. The identified compounds are listed in Table I-2, semi-quantitative phase fractions are included which were obtained from relative peak heights. As can be seen from Figure I-2, there are various phases within the material which give rise to many peaks and since some are overlapping with each other, it can be challenging to identify all the existing phases. Phases which have been marked with ++ in Table I-2 have a clearer signal, however the other possible phases have more overlapping peaks and require complementary methods to ensure their existence.

In Table I-2, "+" or "++" are the operator's interpretation of the results. The notation "++" means that the peak is clearly present, and that the specific compound is the only one that fits the peaks. The notation "+" means that the peak could possibly correspond to this compound. Sources of uncertainty in the identification of compounds can be, for example: difficulty in finding the compound best matching the peaks; compounds having diffraction patterns with overlapping peaks (meaning that complementary methods are necessary to confirm whether or not a specific phase has been detected), and; in some case the peak is too weak that the compound may or may not exist. For more detailed analysis of phase fractions, complementary methods and then Rietveld refitment of the diffraction pattern would be required.

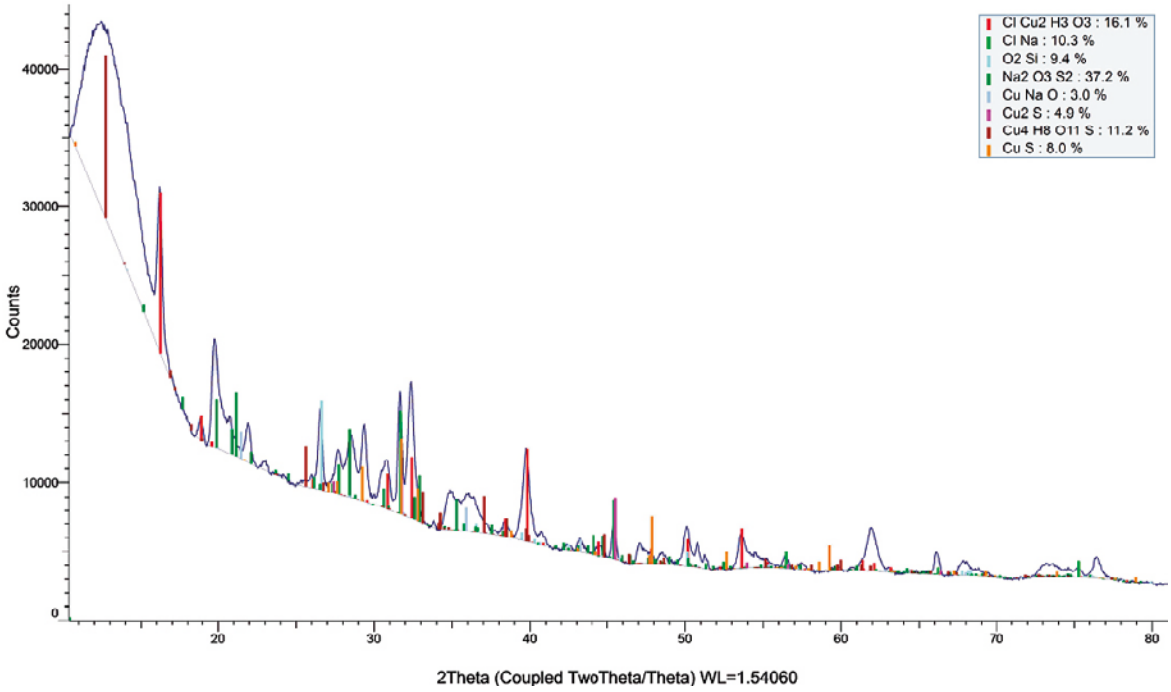

Figure I-2. *The obtained XRD patterns for the sample and the peaks corresponding to each phase.*

Table I-2. Identified compounds and semiquantitative phase fractions: ++ = Peak correlates well with suggested compound, + = weaker peaks/peaks which may also correspond to similar phases.

Phase	SQ volume fractions
$Cu_2Cl(OH)_3$	~ 16 % ++
NaCl	~ 10 % ++
$Cu_4H_8O_{11}S$	~ 11 % ++
CuNaO	~ 3 % ++
SiO_2	~ 9 % +
$Na_2S_2O_3$	~ 37 % +
CuS	~ 5 % +
Cu_2S	~ 8 % +

Two X-ray diffraction measurements were performed on the sample. For the second analysis the powder was stirred and ground once more, before being placed again on the sample holder to ensure that the sample was uniform. Figure I-3 shows the comparison between the two diffraction patterns obtained. As seen in the figure, the major peaks observed, and the intensities measured look very similar. The slight difference in the background and intensity observed especially at low angles can be due to the flatness of the distributed powder on the sample holder or possibly larger grains in some part of the powder.

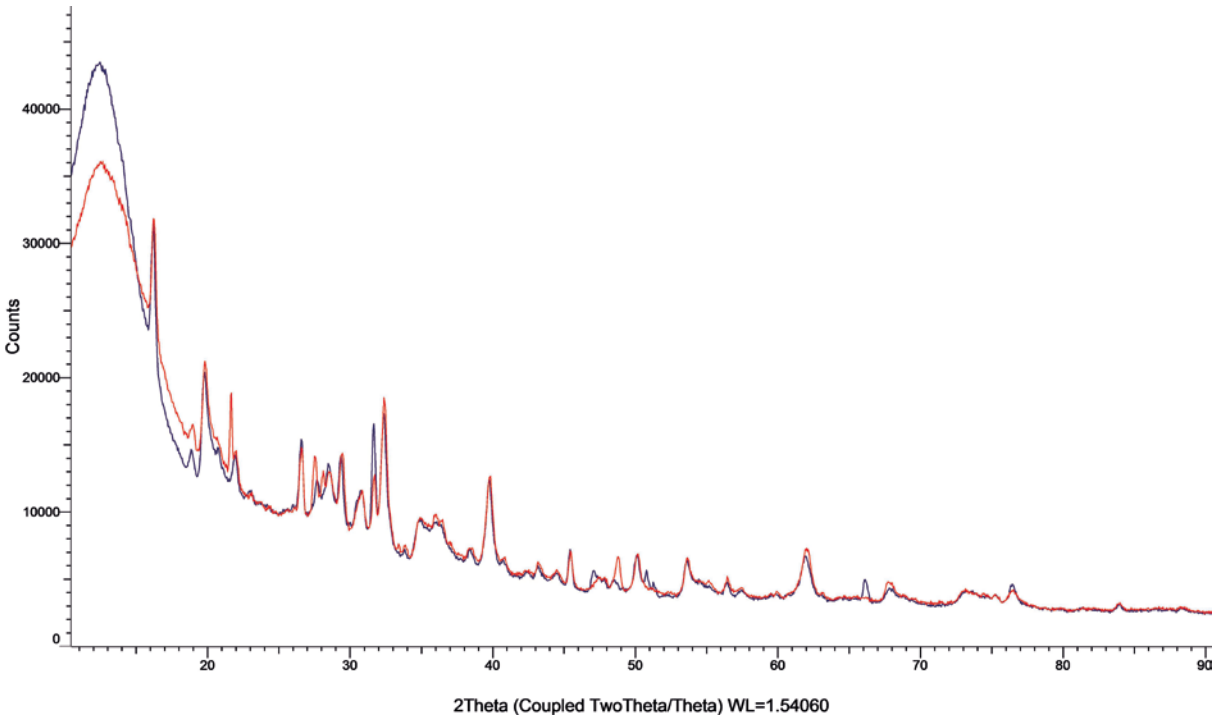

Figure I-3. *Comparison between two XRD patterns measured with the same setting on the sample, after extra mixing to ensure the sample was uniform.*

Estimation of corrosion depths from XRF

Ident	Na2O	MgO	Al_2O_3	SiO_2	SO_3	Cl	K_2O	CaO	TiO_2	Fe_2O_3	CuO	MnO	P_2O_5	Distance	Id	Position	Average CuO (wt%)	Mass CuO (g)	Mass Cu (g)	Volume copper (cm^3)
LOT A3 #9E 0–2mm d5c751	1.5	3.4	19.6	65.1	2.0	0.1	0.5	2.1	0.2	4.7	0.813	0.0	0.0	1	LOT A3 #9E	0–2 mm	0.83	0.86	0.69	0.077
LOT A3 #9E 0–2mm d5c751	1.5	3.3	19.5	64.6	2.5	0.1	0.6	2.3	0.2	4.6	0.838	0.0	0.0	1						
LOT A3 #9E 2–10mm d5c752	1.6	2.5	19.6	66.7	1.5	0.1	0.6	1.8	0.2	4.7	0.63	0.0	0.0	6		2–10 mm	0.69	3.11	2.48	0.277
LOT A3 #9E 2–10mm d5c752	1.5	2.6	20.0	66.2	1.4	0.1	0.6	1.7	0.2	4.9	0.746	0.0	0.0	6						
LOT A3 #9E 10–20mm d5c753	1.6	2.4	20.0	67.2	1.5	0.1	0.6	1.6	0.2	4.7	0.033	0.0	0.0	15		10–20 mm	0.03	0.22	0.18	0.020
LOT A3 #9E 10–20mm d5c753	1.6	2.4	20.1	67.1	1.5	0.1	0.5	1.6	0.2	4.7	0.035	0.0	0.0	15						
LOT A3 #9E 20–50mm d5c754	1.7	2.3	20.2	66.5	1.8	0.1	0.6	2.0	0.2	4.6	0.003	0.0	0.0	35					Sum:	0.374
LOT A3 #9E 20–50mm d5c754	1.7	2.3	20.3	66.5	1.8	0.1	0.6	2.0	0.2	4.5	0.001	0.0	0.0	35					Corrosion thickness (µm):	11.0
LOT A3 #9E 50–70mm d5c755	1.7	2.3	20.6	67.8	0.3	0.2	0.6	1.7	0.2	4.6	0.002	0.0	0.0	60						
LOT A3 #9E 50–70mm d5c755	1.7	2.3	20.6	67.8	0.3	0.2	0.6	1.7	0.2	4.6	0.001	0.0	0.0	60						
LOT A3 #9E 70–100mm d5c756	1.7	2.3	20.8	68.2	0.3	0.2	0.6	1.2	0.2	4.6	0.002	0.0	0.0	85						
LOT A3 #9E 70–100mm d5c756	1.7	2.3	20.8	68.3	0.3	0.2	0.6	1.2	0.2	4.6	0.001	0.0	0.0	85						

															Id	Position	Average CuO (wt%)	Mass CuO g)	Mass Cu (g)	Volume copper (cm^3)
LOT A3 #11N 0–2mm d5c757	1.6	3.2	20.1	65.9	1.2	0.1	0.5	1.6	0.2	4.6	0.834	0.0	0.0	1.0	LOT A3 #11N	0–2 mm	0.80	0.83	0.66	0.074
LOT A3 #11N 0–2mm d5c757	1.6	3.2	20.0	66.1	1.2	0.1	0.6	1.7	0.2	4.6	0.763	0.0	0.0	1.0						
LOT A3 #11N 2–10mm d5c758	1.6	2.7	20.0	66.7	1.3	0.2	0.6	1.6	0.2	4.7	0.524	0.0	0.0	6.0		2–10 mm	0.50	2.26	1.80	0.201
LOT A3 #11N 2–10mm d5c758	1.6	2.7	20.0	66.6	1.5	0.1	0.5	1.7	0.2	4.7	0.474	0.0	0.0	6.0						
LOT A3 #11N 10–20mm d5c759	1.6	2.5	19.8	66.4	2.1	0.1	0.5	1.9	0.2	4.8	0.041	0.0	0.0	15.0		10–20 mm	0.05	0.30	0.24	0.027
LOT A3 #11N 10–20mm d5c759	1.6	2.5	19.8	66.5	2.0	0.1	0.6	1.8	0.2	4.7	0.052	0.0	0.0	15.0						
LOT A3 #11N 20–50mm d5c75a	1.7	2.4	20.4	67.0	1.3	0.2	0.5	1.8	0.2	4.6	0.001	0.0	0.0	35.0					Sum:	0.302
LOT A3 #11N 20–50mm d5c75a	1.7	2.4	20.5	66.9	1.2	0.2	0.6	1.8	0.2	4.6	0.001	0.0	0.0	35.0					Corrosion thickness (µm):	8.9
LOT A3 #11N 50–70mm d5c75b	1.7	2.3	20.8	67.8	0.3	0.2	0.6	1.5	0.2	4.6	0	0.0	0.0	60.0						
LOT A3 #11N 50–70mm d5c75b	1.7	2.3	20.8	67.8	0.3	0.2	0.6	1.6	0.2	4.6	0.001	0.0	0.0	60.0						
LOT A3 #11N 70–100mm d5c75c	1.7	2.3	20.7	68.2	0.3	0.2	0.6	1.1	0.2	4.7	0.021	0.0	0.0	85.0						
LOT A3 #11N 70–100mm d5c75c	1.7	2.3	20.8	68.2	0.3	0.2	0.6	1.1	0.2	4.7	0.02	0.0	0.0	85.0						

															Id	Position	Average CuO (wt%)	Mass CuO (g)	Mass Cu (g)	Volume copper (cm^3)
LOT A3 #15 0–2mm d5c745	1.4	3.2	18.6	62.1	4.9	0.1	0.5	3.3	0.2	4.7	0.88	0.02	0.0	1.0	LOT A3 #15					
LOT A3 #15 0–2mm d5c745	1.4	3.1	18.8	62.9	4.3	0.1	0.5	3.0	0.2	4.8	0.88	0.02	0.0	1.0		0–2 mm	0.88	0.91	0.73	0.082
LOT A3 #15 2–10mm d5c746	1.5	2.6	19.3	65.6	2.3	0.1	0.6	2.2	0.2	4.9	0.78	0.01	0.0	6.0						
LOT A3 #15 2–10mm d5c746	1.5	2.5	19.3	65.1	2.8	0.1	0.5	2.3	0.2	4.9	0.73	0.01	0.0	6.0		2–10 mm	0.75	3.40	2.72	0.303
LOT A3 #15 10–20mm d5c747	1.5	2.2	18.8	63.8	4.7	0.2	0.6	3.1	0.2	4.8	0.09	0.01	0.0	15.0						
LOT A3 #15 10–20mm d5c747	1.5	2.2	18.8	63.6	4.8	0.2	0.5	3.1	0.2	4.8	0.09	0.01	0.0	15.0		10–20 mm	0.09	0.56	0.45	0.050
LOT A3 #15 20–50mm d5c748	1.6	2.2	19.7	67.7	1.3	0.2	0.6	1.7	0.2	4.8	0.00	0.01	0.0	35.0						
LOT A3 #15 20–50mm d5c748	1.6	2.3	19.6	67.4	1.5	0.2	0.6	1.7	0.2	4.9	0.00	0.02	0.0	35.0					Sum:	0.435
LOT A3 #15 50–70mm d5c749	1.7	2.3	20.1	68.3	0.3	0.2	0.5	1.6	0.2	4.8	0.00	0.02	0.0	60.0					Corrosion thickness (µm):	12.8
LOT A3 #15 50–70mm d5c749	1.6	2.2	20.0	68.7	0.3	0.2	0.6	1.3	0.2	4.8	0.00	0.01	0.0	60.0						
LOT A3 #15 70–100mm d5c750	1.6	2.2	20.0	68.7	0.3	0.3	0.6	1.3	0.2	4.9	0.00	0.01	0.0	85.0						
LOT A3 #15 70–100mm d5c750	1.6	2.2	19.9	68.5	0.6	0.3	0.6	1.4	0.2	4.8	0.01	0.01	0.0	85.0						

Ident	Na2O	MgO	Al_2O_3	SiO_2	SO_3	Cl	K_2O	CaO	TiO_2	Fe_2O_3	CuO	MnO	P_2O_5	Distance	Id	Position	Average CuO (wt%)	Mass CuO (g)	Mass Cu (g)	Volume copper (cm^3)
LOT A3 #16 0–2mm d5c74b	1.5	2.9	19.2	64.3	3.1	0.1	0.5	2.5	0.2	4.8	0.87	0.02	0.0	1.0	LOT A3 #16					
LOT A3 #16 0–2mm d5c74b	1.5	3.0	19.2	64.1	3.1	0.1	0.5	2.5	0.2	4.9	0.89	0.02	0.0	1.0		0–2 mm	0.88	0.92	0.73	0.082
LOT A3 #16 2–10mm d5c74c	1.5	2.4	19.0	65.2	3.0	0.1	0.6	2.5	0.2	4.7	0.79	0.01	0.0	6.0						
LOT A3 #16 2–10mm d5c74c	1.5	2.4	19.3	65.0	2.9	0.1	0.5	2.4	0.2	4.8	0.76	0.01	0.0	6.0		2–10 mm	0.77	3.49	2.79	0.312
LOT A3 #16 10–20mm d5c74d	1.6	2.3	19.4	66.1	2.5	0.2	0.6	2.1	0.2	5.0	0.14	0.01	0.0	15.0						
LOT A3 #16 10–20mm d5c74d	1.6	2.3	19.1	66.3	2.6	0.1	0.6	2.2	0.2	4.8	0.12	0.01	0.0	15.0		10–20 mm	0.13	0.84	0.67	0.074
LOT A3 #16 20–50mm d5c74e	1.6	2.2	19.7	68.3	0.8	0.2	0.6	1.6	0.2	4.7	0.00	0.02	0.0	35.0						
LOT A3 #16 20–50mm d5c74e	1.6	2.3	20.2	68.1	0.6	0.2	0.6	1.3	0.2	4.9	0.00	0.02	0.0	35.0					Sum:	0.468
LOT A3 #16 50–70mm d5c74f	1.6	2.2	20.0	68.7	0.3	0.2	0.6	1.3	0.2	4.9	0.00	0.02	0.0	60.0					Corrosion thickness (µm):	13.8
LOT A3 #16 50–70mm d5c74f	1.7	2.2	19.9	68.5	0.3	0.2	0.6	1.6	0.2	4.8	0.00	0.02	0.0	60.0						
LOT A3 #16 70–100mm d5c74a	1.7	2.2	19.9	68.8	0.3	0.3	0.6	1.3	0.2	4.8	0.03	0.01	0.0	85.0						
LOT A3 #16 70–100mm d5c74a	1.7	2.2	19.9	68.7	0.3	0.2	0.6	1.3	0.2	4.8	0.04	0.01	0.0	85.0						

Ident	Na2O	MgO	Al_2O_3	SiO_2	SO_3	Cl	K_2O	CaO	TiO_2	Fe_2O_3	CuO	MnO	P_2O_5	Distance	Id	Position	Average CuO (wt%)	Mass CuO (g)	Mass Cu (g)	Volume copper (cm^3)
LOT A3 #33E 0–2mm d5c75d	0.8	2.3	20.5	67.5	0.6	0.1	0.5	2.8	0.2	4.7	0.058	0.0	0.0	1.0	LOT A3 #33E					
LOT A3 #33E 0–2mm d5c75d	0.8	2.2	20.4	67.9	0.5	0.1	0.6	2.6	0.2	4.6	0.044	0.0	0.0	1.0		0–2 mm	0.05	0.05	0.04	0.005
LOT A3 #33E 2–10mm d5c75e	0.8	2.2	20.3	68.1	0.6	0.1	0.6	2.6	0.2	4.6	0.002	0.0	0.0	6.0						
LOT A3 #33E 2–10mm d5c75e	0.8	2.3	20.5	67.9	0.6	0.1	0.5	2.5	0.2	4.6	0.002	0.0	0.0	6.0		2–10 mm	0.00	0.01	0.01	0.001
LOT A3 #33E 10–20mm d5c75f	0.8	2.2	20.3	68.1	0.6	0.1	0.6	2.5	0.2	4.6	0.001	0.0	0.0	15.0						
LOT A3 #33E 10–20mm d5c75f	0.8	2.2	20.3	68.0	0.6	0.1	0.6	2.6	0.2	4.6	0.001	0.0	0.0	15.0		10–20 mm	0.00	0.01	0.01	0.001
LOT A3 #33E 20–50mm d5c760	0.8	2.3	20.7	67.7	0.5	0.1	0.5	2.6	0.2	4.6	0.001	0.0	0.0	35.0						
LOT A3 #33E 20–50mm d5c760	0.8	2.3	20.8	67.6	0.5	0.1	0.6	2.5	0.2	4.6	0.001	0.0	0.0	35.0					Sum:	0.006
LOT A3 #33E 50–70mm d5c761	0.9	2.3	20.8	67.8	0.3	0.1	0.5	2.5	0.2	4.6	0	0.0	0.0	60.0					Corrosion thickness (µm):	0.2
LOT A3 #33E 50–70mm d5c761	0.8	2.3	20.8	67.9	0.3	0.1	0.6	2.5	0.2	4.6	0.001	0.0	0.0	60.0						
LOT A3 #33E 70–100mm d5c762	0.9	2.2	20.8	67.9	0.3	0.1	0.5	2.4	0.2	4.6	0.004	0.0	0.0	85.0						
LOT A3 #33E 70–100mm d5c762	0.8	2.3	20.9	67.9	0.3	0.1	0.5	2.4	0.2	4.6	0.004	0.0	0.0	85.0						

Ident	Na2O	MgO	Al_2O_3	SiO_2	SO_3	Cl	K_2O	CaO	TiO_2	Fe_2O_3	CuO	MnO	P_2O_5	Distance	Id	Position	Average CuO (wt%)	Mass CuO (g)	Mass Cu (g)	Volume copper (cm^3)
LOT A3 #35N 0–2mm	1.1	2.3	20.5	67.7	0.6	0.1	0.6	2.3	0.2	4.6	0.09	0.01	0.0	1.0	LOT A3 #35N					
LOT A3 #35N 0–2mm	1.1	2.3	20.4	67.6	0.6	0.1	0.6	2.4	0.2	4.5	0.11	0.01	0.0	1.0		0–2 mm	0.10	0.11	0.08	0.009
LOT A3 #35N 2–10mm	1.1	2.3	20.3	67.8	0.7	0.1	0.6	2.3	0.2	4.6	0.01	0.01	0.0	6.0						
LOT A3 #35N 2–10mm	1.1	2.3	20.2	68.1	0.7	0.1	0.6	2.2	0.2	4.5	0.01	0.01	0.0	6.0		2–10 mm	0.01	0.04	0.03	0.004
LOT A3 #35N 10–20mm	1.1	2.3	20.2	67.7	0.7	0.1	0.6	2.5	0.2	4.6	0.02	0.01	0.0	15.0						
LOT A3 #35N 10–20mm	1.1	2.2	20.2	67.9	0.7	0.1	0.6	2.4	0.2	4.6	0.00	0.01	0.0	15.0		10–20 mm	0.01	0.08	0.07	0.008
LOT A3 #35N 20–50mm	1.1	2.3	20.9	67.7	0.4	0.1	0.6	2.1	0.2	4.5	n/a	0.01	0.0	35.0						
LOT A3 #35N 20–50mm	1.2	2.3	20.8	67.7	0.4	0.1	0.6	2.1	0.2	4.5	0.00	0.01	0.0	35.0					Sum:	0.021
LOT A3 #35N 50–70mm	1.1	2.3	20.7	68.0	0.3	0.1	0.6	2.0	0.2	4.6	n/a	0.01	0.0	60.0					Corrosion thickness (µm):	0.6
LOT A3 #35N 50–70mm	1.1	2.3	20.7	68.0	0.3	0.1	0.6	2.1	0.2	4.6	n/a	0.01	0.0	60.0						
LOT A3 #35N 70–100mm	1.1	2.3	20.7	68.1	0.3	0.1	0.6	2.0	0.2	4.6	n/a	0.01	0.0	85.0						
LOT A3 #35N 70–100mm	1.1	2.3	20.7	68.1	0.3	0.1	0.6	2.0	0.2	4.6	n/a	0.01	0.0	85.0						

Ident	Na2O	MgO	Al_2O_3	SiO_2	SO_3	Cl	K_2O	CaO	TiO_2	Fe_2O_3	CuO	MnO	P_2O_5	Distance	Id	Position	Average CuO (wt%)	Mass CuO (g)	Mass Cu (g)	Volume copper (cm^3)
LOT S2 #9E 0–2mm d5c769	1.5	2.3	18.9	61.8	6.1	0.1	0.5	3.6	0.2	4.5	0.44	0.0	0.0	1	LOT S2 #9E					
LOT S2 #9E 0–2mm d5c769	1.5	2.2	18.2	59.3	7.9	0.1	0.6	5.0	0.2	4.5	0.48	0.0	0.0	1		0–2 mm	0.46	0.48	0.38	0.043
LOT S2 #9E 2–10mm d5c76a	1.6	2.4	20.1	66.3	1.9	0.1	0.5	1.8	0.2	4.8	0.14	0.0	0.0	6						
LOT S2 #9E 2–10mm d5c76a	1.6	2.3	19.8	66.5	2.0	0.1	0.6	1.9	0.2	4.7	0.13	0.0	0.0	6		2–10 mm	0.14	0.62	0.50	0.055
LOT S2 #9E 10–20mm d5c76b	1.7	2.4	20.5	67.1	1.2	0.1	0.6	1.6	0.2	4.6	0.06	0.0	0.0	15						
LOT S2 #9E 10–20mm d5c76b	1.7	2.4	20.5	67.1	1.1	0.1	0.6	1.6	0.2	4.6	0.06	0.0	0.0	15		10–20 mm	0.06	0.40	0.32	0.035
LOT S2 #9E 20–50mm d5c76c	1.7	2.3	20.5	67.1	1.2	0.1	0.6	1.7	0.2	4.6	0.01	0.0	0.0	35						
LOT S2 #9E 20–50mm d5c76c	1.7	2.3	20.6	67.1	1.2	0.1	0.6	1.7	0.2	4.6	0.01	0.0	0.0	35					Sum:	0.134
LOT S2 #9E 50–70mm d5c76d	1.7	2.3	20.7	68.1	0.3	0.1	0.6	1.4	0.2	4.6	0.00	0.0	0.0	60					Corrosion thickness (µm):	3.9
LOT S2 #9E 50–70mm d5c76d	1.7	2.3	20.7	68.1	0.4	0.1	0.6	1.4	0.2	4.6	0.00	0.0	0.0	60						
LOT S2 #9E 70–100mm d5c76e	1.7	2.3	20.7	68.2	0.3	0.1	0.6	1.3	0.2	4.6	0.00	0.0	0.0	85						
LOT S2 #9E 70–100mm d5c76e	1.7	2.3	20.7	68.2	0.3	0.1	0.6	1.3	0.2	4.6	0.00	0.0	0.0	85						

Ident	Na2O	MgO	Al_2O_3	SiO_2	SO_3	Cl	K_2O	CaO	TiO_2	Fe_2O_3	CuO	MnO	P_2O_5	Distance	Id	Position	Average CuO (wt%)	Mass CuO (g)	Mass Cu (g)	Volume copper (cm^3)
LOT S2 #11W 0–2mm d5c76f	1.6	2.4	19.4	64.0	4.0	0.1	0.5	2.7	0.2	4.8	0.41	0.0	0.0	1.0	LOT S2 #11W					
LOT S2 #11W 0–2mm d5c76f	1.6	2.3	19.1	63.9	4.2	0.1	0.6	2.9	0.2	4.6	0.40	0.0	0.0	1.0		0–2 mm	0.41	0.42	0.34	0.038
LOT S2 #11W 2–10mm d5c770	1.6	2.4	20.1	66.8	1.8	0.1	0.6	1.7	0.2	4.7	0.17	0.0	0.0	6.0						
LOT S2 #11W 2–10mm d5c770	1.6	2.4	19.9	66.5	1.8	0.1	0.6	1.9	0.2	4.8	0.17	0.0	0.0	6.0		2–10 mm	0.17	0.77	0.62	0.069
LOT S2 #11W 10–20mm d5c771	1.7	2.4	20.5	67.1	1.1	0.1	0.6	1.6	0.2	4.6	0.07	0.0	0.0	15.0						
LOT S2 #11W 10–20mm d5c771	1.7	2.4	20.5	67.1	1.1	0.1	0.6	1.6	0.2	4.6	0.06	0.0	0.0	15.0		10–20 mm	0.07	0.43	0.34	0.038
LOT S2 #11W 20–50mm d5c772	1.7	2.3	20.5	67.1	1.2	0.1	0.6	1.7	0.2	4.6	0.00	0.0	0.0	35.0						
LOT S2 #11W 20–50mm d5c772	1.7	2.3	20.5	67.2	1.2	0.1	0.6	1.7	0.2	4.6	0.00	0.0	0.0	35.0					Sum:	0.144
LOT S2 #11W 50–70mm d5c773	1.7	2.3	20.8	68.0	0.3	0.1	0.6	1.3	0.2	4.6	0.00	0.0	0.0	60.0					Corrosion thickness (µm):	4.3
LOT S2 #11W 50–70mm d5c773	1.7	2.3	20.8	68.0	0.3	0.1	0.6	1.3	0.2	4.6	0.00	0.0	0.0	60.0						
LOT S2 #11W 70–100mm d5c774	1.7	2.3	20.8	68.0	0.3	0.1	0.6	1.3	0.2	4.6	0.00	0.0	0.0	85.0						
LOT S2 #11W 70–100mm d5c774	1.7	2.3	20.8	68.0	0.3	0.1	0.6	1.3	0.2	4.6	0.00	0.0	0.0	85.0						

															Id	Position	Average CuO (wt%)	Mass CuO (g)	Mass Cu (g)	Volume copper (cm^3)
LOT S2 #15S 0–2mm	1.5	2.2	17.9	58.0	9.0	0.1	0.5	5.4	0.2	4.6	0.59	0.01	0.0	1.0	LOT S2 #15S					
LOT S2 #15S 0–2mm	1.4	2.1	17.4	57.1	10.0	0.1	0.5	5.9	0.2	4.5	0.60	0.01	0.0	1.0		0–2 mm	0.60	0.62	0.50	0.055
LOT S2 #15S 2–10mm	1.6	2.4	19.4	65.2	3.2	0.2	0.6	2.5	0.2	4.5	0.18	0.01	0.0	6.0						
LOT S2 #15S 2–10mm	1.6	2.4	19.5	65.1	3.4	0.2	0.5	2.5	0.2	4.6	0.18	0.01	0.0	6.0		2–10 mm	0.18	0.82	0.65	0.073
LOT S2 #15S 10–20mm	1.6	2.3	19.5	65.4	3.2	0.2	0.6	2.5	0.2	4.5	0.07	0.01	0.0	15.0						
LOT S2 #15S 10–20mm	1.6	2.3	19.6	65.1	3.3	0.2	0.5	2.4	0.2	4.6	0.06	0.01	0.0	15.0		10–20 mm	0.06	0.39	0.31	0.035
LOT S2 #15S 20–50mm	1.8	2.4	20.7	67.9	0.5	0.2	0.6	1.3	0.2	4.5	0.01	0.02	0.0	35.0						
LOT S2 #15S 20–50mm	1.8	2.4	20.7	67.9	0.5	0.2	0.6	1.3	0.2	4.5	0.01	0.01	0.0	35.0					Sum:	0.163
LOT S2 #15S 50–70mm	1.7	2.3	20.7	68.1	0.3	0.2	0.6	1.3	0.2	4.6	n/a	0.01	0.0	60.0					Corrosion thickness (µm):	4.8
LOT S2 #15S 50–70mm	1.7	2.3	20.7	68.1	0.3	0.2	0.6	1.3	0.2	4.6	0.00	0.02	0.0	60.0						
LOT S2 #15S 70–100mm	1.7	2.3	20.5	68.2	0.3	0.2	0.6	1.3	0.2	4.7	0.00	0.02	0.0	85.0						
LOT S2 #15S 70–100mm	1.7	2.3	20.6	68.2	0.3	0.2	0.6	1.3	0.2	4.7	n/a	0.01	0.0	85.0						

Ident	Na2O	MgO	Al_2O_3	SiO_2	SO_3	Cl	K_2O	CaO	TiO_2	Fe_2O_3	CuO	MnO	P_2O_5	Distance	Id	Position	Average CuO (wt%)	Mass CuO (g)	Mass Cu (g)	Volume copper (cm^3)
LOT S2 #25E 0–2mm	1.7	2.3	20.0	67.0	1.6	0.1	0.6	1.9	0.2	4.5	0.09	0.01	0.0	1.0	LOT S2 #25E					
LOT S2 #25E 0–2mm	1.7	2.3	20.1	66.8	1.6	0.1	0.6	2.0	0.2	4.6	0.08	0.01	0.0	1.0		0–2 mm	0.08	0.08	0.07	0.008
LOT S2 #25E 2–10mm	1.8	2.3	20.2	68.0	0.8	0.2	0.6	1.4	0.2	4.5	0.01	0.01	0.0	6.0						
LOT S2 #25E 2–10mm	1.8	2.3	20.3	67.8	0.8	0.2	0.5	1.4	0.2	4.5	0.01	0.01	0.0	6.0		2–10 mm	0.01	0.05	0.04	0.005
LOT S2 #25E 10–20mm	1.7	2.3	20.1	68.3	0.7	0.2	0.6	1.4	0.2	4.4	0.00	0.01	0.0	15.0						
LOT S2 #25E 10–20mm	1.7	2.4	20.2	67.9	0.8	0.2	0.6	1.4	0.2	4.6	0.00	0.01	0.0	15.0		10–20 mm	0.00	0.01	0.01	0.001
LOT S2 #25E 20–50mm	1.7	2.4	20.7	67.8	0.6	0.2	0.6	1.4	0.2	4.5	0.00	0.01	0.0	35.0						
LOT S2 #25E 20–50mm	1.7	2.4	20.7	67.8	0.6	0.2	0.6	1.4	0.2	4.5	0.00	0.01	0.0	35.0					Sum:	0.013
LOT S2 #25E 50–70mm	1.7	2.3	20.6	67.7	0.6	0.1	0.6	1.5	0.2	4.7	n/a	0.01	0.0	60.0					Corrosion thickness (µm):	0.4
LOT S2 #25E 50–70mm	1.7	2.3	20.6	67.7	0.6	0.1	0.6	1.5	0.2	4.6	n/a	0.01	0.0	60.0						
LOT S2 #25E 70–100mm	1.7	2.4	20.7	67.9	0.4	0.2	0.5	1.3	0.2	4.6	n/a	0.01	0.0	85.0						
LOT S2 #25E 70–100mm	1.7	2.4	20.7	68.0	0.4	0.2	0.6	1.3	0.2	4.6	n/a	0.01	0.0	85.0						

															Id	Position	Average CuO (wt%)	Mass CuO (g)	Mass Cu (g)	Volume copper (cm^3)
LOT S2 #33S 0–2mm d5c781	1.6	2.3	20.6	68.0	0.4	0.1	0.6	1.4	0.2	4.7	0.04	0.0	0.0	1.0	LOT S2 #33S					
LOT S2 #33S 0–2mm d5c781	1.6	2.3	20.6	68.0	0.4	0.1	0.6	1.5	0.2	4.7	0.05	0.0	0.0	1.0		0–2 mm	0.05	0.05	0.04	0.004
LOT S2 #33S 2–10mm d5c782	1.6	2.3	20.2	68.0	0.8	0.1	0.6	1.7	0.2	4.6	0.00	0.0	0.0	6.0						
LOT S2 #33S 2–10mm d5c782	1.6	2.3	20.2	67.7	0.8	0.1	0.6	1.8	0.2	4.7	0.00	0.0	0.0	6.0		2–10 mm	0.00	0.01	0.01	0.001
LOT S2 #33S 10–20mm d5c783	1.6	2.3	20.3	67.9	0.7	0.1	0.6	1.7	0.2	4.6	0.00	0.0	0.0	15.0						
LOT S2 #33S 10–20mm d5c783	1.6	2.3	20.3	68.1	0.7	0.1	0.6	1.5	0.2	4.7	0.00	0.0	0.0	15.0		10–20 mm	0.00	0.00	0.00	0.000
LOT S2 #33S 20–50mm d5c784	1.6	2.3	20.9	67.7	0.4	0.1	0.6	1.5	0.2	4.7	0.00	0.0	0.0	35.0						
LOT S2 #33S 20–50mm d5c784	1.6	2.3	20.9	67.7	0.4	0.1	0.6	1.5	0.2	4.6	0.00	0.0	0.0	35.0					Sum:	0.005
LOT S2 #33S 50–70mm d5c785	1.6	2.3	20.9	68.1	0.3	0.1	0.6	1.4	0.2	4.6	0.00	0.0	0.0	60.0					Corrosion thickness (µm):	0.2
LOT S2 #33S 50–70mm d5c785	1.6	2.4	20.8	68.0	0.3	0.1	0.6	1.4	0.2	4.6	0.00	0.0	0.0	60.0						
LOT S2 #33S 70–100mm d5c786	1.6	2.4	20.8	68.1	0.3	0.1	0.6	1.4	0.2	4.6	0.00	0.0	0.0	85.0						
LOT S2 #33S 70–100mm d5c786	1.6	2.3	20.8	68.2	0.3	0.1	0.6	1.4	0.2	4.5	0.00	0.0	0.0	85.0						

Ident	Na2O	MgO	Al_2O_3	SiO_2	SO_3	Cl	K_2O	CaO	TiO_2	Fe_2O_3	CuO	MnO	P_2O_5	Distance	Id	Position	Average CuO (wt%)	Mass CuO (g)	Mass Cu (g)	Volume copper (cm^3)
LOT S2 #35W 0–2mm	1.6	2.3	20.5	67.8	0.7	0.1	0.6	1.5	0.2	4.6	0.07	0.01	0.0	1.0	LOT S2 #35W					
LOT S2 #35w 0–2mm	1.7	2.3	20.3	67.7	0.8	0.1	0.6	1.6	0.2	4.5	0.26	0.01	0.0	1.0		0–2 mm	0.16	0.17	0.14	0.015
LOT S2 #35w 2–10mm	1.6	2.3	20.3	68.2	0.6	0.1	0.6	1.5	0.2	4.6	0.01	0.02	0.0	6.0						
LOT S2 #35W 2–10mm	1.6	2.3	20.3	67.7	0.7	0.1	0.6	1.7	0.2	4.7	0.00	0.01	0.0	6.0		2–10 mm	0.00	0.02	0.02	0.002
LOT S2 #35W 10–20mm	1.6	2.3	20.3	68.1	0.7	0.1	0.6	1.5	0.2	4.6	0.00	0.01	0.0	15.0						
LOT S2 #35w 10–20mm	1.7	2.3	20.2	68.3	0.6	0.1	0.6	1.5	0.2	4.5	0.00	0.01	0.0	15.0		10–20 mm	0.00	0.01	0.01	0.001
LOT S2 #35w 20–50mm	1.7	2.3	20.8	67.9	0.5	0.1	0.6	1.4	0.2	4.5	0.00	0.01	0.0	35.0						
LOT S2 #35W 20–50mm	1.7	2.4	20.8	67.8	0.5	0.1	0.6	1.4	0.2	4.5	n/a	0.01	0.0	35.0					Sum:	0.018
LOT S2 #35W 50–70mm	1.7	2.3	20.7	67.8	0.6	0.1	0.6	1.5	0.2	4.6	n/a	0.01	0.0	60.0					Corrosion thickness (µm):	0.5
LOT S2 #35W 50–70mm	1.7	2.3	20.7	67.8	0.6	0.1	0.6	1.5	0.2	4.6	n/a	0.01	0.0	60.0						
LOT S2 #35W 70–100mm	1.7	2.3	20.6	67.9	0.6	0.1	0.6	1.5	0.2	4.6	n/a	0.01	0.0	85.0						
LOT S2 #35W 70–100mm	1.7	2.3	20.6	67.9	0.6	0.1	0.6	1.4	0.2	4.6	n/a	0.01	0.0	85.0						

Ident	Na2O	MgO	Al_2O_3	SiO_2	P_2O_5	SO_3	Cl	K_2O	CaO	TiO_2	MnO	Fe_2O_3	CuO
LOT A2 MX80 Referens block 4	1.7	2.3	20.5	67.5	0.0	0.7	0.0	0.7	1.7	0.2	0.0	4.6	0
LOT A2 MX80 Referens block 4	1.6	2.4	20.6	67.8	0.0	0.7	0.0	0.5	1.6	0.2	0.0	4.6	0.001
LOT A2 MX80 Referens block 29	1.7	2.4	20.5	67.6	0.0	0.7	0.0	0.7	1.7	0.2	0.0	4.6	0.001
LOT A2 MX80 Referens block 29	1.7	2.3	20.5	67.7	0.0	0.7	0.0	0.7	1.7	0.2	0.0	4.5	0.001
LOT A2 MX80 Referens block 29	1.6	2.4	20.8	67.3	0.0	0.9	0.0	0.5	1.7	0.2	0.0	4.6	n/a
LOT A2 MX80 Referens block 29	1.6	2.4	20.8	67.3	0.0	0.7	0.0	0.5	1.8	0.2	0.0	4.7	n/a
LOT A2 MX80 Referens block 24	1.7	2.3	20.5	67.7	0.0	0.7	0.0	0.6	1.7	0.2	0.0	4.5	0
LOT A2 MX80 Referens block 24	1.7	2.3	20.4	67.6	0.0	0.8	0.0	0.7	1.7	0.2	0.0	4.6	0
LOT A2 MX80 Referens block 24	1.6	2.4	20.8	67.5	0.0	0.8	0.0	0.5	1.7	0.2	0.0	4.6	n/a
LOT A2 MX80 Referens block 24	1.6	2.4	21.0	66.7	0.0	0.9	0.0	0.5	1.9	0.2	0.0	4.6	n/a

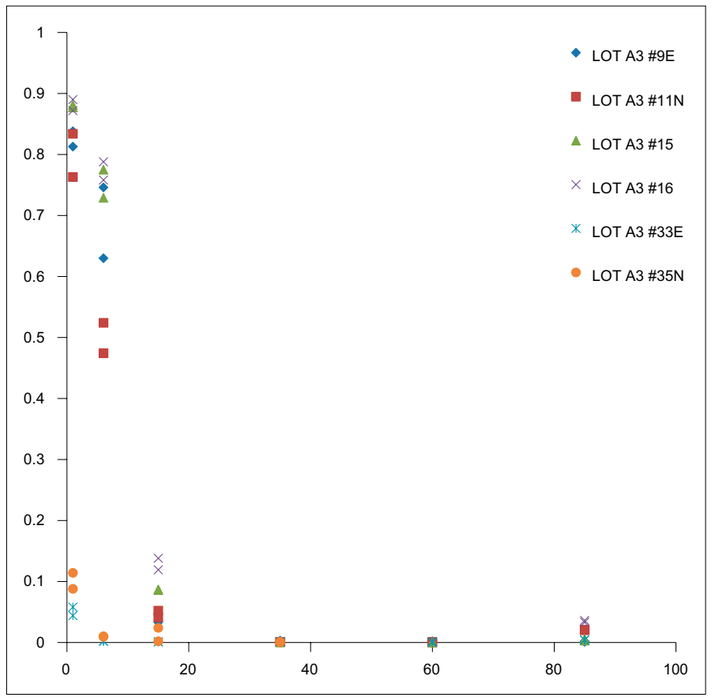

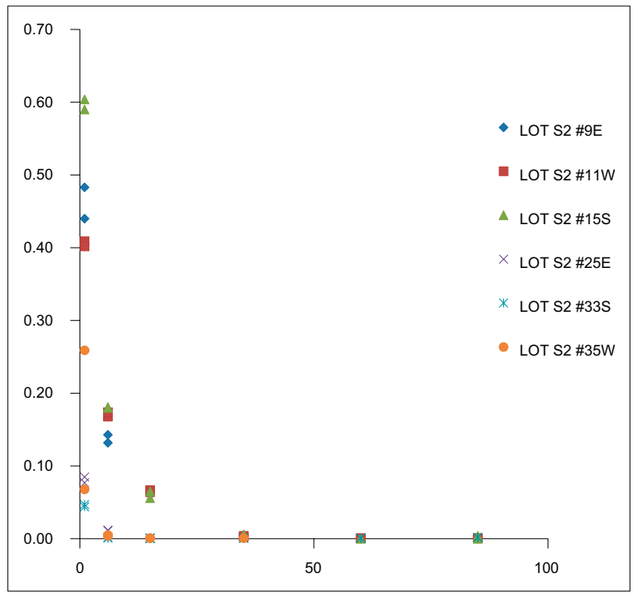

Appendix K

Integrated corrosion depths of pipes

Integrated corrosion depth in LOT S2			
Data from Figure 1-3		**Data from Figure 4-1**	
T (°C)	**Length (mm)**	**Corr/temp**	**Corr/area**
25.0	23.0	0.3	0.1
35.0	13.0	0.4	0.1
45.0	6.0	0.7	0.0
55.0	17.0	1.1	0.2
65.0	14.0	1.7	0.2
75.0	13.0	2.7	0.4
85.0	14.0	4.1	0.6
			1.5

Integrated corrosion depth in LOT A3			
Data from Figure 1-3		**Data from Figure 4-1**	
T (°C)	**Length (mm)**	**Corr/temp**	**Corr/area**
25.0	24.0	0.3	0.1
35.0	9.0	0.5	0.0
45.0	4.0	0.7	0.0
55.0	4.0	1.1	0.0
65.0	3.0	1.7	0.1
75.0	3.0	2.7	0.1
85.0	13.0	4.1	0.5
95.0	12.0	6.3	0.8
105.0	14.0	9.8	1.4
115.0	14.0	15.1	2.1
			5.1

Arkitektkopia AB, Bromma, 2020

SKB is responsible for managing spent nuclear fuel and radioactive waste produced by the Swedish nuclear power plants such that man and the environment are protected in the near and distant future.

skb.se